„HENRI COANDĂ”
AIR FORCE ACADEMY

ROMANIA

ASSOCIATION for
RESEARCH and EDUCATION

„GENERAL M. R. STEFANIK”
ARMED FORCES ACADEMY

SLOVAK REPUBLIC

# AFASES 2015

ISSN, ISSN-L: 2247-3173

## Volume II

**20 th “Henri Coandă”**
**Air Force Academy Anniversary**
**1995-2015**

**Publishing House of "Henri Coanda" Air Force Academy**

**Str. Mihai Viteazu 160, Brasov 500183, ROMANIA**
**Phone: +40 268 423 421, Fax: +40 268 422 004**
**Webpage: www.afahc.ro/ro/editura/editura.html**
**E-mail: editura@afahc.ro**

# *INTERNATIONAL SCIENTIFIC COMMITTEE*

***Presidents ship:***

Air Flotilla General **Vasile BUCINSCHI**, PhD

Brigadier General **Boris ĎURKECH**, PhD

***Members:***

Brigadier General **Ghiță BÂRSAN**, PhD

Professor Eng. **Milan SOPOCI,** PhD

Associate Professor **Mária PETRUFOVÁ**, PhD

Associate Professor Eng. **Miroslav ŠKOLNÍK**, PhD

Associate Professor Eng. **Marcel HARAKAL**, PhD

Professor Dr. Hab. **Marek WALANCIK**, PhD

Professor **Barry JACKSON**, PhD

Professor **Florentin SMARANDACHE,** PhD

Associate Professor **Ludovic Dan LEMLE**, PhD,

Professor **Yiwen JIANG**, PhD

Professor **Gherman A. DE LA REZA**, PhD

Professor Eng. **Juraj MIČEK,** PhD

Assistant Professor **Ozgur Koray SAHINGOZ,** PhD

Professor **Mircea LUPU**, PhD

Professor **Corneliu UDREA**, PhD

Professor **Victor Valeriu PATRICIU**, PhD

Professor **Stefan-Gheorghe PENTIUC**, PhD

Professor **Răzvan - Lucian ANDRONIC,** PhD

Professor **Ciprian Ioan RĂULEA,** PhD

Professor **Constantin -Edmond CRACSNER,** PhD

Professor **Cătălin Marius GHERASIM,** PhD

Associate Professor **Rudolf HORAK**, PhD

Associate Professor **Jaromir MARES**, PhD

Professor **Aurel CRIŞAN**, PhD

Colonel **Mihail ANTON**, PhD

Professor **Gavrilă CALEFARIU**, PhD

Professor **Constantin DUGULEANĂ**, PhD

Professor **Philippe DONDON**, PhD

Professor **Maria IOANIDES,** PhD

Professor **Melissa LUKA**, PhD

Professor **Daniela ROSCA**, PhD

Professor **Robert SZABOLCSI**, PhD

Professor Eng. **Alex STEFAN,** PhD

Professor **Maria TUDOR,** PhD

Associate Professor **Anca PETRE**, PhD

Professor **Petrică VIZUREANU**, PhD

Associate Professor Eng. **Sławomir AUGUSTYN**, PhD

Professor **Marek MARKIEWICZ,** PhD

Professor Eng. **Marian PEARSICA**, PhD

Professor Eng. **Constantin ROTARU,** PhD

Professor **Traian ANASTASIEI,** PhD

Associate Professor Eng. **Doru LUCULESCU**, PhD

Professor Eng. **Mircea BOŞCOIANU**, PhD

# *ORGANIZING COMMITTEE*

***President*:**

LTC **Laurian GHERMAN**,PhD

***Members*:**

Prof. **Ion DINESCU**, PhD
Maj. **Cătălin CIOACĂ**, PhD
Capt. Cmd. **Ionică CÎRCIU**, PhD
Maj. **Cornel ARAMĂ**, PhD
Assist. Prof. **Liliana MIRON**, PhD
Assist. Prof. **Constantin STRÎMBU**, PhD
Assist. Prof. **Cristian CONSTANTINESCU**, PhD
Assist. Prof. **Gheorghe RADU**, PhD
Math. **Carmen URSOIU**
Lt.Col. **Cristian ENE**
Assoc. Prof. **Diana ILIŞOI**, PhD
Assist. Prof **Mihaela SMEADĂ**, PhD
Assist. **Bogdan Gheorghe MUNTEANU**, PhD
Assist. **Daniela NAGY**, PhD
Psychologist **Mihaela OANCEA**
Cmd. **Marian BOBE**

***Logistics:***

Col **Dumitru DINU**
Lt Col **Bogdan CHIOSEAUA**
Lt **Cosmin TĂTULESCU**
WO **Marian MIHALACHE**
WO **Sergiu OBREJA**
WO **Daniel CHERCIU**

***Secretariat:***

Maj **Criste RĂU**
Eng. **Mariana GHINDĂOANU**

"HENRI COANDA"
AIR FORCE ACADEMY
ROMANIA

"GENERAL M.R. STEFANIK"
ARMED FORCES ACADEMY
SLOVAK REPUBLIC

INTERNATIONAL CONFERENCE of SCIENTIFIC PAPER
AFASES 2015
Brasov, 28-30 May 2015

# CONTENTS

## VOLUME I


| *AIR FORCE* | *Pag* |
|---|---|
| **Jacques ABEN, Julien MALIZARD**<br>***THE SPIRIT OF DEFENCE AND ITS DETERMINANTS*** | **13** |
| **Traian ANASTASIEI**<br>***CONNECTIONS OF AIR POWER*** | **25** |
| **Daniel-Nicolae BĂNICĂ**<br>***EUROPEAN ANTIMISSILE DEFENSE SYSTEM –POST SECOND PHASE IMPLEMENTATION PERSPECTIVE IN THE CONTEXT OF NATO-RUSSIA RELOCATION*** | **33** |
| **Oliver CIUICĂ, Eduard MIHAI**<br>***HUMAN ERROR – COCKPIT VULNERABILITIES*** | **43** |
| **Iulia-Mădălina DUMITRU, Mircea BOŞCOIANU**<br>***HUMAN FACTORS CONTRIBUTION TO AVIATION SAFETY*** | **49** |
| **Ion MAGDALENA**<br>***UNMANNED AIR VEHICLES IN ROMANIA. STEPS TO THE FUTURE*** | **55** |
| **Diana MANOLACHE, Ciprian CHIŞ**<br>***NATO BOMBING IN THE FORMER REPUBLIC OF YUGOSLAVIA*** | **61** |
| **Eduard MIHAI, Oliver CIUICĂ**<br>***FOUNDATION OF THE EARLY PILOTING SCHOOLS IN ROMANIA*** | **71** |
| **Ovidiu-Gheorghe MOŞOIU**<br>***ECONOMIC COOPERATION AND REVITALIZING THE NATIONAL DEFENSE INDUSTRY, DETERMINANT FACTORS IN STRENGTHNING THE FUNDAMENTAL NATIONAL INTERESTS IN THE EUROPEAN COMMUNITY AND NATO*** | **77** |
| **Ilie PĂUN**<br>***THE INTEROPERABILITY OF THE INTELLIGENCE SYSTEM – A SALIENT PREREQUISITE FOR ACQUIRING INTELLIGENCE COMPATIBILITY*** | **85** |
| **Vasile PRISACARIU, Ionică CÎRCIU, Sebastian POP**<br>***INSTRUMENTS FOR THE EVALUATION OF THE AERODYNAMIC PERFORMANCE OF WIND TUNNELS*** | **93** |
| **Marius RĂDULESCU, Vasile ŞANDRU**<br>***SHORAD SOLUTIONS FOR THE AIR FORCES SYSTEMS UP-GRADE*** | **99** |
| **Róbert SZABOLCSI**<br>***NIGHT WATCHBIRD UAV SYSTEM: AN EFFECTIVE TOOL IMPROVING FORCE PROTECTION CAPABILITIES IN THE WAR THEATRES*** | **105** |
| **Daniel ŞTEFĂNESCU**<br>***NATO STRATEGY TO DEFEAT ENEMY FORCES IN THE HYBRID WAR*** | **113** |

## *MANAGEMENT*


| | |
|---|---|
| **Constantin-Valentin BORDEI**<br>***THE CHARACTERISTICS OF THE TERRORIST TARGETS IDENTIFICATION PROCESS*** | **119** |
| **Paul-Marian FUSEA**<br>***THE MILITARY AUTHORITY – THE DECISIONAL SUPPORT OF THE MILITARY ADMINISTRATION*** | **125** |
| **Marius MILANDRU**<br>***LOGISTIC DECISION MAKING PROCESS INSIDE THE MILITARY ORGANISATION USING EXPERT SYSTEMS*** | **131** |
| **Elena POPOVICI, Rosa Elena PINOS NEIRA**<br>***INSTITUTIONAL GOVERNANCE STRATEGIES OF HUMAN RESOURCES IN THE PUBLIC INSTITUTIONS OF THE REPUBLIC OF ECUADOR*** | **137** |
| **Mădălin SLĂNICEANU**<br>***RESEARCH ON CADEDTS' PREFERENCES AND REQUIREMENTS REGARDING THE GUIDED PHYSICAL TRAINING AND SPORT ACTIVITY*** | **141** |
| **Milan SOPÓCI, Marek WALANCIK**<br>***CONCEPTION OF COMPETENCES DEVELOPMENT OF AIR DEFENCE OF ARMED FORCES*** | **147** |


## *SOCIO - HUMANITIES*


| | |
|---|---|
| **Florin-Marian ANTONESCU, Petronela-Sorina VÎRBAN**<br>***RELATIONSHIP MOTIVATION - VOCATIONAL MATURITY TO STUDENTS TO PRACTICE SPORTS CONTACT*** | **153** |
| **Ramona-Cristina BALANESCU**<br>***THE PROJECT-BASED LEARNING IN THE HIGHER EDUCATION - THEORETICAL AND PRACTICAL ASPECTS*** | **159** |
| **Angela BLOGUȚ**<br>***STRESSING FACTORS IN AVIATION*** | **165** |
| **Ileana-Mihaela CHIRIȚESCU**<br>***ADOLESCENT DEVELOPMENT: NEEDS, DESIRES, REQUIREMENTS*** | **171** |
| **Cătălin CIOACĂ, Horațiu MOGA**<br>***THE ARTICULATION AND AGGREGATION OF INTERESTS IN THE ANALYSIS OF INFORMATION TECHNOLOGIES COOPERATION*** | **175** |
| **Georgiana CORCACI**<br>***SATISFACTION AND PERFORMANCE WORK -DIMENSIONS RELEVANT FOR THE ORGANIZATIONAL YIELD*** | **185** |
| **Constantin-Edmond CRACSNER, Lidia MOGOŞAN**<br>***IRRATIONAL BELIEFS, PROFESSIONAL STRESS AND PERSONALITY IN THE MILITARY*** | **191** |
| **Elena-Oliviana EPURESCU**<br>***CAREER COUNSELOR'S/CONSULTANT'S ROLE FOR A PROFESSION*** | **203** |
| **Diana ILIŞOI, Ana-Maria FURTUNĂ**<br>***STRESS IN MILITARY FIELD*** | **209** |
| **Cristian-Vlad IRIMIA**<br>***HUMAN SECURITY PSYCHO-MORAL CONSIDERATIONS*** | **213** |

| | |
|---|---|
| **Irina IOANA**<br>***THE TERRORISM AND ITS PSYCHOLOGICAL EFFECTS*** | **219** |
| **Cosmin IVANCIU**<br>***GUNS FOR HIRE: PRIVATE MILITARY COMPANIES AND THEIR STATUS UNDER INTERNATIONAL HUMANITARIAN LAW*** | **227** |
| **Nicoleta LITOIU**<br>***FACILITATION OF LEARNING AT A DISTANCE TRAING PROGRAM*** | **235** |
| **Nicoleta LITOIU**<br>***PROFESSIONAL TRAINING PROGRAMS FOR PRACTICIONERS IN CAREER COUNSELING*** | **243** |
| **Roxana MAIER, Alina MARIAN**<br>***THE TEACHER-PARENT EDUCATIONAL PARTNERSHIP, HEALTH PROMOTION PROGRAM - SPECIFIC CASE - DENTAL HEALTH*** | **249** |
| **Loredana MANASIA**<br>***CREATING A-HA MOMENTS IN TEACHING PRACTICE. ROUTINE VERSUS ADAPTIVE METACOGNTIVE BEHAVIORS IN TEACHERS*** | **255** |
| **Gabriela-Carmen OPROIU**<br>***THEORETICAL APPROACHES ON LEARNING FACILITATION IN MENTORING*** | **263** |
| **Anca PĂUNESCU, Laviniu LĂPĂDAT**<br>***MEDIATIZATED WORD. INFORMATION. EDUCATION. MANIPULATION*** | **269** |
| **Silviu PETRE, Gheorghe SĂVOIU**<br>***SEARCHING FOR SHREADS OF ORDER. THE STRUCTURE OF TODAY'S INTERNATIONAL SYSTEM*** | **277** |
| **Lavinia-Maria PRUTEANU, Viorel ROBU**<br>***ASPECTS OF PROFESSIONAL BURNOUT AMONG NURSES*** | **287** |
| **Monica A.P. PURCARU, Gabriela CÂMPEAN**<br>***FIGHTING SCHOOL FAILURE IN MATHEMATICS*** | **293** |
| **Răzvan George ŞTEFAN**<br>***ETHICS ON THE HORIZON. TOWARDS A COMPLEX ASSUMPTION OF A SECURITY CULTURE*** | **301** |
| **Marilena TICUŞAN, Hurjui ELENA**<br>***CRITICAL THINKING IN DEVELOPMENT OF CREATIVITY*** | **309** |
| **Marilena TICUŞAN**<br>***EDUCATIONAL ASPECTS OF ASSESSMENT OF CREATIVITY*** | **315** |

"HENRI COANDA"
AIR FORCE ACADEMY
ROMANIA

"GENERAL M.R. STEFANIK"
ARMED FORCES ACADEMY
SLOVAK REPUBLIC

INTERNATIONAL CONFERENCE of SCIENTIFIC PAPER
AFASES 2015
Brasov, 28-30 May 2015

# VOLUME II

## *ELECTRICAL AND ELECTRONICAL ENGINEERING*


| | |
|---|---|
| **Philippe DONDON, Ecaterina-Liliana MIRON**<br>***EFFECT OF LIGHT DEPENDANT RESISTOR MISMATCHING AND IMPACT OF NON LINEARITY IN A SMALL SCALE SOLAR TRACKING SYSTEM*** | **321** |
| **Florin-Andrei GEORGESCU, Mihai DATCU, Dan RĂDUCANU**<br>***GABOR AND WEBER LOCAL DESCRIPTORS PERFORMANCE IN MULTISPECTRAL EARTH OBSERVATION IMAGE DATA ANALYSIS*** | **331** |
| **Gheorghe MORARIU, Mihai MIRON**<br>***FRACTAL ANTENNA WITH HEXAGONAL RESONATORS*** | **337** |
| **Dan STOICA, Adina BOTEANU, Mihai ENACHE, Albert PLOŞNIŢĂ**<br>***INFLUENCE OF THE INTERCONNECTING CABLES ON EQUIPMENTS ELECTROMAGNETIC EMISSIONS SPECTRUM*** | **341** |
| **Constantin STRÎMBU**<br>***ABOUT POLY-PHASE VOLTAGE RECTIFIERS OPERATION*** | **347** |
| **Mihai TIMIS, Alexandru VALACI, Calin MONOR**<br>***IMPROVEMENTS METHODS FOR DESIGN OF MULTIFUNCTIONAL REGISTERS WITH DECODED MODE SIGNALS*** | **351** |
| **Grigore VASILIU**<br>***VALIDATION OF SPECTRAL ANALYSIS RESULTS USING PLC IMPLEMENTED AI TECHNIQUES*** | **357** |


## *MECHANICAL ENGINEERING. MATERIALS AND TECHNOLOGY*


| | |
|---|---|
| **Cornel ARAMĂ, Mariana SAVA, Lavinia CUCU**<br>***ANALYSIS OF THE LIGHT OFF-ROAD VEHICLE ENDOWMENT POSSIBILITIES IN ORDER TO USE IT FOR AIR FORCE MISSIONS*** | **363** |
| **Sławomir AUGUSTYN, Bogumił ZNOJEK**<br>***THE NEW VISION IN DESIGNING OF AIRPORT*** | **369** |
| **Sławomir AUGUSTYN, Telesfor-Marek MARKIEWICZ**<br>***THE USING OF NANOCOMPOSITE HEATING SYSTEM FOR AVIATION DESIGNING*** | **373** |
| **Bogdan BARABAŞ, Adriana FLORESCU, Sorin BARABAŞ**<br>***SAVING ENERGY ESTIMATION FOR USE OF HOLLOW ROLLERS IN BEARINGS UTILIZED IN WIND ENERGY TURBINES*** | **377** |
| **E.S. BÂRCĂ, A.G. PLĂIAŞU, Mihaela VLADU, Marioara ABRUDEANU, G. MAHU, Corneliu MUNTEANU**<br>***STRESS DISTRIBUTION FOR A PISTON WITH AN $AL_2O_3$ TOP LAYER DEPOSITED ON THE PISTON HEADS WHICH ABSORBS GAS PRESSURE*** | **383** |

| | |
|---|---|
| **Bogdan-Alexandru BELEGA, Trung Duc NGUYEN**<br>***ANALYSIS OF FLOW IN CONVERGENT-DIVERGENT ROCKET ENGINE NOZZLE USING COMPUTATIONAL FLUID DYNAMICS*** | **389** |
| **Bogdan-Alexandru BELEGA, Amado ŞTEFAN**<br>***DYNAMIC ANALYSIS OF COMPOSITE WINGS*** | **395** |
| **Ion DINESCU**<br>***CHARACTERISTICS OF SLUDGE RESULTED FROM BALL-BEARINGS RECTIFICATION*** | **401** |
| **Lica FLORE, Albert Arnau CUBILLO**<br>***DYNAMIC MECHANICAL ANALYSIS OF AN AIRCRAFT WING WITH EMPHASIS ON VIBRATION MODES CHANGE WITH LOADING*** | **405** |
| **Adriana FLORESCU, Bogdan BARABAŞ, Sorin BARABAŞ**<br>***TRENDS IN IMPLEMENTATION OF RISK MANAGEMENT IN SMEs*** | **411** |
| **Ciprian-Marius LARCO, Ştefan-Mircea MUSTAŢĂ, Radu-Călin PAHONIE**<br>***COMPOSITE MULTILAYER STRUCTURES OBTAINED BY EXPLOSIVE METHO*** | **419** |
| **Doru LUCULESCU, Vasile PRISACARIU**<br>***KINEMATICS OF THE LANDING GEAR SYSTEMS OF AIRCRAFT*** | **425** |
| **Tomáš LUKÁČ, Vladimír HORÁK, Linh Do DUC, Dalibor ROZEHNAL**<br>***EXPERIMENTAL SETUP FOR STUDYING PROPERTIES OF POWER GASES*** | **429** |
| **Mihai MIHAILA-ANDRES, Paul Virgil ROSU**<br>***THERMO-GAS DYNAMIC ANALYSIS OF UPPER-STAGE ROCKET ENGINE NOZZLE*** | **437** |
| **Angi NORBERT, Razvan UDROIU**<br>***DESIGN OF A LSA AIRCRAFT USING ADVANCED SOFTWARE*** | **445** |
| **Geanina-Laura PINTILEI, Marioara ABRUDEANU, Corneliu MUNTEANU, Ionuţ-Vasile CRISMARU, Mihaela VLADU, Iustin POPA**<br>***THE BEHAVIOR OF AN $AL_2O_3$ COATING DEPOSITED BY PLASMA ELECTROLYTIC OXIDATION ON ALUMINUM ALLOYS AT HIGH TEMPERATURE REGIME*** | **451** |
| **Geanina-Laura PINTILEI, Marioara ABRUDEANU, Corneliu MUNTEANU, Ionuţ-Vasile CRISMARU, Iustin POPA, Mihaela VLADU**<br>***THE INFLUENCE OF Al2O3 DEPOSITED COATING BY PLASMA ELECTROLYTIC OXIDATION TO THE BEHAVIOR OF AN ALUMINUM ALLOY SUBJECTED TO MECHANICAL SHOCK*** | **455** |
| **Corina-Monica POP, Gheorghe-Leonte MOGAN**<br>***ROBOTIC GRIPPERS FOR HANDLING BOOKS IN LIBRARIES*** | **461** |
| **Lucian-Eugen RAD, Thomas HEITZ, Anghel CHIRU**<br>***SPECIFIC TESTS FOR COMPOSITE STEERING COLUMNS*** | **467** |
| **Constantin ROTARU, Ionică CÎRCIU, Raluca-Ioana EDU, Oliver CIUICĂ, Eduard MIHAI**<br>***NONLINEAR EFFECTS OF THE SIDEWASH GRADIENT ON AN AIRPLANE VERTICAL TAIL*** | **475** |
| **Amado ŞTEFAN, Ciprian LARCO, Radu-Călin PAHONIE, Ionut NICOLAESCU**<br>***COUPLED TRANSIENT ANALYSIS OF A UAV COMPOSITE WING*** | **481** |
| **Stoyko STOYKOV, Milen ATANASOV**<br>***CALCULATING TECHNICAL SCATTERING FULL ERROR FOR EXTERNAL SUSPENDED BOMBS AT FREE RELEASE*** | **487** |

| | |
|---|---|
| **George SURDU, Ioan VEDINAŞ, Georgică SLĂMNOIU, Şomoiag PAMFIL**<br>***PROJECTILE'S DRAG COEFFICIENT EVALUATION FOR SMALL FINITE DIFFERENCES OF HIS GEOMETRICAL DIMENSIONS USING ANALYTICAL METHODS*** | **491** |
| **Fulga TANASA, Madalina ZANOAGA, Yevgen MAMUNYA**<br>***CONDUCTIVE THERMOPLASTIC POLYMER NANOCOMPOSITES WITH ULTRALOW PERCOLATION THRESHOLD*** | **497** |
| **Michael Damianov TODOROV**<br>***AERODYNAMIC CHARACTERISTICS OF AIRFOIL WITH SINGLE SLOTTED FLAP FOR LIGHT AIRPLANE WING*** | **509** |
| **Alexandru-Nicolae TUDOSIE**<br>***MATHEMATICAL MODEL FOR A JET ENGINE WITH ANTI-STALL AUTOMATIC VALVE AIDED COMPRESSOR*** | **515** |
| **Alexandru-Nicolae TUDOSIE, Mihai-Cătălin OLTEANU**<br>***PNEUMATIC ANTI-STALL AUTOMATIC SYSTEM FOR A JET ENGINE COMPRESSOR*** | **523** |
| **Sebastian-Marian ZAHARIA**<br>***FATIGUE LIFE SIMULATION OF THE SPECIMENS MADE OF MECHANICAL COMPONENT*** | **531** |
| **Sebastian-Marian ZAHARIA**<br>***RELIABILITY AND STATISTICAL ANALYSIS OF THE FATIGUE LIFE OF THE TAPERED ROLLER BEARINGS*** | **535** |
| **Mădălina ZĂNOAGĂ, Fulga TANASA, Raluca DARIE**<br>***NOVEL POLYPROPYLENE-CLAY HYBRID MATERIALS FOR AUTOMOTIVE INDUSTRY. EFFECT OF THE COMPATIBILIZING AGENT*** | **541** |
| ***RENEWABLE ENERGY AND ENVIRONMENT*** | |
| **Timur CHIS**<br>***THE LIFE CYCLE AS AN OFFSHORE PIPELINE*** | **547** |
| **Bogdan CIORUȚA, Mirela COMAN**<br>***INNOVATIVE POSSIBILITIES TO REPRESENT THE BAIA MARE URBAN SYSTEM SOILS POLLUTION WITH HEAVY METALS USING G.S. SURFER*** | **551** |
| **Marcela HRENIUC, Mirela COMAN, Bogdan CIORUȚA**<br>***CONSIDERATIONS REGARDING THE SOIL POLLUTION WITH OIL PRODUCTS IN SĂCEL - MARAMUREŞ*** | **557** |
| **Raluca NICOLAE (MĂNESCU), Anişor NEDELCU**<br>***SOME PATTERNS OF APPLICATION OF FMEA METHOD FOR STUDYING THE QUALITY OF A PRODUCT*** | **563** |
| **Ramona PAKOCS, Nouraş-Barbu LUPULESCU**<br>***NEED TO IMPLEMENT A HIGHLY-PERFORMING INTELLECTUAL-PROPERTY MANAGEMENT IN THE TECHNICAL-ENGINEERING FIELD*** | **567** |

| | |
|---|---|
| **Ramona PAKOCS , Nouraş-Barbu LUPULESCU**<br>***RISK MANAGEMENT AND ASSESSMENT OF THE MANUFACTURING AND MARKETING RISK-FACTORS, WITHIN INDUSTRIAL COMPANIES*** | **575** |
| **Adrian PETRU, Aurel LUNGULEASA**<br>***EFFECTS OF THE LASER POWER ON WOOD COLOURATION*** | **581** |
| **Adrian ROŞCA, Petre CÎRDEI**<br>***MATHEMATICAL MODEL FOR PORK BONELESS NECK TENDERIZING TO PRODUCE ROMANIAN TRADITIONAL PRODUCT "CEAFĂ PERPELITĂ"*** | **585** |
| **Daniela ROŞCA, Adrian ROŞCA**<br>***THE INFLUENCE OF CYCLIC VACUUMING AND PRESSURING PROCESS ON TENDERIZING SHEEP PASTRAMI*** | **591** |
| **Cosmin SPÎRCHEZ, Aurel LUNGULEASA**<br>***THE INFLUENCE HEAT TRANSFER COEFFICIENT ON WOOD CONSTRUCTION*** | **597** |


## *APPLIED MATHEMATICS, COMPUTER SCIENCE, IT&C*


| | |
|---|---|
| **Gabriel ANASTASIU, Elena ANASTASIU**<br>***TRANSMISSION CODING SYSTEM USING HAMMING ENCODING FHSS*** | **601** |
| **Cristian BUCUR**<br>***USING BIG DATA FOR INTELLIGENT BUSINESSES*** | **605** |
| **Mihaela DUMITRACHE, Camelia GHELDIU**<br>***THE EQUATION OF DISPERSION AND THE DISPLACEMENT VECTOR IN THE ANTISYMMETRIC CASE*** | **613** |
| **Miroslav HRUBÝ**<br>***SUBJECT INFORMATION TECHNOLOGY IN MILITARY EDUCATION*** | **617** |
| **Hošek JAROMÍR, Alexandr ŠTEFEK**<br>***SIMPLE SOFTWARE FOR EDUCATION*** | **621** |
| **Mircea LUPU, Cristian-George CONSTANTINESCU, Gheorghe RADU**<br>***AIRPLANES OR RACKETS FLIGHT STABILIZATION OPTIMAL CONTROL IN CASE OF PITCH PERTURBATIONS*** | **625** |
| **Ioan MILOSAN**<br>***MATHEMATICAL MODELING BY USING A C++ SOFTWARE*** | **631** |
| **Ioan MILOSAN**<br>***OPTIMIZATION OF INDUSTRIAL PROCESSES USING A SPECIAL SOFTWARE*** | **639** |
| **Gabriela MOGOS**<br>***COMPARATIVE ANALYSIS OF QUANTUM KEY DISTRIBUTION PROTOCOLS WITH TWO, THREE AND FOUR-STATE SYSTEMS*** | **645** |
| **Ana-Maria RÎTEA, Sorina-Mihaela STOIAN**<br>***SOME FEATURES ABOUT STATIONARY DISTRIBUTION OF PROBABILITIES AND APPLICATIONS*** | **649** |
| **Ştefania-Iuliana ŞOIMAN, Gheorghe RADU, Ştefan-Gheorghe PENTIUC, Ionuț BALAN**<br>***PERFORMANCE ANALYSIS OF PARALLEL SVM TRAINING ON CLUSTER HAVING SIMILAR IBM ROADRUNNER ARCHITECTURE*** | **655** |

"HENRI COANDA"
AIR FORCE ACADEMY
ROMANIA

"GENERAL M.R. STEFANIK"
ARMED FORCES ACADEMY
SLOVAK REPUBLIC

INTERNATIONAL CONFERENCE of SCIENTIFIC PAPER
AFASES 2015
Brasov, 28-30 May 2015

# EFFECT OF LIGHT DEPENDANT RESISTOR MISMATCHING AND IMPACT OF NON LINEARITY IN A SMALL SCALE SOLAR TRACKING SYSTEM

**Philippe Dondon*, Ecaterina-Liliana Miron****

*Université de Bordeaux, IPB, Talence, France, **Faculty of Aeronautical Management, "Henri Coandă" Air Force Academy, Brasov, Romania

***Abstract:*** *The design of a didactical small scale "green" house and its power production systems has been previously presented in [1]. As power generation is one of the challenges in Sustainable Development, some scaled accessories have been included on house surroundings. In particular, a small scale simplified solar tracking analogue system based on LDR sensors, has been designed and installed [2]. A mixed SPICE modelling of the system, including geometrical, optical, electronic linear and nonlinear aspects has been built. This new paper focuses on effects of Light Dependant Resistor mismatching, and impact of non-linearity on the solar tracking performances. Firstly, the principle of tracking and its SPICE modelling are shortly described; Secondly, impacts of each imperfection are detailed and simulated. Finally, impacts are quantified and discussed before conclusion.*

***Key words****: Sun tracking, Mixed SPICE modelling, Analogue design, Sustainable development*

## 1. INTRODUCTION

**1.1 Small scale house project state of art.** Within the framework of an innovative sustainable development project, the design a functional realistic small scale house, built in genuine materials took almost three years. The building (with true materials) of small scale house itself is finished. It required more than 1500 hours of work and was detailed in [1]. Figure 1 shows a picture of the finished small scale model (at 1/20 scale).

The small scale model will be used as:

- Demonstrator (sustainable development exhibition in town halls or local sustainable development events)
- Pedagogical support for practical lessons and electronic projects, for sensitizing engineering students to green power management, power saving and low power electronic in first and 2nd year study

**1.2 Study background.** We designed several electronic boards and their electronic control circuits, as indicated hereafter, in order to make the "green" house model, didactical and fully functional:

- A small scale home automation including weather station, low voltage LED lighting for the terrace, roof solar panel and battery cells management, "air conditioned" system powered by an hydrogen fuel stack (i.e. scaled Canadian well under the house), an electrical

heater circuit house and its temperature control.
- A solar tower and its performance measurement system,
- A small scale simplified solar tracking system for a solar panel…

Figure 1: View of house and surroundings.

The present paper focuses on intrinsic imperfection of this last accessory. Modelling and design has already been detailed [2]. However, effects of mismatching and other imperfection must be taken in consideration for a fine analysis of the system's behavior. For a better understanding, we bring back to mind in §2. and §3. some important points.

## 2. SUN TRACKING CIRCUIT PRINCIPLE

**2.1 Generalities.** The didactical designed circuit is obviously a simplified version of a true system [3], [4], [5]. Main goals were to illustrate feedback theory taught in our electronic engineering school and more generally to introduce sustainable development in scientific studies.

**2.2 Principles and schematic.** The small scale "green house" is used for in-door demonstration and applications. Thus, a halogen spot light is used to "replace" the sun light.

The system consists of an analogue system with one rotation axis control (horizontal plan) [6], [7] to simplify the approach. Figure 2 shows the sun tracking principle.

When the solar panel is aligned in "sun" direction, the received left and right lights flux L1 and L2 are equal (Cf. figure 3). When it is not, one of the two LDR receives more flux than the other. This generates an analogue difference voltage $V_{diff}$ ("left minus right") and the feedback loop moves the servo motor into the right direction until to cancel the voltage $V_{diff}$.

A classical hobbyist servo Futaba (or equivalent) is used to move the panel. According to standards, the rotation angle α is proportional to an input control signal $V_{pwm}$ with the following characteristics: two voltage level signal 0, +5V, period 20ms, pulse width variable from 1ms to 2ms for a 0° to 180° rotation. Thus, a DC to PWM converter is required between subtraction block and Servo input (Cf. figure 2).

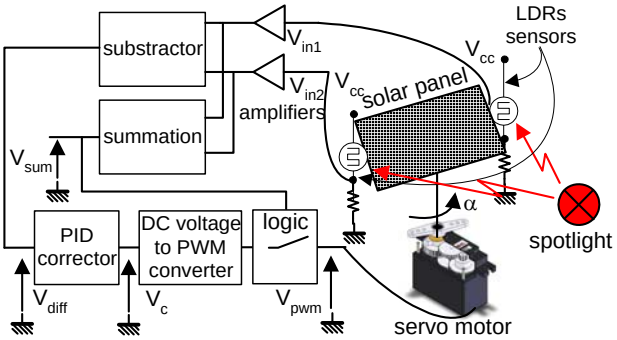


Figure 2: Sun tracking system block diagram

Two light sensors LDR1 and LDR2 (LDR: Light Dependant Resistors,), are located on left and right side of the panel. They receive the "sun" light.

A summation $V_{sum}$ of the two sensors voltages is used to distinguish dark and sunny situation; and power consumption is minimized during the "night" by turning off the servo voltage supply.

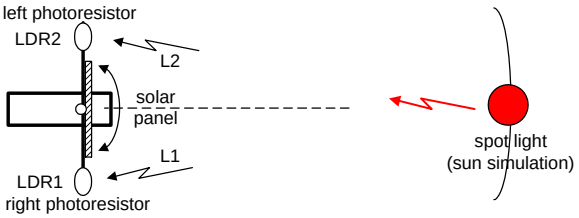


Figure 3: Solar panel alignment

## 3. MODELLING OF TRACKING SYSTEM

**3.1 Generalities.** L1, L2 represents the received light (in Lux) on each LDR, $\alpha_{ref}$ the "sun" angular position, $\alpha_e$ the error angle, $\alpha$ the angle given by the servo motor (referenced as indicated in figure 5). Thus, the tracking system can be modelled as follow:

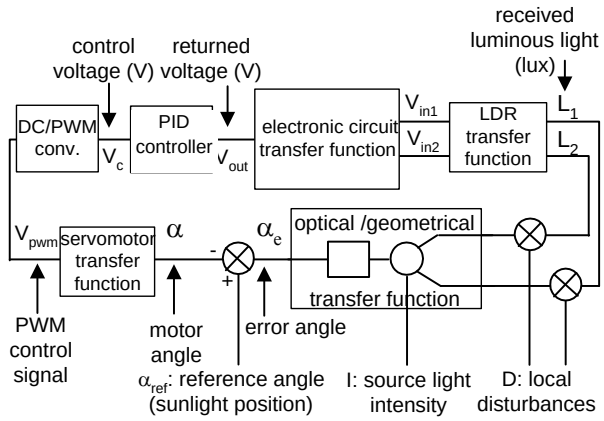


Figure 4: System identification

- $\alpha_{ref}$ is the main input of the feedback system.
- Source light intensity input (I) can be seen as a parasitic input which represents fluctuation of source intensity (fog, sky partially cloudy, etc).
- Local disturbances input (D) represent disturbances that can occur individually, on each LDR optical way. (object passing over the LDR etc).

We set up:

$$L_0 = I / D^2 \text{ and } \alpha_0 = \text{artg}\,(l/2.D) \qquad (1)$$

Where, I is the light intensity of the source (in Candela), D the distance light source/solar panel, and *l* the distance between LDR sensors (in cm).

With these conditions, received flux is given by [2]:

$$L_1 = L_0 \cos(\Theta o - \alpha_e)$$
$$L_2 = L_0 \cos(\alpha_e + \Theta o)$$
(2)

Nominal values in our small scale system are D=1m and l=10cm and $L_0$=1000 lux.

**3.2 Tracking system global modelling.** The global equivalent mixed Spice schematic previously built in [2] is given in figure 6.

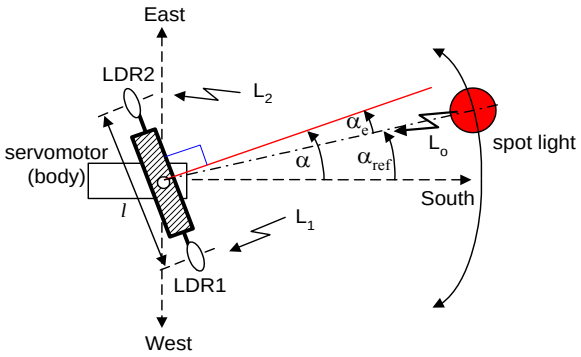


Figure 5: Reference angles (top view) modelling

**3.3 LDR detailed modelling.** LDR sensors are intrinsically nonlinear. Our commercial LDRs samples (VT90N) vary over 3 decades as a non-integer power of the received light (i.e. from $L^{-0.5}$ to $L^{-0.7}$), thus:

$$LDR(\Omega) = k.\frac{1}{L^y} \qquad (3)$$

(with 0.5<y<0.7, and L in Lux)

The corresponding Spice modelling is given in figure 7. LDR, modelled by a Voltage Controlled Resistor block ("VCR"), is inserted in a resistor bridge supplied under +5V. Capacitor C4 represents the average time constant of the LDR as defined in [2].

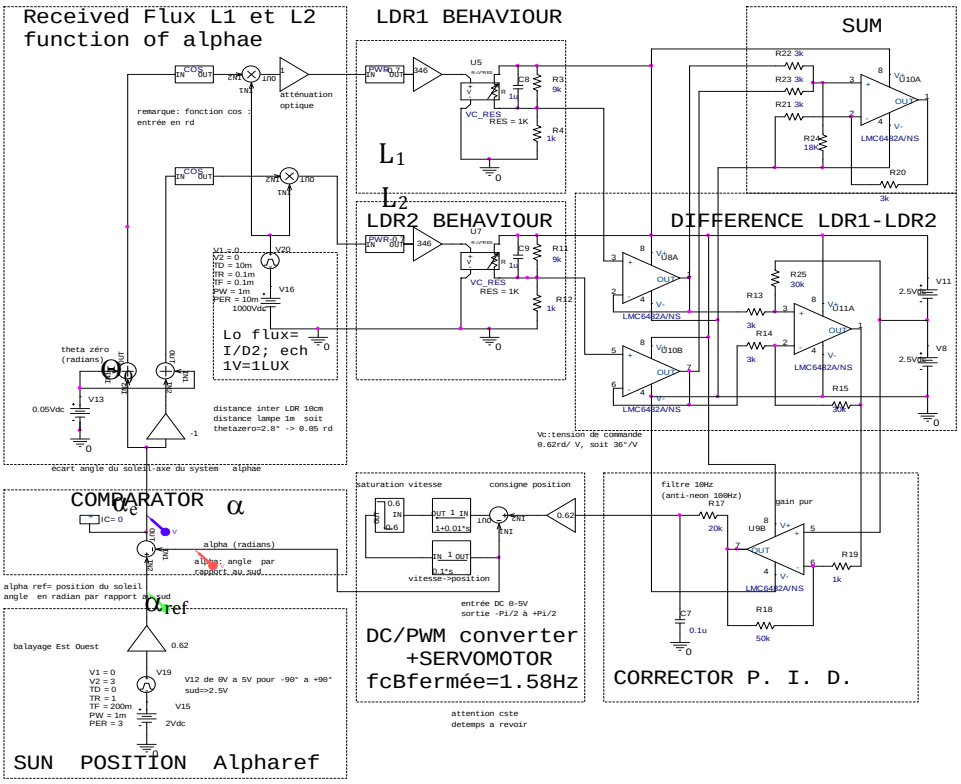


Figure 6: Global SPICE modelling

**3.4 LDR detailed modelling.** LDR sensors are intrinsically nonlinear. Our commercial LDRs samples (VT90N) vary over 3 decades as a non-integer power of the received light (i.e. from $L^{-0.5}$ to $L^{-0.7}$), thus:

$$LDR(\Omega) = k.\frac{1}{L^{y}} \quad (3)$$

(with 0.5<y<0.7, and L in Lux)

The corresponding Spice modelling is given in figure 7. LDR, modelled by a Voltage Controlled Resistor block ("VCR"), is inserted in a resistor bridge supplied under +5V. Capacitor C4 represents the average time constant of the LDR as defined in [2].

## 4. IDENTIFICATION OF IMPERFECTIONS

Since the tracking system is basically a feedback circuit, imperfections of active blocks are obviously greatly reduced. However, quality of sensors (which belong to the return loop) can impact directly the performances of the system (accuracy, stability etc.).

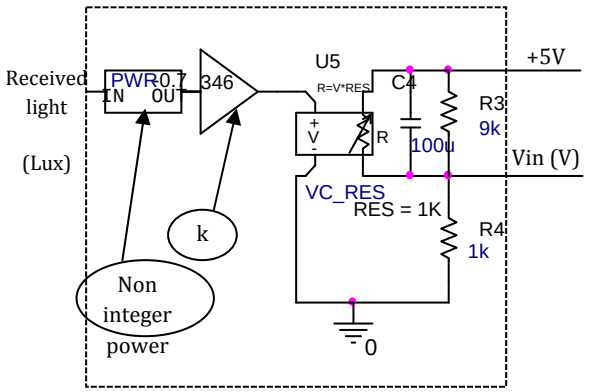


Figure 7: LDR generic modelling

In order to reduce this impact, the two LDR sensors were obviously sorted and a selection of two "similar" LDR was done. However, we estimate the residual global mismatching up to 10%.

Thus, it is important first to identify the different imperfections sources and to predict their effects and finally to suggest some possible compensations.

The main imperfections identified are as follow.
- Intrinsic non linearity of the LDR
- Mismatching between LDRs:
  - Variation in k factor
  - Dispersion of the *y* exponent from -0.5 to -0.7
  - Dispersion of time response
  - Optical attenuation on LDR protection layer due to the dirt.
- LDRs ambient temperature variations

## 5. ANALYSIS OF LDR SENSOR'S NON LINEARITY

**5.1. Impact of non-linearity.** Non linearity leads to several consequences:
- A non-constant sensitivity over the full luminous flux range,
- A higher difficulty to match the two sensors response
- A possible instability depending on light level $L_0$.

**5.2. Non linearity SPICE simulations.** Due to non-linearity, open loop gain depends on $L_0$ value. And the frequency response of the closed loop, with a parametric sweep for $L_0$ = 10, 100, 1000 and 10000 Lux is like indicated in figure 8. Gain in bandwidth is obviously close to 1, and a resonant frequency appears at high source intensity level.

## 6. ANALYSIS OF LDR SENSOR'S MISMATCHING

**6.1 Impact of mismatching.** Mismatching leads to several consequences:
- A possible permanent position angle error,
- Local instability.

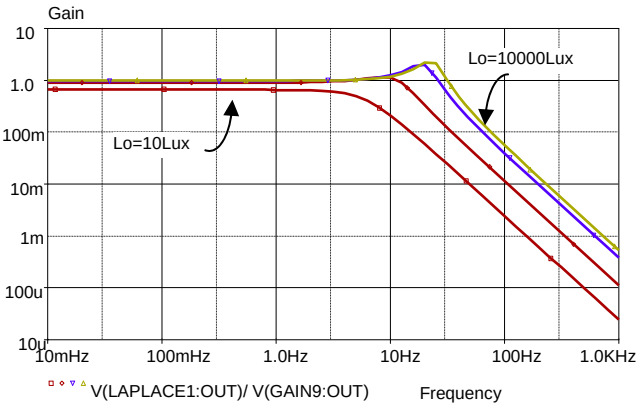


Figure 8: Closed loop gain

### 6.2 Impact of "k" factor

#### 6.2.1 Analysis method

In a Log/log representation of LDR characteristic, varying k corresponds to a change of vertical offset (Cf. figure 9). A parametric sweep corresponding to a 10% variation on the LDR1sensor is performed.

#### 6.2.2 SPICE simulations

For these simulations, the system is initially pointed to south direction. A preliminary simulation is done as indicated hereafter:

- Tracking system in open loop. DC sweep from $L_0$ = 10 to 10000 Lux (full luminous range) with a parametric sweep of k value from 306 to 386 on LDR1 (Symmetric compared to the nominal value) to produces a voluntary mismatching.

Figure 9 shows the corresponding simulated behaviour of the LDR. Once LDR behavior checked, another simulation is run:

- a DC sweep from L0 = 10 to 10000 Lux in closed loop with the same parametric sweep of k.

Using the «Spice performance analysis» option, once can extract the average error angle $\alpha_e$ vs. k (Cf. figure 10).

A variation of ±11% of k value around the nominal value leads to a huge error $\alpha_e$ of ±1rd (i.e. ±57 °).

### 6.3 Impact of *y* exponent

#### 6.3.1 Analysis method

We perform a parametric sweep of exponent number *y*, in the "power block" ABM spice element. In Log/log representation of LDR characteristic, variation of power order *y* corresponds to a change in curve slope (cf. figure 11).

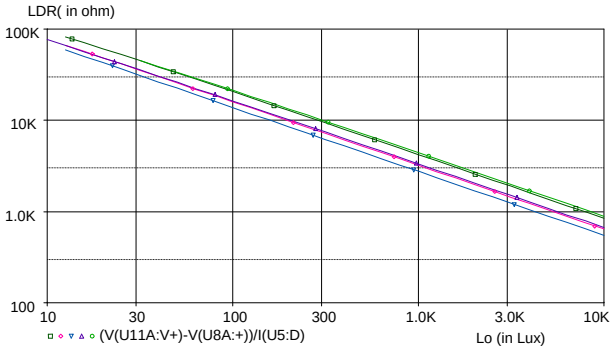


Figure 9: LDR(Ω) = f($L_0$ ) Lux parametric analysis k

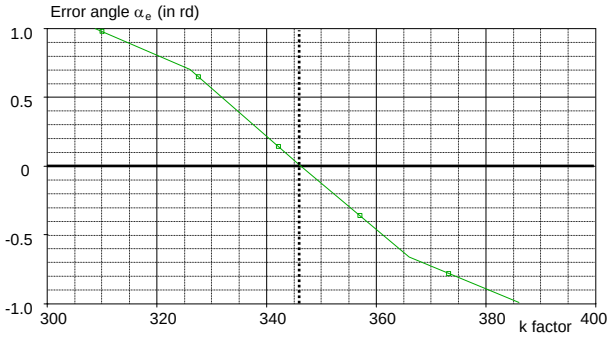


Figure 10: Error angle $\alpha_e$ = f(k)

#### 6.3.2 SPICE simulations

A first simulation is done as indicated hereafter:

- Tracking system in open loop. DC sweep from $L_0$ = 10 to 10000 Lux with a parametric sweep of exponent *y* of LDR1 from -0.65 to -0.75 (symmetric compared to the nominal value -0.7). Figure 11 shows the corresponding simulated behavior of the LDR.

Once LDR behavior checked, a second simulation is run:

- DC sweep from $L_0$ = 10 to 10000 Lux in closed loop with the same parametric sweep of *y*.

Using the «Spice performance analysis» option, once can obtain an average error angle $\alpha_e$ around $L_0$= 300 Lux. (as $\alpha_e$ depends on absolute value Lo).

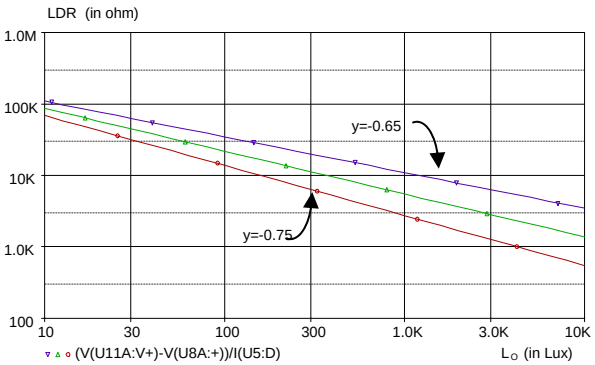


Figure 11: LDR(Ω) = f ($L_0$) Lux (parameter *y*)

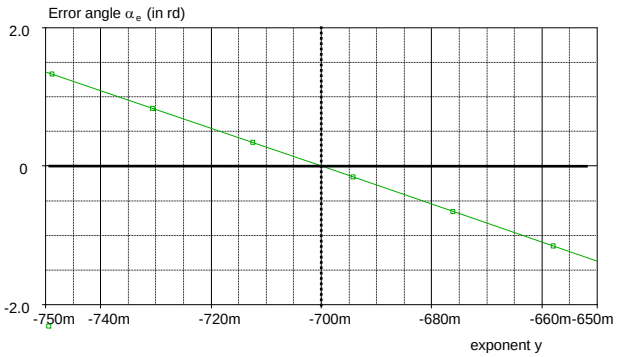


Figure 12: Error angle $\alpha_e$ = f(y) vs. *y* exponent

A +/-5% variation of *y* around -0.7, produces a huge deviation of angle error +/- 1 rd (i.e. 57°). The relative impact of *y* is greater than the one of k.

### 6.4 Impact of response time

#### 6.4.1 Analysis method

A parametric sweep of 10% on capacitor value C4 is performed.

#### 6.4.2 SPICE simulations

A mismatching on capacitor value does not have any impact in DC mode. But it may have an impact. Thus, the following transient analyses are performed:

- Response to a $\alpha_{ref}$ step pulse. The pulse characteristics are rise time 10ms, pulse width 4s, step of +/-1/2 rd around 0 (south position). $L_0$= 1000Lux, Figure 13 shows the response in closed loop, when capacitors are equal to 100µF and perfectly matched.

A 10% variation on capacitor value does not have significant effect. So, an extreme capacitor mismatching is simulated (100µF for

LDR2 and 1µF LDR1) to check asymptotic behavior.

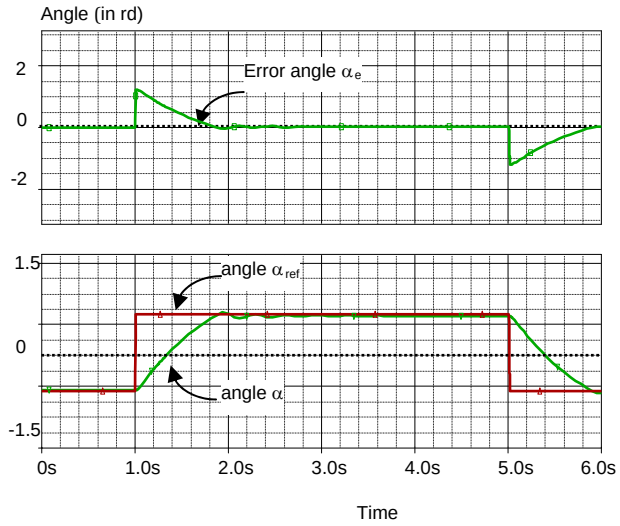


Figure 13: Transient simulations (C matched)

Figure 14 shows the response curve. The transient shape changes a little bit but the global behavior remains correct.

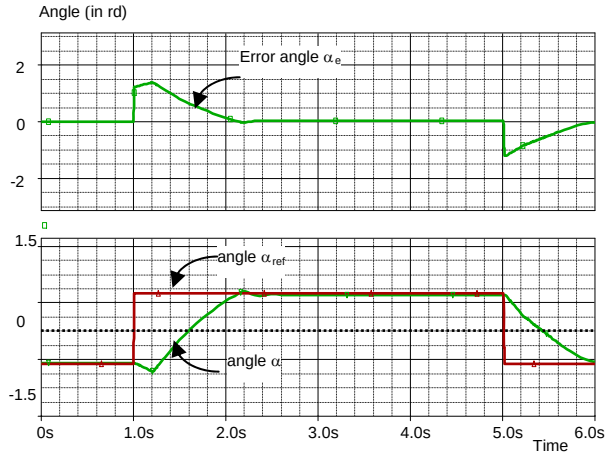


Figure 14: Transient simulations (C huge mismatch)

- Response to a 100Hz squared stimuli on $L_0$: It represents the parasitic 100Hz flicker noise coming from fluorescent neon tubes in the room, during in door experimentation. The simulation conditions are rise time 0.1ms, pulse width 1ms, period 10ms, nominal value $L_0$=1000 Lux, $\mu_{ref}$=0.

A 10% variation on capacitor value does not have significant effect. Like previously, the same extreme capacitor mismatching is simulated to check asymptotic behaviour.

Figure 15 shows the response curve. A permanent small error angle $\alpha_e$ (less than 4.5°) is observed.

Thus, the system is almost insensitive to this noise since mismatching between LDR time response remains small (less than 10%).

In fact, the previous simulations do not represent realistic phenomenon and should not be necessary for a real system, because all natural phenomenon are extremely slow: sun goes always in the same direction; there is no sudden movement of the sun or sudden change of light intensity in the Nature.

However, simulations were required to check reaction of the system since it works with "in door" conditions, which are different from reality.

### 6.5 Impact of optical attenuation

#### 6.5.1 Modelling of optical attenuation.

A 0.9 attenuator SPICE element is placed in series on LDR1 received light input to produce voluntarily a difference in optical ways between LDR1 and LDR2.

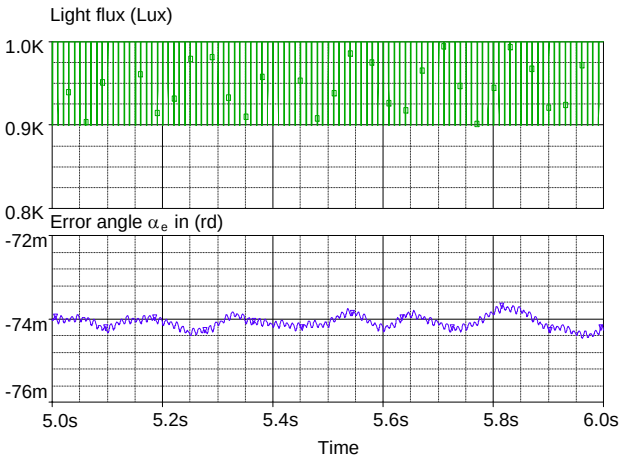


Figure 15: Transient simulations

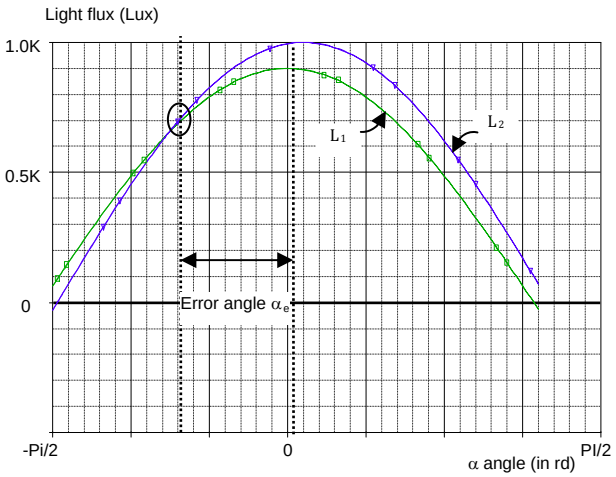


Figure 16: DC Sweep Simulations

### 6.5.2 SPICE simulations

Theses simulations investigate the static behavior in open loop, when submitting the system to a DC sweep of α angle from -90° to +90° (i.e. full rotation from East to West). The spot light is locked in south position ($\alpha_{ref}$ = 0°), D=1m and $L_0$=1000 Lux.

As the distance between sensors is an important parameter, two cases have been tested:

- Distance between LDR sensors l=10cm

(i.e $\Theta_0 \approx 2.8°$) (Cf. figure 16).

- Distance between LDR sensors l=60cm

(i.e. $\Theta_0 \approx 18°$) (Cf. figure 17).

Figure 16 shows the received light L1 and L2 vs. angle α. It can be read as follow:

$L_1$, $L_2$ reach their maximum values $L_0$ (here =1000 lux) when the spotlight is exactly in front of them (Respectively $\alpha_e=\Theta_o$ and $\alpha_e=-\Theta_o$). And they tend toward 0 when α reaches ± 90° (Sunset or sunrise situation). When feedback loop operates normally, the system tends to make the two received lights flux, equal. This happens on figure 16 (resp. 17) at the intersection between the two curves $L_1$ and $L_2$. Thus, the corresponding error angle can be deduced.

Here, we obtain $\alpha_e \approx 45°$.

Vertical scale: received light in Lux

Green curve: L1 (after optical attenuation x0.9)

Blue curve: L2 (no attenuation)

Figure 17 shows also the received light L1 and L2 vs. angle α. Distance between sensors is 6 times greater than in figure 16 (i.e. 60cm). In this situation, error angle $\alpha_e$ is reduced to around 15°; the more sensors are spaced, the less is the static angle error due to optical mismatching.

Vertical scale: received light in Lux

- Red curve: L1 (before attenuation)
- Green curve: L1 (after optical attenuation x0.9)
- Blue curve: L2

### 6.6 Temperature impact

The ambient temperature changes from morning to afternoon. Unfortunately, LDRs are sensitive to temperature [8]: the LDR resistance value decreases as the temperature rises.

The relationship between temperature and resistance was not completely investigated but it appears that the resistance of an LDR is a function of both light flux and temperature.

For our "in door" application with a spot light of 75 to 100W, 1meter far, and distance between sensor 10cm, this is not really a problem. However, for outdoor uses, when the component is oriented towards the sun, the LDR resistance becomes very low, and the effects of temperature variation could appear more significant.

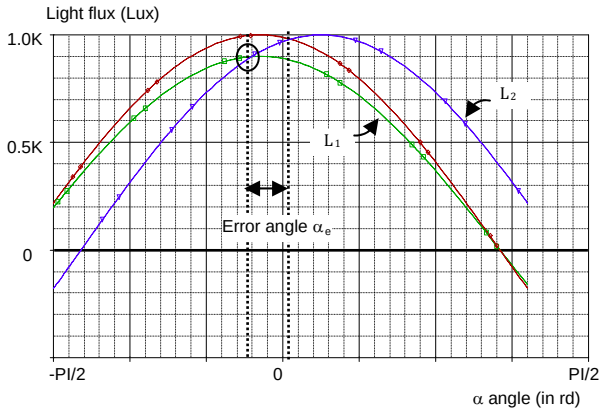


Figure 17: DC sweep Simulations

## 7. EXPERIMENTS

It is difficult, from experimental point of view, to reproduce exactly the simulated mismatching because it could require a lot of mismatched LDR and many repetitive tests.

We only performed some tests with a few "no sorted" LDRs. Due to the test bench, a fine measurement of accuracy is difficult to obtain. However, when LDR are mismatched, the main tendencies and order of magnitude of error angle αe predicted by simulation are experimentally checked.

When the two LDR are matched, the system tracks correctly the light source with accuracy better than 5°, which is enough for demonstrating the theoretical principle of tracking and for public exhibition purposes.

## 8. DISCUSSION AND COMMENTS

Angle accuracy of the system is affected by all the imperfections. Among the four parameters, non-integer power exponent *y* is the most influent. Instability risk comes from the nonlinear intrinsic behavior of LDR. Distance *l* between LDR sensors is an important factor: the more they are spaced, the less is the static angle error.

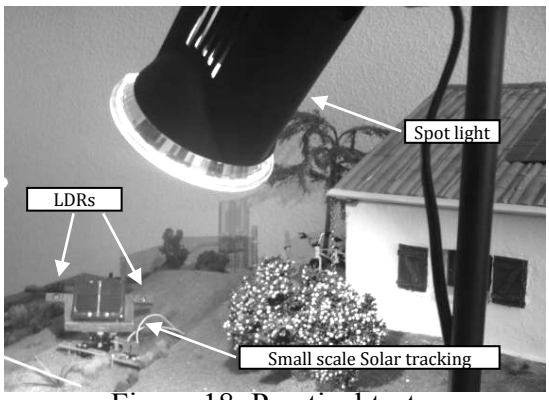


Figure 18: Practical test

The small scale solar tracking system will operates whatever the situation, but with a more or less important static permanent error. From simulations, a maximum error of 5° requires a global matching better than 1% between LDR sensors.

As perfect matching between sensors is never possible, some improvements can help to reduce the error. Two kind of improvement can be investigated. Whatever the strategy, a preliminary strong sorting of LDR sensors is required. Then, a linearization circuit can be added, if necessary. It can be done in two ways:

- by using a micro controller with a tabulated conversion table (a new design is already planned)
- by using analogue circuits with voltage dependant gain circuit (diode or multiplier) and OP amps for offset and gain adjustments.

## 9. CONCLUSION

A small scale solar tracking system was designed and an equivalent mixed modelling was presented. Effects and impacts of major imperfections were studied and quantified.

Possible improvements to compensate imperfections have been suggested. However, the presented system is not mass produced; it is only a unique experimental device. Thus, there was no need to include such improvements in the present design till now. The tracking system is now installed in on our small scale greenhouse modelling. And some exhibitions have been planned for general public sensitizing in the near future.

## REFERENCES


[1] Ph. Dondon- P. Cassagne- M. Feugas- C.A. Bulucea- D.Rosca-V. Dondon- R. Charlet de Sauvage "*Concrete experience of collaboration between secondary school and university in a sustainable development project: design of a realistic small scale house to study electronic and thermal aspect of energy management.*" WSEAS Transactions on ENVIRONMENT and DEVELOPMENT Issue 10, Vol 7, oct 2011, ISSN: 1790-5079 p 225-235

[2] Ph. Dondon, L. Miron « *Modelling and design of a small scale solar tracking system -Application to a green house model-* » WSEAS Transactions on ENVIRONMENT and DEVELOPMENT Issue 10, Vol 7, oct 2013, ISSN: 1790-5079 p 225-235

[3] « *Choix d'un suiveur solaire* » http://www.energieplus-lesite.be/energieplus/page_16690.htm?reload

[4]http://www.exosun.fr/index.php

[5] T. Bendib, B. Barkat, F. Djeffal, N. Hamia et A. Nidhal « *Commande automatique d'un système de poursuite solaire à deux axes à base d'un microcontroleur PIC16F84A* » Revue des Energies Renouvelables Vol. 11 N°4 (2008) 523 – 532

[6] C.S. Chin, A. Babu, W. McBride. «*Design, Modelling and testing of a Standalone Single-Axis Active Solar Tracker using MATLAB/Simulink* » Renewable Energy journal, 01/2011; ISSN 0960-1481

[7]PC Control Ltd web site: http://www.pc-control.co.uk/howto_tracksun.htm

[8]Brighton Webs Ltd. web site: http://www.brighton-webs.co.uk/electronics/light_dependent_resitor.htm

"HENRI COANDA"
AIR FORCE ACADEMY
ROMANIA

"GENERAL M.R. STEFANIK"
ARMED FORCES ACADEMY
SLOVAK REPUBLIC

INTERNATIONAL CONFERENCE of SCIENTIFIC PAPER
AFASES 2015
Brasov, 28-30 May 2015

# GABOR AND WEBER LOCAL DESCRIPTORS PERFORMANCE IN MULTISPECTRAL EARTH OBSERVATION IMAGE DATA ANALYSIS

**Florin-Andrei Georgescu*, Mihai Datcu**, Dan Răducanu*****

*Military Technical Academy, Bucharest, Romania & Politehnica University of Bucharest, Romania, **Politehnica University of Bucharest, Romania & German Aerospace Center (DLR), Oberpfaffenhofen, Germany, ***Military Technical Academy, Bucharest, Romania

***Abstract:*** *During the last decades, both the satellite sensors and remote sensing imagery are evolving so fast that the methods and techniques of processing and analyzing Earth Observation (EO) data usually are staying one step behind. In the current paper, the authors goal was to prove the usability of Gabor and Weber Local Descriptors (WLD) in multispectral image classification. The extracted Gabor and WLD features were tested with Support Vector Machines (SVM), k-Nearest Neighbors (k-NN) and k-Means classifiers.*

***Keywords:*** *benchmarking, remote sensing, classification, Gabor filtering, Webber Local Descriptors, feature extraction*

## 1. INTRODUCTION

In the field of remote sensing and EO image data processing it is important to have at disposal a large variety of tools that can extract the maximum relevant information from an image [2]. The applicability of remote sensing image classification goes beyond the walls of the laboratory environment and can be used with success in crises and disaster management, in local administration and even in military applications. Also the multispectral images provide us relevant information about the land cover and land use.

Until now, there is no general rule that can be applied to create a universal information retrieval procedure regardless of the data being analyzed [3]. In most of the cases we must use specific algorithms for specific types of data.

Most of the times, the image indexing methods are based on identification and classification of image texture, image intensity or by using statistical models. The results are then grouped in a few generic classes (3-6) like crops, buildings, streets, vegetation, forest etc. [6]

In this paper, the authors are presenting a benchmark of extracted Gabor and WLD image descriptors when using SVM, k-NN and k-Means classifiers. This benchmark idea is to gather relevant results on the performance of classifiers when dealing with Gabor and WLD image descriptors in the context of multispectral image analyses. The goal is to determine the best classifier that fits best the image content given the analyzed features.

## 2. FEATURE SPACE AND IMAGE DESCRIPTORS

Usually, in order to proceed with image classification there are a few steps that must be taken into account. Some of these steps refer to image pre-processing, image feature extraction and image classification.

The image pre-processing step require that the analyzed image to be geometrically and radiometric correct. Also in the image pre-processing step, the multispectral data is filtered and then is cut into image patches of conveyable size. These patches are used in the image feature extraction step where the mean and standard deviation of each patch is computed. After obtaining all the statistical image descriptors for each patch we are ready for the image classification.

**2.1 Gabor features.** It is known that texture classification plays an important role in computer vision and its applications. Among various feature extraction methods, filter bank method such as Gabor filters has emerged as one of the most popular one. This filter bank is defined by its parameters including frequencies, orientations, frequency ratio and smooth parameters of Gaussian envelope. [5]

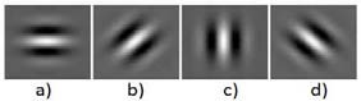


Figure 1. Gabor Filter example in spatial domain, with 4 orientations θ= 0°, 45°, 90° and 135° and scale parameters $\sigma_x = \sigma_y = 3$ pixels.

Considering the texture characteristics and other related studies, one can conclude that the human visual system responds to texture properties such as repetition, directionality and complexity [4], so the 2D Gabor filter can be expressed as in equation (1) using λ, θ, □, σ, γ parameters that represent wavelength, orientation angle (in radians), phase offset, standard deviation and filter scale. In our study we made use of Gabor filter banks with 4 orientations and 3 scales that we apply on each band of the extracted patch.

$$g_{\lambda,\theta,\varphi,\sigma,\gamma}(x,y) = e^{-(x'^2+\gamma^2 y'^2)/2\sigma^2}\cos(2\pi x'/\lambda + \varphi) \quad (1)$$

$$\frac{\sigma}{\lambda} = \frac{1}{\pi}\sqrt{\frac{\ln 2}{2}\cdot\frac{2^b+1}{2^b-1}} \quad (2)$$

$$b = \log_2 \frac{\frac{\sigma}{\lambda}\pi + \sqrt{\ln 2/2}}{\frac{\sigma}{\lambda}\pi - \sqrt{\ln 2/2}} \quad (3)$$

$$x' = x\cdot\cos\theta + y\cdot\sin\theta$$
$$y' = -x\cdot\sin\theta + y\cdot\cos\theta \quad (4)$$

**2.2 Weber Local Descriptors (WLD).** The Weber's law (Ernst Weber) states that the change of a stimulus that will be just noticeable is a constant ratio of the original stimulus. [1] If the change is smaller than this constant ratio, it cannot be recognized. In equation (5), $\Delta I$ represents the barely perceptible difference of two stimulus, $I$ represents the initial intensity of the stimulus and the $k$ meaning is that the ratio stays constant regardless of $I$ variations. This equation is known as Weber ratio. [4]

$$\frac{\Delta I}{I} = k \quad (5)$$

$$v_s^{00} = \sum_{i=0}^{p-1}(\Delta x_i) = \sum_{i=0}^{p-1}(x_i - x_c) \quad (6)$$

$$G_{ratio}(x_c) = \frac{v_s^{00}}{v_s^{01}}, \quad (7)$$

$$\zeta(x_c) = \arctan\left(\frac{v_s^{00}}{v_s^{01}}\right) = \arctan\left(\sum_{i=0}^{p-1}\frac{(x_i - x_c)}{x_c}\right) \quad (8)$$

$$\theta(x_c) = \arctan 2\left(\frac{v_s^{11}}{v_s^{10}}\right) \quad (9)$$

$$v_s^{10} = x_5 - x_1 \quad \text{and} \quad v_s^{11} = x_7 - x_3 \quad (10)$$

The equations (8) and (9) are used when we speak about multispectral data. In the case of Synthetic Aperture Radar (SAR) data, the situation is slightly different and an adapted WLD must be used [1].

## 3. REMOTE SENSING IMAGE CLASSIFICATION

Remote sensing image classification is a continuous expanding domain and makes use of the multimedia image classification techniques that are modified and adapted to handle EO data. As it is well known, the procedures employed can be unsupervised (where no user effort is required), supervised (the user must prepare a training set) and

object-based (based on multi resolution segmentation). In the present study we chosen a patch based approach for image content classification and we used supervised SVM and k-NN and unsupervised k-Means on Gabor and WLD image feature descriptors.

SVM represents a set of supervised learning methods used in automatic classification. The inputs of the algorithm are the training sets (stored into a database) and a test set (the computed patches). Also, the same principle is used in the k-NN classification, despite the of unsupervised k-Means case, were the user only specifies the number of classes he desire to obtain.

## 4. EXPERIMENTAL RESULTS

During the experimental stage, we used supervised SVM and k-NN classification and unsupervised k-Means classification along with Gabor and WLD local descriptors.

In the frame of the experimental setup we are using a WorldView2 multispectral image that illustrates the area of Bucharest, Romania (Figure 3). The scene covers almost 25 square kilometers and is characterized by 2 m spatial resolution, 8 spectral bands and 8 bits radiometric resolution representation. In our experiment, the image was resampled using nearest neighbors method in order to enhance the spatial resolution from 2 m to 1 m.

In the image classification process we used conveyable patches of 50 pixels size that covers 2.5 square kilometers. During testing we considered 5 semantic categories, as shown in Figure 2 and Figure 7. In Figure 7 is the representation of manual annotation map used in the qualitative evaluation of the study.

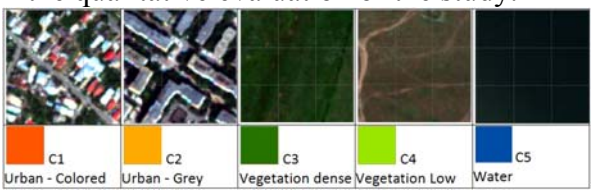


Figure 2. Land cover semantic categories and associated color representation used in classification.

In the case of supervised classification we used 20 samples per class, meaning a total of 100 samples, from the input image. The selected samples represent 0.01% from the total number of patches. In the case of the unsupervised classification no supplementary operations were needed.

Figure 3. WorldView2 image, Bucharest, Romania, 8 spectral bands, 8 bit radiometric resolution

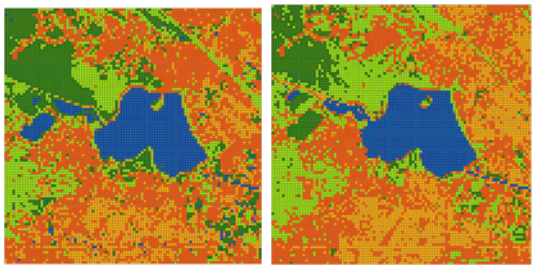

Figure 4. SVM Classification Gabor filter (a) vs. WLD (b)

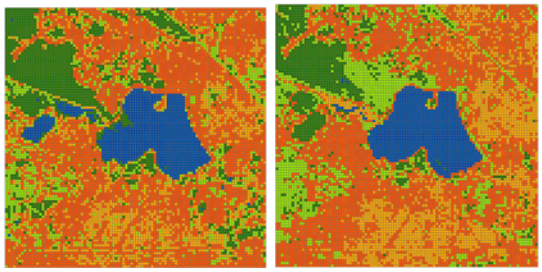

Figure 5. k-NN Classification Gabor filter (a) vs. WLD (b)

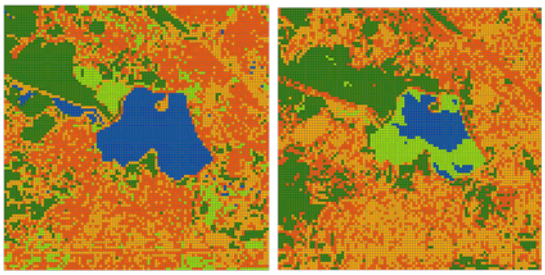

Figure 6. k-Means Classification Gabor filter (a) vs. WLD (b)

| | SVM | | k-NN | | k-Means | |
|---|---|---|---|---|---|---|
| Class | Precision | Recall | Precision | Recall | Precision | Recall |
| C1 | 80.0 % | 64.3 % | 83.6% | 55.4 % | 69.7% | 58.3 % |
| C2 | 48.3 % | 57.8 % | 32.5% | 40.0 % | 40.3% | 31.5 % |
| C3 | 55.7 % | 76.6 % | 49.3% | 72.8 % | 57.4% | 74.4 % |
| C4 | 59.2 % | 51.7 % | 30.0% | 36.8 % | 15.5% | 27.3 % |
| C5 | 87.9 % | 84.5 % | 81.3% | 91.0 % | 90.4% | 96.6 % |

Table 1. Confusion matrix for Gabor features classification with SVM, k-NN and k-Means

| | SVM | | k-NN | | k-Means | |
|---|---|---|---|---|---|---|
| Class | Precision | Recall | Precision | Recall | Precision | Recall |
| C1 | 63.4 % | 54.2 % | 77.5% | 52.3 % | 46.0% | 45.2 % |
| C2 | 50.9 % | 51.0 % | 42.9% | 49.2 % | 54.3% | 32.7 %8 |
| C3 | 34.6 % | 82.5 % | 37.2% | 79.3 % | 44.8% | 43.4 % |
| C4 | 68.7 % | 43.0 % | 53.7% | 46.1 % | 0.3% | 0.9% |
| C5 | 93.7 % | 96.3 % | 82.1% | 99.3 % | 36.5% | 100 |

Table 2. Confusion matrix for WLD features classification with SVM, k-NN and k-Means

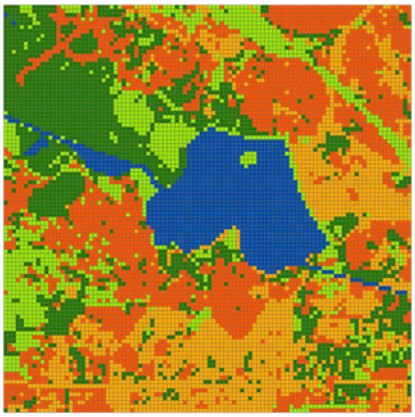

Figure 7. Reference annotation map

In Figure 4, Figure 5 and Figure 6 are shown the results of the classification benchmarking, as well in the Table 1 and Table 2 we can see the confusion matrixes resulted from the classifications.

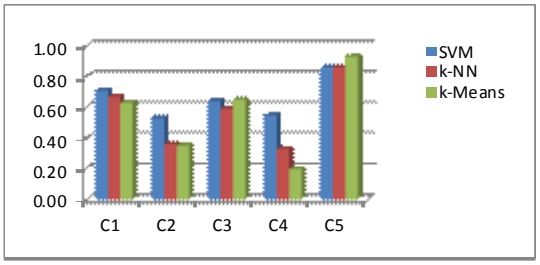


Figure 8. F-measure for Gabor features classification

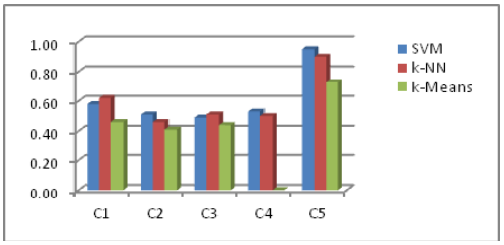


Figure 9. F-measure for WLD features classification

## 5. CONCLUSIONS & ACKNOWLEDGMENT

This paper has the purpose to demonstrate the usability of local descriptors in the case of multispectral EO image classification. As it can be seen from the confusion matrixes, the correct classification scores are very high in the case of classification with SVM and k-NN and not so accurate when using unsupervised k-Means. The reason we used in our tests not only supervised but also unsupervised classification methods is that we wanted a method to validate the class separation performance.

As it can be seen from the F-measure charts, Figure 8 and Figure 9, in the multispectral image classification is important not only the feature extraction method but also the classification method we use. The best results are obtained using SVM and k-NN supervised classification for Gabor and WLD also.

This paper has been financially supported within the project entitled “Horizon 2020 - Doctoral and Postdoctoral Studies: Promoting the National Interest through Excellence, Competitiveness and responsibility in the Field of Romanian Fundamental and Applied Scientific Research”, contract number POSDRU/159/1.5/S/140106. This project is co-financed by European Social Fund through

Sectorial Operational Programme for Human Resources Development 2007-2013. Investing in people!

## REFERENCES

1. Cui, S., Dumitru, C. O., Datcu, M., "Very High Resolution SAR Image Indexing Based on Ratio Operator", IEEE, GRS Letter, February 9, 2012.
2. Cui, S., Datcu, M., "Cascade Active Learning for Evolution Pattern Extraction From SAR Image Time Series", Multi Temp 2013
3. Dumitru, C.O. , Datcu, M., "Information Content of Very High Resolution SAR Images: Study of Dependency of SAR Image Structure with Incidence Angle", International Journal on Advances in Telecomunications, vol 5 no 3 & 4, 2012
4. Jie, C., Shiguang, S., Chu, H., Guoying, Z. Matti, P., Xilin, C., Wen, G., "WLD: A robust Local Image Descriptor", IEEE Transactions on Pattern Analysis and machine intelligence, 2009
5. Pakdel, M., Tajeripour, F., Texture Classification Using Optimal Gabor Filters, 1st International eConference on Computer and Knowledge Engineering (ICCKE), October 13-14, 2011
6. Popescu, A.A., Gavat, I., Datcu, M., "Contextual Descriptors for Scene Classes in Very High Resolution SAR Images", IEEE Geoscience and Remote Sensing Letters, Vol. 9, No.1, January 2012

# ENGINEERING SCIENCES

"HENRI COANDA"
AIR FORCE ACADEMY
ROMANIA

"GENERAL M.R. STEFANIK"
ARMED FORCES ACADEMY
SLOVAK REPUBLIC

INTERNATIONAL CONFERENCE of SCIENTIFIC PAPER
AFASES 2015
Brasov, 28-30 May 2015

# FRACTAL ANTENNA WITH HEXAGONAL RESONATORS

**Gheorghe Morariu***, **Mihai Miron***

*Electronics & Computers Department, Transilvania University of Brasov, Romania

***Abstract:*** *The paper presents a model of fractal antennae having hexagonal resonators with slots. The content highlights the principles, the calculation model and technical design features accompanied by experimental results. Covering a very wide frequency band, having a satisfactory gain and relatively small geometric dimensions, this antenna is recommended in mobile telephony and multiservice.*

***Keywords:*** *fractal, antenna, resonator, directivity, field intensity.*

## 1. INTRODUCTION

A fractal element antenna uses the fractal geometric structure as a virtual combination of capacitors and inductors. This allows the antenna to have multiple resonance frequencies that can be selected and corrected by chosen fractal model. Recent years have shown in many studies [1], [2], [3] that the use of fractal element antennas in the antennas construction confers superior performances and properties, validating the idea that geometry is a key issue in unique determination of the electromagnetic behavior of antennas that are independent of frequency [6].

## 2. ANTENNA DESIGN

**2.1 Principles and the calculation model**. The theoretical model of reference is fractal with discs, while the calculation procedure of electrical quantities is similar to fractal sector antenna with disk-shaped resonators, stressing that discoid surfaces were approximated with hexagonal surfaces.

**2.2 Antenna architecture**. The geometrical shape used both for the fractal construction and for the radiating surface of the antenna, it is the hexagon. Fractal has in this case three iterations and the scaling factor is two. In the first iteration six new hexagons are created (one on each side of the basic shape, having the edge dimension equal to half of the generator side), and in the second iteration are kept only three hexagons, on the sides that are towards the outside of figure (Fig. 1).

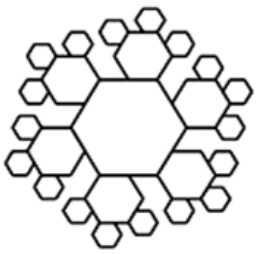

Fig. 1. The architecture of the fractal antenna with hexagonal resonators.

In the final shape of the radiating surface are placed two such fractals. Hexagonal surfaces on the top floor are approximated by discs. Each hexagonal surface contains a

resonant slot disposed symmetrical on rectangular axes of the hexagonal surface. For one of fractals slots are placed horizontally and vertically to other one (Fig. 2).

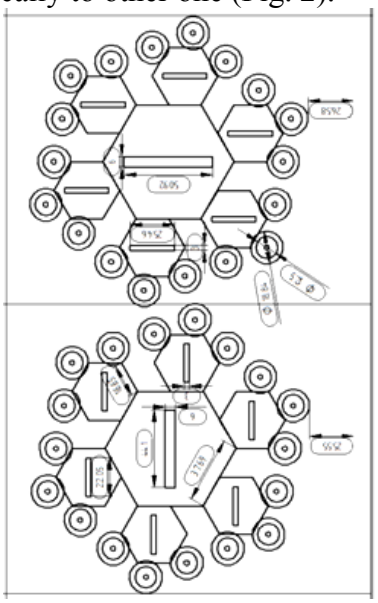

Fig. 2. Fractal antenna with hexagonal resonators – slots disposing.

**2.3 Dimensioning of planar resonant slot.** The electromagnetic wave equation of the planar resonant cavity is:

$$\frac{\partial^2 H_z}{\partial x^2} + \frac{\partial^2 H_z}{\partial y^2} + \mu\varepsilon\omega^2 H_z = 0 \qquad (1)$$

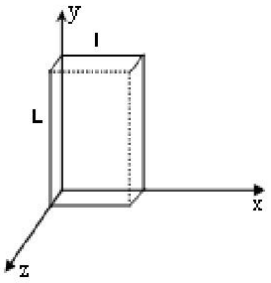


Fig. 3. Model of the planar resonant slot.

Considering the following conditions:

$E_z = 0$, $x = 0$ and $x = l$;

$E_z = 0$, $y = 0$ and $y = L$,

the $H_z$ value can be calculated:

$$H_z = H_0 \cos(n\pi \frac{x}{l}) \cos(m\pi \frac{y}{L}) \qquad (2)$$

for $0 \le x \le l$ and $0 \le y \le L$.

Specific resonance pulsation for the propagation mode is:

$$\omega = \frac{\pi}{\sqrt{\varepsilon\mu}} \sqrt{\frac{n^2}{l^2} + \frac{m^2}{L^2}} \qquad (3)$$

$$\lambda_{rez} = \frac{2\pi\sqrt{\varepsilon_r}}{\sqrt{\frac{n^2}{l^2} + \frac{m^2}{L^2}}} \qquad (4)$$

The $H_{01}$ propagation mode is dominant, rendering n=0 and m=1.

$$L = \frac{\lambda_r}{2} \qquad (5)$$

$$\omega_r = \frac{4\pi}{\lambda_r\sqrt{\varepsilon\mu}} = \frac{4\pi}{\lambda_r\sqrt{\varepsilon_r}\sqrt{\varepsilon_0\mu_0}} = \frac{4\pi c}{\lambda_r\sqrt{\varepsilon_r}} \qquad (6)$$

$$f_r = \frac{2c}{\lambda_r\sqrt{\varepsilon_r}} \qquad (7)$$

The resonant frequencies of the slots for H wave propagation mode (obtained for $\varepsilon_r \cong 2.25$ and expressed in GHz) are shown in the following table.

Table 1. The resonant frequencies of the slots; Propagation mode $H_{i0}$, i = 1÷3.

| i | $L_1$ [mm] | $L_2$ [mm] | $\square_{r1}$ [mm] | $\square_{r2}$ [mm] | $f_{1n}$ [GHz] | $f_{2n}$ [GHz] |
|---|---|---|---|---|---|---|
| 1 | 51 | 25.4 | 162.56 | 81.28 | 1.84547 | 3.69094 |
| 1 | 44 | 22 | 140.8 | 70.4 | 2.13068 | 4.26136 |
| 2 | 51 | 25.4 | 81.28 | 40.64 | 3.69094 | 7.38189 |
| 2 | 44 | 22 | 70.4 | 35.2 | 4.26136 | 8,52272 |
| 3 | 51 | 25.4 | 54.187 | 27.09 | 5.53641 | 11.0728 |
| 3 | 44 | 22 | 46.933 | 23.47 | 6.39204 | 12.7840 |

**2.4 Dimensioning of resonant surfaces having hexagonal shape**. To calculate the resonance frequencies was used the calculation method of the resonant frequencies of disc resonators [4], [5] weighted by equivalent radius of the hexagonal surface (Fig. 4) for fundamental mode $E_{110}$.

Corresponding to this resonant mode, the fundamental frequency was calculated using the first solution of Bessel function $J_0$ - $X_{01}$ = 2.402, resulting in resonance wavelengths:

$$\lambda_{rez} = \frac{2\pi r_{ef}}{X_{01}}\sqrt{\varepsilon_r} \qquad (8)$$

where $r_{ef}$ is the circle radius with surface area equivalent to hexagon surface area having value 0.91r (r - hexagon edge).

The successive resonant wavelengths $\lambda_{rez}$ have divided by two.

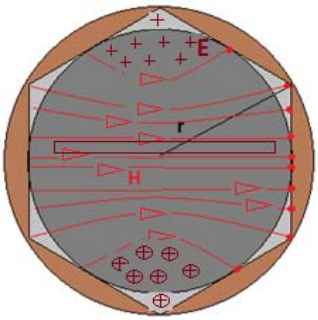


Fig. 4. Hexagonal resonator surface.

Fig. 5. The antenna radiant surface.

Figure 6 shows the resonators phasing and the feeder adaptation circuit.

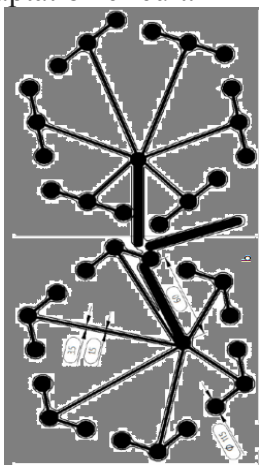

Fig. 6. Phasing and adaptation circuits.

## 3. EXPERIMENTAL RESULTS

The most representative experimental data results were obtained by spectral analysis (scalar) and vectorial analysis (with VNA) and are shown in Fig. 7 – 11 (experimental diagrams).

Fig. 7 shows the directivity diagrams for both type of polarization: horizontal and vertical.

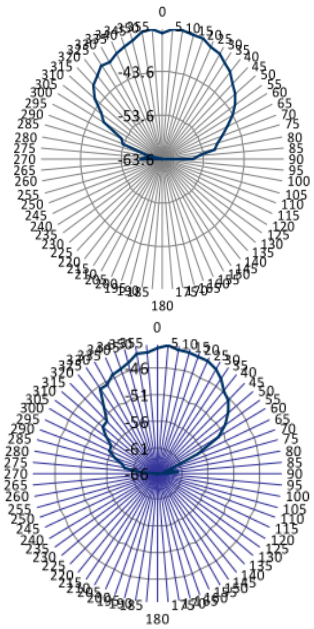


Fig. 7. Fractal antenna with hexagonal resonators: Directivity diagram for horizontal and vertical polarization.

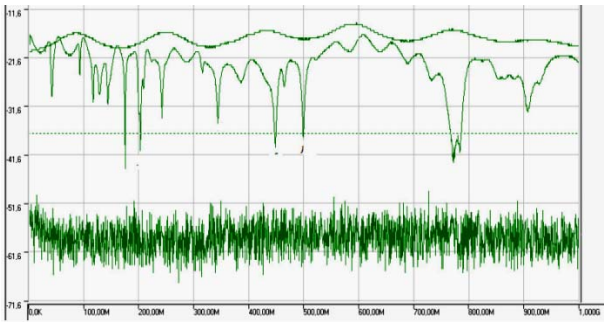

Fig. 8. Fractal antenna with hexagonal resonators: The reflection coefficient variation.

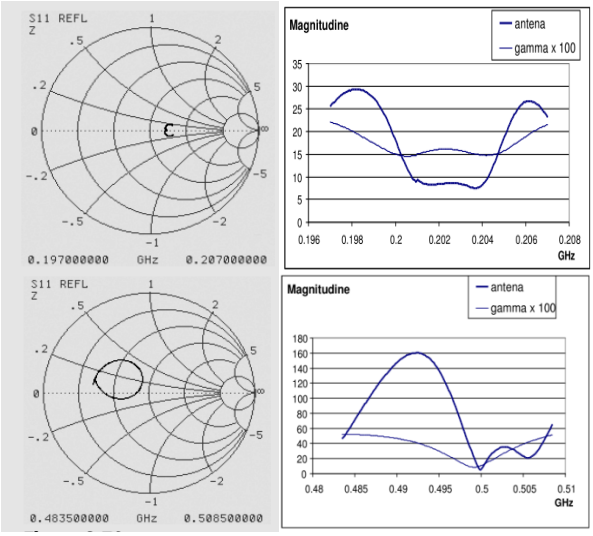


Fig. 9. Fractal antenna with hexagonal resonators – VNA analysis in the frequency band 0.19 - 0.51GHz.

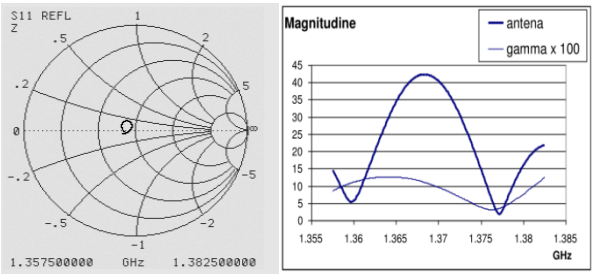


Fig. 10. Fractal antenna with hexagonal resonators – VNA analysis in the frequency band 1.35- 1.39 GHz.

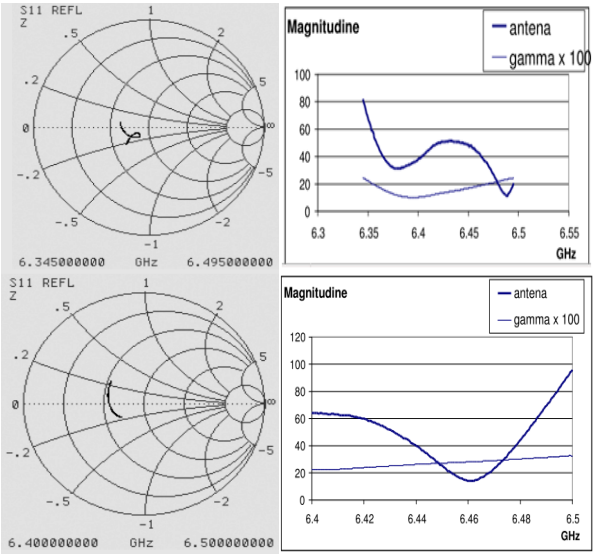


Fig. 11. Fractal antenna with hexagonal resonators – VNA analysis in the frequency band 6.34 - 6.5GHz.

## 4. CONCLUSIONS

This fractal antenna belonging to the class of fractal antennas (theoretically independent of frequency antennas) operate in 100MHz - 6GHz frequency band with a 3 - 9dB gain.

Through a narrower adjustment of the phasing lines between fractal radiating elements and the feeder adaptation, can be obtained a narrower frequency band with a gain of 8 - 10dB.

The antenna operates with small differences in circular polarization and vertical/ horizontal. Due assessment results, this model of antenna achieved at a smaller scale can be used in mobile phones or base stations respecting the dimensions determined in the paper.

## REFERENCES

1. Kumar, R., Malathi, P. *On the Design of CPW - Fed Ultra Wideband Triangular Wheel Shape Fractal Antenna*, IJMOT, vol. 5 no. 2, p. 89-93, (2010).
2. Kumar, R., Chaubey, P. N. *On the Design of Tree-type Ultra Wideband Fractal Antenna for DS-CDMA System*, Journal of Microwaves, Optoelectronics and Electromagnetic Applications, Vol. 11, No.1, p. 107-121, (2012).
3. S. Best, S. *A Comparison of the Resonant Properties of Small Space-Filling Fractal Antennas,* IEEE Antennas and Wireless Propagation Letters 2 (1): p. 197–200, (2003).
4. Kumar, R., Sawant, K. K. *On the Design of Circular Fractal Antenna with UShape Slot in CPW-Feed*, Wireless Engineering and Technology, , No.1, p. 81-87, (2010).
5. Morariu, G., Alexandru, M., Miron, M., Romanca, M., Machedon-Pisu, M., Dobrescu, A. *Experiment-supported Study on the Bipolar Disk Microstrip Antenna,* DAAAM International Vienna, Austria, Annals of DAAAM & Proceedings, (2009).
6. Hephzibah, L., B., Srinivasan, A., Rajalakshmi, B. *Wideband Fractal Microstrip Antenna for Wireless Application*, ICT Journal, Volume 3 No. 3, (2013).

"HENRI COANDA"
AIR FORCE ACADEMY
ROMANIA

"GENERAL M.R. STEFANIK"
ARMED FORCES ACADEMY
SLOVAK REPUBLIC

INTERNATIONAL CONFERENCE of SCIENTIFIC PAPER
AFASES 2015
Brasov, 28-30 May 2015

# INFLUENCE OF THE INTERCONNECTING CABLES ON EQUIPMENTS ELECTROMAGNETIC EMISSIONS SPECTRUM

**Dan Stoica*, Adina Boteanu *, Mihai Enache*, Albert Ploşniță***

*Information Systems and Communications Test & Evaluation Scientific Research Center, Military Equipment and Technologies Research Agency, Bucharest, Romania

***Abstract:*** *This paper presents the results of some experimental activities carried out in our specialized electromagnetic compatibility laboratory for equipments emissions analysis. It is in the interest of all sensitive information processing equipments owners to invest in data security measures but with respect to a reasonable budget. At the present the most common methods to prevent electromagnetic data leakage are represented by electromagnetic shielding solutions. Not always these solutions are the most efficient way to solve data security problem, especially from economical point of view. Our paper presents some aspects regarding interconnecting cables influence on the system vulnerability. It represents a starting phase in a bigger project that aims to adapt and optimize shielding methods for data electromagnetic leakage prevention.*

***Keywords:*** *shielding screen, electromagnetic, EMC*

## 1. INTRODUCTION

Electromagnetic interferences represent the energy levels introduced by electronic or electrical devices that have a negative effect on other equipments, regarding their functionality. Any electronic equipment is affected by interferences in a moderate or more sever manner.

Electromagnetic screening represents the most common solution used to protect equipments or their components from the outside electromagnetic environment and vice versa. It represents also a good way to secure data processing equipments by preventing electromagnetic emissions leakage.

The idea behind these techniques is to ensure high attenuation of the electromagnetic radiated field that passes through a screen in order to reduce the data integrity carried out by these emanations [10].

In the design phase it is necessary to analyze, select and optimize all the adequate shielding techniques, in order to fulfil special EMI/EMSEC protection requirements at the lowest design level possible.

For this reason, electromagnetic shielding solutions design and implementation is a complex task to achieve, and it sometimes involves special design and simulation software. Sometimes, the electromagnetic protection solution is very simple and consists in efficient methods appliance like components isolation, equipment grounding or replacing the original cables with proper shielding ones.

We believe that EMC testing and analysis could be also optimized by offering more

This work was supported by a grant of the Romanian National Authority for Scientific Research, Programe for research - Space Technology and Advanced Research - STAR, project number 48/2012

detailed information about interference sources, conducting specific tests.
This paper presents a case study regarding video displays interconnecting cables. The aspects concluded could be extended to other typical IT and communications equipments sources.

## 2. SHIELDING THEORY

The shielding effectiveness, noted *SE*, is an important parameter [1-6] for the characterization of an electromagnetic screen and is defined as the report between the field's intensity (electric or magnetic) measured without screen $E_s$ and with screen $E_0$.

$$SE = 20 \cdot log\left(\frac{E_s}{E_0}\right) \quad (1)$$

or

$$SE = 10 \cdot log\left(\frac{P_i}{P_t}\right) \quad (2)$$

In the same time SE could be obtained as a ratio between the field strength, at a given distance from the source, without the shield interposed ($P_i$) and the field strength with the shield interposed ($P_t$).

A screen action on the electric or magnetic field through the following mechanisms:

- absorption (characterized by the factor of attenuation through absorption *A*)
- reflection (characterized through the factor of attenuation through reflection *R*)
- multiple scintillations (with significant effects in the thin screen's case) (characterized through the factor of attenuation through scintillations *Rr*).

Expressing the attenuations *A*, *R* and $R_r$ in dB, it's obtained, through their summarization, the (total) efficacy *SE* of the screen.

$$SE = A + R + R_r \quad (3)$$

where:

R - the factor of attenuation through reflection at the frontier surfaces,

A - the factor of attenuation through absorption within the screen (the transformation of the electromagnetic energy in heat through the losses due to currents circulation through the screen),

Rr - the factor of attenuation that considers the multiple scintillations in the inside of the screen.

The efficacy of the screening depending on: the perturbation source's frequency, the material of the screen (generally: copper, iron, aluminum), the field's type that must be attenuated (electric, magnetic, TEM), the screen's geometry (parallelepiped, cylindrical, spherical, etc.), the incidence angle of the field, etc.

Frequently though, it's worked with the inverted value, $\delta$ $(\delta = 1/\alpha_a)$, called, penetration depth. This represents the distance from the incidence surface in the conducting material to which the field applied on the surface decreases to level 0.368 (e-1=0.368) compared to the value from the incidence surface of the material.

Analytically, the penetration depth is described through the relation:

$$\delta = \frac{1}{\sqrt{\pi f \mu \sigma}} \quad (4)$$

from where results that the value varies proportionally inverse with the electromagnetic field applied on the screen's surface and with the material's conductivity the screen's made of.

Attenuation by reflection is the difference between the incident wave E0 and the out wave of the screen Ed:

$$R = 20 \cdot log\frac{E_0}{E_d} = 20 \cdot log\frac{|Z_1|}{4 \cdot |Z_2|} \quad [dB] \quad (5)$$

The reflection losses do not depend on the thickness of the screen just on the screen impedance values or environmental impedance.

The attainment of an efficient screening implies, among others, the use of a material that has low permeation depth.

In conclusion, the electromagnetic shielding solution will be adapted to the specific protection requirements by choosing material type and construction. As a first step in our project we wanted to evaluate these requirements and the influence of the products parameters (length, position and grounding) on the overall system vulnerability.

This work was supported by a grant of the Romanian National Authority for Scientific Research, Programe for research - Space Technology and Advanced Research - STAR, project number 48/2012

## 3. CONFIGURATION SETUP

In our testing activity, we focused on VGA card signals analysis and measurements, conducting investigations on a reference electromagnetic shielded central unit, in order to minimize electromagnetic noise background during emissions tests. All tests was carried inside our specialized laboratory using measurements equipments like oscilloscope, spectrum analyzer, antennas, shielded cables, connectors and specialized software applications.

VGA typical electric signals are composed by synchronization (H, V) signals and data channels (R, G and B). We have been tested different display settings and various images.

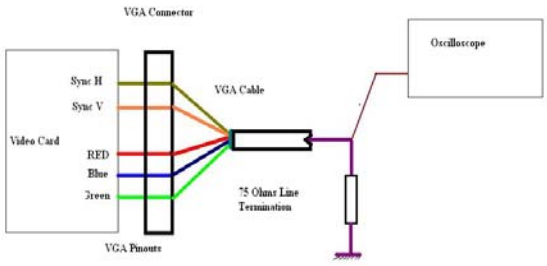


Figure 1. VGA card signals measurements and image setup

For instance, in this paper are presented the results obtained for a 32 bits VGA card working on 1280x1024@75 Hz resolution, using a simple test image that consists in a black background with 3 parallel red horizontal lines.

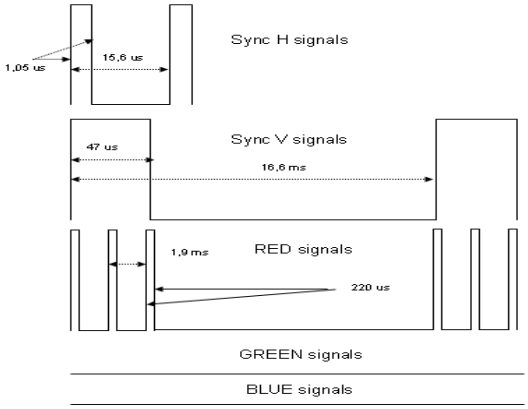


Figure 2. VGA card signals measured parameters for reference image

The measurement results are displayed in figure 2. These values represent reference parameters that will be compared with received signals during EMC tests.

Analyzed signal sources could be present in the equipment radiated emissions as a normal consequence of electromagnetic field propagation. Such correlated emissions may occur as a direct base-band or high harmonic radiation and also as a modulation of other high frequency signals present in the internal equipment components.

Based on initial measurement results we tried to identify in the 50 – 1000 MHz band correlated emissions with these signal sources. Tests were conducted in accordance with standard EMC radiation procedures, using current measurement platform, presented in fig. 3.

In order to minimize effects of other signals we used a shielded computer central unit (TEMPEST product), containing measured VGA card for exciting 2 different standard VGA cables: 1.8 meter length, 1 meter length, in both planes of polarization.

This work was supported by a grant of the Romanian National Authority for Scientific Research, Programe for research - Space Technology and Advanced Research - STAR, project number 48/2012

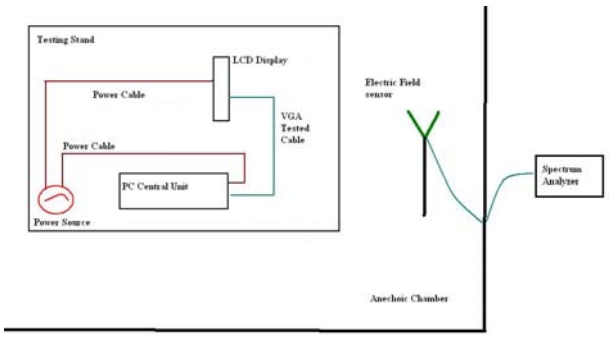


Figure 3. Emission radiation measurement setup

## 4. EXPERIMENTAL RESULTS

Electromagnetic field measurements were conducted in an semi-anechoic chamber, using a receiver system composed by a bi-conilog antenna and a wideband EMI receiver. We made spectrum measurements for each cable as it's presented below (figure 4, 5).

All these data represents electromagnetic spectrum radiated by the equipment and its cables. As we said before we used a shielded central unit with shielded and filtered power cable and the VGA cables 75 ohms ended.

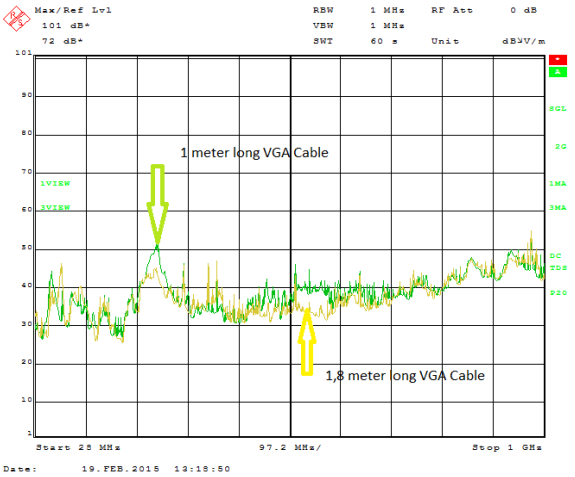


Figure 4. Radiated Emissions levels in 28-1000 MHz for different cable lengths

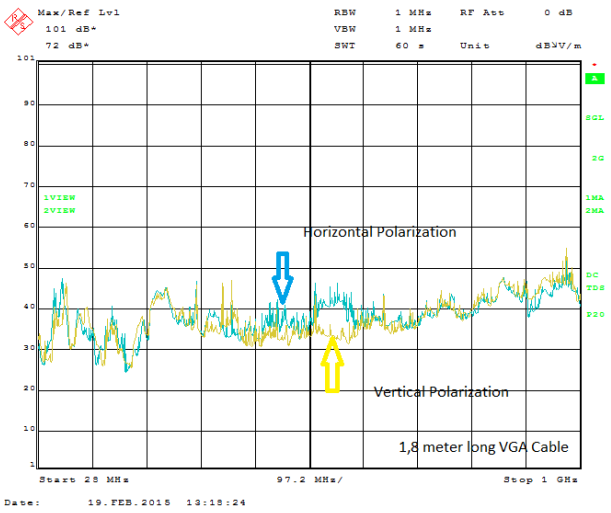


Figure 5. Radiated Emissions levels in 28-1000 MHz polarization V and H

As other research works in the display data units eavesdropping field [7-9] we identified correlated emissions with reference video signal around pixel frequency, respectively 134.18 MHz (for 1280x1024@75 Hz resolution). Manual searches conducted for each configuration, in this spectrum band, have shown results displayed in figure 5.

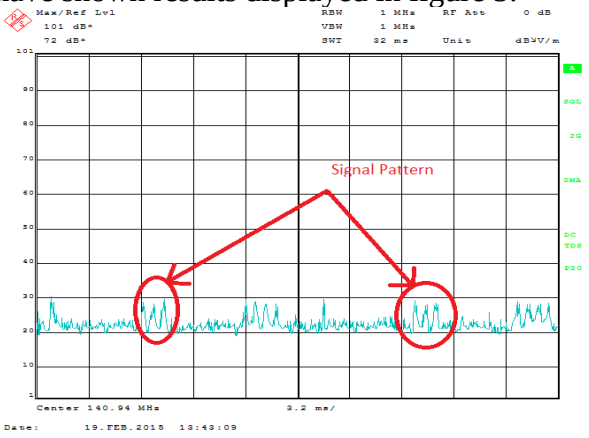


*a)*

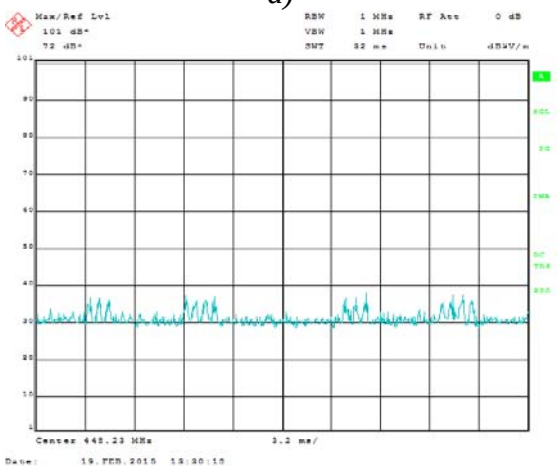

b)

This work was supported by a grant of the Romanian National Authority for Scientific Research, Programe for research - Space Technology and Advanced Research - STAR, project number 48/2012

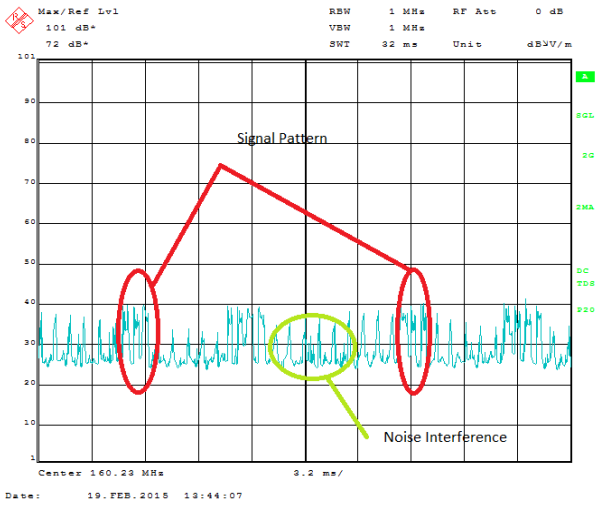


c)

Figure 6. Time domain manual measurement for investigated emissions: a) 1,8 meter cable, 140 MHz emission; b) 1 meter cable, 448 MHz emission c) H-plane polarization, 160 MHz emission

In all three configuration setups (140 MHz emission, 448 MHz emission, 160 MHz emission) the equipment presented evident vulnerabilities, even if the measured spectrum seems to be different for each one. As it is presented in figure 6, each EUT could be identified by video card signals intercepted by his own unintentional emissions. The difference between them is that EUT present the main vulnerability at different frequencies. It could be explained by the multiple interference sources presence in the same time on the same transmission cable. An emission is better propagated if the electrical length of the equivalent antenna is closer to the wavelength fraction (with respect to the ground).

The EMC standard measurements in the 100-500 MHz band require resolution bandwidth of 100 KHz and a minimum dwell time of 15 ms. These conditions assure to evaluate effect of mostly present signal sources inside equipment, but will not offer correct bandwidth for wideband signals analysis. Considering all these aspects we performed personalized tests for properly electromagnetic data acquisition.

Recorded data on spectrum analyzer it's not enough to conduct proper offline frequency domain analysis in larger bandwidths, because of storage hardware limitations. All tests carried out limited data records to 500 points/measurement, far from resolution needs on this scenario.

In figure 7 are presented some image reconstruction results obtained in our testing laboratory by EUT unintentional emission processing and analysis.

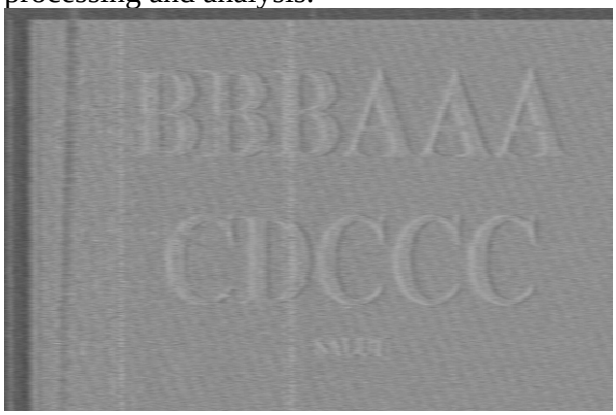

Figure 7. Software reconstruction of initial image from VGA cables unintended emanations

## 5. CONCLUSION

This paper describes a work covering some aspects of the EMC and EMSEC testing and evaluation techniques for improving customer feedback.

EMC or EMSEC evaluations are not formal testing activities and customer epected

This work was supported by a grant of the Romanian National Authority for Scientific Research, Programe for research - Space Technology and Advanced Research - STAR, project number 48/2012

feedback is not always satisfying if is reduced to yes/no, or compliant/incompliant especially in development and integration stages of the product.

As we presented already, the influence of the interconnecting cables on the overall system vulnerability exists but it's more significant in the EMSEC field than EMC.

There are ways to improve an existing system quality, from this point of view, by simply replacing a regular cable with a shielded one or just increasing cables length for wideband signals.

The present paper is a first step approach to the problem of electric and electronic equipments interference signal sources detection and identification. The electromagnetic protection measures should be chosen according to the firstly evaluated equipment vulnerabilities.

## REFERENCES


1. Armstrong R., *Measurement of shielding in electrically large metallic enclosures*, University of York, February 2013
2. Celozzi, S., Araneo, R., Lovat, G. *Electromagnetic Shielding* IEEE Press, Wiley-Interscience a John Wiley & Sons, Inc. Publication, Mar.2008, ISBN : 978-0-470-05536-6
3. Chung, D. D. L., *Electromagnetic interference shielding effectiveness of carbon materials*, Carbon, vol. 39, no. 2, pp. 279-285, Feb. 2001.
4. Clayton R. Paul, *Introduction to electromagnetic compatibility*, Second edition, John Wiley & Sons, Inc. Publication, February 2006, ISBN : 978-0-471-75500-5
5. Erhart Moller, *Protective Measures Against Compromising Electro Magnetic Radiation Emitted by Video Display Terminals*.
6. Gainsville, VA: Interference Control Technology, 1988
7. Markus G. Kuhn, Ross J. Anderson, Soft Tempest: *Hidden Data Transmission Using Electromagnetic Emanations*. Information Hiding Proceedings, 1998.
8. Markus G. Kuhn, *Compromising emanations: eavesdropping risks of computer displays*, Technical Report, 2003.
9. Robinson, M. P., Thomas, D. W. P., Dawson, J. F., Porter, S. J., Christopoulos, C., *Design of EMC shielding*, 1997 The Institution of Electrical Engineers, Savoy Place, London WC2R OBL, UK
10. White, D. R. J., Mardiguian, M., *Electromagnetic Shielding: A Handbook Series on EMI and Compatibility*, vol. 3.


This work was supported by a grant of the Romanian National Authority for Scientific Research, Programe for research - Space Technology and Advanced Research - STAR, project number 48/2012

"HENRI COANDA"
AIR FORCE ACADEMY
ROMANIA

"GENERAL M.R. STEFANIK"
ARMED FORCES ACADEMY
SLOVAK REPUBLIC

INTERNATIONAL CONFERENCE of SCIENTIFIC PAPER
AFASES 2015
Brasov, 28-30 May 2015

# ABOUT POLY-PHASE VOLTAGE RECTIFIERS OPERATION

**Constantin Strîmbu***

*Faculty of Aeronautic Management, "Henri Coandă" Air Force Academy, Brasov, Romania

***Abstract:*** *Some issues regarding the analysis of poly-phase voltage rectifier operation will be presented in this paper. The switch is an uncontrolled-type, a diode in this case, which is considered as an ideal one. The expressions of the parameters characterizing the rectifier operation are computed in the paper. Their variations depending on load are also discussed*

***Keywords:*** *poly-phase, rectifier, diode,*

## 1. INTRODUCTION

A poly-phase switch, equipped with *m* individual uncontrolled switches (diodes) will be discussed. The input of this device consists in the following poly-phased voltage system:

$$\begin{cases} u_{1,0} = U_M \sin \omega t \\ u_{2,0} = U_M \sin\left(\omega t - \dfrac{2\pi}{m}\right) \\ \ldots\ldots\ldots\ldots\ldots\ldots\ldots\ldots \\ u_{p,0} = U_M \sin\left[\omega t - (p-1)\dfrac{2\pi}{m}\right] \\ \ldots\ldots\ldots\ldots\ldots\ldots\ldots\ldots \\ u_{m,0} = U_M \sin\left[\omega t - (m-1)\dfrac{2\pi}{m}\right] \end{cases} \quad (1)$$

The schematic of an angle-phase voltage rectifier is presented in figure 1.

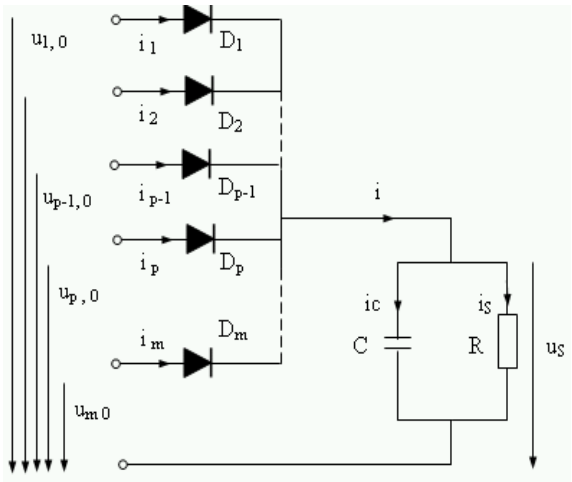


Fig.1. Poly-phase voltage rectifier with diode

The steady-state signals expressions are the following [1,3]:

The diode $D_p$ is "on":

$$\omega t \in \left( (p-1)\frac{2\pi}{m} + \alpha_p \, , (p-1)\frac{2\pi}{m} + \beta \right)$$

$$\begin{cases} u_S = u_p = U_M \sin\left[\omega t - (p-1)\dfrac{2\pi}{m}\right] \\ i_S = I_M \sin\left[\omega t - (p-1)\dfrac{2\pi}{m}\right] \\ u_{D,p} = 0 \\ i_C = \omega C U_M \cos\left[\omega t - (p-1)\dfrac{2\pi}{m}\right] \\ i_{D,p} = I_M \sin\left[\omega t - (p-1)\dfrac{2\pi}{m} + \xi\right] \end{cases} \quad (2)$$

The diode $D_p$ is "off":

$$\omega t \in \left( (p-1)\frac{2\pi}{m} + \beta \, , p\frac{2\pi}{m} + \alpha_p \right)$$

$$\begin{cases} u_s = U_M \sin\varphi \, e^{-\frac{\left[\omega t - (p-1)\frac{2\pi}{m} - \beta\right]}{\omega R C}} = \\ = U_M \sin\xi \, e^{-\left[\omega t - (p-1)\frac{2\pi}{m} - \beta\right]\operatorname{ctg}\xi} \\ i_S = I_M \sin\varphi \, e^{-\frac{\left[\omega t - (p-1)\frac{2\pi}{m} - \beta\right]}{\omega R C}} = \\ = I_M \sin\xi \, e^{-\left[\omega t - (p-1)\frac{2\pi}{m} - \beta\right]\operatorname{ctg}\xi} \end{cases} \quad (3)$$

The firing angle is computing by solving the equation:

$$\sin\xi \, e^{-\frac{\left(\frac{2\pi}{m} + \alpha_p - \beta\right)}{\omega R C}} = \sin\alpha_p \quad (4)$$

The turn-off angle - $\beta$ - expression comes out from the condition: $i_{V,p}\left(\omega t = \beta + (p-1)\dfrac{2\pi}{m}\right) = 0$ resulting:

$$\beta = \pi - \xi = -\operatorname{arctg}(\omega R C) \quad (5)$$

The graphic representations of the signals $(u_i, u_s, i_S, i_C, i)$ as functions of load $\xi = \operatorname{arctg}(\omega RC)$ are shown in the figures below. A three-phase $(m = 3)$ was considered in the above mentioned plots, related to the load values presented in table 1.

Table 1

| C [μF] | R [Ω] | tgξ | ξ [rad] | ξ [°] |
|---|---|---|---|---|
| 1000 | 10 | 3.14159 | 1.26262 | 72.34321 |
| 1000 | 50 | 15.70796 | 1.50722 | 86.35735 |
| 1000 | 100 | 31.41592 | 1.53897 | 88.17683 |

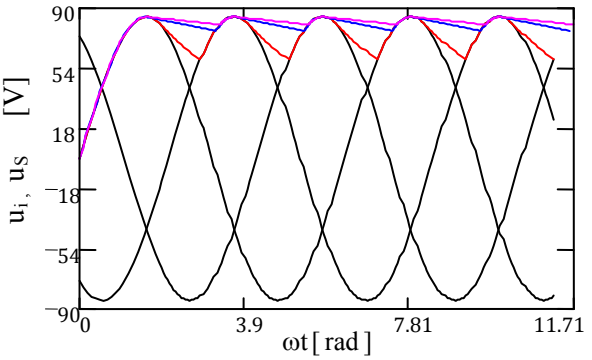


Fig.2 $u_i$ and $u_S$ variation for different load and m=3

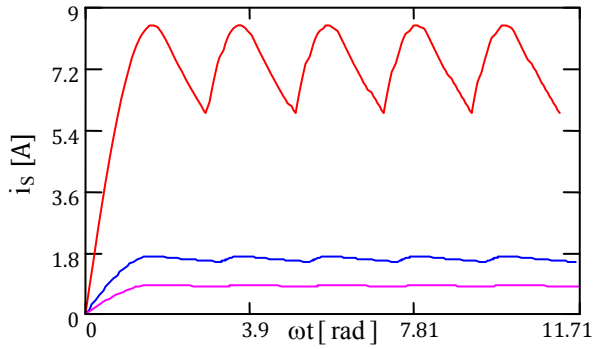


Fig.3 $i_S$ variation for different load and m=3

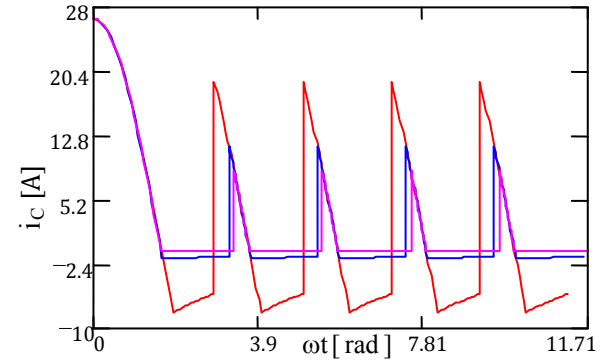


Fig.4 $i_C$ variation for different load and m=3

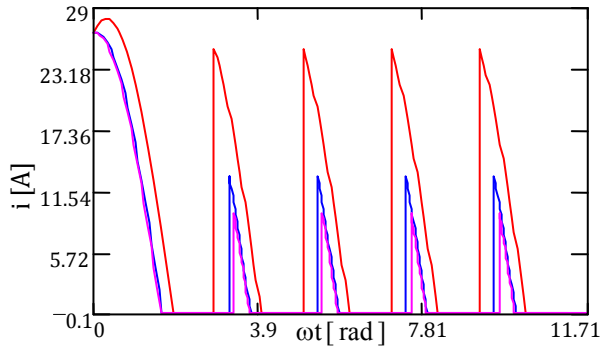


Fig.5 i variation for different load and m=3

## 2. CIRCUIT ANALYSIS

### 2.1 Variations of angles $\alpha_p$ and $\beta$

It results from (5) the following restrictions upon the circuit parameters in order to obtain a interrupted current regime:

$$\xi = \operatorname{arctg}(\omega R C) > \frac{\pi}{2} - \frac{\pi}{m} \qquad (6)$$

$$m \geq 3 \ , \xi_{min} = \frac{\pi}{2} - \frac{\pi}{m}$$

The non-interrupted current regime is characterized by the fact that a diode turning-off is determined by the turning-on of another one. A necessary condition to be satisfied for the rectifier operation in this working regime is the following:

$$\beta > \frac{\pi}{2} + \frac{\pi}{m} \qquad (7)$$

Related to the interrupted current operation, considering a given number of phases – m – of the input voltage system, the capacitive load value is inferior limited by (6). Taking into consideration that $\alpha_p$ has an increasing variation with capacitive load value, it results that a minimum value of this parameter has to exist:

$$\alpha_{p,min} = \frac{\pi}{2} - \frac{\pi}{m} \qquad (8)$$

The variation of turning-on and off angles as function of rectifier parameters $\xi = \operatorname{arc\,tg}(\omega RC)$ and number of phases, m, is plotted in figure 6.

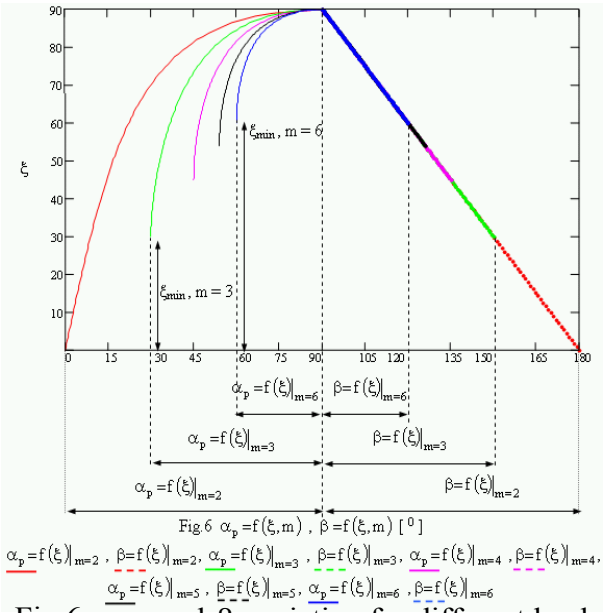


Fig.6 $\alpha_p$ and $\beta$ variation for different load and m=3

### 2.2 The Voltages and Currents Average Values

According to [2], the following parameters are defined:

$(U_{d,m})_{\alpha_p}$ - average value of the output voltage:

$$(U_{d,m})_{\alpha_p} = \frac{m U_M}{2\pi}\left[\cos\alpha_p + \frac{1}{\cos\xi} * \left[1 - \sin^2\xi\, e^{-\left(\alpha_p + \varphi + \pi\frac{2-m}{m}\right)\operatorname{ctg}\varphi}\right]\right] \qquad (9)$$

$(U_{def,m})_{\alpha_p}$ - RMS value of the output voltage:

$$\left(U_{def,m}\right)_{\alpha_p} = \frac{U_M\sqrt{m}}{2\sqrt{\pi}} * \\ * \sqrt{\pi - \xi - \alpha_p + \sin\left(\alpha_p + \xi\right)\cos\left(\alpha_p - \xi\right) + A} \quad (10)$$

$$A = \frac{\sin^3\xi}{\cos\xi}\left[1 - e^{-2\left(\alpha_p + \xi + \pi\frac{2-m}{m}\right)ctg\xi}\right]$$

$\left(I_m\right)_{\alpha_p}$ - average value of the current flowing through the diode:

$$\left(I_m\right)_{\alpha_p} = \frac{m}{2\pi}\frac{U_M}{R}\left[\cos\left(\alpha_p + \xi\right) + 1\right] = \\ = m\left(I\right)_{\alpha_p} \quad (11)$$

$\left(I_{S,m}\right)_{\alpha_p}$ - average value of the load (R) current:

$$\left(I_{S,m}\right)_{\alpha_p} = \frac{m I_M}{2\pi}\left[\cos\alpha_p + \frac{1}{\cos\xi} * \right. \\ \left. * \left[1 - \sin^2\varphi\, e^{-\left(\alpha_p + \xi + \pi\frac{2-m}{m}\right)ctg\varphi}\right]\right] = \quad (12)$$

$$= \frac{\left(U_{d,m}\right)_{\alpha_p}}{R}$$

## 3. CONCLUSIONS & ACKNOWLEDGMENT

The following conclusions derive from the study of voltage poly-phased rectifiers, provided with non-controlled switches (diodes):

1. The non-interrupt current regime is possible only if the rectifier load respects (6);
2. After the second switch of the diode, the circuit reaches its steady state regime;
3. The diode turn-on angle $\alpha_p$ has an increasing variation of load (R);
4. The diode turn-off angle $\beta$ has an decreasing variation of load (R);

## REFERENCES

1. Cerbulescu, D. *Convertoare statice de putere: Redresoare* Craiova: Editura Scrisul Românesc (1995).
2. Matlac, I. *Convertoare electroenergetice* Timişoara: Editura Facla (1987).
3. Strîmbu, C. About single-phase voltage rectifiers operation. *AFASES 2014, 22-24 May Brasov, 2014.*.

"HENRI COANDA"
AIR FORCE ACADEMY
ROMANIA

"GENERAL M.R. STEFANIK"
ARMED FORCES ACADEMY
SLOVAK REPUBLIC

INTERNATIONAL CONFERENCE of SCIENTIFIC PAPER
AFASES 2015
Brasov, 28-30 May 2015

# IMPROVEMENTS METHODS FOR DESIGN OF MULTIFUNCTIONAL REGISTERS WITH DECODED MODE SIGNALS

**Mihai Timis*, Alexandru Valachi*, Calin Monor***

*Automatic Control and Computer Engineering,"Gh.Asachi", Iasi, Romania

***Abstract:*** *This paper presents the research results regarding a comparison between two multifunctional registers types, with coded or decoded command validation signals. Also, the implementation costs, time parameters and the applicability in Finite State Machine - FSM synthesis are presented as conclusion.*

***Keywords:*** *Multifunctional Registers, Moore Sequential System, Veitch – Karnaugh, Logic Gates, Truth Table, Priority Inputs Signals, FSM – Finite State Machine.*

## 1. INTRODUCTION

In this paper the authors continue the research of synthesis multifunctional registers, described in research papers [1],[2],[3]. The authors present in [1] the set of priority criteria orders for the multifunctional registers, denoted as RMF with the validation decode signals.

In this paper, the authors undertake a comparison between two multifunctional registers types, with the coded or decoded command validation signals. From this point of view, the authors analyze the implementation costs, time parameters and the applicability in FSM synthesis. The basic idea is to synthesis any digital systems using digital registers with multifunctional support. This means we use only the increment, parallel load, reset, decrement, shift signals. In this way, the system is costless which means optimal. This part of our design can be found inside a digital processor. The technology used is CMOS. The implementation cost represents the total number of the CMOS digital logic gates used. We assume that optimal design implementation means less digital circuit used compared with the already existing implementations, see [2],[3],[4].

## 2. MULTIFUNCTIONAL REGISTERS WITH DECODED MODE SIGNALS

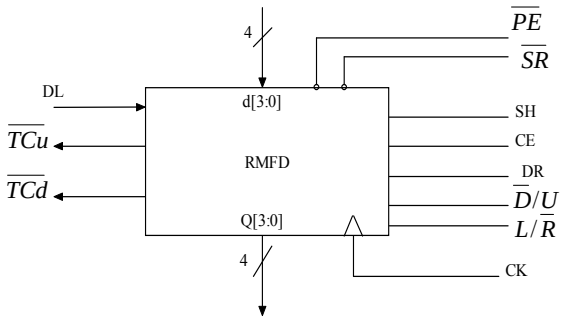


Figure 1 - RMF(decoded mode inputs)

Signals description:

Mode inputs: $\overline{SR}$ - Reset (High Priority), $\overline{PE}$ - Parallel Enable, SH – Logical

Shift( $L/\overline{R}=0-Right$ , $L/\overline{R}=1$-Left), CE – Count Enable(Low Priority) ($U/\overline{D}=0\rightarrow Down, U/\overline{D}=1\rightarrow UP$)

Data: d[3:0] – input data in parallel load mode, Q[3:0] –output data, DR,DL – serial input data, left shift, right shift, $\overline{TC_u}$ - Terminal Count Up (Q[3:0]=1111, last state), $\overline{TC_D}$ - Terminal Count Down (Q[3:0]=0000, last state).

CK – clock input, active on positive edge signal.

The functional behavior is described in Table 1.

| Mode | $\overline{SR}\,\overline{PE}$ SH CE $L/\overline{R}$ $U/\overline{D}$ CK | $Q[3:0]_{n+1}$ |
|---|---|---|
| Hold | 1 1 0 0 - - | $Q[3:0]_n$ |
| Reset | 0 - - - - - ↑ | 0000 |
| Parallel Load | 1 0 - - - - ↑ | $d[3:0]_n$ |
| Shift Right | 1 1 1 - 0 - ↑ | $DRQ[3:1]_n$ |
| Shift Left | 1 1 1 - 1 - ↑ | $Q[2:0]_n DL$ |
| Count Down | 1 1 0 1 - 0 ↑ | $[Q_n-1]_n$ mod |
| Count UP | 1 1 0 1 - 1 ↑ | $[Q_n+1]_n$ mo |

Table1 – RMF functionality

Observation: From paper [1], we consider only 4 bits for input/output data. This limitation doesn't affect the presented research idea.

Based on functionality modes and priority orders, we deduced the following equations (Di- data inputs on flip-flop D, Qi- outputs from flip-flop D).

$$D_i=\overline{SR}\cdot(PE\cdot d_i+\overline{PE}\cdot(SH\cdot(\overline{L/\overline{R}\cdot Q_{i+1}+L/\overline{R}\cdot Q_{i-1}})+\overline{SH}\cdot(CE\cdot(\overline{U/\overline{D}\cdot(\overline{Q_i}\oplus\varphi_i)+U/\overline{D}\cdot(Q_i\oplus\psi_i)})+\overline{CE}\cdot Q_i)))$$

$$D_3=\overline{SR}\cdot(PE\cdot d_3+\overline{PE}\cdot(SH\cdot(\overline{L/\overline{R}\cdot DL+L/\overline{R}\cdot Q_2})+\overline{SH}\cdot(CE\cdot(\overline{U/\overline{D}\cdot(\overline{Q_3}\oplus\varphi_3)+U/\overline{D}\cdot(Q_3\oplus\psi_3)})+\overline{CE}\cdot Q_3)))$$

$$D_0=\overline{SR}\cdot(PE\cdot d_0+\overline{PE}\cdot(SH\cdot(\overline{L/\overline{R}\cdot Q_1+L/\overline{R}\cdot DR})+\overline{SH}\cdot(CE\cdot(\overline{U/\overline{D}\cdot(\overline{Q_0}\oplus\varphi_0)+U/\overline{D}\cdot(Q_0\oplus\psi_0)})+\overline{CE}\cdot Q_0)))$$

where $i\in\{1,2\}$ and $\varphi_i,\psi_i$ represent the "$i^{th}$" rank function for the down- or adder binary counter.

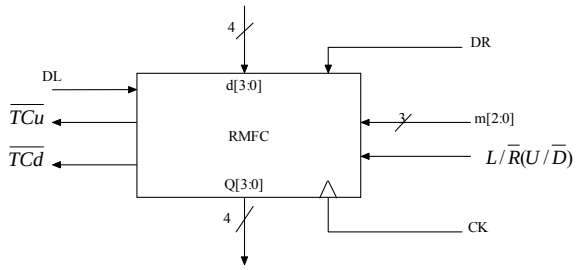


Figure 2 – RMFC design

$$\varphi_i=\prod_{k=0}^{i-1}\overline{Q_k}\ ,\ \psi_i=\prod_{k=0}^{i-1}Q_k$$

or

$$\varphi_i=\varphi_{i-1}\cdot\overline{Q_{i-1}}\ ,\qquad \psi_i=\psi_{i-1}\cdot Q_{i-1}\qquad \text{and}\qquad \varphi_0=\psi_0=1$$

We used a MUX2x1, described in figure 3, [1].

Taking into consideration the dynamic parameters for the digital circuits, like propagation delay times, set up times, hold times, one obtains the minimum expression for the clock period (equation (8) in [1]).

$$\underline{T_i}=\underline{t_{s\_u}}(D)+\overline{t_b}+\overline{t_p}(\varphi_i,\psi_i)+\overline{t_p}(86)+4\overline{t_p}(MUX)=$$

$$=\underline{t_{s\_u}}(D)+\overline{t_b}+i\cdot\overline{t_p}(08)+\overline{t_p}(86)+4\overline{t_p}(MUX)=230n\sec$$

or $\overline{f_1}=4{,}35MHz$ (2)

In the same paper [1], we calculated the same maximum clock parameters $(\overline{T},\overline{f})$ for another priority order criteria when the best values were obtained.

So, the conclusion from [1] is that dynamic parameters depends on the priorities allocation modes.

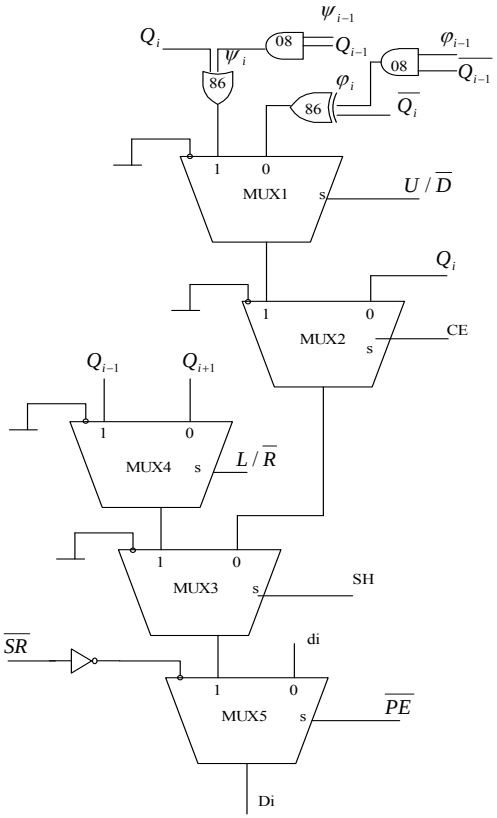


Figure 3 – RMF digital implementation

## 3. SYNTHESIS FOR THE SEQUENTIAL SYSTEM USING RMF WITH DECODED MODE SIGNALS

The unused mode or data inputs are disabled by connection to ground (0 logic). The truth table was completed as: if priority command signal is activated, the next low priority signals are *x* (0 or 1 logic)

$U/\overline{D}$ has 0 logic value for the DEC mode and 1 logic value for INC mode in the Hold state, the commands are disabled

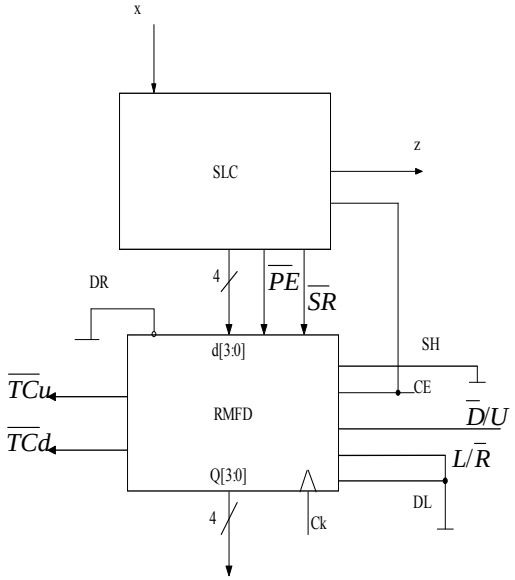


Figure 4 - Automata implementation architecture with RMFD

Considering the (1) priority order ($\overline{SR}$ - High Priority, SH – Low Priority), using Tables 2, results the next truth table, figure 5.

| X / $Q_2Q_1Q_0$ | $Q[2:0]_{n+1}$ | | $\overline{SR}$ | | $\overline{PE}$ | | CE | | Z |
|---|---|---|---|---|---|---|---|---|---|
| | 0 | 1 | 0 | 1 | 0 | 1 | 0 | 1 | - |
| 000 | 001 | 101 | 1 | 1 | 1 | 0 | 1 | - | 0 |
| 001 | 010 | 110 | 1 | 1 | 1 | 0 | 1 | - | 0 |
| 011 | 001 | 100 | 1 | 1 | 0 | 1 | - | 1 | 1 |
| 010 | 001 | 011 | 1 | 1 | 1 | 1 | 1 | 1 | 1 |
| 110 | 010 | 100 | 1 | 1 | 0 | 0 | - | - | 0 |
| 111 | 000 | 000 | 0 | 0 | - | - | - | - | 0 |
| 101 | 001 | 100 | 1 | 1 | 0 | 1 | - | 1 | 0 |
| 100 | 100 | 100 | 1 | 1 | 1 | 1 | 0 | 0 | 0 |

Table 2

| | $d_2$ | | $d_1$ | | $d_0$ | | | |
|---|---|---|---|---|---|---|---|---|
| $U/\overline{D}$ | | | | | | | | |
| X / $Q_2Q_1Q_0$ | 0 | 1 | 0 | 1 | 0 | 1 | 0 | 1 |
| 000 | - | 1 | - | 0 | - | 1 | 1 | - |
| 001 | - | 1 | - | 1 | - | 0 | 1 | - |
| 011 | 0 | - | 0 | - | 1 | - | - | 1 |
| 010 | - | - | - | - | - | - | 0 | 1 |
| 110 | 0 | 1 | 1 | 0 | 0 | 0 | - | - |
| 111 | - | - | - | - | - | - | - | - |
| 101 | 0 | - | 0 | - | 1 | - | - | 0 |
| 100 | - | - | - | - | - | - | - | - |

Figure 5 – Truth Table

Using the Veitch-Karnaugh method, results the following equations:

$$\overline{SR} = \overline{Q_2}\,\overline{Q_1}\,\overline{Q_0}$$

$$\overline{PE} = \overline{\bar{x}\cdot[Q_1Q_0 + Q_2Q_1 + Q_0Q_2] + x\cdot(Q_2 \oplus \overline{Q_1})}$$

$$CE = \overline{Q_2\,\overline{Q_0}\cdot\overline{Q_1}}$$

$$\overline{D}/U = \overline{\bar{x}\cdot Q_1 + xQ_2}$$

$$Z = \overline{Q_2}Q_1$$

$$d_3 = 0$$

$$d_2 = x\cdot\overline{Q_0}$$

$$d_1 = \overline{Q_0} \oplus x$$

$$d_0 = \bar{x}\cdot Q_0 + x\cdot\overline{Q_2}\,\overline{Q_0} \qquad (3)$$

If the SLC system would be implemented with logic gates as: AND (2 inputs), OR(2 inputs), XOR(2 inputs), NAND(2 inputs), 23 elementary circuits will be obtained, $C_{dec} = 23$.

## 4. SYNTHESIS OF SEQUENTIAL SYSTEM USING RMF WITH CODED MODE SIGNALS (RMFC)

If we consider the same Moore automata, we use only the Hold, Reset, INC/DEC, Parallel Load functions as:

- $m_2 \equiv 0$ (use only 2 codify bits)
- DL=DR=0 (the Shift function isn't used)
- $d_3 = 0$ (the automaton has only 8 states)

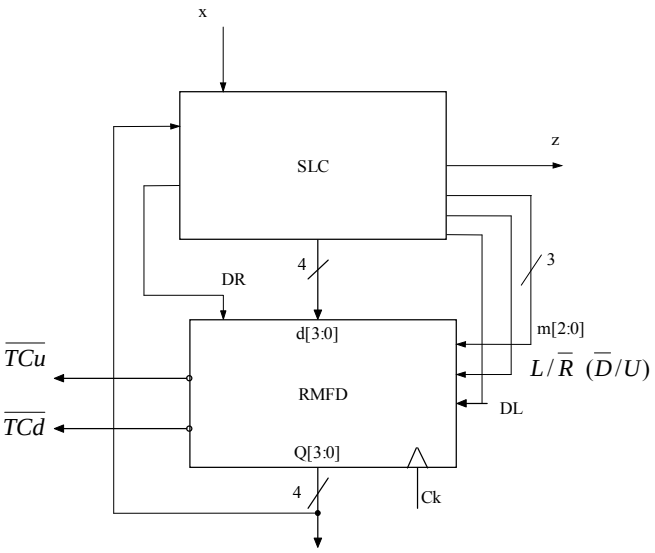


Figure 6 - Architecture of automata implemented with RMFC

The codifying function is defined in Table 3.

. □

| $m_2m_1m_0$ | Mode | $L/\overline{R}(U/\overline{D})$ |
|---|---|---|
| 000 | HOLD | - |
| 001 | Reset | - |
| 010 | Paralle l Load | - |
| 011 | Count Up | 1 |
| 011 | Count Down | 0 |

Table 3 – Mode Coding

The proposed system use only one RMFC and SLC which generates the output *z* signals, m[2:0], $L/\overline{R}(U/\overline{D})$.

The RMFC implementation became the one illustrated in Table 4.

| | | | $Q[2:0]_{n+1}$ | | |
|---|---|---|---|---|---|
| $m_1m_0$ | Z | | | | |
| X / $Q_2Q_1Q_0$ | 0 | 1 | 0 | 1 | - |
| 000 | 001 | 101 | 011 | 010 | 0 |
| 001 | 010 | 010 | 011 | 010 | 0 |
| 011 | 001 | 100 | 010 | 011 | 1 |
| 010 | 001 | 011 | 010 | 011 | 1 |
| 110 | 010 | 100 | 010 | 010 | 0 |
| 111 | 000 | 000 | 001 | 001 | 0 |
| 101 | 001 | 100 | 010 | 010 | 0 |
| 100 | 100 | 100 | 000 | 000 | 0 |

$L/\overline{R}(U/\overline{D})$ $d_2$ $d_1$ $d_0$

| $X$ / $Q_2Q_1Q_0$ | 0 | 1 | 0 | 1 | 0 | 1 | 0 | 1 |
|---|---|---|---|---|---|---|---|---|
| 000 | 1 | - | - | 1 | - | 0 | - | 1 |
| 001 | 1 | - | - | 1 | - | 1 | - | 0 |
| 011 | - | 1 | 0 | - | 0 | - | 1 | - |
| 010 | 0 | 1 | - | - | - | - | - | - |
| 110 | - | - | 0 | 1 | 1 | 0 | 0 | 0 |
| 111 | - | - | - | - | - | - | - | - |
| 101 | - | 0 | 0 | - | 0 | - | 1 | - |
| 100 | - | - | - | - | - | - | - | - |

Table 4 – State transition matrix

Using one of the synthesis methods (Veitch-Karnaugh, Quine-McCluskey), we obtain the following equations:

$$m_1 = \overline{Q_2} + Q_1 \oplus Q_0$$

$$m_0 = \overline{Q_2} \cdot (x \oplus \overline{Q_1}) + x \cdot Q_2 Q_0 + Q_1 \cdot (Q_2 \oplus \overline{Q_0})$$

$$z = \overline{Q_2} Q_1$$

$$U/\overline{D} = x \oplus \overline{Q_1}$$

$$d_2 = x \cdot \overline{Q_0}$$

$$d_1 = x \oplus \overline{Q_0}$$

$$d_0 = \bar{x} Q_0 + x \overline{Q_1} \cdot \overline{Q_0}$$

If the above equations are implemented with the same elementary circuits, results costs C=18.

## 3. CONCLUSIONS & ACKNOWLEDGMENT

In this paper, the authors made a comparison between the 2 types of RMF: RMFD – Multifunctional Registers with validation signals of decoded commands and RMFC – Multifunctional Registers with coded mode signals.

The authors, already presented RMFD in [1] and the conclusion is that the maximum frequencies depends on the priority allocation order for the mode signals. In general, from our simulations, we can affirm that maximum allowed frequency is 5MHz.

From the comparison of 2 multifunctional register types, RMFD and RMFC results: RMFC allows a maximum frequency (lower than RMFD) but a cost greater than RMFD (See Tables 4 and 5, for the 2 modes of priorities assignments).

In section 3, the authors synthesized a Moore automata and proposed an original contribution to the states coding, taking into account that the most used RMF functions must be used most often (INC/DEC most often and Parallel Load as little).

The logical structure (SL) will contain less elementary circuits for the RMFC implementation as compared with RMFD, so there is cost compensation (RMFC more expensive than RMFD).

To design automation with separate inputs, which can be activated simultaneously, it is necessary to use RMFD.

| Synthesis method | Implementation Costs (number of logic gates) | Clock frequency |
|---|---|---|
| RMFC | 18 | 5 Mhz |
| RMFD | 23 | 4.35Mhz |

## REFERENCES

[1] Al. Valachi, M. Timis, B. Aignatoaie, S. Tarcau, "Orders Priorities Settings Criteria for Multifunctional Registers," Electronics and Electrical Engineering ISSN 1392 – 1215, T 120, System Engineering, Computer Technology, The 14th International Conference ELECTRONICS'2010 Kaunas and Vilnius University – Lituania,

http://www.ee.ktu.lt/page.php?227 - T120, page.87.

[2] Drane, Theo, Cheung, Wai-chuen, Constantinides, G. "Correctly rounded constant integer division via multiply-add", in Circuits and Systems (ISCAS), 2012 IEEE International Symposium on Circuits and Systems, Seul - Korea, May 2012, pages 1243 – 1246.

[3] C. H. Roth, Fundamentals of Logic Design, West Publishing Company, 1999.

[4] Al. Valachi, R.Silion, M. Timis, “Improvement of FSM Synthesis using MSI and LSI Circuits,” Advances in Electrical and Computer Engineering. Academy of Technical Sciences of Romania, “Stefan cel Mare” University of Suceava, vol 5(12), no.1/23, 2005.

[5] Shepherd, B.J., "Right Shift for Low-Cost Multiply and Divide", in IEEE Transactions on Computer Arithmetic (Volume:C-20 , Issue: 12 ), august 2006, pages 1586 – 1589.

[6] Oberman, S.F., Flynn, M., "Division algorithms and implementations", in IEEE Transactions on Computer Arithmetic (Volume:46, Issue: 8 ) Comput. Syst. Lab., Stanford Univ., CA, USA, august 2002, pages 833 – 854.

[7] Lin Yuan, Gang Qu, Villa, T., Sangiovanni-Vincentelli,A., "An FSM Reengineering Approach to Sequential Circuit Synthesis by State Splitting", in IEEE Transactions on Computer-Aided Design of Integrated Circuits and Systems(Volume:27,Issue: 6 ), may 2008, pages 1159 – 1164.

[8] M.Timis, A.Valachi, P.Cascaval, R.Silion, “A Comparison between Coded-Decoded Mode Signals on Multifunctional Registers“, 12th International Conference on Development and Application Systems, Suceava, Romania, 2014.

"HENRI COANDA"
AIR FORCE ACADEMY
ROMANIA

"GENERAL M.R. STEFANIK"
ARMED FORCES ACADEMY
SLOVAK REPUBLIC

INTERNATIONAL CONFERENCE of SCIENTIFIC PAPER
AFASES 2015
Brasov, 28-30 May 2015

# VALIDATION OF SPECTRAL ANALYSIS RESULTS USING PLC IMPLEMENTED AI TECHNIQUES

**Grigore Vasiliu***

*Faculty of Automatic Control, Computers, Electrical Engineering and Electronics, "Dunărea de Jos" University, Galati, Romania

***Abstract:*** *The purpose of this paper is the processing of a trace image of steel, which results from a spectral measurement system, using a programmable logic controller (PLC). The spectral analysis of the steel is made by investigating the trace image, generated by an electric arc, in a PLC. The PLC makes simple images to be processed, so it can recognize some traces undetectable by the measurement results. The validation or the invalidation of the final result is provided by the data analysis obtained from the processing, with artificial intelligence techniques, (like fuzzy techniques) of the arc trace image. The image processing with PLC is slow, but possible because the processing time isn't critical, as in real-time application. Using this method, huge amounts of energy can be saved (in order to avoid an unnecessary batch of the steel processing).*

***Keywords:*** *spectral measurement system, programmable logic controller, image processing,*

## 1. INTRODUCTION

Spectral system of steel analysis must be very sure when it is offered the measurement result. The PLC are the most accurate control numerical systems. The autonomous measurement systems have to proceed successfully a lot of operations usually executed by a human operator. One of these operations is to validate the analysis results of a spectrometer arc, if the trace image aspect results after the electric arc between a wolfram electrode and a measurement probe. The electric arc represents the information source for the composition of the measurement probe. The continuous frequency of the source spectrum, represented by the arc contains the specific information: figure no. 1 [14].

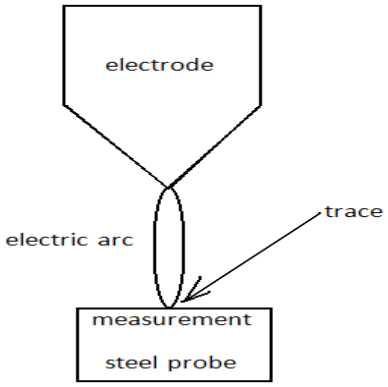


Fig. 1. Trace image after spectral analysis

The validation of spectral analysis results using artificial intelligence techniques implemented with PLC, it is possible due to the following aspects:

1. The objective of this research was not a complex image processing analysis (medium

resolution images). The final result was to obtain a validation decision, or an invalidation decision.
2. The continuous expansion of the numerical systems of the PLC family, through:
- the expansion of the instruction set
- the possibility to generate complex program structures through the defining of some functional blocks.
- the expansion of the hardware variables number which can be implemented in this system
- complex interfaces which can process the dates from the process (the acquisition of a medium resolution images, for processing, using the available resources of the system)[8].

## 2. THE INDUSTRIAL BENEFITS OF THE TRACE IMAGE PROCESSING

**2.1 The recognition of the small black dots.** The text one of the advantages of visual analyze of the trace image[5], is the recognition of the small black dots from the trace image, (figure no. 2) which indicates the presence of the carbon disulphide in the metallic structure, which does not affects the material procentual composition, but after the lamination, the material properties are compromised.

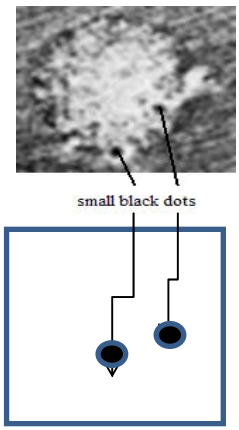


Fig. 2. Recognition of small black dots
2.a. Initial arc image trace
2.b. The points recognition

In figure no. 2, in the second image, the only thing that remains are the black dots; the rest of the dots will be replaced by the white dots [9]. Due to this way of action, it will result the cracking of the steel sheet, followed by the whole lot cassation. Because of this simple recognition of the black dots in the metal sample, which is the composition of 200 tons of steel, the unnecessary lamination of the whole lot is prevented.

**2.2 The black dots detection method (representing the carbon disulphide, figure no. 3):**

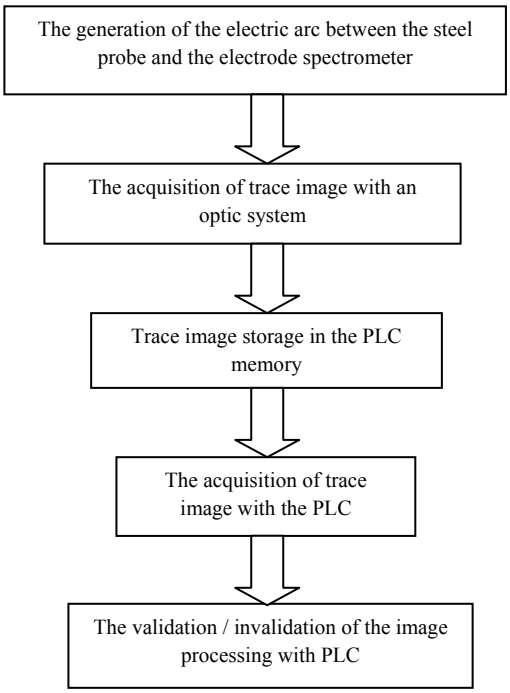


Fig. 3. The black dots detection method

This information can be obtained only through the trace image analysis[1,2]. It will not result from the spectral analysis.

For the recognition of the carbon disulphide dots (black dots of small size), a specific technique, similar to the well-known selective technique, was implemented. How does this technique works? It was calculated the sum of all the pixels intensity from the image, following the dots counting with maximum intensity (dots with much higher intensity than the average sum). If the resulted number is relatively small and the dots are situated next to each other, then the presence of a carbon disulphide dot is validated. Similar, the second major point of this paper was analyzed: images with good contrast and images with poor contrast. The images with poor contrast appear only if in the area there are some cracks in the sample probe, visually unnoticed, due to the grinding process of the surface. Before the attained electric arc between the electrode and the probe, the

surface of the probe, where the trace image will appear, must be well polished. Through this process of grinding, the possible cracks which may result from the probe solidification are covered. But, when the process of the attaining electric arc is over, these cracks compromise the measurement results.

**2.3 The recognition of nonviable images using the brightness and the contrast.** Examples of viable images and nonviable images [15]:

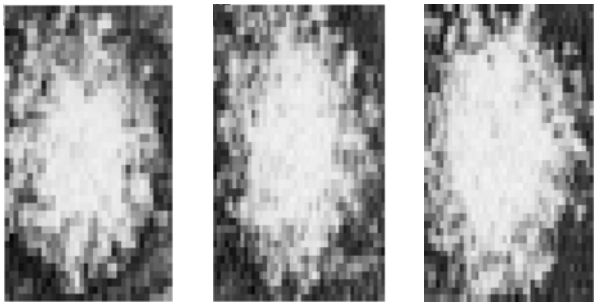

Fig. 4. Viable arc trace images

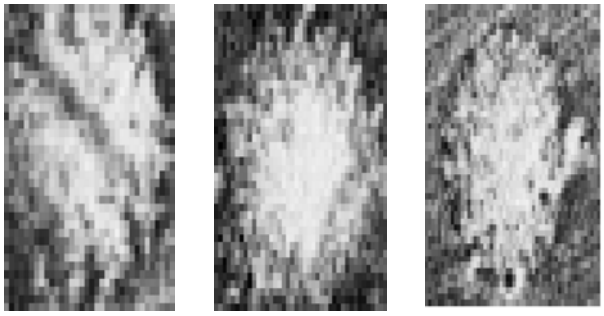

Fig. 5. Nonviable arc trace images

## 3. MATHEMATICAL ASPECTS

**3.1 Introduction.** The image processing is made using the selective main method, where the images are loaded dot by dot in the PLC. The first phase, is to calculate the average sum for all the pixels of light intensity. The second phase is to reload the image, and after that to count of the pixels which are that are above a certain value. If the counting is within a certain value range, it means that we have a carbon disulphide point.

**3.2 Harris detector.** Harris detector is used due to its specific pixels recognition ability. A particular property is the detection of pixels which low variations of light intensity. The detection process is made by the analyzing of the local auto-correction function properties for a general position [4]. The auto-correction function c is defined by :

$$c(x,y,\Delta x,\Delta y) = \sum_{(u,v)\in W(x,y)} w(u,v)[I(u+\Delta x, v+\Delta y) - I(u,v)]^2 \quad (1)$$

Where w(u,v), is the Gaussian nucleus

$$e^{-\frac{(u-x)^2-(v-y)^2}{2\sigma^2}} \quad (2)$$

and W(x,y) is a media of the points which are situated next to each other [3]. According the Taylor series, from the very first term up to the last one:

$$I(u+\Delta x, v+\Delta y) \quad (3)$$

$$A(x,y) = \begin{bmatrix} \sum_W w(u,v) I_x(x,y)^2 & \sum_W w(u,v) I_x(x,y) I_y(x,y) \\ \sum_W w(u,v) I_x(x,y) I_y(x,y) & \sum_W w(u,v) I_x(x,y)^2 \end{bmatrix} \quad (4)$$

$$R(A) = det(A) - k[Tr(A)]^2 \quad (5)$$

The Harris detection method has been implemented using programmable logic controller for the recognition of the dots which contains carbon disulphide.

**3.3 Fuzzy aspects in image traces of carbon disulphide.** A simple fuzzy selector can solve the problem of the arc trace recognition by processing a set of logic statements [11]. First, it is compared the dot from the initial loaded image with an average dot sum, obtained after the whole image was

loaded. If it is smaller, it is replaced by the white color [7]. If it is bigger, it is replaced by the black color, and it is counted (one black dot was found). Also, if the nearest dot is black too, the counter increases [12]. In the image with black and white dots, it will be considered as impurities of the carbon disulphide, only the areas where the number of black dots is within a certain value range. This range is offered by the human operator experience.

## 4. EXPERIMENTAL RESULTS

The experimental results were taken using trace images, from some probes of ArcelorMittal Steel, Galati. The image processing was realized using the PLC DirectLogic 205. For receiving the trace images, a video camera was used, in order to transform the image in a pixels matrix with a grey tone, from white to black (for 8 bits per pixel – 256 tones). It had been used 8 numerical inputs and one numerical output, for the next character request. A more efficient technique, included into the DL205 system, is the transfer of these images through the Ethernet ports, implemented on a UC of the DL260 system (it also contains instructions for the neuro-fuzzy implementations techniques) and also through an Ethernet port embedded in the specialized module H2-ECOM.There are video cameras which can be connected directly on the internet, frequently used for surveillance systems. The image acquisition and processing doesn't have to be achieved in a very short time, because the resulted data is not used for a real time application. The most important aspect is that the final decision must be correctly, due to the data processing. Also, the necessary time for the neuro-fuzzy algorithms in order to provide results, isn't critical, as the neuro-fuzzy algorithm implementation can be made by using an adjustable number of iterations which can ensure the validation of the final result, according to the desired level of safety. Though the carbon and sulphur concentrations are correctly in the P1 , P2, ... , P9 spectral analyses cases (see table no. 1) the recognition of the small black dots, using Harris detector method, implemented using programmable logic controller, has been validated by the appearance of some fissures in the steel during the lamination process (figure no. 6).

| Sample | C | Si | P | S |
|---|---|---|---|---|
| P1 | 0.025 | 0.004 | 0.005 | 0.015 |
| P2 | 0.037 | 0.043 | 0.012 | 0.027 |
| P3 | 0.049 | 0.150 | 0.024 | 0.035 |
| P4 | 0.102 | 0.180 | 0.033 | 0.231 |
| P5 | 0.195 | 0.190 | 0.051 | 0.412 |
| P6 | 0.243 | 0.250 | 0.054 | 0.324 |
| P7 | 0.416 | 0.310 | 0.061 | 0.457 |
| P8 | 0.523 | 0.510 | 0.075 | 0.763 |
| P9 | 0.862 | 1.912 | 0.093 | 0.934 |

Table no. 1 The results of the spectral analyses of the P1, P2,... P9 samples.

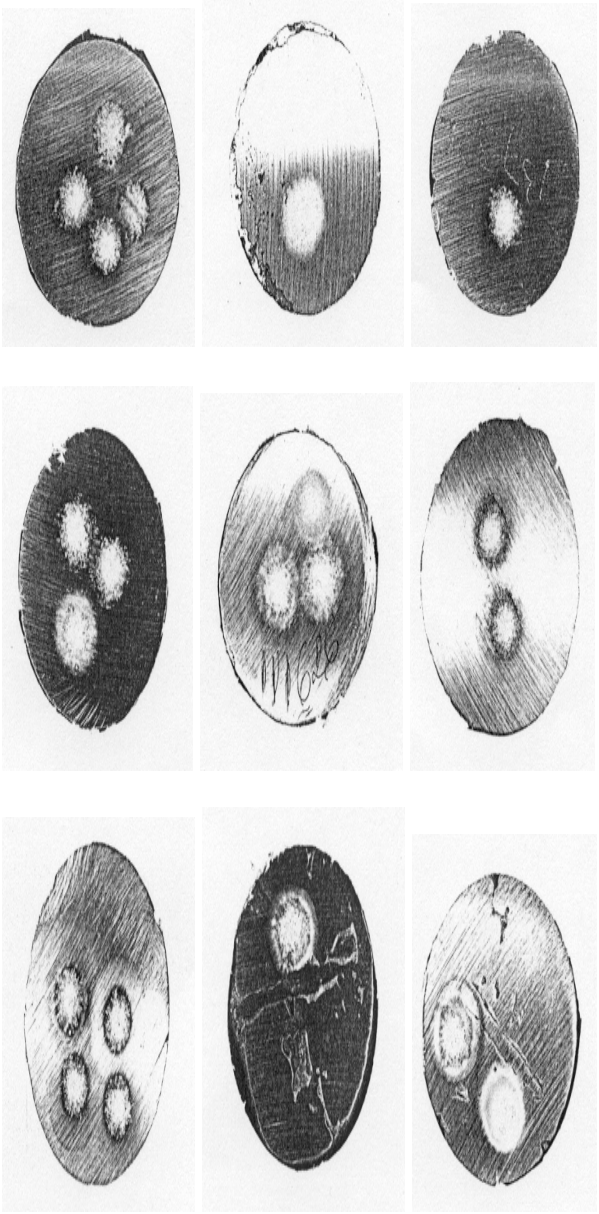

Figure no. 6 The images of the P1, P2, ... P9 samples.

## 5. CONCLUSIONS

The proposed objectives can be achieved, for a certain degree of image resolution, which is taken from the optic systems of the PLC memory, by using the adequate interfaces [6]. Using this method, the PLC can successfully replace the human operator, and, with correct learning algorithms, the PLC can reach, in time, more superior outcomes. The human operator job which works in a spectral laboratory, can be replaced by a PLC network, as an autonomous spectrum analyzer.[10] This system, can ensure a high precision of the final result, by executing, at the highest standard, the calibration and the testing operations. Neuro-fuzzy techniques can be implemented through modern PLC networks, with are comparable microcontroller networks. Nowadays, the speed transfer between PLC networks had increased extraordinary [13].

## REFERENCES

1. Ayache,N. Lustman,F.,*"Fast and Reliable Passive Trinocular Stereovision"*. ICCV (1987).

2. Beaudet, P., R., *"Rotationally Invariant Image Operators"*, IJCPR, (1987).

3. Burlacu, A., Lazăr C., *"Visual feature tracking using Kalman filter"*, ICCSCS, Bucharest. (2009).

4. Burlacu, A Ph.D. Thesis : *"Imagine processing algorithms for object movement applications"*. (2009).

5. Canny,J.F.*"Finding Edges and Lines in Images"*. MIT(1983).

6. Charnley, D., Blissett, R. J., *"Surface Reconstruction from Outdoor Image Sequences"*. AVC88 (1988).

7. Filipescu, Adrian, I. Susnea, I. et al. *"Control of mobile platforms as robotic assistants for elderly." ASCC 7th*. IEEE,. (2009).

8. Harris, C. G. Pike, J. M,*"Positional Integration from Image Sequences"* AVC87, (1988).

9. Kitchen, L., Rosenfeld, A., *"Grey-level Corner Detection"*. PRL (1982).

10. Sargur, S.,*"High-Performance Reading Machines"*. Pr.IEEEvol80 (1992).

11. Susnea, I., Vasiliu, G., Filipescu, A.,*"Real-Time, Embedded Fuzzy Control of the Pioneer 3-DX Robot for Path Following"*. WSEAS. (2008).

12. Susnea, I., Vasiliu, G., et al.*"Virtual pheromones for real-time control of autonomous mobile robots"*. S.I.C., Bucarest,. (2009).

13. Susnea, I. *"Distributed Neural Networks Microcontroller Implementation and Applications"*, S.I.C., Bucarest, (2012)

14. Vasiliu, G. *Ph.D. Thesis :* "Research on increasing the precision of multichannel measurement systems, with aplications in electrical and electronics engineering". (2005).

15. Vasiliu, G., Susnea, I. "*Computerised systems of measurement*". Matrix Rom, Bucarest, (2009).

"HENRI COANDA"
AIR FORCE ACADEMY
ROMANIA

"GENERAL M.R. STEFANIK"
ARMED FORCES ACADEMY
SLOVAK REPUBLIC

INTERNATIONAL CONFERENCE of SCIENTIFIC PAPER
AFASES 2015
Brasov, 28-30 May 2015

# ANALYSIS OF THE LIGHT OFF-ROAD VEHICLE ENDOWMENT POSSIBILITIES IN ORDER TO USE IT FOR AIR FORCE MISSIONS

**Cornel Aramă *, Mariana Sava, Lavinia Cucu**

* Faculty of Aeronautics Management, "Henri Coandă" Air Force Academy Brasov, Romania

***Abstract:*** *The possibility to use a fast, maneuverable and high passing capacity mobile platform, characterized by a large modularity, in order to be endowed with different special equipments has been analyzed by several researchers, who have focused their studies on the performances of each model.*
*The following paper presents a study on two possibilities of endowing a light off-road articulated prototype vehicle, DAC 2.65 FAEG, in order to fulfill some specific missions for Air Force: an UAV mobile cell for forward reconnaissance missions and a combat mobile cell against low altitude targets.*
*In order to establish the best solution to endow this suggested mobile platform, the researchers are going to use the advanced multi-criteria analysis method. The final result will be interesting due to the fact that the suggested vehicle prototype has a high modularity towards being endowed with different special equipments.*

***Keywords:*** *mobile platform, unmanned air vehicle (UAV), combat mobile cell, advanced multi-criteria analysis*

## 1. INTRODUCTION

The global current security situation is an environment which is characterized by asymmetric conflicts where one of the engaged parties has been specializing in classic or urban guerrilla war and the military-developed countries have been improving their antiterrorist fighting continuously.

This is the reason why the weapons industry is focusing more and more on the combat mobile cells production which has to display a more increased viability in antiterrorist or guerrilla fights. From our point of view a combat/fighting mobile cell, seen as an acting system, must comprise the following main parts (Figure 1.1):

- the terrestrial subsystem consisting of crew, intelligent equipment (gadgets such as: computer, sensors, communication and reception data gadgets etc.), maintenance equipment, military assets and the mobile platform;
- the air subsystem consisting of UAV, the intelligent equipment for acquisition, communication and control data, and possibly, depending on the constructive variant, special equipment for self-destruction;
- the interface between air and terrestrial subsystems.

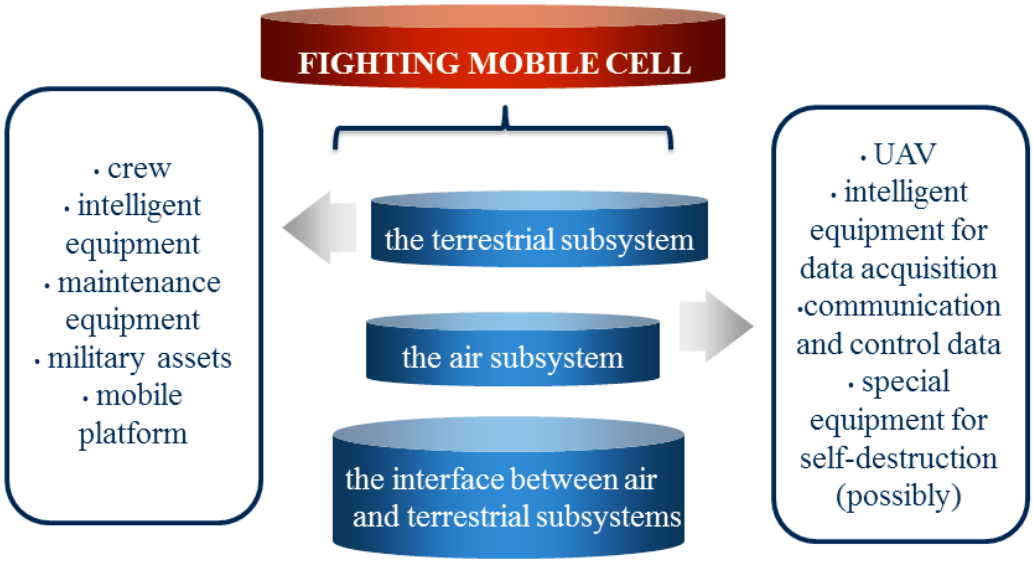


Fig. 1.1 The general structure of a combat/fighting mobile cell

Due to the possibility of working directly on the prototype vehicle, this paper presents a study on two possibilities of endowing a light off-road articulated prototype vehicle, DAC 2.65 FAEG, in order to fulfil some specific missions for Air Force: an UAV Forward Reconnaissance Mobile Cell - FRMC (Figure 1.2) and a Combat Mobile Cell Against Low Altitude Targets - CMCALAT (Figure 1.3).

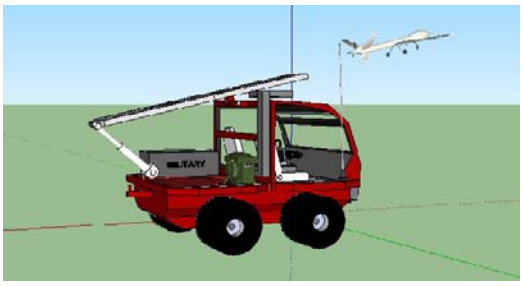

Fig. 1.2 An UAV Forward Reconnaissance Mobile Cell (concept)

Fig. 1.3 A Combat Mobile Cell Against Low Altitude Targets (concept)

## 2. A SHORT PRESENTATION OF THE MOBILE PLATFORM

A light off-road articulated vehicle is a vehicle with a maximum weight of less than three tones and consisting of two equal vats connected to each other through a central pivoting bearing which allows moving both parts around the vehicle longitudinal central axis (Figure 2.1). [1]

Fig. 2.1 The light off-road articulated vehicle DAC 2.65 FAEG

The main technical characteristics of the light off-road articulated vehicle DAC 2.65 FAEG are [1]:

- 4 Wheel Drive off-road utility vehicle consisting of two vats connected with a "Center Rotational Articulation"; the first vat has the power unit (the most part) and the driving control point and the second vat is empty and it could be used for special equipment; remarkable crossing capacity due to 4x4 system and to the central pivoting

bearing which allow the vehicle to follow the ground conformation permanently by keeping all the wheels in contact with land; moreover, the vehicle has enormous approach and rear overhang angles which allow it to attack very high obstacles;
- no suspension but center articulation - 45 degrees of travel;
- it could be equipped as an amphibious vehicle (optional) because it is calculated to move on the water by using the wheels alone or combined with a propeller or a system of propellers which are trained by a power take-off from the rear axle differential;
- 4 Wheel Power Steering; very good maneuverability (swiveling radius less 10 m) due to the possibility of steering by using all the wheels;
- very good stability due to very low center of gravity;
- simple and robust construction;
- the theoretical impossibility to be stuck in mud due to very wide wheels which determine a very high upward force, the wheels which are operated directly from a covered body and due to the simple conformation of the "belly" of the vehicles which allow it to crawl without any problems on the muddy ground.

This type of vehicle is very rare. Generally, it has stayed at a prototype stage. Unfortunately, this was the main reason why, while being exploited, some technical problems which must be solved were identified:
- little ground clearance which could create problems when the obstacles are attacked between the front wheels; the obstacles have to be attacked only by one wheel at a time;
- finding an engine capable to move the vehicle because this one must have a small volume, high power and it has to be easily maintained at the nominal temperature; it is working into a tough, not ventilated environment (into the first vat);
- the necessity of an automatic transmission which is going to work into a tough, not ventilated environment as well;
- the lack of suspension which could create comfort difficulties for the occupants of the vehicles;
- the lack of a covered body (because of the necessity to decrease the total weight) which can cause discomfort to the passengers.

## 3. THE OPERATIONAL MILITARY REQUIREMENTS FOR SUGGESTED ENDOWMENTS VARIANTS

This kind of vehicle has large possibilities to be endowed in order to fulfil a lot of missions from the civilian and military fields. This is due to the fact that the rear vat is almost empty and it can be endowed in different structures without difficulties. The low center of gravity offers the possibility to attach vertical equipment without affecting too much its stability.

The generally operational military requirements which influence the two types of mission which could be conducted by the endowed variants from this study are (the ones which are not relevant to the study have been removed because they are identical for both missions):
- constructive simplicity;
- high reliability;
- compactness;
- tactical-operational mobility – marching;
- low overall dimensions;
- low weight;
- easy exploitation to fulfil the missions;
- high maintainability;
- high ergonomics for the crew;
- protection of transported materials;

- crew protection;
- transportability;
- efficiency of combat actions – the results that can be obtained;
- profitability – the fast and restoration costs of fighting capacity.

In order to fulfil an advanced multi-criteria analysis method the researchers will select from this list the most important military operational requirements. The aim of the study is to establish the most viable structure for this kind of vehicle in order to use it in the military field.

## 4. ESTABLISHING THE BEST STRUCTURE FOR THE SUGGESTED VEHICLE BY USING THE ADVANCED MULTI-CRITERIA METHOD

The advanced multi-criteria analysis method is a general method of comparing some item categories. This method is going to be used in order to obtain some useful conclusions for the endowment of the mobile platform which has been suggested to be part of the mobile combat cell which is going to be used in air force missions.

It is known that it is better to combine the multi-criteria analysis method with the "brainstorming" method especially when launching new items on the market. The steps of the creative process which are developed into this method are the market necessities study, the identification of the project theme, the launching of different new variants for the implementation of the project and the evaluation of the solutions suggested by the multi-criteria analysis method.

In this situation, the market necessities involve the endowing of the mobile platform (the light articulated off-road vehicle DAC 2.65 FAEG) with a most viable structure in order to fulfil air force missions. Thus, the project theme and the new endowment variants for the project have been identified. The suggested variants are:

- UAV Forward Reconnaissance Mobile Cell and
- Combat Mobile Cell against Low Altitude Targets.

**4.1 The Criteria Establishment.** The chosen criteria necessary in order to achieve this analysis require a precise definition because they have to allow the limiting of some characteristics that are imposed as an analyzing object in order to result in a characterization without any ambiguities [5]. In this research seven operational requirements were selected as criteria for the advanced multi-criteria analyzing method. Thus, the selected criteria are:

- constructive simplicity;
- compactness;
- easy exploitation to fulfil the missions;
- high maintainability;
- high ergonomics for the crew;
- efficiency of combat actions;
- profitability.

**4.2 Determining the weight of each criterion.** The weight factors need to be calculated in order to determine the weight of each criterion. The criteria taken into consideration are written down into a table both on the rows and columns using the following abbreviation:

- constructive simplicity – CS;
- compactness – CO;
- easy exploitation to fulfil the missions – EE;
- high maintainability – HM;
- high ergonomics for the crew – HE;
- efficiency of combat actions – EC;
- profitability – PR.

Within this table, the criteria are compared to one another by using the notations: value 1 when the row criterion is more important than column criterion, value 0,5 when both of them are equally important and value 0 when the column criterion is more important than the row criterion.

The classification of the criteria is made by the amount of the row points for each criterion. If two or more criteria have the same number of points, the position into the classification will be the value of their semi-sum (in case there are more criteria, the arithmetic average). The criterion with the most number of points will be on the first place, and the criterion with the least number of points will occupy the last place.

Table 4.1

| Criteria | CS | CO | EE | HM | HE | EC | PR | Points of the criterion | Level (classification) | Weight factor [$\gamma_i$] |
|---|---|---|---|---|---|---|---|---|---|---|
| **CS** | 0,5 | 1 | 0 | 0 | 0 | 0 | 0 | **1,5** | **6** | **0,47** |
| **CO** | 0 | 0,5 | 0 | 0 | 0 | 0 | 0 | **0,5** | **7** | **0,10** |
| **EE** | 1 | 1 | 0,5 | 0,5 | 1 | 0 | 0,5 | **4,5** | **3** | **2,36** |
| **HM** | 1 | 1 | 0 | 0,5 | 0 | 0 | 0 | **2,5** | **5** | **0,93** |
| **HE** | 1 | 1 | 0 | 1 | 0,5 | 0 | 0 | **3,5** | **4** | **1,53** |
| **EC** | 1 | 1 | 1 | 1 | 1 | 0,5 | 1 | **6,5** | **1** | **5,42** |
| **PR** | 1 | 1 | 1 | 1 | 1 | 0 | 0,5 | **5,5** | **2** | **3,55** |

The weight factors can be calculated by using different formulas. The FRISCO formula was used in order to find out the coefficients because it is globally recognized as the most performant and it is very practical.

$$\gamma_i = \frac{p + m + \Delta p + 0,5}{-\Delta p' + \frac{N_{crt}}{2}}$$

where:

p – the amount of the row points for the element taken into account;

m – the number of the criteria which were surpassed by the criteria taken into account;

Δp – the difference between the score of the item taken into account and the score of the item from the last level; if the item taken into account is placed on the last place, Δp will have the value 0;

Δp' – the difference between the score of the item taken into account and the score of the item from the first level; if the item taken into account is on the first place, Δp' will have the value 0; $N_{crt}$ – the number of the criteria taken into account. Thus, the result is the table 4.1.

**4.3 The identification of the variants, granting the N grade and the establishing of the consequences matrix.** This comparative analysis aims at comparing and establishing the best structure of the light off-road articulated prototype vehicle, DAC2.65 FAEG type, in order to be used mainly for the air force mission. The suggested and analyzed solutions are the Forward Reconnaissance Mobile Cell (FRMC) and the Combat Mobile Cell against Low Altitude Targets (CMCALAT).

Table 4.2

| Combat variant | | FRMC | | CMCALAT | |
|---|---|---|---|---|---|
| **Criterion** | **Weight factor** [$\gamma_{ij}$] | **Importance grade** [$N_i$] | $N_i x \gamma_i$ | **Importance grade** [$N_i$] | $N_i x \gamma_i$ |
| **EC** | 5,42 | 9 | 48,78 | 8 | 43,36 |
| **PR** | 3,55 | 9 | 31,95 | 8 | 28,4 |
| **EE** | 2,36 | 8 | 18,88 | 10 | 23,6 |
| **HE** | 1,53 | 8 | 12,24 | 10 | 15,3 |
| **HM** | 0,93 | 8 | 7,44 | 9 | 8,37 |
| **CS** | 0,47 | 7 | 3,29 | 8 | 3,76 |
| **CO** | 0,10 | 7 | 0,7 | 9 | 0,9 |
| **The final classification** | | | **123,28** | | **123,69** |
| **The place** | | | **2** | | **1** |

The grade which was granted to each criterion is a number from 1 to 10. At the same time, it is also called importance grade or contribution to a criterion grade and it granted to each variant based on the technical and tactical characteristics, according to each criterion. The grades $N_i$ which were granted to each variant are shown in table 4.2.

The importance grades are invariably influenced by the weight factors. To this end, the wedge between the importance grades and the weight factors must be calculated for each criterion. The sum of the $N_i \ x \ \gamma_i$ wedges will logically establish the final classification. These calculations are shown into table 4.2, too.

**4.4 The results interpretation.** As it could be seen in table 4.2, the CMCALAT variant is the best structure for the DAC 2.65 FAEG vehicle according to this analysis. What is interesting is that the difference between the suggested variants is extremely small. This fact can suggest that it is better to redo the calculations and reopen the discussions in order to eliminate as much as possible the subjectivity of the expert appreciations.

For instance, at first glance, one could notice that two criteria which may have major influences on the last decision were omitted: the cost and the easiness of purchasing the special equipment.

As presented in the table 4.1 the criterion efficiency of combat actions – EC resulted as the most important from the weight factors point of view. It is logical. But maybe it is better to make the difference between the missions which can be executed by the FRMC, tactically thinking, combat service missions and the missions which can be executed by the CMCALAT, which are combat missions. If the UAV used by the FRMC is a flying bombe type, the FRMC can fulfil combat missions too.

And this is how this analysis can become more complex and it can be the subject of some next research.

## REFERENCES


1. Aramă, Cornel, Aramă A., *"Investigations of the Possibilities to Improve the Dynamic Performances of DAC 2.65 FAEG Light Off-road Articulated Vehicle",* The 15th International Conference of Scientific Papers*"Scientific Research and Education in the Air Force"* AFASES 2013*, "Henri Coandă"* Air Force Academy, Braşov*,* Section: *"Engineering Sciences-Mechanical Engineering Materials and Technology"* May 2013.
2. Aramă, Cornel, Aramă, A., *"A Study Regarding the Analysis of the Fulfillment of the Operational Military Requirements by the Light Off-Road Articulated Vehicle","Review of the Air Force Academy"*, The Scientific Informative Review, No 1(23)/2013, "Henri Coandă" Air Force Academy Printed House, B+, May 2013.
3. Aramă, Cornel, "*Investigation of Possibilities to Improve the Performances of Special Vehicles*", "*Transylvania*" University Braşov, Doctoral Degree thesis, 2006.
4. Bobancu □., *"Creativitate □i inventică",* - course, *"Transylvania"* University of Bra□ov, 2014.
5. Sava, Mariana, "*Analiza viabilităţii radarelor moderne mobile*", Bachelors Degree thesis, "*Henri Coandă*" Air Force Academy, Braşov, July 2014.

"HENRI COANDA"
AIR FORCE ACADEMY
ROMANIA

"GENERAL M.R. STEFANIK"
ARMED FORCES ACADEMY
SLOVAK REPUBLIC

INTERNATIONAL CONFERENCE of SCIENTIFIC PAPER
AFASES 2015
Brasov, 28-30 May 2015

# THE NEW VISION IN DESIGNING OF AIRPORT

**Sławomir Augustyn*, Bogumił Znojek****

*National Defense University, Warsaw, Poland, **Aviation & Air Defense Institute, Poland

***Abstract:*** *The article shows a new approach to the vision in design of aviation. This approach allows for analysis and assessment in the forecasting of the aviation project. Moreover, this aspect influences on safety and security of aircraft. Due to the extensive theme, the subject of research was limited to select all technical sciences are as associated with medicine in the project process of the aircraft.*

***Key words****: aviation design, safety and security system, project process.*

## 1. INTRODUCTION

Different institutions in the aviation business, e.g. research facilities, aircraft constructers, politicians and experts published different treatises about the future in aviation. One of these is the „Vision 2050" of the IATA, which deals with the concept of an airport without a control tower operator.

In this vision the function of the control tower operator is just to be the supervisor. Ground-based computers send all the necessary information to the aircrafts. With this technology, which uses digital data link, all the planes can stagger themselves automatically. The work of the human being would just be to monitor the current operations and in case of problems he would intervene and rectify the issue.

The reason of thinking about this is the expectation of a continuous rising air transport market. The IATA assumes a increasing of the number of passengers worldwide from 2.8 billion in 2011 to 16 billion in 2050. Therefore it's necessary to have a more efficient infrastructure and more sustained technologies. A higher utilization of the airborne and airports will be required, which on the other hand will be a bigger challenge for the ATC [3].

Reasons for loss of capacity like a bad outside view of the control tower operator will not be tolerated anymore because the revenue losses of all involved persons at the airport would be huge. On the other side the unpredictable workload of the air traffic controller because of the increased complexity is the reason for the research on a possible automation of the controllers work. With availability of fully developed technology and the related procedures, which could exceed the certainly existing performance barriers of a human being, the aviation of tomorrow can be operated safer, more secure, more efficient and cheaper to satisfy the increasing mobility needs of the people.

To understand which work areas of the control tower operators could be automated, we have to know what the challenges the controllers face today are. The function of the controllers is to prevent the collision of aircrafts with other users of the traffic events.

This can be other planes or ground vehicles. Furthermore they are responsible to guarantee a regular traffic flow. Last but not least they have to provide information and give instructions to everyone at the airport [1].

An integration of the apron control in the whole system is appropriate and will be arranged. A handover of the aircraft between the individual instances of the airport close-up range will be not omitted because of the standardization of the total system and won't be considered in below.

The following explanations describe some of the automation of control tower operator's tasks after the landing of an aircraft all the way from the parking position to the start position before the takeoff.

**1.1. Infrastructure of airport.** The central control device of all the processes is a central processing unit (see figure 1), which is located at the airport. Essentially it matches a strong-networked server room. It determines the planned and actual movement data of every participant and provides it on request. Thereby it takes one of the essential tasks of the control tower operator [2]. The location of the central processing unit on the airport depends of its size and labor-extensive, which are related to its converted traffic volume.

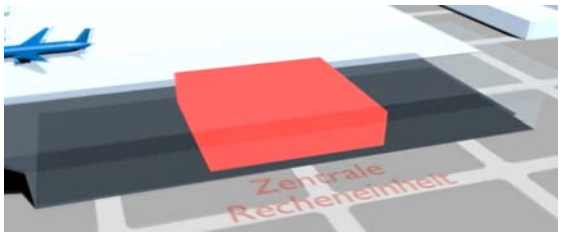


**Fig. 1:** Zentrale Recheneinheit (centralprocessingunit)
Source: Extractofthepräsentationvideo (Stefan Reitmann)

The communication between the central processing unit with all the personnel on the airport is considered in detail because this is another task of control tower operators today. The communicative work which is actually accomplished via radiotelephone have to be adopted an equivalent way.

Because the central processing unit gets all the current movement data of all the personnel, it must have a data communication between it and every aircraft and every ground-vehicle inside of the airport close range. The current position data and the expected trajectory data have to get transmitted. Since there will be a permanent and tight data flow, a high volume air network like the today's cable less internet is required. It has to be interruption resistant and have a wide coverage to ensure a safe operation.

A precise identification of the position is indispensable to ensure a working procedure because the location and routing data are fed into, processed, manipulated and relayed by the central processing unit. The reproduction and control of a high complex traffic event increases with its degree of accuracy also the value of the safety of the total system. Independent of the condition of the atmosphere or extreme weather conditions, e.g. a strong cloud layer, a permanent and nearly perfect position determination must ensure. Furthermore geographical location shouldn't be an obstacle in the locating.

Because the signals are spreading in the form of electromagnetic waves, a suitable frequency should be chosen, which over clouding, rainfall and other interferences should not affect. Basic principle is the satellite-based navigation, e.g. used by Global Positioning System (GPS) or GALILEO. The number of navigation satellites should be chosen so that at any position at each time at the airport close range and its surroundings the same availability is given. To avoid receiving gaps, e.g. very special infrastructure, ground-based systems should be added [4].

To realize the data connection between aircraft and central processing unit, the plane should have antenna systems.

Indispensable for the rolling operation on the ground is an adaption of the display instruments on a certain scale. To have a good overview of all the vehicles, which are moving in a fixed cellular structure, it needs to have a dynamical map illustration. The Electronic Flight Bag (EFB) has a central role there. It evaluates the position and path data of all participants, which is transmitted by the central processing unit as a result the pilot adapts his control.

## 2. PROCESS PLANNING OF AIRPORT

Even before the landing the EFB visualizes the pilot the taxi path to the parking position. Additionally a dynamical light guidance is visible. This means that the midline lighting of the taxiways and runways are activated. This is also the backup for the case of a malfunctioning EFB or a problem with the data transmission to the central processing unit.


**Fig 2:** Zellen-Struktur des Flugplatzes
( cellular structure of the airport)
Source: Extract of the präsentation video
( Stefan Reitmann)

The movement areas of the airport have a cellular structure (see Fig. 2). The taxiway of an aircraft or a ground-vehicle can be described very well as a sequence of cells. In a dynamic manner, similar to the above described dynamic light guidance, cells are closed for the moving processes. Taxiways of aircrafts have a priority compared to plan movements of ground-vehicles (this does not include emergency vehicles)[2].

The determination of the position based on satellites (e.g.GALILEO). The cellular structure of the airport has to be exactly calibrated. The cell will get released after the aircraft passed it. In this theory, a shell which is adjusted to the structure of the aircraft, determines the length and width of the corridor which is blocked for the roll event.

The EFB shows useable conflict-free taxiways to the parking position. An optimization algorithm calculates the best solution in relation to fuel consumption, conflict frequency and time. The pilot has similar to a navigation system the chance to choose a fuel poorer or faster variant to react on delay. The Ground-vehicles are handled equally concerning their movements on the apron and taxiways. For flexibility reasons the parking position of an aircraft is seen as a complete sector, which is completely released by the central processing unit. All the handling vehicles can move here on view. Concrete routes for routine actions like the aircraft clearance are cumbersome. All ground-vehicles can drive back to their parking position after the aircraft clearance without a separate request, provided that they don't leave the neutral area [3].

For movements, which don't concern aircraft clearance, they have to set a ride request over their navigation system. The route selection and the visualization will result also on the navigation display. Possible conflicts are shown and if applicable illustrated during the ride via visual and acoustic signal. An example for this will be a crossing plane, which has priority. The navigation display also shows all the routes of all the other ground-vehicles to get a good overview for possible conflict situations.

The Push-Back-Process will be replaced by an independently reversing of the aircraft. Therefore every plane uses electric motors in the gears to drive the whole way from the gate to the starting position respectively from the runway to the gate independently.

The advantage is the reduction of push-back-vehicles to a minimum (for emergencies). The aircraft is able to wait to start the engines until it arrives in the starting position, because the electric motors will get

their energy from the Auxiliary Power Unit (APU). The firms Honeywell Aerospace and Safran with the Electric Green Taxiing System (EGTS) provide exemplary pilot projects [3].

The safety aspect is essential, because situations, which unpredictably break the routine processes, will never be managed without the coordination from human beings. For this reason a safety and fire fighter central will stay at the airport, which is not automated. In critical situations the safety commissioner triggers the fire fighters and other operation vehicles. This matches almost with today's situation. In the vision the task of observation of the movement area is transferred from the control tower operator to the safety commissioner. Consequently his workplace must have the sufficient opportunities to monitor the movement area.

The safety commissioner will cancel the usability of cells in case of trouble on the movement area such as ice on the taxiways or a remained lying aircraft. This is the input for the central processing unit. If the fire fighters have to disengage to solve the trouble, the relevant cells will be blocked.

The safety commissioner has also the opportunity to block the whole airport. In this case all vehicles have to stop immediately (except of aircrafts on the runway, to ensure the possibility of an emergency landing and emergency vehicles). In case that winter services are necessary, the critical area is blocked for this time interval.

If a ground-vehicle loses contact/ communication lost to the central processing unit it has to stay in the neutral airport area. Another ground-vehicle will do the task if it immediately. The heart of the airport, the central processing unit must have a hot reserve. This identical unit does exactly the same tasks like the primary unit. If this primary unit would break down, the reserve would stand in, so performance losses are prevented. This secondary unit shouldn't be stored at the same place like the primary unit. If both units break down, the airport will be closed immediately until one of them is working again.

## 3. CONCLUSION& ACKNOWLEDGMENT

To realize the vision it is not just necessary to manage the mentioned challenges. With the view in year 2050 there will be new unpredictable hurdles, which couldn't get solved jet. It is viewable that to reach this vision research and industry have to work better together. On the other hand cooperation has to be international, because it will just bring a benefit if everybody will use the new system.

Special thanks must go to Professor J. Lewitowicz and Professor W. Gąsowski my mentors of engineering aviation, who were source of endless encouragement and motivation, patient in the extreme during my long hours at the computer, but with a keen eye and perceptive mind.

## REFERENCES

1. Augustyn S., Human factors in aviation safety investigations. Kosice: ActaAvionica 2011.
2. Main seminar of the course of studies "Transport Engineering", Technical University Dresden, Group vision development
3. International Air Transport Association (IATA), Vision 2050, Singapore, February 12 2011
4. International Air Transport Association (IATA). (2011). *Vision 2050.* Abgerufen am 26. April 2013 von http://www.iata.org/pressroom/facts_figures/Documents/vision-2050.pdf
5. EGTS International. (2013). *Electric Green Taxiing System*. Abgerufen am 26. Juni 2013 http://www.greentaxiing.com/index.html

"HENRI COANDA"
AIR FORCE ACADEMY
ROMANIA

"GENERAL M.R. STEFANIK"
ARMED FORCES ACADEMY
SLOVAK REPUBLIC

INTERNATIONAL CONFERENCE of SCIENTIFIC PAPER
AFASES 2015
Brasov, 28-30May 2015

# THE USING OF NANOCOMPOSITE HEATING SYSTEM FOR AVIATION DESIGNING

**Sławomir Augustyn*, Telesfor Marek Markiewicz****

*National Defense University, Warsaw, Poland, **Aviation Institute & Air Defense, Poland

***Abstract:*** *The publication shows the preliminary possibility of nanocomposite heating system using for aviation designing. Carbon nanotubes are the quintessence of nanotechnology advances mainly due to their specific thermal, physical and mechanical properties. They are used to create totally new materials and occur as strengthening phase, for example, to medicine or build the wings and fuselages of aircraft as well as to their self-healing.*

***Key words****: nanocomposite heating system, safety & security system, aviation design.*

## 1. INTRODUCTION

Materials for the construction of an airframe, aircraft engine containing carbon nanotubes with the use of the right proportion in combination with other structural materials (polymers, sintered metal) give more flexibility [2]. The main fields of nanocomposite heating system applicable to medicine, rehabilitation, paramedical rescue services, aviation construction, building industry, means of motor, air and railway conveyance, household equipment, agriculture and special applications etc. [4].

## 2. THE PRINCIPLE OF NANOCOMPOSITE HEATING SYSTEM OPERATION

The heating technology elaborated in the nanocomposite heating system laboratories allows attaining properties and qualities of heating systems, hitherto unattainable. Traditional paths (cylinders) or electrically conducting resistance wires have been replaced with uniform heating composite containing modified carbon nanomaterials (figure.1) [3]. The result of our efforts is heating mats and coatings distinguished from:
- an uniform temperature distribution all over the surface being heated,
- the short reaction times in order to attain the temperature desired,
- the safe supply voltages under 24V for surface temperatures 0 - 70˚C,
- an adjustment of the technology to the expected rigidity or elastic properties of materials [5].

The nanocomposite heating system is based upon carbon nanomaterials modified in our labs and used for manufacturing polymer nanocomposites to produce heating effects.

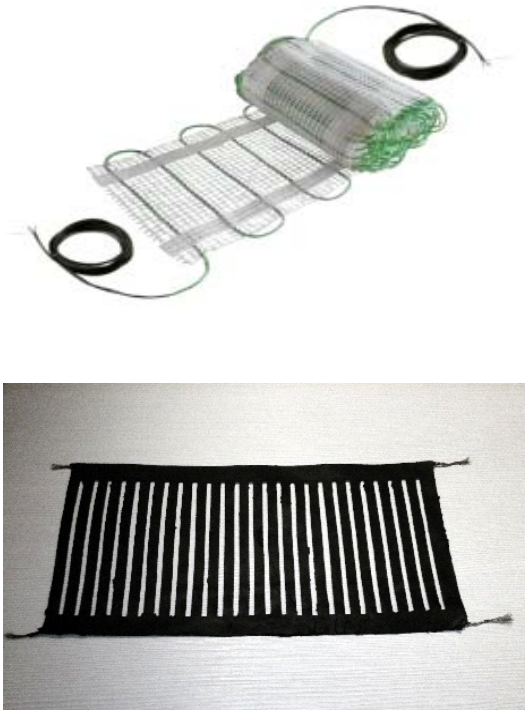

**Figure 1.** Traditional heating system vs. Nanocomposite Heating System

Such nanocomposites are distinguished with increased electrical resistance. They can be laid on many materials, e.g. polymer products and natural products.

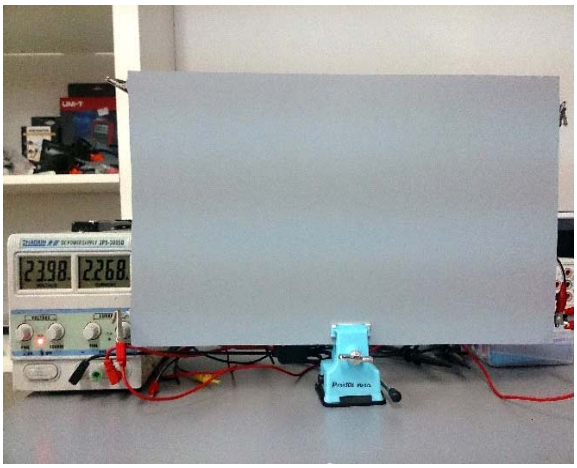

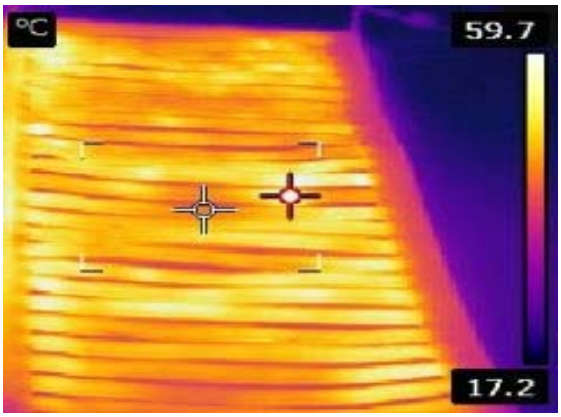


**Figure 2.** Thermal camera picture of nanocomposite heating mat (the surface temperature 60°C, current 24V)

By applying various types of polymers as carriers, it is possible to lend elasticity or rigidity to the heating coatings being laid. Simple current control systems: voltage controller to hold no more than 24V, temperature sensor, thermostat and electronic program selector can secure an accurate control and selection of temperature ranges from 0 to 60°C (figure 2).

The use of heating mats system and coatings will mean energy saving due to a uniform temperature distribution all over the heating surface (figure 3). No energy overuse is needed to heat up ‘voids’, which happens while using conventional technologies with resistance wire windings. Because the heat radiation is emitted from the entire working surface, the heat comfort is attained earlier and an item of consumer goods subject is heated faster and uniformly. For each user, such a functionality will also mean money saving.

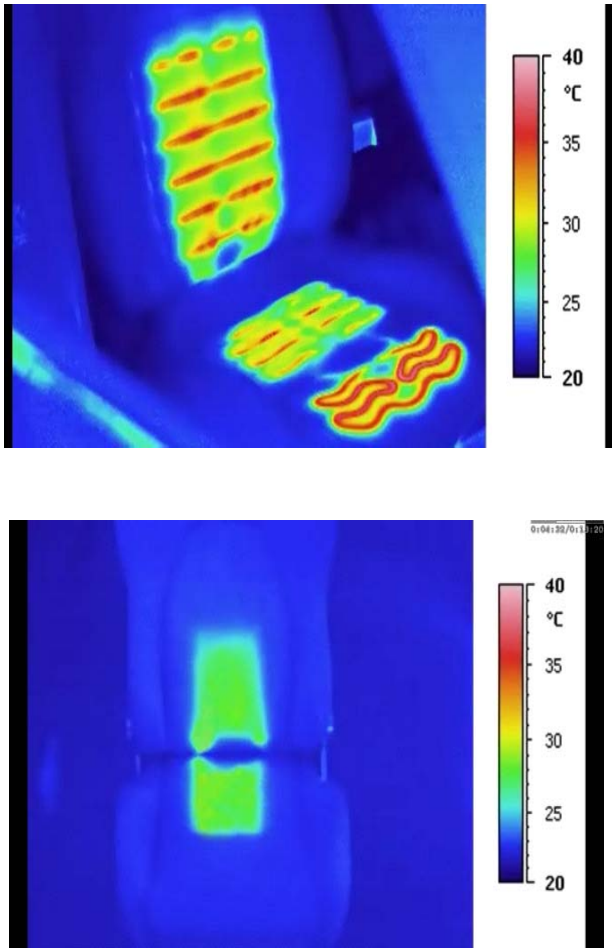


**Figure 3.** The Classical Seat Heating System vs. Nanocomposite Heating System (the thermovision camera pictures)

## 2. CONCLUSION& ACKNOWLEDGMENT

The introduction of Nanocomposite Heating System as new technology does not affect the previous functional quality of products and sub-assemblies. To end of them with heating properties means gaining access to new fields of application, previously either unattainable or which demanded the purchasing and fitting extra heating devices. What the more this system gives high efficiency and reliability during the working life because the functional heating elements this of new system is longer than in the case of classical heating with systems based upon leads and resistance wires.

The heating mass of paint does not contain any paths or electrical resistance circuits; hence, there is no risk of their burning or breaking. The entire heating surface/mat will keep on working to heat until torn apart.

An innovative and specialized product with new qualities will allow having the offer targeted at a wider field of application. Safe and low supply voltages of heating mats and coatings will make the user more aware of their safe and trouble-free operation. There is no risk when the product is used in consumer goods within the children's reach - even if destroyed or flooded.

Special thanks must go to Professor J. Lewitowicz and Professor W. Gąsowski my mentors of engineering aviation, who were source of endless encouragement and motivation, patient in the extreme during my long hours at the computer, but with a keen eye and perceptive mind.

## REFERENCES

[1] Air University Center for Strategy and Technology, *Blue Horizons 2007: "Horizon 2010"*. Project Report, Maxwell AFB, AL: Air University Center for Strategy and Technology, 2007.

[2] Augustyn S.: *The decision model of an aircraft crew in safety system*. International Journal of Computer and Information Technology, Vol. 2, Issue 2. 2013.

[3] Chung D. D. L.: *Composites get smart*. Materials today, January 2002.

[4] Craig B. D.: *AFRL Nanotechnology R&D Efforts to Advance Aerospace Systems for the Next Century*, The AMPTIAC Quarterly, Vol. 8, No. 2
[5] ITP-System, Specification Materials. DąbrowaGórnicza 2014, www.itp-system.pl
[6] Lewitowicz J.: *The basic of maintenance and operation aircraft, The problems of maintenance and operation to design and upgraded of aircraft*, Air Force Institute of Technology, Nr 6, Warsaw ITWL 2012.
[7] Peddel J., Turner S.: *Stealth and signature management – capability, technology and cost.*NavalForces, Nr 4/2002.

"HENRI COANDA"
AIR FORCE ACADEMY
ROMANIA

"GENERAL M.R. STEFANIK"
ARMED FORCES ACADEMY
SLOVAK REPUBLIC

INTERNATIONAL CONFERENCE of SCIENTIFIC PAPER
AFASES 2015
Brasov, 28-30 May 2015

# SAVING ENERGY ESTIMATION FOR USE OF HOLLOW ROLLERS IN BEARINGS UTILIZED IN WIND ENERGY TURBINES

**Bogdan Barabas*, Adriana Florescu*, Sorin Barabas***

*Faculty of Engineering Technology and Industrial Management, Transilvania University of Brasov, Romania

***Abstract:*** *The main objective of this paper is to establish the benefits obtained by implementing hollow rollers in the construction of large sized bearings, mounted in wind turbines by using innovative constructive solutions. Using hollow rollers has the immediate effect of decreasing inertia rotor system, with significant results in increased energy efficiency. This is due to decreased friction forces between rollers and raceways and by the uniform contact stress occurring at the ends of the rollers. Favorable results are expected in the economic field, by reducing material consumption and by increasing the durability of bearings. Using hollow rollers instead of solid rollers has an impact on working temperature, on vibrations and noise which decrease. Implementation of types of hollow rollers of cylindrical tubular type, instead of expensive rollers with logarithmic profile, will bring significant price decreases*

***Keywords:*** *saving energy, hollow rollers, dynamic dispatch*

## 1. INTRODUCTION

Use of bearings with hollow rollers in wind energy turbines is an innovative concept in saving green energy by increasing efficiency, with great benefits in maintenance technology and economic profits.

There have been attempts to use several hollow rollers in a bearing for different reasons but so far, from what we investigated; implementation of large bearings with hollow rollers in construction of wind power systems is new and not used.

An evaluation of the production tendencies, as well as a research of the development market pointed out the demand of the beneficiaries in the maintenance of working systems. The difficulties appeared in maintenance (poor lubrication, highly qualified assistance), as well as eliminating problems as vibration or noise, can be reduced or even removed, using bearings with hollow rollers.

Increase energy efficiency (wind power) is based on decreasing moment of inertia of rotor hence its inertial mass. That will lead directly to increase rotational speed of main shaft so will enable faster start at low speed wind of power plant. With decreasing inertia, the starting, the speed control during energy production, and stopping the turbine when required are more well done.

In Romania, the renewable energy production reached a record level at the end of last year when the total capacity of projects in the system reached 4255 MW, 82% higher

than the end of the year 2012, according to the National Authority in Energy Regulation data, the producers of renewable energy receive subventions as green certificates which all the consumers pay. To regulate the growth of invoices the government decided on July 1st 2013 to delay until 2017-2020 some green energy certificates. Romania assumed that 24% of electricity consumption from the year 2020 to come from renewable sources but the National Authority in Energy Regulation announced that this target was already achieved on January 1st 2014.[10]

## 2. ENERGY SAVING PROFILE OF WIND POWER SYSTEM

The energy saving profile was achieved using control dynamic dispatch. The optimal setting of parameters with influence in power system was made by optimization techniques and probabilistic approach. The quantification of energy saving revealed important gains in correlation with the objectives proposed: maximization energy output and constrained economic dispatch, namely, cost per KW. The proposed real-time control system is based on the following constraints: reduction of material consumption, inertia reducing, increase of durability, decrease of environmental costs and simplification of large bearings technology. (Fig.1)

Estimation of energy saving for wind turbine using bearings with hollow roller was made after constraints application [2]:

$$P_{SE} = P_T \times \sum_{i=1}^{n} P_{SE(Fi)} \quad (1)$$

where: $P_{SE}$ is energy saving for a wind turbine;

$P_T$ is output energy before implementation of bearings with hollow rollers;

$P_{SE(Fi)}$ is estimated value of saving energy of each constraint.

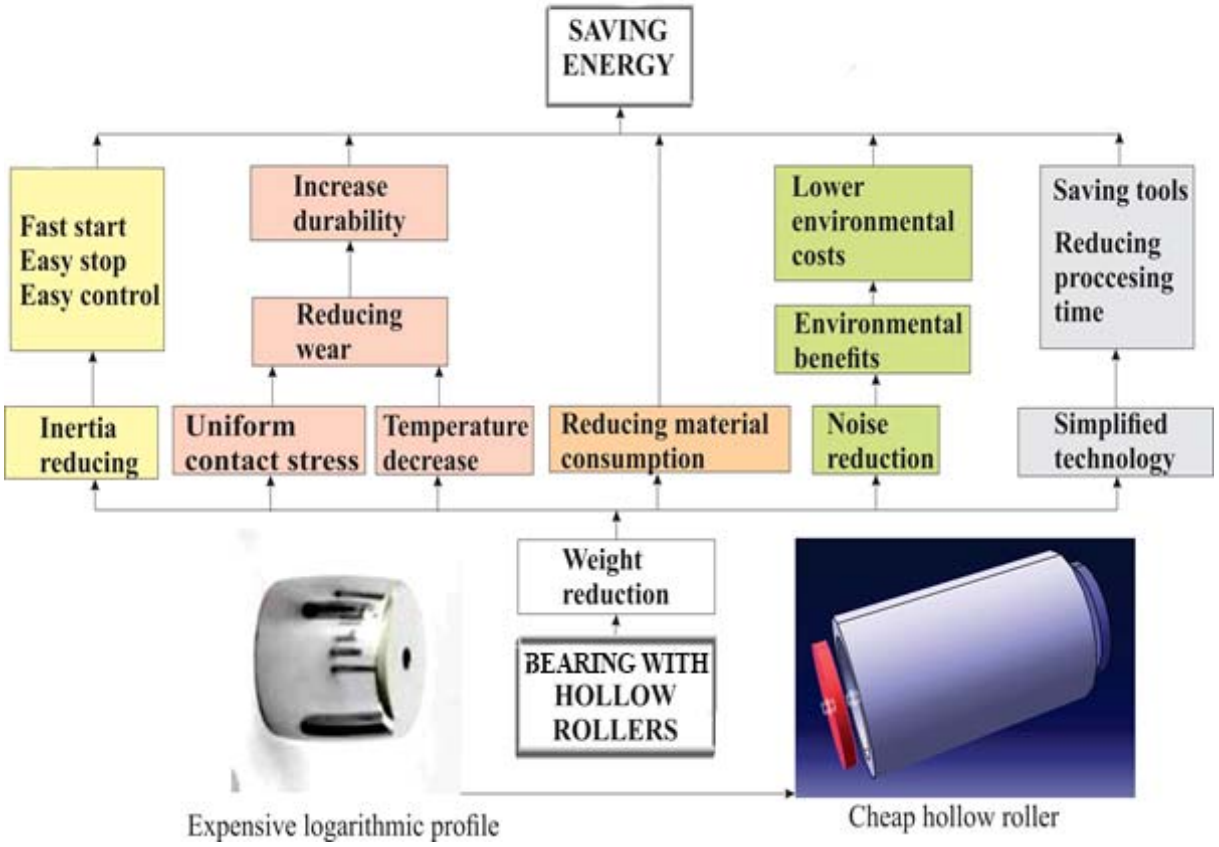


Figure 1 – The parameters who influences the saving energy in case of implementation in wind energy system of bearings with hollow rollers

## 3. MATHEMATICAL MODELING OF SAVING ENERGY OF WIND TURBINE

**3.1 Inertia reducing.** Reduction of inertia of system is one of most important effect of using of hollow rollers. Fast start, easy stop and easy control bring an increase of energy efficiency [6].

At very low wind speeds, there is insufficient torque exerted by the wind on the turbine blades to make them rotate. However, as the speed increases, the wind turbine will begin to rotate and generate electrical power.

The speed at which the turbine first starts to rotate and generate power is called the *cut-in speed* and is typically between 3 and 4 meters per second. As the speed increases above the rate output wind speed, the forces on the turbine structure continue to rise and, at some point, there is a risk of damage to the rotor. As a result, a braking system is employed to bring the rotor to a standstill. This is called the *cut-out speed* and is usually around 20-25 meters per second.

$$J_r \cdot \dot{\omega} = M_a - M_g \quad (2)$$

where: $J_r$ is rotor moment of inertia
$\omega$ is rotor speed;
$M_a$ is aerodynamic torque;
$M_g$ is generator torque.

$$J = \sum m_i \cdot r_i^2 \quad (3)$$

$$P_T = \omega \cdot M_g \quad (4)$$

$$M_a = \gamma \cdot \mathbf{R}^3 \cdot \mathbf{v_w^2} \quad (5)$$

where: $r_i$ is the radial distance from the inertia axis to the particle of mass $m_i$ and the summation is taken over all particles;
$\gamma$ is a constant depending by turbine construction;
R is rotor radius;
$V_w$ is the wind speed.

Influence of inertial mass on the speed is evident according to relations (2) and (3). Direct relation between wind speed and inertia lead to a decrease of cut-in speed in case of decrease of inertial mass of rotor. (Fig.2) [7].

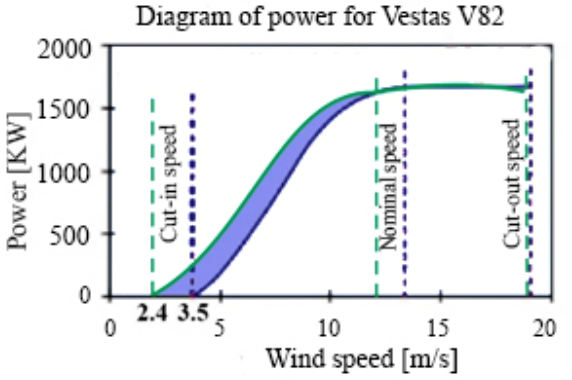


Figure 2 - Typical wind turbine power output equipped with bearings with filled rollers (blue) and expected power output for wind turbine equipped with bearings with hollow rollers (green)

In Fig. 2, with blue is quantity of gained power at a single starting, in case of wind turbine with bearings with hollow rollers and depend of power coefficient of every turbine. For Vestas V82, the computational model in conjunction with experimental observation (the cut-in speed decrease from 3.5 m/s to 2.4 m/s) lead to concrete values of gain energy at single start-up at 250 KWh. For 15 start-up/month gain energy for one turbine is approx. 45MWh in one year that means 3% of entire capacity of turbine.

**3.2 Increase durability**. It is based on temperature decrease in the system, on reducing wear due to uniform contact stress to the end of the rollers. For large bearing durability in millions rotation is [4, 5]:

$$L_{na} = a_1 \times a_2 \times a_3 \times a_v \times a_r \times a_c \times a_a \times \left(\frac{C}{P}\right)^p \quad (6)$$

where: $L_{na}$ is nominal durability in millions rotations[9];

$a_1$ is factor of reliability;

$a_2$ is factor for material;

$a_3$ is factor for running conditions;

$a_v$ is speed factor;

$a_r$ is a roughness factor;

$a_c$ is a factor for lubricant;

$a_a$ is factor of coaxiality ;

C - basic dynamic load [N];

P - equivalent dynamic load [N];

p - exponent for roller bearings: p=10/3;

The ratio $\left(\frac{C}{P}\right)$ is direct dependent on contact stress.

Were chosen rollers with $D_{ext}$ = 120 mm and L = 220mm from SAE 3310, carburized at 65HRC. The diameter of bearing has the $D_{rul}$ = 1900 mm. For the inside diameter (hole diameter) were chosen four cases according to the following values: $Di_1$ = 60 mm, $Di_2$ = 80 mm, $Di_3$ = 90 mm**,** $Di_4$ = 100 mm**.**

For bearing with solid rollers and for all bearings with hollow rollers was made the finite element analysis with Nastran software. The results was showed in diagram in Fig.3 [3]

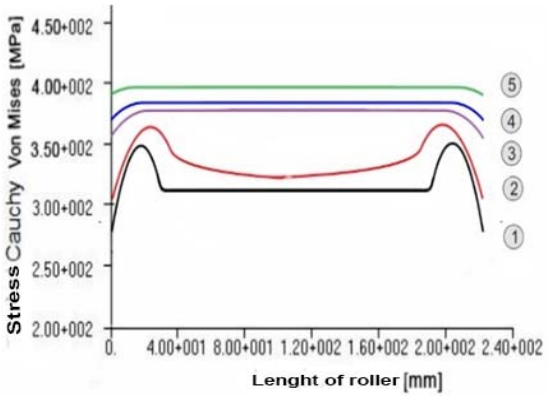


Figure 3 - Graph of contact stress in roller depending on cavity-results obtained by finite element analysis-1) solid roller D = 120mm, 2) hollow roller Di = 60mm, 3) hollow roller Di = 80mm, 4) hollow roller Di = 90mm 5) hollow roller Di = 100mm

Curve 1 belongs radial cylindrical roller bearing straight and solid (Fig.3). It can be seen that even if the end tensions does not exceed the permissible limits, bearing wear unevenly, leading to sliding movements. As shown, sliding produces frictions and leading to heat of bearing, fluidization of lubricant, shortening its durability. Curve 1 (Di = 60 mm), rollers respond the requirement to reduce inertial mass in a small measure, without an essential contribution to increasing the efficiency of large bearing assemblies. Both deformations and tensions are similar to the solid roller (Fig. 3). Curve 3 (Di = 80mm), curve 4 (Di = 90mm) and curve 5 (Di = 100mm) have end tensions, completely reduced. The bearing has uniform wear that increases durability, (stress-free to the end of roller) and respond perfectly to requirements reduction of inertial mass. [1, 8] The reduction of irregular wear is made using hollow rollers. Their degree of cavity increase or decrease masses, forces and inertial and centrifugal moments. Their mounting on large bearing do not present any difficulties. The processing is identical with that of the cylindrical rollers and much more easy and cheap then processing cylindrical rollers with logarithmic profile. Switching to bearing with hollow rollers doesn't require major changes in technology. Both the dynamic analysis performed with the help of finite element method as well as the results of the analytical model calculations lead to the conclusion that hollow cylindrical rollers can replace rollers with logarithmic profile, more expensive and heavy, bringing in the same time an increase of life of the bearing through the reduction of uneven wear of rolling elements. The uniform stress combined with vibrations reduction and low temperature operation (in cavity of rollers can be stored an additional amount of lubricant) lead to gain energy for one turbine aprox.7%. Expected life of bearing with hollow rollers only can be predicted at 21-22 years (eq.6) as against 20 years for classic bearing.

**3.3 Reducing material consumption.** For a roller with $D_i$= 80mm the difference between a solid roller and a hollow roller is approx. 35 kg. (Table 1)

Table 1 Weight of rollers with different hollowness

| $D_i$ roller [mm] | 0 | 60 | 80 | 90 | 100 |
|---|---|---|---|---|---|
| Weight [Kg] | 78,22 | 58,67 | 43,46 | 34,22 | 23,90 |

For a bearing with 20 rollers the difference is approx. 700 kg, with 30% lighter in weight. For a product with 20 years life the saving energy for product for 1 year is approx. 1.5 % if we approximate the gained weight with gained energy. The saving energy in environmental domain is based on noise reduction due to possibility of use of phono-absorbant foam with lubricant in cavity of rollers. The saving energy in technology domain for one product for one year is based to reducing of tools consumption. The both require complex computation and are approximate at 2% and respectively at 6 %. The total energy saving is approx. 26%.

## 4. CONCLUSIONS & ACKNOWLEDGEMENT

Total saving energy is estimated to a 1.65MW/h x 26% = 0.43 MW/h. This saving energy is gained through the use of one bearing of hollow roller with $D_{ext}$ =1900mm. The roller diameter is D=120 mm and the cavity has diameter $D_i$=80 mm. Main area, on which it pursues a growth effect is energy performance by implementing a new bearing with hollow rollers in large assemblies of wind energy, leading to increase their sustainability through capacity building maintenance.

Reducing subsidies in this area makes the proposed bearing with hollow rollers, to be of great interest as it leads to significant savings by reducing maintenance cost price of wind power stations by increasing sustainability and energy efficiency.

Market study, technical, financial and operating reports has encouraging results.

This work was partially supported by the strategic grant POSDRU/159/1.5/S/137070 (2014) of the Ministry of Labor, Family and Social Protection, Romania, co-financed by the European Social Fund – Investing in People, within the Sectorial Operational Programme Human Resources Development 2007-2013.

## REFERENCES

1. Abu-Jadayil, W.M., Jaber, N.M., "*Numerical prediction of optimum hollowness and material of hollow rollers under combined loading*". Materials and Design no.31, ISSN: 0261-3069, 2010, pag.1490–1496.
2. Bhateja, C.P., Hahn, R.S.,"*A Hollow Roller Bearing for Use in Precision Machine Tools*", CIRP Annals, Man. Technology, Volume 29, Issue 1, 1980, pag. 303-307.
3. Baraba□, S.A., □erban, C.,"*Heat treatment for 20NiCrMo7 and 15NiCr13 steels used in construction of extralarge bearings*". Recent Journal Vol. 11 No. 2 (29), July 2010 ISSN 1582-0246.
4. Blau, J.P.,"*ASM Handbook, Friction, Lubrication, and Wear Technology*". ASM International, Vol. 18, 1992.
5. Doll, G. L., Kotzalas, M. N. and Kang, Y. S. Life-Limiting Wear of Wind Turbine Gearbox Bearings: Origins and Solutions Timken Company
6. Hosseini, S.A.A., Khadem, S.E.,"*Free vibrations analysis of a rotating shaft with nonlinearities in curvature and inertia*". Mechanism and Machine Theory, pag. 272–288, 2009.
7. Kakuta, K.,"*High Speed Rolling Bearings for Gas Turbines*". Japanese Journal of Tribology, Vol. 35, 1990, pag. 877-889.
8. Wei, Y., Balendra, R.,"*FE analysis of a novel roller form: a deep end-cavity roller for roller-type bearings*". Journal of Materials Processing Technology 145, 2004, pag. 233–241.

9. ***Tapered roller Bearing Catalogue, INA Schaeffler.
10. http://www.reportsandintelligence.com/global-waterjet-cutting-machine-2014.

"HENRI COANDA"
AIR FORCE ACADEMY
ROMANIA

"GENERAL M.R. STEFANIK"
ARMED FORCES ACADEMY
SLOVAK REPUBLIC

INTERNATIONAL CONFERENCE of SCIENTIFIC PAPER
AFASES 2015
Brasov, 28-30 May 2015

# STRESS DISTRIBUTION FOR A PISTON WITH AN $AL_2O_3$ TOP LAYER DEPOSITED ON THE PISTON HEADS WHICH ABSORBS GAS PRESSURE

**E.S. Bârcă*, A.G. Plăiaşu*, Vladu Mihaela*, M. Abrudeanu*, G. Mahu**, C. Munteanu****

*Faculty of Mechanics and Technology, University of Pitesti, Romania, **Faculty of Mechanics, Technical University "Gheorghe Asachi", Iasi, Romania

***Abstract:*** *Thin layer deposition is considered to be a method to bring internal combustion engines one step closer to the ideal engine inside which is taking place the adiabatic process. The piston is allowed to move on a single axis and is considered to be leaning in its bearings. The only force acting was considered to be due to flue gas pressure while the piston is at TDC. Thin layer deposition has been carried out on the piston and then analyzed with the finite element method using the ANSYS 13 software in order to determine the state of stress. There were designed CAD models of the piston and of the piston with top layer which were imported in ANSYS 13 software in order to carry out the analysis.*

***Keywords:*** *thin layer, $AL_2O_3$, ICE piston, finite element analysis*

## 1. INTRODUCTION

The effects of the thin layers as thermal barrier have been studied in both naturally aspired and turbocharged Diesel engines in order to observe what improvement the deposited layer brings. The usual thickness of the deposited layer varies between 100 and 500 μm, consisting out of a intermediate layer with a thickness of 0.15mm and the ceramic layer with an 0.35mm thickness. [1-4]

The increased harshness of the obtained surface has a positive effect over the contact wear resistance thus the engine can operate with a higher compression ratio. One advantage the deposition brings is that after the thermal deposition the obtained layer no longer needs subsequent machining. [5]

Practical and mathematical studies over the thermal behavior of the piston with deposited top layer have shown that the temperature inside the base material is lower compared with the temperature the piston without deposited layer have. Also is concluded that the top layer may have a high potential to increase performance and reduce unwanted emissions. [6]

Another study is carried out by H. Mindivan and provides a review on the wear behavior of a layer of Al2O3 formed in situ in a matrix of a hypereutectic Al18Si with the purpose to improve the wear resistance of the piston. The study highlighted the effect it has the spraying distance and the characteristics of molten particles on wear behavior of the layer. The number of Al2O3 particles formed in situ by plasma deposition raises by increasing the spraying distance and decreases the speed and temperature of the molten particle. This led to

improved hardness increased wear resistance. [7]

## 2. FINITE ELEMENT ANALYSES RESULTS

For the piston with an $Al_2O_3$ ceramic coating it was used the coordinate system presented in Fig. 1. – a. in order to present the stress distribution. Based on this coordinate system there are presented normal and tangential stress distributions. Fig.1. b) shows a section through the mesh network carried out in the analysis.

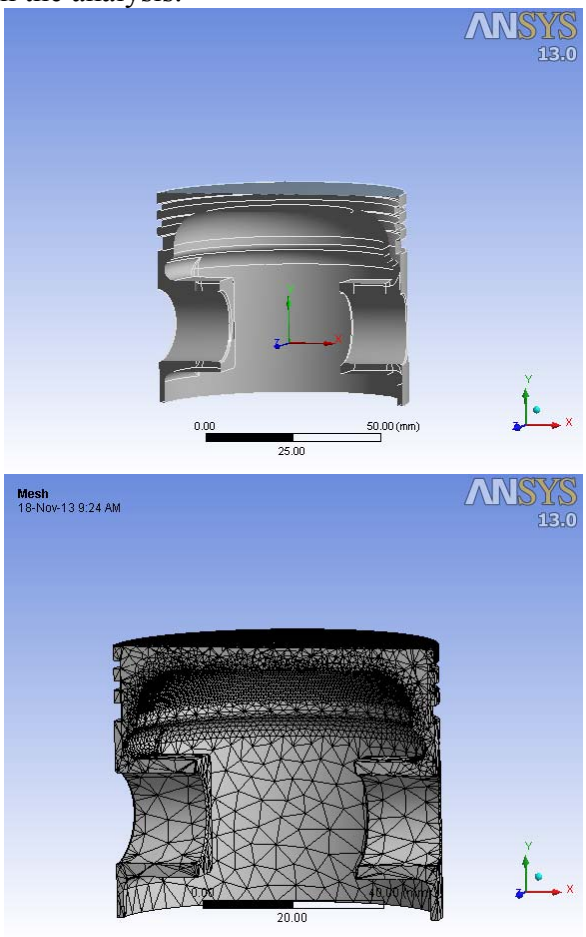


Fig.1. Section through CAD model used in the analysis of $Al_2O_3$ coated piston: a) coordinate system used in the analysis and b) mesh network

In the following there are presented the obtained results for the structural analysis made on the piston with an $Al_2O_3$ thin layer on the working surface.

Fig.2 presents the primary stress vector distribution in the base material of the piston. With red there is presented maximum primary stress vector ($\sigma_1$). The green color highlights medium primary stress vector ($\sigma_2$), and the blue color highlights minimum primary stress vector ($\sigma_3$). It can be noticed that the maximum primary stress value is found on the upper surface of the deposited layer near the edge area and on the inner surface of the piston head. In these regions the maximum primary stress produces the stretching of the material. On the central area of the upper surface of the deposited layer acts the minimum primary stress, thus resulting in the compression of the thin layer. Medium primary stress is found mainly at the interface of the layer with the base material.

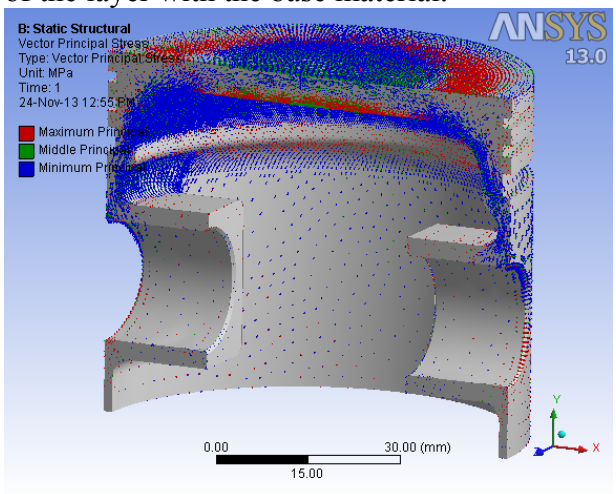


Fig.2. Primary stress distribution vectors in the piston's material with an $Al_2O_3$ top layer

Fig.3 shows the equivalent stress distribution for the piston with an $Al_2O_3$ top layer. The equivalent stress is calculated with equivalence theorem of Von Mises or the Von Mises yield criterion. The equivalent stress provides a correspondence between a complex state of stresses consisting of normal and tangential stresses and a normal stress which presents the same risk. In the case of the piston with an $Al_2O_3$ deposited on the piston head, the maximum equivalent stress occurs at the pin bosses and has a value of 68.17 MPa. In the layer area the maximum equivalent stress has a value of 53 MPa (Fig.3.a). In the base material in the piston head region is found maximum equivalent stress with a value of 45.5 MPa (Fig.3.b).

Normal and tangential stress determination was made according to the direction and characteristic plane of the pistons real load. Normal stress was determined for the x,y and z directions as shown in Fig.1.a) in coordinate

system. Tangential stresses were expressed in planes parallel to the plane belonging to the trihedral respectively xy, zy and xz.

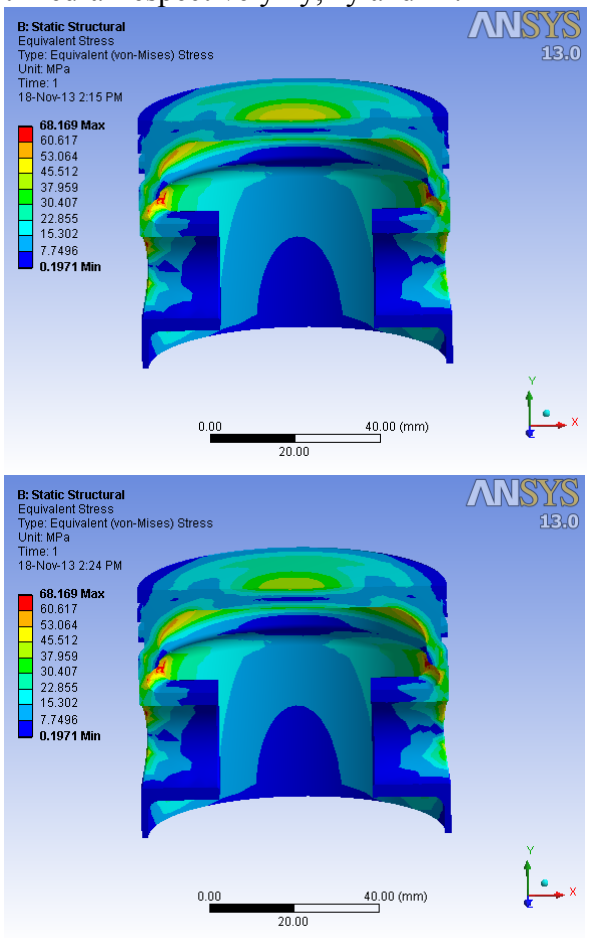


Fig.3. Equivalent stress distribution for the piston with an $Al_2O_3$ top layer: a) with top layer and b) with top layer removed

In Fig.4 there is presented the tangential stress distribution for the planes parallel with the XY plane for the piston with an $Al_2O_3$ top layer. The maximum tangential stresses in this plane have two components $\tau_1$ and $\tau_2$. The $\tau_1$ component of the tangential stress has a value of 26, 285 MPa, and the $\tau_2$ component has a value of 26,331 MPa. These are found in the radius of curvature area between the piston head and the piston rings area and in the radius of curvature of the pin bosses. They have opposite directions and at a 45º angle to the main directions.

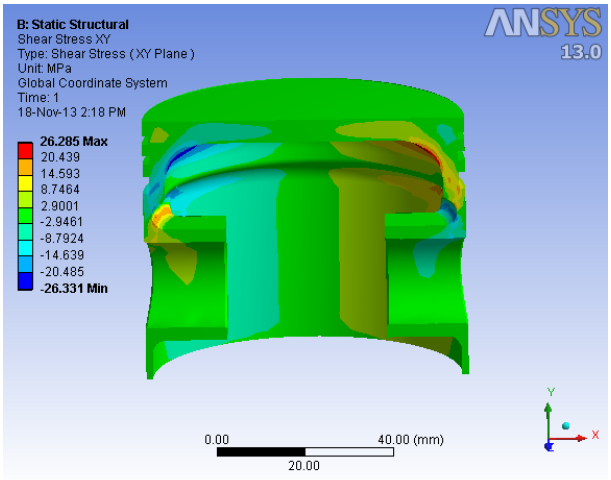


Fig.4. Tangential stress distribution for the xy plane for a piston with an $Al_2O_3$ top layer

Fig.5 shows the tangential stress distribution in planes parallel with the yz plan. Maximum tangential stress components for this plane are found in radius of curvature area between the pin bore and the lower part of the piston skirt ($\tau 1$ = 29,063 MPa) and in the radius of curvature area of the piston head and the port rings region ($\tau 2$ = 27,502 MPa) and are disposed at an angle of 90º to each other from which can be deduced the fact that they are expressed on the main directions with different orientation.

The tangential stress distribution components for the xy plane of the piston head with an $Al_2O_3$ top layer are found both inside and on the upper surface of the deposited layer and in the inner region of the piston pin bore (Fig. 6.). The $\tau_1$ component value is 25,344 MPa and the value of the $\tau_2$ component is 28,208 MPa. These components are located in planes found at 45º towards the primary direction $\sigma_1$.

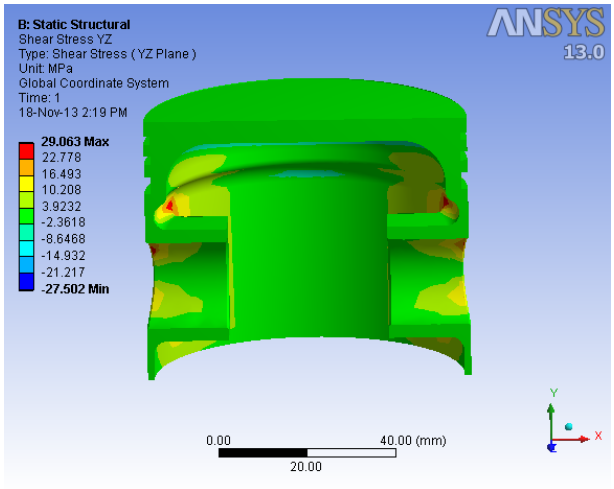


Fig.5. Tangential stress distribution for the yz plane for the piston with an $Al_2O_3$ top layer

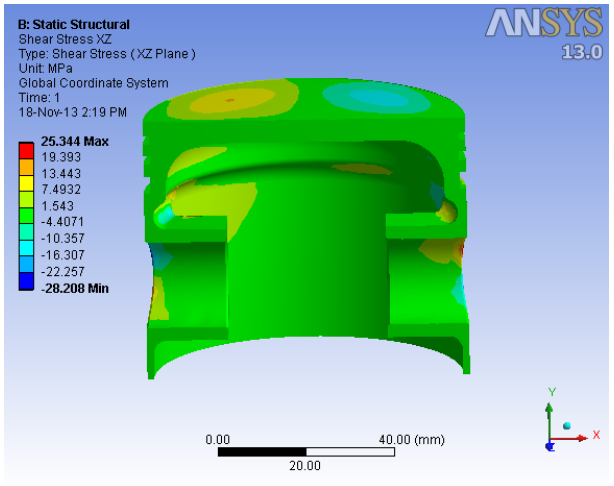


Fig.6. Tangential stress distribution for the xz plane for the piston with an $Al_2O_3$ top layer

Fig.7 shows the normal stress distribution for the x axis direction in the case of the piston with an $Al_2O_3$ top layer. The compression component of the normal stress after this direction has a maximum value of 42.351 MPa, value found on the upper surface of the piston head respectively in the deposited layer. The stretching component of the normal stress is found on the inner surface of the piston head and on the upper surface of the deposited layer in the edge area and has a maximum value of 60.043 MPa. The compression component that occurs in the x axis direction is due to minimal primary stress $\sigma_3$, and the stretching component is due to maximum primary stress $\sigma_1$.

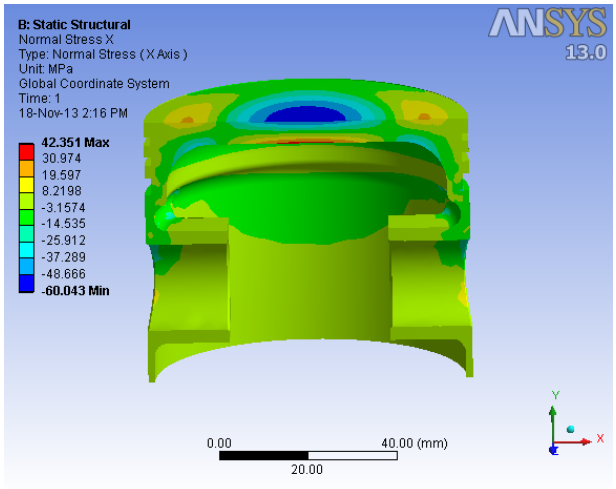


Fig.7. Normal stress distribution for the x axis direction for the piston with an $Al_2O_3$ top layer

For the y axis direction the normal stress distribution is presented in Fig. 8. For this direction the normal stress acts mainly in the radius of curvature area between the pin bolt and the piston's skirt where the maximum value of the compression component is 74,869 MPa and in the lower part of the pin bore and the port rings area where the stretching component has a maximum value of 41,848 MPa. Normal stress after this direction is produced mainly by the primary stresses $\sigma_1$ and $\sigma_3$.

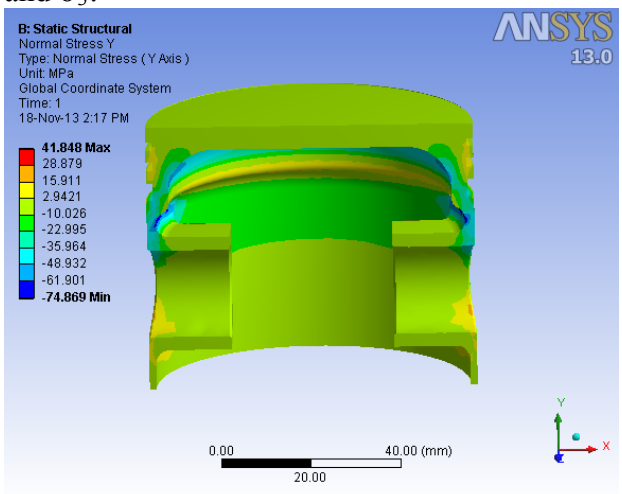


Fig.8. Normal stress distribution for the y axis direction for the piston with an $Al_2O_3$ thin layer

Normal stress distribution for the z axis direction is shown in Fig. 9. The maximum value of the compression component for this direction is 60.069 MPa, and the maximum value of the stretching component is 86.424 MPa. The compression on the upper surface of

the deposited top layer and the stretching in the pin bore region are produced by the primary stress $\sigma_3$. The stretching that appears on the inner surface of the piston head is produced by the primary stress $\sigma_2$.

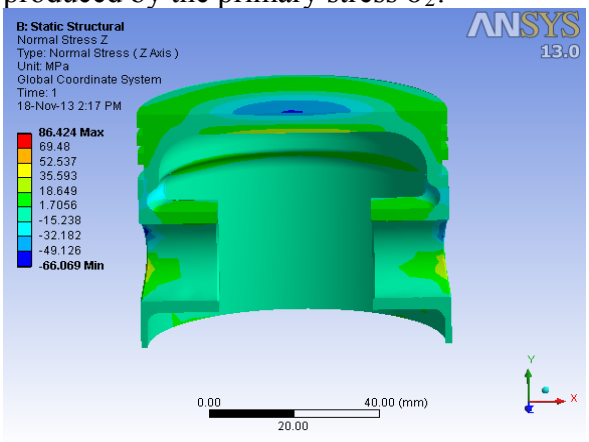


Fig.9. Normal stress distribution for the z axis direction for the piston with an $Al_2O_3$ top layer

Fig.10 presents the deformation that appears inside the piston following the loads that have been applied.

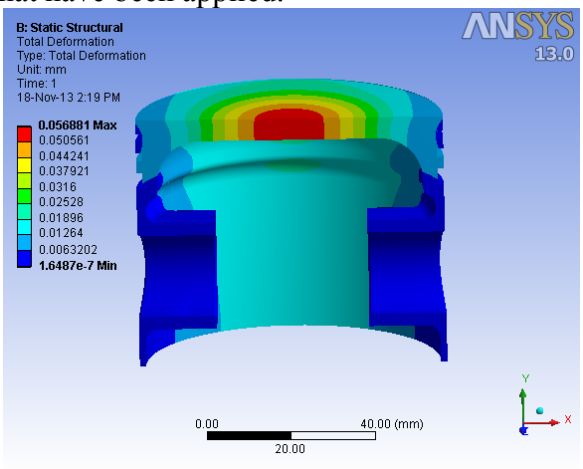


Fig.10. Present deformation in case of the piston with an $Al_2O_3$ top layer

The maximum value of the deformation is found in the piston head region and has a value of 0.57 mm.

Fig.11 presents the elastic deformation that appears in this piston, reording a maximum value of 9.6013 x $10^{-4}$ mm/mm in the radius of curvature area between the pin bore and the skirt. The elastic deformation that is found in the deposited layer has a maximum value of 7.4739 x$10^{-4}$ mm/mm.

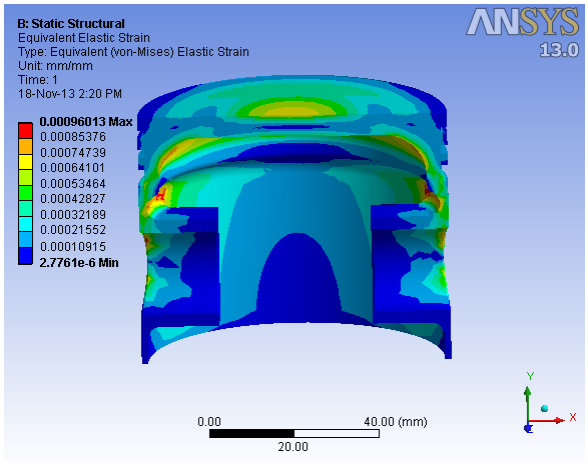


Fig.11. Elastic deformation that is found in the piston with an $Al_2O_3$ top layer

## 3. CONCLUSIONS & ACKNOWLEDGMENT

The finite element analysis strated with the CAD models of the piston and of the piston with top layer. These models were designed in SOLIDWORKS and then imported in the ANSYS 13 software. The first module, in which the data were inserted in, was the Data Engineering module. In this module, properties of the piston and of the deposited layer such as: material properties, young's module, tensile strength, density and Poisson's constant were defined. The Mechanical module was used to develop the mesh models for each individual model.

From the finite analysis we can conclude that the $Al_2O_3$ layer has a good mechanical behavior, which recommends it for this kind of thin layers. By applying this kind of thin layer,

the base material is less stressed conducing to a better wear resistance due to flue gas pressure and thermal stress.

This work was supported by the strategic grant POSDRU/159/1.5/S/138963 - PERFORM, co-financed by the European Social Fund – Investing in People, within the Sectoral Operational Programme Human Resources Development 2007-2013.

## REFERENCES

1. Prasad, C.M.V., Krishna, M.V., Reddy, C.P. & Mohan, K. R. (2000), Performance Evaluation Of Non-Edible Vegetable Oils As Substitute Fuels In Low Heat Rejection Diesel Engines, Proceedings of the institution of mechanical Engineers, 214,2; ProQuest Science Journals.
2. Charlton, S.J., Campbell, N.A., Shephard, W.J., Cook, G. & Watt, M. (1991), An Investigation of Thermal Insulation of IDI diesel Engine Swirl Chamber, Proc. Instn. Mech. Engrs., Vol.205
3. Chang, S.I. & Rhee, K.I. (1983), Computation of Radiation Heat Transfer in Diesel Combustion, SAE International of Highway Meating, Wisconsin; 327-341, USA
4. Parlak, A., Yaşar, H. & Şahin, B. (2003), Performance And Exhaust Emission Characteristics Of A Lower Compression Ratio LHR Diesel Engine, Energy Conversion and Management, 44, 163-175
5. Hanbey Hazar, Characterization of MoN coatings for pistons in a diesel engine, journal homepage: www.elsevier.com/locate/matdes, Materials and Design 31 (2010) 624–627
6. Mesut Durat, Murat Kapsiz, Ergun Nart, Ferit Ficici, Adnan Parlak, The effects of coating materials in spark ignition engine design, journal homepage: www.elsevier.com/locate/matdes, Materials and Design 36 (2012) 540–545
7. H. Mindivan, C. Tekmen, B. Dikici, Y. Tsunekawa, M. Gavgali, Wear behavior of plasma sprayed composite coatings with in situ formed Al2O3, journal homepage: www.elsevier.com/locate/matdes, Materials and Design 30 (2009) 4516–4520

"HENRI COANDA"
AIR FORCE ACADEMY
ROMANIA

"GENERAL M.R. STEFANIK"
ARMED FORCES ACADEMY
SLOVAK REPUBLIC

INTERNATIONAL CONFERENCE of SCIENTIFIC PAPER
AFASES 2015
Brasov, 28-30 May 2015

# DYNAMIC ANALYSIS OF COMPOSITE WINGS

**Bogdan-Alexandru Belega*, Amado Ştefan***

*Military Technical Academy, Bucharest, Romania

***Abstract:*** *The present paper has been designed to geometrical modelling and FEM structural analysis of fiber glass/epoxy wing airframe. It presents a dynamic analysis of wing endured at two shocks, one horizontal and one vertical, with the same law of variation of the acceleration. During the simulation, the law of variation of the acceleration was used for symmetrical wing section that is recessed.*

***Keywords:*** *airfoil, plain weave, E-glass, airframe, FEM, shock*

## 1. INTRODUCTION

Plastics reinforced with glass fibers were used for the first time due to their outstanding qualities compared to conventional materials, 60 years ago.

Increasingly high performance required of strength structures generally, especially those for aeronautics and military applications require very severe condition during their operation.

Priorities are the considerations functional optimization of aerodynamic at profiles aeronautical structures and satisfying the restrictive conditions related to: special mechanical strength in a broad range of the environmental temperature, vibration, fatigue, stiffness, minimum weight and maximum reliability.

For the case of UAVs, in their construction it is used particularly balsa wood, which has a good resistance in flight conditions and is also characterized by a low weight. The disadvantage of this construction occurs when the UAV has a shock due to a crash or other similar situations. The use of composite materials based on fiber glass (carbon, Kevlar) although they have a higher density than wood, lead to the structural resistance much higher in case of shocks.

## 2. THEORETICAL ASPECTS

**2.1 Important equations.** The process of approximating the solution of the equations of motion by considering only the first few modes of the system's natural frequencies is called normal mode or modal superposition analysis and in the Advanced Dynamic Module, all forced vibration response problems are based on this procedure.

The equations of motion for a linear dynamic system are:

$$[M]\{\ddot{u}\}+[C]\{\dot{u}\}+[K]\{u\}=\{f(t)\} \qquad (1)$$

where: $[M]$ is mass matrix, $[C]$ is damping matrix, $[K]$ is stiffness matrix, $\{f(t)\}$ is time varying load vector and are the displacement, velocity, and acceleration vectors, respectively.

For linear dynamic problems, the system of equations of motion (1) can be decoupled into "nf" single degree of freedom equations in

terms of the modal displacement vector $\{x\}$, where:

$$\{u\} = [\Phi]\{x\} \tag{2}$$

and $[\Phi]$ is the matrix of the lowest "nf" eigenvectors obtained from the solution of:

$$[K]\{u\} = \omega^2 [M]\{u\} \tag{3}$$

Substituting for $\{u\}$ from (2) into (1) and pre-multiplying it by $[\Phi]^T$ , will yield:

$$\begin{aligned}&[\Phi]^T [M][\Phi]\{\ddot{x}\} + [\Phi]^T [C][\Phi]\{\dot{x}\} + \\ &+ [\Phi]^T [K][\Phi]\{x\} = [\Phi]^T \{f(t)\}\end{aligned} \tag{4}$$

With the mode shapes satisfying the orthogonality conditions, (4) becomes:

$$[I]\{\ddot{x}\} + [\lambda]\{\dot{x}\} + [\Delta^2]\{x\} = [\Phi]^T \{f(t)\} \tag{5}$$

Equation (5) represents "nf" uncoupled single degree of freedom (second-order differential) equations as shown below:

$$\ddot{x}_i + 2\xi\dot{x}_i + \omega_i^2 x_i = \{\phi\}_i^T \{f(t)\} \tag{6}$$

These equations can be evaluated using step-by-step integration or other techniques, and the displacements {u} and other system responses can then be determined by performing the transformation shown in equation (2).

**2.2 Damping Effects.** The damping matrix $[C]$ is assumed to satisfy the orthogonality conditions. It should be noted that in the majority of cases, (a) the exact damping matrix is unknown, and (b) the effect of any non-orthogonality is usually small. In the Post Dynamic module, the following damping options are available.

*Rayleigh damping* is of the form:

$$[C] = \alpha[M] + \beta[K] \tag{7}$$

This form of $[C]$ is orthogonal with respect to the system eigenvectors and the modal damping coefficient for the $i^{th}$ mode $C_i$ may be calculated:

$$C_i = 2\xi_i\omega_i = \alpha + \beta\omega_i^2 \tag{8}$$

and in terms of the modal critical damping ratio

$$\xi_i = \frac{\alpha}{2\omega_i} + \frac{\beta\omega_i}{2} \tag{9}$$

where $\alpha$ and $\beta$ are the Rayleigh damping coefficients.

*Modal damping* is defined as a fraction of critical damping

$$\xi_i = \frac{C_i}{C_c} \tag{10}$$

**2.3 Modal Acceleration Method (MAM) in Time History.** The process of mode truncation, as was explained before, introduces some error in the response. The Modal Acceleration Method (MAM), in the Time History Analysis, approximates the effects of the truncated modes by their equivalent static effects. This approximation can be expressed for the displacement by:

$$U_c = [K]^{-1}\{R_c\}$$

where, $K$ is the structural stiffness matrix and $R_c$ represents the static loading. It can be shown that this static load vector can be computed in terms of the included modes, according to:

$$R_c = \left[I - M\Phi\Phi^T\right]\{P(T)\} \tag{11}$$

where, $M$ and $\Phi$ are the mass matrix and modal matrix, respectively, $\{P(t)\}$ is the applied dynamic load, and $\Phi^T$ is the mass matrix transpose. Thus by considering only a few numbers of modes, for even very complicated geometry, it can evaluate the response accurately.

**2.4 Uniform Translational Base Motion.** The equations of motion for a linear dynamic system with uniform base acceleration $\ddot{u}_b(t)$, can be written as:

$$[M]\{\ddot{u}_r\} + [C]\{\dot{u}_r\} + [K]\{u_r\} = \{f_e(t)\} \tag{12}$$

where $\{u_r\}$ is the structure displacement relative to the base, and $\{f_e(t)\}$ is an effective load due to the base motion:

$$\{f_e(t)\} = -[M]\{I_b\}\ddot{u}_b(t) \tag{13}$$

The vector $\{I_b\}$ is an influence vector relating base motion to rigid body structure displacements according to:

$$\{U\} = \{u_r\} + \{I_b\}u_b(t) \tag{14}$$

As previously described, (12) can be transformed into uncoupled equations in terms of the modal displacements $\{x\}$ where:

$$\{u_r\} = [\Phi]\{x\} \tag{15}$$

and the equation of motion (12) becomes

$$\begin{aligned}&[I]\{\ddot{x}\} + [\lambda]\{\dot{x}\} + [\Delta^2]\{x\} = \\ &= -[\Phi]^T [M]\{I_b\}\ddot{u}_b(t) = -\{\Gamma\}\ddot{u}_b(t)\end{aligned} \tag{16}$$

where $\{\Gamma\}$ is the modal participation factor for the lowest "nf" eigenvectors, i.e.,

$$\{\Gamma\} = [\Phi]^T [M] \{I_b\} \quad (17)$$

## 3. NUMERICAL ANALYSIS

The UAV wing has been consider up of *100%* composite materials, e-glass type woven fabric is used. These are plain weave balanced fabrics with *0..90* degrees fiber orientation. For the matrix material epoxy is used. The airfoil is E197, the wingspan is *1000mm*, root chord length has *150mm*, and the end chord is *80mm* (figure 1). The wing has eleven ribs, two spars and two cylindrical reinforcement tubes.

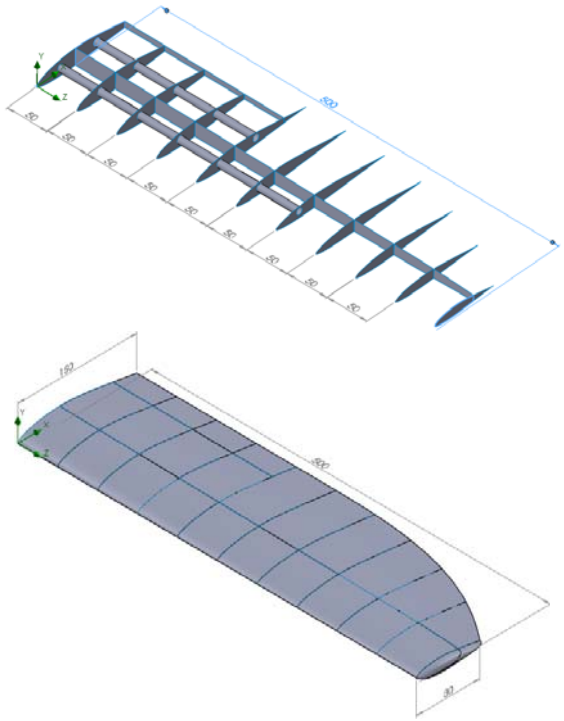

Figure 1 - The wing structure – geometry model

Shell and the ribs have three layers of fabric with a thickness of *0.36mm* and the rest of the resistance structure is made with 5 layers with a total thickness of *0.6mm*. Estimated total mass of the half-wing is *0.180kg*.

The fibers used in the UAV are plain weave fabrics (table 1), which have a complicated structure and detailed mesh scale models are required for the analysis (representative cell in figure 2).

Table 1

| | E-glass | Vinyl ester |
|---|---|---|
| $E_f$ longitudinal [GPa] | 73 | 3,4 |
| $\nu_f$ | 0,20 | 0,35 |

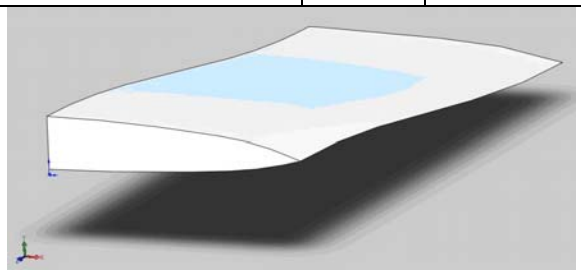

a - the wire of fabric

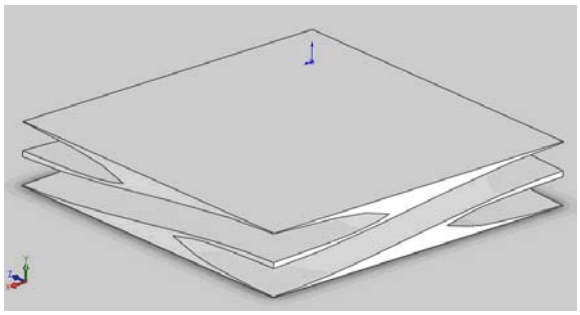

b - matrix

Figure 2 - The basic construction of the representative cell

A procedure for obtaining modules of elasticity and Poisson's ratio is to impose an average stress on cell faces, which leads to the following values of the equivalent mechanical constants for the representative cell.

Based on numerical and experimental determinations, resulting average values:

$$E_x = E_y = 12GPa \qquad E_z = 8GPa$$

$$v_{yz} = v_{xz} = 0.2 \qquad v_{xy} = 0.15$$

z axis being normal to the plane of the fabric. The density is $1800\frac{kg}{m^3}$.

Modal damping factor is $0.05$. In figure 3 is presented the base excitation law, in terms of time-acceleration. Shock begins at the $0.01s$ and ends at the $0.019s$. Maximum acceleration is 180g and lasts for a period of 0.007 s.

A triangle shell thin element with 6 nodes is used for meshing, with $2mm$ element size, resulting 184262 nodes and 92215 elements.

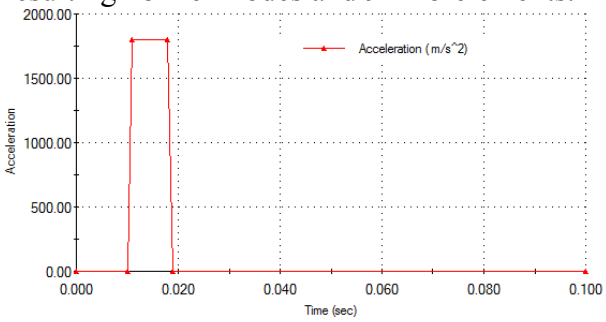


Figure 3 - The law of variation of the acceleration

There have been considered two cases of shock: one along the x-axis (as shown in Figure 3 - along the chord of the wing) and a shock along the y-axis (perpendicular to the chord).

In case of shock along the x-axis is observed the bending of the wing in longitudinal plane, maximum efforts being taken by the secondary longeron in interlocking area, the area who is stretched (Figure 4 - time $0.019s$ - at the end of the maximum acceleration). We are also observed compressive stress on the fuselage, in the area of the leading edge, near the symmetry plane of the wing.

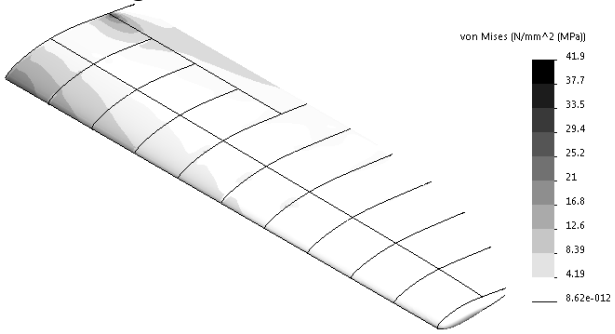


Figure 4 - Equivalent von Mises stress distribution on the wing for horizontal shock

Figure 5 presents the positions of nodes of interest, nodes where tensions take maximum values, all in the plane of symmetry. Node 2610 is positioned on the leading edge, 5457 on the upper side of the primary longeron, 6377 and 7883 on the upper side and underside of the secondary longeron. Figure 6 presents the variation in time of von Mises equivalent stress during shock, in specified nodes.

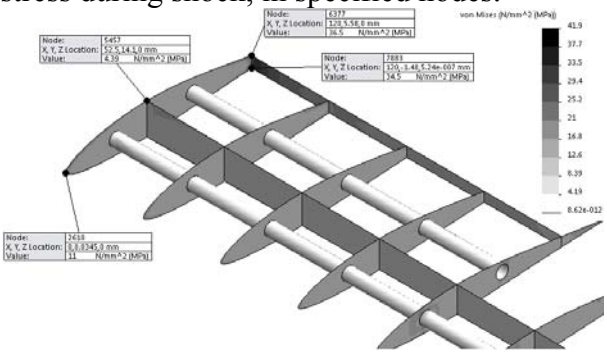

Figure 5 - The distribution of equivalent tensions on the strength structure and the position of the nodes of interest

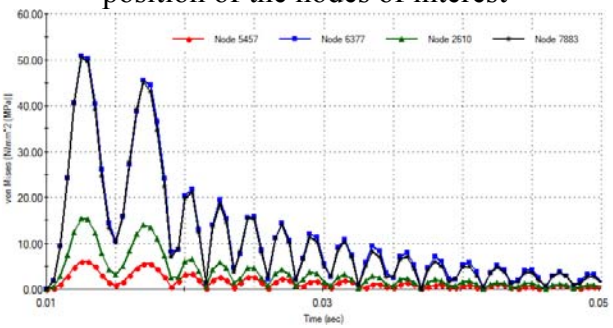


Figure 6 - Variation von Mises equivalent stress in the plane of symmetry

Be noticed close values of equivalent stress in secondary longeron, which undergoes the bending in the longitudinal plane of the wing. A high value of the stresses stands at joining between the main reinforcing bar and the last three of its ribs. In Figure 7 are the nodes of interest and in Figure 8 are presented variations of equivalent tensions in these nodes.

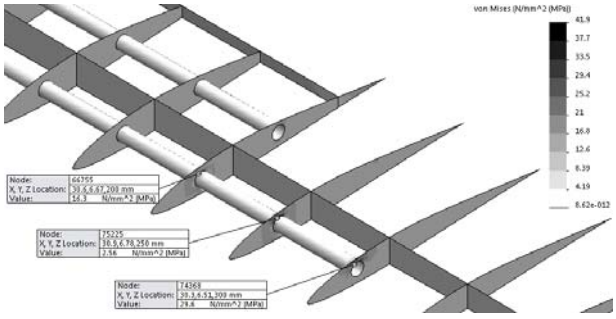

Figure 7 - Stress and nodes of interest in the main reinforcing bar

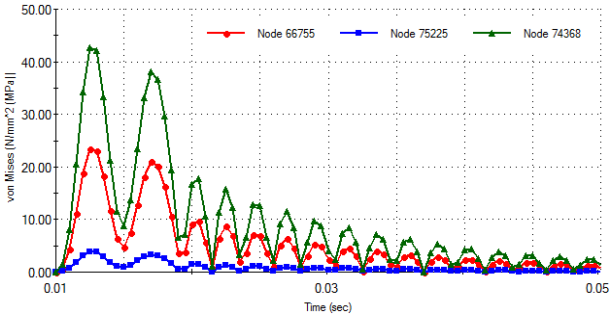


Figure 8 - Variation in time of equivalent von Mises stress

In case of vertical shock due to lower rigidity of the wing in this direction, the maximum stress are in the plane of symmetry (a catching wing), as shown in Figure 9 (time *0.019s*). In Figure 10 are shown stress of structural strength and positions of nodes which varies in time.

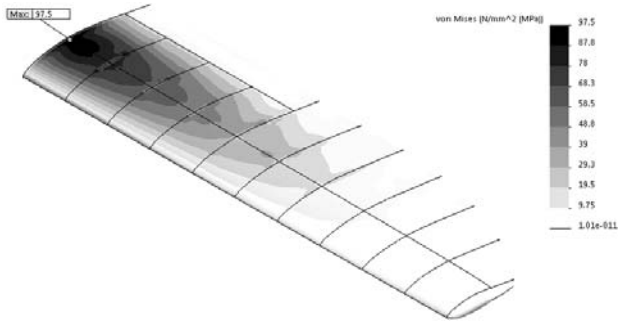

Figure 9 - Equivalent von Mises stress distribution on the wing for vertical shock

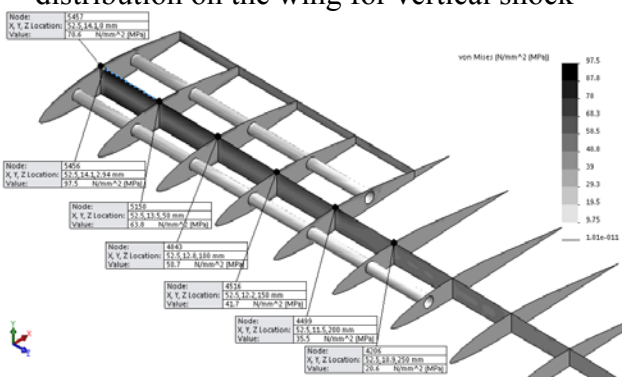

Figure 10 - Equivalent von Mises stress distribution on the structural strength and nodes of interest

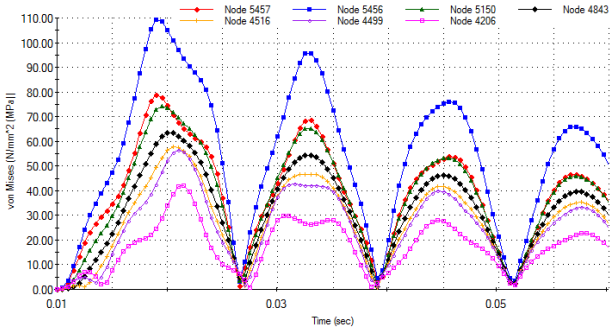


Figure 11 - Equivalent von Mises stress distribution on the structural strength and nodes of interest

We ascertain that the main longeron stress are the highest in the strength structure, the upper surface being stretched and compressed the underside. Stresses are highest in the plane of symmetry, decreasing towards the end of the wing.

## 4. CONCLUSIONS & ACKNOWLEDGMENT

Although vertical shock produce higher stress (dual in this case) compared with horizontal shock, in case of UAVs are very unlikely to occur with acceleration size used in shaping. In the case of horizontal shock, stresses produced are six times lower than the experimentally determined fracture stress ($310-330MPa$). In shaping, however, not taken into consideration the delamination, which can occur in the most requested, the maximum stress exceeds fracture stress of the resin.

This paper has been financially supported within the project entitled "Horizon 2020 - Doctoral and Postdoctoral Studies: Promoting the National interest through Excellence, Competitiveness and Responsibility in the Field of Romanian Fundamental and Applied Scientific Research", contract number POSDRU/159/1.5/S/140106. This project is

co-financed by European Social Fund through Sectorial Operational Programme for Human Resources Development 2007 - 2013. Investing in people!

## REFERENCES

1. Geier, M., Duedal, D., *Guide practique des materiaux composites.* Technique et Documentation Lavoisier, Paris, 1985.
2. Reddy, J. N., *Mechanics of Composites Structures Issue.* Mc Graw Hill, New York, 1980.
3. Constantinescu, I.N., Picu, C., Hadăr, A., Gheorghiu, H., *Rezistența materialelor pentru ingineria mecanică,* Editura BREN, București, 2006.
4. User Guide – Advance Module – CosmosM.

"HENRI COANDA"
AIR FORCE ACADEMY
ROMANIA

"GENERAL M.R. STEFANIK"
ARMED FORCES ACADEMY
SLOVAK REPUBLIC

INTERNATIONAL CONFERENCE of SCIENTIFIC PAPER
AFASES 2015
Brasov, 28-30 May 2015

# DYNAMIC ANALYSIS OF COMPOSITE WINGS

**Bogdan-Alexandru Belega*, Amado Ştefan***

*Military Technical Academy, Bucharest, Romania

***Abstract:*** *The present paper has been designed to geometrical modelling and FEM structural analysis of fiber glass/epoxy wing airframe. It presents a dynamic analysis of wing endured at two shocks, one horizontal and one vertical, with the same law of variation of the acceleration. During the simulation, the law of variation of the acceleration was used for symmetrical wing section that is recessed.*

***Keywords:*** *airfoil, plain weave, E-glass, airframe, FEM, shock*

## 1. INTRODUCTION

Plastics reinforced with glass fibers were used for the first time due to their outstanding qualities compared to conventional materials, 60 years ago.

Increasingly high performance required of strength structures generally, especially those for aeronautics and military applications require very severe condition during their operation.

Priorities are the considerations functional optimization of aerodynamic at profiles aeronautical structures and satisfying the restrictive conditions related to: special mechanical strength in a broad range of the environmental temperature, vibration, fatigue, stiffness, minimum weight and maximum reliability.

For the case of UAVs, in their construction it is used particularly balsa wood, which has a good resistance in flight conditions and is also characterized by a low weight. The disadvantage of this construction occurs when the UAV has a shock due to a crash or other similar situations. The use of composite materials based on fiber glass (carbon, Kevlar) although they have a higher density than wood, lead to the structural resistance much higher in case of shocks.

## 2. THEORETICAL ASPECTS

**2.1 Important equations.** The process of approximating the solution of the equations of motion by considering only the first few modes of the system's natural frequencies is called normal mode or modal superposition analysis and in the Advanced Dynamic Module, all forced vibration response problems are based on this procedure.

The equations of motion for a linear dynamic system are:

$$[M]\{\ddot{u}\}+[C]\{\dot{u}\}+[K]\{u\}=\{f(t)\} \qquad (1)$$

where: $[M]$ is mass matrix, $[C]$ is damping matrix, $[K]$ is stiffness matrix, $\{f(t)\}$ is time varying load vector and are the displacement, velocity, and acceleration vectors, respectively.

For linear dynamic problems, the system of equations of motion (1) can be decoupled into "nf" single degree of freedom equations in

terms of the modal displacement vector $\{x\}$, where:

$$\{u\} = [\Phi]\{x\} \tag{2}$$

and $[\Phi]$ is the matrix of the lowest "nf" eigenvectors obtained from the solution of:

$$[K]\{u\} = \omega^2 [M]\{u\} \tag{3}$$

Substituting for $\{u\}$ from (2) into (1) and pre-multiplying it by $[\Phi]^T$ , will yield:

$$\begin{aligned}&[\Phi]^T [M][\Phi]\{\ddot{x}\} + [\Phi]^T [C][\Phi]\{\dot{x}\} + \\ &+ [\Phi]^T [K][\Phi]\{x\} = [\Phi]^T \{f(t)\}\end{aligned} \tag{4}$$

With the mode shapes satisfying the orthogonality conditions, (4) becomes:

$$[I]\{\ddot{x}\} + [\lambda]\{\dot{x}\} + [\Delta^2]\{x\} = [\Phi]^T \{f(t)\} \tag{5}$$

Equation (5) represents "nf" uncoupled single degree of freedom (second-order differential) equations as shown below:

$$\ddot{x}_i + 2\xi\dot{x}_i + \omega_i^2 x_i = \{\phi\}_i^T \{f(t)\} \tag{6}$$

These equations can be evaluated using step-by-step integration or other techniques, and the displacements {u} and other system responses can then be determined by performing the transformation shown in equation (2).

**2.2 Damping Effects.** The damping matrix $[C]$ is assumed to satisfy the orthogonality conditions. It should be noted that in the majority of cases, (a) the exact damping matrix is unknown, and (b) the effect of any non-orthogonality is usually small. In the Post Dynamic module, the following damping options are available.

*Rayleigh damping* is of the form:

$$[C] = \alpha[M] + \beta[K] \tag{7}$$

This form of $[C]$ is orthogonal with respect to the system eigenvectors and the modal damping coefficient for the $i^{th}$ mode $C_i$ may be calculated:

$$C_i = 2\xi_i\omega_i = \alpha + \beta\omega_i^2 \tag{8}$$

and in terms of the modal critical damping ratio

$$\xi_i = \frac{\alpha}{2\omega_i} + \frac{\beta\omega_i}{2} \tag{9}$$

where $\alpha$ and $\beta$ are the Rayleigh damping coefficients.

*Modal damping* is defined as a fraction of critical damping

$$\xi_i = \frac{C_i}{C_c} \tag{10}$$

**2.3 Modal Acceleration Method (MAM) in Time History.** The process of mode truncation, as was explained before, introduces some error in the response. The Modal Acceleration Method (MAM), in the Time History Analysis, approximates the effects of the truncated modes by their equivalent static effects. This approximation can be expressed for the displacement by:

$$U_c = [K]^{-1}\{R_c\}$$

where, $K$ is the structural stiffness matrix and $R_c$ represents the static loading. It can be shown that this static load vector can be computed in terms of the included modes, according to:

$$R_c = \left[I - M\Phi\Phi^T\right]\{P(T)\} \tag{11}$$

where, $M$ and $\Phi$ are the mass matrix and modal matrix, respectively, $\{P(t)\}$ is the applied dynamic load, and $\Phi^T$ is the mass matrix transpose. Thus by considering only a few numbers of modes, for even very complicated geometry, it can evaluate the response accurately.

**2.4 Uniform Translational Base Motion.** The equations of motion for a linear dynamic system with uniform base acceleration $\ddot{u}_b(t)$, can be written as:

$$[M]\{\ddot{u}_r\} + [C]\{\dot{u}_r\} + [K]\{u_r\} = \{f_e(t)\} \tag{12}$$

where $\{u_r\}$ is the structure displacement relative to the base, and $\{f_e(t)\}$ is an effective load due to the base motion:

$$\{f_e(t)\} = -[M]\{I_b\}\ddot{u}_b(t) \tag{13}$$

The vector $\{I_b\}$ is an influence vector relating base motion to rigid body structure displacements according to:

$$\{U\} = \{u_r\} + \{I_b\}u_b(t) \tag{14}$$

As previously described, (12) can be transformed into uncoupled equations in terms of the modal displacements $\{x\}$ where:

$$\{u_r\} = [\Phi]\{x\} \tag{15}$$

and the equation of motion (12) becomes

$$\begin{aligned}&[I]\{\ddot{x}\} + [\lambda]\{\dot{x}\} + [\Delta^2]\{x\} = \\ &= -[\Phi]^T [M]\{I_b\}\ddot{u}_b(t) = -\{\Gamma\}\ddot{u}_b(t)\end{aligned} \tag{16}$$

where $\{\Gamma\}$ is the modal participation factor for the lowest "nf" eigenvectors, i.e.,

$$\{\Gamma\} = [\Phi]^T [M] \{I_b\} \quad (17)$$

## 3. NUMERICAL ANALYSIS

The UAV wing has been consider up of *100%* composite materials, e-glass type woven fabric is used. These are plain weave balanced fabrics with *0..90* degrees fiber orientation. For the matrix material epoxy is used. The airfoil is E197, the wingspan is *1000mm*, root chord length has *150mm*, and the end chord is *80mm* (figure 1). The wing has eleven ribs, two spars and two cylindrical reinforcement tubes.

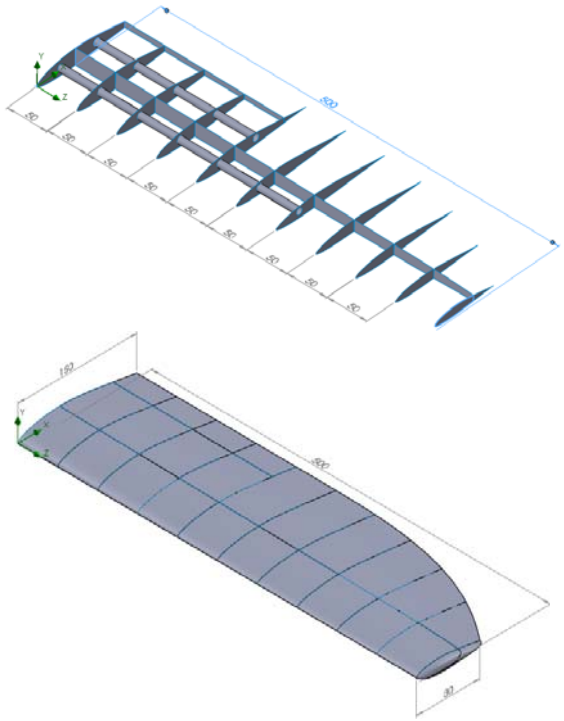

Figure 1 - The wing structure – geometry model

Shell and the ribs have three layers of fabric with a thickness of *0.36mm* and the rest of the resistance structure is made with 5 layers with a total thickness of *0.6mm*. Estimated total mass of the half-wing is *0.180kg*.

The fibers used in the UAV are plain weave fabrics (table 1), which have a complicated structure and detailed mesh scale models are required for the analysis (representative cell in figure 2).

Table 1

| | E-glass | Vinyl ester |
|---|---|---|
| $E_f$ longitudinal [GPa] | 73 | 3,4 |
| $\nu_f$ | 0,20 | 0,35 |

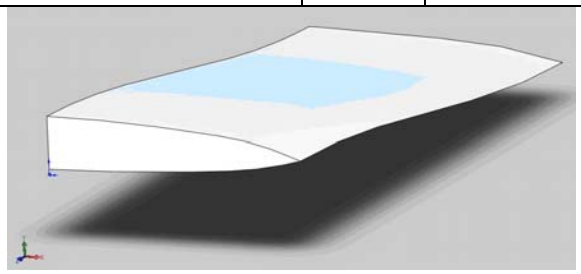

a - the wire of fabric

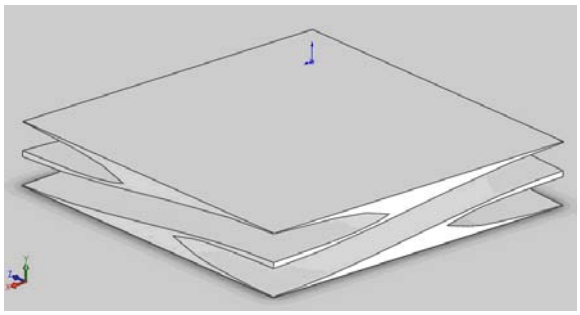

b - matrix

Figure 2 - The basic construction of the representative cell

A procedure for obtaining modules of elasticity and Poisson's ratio is to impose an average stress on cell faces, which leads to the following values of the equivalent mechanical constants for the representative cell.

Based on numerical and experimental determinations, resulting average values:

$$E_x = E_y = 12GPa \qquad E_z = 8GPa$$

$$v_{yz} = v_{xz} = 0.2 \qquad v_{xy} = 0.15$$

z axis being normal to the plane of the fabric. The density is $1800\frac{kg}{m^3}$.

Modal damping factor is $0.05$. In figure 3 is presented the base excitation law, in terms of time-acceleration. Shock begins at the $0.01s$ and ends at the $0.019s$. Maximum acceleration is 180g and lasts for a period of 0.007 s.

A triangle shell thin element with 6 nodes is used for meshing, with $2mm$ element size, resulting 184262 nodes and 92215 elements.

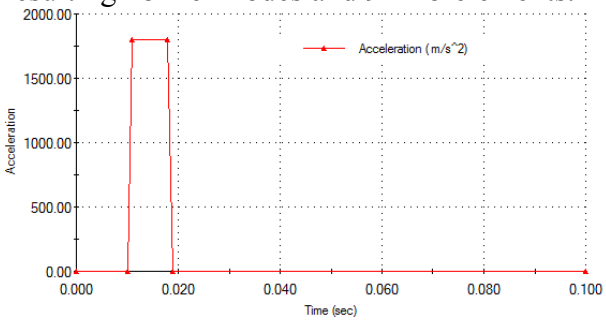


Figure 3 - The law of variation of the acceleration

There have been considered two cases of shock: one along the x-axis (as shown in Figure 3 - along the chord of the wing) and a shock along the y-axis (perpendicular to the chord).

In case of shock along the x-axis is observed the bending of the wing in longitudinal plane, maximum efforts being taken by the secondary longeron in interlocking area, the area who is stretched (Figure 4 - time $0.019s$ - at the end of the maximum acceleration). We are also observed compressive stress on the fuselage, in the area of the leading edge, near the symmetry plane of the wing.

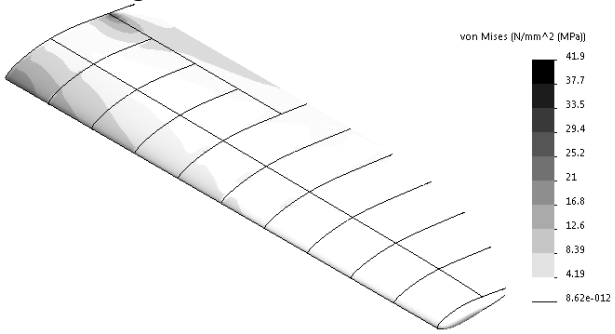


Figure 4 - Equivalent von Mises stress distribution on the wing for horizontal shock

Figure 5 presents the positions of nodes of interest, nodes where tensions take maximum values, all in the plane of symmetry. Node 2610 is positioned on the leading edge, 5457 on the upper side of the primary longeron, 6377 and 7883 on the upper side and underside of the secondary longeron. Figure 6 presents the variation in time of von Mises equivalent stress during shock, in specified nodes.

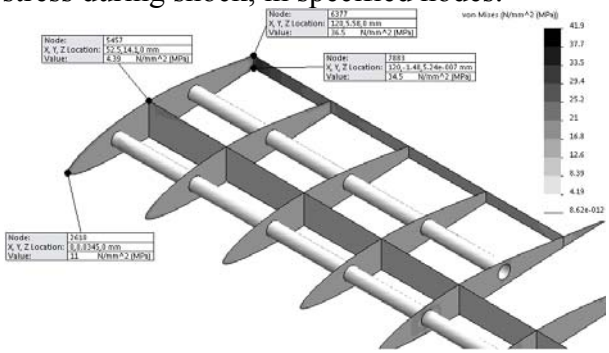

Figure 5 - The distribution of equivalent tensions on the strength structure and the position of the nodes of interest

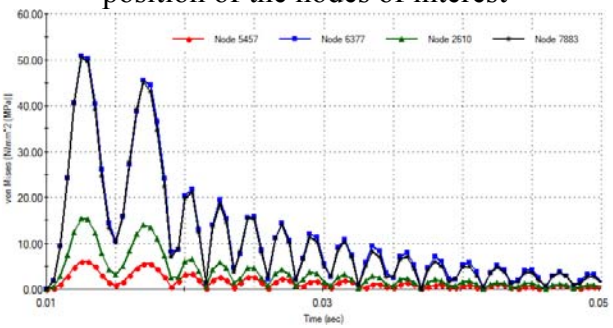


Figure 6 - Variation von Mises equivalent stress in the plane of symmetry

Be noticed close values of equivalent stress in secondary longeron, which undergoes the bending in the longitudinal plane of the wing. A high value of the stresses stands at joining between the main reinforcing bar and the last three of its ribs. In Figure 7 are the nodes of interest and in Figure 8 are presented variations of equivalent tensions in these nodes.

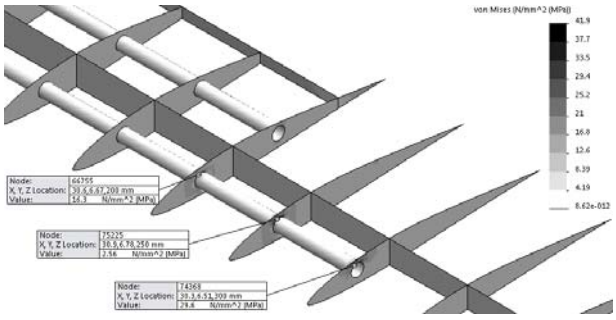

Figure 7 - Stress and nodes of interest in the main reinforcing bar

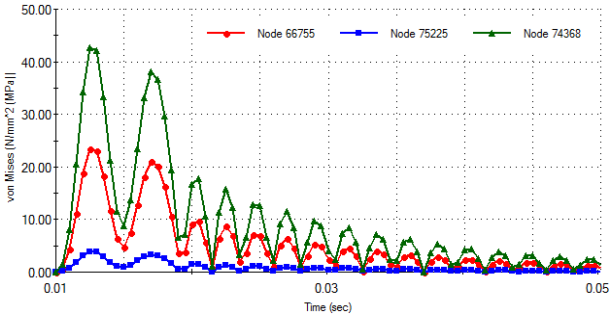


Figure 8 - Variation in time of equivalent von Mises stress

In case of vertical shock due to lower rigidity of the wing in this direction, the maximum stress are in the plane of symmetry (a catching wing), as shown in Figure 9 (time *0.019s*). In Figure 10 are shown stress of structural strength and positions of nodes which varies in time.

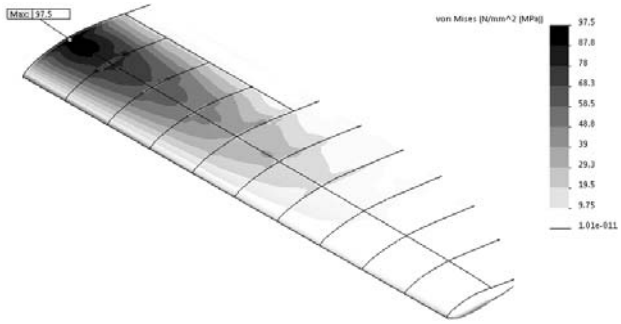

Figure 9 - Equivalent von Mises stress distribution on the wing for vertical shock

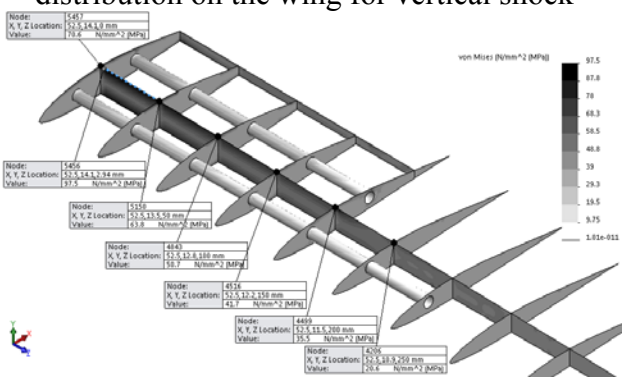

Figure 10 - Equivalent von Mises stress distribution on the structural strength and nodes of interest

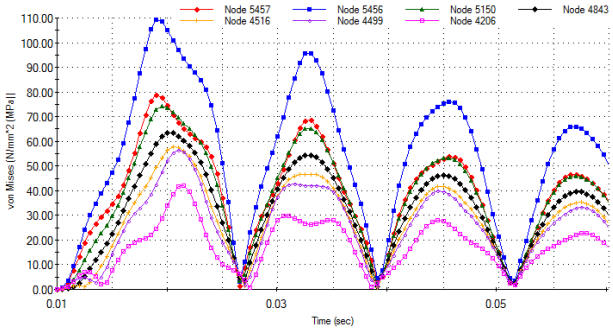


Figure 11 - Equivalent von Mises stress distribution on the structural strength and nodes of interest

We ascertain that the main longeron stress are the highest in the strength structure, the upper surface being stretched and compressed the underside. Stresses are highest in the plane of symmetry, decreasing towards the end of the wing.

## 4. CONCLUSIONS & ACKNOWLEDGMENT

Although vertical shock produce higher stress (dual in this case) compared with horizontal shock, in case of UAVs are very unlikely to occur with acceleration size used in shaping. In the case of horizontal shock, stresses produced are six times lower than the experimentally determined fracture stress ($310-330MPa$). In shaping, however, not taken into consideration the delamination, which can occur in the most requested, the maximum stress exceeds fracture stress of the resin.

This paper has been financially supported within the project entitled "Horizon 2020 - Doctoral and Postdoctoral Studies: Promoting the National interest through Excellence, Competitiveness and Responsibility in the Field of Romanian Fundamental and Applied Scientific Research", contract number POSDRU/159/1.5/S/140106. This project is

co-financed by European Social Fund through Sectorial Operational Programme for Human Resources Development 2007 - 2013. Investing in people!

## REFERENCES

1. Geier, M., Duedal, D., *Guide practique des materiaux composites.* Technique et Documentation Lavoisier, Paris, 1985.
2. Reddy, J. N., *Mechanics of Composites Structures Issue.* Mc Graw Hill, New York, 1980.
3. Constantinescu, I.N., Picu, C., Hadăr, A., Gheorghiu, H., *Rezistența materialelor pentru ingineria mecanică,* Editura BREN, București, 2006.
4. User Guide – Advance Module – CosmosM.

"HENRI COANDA"
AIR FORCE ACADEMY
ROMANIA

"GENERAL M.R. STEFANIK"
ARMED FORCES ACADEMY
SLOVAK REPUBLIC

INTERNATIONAL CONFERENCE of SCIENTIFIC PAPER
AFASES 2015
Brasov, 28-30 May 2015

# CHARACTERISTICS OF SLUDGE RESULTED FROM BALL-BEARINGS RECTIFICATION

**Ion Dinescu**

*Faculty of Aeronautical Management, "Henri Coandă" Air Force Academy, Brasov, Romania

***Abstract:*** *The paper is presenting some of the researches made on sludge resulted after a processing of ball bearings, by grinding. Due to the high quantity of sludge, it must be considered the power which can result, because it is already there. The power from ball-bearing steel is compared with powders produced by famous companies from the world.*

***Keywords:*** *sludge, powder, ball-bearing, rectification.*

## 1. INTRODUCTION

As a result of processing of the component parts from a ball-bearing, there is resulting an important amount of sludge. This sludge is containing particles detached from the rectified piece and also granules from the abrasive disk.

Nearby these components, which are in solid state, the sludge is containing also a fluid component coming from the cooling fluid. But the most important component is from ball-bearings steel, which is a medium alloyed steel containing a high level of carbon.

Missile aeromechanics technologies have benefits that include enhanced flight performance, reduced weight, increased Mach number, reduced cost, higher reliability, and reduced observables [6].

In the following passages there are presented some characteristics of the sludge resulted from working processes

## 2. HOW TO OBTAIN THE POWDER

The studies sludge is obtained during the grinding of the components from the ball-bearings. Grinding is a technological proceeding where the surfaces of features are treated with the help of grinding stones, with the purpose of obtaining a precise dimension and higher quality of the surface.

Grinding stock is eliminated through very fine splinters. Fineness is depending on: grinding regime, cutting oil, working material, and the characteristics of grinding stones (hardness, binding matter, and granulation). During rectification, the grinding stones are working as the milling cutter. The difference between these two is that according to the tooth of milling cutter, hard grains are dispersed in an arbitrary manner, and this working with very different departure angle [1]. This can be observed in figure 1.

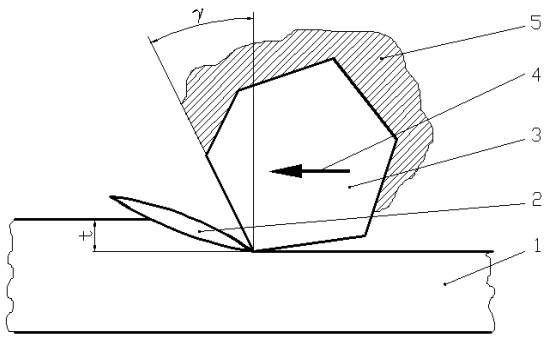


1 – feature; 2 – splinter; 3 – grain; 4 – binding matter; 5 – direction of cutting;
γ – departure angle; t – cutting depth.

**Fig. 1.** The geometry of cutting with abrasive grains

Because most of grains are cutting with different departure angles, in the cut surfaces we will find plastically deformations which will influence the sludge quality. For this study it was used a sludge resulted from rough-grinding and roughing.

The sludge is containing the following elements: [2, 4]

- *particles from the grinding stone*; these particles are $SiO_2$, carbides, and are very hard; these there are influencing, in a certain way, the characteristics of the powder obtained from the sludge;
- *grinding compound*; this fluid, normally, is containing a water emulsion and has the role of preventing the overheating of the feature, evacuation of falling splinters and grains, and decreasing of friction;
- *splinters from the piece*, in fact splinters from steel for ball-bearings.

Ball-bearing steels are alloyed steels, with a high percentage of carbon. The chemical composition of ball-bearing steel (RUL) are presented in Table 1.

**Table 1**. The chemical composition of ball-bearing steels (RUL) according to STAS

| **Steel** | **Chemical composition**, [%] | | | | | | | |
|---|---|---|---|---|---|---|---|---|
| | **C** | **Mn** | **Si** | **Cr** | **S** [max.] | **P** [max.] | **Ni** [max.] | **Cu** [max.] |
| RUL 1 | 0.95-1.10 | 2.20-0.45 | 0.17-0.37 | 1.30-1.65 | 0.20 | 0.027 | 0.30 | 0.25 |
| RUL 2 | 0.95-1.10 | 0.90-1.20 | 0.40-0.65 | 1.30-1.65 | 0.20 | 0.027 | 0.30 | 0.25 |

## 3. THE CHEMICAL COMPOSITION OF THE POWDER

The chemical composition and the purity of powders are depending on working material and the technological processes for fabrication [3]. The obtained powder of the sludge from ball-bearings is containing impurities like:

- hard grains from the grinding stone;
- textile residues, thrown by the workers on the gathering belt;
- film around the splinter, film which is coming from the cooling-fluid;
- particles coming from the bounding material used when the abrasive disk was made .

The impurities can generate different influences:

- *a negative one*: modifies pressability, is griping matrix, is providing deformations during sinterisation, there are resulting chemical reactions during sinterisation; these are diminishing the final properties of features;
- *a positive one*: less often by increasing the hardness of features.

The percentage of impurities in sludge is about 14-16% depending on the type of working, smoothing, grinding, finish grinding.

The chemical composition of the sludge is depending on working material (ball-bearing steel) grinding regime. At the smoothing grinding the percentage of hard abrasive particles is higher as with finish-grinding, but it is also depending on the processing where the sludge is transformed in powder.

The sludge obtained with ball-bearings processing is containing a series of elements. These are presented in Table 2. [1, 3, 5]

**Table 2.** Chemical composition of sludge

| **The type of sludge** | **Chemical composition**, [%] | | | | | | | | | |
|---|---|---|---|---|---|---|---|---|---|---|
| | **C** | **Mn** | **Cr** | **Ni** | **Cu** | **Al** | **Si** | **P** | **S** | **Loss of mass in $H_2$** |
| From smoothing grinding | 0.90 | 0.33 | 1.74 | 0.21 | 0.76 | 2.64 | 1.90 | 0.03 | 0.03 | 6.98 |
| Finishing grinding | 0.72 | 0.33 | 1.74 | 0.21 | 0.66 | 2.62 | 1.70 | 0.03 | 0.03 | 4.33 |

This percentage presented in Table 2 can be explained like this:

- smoothing grinding is leading to a higher quantity of impurities, which, at their turn, are increasing the percentage of carbon, silicon, aluminum, cooper;
- in the case of finishing grinding impurities can be found in a lower degree;
- when, from the sludge, there are separated abrasive particles, then the percentage of carbon is decreasing till 0.40%-0.60% and silicon it's almost reaching the normal limits of RUL steel, and aluminum it is also substantially decreasing till 1%.

Researches on sludge were made with spectral-chemical analysis, with the help of Spectrograph Q24 – with a prism, produced by Carl Zeiss Company – Germany.

## 4. THE POWDER HUMIDITY

An important characteristic for further processing of sludge is humidity.

This was determined as following:

- 100g of sludge ($m_0$=100g) was weight with analytical balance;
- the sludge was dried in oven at temperature of 170ºC;
- the dry sludge was weight ($m_1$) and calculated the humidity (u) with the relation 1.1. [5]

$$u = \frac{m_0 - m_1}{m_0} \times 100, \ [\%] \qquad (1.1)$$

The sludge humidity has got the values between 42% and 48% (u=42-48%) and in is depending on different factors, for example:

- the place where sludge is collected, collecting band or filtrate;
- the nature of cooling fluid used for grinding.

The humidity isn't influencing the chemical composition, the chemical properties or other characteristics of powder, because at the high temperature of soaking, the possible oil residue what remains, will be burned out.

## 5. THE CHEMICAL COMPOSITION OF THE POWDER

To be able to use the powder incorporated in the sludges, this must come to a technological process. The powder chemical composition depends, evidently, on the sludge's composition. The sludge processing will result in a changing of percentage for a few elements.

The results of the chemical analysis are presented in the Table 3.

Unseparated powder is representing the powder from where impurities were not separated, and separated powder is representing the powder from where impurities were cleaned [4, 5].

**Table 3.** Chemical composition of powder

| Powder | C | Cr | Ni | Mn | Al | Cu | Si | P | S | $O_2$ |
|---|---|---|---|---|---|---|---|---|---|---|
| | [%] | | | | | | | | | |
| Unseparated | 0.57 | 1.74 | 0.21 | 0.33 | 2.32 | 0.50 | 1.60 | 0.027 | 0.01 | 0.36 |
| Separated | 0.40 | 1.74 | 0.20 | 0.31 | 1.84 | 0.45 | 1.40 | 0.014 | 0.001 | 0.20 |

As a comparison between powders produced by prestigious companies from all over the world and the chemical composition of these powders obtained from the sludge resulted from ball-bearings, there is presented in Table 4 [2, 5].

**Table 4.** Chemical composition from different powders

| Different powders | C | Cr | Ni | Mn | Al | Cu | Si | P | S | $O_2$ |
|---|---|---|---|---|---|---|---|---|---|---|
| | [%] | | | | | | | | | |
| RUL Separated | 0.40 | 1.74 | 0.20 | 0.31 | 1.84 | 0.45 | 1.40 | 0.014 | 0.001 | 0.20 |
| FREM 400-24 | 0.05 | - | - | 0.40 | - | - | 0.35 | 0.02 | 0.02 | 0.50 |
| ULTRPAC A | 0.02 | - | 1.75 | 0.20 | - | 1.50 | 0.05 | 0.02 | 0.01 | 0.22 |
| NC 100-24 | 0.02 | - | - | - | - | - | 0.25 | - | - | 0.30 |
| ATOMET 4601 | 0.003 | 0.05 | 1.8 | 0.20 | - | 0.02 | 0.003 | 0.01 | 0.01 | 0.10 |
| SUMIRON 4100 S | 0.008 | 0.93 | - | 0.69 | - | - | 0.002 | - | - | 0.08 |
| RZ 400 | 0.03 | - | - | 0.25 | - | - | 0.10 | 0.03 | 0.02 | 0.35 |

As we can observe it from Table 4, RUL powder separated is similar from chemical point of view with powders produced by famous companies from the world. [2, 3, 5]

## 6. CONCLUSIONS & ACKNOWLEDGMENT

With grinding of ball-bearings there is resulting an important amount of sludge. This sludge is mostly containing splinters from the rectified part, and also some impurities.

By detaching these impurities there can be obtained a powder, from ball-bearing steel, which from chemical point of view is similar to powders produced by famous companies in the world.

## REFERENCES


1. Dinescu, I. *Investigations about the determination of the powder's physical properties which result from the processing bearings*, Bulletin of the Transylvania University of Brasov, Romania, Series A, Vol. XXXII, 1990.
2. Dinescu, I., Maniu, Al. *Investigations about the pressability of the powder result from the processing bearings*, Bulletin of the Transylvania University of Brasov, Romania, Series A, Vol. XXXII, 1990.
3. Dinescu, I. *Researches on the powders resulting from ball-bearing rectification*, Proceedings First International Conference on Materials and Manufacturing Technologies, MATEHN '94, Technical University of Cluj-Napoca, Romania, 18-20 May, 1994, p. 385-390.
4. Dinescu, I., s.a. *Theoretical and Practical Researcher concerning New Recycling Technologies for Steel Powder from the Sludge Obtained after Rectifing Bearing Elements*, Second International Conference on The Recycling of Metals, Organized by the European of ASM International Europe and its Recycling Division, Amsterdam, Nederland, 19-21 October, 1994, p. 295-304.
5. Dinescu, I. *Characteristics of powder resulted from ball-bearing steel processing*, Proceedings of the International Conference on Powder Metallurgy, RoPM '96, Technical University of Cluj-Napoca, Romania, 4-7 July, 1996, ISBN 973-97485-5-4, p. 205-208.
6. Prisacariu V., *The aerodynamic analysis of the profiles for flying wings,* Journal of Defense Resources Management, vol.4 Issue 1(6)/2013, ISSN:2068-9403, eISSN: 2247-6466, ISSN-L:2247-6466, p.211-218.

"HENRI COANDA"
AIR FORCE ACADEMY
ROMANIA

"GENERAL M.R. STEFANIK"
ARMED FORCES ACADEMY
SLOVAK REPUBLIC

INTERNATIONAL CONFERENCE of SCIENTIFIC PAPER
AFASES 2015
Brasov, 28-30 May 2015

# DYNAMIC MECHANICAL ANALYSIS OF AN AIRCRAFT WING WITH EMPHASIS ON VIBRATION MODES CHANGE WITH LOADING

**Lica Flore*, Albert Arnau Cubillo****

*Institute for Theoretical and Experimental Analysis of Aero-Astronautical Structures STRAERO S.A., Bucharest, Romania, **Politehnica University of Bucharest, Romania

***Abstract:*** *This paper presents the results of a study of the dynamical behavior on an aircraft wing structure. The study has consisted in a set of dynamical tests in which the vibration parameters of the structure have been determined. The aim of this research is dual: to study the viability of performing vibration testing with strain gages instead of accelerometers and to determine the change in the dynamic behavior of the structure when loading is applied. The report presents the conclusions derived from the analysis of the generated data correlating the results with the available structural theory.*

***Keywords:*** *dynamic testing, strain gage, ground vibration test, modal analysis, jump phenomena*

## 1. INTRODUCTION

Dynamic testing is an extended practice in aviation certification whenever any changes are performed on an aircraft that change its structural behavior. These tests are usually referred to as Ground Vibration Testing or GVT.

The purpose of GVT is to validate and improve the structural dynamic models. This is performed through the experimental determination of the low-frequency vibration modes. These models are later used to predict dynamic aero-elastic behavior and plan the safety-critical flight testing phase. [2, 7]

Basically, two techniques are used to determine the vibration modes of a structure. A first technique is the phase-resonance method; in this approach a sine force is applied through one or multiple shakers at a single frequency in order to excite the structure at each of its natural frequencies at a time. When such condition is met, the structure acts like a single degree of freedom (DOF) system. [8]

Another, newer, approach is to use phase-separation techniques; these methods allow for the extraction of the different frequency response functions (FRF) of a structure simultaneously while using random excitation in one or more shakers. [10]

Because of the extra complexity that the phase-separation techniques present and provided that the sufficient testing time has been available, the method used to study the structure has been the phase-resonance method using one shaker. This allowed for increased precision in the results with lower post-processing complexity.

It is one of the main focuses of the article to determine if the results obtained through GVT can be obtained with the use of strain gages instead of accelerometers. This presents an advantage provided that the use of gages is

more economical. Such application of strain gages has been considered in [4].

Moreover, the aim of the study is to determine the change in the dynamic behavior of the structure as loading is applied, intending to simulate the real operating conditions of the aircraft. This analysis could be relevant in further study of aero-elastic phenomena. The available bibliography predicts an increase in frequency in the vertical vibration modes and a decrease in the torsion modes. [1] The study of the lagging modes is not in the scope of this research because they do not significantly influence the aero-elastic effects.

## 2. EQUIPMENT USED AND TEST CONFIGURATION

During the experiments performed on the studied wing, two acquisition systems have been used to monitor the dynamic behavior of the structure. The systems used have been the Prodera installation and the HBM installation.

**2.1 Prodera installation.** The Prodera installation is the modal analysis equipment that uses 16 unidirectional accelerometers simultaneously to determine the vibration parameters of a structure. Its software allows modeling the experiment configuration in order to provide graphical representation during or after each test. This system features also post-processing tools that allows calculating the parameters of a vibration mode using the phase-resonance method.

**2.2 HBM installation.** Parallel to the Prodera installation, another acquisition system has been used in order to provide redundancy in the measures to validate the results obtained with Prodera; and also to monitor the dynamic tests using the strain gages embedded in the structure. The HBM installation has been used with 3 accelerometers of type B&K model 4507B005 and 34 strain gauges.

**2.3 Test specimen.** The studied structure is an IAR-99 aircraft wing structure. The specimen has been tested without control surfaces installed and with the lower surface inspection hatches removed. No pods for external equipment have been mounted at the time of the test either. The structure has been tested vertically and excited with a 200N shaker mounted in the horizontal direction (vertical in relation to the wing).

Despite the position of the wing during testing, the vertical direction for the wing is considered as if the wing was mounted on an aircraft horizontally. The vertical modes refer to the flapping modes of the wing.

The wing has been tested by clamping the wing-fuselage attachments to a steel base on the ground that can be considered rigid.

The static loading has been applied using a spring. This allowed for the loading of the structure with the minimum influence on the vibration modes because the mechanism is flexible. A drawing of the tested model is shown in Figure 1.

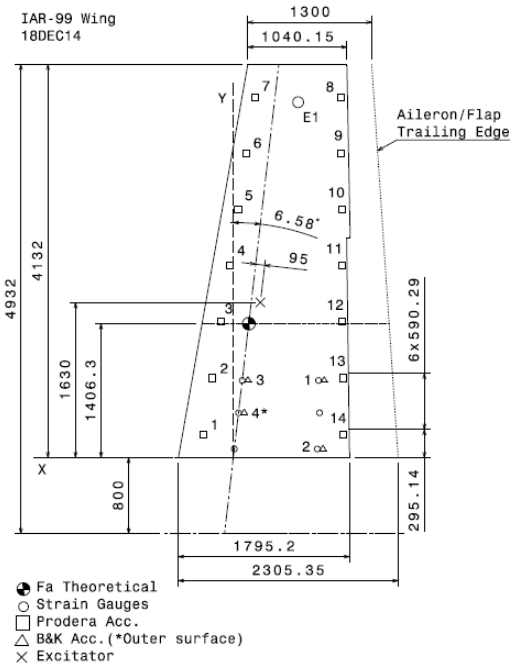


**Figure 1.** Design of the tested wing and location of the analyzed sensors.

**2.4 Sensor locations.** The distribution of the accelerometers is shown in Figure 1. The 16 accelerometers in the Prodera installation are located on the inner surface of the wing at equal distance from the wing root to determine the different mode shapes of the structure. The accelerometers linked to the spider acquisition system (HBM) are located both in the inner and outer surfaces; the gages are installed in the outer and inner surfaces and also in some internal structural elements.

## 3. EXPERIMENTAL RESULTS

Different dynamic testing has been performed on the wing structure in order to determine the vibration parameters for the different modes. This testing is presented divided according to the loading of the wing at each test. Two test cases have been considered to establish a correlation between the modal frequencies and the loading of the wing.

The results have been post-processed using respectively Prodera and HBM Catman software [5] in order to determine mode shape, frequency, damping factor and generalised mass for each vibration mode. In order to calculate these parameters the complex power method has been used in Prodera [6].

**3.1 Tests without loading.** A first set of tests has been performed without any loading on the wing in order to determine the vibration modes of the structure as a reference for further analysis. This has been the most extensive loading case in terms of number of tests because the different vibration modes have been analyzed. The viability of using strain gages in dynamic analysis is studied with no loading. The average results for the tests without loading are presented in Table 1.

**Table 1** Average testing results obtained without loading.

| | 1st mode | 2nd mode | 3rd mode | 4th mode |
|---|---|---|---|---|
| Type | Bending | Bending | Torsion | n/a |
| Freq. | 9.61Hz | 47.11Hz | 50.27Hz | 98.72Hz |
| $\gamma$ | 0.0233 | 0.0072 | 0.010 | n/a |
| $\tilde{\mu}$ | 746kgm$^2$ | 431kgm$^2$ | 288kgm$^2$ | n/a |

**3.2 Tests at 1.5kN loading.** The maximum loading that has been applied to the structure has been the operational limit of the spring used. The obtained results are shown in Table 2.

**Table 2** Average testing results for the loading case at 1.5kN.

| | 1st mode | 2nd mode | 3rd mode | 4th mode |
|---|---|---|---|---|
| Type | Bending | Bending | Torsion | n/a |
| Freq. | 11.25Hz | 49.49Hz | 50.81Hz | n/a |
| $\gamma$ | 0.0169 | 0.0065 | n/a | n/a |
| $\tilde{\mu}$ | 4819kgm$^2$ | 380kgm$^2$ | n/a | n/a |

During the post-process of the results with Prodera it has been possible to detect errors in the calculation of parameters due to the wrong interpolation of the results. In order to correct the modal parameters an software has been developed that interpolates the results and recalculates the modal parameters using the formulation used in [9] shown below:

$$\gamma_i = -\left.\frac{dS}{d\omega}\right|_{\omega=\omega_i} \quad (1)$$

$$\mu_i = \frac{\gamma_i}{\omega_i^2} \quad (2)$$

$$\zeta_i = \frac{R(\omega_i)}{\omega_i \gamma_i} \quad (3)$$

Where $\gamma$ is the generalized stiffness, $\mu$ the generalized mass, $\zeta$ the damping factor, $\omega$ the pulsation, $R(\omega)$ and $S(\omega)$ the real and imaginary parts of the complex power and $\omega_i$ the $i^{th}$ resonance frequency. The normalized generalized parameters can then be obtained with the amplitude of the reference transducer $A_n$ (located close to the excitation point).

$$\tilde{\mu} = \frac{\mu}{A_n^2} \quad (4)$$

$$\tilde{\gamma} = \frac{\gamma}{A_n^2} \quad (5)$$

These results have been later compared with Prodera to analyze the dependence of the calculated modal parameters with the interpolation method used in the complex power method.

## 4. CRITICAL ANALYSIS

The analysis of the results according to the focus of this article is presented in this section. The emphasis is put in the determination of the modal parameters of the different vibration modes for the studied wing. These parameters are modal frequency, damping factor, mode shape and generalized mass. The analysis is performed using the results presented before for the different load cases.

**4.1 Vibration modes.** It has been possible to identify 4 vibration modes in the range of frequencies from 0 to 100Hz. These modes have been 2 flapping (or vertical) modes at 9.61 and 47.11Hz; and 1 torsion mode at 50.27Hz. A 4$^{th}$ mode has been detected at 98.72Hz but has not been properly characterized. This mode is outside of the frequency range of interest. Such results have been compared with the analysis performed in [3] for the same tests.

It has been possible to determine the modal shape through two analysis methods. The first method has used the HBM system to compare the signals of the available accelerometers; the phase analysis of the accelerometer response provided information on the way the structure vibrated. Figure 2 shows a signal analysis for a torsion mode characterized.

The second method used the code implemented in the Prodera installation to perform the same process through the 14 accelerometers connected to the system.

**4.2 Calculated modal parameters.** An estimation of the modal parameters has been possible through the Prodera installation. The system integrates post-processing software that calculates the modal parameters using the representation of the complex power in the vicinity of the studied natural frequency. This representation allows for the calculation of the slope of the imaginary power and the value of the real power at the resonance point. Through these values it is then possible to calculate the damping factor, the generalized mass and the generalized stiffness. The obtained results for these values are presented in Table 1 and in Table 2.

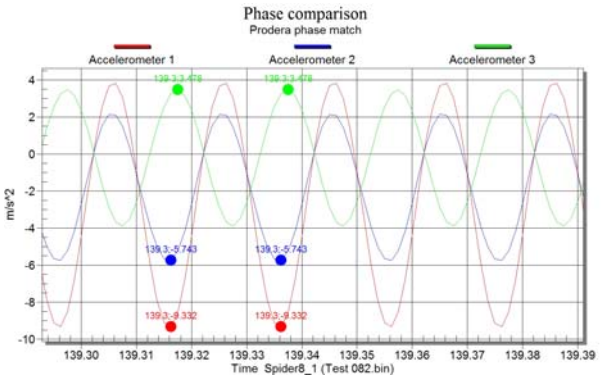


**Figure 2.** Signal analysis for a torsion mode in HBM Catman. Note the front accelerometer in anti-phase with the two accelerometers located in the trailing edge part of the wing.

The analysis of these values leads to the conclusion that the results obtained are coherent. The damping factor is a function that increases with frequency while the generalized mass decreases. The experimental values obtained follow this trend apart from specific anomalies.

**4.3 Correlation between acceleration and deformation.** The study of the acceleration deformation correlation has been performed using HBM software to compare the power spectrum of a representative accelerometer with a strain gage mounted close to the position of the accelerometer.

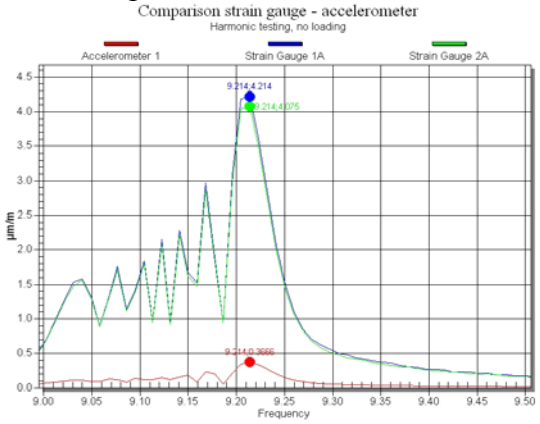


**Figure 3.** Frequency spectrum comparison for an accelerometer and 2 strain gages (No amplitude scale is provided for the accelerometer).

The obtained results, exemplified in Figure 3, show that there is a good correlation between the strain gage and the accelerometer results. A major drawback has been detected in the amplitude of the strains sensed. The average strains sensed have a value around 4 micro-strains for the performed tests. These

values might not be big enough for a precise characterization of the structure vibration.

**Table 3** Comparison between accelerometer and strain gage natural frequencies [Hz].

| Mode | 1st | 2nd | 3rd | 4th |
|---|---|---|---|---|
| | No loading | | | |
| Acc. | 9.61 | 47.11 | 50.27 | 98.72 |
| Gage | 10.11 | 47.77 | 50.75 | n/a |
| Difference | 5.2% | 1.4% | 1.0% | |
| | 1.5kN loading | | | |
| Acc. | 11.25 | 49.49 | 50.81 | n/a |
| Gage | 11.14 | 49.53 | 50.85 | n/a |
| Difference | -1.0% | 0.1% | 0.1% | |

Despite the precision problem for the strain gages it has been possible to determine the natural frequencies of the structure with the gages. The comparative results with the accelerations are presented in Table 3.

**4.4 Effect of loading.** The effect of loading in the structure has had the expected result. When a structure is loaded, the stress increases the stiffness of the structure; therefore, the expected vibration modes are expected to be found at a higher frequency. This has been corroborated in the experiments, as can be seen in Table 3, for all modes except for the torsion one. In the torsion mode, the variation of frequency is too small to determine whether the recorded difference is caused by loading or by the precision of the instruments.

**4.5 Structural non-linarites detected.** During the testing phase it has been possible to identify instability in the first bending mode that led to believe that a non-linearity was involved. The effect manifested as a sudden change of vibration amplitude close to the mode frequency during harmonic testing. This sudden change occurred without noticeable external cause and it changed its behavior depending on whether the test was performed increasing frequency or decreasing it.

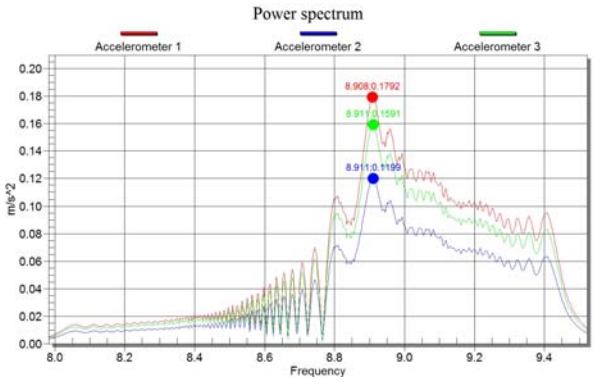


**Figure 4.** Behavior of the detected non-linearity for the first bending mode during a harmonic test with increasing frequency.

Figure 4 illustrates how the acceleration recorded during the test suddenly steps up when passing close to the calculated resonance frequency (around 8,9Hz). This behavior is known as jump phenomenon and it occurs in softening or hardening springs. In these cases, the amplitude - frequency diagram of the system presents a region of instability in which two possible dynamic states coexist; depending on whether the analysis is conducted increasing or decreasing frequency, the amplitude will be different up to a point in which the system brusquely changes its vibration characteristics. This jump usually occurs at different frequencies depending on the direction of the test; these two frequencies define the instability region. An example of the jump phenomena detected during testing is presented in Figure 5 for the first bending mode.

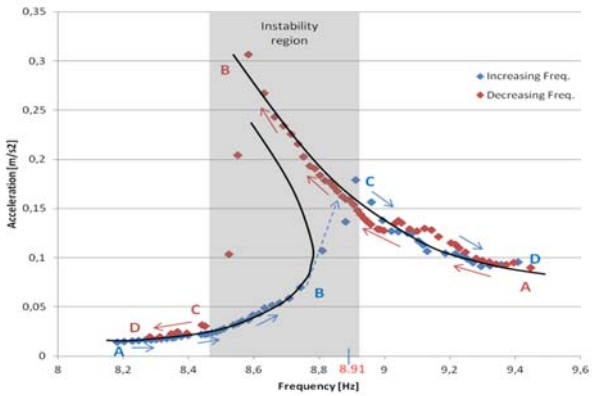


**Figure 5.** Jump phenomena depicted for the first bending mode using data from accelerometer 1.

According to the definitions found in the bibliography, the jump phenomenon found in the first bending mode is of softening spring type.

## 5. CONCLUSIONS & ACKNOWLEDGEMENTS

Some conclusions can be drawn from the analysis presented. Firstly, the results obtained using the frequency response function in the Prodera installation have been slightly lower than the results obtained with the power spectrum performed with the HBM system. This difference is around 4%.

The calculations performed parallel to Prodera to determine the modal parameters led to the following results. The difference obtained for the natural frequencies are up to 5%; for the damping factor the maximum difference is around 5%; the normalized generalized mass presents a maximum difference of 23%.

These results have been calculated with an accelerometer close to the excitation point but not in the exact point of excitation. This fact could explain the difference in the normalized generalized mass, very influenced by the amplitude of the excitation point. The utilization of an accelerometer in the excitation position should improve the results.

The use of strain gages is enough to study the vibration analysis if the precision of the gage is good enough and if the natural frequency is the only required parameter.

The recorded evolution with the loading of the damping factor and the natural frequency has been coherent with the expected behavior, with a variation of around 16%.

Non-linearity can be observed in harmonic testing if the frequency is slowly changed in the affected modes (0,004Hz/s).

## REFERENCES

1. Bisplinghoff, R.L., Ashley, H. and Halfman, R.L. *Aeroelasticity*. Courier corporation (2013).
2. Dieckelman, R.J., Hauenstein, A.J. and Ritzel, R.P. *Modern sine excitation GVT techniques.* Proceedings of the 20th International Modal Analysis Conference. Issue (2002).
3. Flore L. *Influenta starii de tensiune asupra caracteristicilor modurilor proprii de vibratie, studiu de caz.* University "Politehnica" of Bucharest (2015).
4. Harris, C.M. and Charles E.C. *Shock and vibration handbook. Vol. 5*. New York: Mc Graw-Hill (1988).
5. HBM Products. *Catman software professional operating manual* (2008).
6. Martinez V., B. and Dijkstra, K. *P-WIN-MODAL v5.1.1 handbook v1.0.* Prodera vibrations (2006).
7. Peeters, B., Hendricx, W., Debille, J. and Climent H. *Modern Solutions for Ground Vibration Testing of Large Aircraft*. Sound and vibration 43.1 (2009).
8. Prickrel, C.R., Foss, G.C., Phillips, A., Allemang, R.J and Brown, D.L. *New concepts GVT.* In M. Peterson, IMAC XXIV International Modal Analysis Conference (2006).
9. Prodera. *Training course in modal analysis.* Prodera vibrations (2002).
10. Salehi, M. and Ziaei-Rad, S. *Ground vibration test (GVT) and correlation analysis of an aircraft structure model.* Iranian Journal of Science and Technology (2007).

"HENRI COANDA"
AIR FORCE ACADEMY
ROMANIA

"GENERAL M.R. STEFANIK"
ARMED FORCES ACADEMY
SLOVAK REPUBLIC

INTERNATIONAL CONFERENCE of SCIENTIFIC PAPER
AFASES 2015
Brasov, 28-30 May 2015

# TRENDS IN IMPLEMENTATION OF RISK MANAGEMENT IN SMEs

**Adriana Florescu*, Bogdan Barabaş*, Sorin Barabaş***

*Faculty of Technological Engineering and Industrial Management, Transilvania University of Brasov, Romania

***Abstract:*** *In the globalized world, the rapid development of technology, increasing competitive advantage, the managerial activities are conducted most often uncertain, decisions are made under conditions of risk. In the small and medium innovative enterprises, decisional problem is more complex, depending on the strategy adopted, obtaining several results, dependent on the dynamics of environmental conditions. In this paper are presented the principles and methods of valuation and risk modeling underlying implementation of risk management in any SME, since the risk assessment results and success strategies decisively influence decisions taken at macro and microeconomic level.*

***Keywords:*** *risk management, modelling, small and medium enterprise, production systems*

## 1. INTRODUCTION

Current society in transformation, knowledge-based, requires finding and implementing some new methods to maintain the competitive advantage and implicit performance standards, in order to adapt to dynamic environmental conditions, in the context of globalization.

The business environment influenced by a lot of factors with event random uncertain requires that many companies, SMEs to integrate risk management into decision-making process in order to increase their competitive advantage. An ineffective risk management can result from economic point of view, both the bankruptcy of many companies on the market, but also at socio-economic and serious environmental problems. For example, through an adequate risk management, many famous industrial accidents (Chernobyl disaster) caused by a number of factors and events could have been prevented. If global risks are not effectively addressed, their social, economic and political fallouts could be far-reaching, as exemplified by the continuing impacts of the financial crisis of 2007-2008, [7].

The results of risk assessment are decisive influence for the decisions and the success adopted strategies at the macro and microeconomic level [1]. Given that risks are inherent in and occurring in all aspects of business management, SMEs should carry out a review regular and continuous of risk management business.

In implementing risk management activities occur most often specific problems and difficulties [5]. Thus, even if the concepts are explained Risk Management, sometimes they are difficult to understand because risk management requires an interdisciplinary approach involving the knowledge from several related fields: economic, technical, sociological or political. Sometimes the message receivers are not specialists in the

field and underestimate the significance of risk management. Risk manager must explain not only the risks and consequences of their methods of prevention, but also to emphasize the importance for risk management organization, positive consequences of the application of risk management policies. The theory is that a manager can have one of three attitudes towards risk: risk assumption, risk rejection or indifference to risk [1]. The need the corresponding approach to business risk level is, in the current round, little aware of small and medium entrepreneurs in Romania. Complex theoretical apparatus required of such an approach is still rather strong preserve of companies or financial institutions, but the small and medium businesses that are mostly of Romanian firms [2, 7]. The implementation of the risk management in SMEs is essential, given the importance of entrepreneurial business development, resulted from the recent studies [*Romanian Entrepreneurship Barometer 2013 EY Romania*]. According to the recorded data, shows the following:

- In the OECD countries, SMEs represent 99% of companies and two-thirds of employees.
- In Romania, SMEs contribute by 66% of the total number of employees of private companies.
- Also, these companies creates jobs at a rate of two times higher than the larger companies in the European Union 85% of all job growth between 2002 to 2010 being due to the SMEs.
- At the same time, we see that Romanian entrepreneurs experiencing significant difficulties: 88% of them find it difficult or very difficult access to finance, 94% wanting the predictability fiscal and regulatory environment, and 59% believe that Romanian mentalities and values do not support the entrepreneurship.

All over the world increased interest in entrepreneurial activity, business is so modeled and SMEs play a decisive role in reviving the overall economy. In terms of positive sentiment towards entrepreneurs, Romania is ranked 18 of 21 countries surveyed in the Entrepreneurship Barometer (Romanian and G20 edition), with only 35% of answers (Figure1).

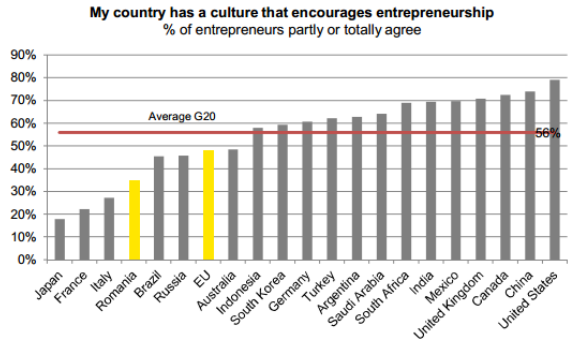


Fig. 1 The entrepreneurial culture [Source: EY Entrepreneurs Speak Out: Romanian Entrepreneurship Barometer and EY G20 Entrepreneurship Barometer]

As risks are inherent, and arise in all aspects of managing a business, SMEs need to conduct a regular and ongoing review of Business Risk Management. This review can be built around Critical Success Factors (CSF) and then expanded to include the risks attaching to those CSFs. CSFs normally contain the key internal and external issues or activities that impact business performance and they should be a mixture of those common to all the businesses in your industry or service sector and those specifically associated with your SME business [*SME Toolkit, „Basel II for SMEs"*].

## 2. THE RISK MANAGEMENT PROCESS

**2.1 Principles.** A risk is an event or condition that, if it occurs, could have a positive or negative effect on a project's objectives. Risk Management is the process of identifying, assessing, responding to, monitoring and controlling, and reporting risks [*EPLC Practices Guide – Risk management*].

The implementation of risk management in any organization need to consider the principles according to which the risk management is viewed as integrated part of decision making and organizational processes creator added value, dynamic, iterative and adaptable to change [*ANSI/PMI 99-001-2004, (2004)*]. The risk management addresses the uncertainty in a way well structured, opportune, based on the best the available information, considering human and cultural factors for continual improvement of the organization.

In accordance with [*AS/NZS 4360:2001 – Risk management*], the implementation of risk management is carried out by the following steps: setting goals; risk identification; risk analysis; assessing and prioritizing risks; risk treatment; communication and consultation; monitoring and review. *ISO/DIS 31000:2008* is a standard governing the issue recently emerged risks. International Organization for Standardization identified a number of principles of risk management in business, [3].

## 3. CASE STUDY. RISK MANAGEMENT PLAN

The activity of identifying of specific components of business risk and ways for managing them has become the need of considering the evolution of Romanian economy, in the current conditions, imposed by the globalization and the internationalization of business firms.

The company analyzed is part of a large industrial group. It is an industrial concern, the market leader in performance operating systems and logistic equipment. Today is a modern company with multiple locations worldwide, all aiming to achieve quality products becoming the preferred partner of customers. The company also provides ancillary services to made products, consisting of a team of experienced engineers. The fundamental concept of the company is to achieve a higher level of quality and service, developing and delivering solutions that fit the needs and expectations of the market.

The company's vision is to achieve a global coverage and to be the market leader. All projects are possible only with the performance of the implementation of complex solutions and quality.

Company objectives are: development of quality products and services; compliance with the dates of delivery; customer loyalty; increase in turnover and profit; developing a good communication between departments of the company; adapting production to market requirements; increase efficiency equipment; increasing the level of training of human resources; compliance with environmental conditions imposed; compliance with of regulations and legislation. To analyze the performance of the company are used as size comparison: the turnover, the number of employees, previous period, the quality of products and services. The target values of these indicators for measuring performance (KPI) are based on strategic objectives and involve both management staff as well as the employees in achieving their. Benefits of using KPIs are not maximized because only 35% of enterprises use in all departments and only 23% design and use in correlation the various areas of activity indicators of the company. Using performance measurement indicators is recommended in terms of risk management.

To highlight the company's financial business development analysis we selected several indicators of balance, in Figure 2.

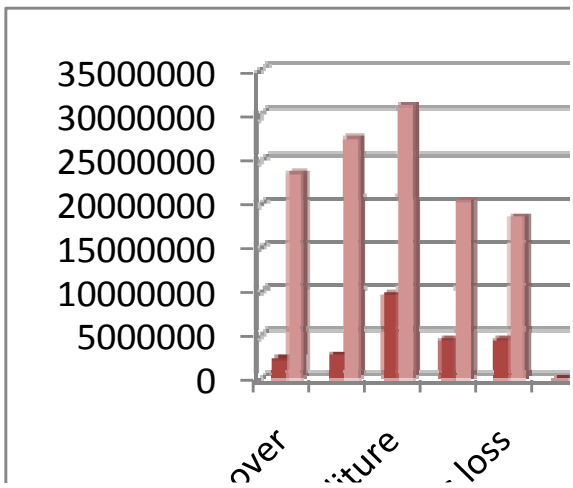


Fig. 2 Financial evolution of the company's

**3.1 Resources allocated.** The organization should develop practical means to allocate adequate resources for risk management, this will be considered: people, skills, experience and competences; resources required for each step in the risk management process; documented processes and procedures; information systems and knowledge management. Gantt chart is a technique often used for scheduling projects (such as project and resource allocation to achieve adequate bond risk management). Gantt charts are designed and implemented with success in operations with a high level of repeats. The activities of several components can be combined in a single graph showing the realization of the aggregate. The graph can show how different activities are performed concurrently to achieve a common goal.

Risk Management clarifies the objectives of the organization and commitment to risk management, specifying: links between risk management policy and other policies that target the enterprise; responsibilities for risk management; how are treated conflicts of interest; the degree of risk acceptance and risk aversion; the processes, methods and tools used for risk management; the resources available to help those responsible for risk management; the way in which risk management performance will be measured and carried; commitment to periodic review and verification policy and structure for risk management and continuous improvement.

Risk management policy should be communicated properly to all levels of the organization.

**3.2 Risk identification.** Assessment and risk modeling is a complex activity that requires multidisciplinary approaches in different branches of science or knowledge of the economic, technological, sociological or political. Risk assessment results and success strategies decisively influence decisions taken at macro and micro. Risk can be defined according to *ISO / IEC Guide 73: 2002* and *ISO/IEC CD2:2008* as the combination of the probability of an event and its consequences.

A difficult situation of the enterprise is characterized "by a serious lack important and progressive mastery obstacles and difficulties", which is caused, on the one hand, the inability of managers to manage effectively the company, and, on the other hand, its development in its economic context. It is important to note that the nature of the difficulties, but the frequency and intensity with which manifests are essential in characterizing such a situation. Difficult financial situation appears, therefore, that a situation likely to upset further work in terms of efficiency and effectiveness. The latter corresponds to reality "normal" enterprise, while plight is associated a reality "abnormal" of the same entity.

The main categories of risks in an enterprise are (Table 1): *financial risks* (interest rates, exchange rates, credits), *strategic risks* (competition, market demand), *operational risks* (regulations, culture, management) and *hazard risks* (employees, properties products, services).

Categories of risk in the company:

01. *The introduction of new products on the production line.* Concern intention of developing locations in Romania entails diversifying production by introducing the production line of products type prototype, which slows down the work of staff.
02. *Interdepartmental Communication.* Failure to company employees share information about the project on all departments involved.
03. *Failure to comply with the terms and conditions of the suppliers of products or services.* Failure to comply with contractual terms and conditions by suppliers failure to meet customer deadlines, possible problems in terms of quality products and services, loss of customer confidence with the company, etc.
04. *Customers.* Lack of optimal communication with customers may result in loss of future contracts, dissatisfaction meet the requirements
05. *The emergence of unforeseen production costs.* Due to the early phase in which the company, running costs of raising plants that have not been taken into account from the beginning costs, thus producing a temporary imbalance the budget.

**3.3 Qualitative and quantitative risk analysis.** In this section are qualitative and quantitative analyses of risk by assessing the impact of risk events on the project objectives and risk score calculation, [2, 6]. Score impact (I) are given in Table 2.

**Table 2.** Score impact

| Level | Score | Description |
|---|---|---|
| *Very low* | 1 | Negligent impact. It is not possible to quantify the impact, which is very low. |
| *Low* | 2 | Minor impact on the project, such as less than 5% deviation from the program or project budget. |
| *Moderate* | 4 | Measurable impact on the project, such as deviations from 5-10% of the program or project budget. |
| *Great* | 8 | Significant impact on the project, such as deviations from 10 to 25% of the program or project budget. |
| *Huge* | 16 | Impact (catastrophic) on the project, such as more than 25% deviation from the program or project budget. |

**a.** ***Qualitative analysis*** of risk by calculating the impact of risk is shown in the following:

*Risk 1*: I=0.4 - Impact of prototype development of type products is high because this activity requires the involvement of specialized personnel and its qualification on the type of product produced. As expected it is impossible to approximate the time of product development, which reduces manufacturing capacity type series from the production line, thus delaying delivery times for this cause blocking of cash flows.

*Risk 2*: I = 0.8 - Lack of communication between departments involved in the projects undertaken by the company has a very high impact; it may cause a breach of the terms of delivery, development of non-compliant, even leading to the loss of a customer.

*Risk 3*: I=0.8 - A high impact it has non terms and conditions by providers of products or services is because it involves the risk of being unable to meet the demand of customers, or deal with, but with delays, with low quality, or some shortcomings, which automatically leads to the possibility of non-compliance of contracts with clients, and loss of confidence and credibility.

*Risk 4*: I=0.8 - As in any company manufacturing activity expenses are occurring, impact can be considered very high as to produce a forecast budget imbalance.

*Risk 5*: I=0.4 - The client is a very important aspect to be taken into account permanently.

It is not enough a quality product at a fair price, or service made on time. Lack of proper and effective communication with customers, or bad communication, conflict, has a high impact because it leads to loss of customer confidence, the credibility of the company, and automatically to loss of customers and financial losses. Therefore it is necessary qualified personnel for this; it represents the company's image.

It is considered impact of risk (I):

0.05 = *Very low*
0.10 = Low
0.20 = *Moderate*
0.40 = *Great* / 0.80 = *Huge*

**b.** Q***uantitative analysis***, the likelihood (P) the risk and the risk impact are given in the Table 3 and Table 4.

**Table 3.** The likelihood (p) the risk

| Level | Score | Description |
|---|---|---|
| *Very low* | 1 | Very low probability of occurrence; Risk monitoring is still required if certain circumstances can lead to a risk with a certain probability of occurrence during the project low |
| *Low* | 2 | Low probability of occurring based on current information available and risk triggering circumstances also have a low probability event. |
| *Average* | 3 | Average probability of occurrence, the risk is likely to occur. |
| *Great* | 4 | High probability of occurrence, based on the circumstances of the project. |
| *Huge* | 5 | High probability of occurrence and the circumstances of the risk occurring are very probable to manifest. |

Risk Analysis Methodologies for the enterprise involves combining qualitative and quantitative techniques. Qualitative analysis techniques are used when there is insufficient data to allow the use of quantitative techniques that apply to more complex activities of the organization, [1, 2, 4].

Risks must be analyzed from two perspectives - the probability and the impact. Also, the risks inherent risks should be analyzed so that, before applying management actions, as well as residual risk remaining after implementation of management actions.

Risk can be defined - according to *ISO / IEC Guide 73: 2002* - as the combination of the probability of an event and its consequences.

The priority score is determined by the probability of occurrence score and impact of the risk score, with the relationship:

*Priority Score = Probability Score x Impact Score*

**Table 4.** Risk impact (quantitative analysis)

| Risk Category / Event | ** (P) | Consequences impact | Risk Score (Px I) |
|---|---|---|---|
| *The introduction of new products on the production line* | **0.9** | The delay deadlines of the other products. | **0.36** |
| *Inter-departmental communication* | **0.7** | The lack of interdepartmental communication can produce deviations from the terms of delivery, development of non-conforming products, leading even to the loss of a customer. | **0.56** |
| *Failure to comply with the terms and conditions of the suppliers of products or services* | **0.5** | Failure to meet the demand of customers, or deal with, but with delays, with reduced quality, or failings; Failure respect of contracts with clients, and loss of confidence and credibility. | **0.4** |
| *The emergence of unforeseen production costs* | **0.5** | Reducing income and deviation from the expected budget plan. | **0.4** |
| *Customers* | **0.1** | The loss of customer confidence, the credibility of the company, and automatically financial losses and loss of customers. | **0.04** |

** Probability (P): Very unlikely = 0.10 / 0.30 = unlikely / 0.50 = Medium / 0.70 = Probable / 0.90 = Very Likely

The most important risks that must be treated it can be seen in Figure 3.

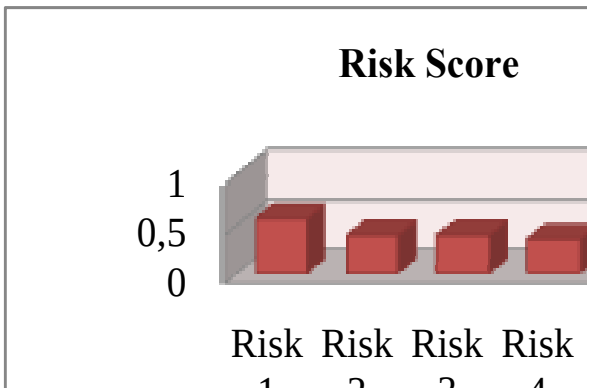


Fig. 3 Risks prioritization

The matrix scores of the priority are given below (Table 5).

**Table 5.** Risk matrix

| Probability of occurrence | | | | | |
|---|---|---|---|---|---|
| 5 | 5 | 10 | 20 | 40 | 80 |
| 4 | 4 | 8 | 16 | 32 | 64 |
| 3 | 3 | 6 | 12 | 24 | 48 |
| 2 | 2 | 4 | 8 | 16 | 32 |
| 1 | 1 | 2 | 4 | 8 | 16 |
| | 1 | 2 | 4 | 8 | 16 |
| | Impact | | | | |

Risk Management Plan contains actions that are applied to avoid, transfer or mitigation risk based on priorities. For each identified risk specified: probability score; score impact; priority score; preventive actions applied to reduce the likelihood of risk; contingency actions (corrective), applied to reduce the impact of emerging risks; data output and resources allocated for each type of action.

The first eight identified risks, in descending order of priority scores are follows: interdepartmental communication; failure to comply with the terms and conditions of the suppliers of products or services; the occurrence of unforeseen production costs; introduction of new products on the production line; customers; competition; provide inconsistent equipment; failure to client deadlines. After analyzing the risks, we can determine the best action for managing each risk. This involves consideration of the impact on business, the probability of occurrence and cost of control or risk reduction. When corrective actions have meaning, options include steps to reduce the potential risk transfer or risk insurance. In the process, we have a clear image of the relevant risks, as they are related to each other and how they can be managed on.

**3.4 Preventive and corrective actions.**

Preventive actions:

- *Risk 1:* Establish a team just type prototype; Separate funding of such projects;
- *Risk 2:* Implementation of rules for transmitting information;
- *Risk 3:* Conclusion of contracts with suppliers including specific contractual clauses regarding timeliness; The choice of suppliers / partners trust;
- *Risk 4:* Building a budget contingency reserve;
- *Risk 5:* Training with customer representatives, specialized training (for communication, sales).

Corrective actions:

- *Risk 1*: Schooling of team made up;
- *Risk 2*: Collection of information by a person involved;
- *Risk 3*: Solutions quick replacement of unsuitable suppliers;
- *Risk 4:* Rebalancing of the budget;
- *Risk 5*: Questioning their customer satisfaction for services received.

Also, implementing the monitoring and control plans, the risks situated in the high domain can be eliminated or minimized to a medium or low level.

It can be noticed that a problem of risk is difficult communication between staff which is part of Departments of Planning, Logistics and Design, in terms of achieving the command products received from customers. As a solution to improve the activity of permanent communication, of transmission of information between these departments and others, decided to re-parcel them under one Department of Planning. Another measure taken is to develop training programs and specialized trainings sites within the company.

Activity of the company is to manufacture systems and equipment logistics on industry, mostly for export. The company capacity is used 100% which shows a profitable business, which initially is continuously developing. This is the reason why the company management attracts more and more contracts, customers who use its services are renowned corporations abroad. Actions taken for the early detection of difficulties and risks that threaten the normal course of business enterprises and to determine their financial status, allowing measures to ensure their economic viability and contributes, of course, to avoid bankruptcy caused by poor management of material resources, financial, human and, not least, information.

## 4. CONCLUSION & ACKNOWLEDGMENT

Risk management is effective when it becomes part of the company culture and employees are interested through key performance indicators in implementation. Given that the negative consequences of risk are most common in business, must be analyzed and implemented effective methods of prevention and mitigation of these undesirable phenomena. Changes in production systems, business development led to the integration of risk management in modern management systems as "key factor" of economic development of any company. Management decisions involve risks that can conduct both behavioral change structures and results. Identifying and managing risks is a complex issue with implications for profit of any company.

Risk management can have positive effects that generate opportunities for earnings a firm or negative, leading to threats, losses. Any type of business is vulnerable to losses due to risks arising from uncontrolled. Risk management should be an ongoing and evolving throughout the organization, which are implemented systematically, and methodically all actions to eliminate or reduce the risks associated with the activities past, present and especially the future of the organization.

This work was partially supported by the strategic grant POSDRU/159/1.5/S/137070 (2014) of the Ministry of Labor, Family and Social Protection, Romania, co-financed by the European Social Fund – Investing in People, within the Sectorial Operational Programme Human Resources Development 2007-2013.

## REFERENCES

1. Bârsan-Pipu, N., Popescu, I., *Risk Management. Concepts. Methods. Applications.* (in Romanian), Transilvania University Publishing House, Brasov, ISBN 973-635-180-7 (2003).
2. Druica E., *Risk and uncertain* (in Romanian), C. H. Beck Publishing House, Bucharest (2006).
3. Garvey, Paul R., *Analytical Methods for Risk Management: A Systems Engineering Perspective*, Taylor & Francis Group,USA, ISBN 9781584886372, (2009).
4. Kleindorfer, R.P., *Industrial Ecology and Risk Analysis, Risk Management and Decision Processes Center*, The Wharton Shool, University Pennsylvania, November (2000).
5. McNulty, M.S. *Applied Risk Analysis of Complex Systems*, the Third Conference on Mathematical Methods in Reliability, pp. 437 – 439 (2002).
6. Marsh & McLennan Companies, *Global Risks 2014*, Ninth Edition, ISBN-13: 92-95044-60-6 (2014).
7. Oprean C., *Methods and techniques of scientific knowledge*, Lucian Blaga University Publishing House (in Romanian), Sibiu (2006).

"HENRI COANDA"
AIR FORCE ACADEMY
ROMANIA

"GENERAL M.R. STEFANIK"
ARMED FORCES ACADEMY
SLOVAK REPUBLIC

INTERNATIONAL CONFERENCE of SCIENTIFIC PAPER
AFASES 2015
Brasov, 28-30 May 2015

# COMPOSITE MULTILAYER STRUCTURES OBTAINED BY EXPLOSIVE METHOD

**Ciprian-Marius Larco*, Ştefan-Mircea Mustață*, Radu-Călin Pahonie***

*Faculty of Mechatronics and Integrated Armament Systems, Military Technical Academy, Bucharest, Romania

***Abstract:*** *The explosive welding process has been understood for decades, the industry has been slow to realize its potential and the possible composites that it makes available. This paper focus on some aspects related to welding process by explosion mechanism in order to obtaining new multi-layer structures used in special industries, such as aeronautics and mechanical engineering.*

***Keywords:*** *composite structures, multilayer structure, explosive welding.*

## 1. INTRODUCTION

The main advantages of multilayer structures obtained by explosion bond, such us elimination of galvanic corrosion, design control of bonding point, weldable bi-metallic transitions, stronger than friction and diffusion welded joints or reduction of mechanical integration, make this composite materials a solution for special vehicles, like aircraft carriers or space satellites.

Several studies concerning the waves at the welding-interface concluded that the particularities of melted and solidified material cannot be explained neither by the mechanism of welding in the solid state, nor by the dissolving mechanism. The deformation of the granules at the interface and the appearance of the waves define that the phenomenon of welding through explosion is based on a hydrodynamic process of inflows. [1,2,3]

In the process of explosion welding of plates, the kinetic energy transforms into thermic energy (accompanied by energy dissipation) at the welding-interface, enough to cause bilateral dissolves throughout the interface. The diffusion of the materials into liquid state takes place gradually, depending on the structure of the welded materials and the distance from the interface. [4]

To illustrate the process of explosion welding of plates, this paper presents a principle method accompanied by a numerical analysis and a practical experiment.

## 2. THE PROCESS

The explosive bonding is a welding process that uses controlled explosive energy to force two or more metals together at high pressures (Fig. 1).

The isotropic layers are joined with a high-quality metallurgical bond, leading to a performant composite system. The time necessary in the explosive welding process is very short, so the reaction zone between the constituent metals is at microscopic level. During the bonding process, several atomic

layers on the surface of each metal become plasma.

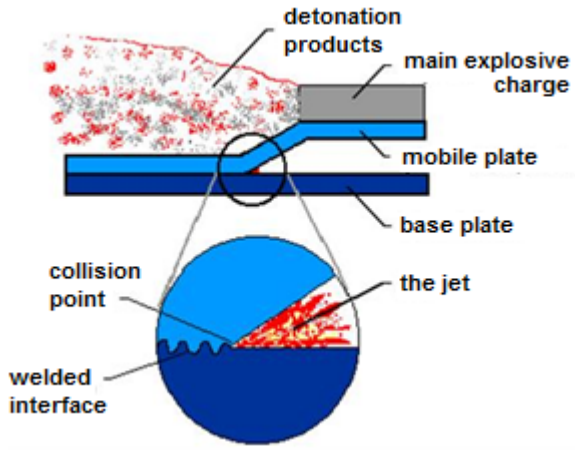


Fig. 1. Explosive bonding process [7]

The collision angle between the two surfaces (typically less than 30°) forces the plasma to jet ahead of the collision front, effectively scrubbing both surfaces.

The remaining thickness stays at near ambient temperature and acts as a huge heat sink. Therefore, the bond line is an abrupt transition from the clad metal to the base metal with virtually no degradation of their initial physical or mechanical properties. The obvious benefit from this process is the joining of metallurgical incompatible systems. Any conventional cladding method, which uses heat, may cause brittle intermetallic compounds to form. [7]

Bonding multiple laminae by explosive welding involves a working knowledge of the process phenomena and the ability to utilize them efficiently. The variables affecting the weld formation must be tightly controlled in order to create the desired composite with quality weld. The characteristics of the wave pattern formed during the explosive process (amplitude and periodicity) are influenced by three major parameters: collision velocity ($V_c$), explosive load and the interface spacing. To control these parameters means to control the welding process. The wave pattern formed at the bond line is most often described as resulting from a fluid-flow collision. The two constituent metals can be considered to act as viscous fluids in the reaction zone and, just as in describing laminar or turbulent flow, a Reynolds number can be determined for the system. [7]

In a fluid-flow collision, the interface turbulence is controlled by the detonation velocity and the collision angle. The interface morphology is important for some specific applications: maintaining a wavy interface to increase transition joint's shear strength or a flat interface in a system, where a reaction zone is minimized for thermal reasons (Fig. 2).

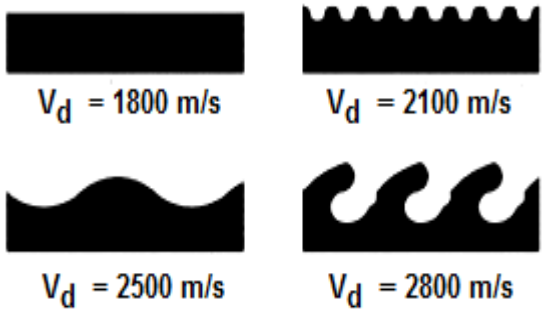


Fig. 2. Explosive Welding Wave Morphology Variation [5]

It has been experimentally established that during the process of welding, important transversal tensions form on the interface, resulting in effect of heating of the interface. This phenomenon could lead to an adequate warming of the superficial shells to produce the welding and can also explain the appearance of the waves at the interface [1].

New testing procedures have revealed that, at the collision of the welding pieces, only a very thin layer of melt forms on the interface. The assigned value of refrigeration of the remained melting layer is $10^5$ $^0$C/s, this value is high because of the line of contact between the components.

The existence of an amorphous layer, inside the welding zone, has been taken into account for different metallic combinations and explained by the scientists as being the main reason of welding through explosion's fundamental mechanism (Mustață, 2003:96-112;Belmas et al.,1996:217-222).

The welding mechanism with jet configuration is able to incorporate the influence of the main technological parameters and can somehow envisage a "working" domain for the welding parameters, for any material combination.

According to these assertions, it is generally accepted that the well-known phenomenon of the point jet formation is a collision and is a fundamental condition for the explosion welding process.

This paper tackles the formed jet that represents the mechanical cleaning agent of the welding areas, removes the impurities and the oxides, allows that the atoms of the two materials collide at interatomic spaces, thus resulting the welding through explosion.

The velocity of a wave is affected by two properties of the material: the elastic properties and its density. The relationship is described by the following equation:

$$v = \sqrt{\frac{C_{ij}}{\rho}} \qquad (1)$$

where $C_{ij}$ is the elastic properties.

The wave speeds differ for different types of solids because of the elastic properties of materials. Elastic properties relate to the tendency of a material to maintain its shape and not deform when a force is applied to it. A material such as steel will experience a smaller deformation than aluminum when a force is applied to it.

At the particle level, a rigid material is characterized by atoms and/or molecules with strong forces of attraction for each other. These forces can be thought of as springs that control how quickly the particles return to their original positions. Particles that return to their resting position quickly are ready to move again more quickly, and thus they can vibrate at higher speeds. Therefore, the waves can travel faster through mediums with higher elastic properties than it can through solids which have lower elastic properties.

Although there are two factors that affect the propagation speed, the elastic properties have a greater influence on the wave speed than the density of the material.

The density of a medium is the second factor that affects the wave speed. Since the density is the mass of a substance per volume, a material that is denser has more mass per volume. Usually, larger molecules have more mass. If a material is denser because its molecules are larger and since the waves are made up of kinetic energy, it takes more energy to make large molecules vibrate than it does to make smaller molecules vibrate. Thus, the waves will travel at a slower rate in the denser object if they have the same elastic properties. If sound waves were passed through two materials with approximately the same elastic properties such as aluminum (10 psi) and gold (10.8 psi), sound will travel about twice as fast in the aluminum (0.632cm/microsecond) than in the gold (0.324cm/microsecond). This is because the aluminum has a density of 2.7gram per cubic cm which is less than the density of gold, which is about 19 grams per cubic cm. The elastic properties usually have a larger effect that the density so it is important to both material properties. [1]

As defined by Crossland [7], the $p$ pressure resulted by every material in the collision point, is obtained by the following formula:

$$p = \rho \cdot u \cdot D \qquad (2)$$

where: $p$ is the shock wave pressure at the interface between plates;

$\rho$ - the density of the material;

$u$ - the material speed at which the materials from the interface move;

$D$ - the speed of the shock wave inside the material, this speed is approximately equal with the speed of the sound (the speed of the longitudinal waves).

Taking account of (1), the pressure ratio of the two materials the dependency is given by:

$$\frac{p_2}{p_1} = \frac{\rho_2}{\rho_1} \cdot \frac{v_2}{v_1} \qquad (3)$$

Besides the impact speed between the mobile and the fix material, the welding through explosion is only possible if at the impact level and collision interface plastic leaks exist. In practice, this condition is defined, as follows: the speed of the collision point, sometimes named the welding speed, must have a lower value than the speed of the sound inside the material.

Also, in order for the welding process to be obtained, the angle of dynamic collision $\beta$ must excel a minimum value. This angle has very low values.

The speed of the collision point is obtained by the following formula:

$$V_c \approx \frac{V_p}{\sin\beta} \qquad (4)$$

where: $V_c$ – is the speed of collision;
$V_p$ – is the speed of propulsion;
$\beta$ – dynamic angle of collision.

The study to obtain some layered materials through the unconventional process mentioned above is essential also because of the energetic independence provided by the technology, such as the adequate energy to detonate an explosive load.

To obtain the process of plating through explosion, after the construction of half-finished materials and bringing them to desirable sizes, the covers of the explosive loadings are being built, with the function to maintain the geometric sizes of the explosive loadings, under the explosive's character and its granulation. In this instance, the boxes belonging to the explosive loadings have been made of cardboard.

After determining the testing conditions, the assembly of the technologic system to create the process of plating through explosion begins. Therefore, the spacers are placed across the base plate.

The experimental technological system, created to generate the process of plating through explosion is shown in fig.1 and fig. 2. (Mustață, 2003:96-112).

The spacers are mechanic elements with the function to create the best distance between the plates to be welded.

Fig. 3. The experimental assembly used for the process of plating through explosion

The Bi-dimensional Mechanical Model from the simulated Explosion Cladding Process is presented in fig.4. [3]

To obtain a multilayered material structure with specific characteristics, through the process of explosion plating, several attempts have been made with aluminum alloy plates type 3105, 3 millimeters thick; between these plates, a stainless steel fiber has been inlayed, with the role of consolidation (Mustață, 2003:96-112).

To form an explosive weld the following conditions need to occur [6]:

- two surfaces that need to be joined are initially spaced at a small distance (stand-off distance).
- an explosive force brings these two surfaces together progressively through a collision front.
- the collision front's velocity must be lower than the speed of sound in the materials, so that the shock wave precedes the bond being formed. If not, the shockwave would interfere with the contact surfaces preventing the bond occurrence.
- the interface pressure at the collision front must exceed the yield strength of the materials, so that plastic deformation will occur.

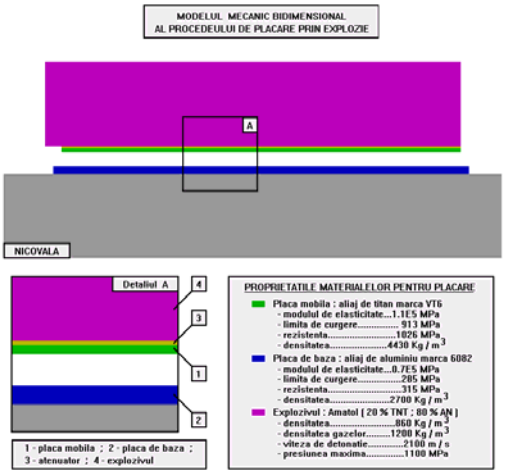


Fig. 4. The bi-dimensional mechanical model from the Explosion Cladding Process

A jet of metal is formed just ahead of the collision front, comprising of the two component surfaces, which is finally ejected from the interface. The surfaces and any surface contaminants are removed in the jet. Behind the collision front, the now clean surfaces bond, under extreme pressure, in the solid state. In cross section, the materials usually bond together in an undulating wave form and the process can weld a parent plate of thickness 0.025mm to over 1m (the maximum flyer plate thickness is one third that of the parent plate). Up to 30m2 can be welded in one explosion.

The stereomicroscopic image of the layered structure obtained by explosion cladding process is presented in fig. 5a,b.

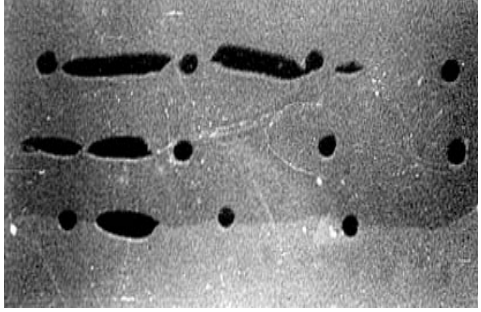

a.

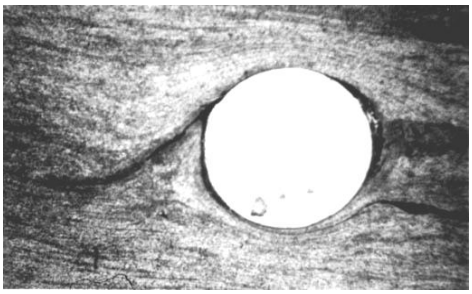

b.

Fig. 5 a,b. The stereomicroscopic images of the structure obtained through the explosion cladding process

The speed's field in the assembly elements can be represented schematically and in principle as in fig.6.

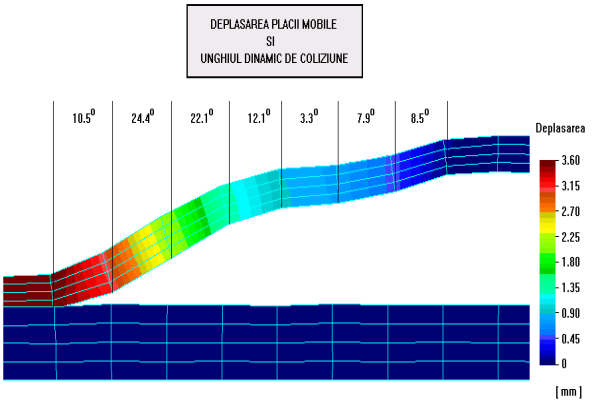


Fig. 6. The mobile plate moving and the dynamic collision angle

Figure 7 presents the graphic of the moving speeds of the nodes in a normal direction the mobile plate. Based on the image obtained throughout the simulation of the explosion plating from the Method Finite Elements process, it can be observed the deformed image of the mobile plate at different moments of time. The types of materials tested, including those obtained by using explosive cladding process, once again underline the fact that the layered materials, can largely meet the requirements.

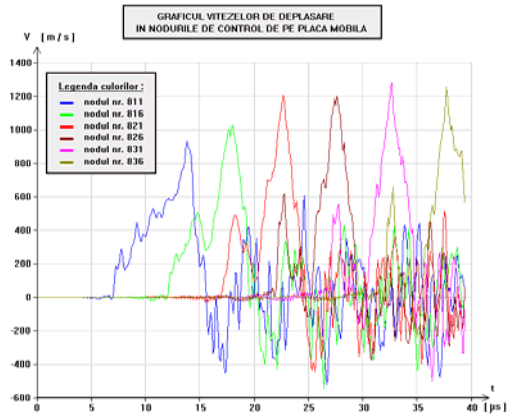


Fig. 7. The moving speeds of the control nodes of the mobile plate.

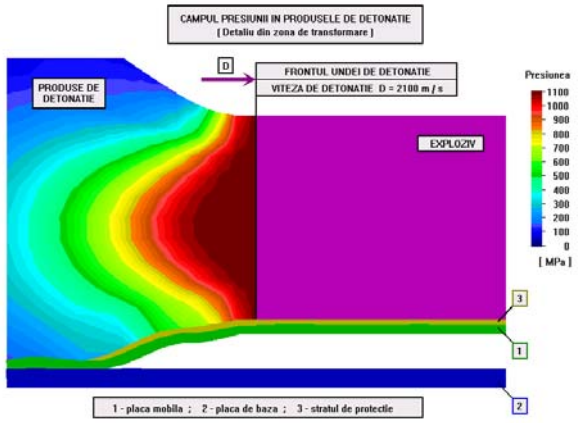


Fig. 8. Presure field in detonation products.

Besides the beneficial effects of explosive cladding technology in fig. 8, some imperfections due to the quality and coated surfaces can be observed.

## 3. CONCLUSIONS & ACKNOWLEDGEMENT

This paper and the experiments presented conclude that, in order to obtain multilayer structures using a nonconventional explosive welding process, various metallic materials are needed in order to obtain a sandwich of different materials, in particular, thin slabs, which sometimes is impossible by using traditional welding processes.

Explosively welded multi-laminates come very close to achieving ideal composite conditions (sharp transition between layers, physical and mechanical properties which are constant or enhanced throughout individual layer thickness, metallurgical bond between layers). These composites will then be available for a wide variety of industrial and strategic applications. The high integrity of the bond allows design engineers to utilize the specific desirable properties of metals more efficiently.

It can be concluded that the trend in the field of research is to obtain new multi-layer materials with high mechanical properties able to satisfy the most demanding technical requirements imposed by peaking technological development.

This paper has been financially supported within the project entitled "*Horizon 2020 - Doctoral and Postdoctoral Studies: Promoting the National Interest through Excellence, Competitiveness and Responsibility in the Field of Romanian Fundamental and Applied Scientific Research*", contract number POSDRU/159/1.5/S/140106. This project is co-financed by European Social Fund through Sectorial Operational Programme for Human Resources Development 2007-2013. Investing in people!

## REFERENCES

1. Meyers M., *Shock Waves and High-Strain-Rate Phenomena in Metals: Concepts and Applications*, Springer Science & Business Media, 2012
2. Reid R.S., *A discussion of the mechanism of interface wave generation in explosive welding*, Int. Journal of Mechanical Sciences, Volume 16, Issue 6, 399–400, 1974
3. Gupta R.C. and Kainth G.S., *Swinging Wake Mechanism for Interface Wave Generation in Explosive Welding of Metals*, J. Appl. Mech. 57(3), 514-521, 1990
4. Chemin C., Qingming T., *Mechanism of wave formation at the interface in explosive welding*, Acta Mechanica Sinica, Volume 5, Issue 2, pp 97-108, 1989
5. Crossland, B., *Explosive welding of materials and its applications*, Clarendon Press, Oxford,1982
6. Belmas R., sa., *Un modèle de points chauds fondé sur l'implosion de la porosite microstructurale*, Propellants explosives and pyrotechnics, 1996-18, (p.217-222)
7. http://www.pacaero.com

"HENRI COANDA"
AIR FORCE ACADEMY
ROMANIA

"GENERAL M.R. STEFANIK"
ARMED FORCES ACADEMY
SLOVAK REPUBLIC

INTERNATIONAL CONFERENCE of SCIENTIFIC PAPER
AFASES 2015
Brasov, 28-30 May 2015

# KINEMATICS OF THE LANDING GEAR SYSTEMS OF AIRCRAFT

**Doru Luculescu*, Vasile Prisacariu***

*Faculty of Aeronautic Management, "Henri Coandă" Air Force Academy, Brasov, Romania

***Abstract:*** *The mechanisms best represented in aircraft design are the bar mechanisms. They are mostly part of the landing gear and of the command systems for aircraft space positioning and for changing flying conditions. The current article is a review of bar mechanisms with reference to the landing gear of aircraft as well as a kinematics functional analysis with software assistance.*

***Keywords:*** *mechanisms, landing gear, software analysis*

## 1. INTRODUCTION

Mechanisms are mechanical systems for transmitting and changing the motion and forces of one or several moving bodies as well as the constraint forces of other bodies; it is the kinematic chain where one kinematics element is fixed [1].

The mechanisms best represented in aircraft design are the bar mechanisms. They are mostly part of the landing gear and of the command systems for aircraft space positioning and for changing flying conditions. [2, 3].

The landing gear is the aircraft component which ensures taxiing in good conditions, prior to takeoff and after landing as well as during parking, see figure 1.1 and 1.2.

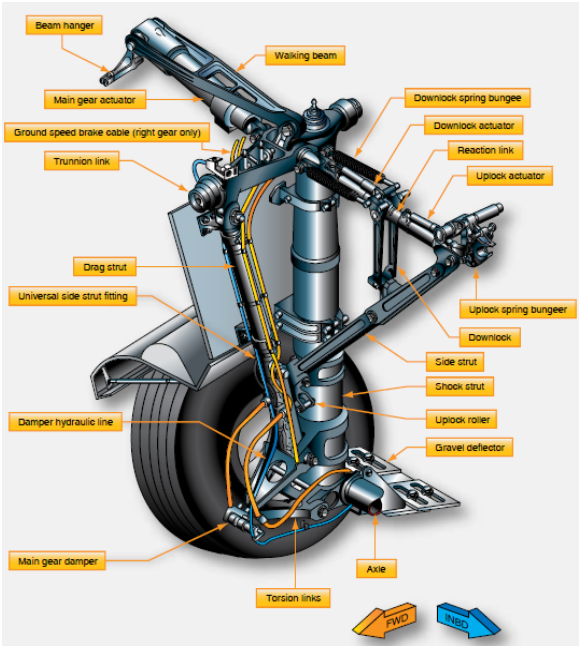


Fig. 1.1 Main landing gear components [5]

Fig. 1.2 Aircraft landing gear [5]

Mostly due to aerodynamic reasons, the majority of modern aircraft exceeding the speed of 350 km/h are equipped with retractable landing gears. The diverse designing requirements turn the design and construction of a retractable landing gear suitable for certain aircraft into complex, difficult tasks. The need of such requirements has led to an increasing number of constructive variants for the design and building of retractable mechanisms as well as to a more systematic approach, - see figures 1.3 and 1.4.

Fig. 1.3 Lockheed Martin Landing Gear - F 16 [6]

Systematization has been used for studying retractable mechanisms, one based on specific classification criteria which emphasize the ranking of these technical systems. Thus, the landing gear can be worthy of being considered a complex system, falling into three categories or subsystems: a *drive mechanism* which is mainly made of a subassembly with the piston in oscillating cylinder and pneumatic or hydraulic drive; a *main mechanism* which supports the gear wheel by means of the undercarriage leg operated by the undercarriage strut; a *wheel spinning mechanism* which can often be studied separately from the other subassemblies.

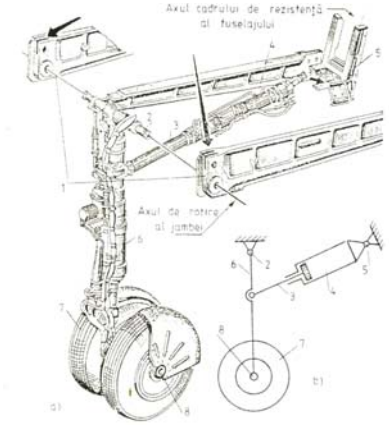


Fig. 1.4 Design of a retractable landing gear [1]

Figure 1.4 shows the following: *1-strut bracing girders, 2-strut rotation axis, 3-actuator rod, 4-strut retraction actuator, 5-assembly for attaching the actuator to the fuselage/wing, 6-landing gear strut, 7-landing gear wheel, 8-axis of the landing gear wheel.*

The most frequently used landing gears are the ones with folding bracing strut, see figure 1.5. The main advantage of this retraction mechanism is that it occupies relatively little space in the fuselage after retraction.

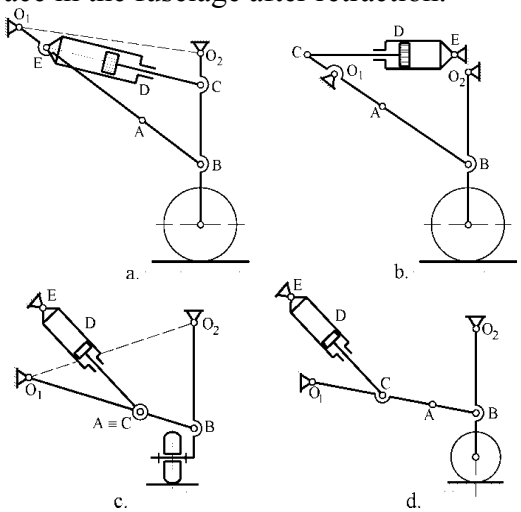


Fig. 1.5 Kinematics diagram of the landing gear with folding bracing strut

From the structural point of view, as shown in figure 1.4 and as previously mentioned, these mechanisms are made up of the drive system (hydraulic or pneumatic) and a four-bar mechanism 4R, $O_1ABO_2$, which is the main mechanism of the retraction system.

All cases clearly demonstrate that the design of the drive mechanism can be done only if certain requirements are met.

One of these requirements is to determine the extreme positions of the elements of the mechanism when the gear is out or retracted. It is a follow-up of the synthesis of the main mechanism of the landing gear. The synthesis will be performed in such a manner that, during its functioning, the mechanism will not reach singular positions.

## 2. KINEMATICS THEORY

Figure 2.1 shows a kinematics diagram of a drive mechanism of the landing gear in which three consecutive positions are presented and the following notations are made $O_1A$= r, $O_1E$= d.

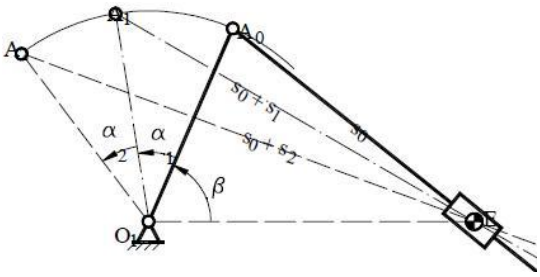


Fig. 2.1 Kinematics diagram of a mechanism with oscillating cylinder for three consecutive positions

Parameters $s_0$, $s_1$ and $s_2$ are known and determine the piston path for all three consecutive positions. Angles $\alpha_1$ and $\alpha_2$ determine the position of the balancer related to the initial position.

The landing gear must show certain advantages and meet certain requirements such as: a minimum number of force elements, a minimum number of mobile elements and joints, no deformity of subassemblies and joints, high reliability, minimum resistance to forward motion, landing shock absorption, reduced weight, easy maintenance, and the best braking capacity.

## 3. KINEMATICS ANALYSIS OF THE LANDING GEAR

We have used Artas SAM 6.1sofware for the kinematics analysis of the landing gear. It is interactive software for design, analysis, synthesis and optimization of plane mechanisms. The software package includes a numerical preprocessor and a post-processing analysis with animation and graphic display of parameters. SAM 6.1 also includes a set of instruments such as design and modeling of mechanisms, CAD interface, and optimization of mechanisms, post-processing and analysis of results, [4].

We propose for analysis a plane mechanism of the landing gear (a constructive solution for both the front strut and the main struts), of the oscillating cylinder type, as shown in figure 3.1.

The mechanism is according to a set of mandatory requirements: supporting points 1 and 5 (the slideway) are at the same absolute altitude, element/bar 3 (the strut) is initially perpendicular to the ground. The component elements have the characteristics in table 3.1.

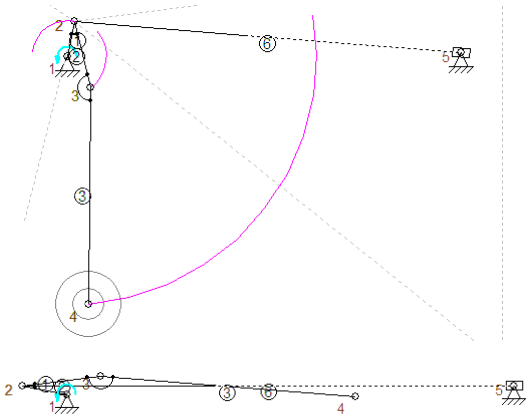

Fig. 3.1 Kinematic diagram of a landing gear

Table 3.1 Characteristics of the landing gear

| Element | Value |
|---|---|
| Element 3, the strut | 560 mm |
| Element 6, bracing strut actuator | 970 mm |
| Element 1, strut spur | 100 mm |
| Node 1 rotation angle | 900 |

Figure 3.2 highlights the variation of absolute motion of node 4 (wheel axis) and nod2 2 (strut spur) while figure 3.3 highlights the speed of these nodes.

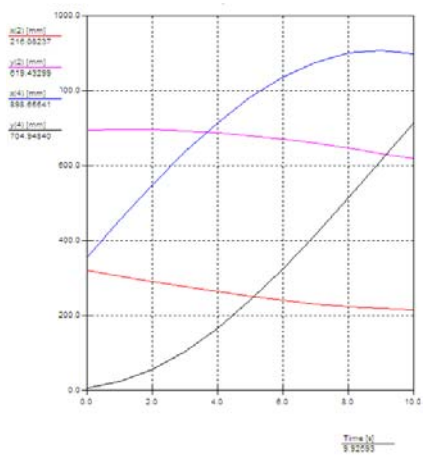

Fig. 3.2 Motion of nodes 2 and 4

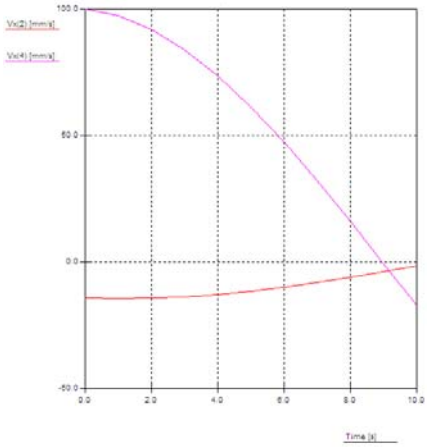

Fig. 3.3. Speeds of nodes 2 and 4

Figure 3.4 highlights the motion of nodes 2 and 4.

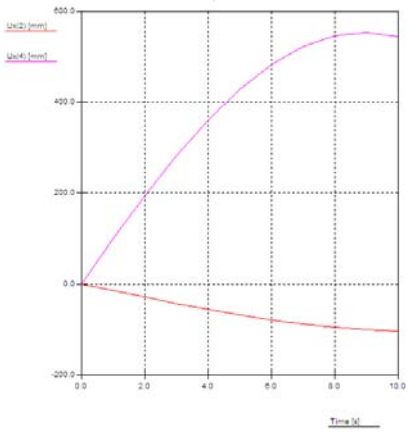

Fig. 3.4 Absolute motion of nodes 2 and 4

Table 3.1 Motion values for nodes 2 and 4

| Nr: [-] | Time [s] | Ux(2) [mm] | Ux(4) [mm] |
|---|---|---|---|
| 0 | 0.000 | 0.000 | 0.000 |
| 1 | 1.000 | -14.322 | 98.716 |
| 2 | 2.000 | -28.719 | 193.318 |
| 3 | 3.000 | -42.796 | 281.214 |
| 4 | 4.000 | -56.168 | 359.991 |
| 5 | 5.000 | -68.468 | 427.490 |
| 6 | 6.000 | -79.357 | 481.858 |
| 7 | 7.000 | -88.539 | 521.605 |
| 8 | 8.000 | -95.760 | 545.641 |
| 9 | 9.000 | -100.822 | 553.305 |
| 10 | 10.000 | -103.588 | 544.388 |

## 4. CONCLUSIONS & ACKNOWLEDGMENT

The kinematics of the mechanisms which are part of the command system of the landing gear needs to be subject to a rigorous dimensional study in order to prevent occurrence of inappropriate phenomena through kinematic parameterization.

The software method allows design and parameterization of the landing gear mechanism at a reliability level similar to the one of studies on the real models.

The authors wish to thank the "Henri Coandă" Air Force Academy of Braşov for supporting the research necessary for writing this article.

## REFERENCES

1 Creţu Mariana-Simona, *Mecanisme, Analiză structurală – teorie şi aplicaţii,* Editura Sitech, Craiova, 2010, ISBN 978-606-11-0760-5, 160p

2 Lazăr I., *Analiza structurală a mecanismelor de aviaţie*, Editura Academiei Tehnice Militare, Bucureşti, 1995, 224 p.

3 Luculescu D., Prisacariu V., *Method for determining the failure of flaps mechanism*, Review of the Air Force Academy, ISSN: 2069-4733 , No 2 (26) 2014, p41-44

4 Artas, *SAM 6.1 The ultimate mechanism designer, manual* 2010, 160p.

5 Federal Administration Aviation, *Aircraft Landing Gear Systems, ( Chapter 13),* 96p, USA, available at http://www.faa.gov/regulations_policies/handbooks_manuals/aircraft/amt_airframe_handbook/media/ama_ch13.pdf

6 Gerd Roloff System General, Airbus Deutschland GmbH, *Aircraft landing gear, The evolution of a system,* 2002, 92p

"HENRI COANDA"
AIR FORCE ACADEMY
ROMANIA

"GENERAL M.R. STEFANIK"
ARMED FORCES ACADEMY
SLOVAK REPUBLIC

INTERNATIONAL CONFERENCE of SCIENTIFIC PAPER
AFASES 2015
Brasov, 28-30 May 2015

# EXPERIMENTAL SETUP FOR STUDYING PROPERTIES OF POWER GASES

**Tomáš Lukáč*, Vladimír Horák*, Linh Do Duc*, Dalibor Rozehnal***

*Faculty of Military Technology, University of Defense, Brno, Czech Republic

***Abstract:*** *The paper deals with the development of the experimental device using for the research and study of the phase behavior and state characteristics of pressurized power gases for liquid propellant powered guns for fast shooting cadence and for long bursts of shooting. Further for the development of the device for the gun's recoil simulation, the device for simulation the sound effect of the RPG-7 launcher for a shooting training, and for the study of using of a liquid gas as the emergency power gas generator for pneumatic systems. Requirements for regulating the duration and timing of the power gas delivery follow the electronically driven and electrically operated solenoid valve. Several kinds of solenoid valves design patterns and principles of driving are closely described. The valve measured characteristics and some results of testing on the proposed experimental device are presented.*

***Keywords:*** *power gas, gas guns, solenoid valve, electrical driving*

## 1. INTRODUCTION

The proposal to develop an experimental device for the purpose of research and study of the phase behavior and state characteristics for various pressurized power gases resulted from the need to obtain experimental data e.g. for:

- The study of the phase behavior and characteristics of power gases for gas guns and verification of mathematical models [1].
- Quantifying limits of use of the liquid propellant powered guns for fast shooting cadence and for long bursts of shooting.
- Development of a variable device for the gun's recoil simulation, whereas increased power gas consumption is supposed.
- Development of a simulation device for the sound effect of the RPG-7 anti-tank grenade launcher for a shooting training [2].
- The study of using of a liquid gas as the emergency power gas generator for pneumatic systems of aircraft and military vehicles.

This device should allow arbitrary regulation of the amount and the rate of flow of a power gas being discharged from a storage tank. Further, the device should be provided with a control system regulating the duration and timing of the power gas delivery.

In liquid propellant powered guns, a mechanical drive is used for the rate valves within the systems of guns. The design involving an electronically driven and electrically operated solenoid valve follows the requirements mentioned above.

## 2. ELECTRICALLY OPERATED VALVES

The valve is controlled by an electric current flowing through a coil, so electrically operated valve is also known as solenoid valve. The most used types of valves are 2/2-way solenoid valves, which switches flow on or off and 3/2-way solenoid valves, which control the flow between the two outlet ports. First number indicates a number of ports and second number indicates number of possible states. For special application are also used 4/2, 5/2, 5/3, 5/4 or 5/5-way valves. According to an internal arrangement of valve control system, solenoid valves are divided to a direct acting and indirect or pilot operated valves. As control current can be used direct or alternating current, where solenoid valves for alternating current systems and applications have a build-in rectifier onboard.

**2.1 Direct acting valves.** Direct acting valves, sometimes referred as electromagnetic solenoid valves, can be used to control a lower pressure because a solenoid can generate only a proportional force according to its dimensions. Lower pressures require a smaller force, needed to switch, open or close a valve. An approximate relationship between the required solenoid force, the fluid pressure, and the orifice area for a direct acting solenoid valve is:

$$F_S = p\,A = p\,\frac{\pi\,d^2}{4} \qquad (1)$$

where $F_S$ is the force acting on the solenoid valve, $p$ is the fluid pressure, $A$ is the valve orifice area, and $d$ is the orifice diameter.

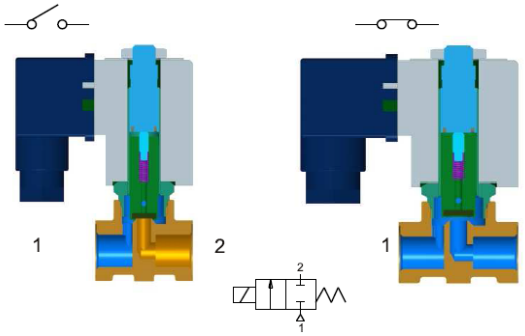


Fig. 1. Direct acting solenoid valve [3]

Fig. 1 shows a cut view of 2/2-way normally closed direct acting valve.

A direct acting solenoid valve typically operates in the range of times from 10 to 30 milliseconds.

**2.2 Indirect acting pilot operated valves.** These valves use fluid pressure to assist operation, which is used to generate the high valve forces and a small solenoid controls usage of fluid pressure. In some solenoid valves the solenoid acts directly on the main valve. Others use a small, complete solenoid valve, known as a pilot, to actuate a larger valve. Piloted valves require much less power to control, but they are noticeably slower. The operation time of a piloted valve depends on its size. Typical values are from 15 to 150 milliseconds. Fig. 2 shows a cut view of 2/2 normally closed pilot operated valve.

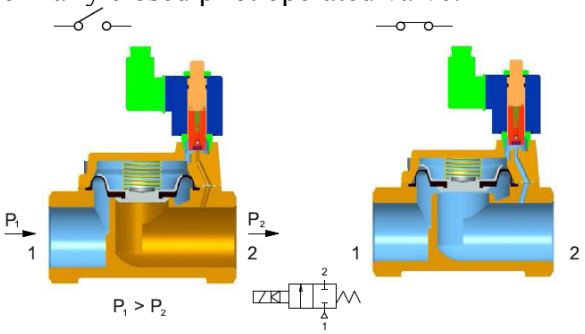


Fig. 2. Pilot operated solenoid valve [3]

Fig. 3 shows an indirect operating valve with forced lifting.

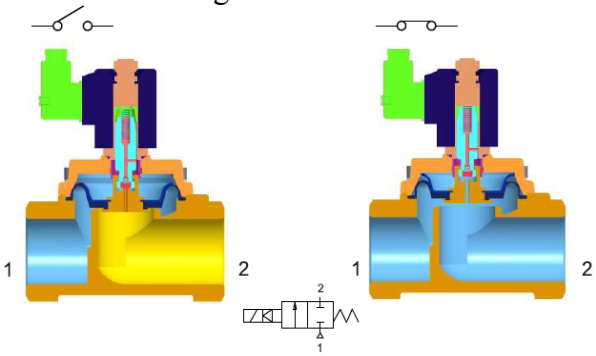


Fig. 3. Indirect operated solenoid valve with forced lifting [3]

**2.3 Valve actuators.** A valve actuator is the mechanism for opening and closing a valve. Power-operated actuators, using gas pressure, hydraulic pressure or electricity, allow a valve to be adjusted remotely, or allow rapid operation of large valves. Power-operated valve actuators may be the final elements of an automatic control loop which automatically regulates some flow, level or other process. Actuators allow an intermediate

positioning. Some valve actuators include switches or other ways to remotely indicate the position of the valve [4].

Both actuator signals and operation commands of the DCS are processed within the actuator controls. This task can in principle be assumed by external controls, e.g. a programmable logic controller (PLC). Controls use the switchgear to switch the electric motor on or off depending on the signals or commands present. Another task of the actuator controls is to provide the distributed control system with feedback signals, e.g. when reaching a valve end position. The electrical connection can be designed as a separately sealed terminal bung or plug/socket connector. For maintenance purposes, the wiring should be easily disconnected and reconnected [5].

Fieldbus technology is increasingly used for data transmission in process automation applications. Electric actuators can therefore be equipped with all common fieldbus interfaces used in process automation. Special connections are required for the connection of fieldbus data cables.

In their basic version most electric actuators are equipped with a hand wheel for operating the actuators during commissioning or power failure [5].

## 3. VALVE MANAGEMENT OPTIONS

Depending on used type of signal to switch or operate a valve, valve control circuits can be divided to analog and digital.

**3.1 Analog valve management.** Analog valve management uses analog signal to operate a solenoid valve. For mono-stable solenoid valve, constant presence of control signal is necessary as the valve is in the switched-on state. The main advantage of this sort of valve management is simple control circuits and easy maintenance. Disadvantage is higher consumption of electricity, depending on solenoid power consumption and the amount of time spent in switched state. In complicated applications with numerous valves, can be power consumption rather high. This disadvantage can be eliminated by using a bi-stable solenoid valves. A bi-stable solenoid valves contains a two solenoids, each for switching valve to one state and its control can be implemented by operating signals. This way of valves control rapidly decreases power consumption of whole system, as solenoids consume power only during the swift process of switching. As control circuits in simple applications can be used dedicated circuits, with or without a feedback, often represented by the time relays. Time relays are made as mechanical adjustable relays or digital programmable relays. Fig. 4 shows mechanical adjustable time relays.


Fig. 4. Mechanical adjustable time relays [6]

Some kinds of digital programmable relays are equipped with digital display to simple adjustment or for showing a working state and time, which is shown on Fig. 5.


Fig. 5. Digital programmable relay [7]

Time relay consists of one or more mechanical relays and timing circuit, which switches relays depending on time variable. Time periods can be adjustable from 10 ms to hundreds of hours and in combination with proper relay function time relay provides simple and effective method for automatization. Basic functions are delay ON/OFF, flasher function is repeating a loop of constant impulses, star/delta change-over allows switching between star and delta connection. Function for impulse generator generates one adjustable impulse.

**3.2 Digital valve management.** In advanced systems are simple control circuits merged in control units, which are able to control several valves at once. Control units include a logical circuit which is capable to operate connected valves and run simple diagnostic or check the states of connected valves. Specialized control units are equipped with RS232, USB or LAN interface and can be programmed and driven through PC to perform advanced tasks and applications, such a manufacturing processes, driving a manipulators or robotic systems. Fig. 6 shows Festo CECX modular automat for motion driving for advanced pneumatic applications.

Fig. 6. Modular controller CECX [8]

In modern automated or computer operated applications is an advantage to use a digital management system. In this case, each valve contains, except a solenoid, or motor in case of actuators a logical circuit onboard which allows us to provide a digital link between control unit and a valve. This system of driving is frequently used to drive valve actuators. It allows more valves or actuators to be connected on one link, depending on bus width, and allows us to build simple installation. Fig. 7 shows an actuator from Siemens Acvatix technology.

Fig. 7. Siemens Acvatix actuator [9]

Communication between valves and control units contains except the operating signals, a data communication, which includes the status reports, advanced control possibilities and makes maintenance and resolving of a problems much easier and faster. Digital connection allows us to connect the valves direct to the dedicated computer or to the module with control electronics, which can be connected to the computer. Operating software with drivers running on the computer can provide a complete control of connected valves, running scheduled tasks, maintenance or system checks. If the Ethernet connection is present, through Ethernet cable or wireless network, operating software can provide LAN or internet access to manage whole system.

## 4. POSSIBILITIES OF MEASUREMENT ON THE EXPERIMENTAL SETUP

The experimental setup for studying the properties of power gases was designed to meet requirements stated in the introduction of this paper. Presented tests were performed with the carbon dioxide.

**4.1 Arrangement of experimental setup.** The block schematic diagram of the presented experimental setup is shown in Fig. 8.

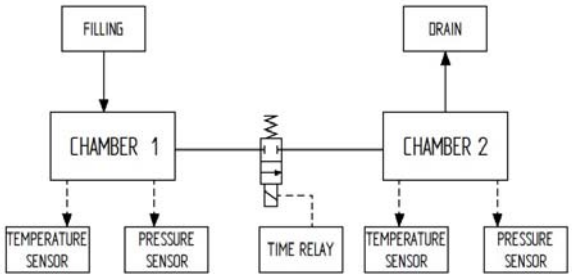


Fig. 8. Block schematic diagram

The experimental device contains two high-pressure chambers of volume 91 $cm^3$ connected by a high pressure hose. Access between chambers is provided through the electrically driven 2/2-way pilot operated solenoid valve GSR Type 46, rated for maximum pressure 10 MPa.

The time courses of pressure within the both chambers are measured by the piezo-resistive pressure sensors DMP 333 with measure range from 0 to 25 MPa.

Temperatures of both chamber walls are measured by resistive temperature sensors Jumo T90 2050 with measure range from -50 to 300 degrees Celsius.

Measured data processing is performed by the software LabVIEW from National Instruments.

The view of the experimental setup is shown in Fig. 9.

Fig. 9. View of experimental setup

**4.2 Discharge characteristics of valve.** These characteristics represent the dependence of the fluid discharged mass $\Delta m$ form the chamber 1 into the surrounding atmosphere versus the time of the valve opening. This time is controlled by the relay ElkoEP PDR-2A.

The valve discharge characteristics for gaseous, liquid and supercritical state of the carbon dioxide are shown in Fig. 10. These characteristics enable us to define the power gas discharged mass for various valve opening times and for various power gas states. The minimum opening time of the valve is 20 ms.

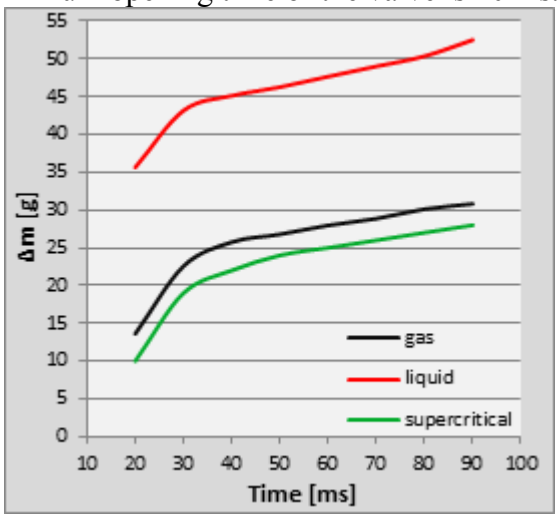


Fig. 10. Valve discharge characteristics

The dependence of the discharged mass on the opening time (see Fig. 10) is nearly linear for higher opening times. The deviation from the linear course is given by the delay of the solenoid valve opening, which is about 10 ms.

Each the discharge measurement has been started with the same initial mass of the carbon dioxide 60 g and the same initial pressure 5.5 MPa. Initial pressure for the supercritical state is 8.2 MPa.

The corresponding dependency of the median discharging fluid mass flow rate during the time of the valve opening is shown in Fig. 11.

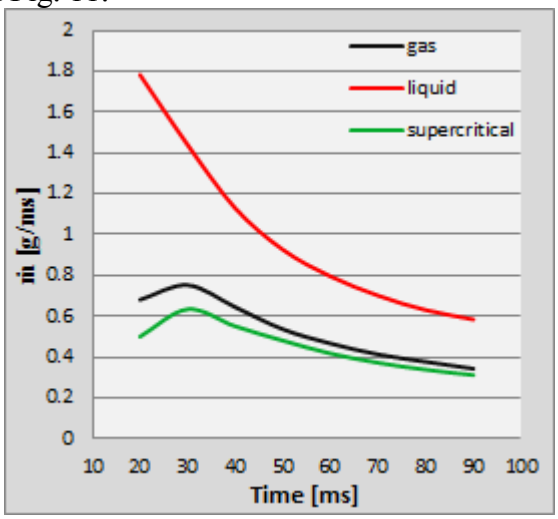


Fig. 11. Discharging mass flow rate

**4.3 Measurement of depressurization.** The time course of pressure within the chamber 1 during the discharge of gaseous $CO_2$ into the surrounding atmosphere is shown in Fig. 12.

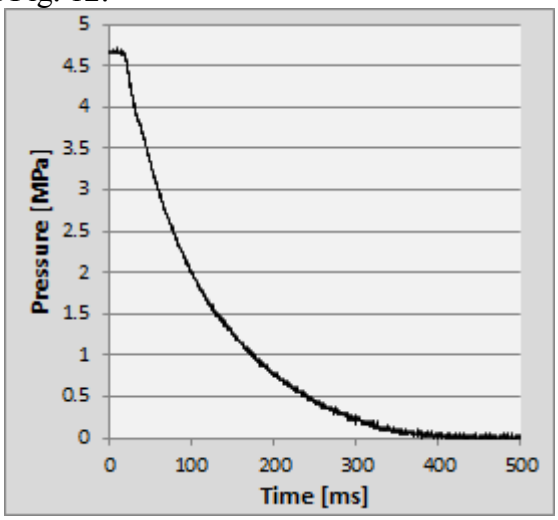


Fig. 12. Depressurization of gaseous $CO_2$

The analogical discharge of a two-phase fluid into the surrounding atmosphere is presented in Fig. 13 for various amounts of the liquid $CO_2$ filled into the chamber 1. The discharge aperture of the chamber 1 is 4 mm. The time courses of pressure from left to right correspond to the liquid $CO_2$ filling 32, 35, and 40 g.

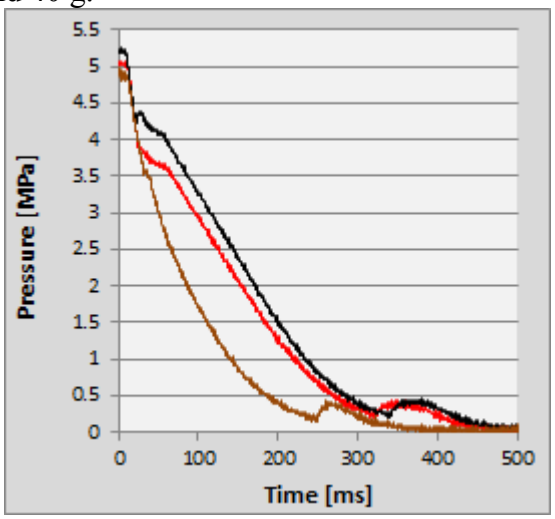


Fig. 13. Depressurization two-phase fluid

The first stage of depressurization, after the valve opening delay, represents discharge of gaseous $CO_2$ above the liquid level. This stage of depressurization corresponds to the pressure course in Fig. 12.

In the second stage between 40 and 80 ms, we can observe thermal non-equilibrium effects of two-phase fluid flow which are present due to rapid depressurization.

If the pressure and temperature drops under the $CO_2$ triple point values, the dry ice is created. The third stage of the discharge process is caused by the formation and following sublimation of the dry ice.

**4.4. Pressurization of second chamber.** When the solenoid control valve is open, the two-phase fluid starts to discharge from the chamber 1 through the valve and the connecting pipe into the chamber 2 (see Fig. 8 and Fig. 9).

Measured time courses of pressure within the both chambers during the pressurization of chamber 2 are shown in Fig. 14 for the initial liquid $CO_2$ filling in the first chamber 40 g.

In the time about 25 ms, we can also observe the thermal non-equilibrium effects of two-phase fluid flow on the chamber 1 pressure curve. In the time about 90 ms, the process of the chamber 2 pressurization is completed. The final value of pressure in the connected chambers is 3.5 MPa.

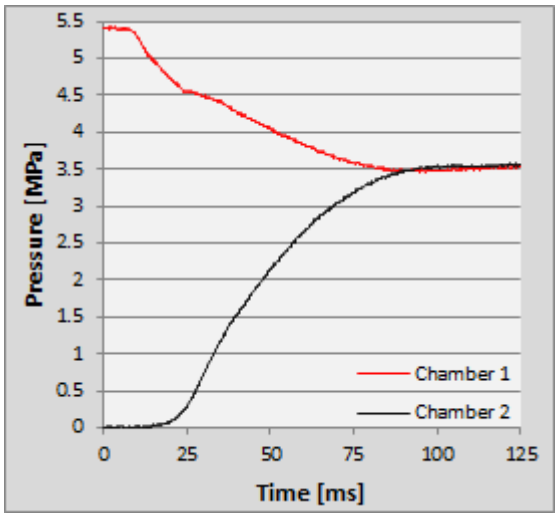

Fig. 14. Time courses of pressure during pressurization of chamber 2

**4.5 Short-interval periodic discharge.** Possibilities of the presented experimental setup to examine various short-interval periodic discharge processes are proved by the example of pressure curves, which is shown in Fig. 15.

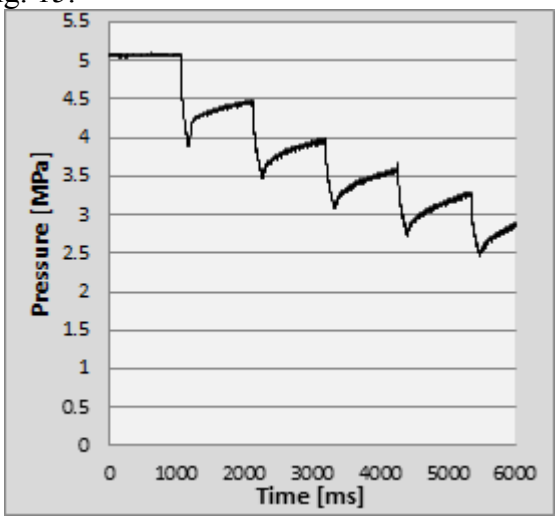

Fig. 15. Periodic discharge

Here, the solenoid control valve opens periodically for 50 ms at intervals of 1 second. The periodic discharge flow to the surrounding atmosphere was stabilized by using the orifice of diameter 1.6 mm that was placed behind the control valve. The initial liquid $CO_2$ filling was 70 g.

We can observe limited pressure stability of the system. The pressure gradually drops due to the decrease in temperature and corresponding decrease in saturated pressure of carbon dioxide.

## 5. CONCLUSIONS & ACKNOWLEDGMENT

The presented experimental setup will be widely used for the research work of authors. It is supposed using mainly for:

- The comprehensive study of properties of power gases for gas guns.
- The study of thermal non-equilibrium effects of two-phase fluid flow during the rapid depressurization.
- The verification of mathematical models of two-phase fluid flow.
- The study of stability of systems using the liquid propellant during the short-interval periodic discharge processes.
- The development of device for the simulation of small gun's recoil and the sound effect of the RPG-7 shooting.
- The study of using of a liquid gas as the emergency power gas generator for pneumatic systems.

The work presented in this paper has been supported by the institutional funding PRO K216 "Support of Research, Experimental Development, and Innovation in Mechanical Engineering" and by the Specific Research Support Project of the Faculty of Military Technology SV K216.

## REFERENCES


1. Horák, V., Do Duc, L., Vítek, R., Beer, S., Mai, Q. H. Prediction of the air gun performance. *Advances in Military Technology*, vol. 9 (2014), no. 1, p. 31-44.
2. Mai, Q. H., Horák, V., Do Duc, L. Sound effect of RPG-7 antitank grenade launcher for shooting training. *Advances in Military Technology*, vol. 9 (2014), no. 2, p. 49-60.
3. *Operation description of solenoid valves*. Mahrlo. (Retrieved November 17, 2014).
4. Nesbitt, B. (ed.), *Handbook of Valves and Actuators*, Chapter 12 Actuators. Elsevier (2007).
5. Cooper, E. *For Gate Valves, Actuation is not Turn Turn Turn. Valve World Americas*, vol. 5 (June 2014), no. 6.
6. *Haustechnik Katalog 3073 DE GB*. Eberle, [online, retrieved January 15, 2015].
7. http://www.safestb2b.com/uploads/digital-electrical-timer-relay-switch-time-ad-c9cf6.jpg, [online, retrieved January 15, 2015].
8. *Modular Controllers CECX Catalog*. Festo, [online, retrieved January 16, 2015].
9. *Acvatix Valves and Actuators Catalog*. Siemens Buildings Technologies, [online, retrieved February 2, 2015].

"HENRI COANDA"
AIR FORCE ACADEMY
ROMANIA

GENERAL M.R. STEFANIK
ARMED FORCES ACADEMY
SLOVAK REPUBLIC

INTERNATIONAL CONFERENCE of SCIENTIFIC PAPER
AFASES 2015
Brasov, 28-30 May 2015

# THERMO-GAS DYNAMIC ANALYSIS OF UPPER-STAGE ROCKET ENGINE NOZZLE

**Mihai Mihaila-Andres*, Paul Virgil Rosu***

*Institute for Theoretical & Experimental Analysis of Aeronautical Structures STRAERO, Bucharest, Romania

***Abstract**: A numerical model for the analysis of thermo-gas dynamics of rocket engine exhaust gases has been developed and described in the present study. This model corresponds to liquid propellant rocket engines designed for upper-stages of multi-stage rockets. The work is focused on the simulation of the rocket plume of the Vinci cryogenic rocket engine. Using available data, an analytical study of the convergent divergent flow was made in order to obtain more sensitive information about the physical properties of the exhaust gases. This new data was used as input for the numerical model and the solution obtained was in good agreement with experimental data both qualitatively and quantitatively.*

***Keywords:** rocket engines, exhaust gases, propulsion, liquid propellant*

## 1. INTRODUCTION

In general, for a multi-stage rocket, the first stage engine should have high thrust because it is the thrust that determines the mass that can be accelerated for a given quantity of propellant. The rest of the stage engines should have high specific impulse (or exhaust velocity) since this will determine the ultimate velocity to which a mass can be accelerated for a given quantity of propellant..

When it comes to the propellants used to create thrust or specific impulse, two types are generally utilized: solid propellants and liquid propellants. The solid propellant rocket engines are used mainly for small and medium launchers, as simple and reliable last stages for orbital launchers or as strap-on boosters for large launchers. The main advantages of the solid propellants are the storage capacity, the low risk handling and the dismissal of a propellant delivery system but there are also two major disadvantages: the engine cannot be controlled once started and the specific impulse is rather low because of the low chemical energy of the solid propellants. The liquid propellants on the other side have the advantage of high specific impulse and the possibility of controlling the flow using a delivery system [1]. The disadvantages are the storage issues and the high risk of handling.

The research presented here is focused on the liquid propellant engines used in the upper-stages of large launchers, more precisely on the thermo-gas dynamics of the exhaust nozzle of the Vinci cryogenic upper-stage engine of Ariane 5. This engine weights 550kg and has an exhaust velocity of 4650m/s and a thrust of 180kN thanks to an expansion ratio of 240 achieved by a nozzle extension deployed after separation of the main stage [2].

The propellant used is a 5.8:1 mixture ratio of liquid-oxygen liquid-hydrogen which creates a pressure of 60bar in the combustion

chamber and can deliver a specific impulse of 465s at an exhaust gas temperature of 3500K for the deployed nozzle exit diameter of 2.15m.

## 2. THERMODYNAMICS OF VINCI ROCKET ENGINE NOZZLE

In order to determine the performance parameters of the Vinci engine to be used in the subsequent numerical simulation of the exhaust gases we need to start from the thrust equation

$$F=\dot{m}u_e+p_eA_e-p_aA_e \quad (1)$$

In this relation $F$ is the rocket thrust, $\dot{m}$ is the mass flow rate through the nozzle, $u_e$ is the exhaust velocity, $p_a$ is the atmospheric pressure, $p_e$ is the pressure at the exit plane of the nozzle and $A_e$ is the area of this exit plane.

Assuming isentropic conditions and the exhaust gas as a perfect gas, the exhaust velocity can be derived by equating the kinetic energy of the exhaust gas to the change in enthalpy of the gas as it cools and expands through the nozzle. Thus, the exhaust velocity will be

$$u_e=\sqrt{2c_p(T_c-T_e)} \quad (2)$$

where $c_p$ is the specific heat at constant pressure, $T_c$ is the temperature of the gas in the combustion chamber and $T_e$ is the temperature of the gas at the exit plane of the nozzle.

Since the thrust equation already contains the exhaust pressure, it is convenient to express the exhaust conditions in terms of this pressure. Under the same assumption of isentropic expansion, the temperatures in the combustion chamber $T_c$ and the temperature at the exit plane $T_e$ can be related by the following equation for isentropic processes

$$\frac{T_e}{T_c}=\left(\frac{p_e}{p_c}\right)^{\frac{\gamma-1}{\gamma}} \quad (3)$$

The index $\gamma$ is the ratio of the specific heat of exhaust gases at constant pressure to that at constant volume. Its value has a significant impact on the resulting thrust. For rocket exhaust gases at high temperature, a typical value would be about 1.2. Using the data presented in the introduction about the Vinci engine, the index $\gamma$ can be computed in this case once we write the thrust equation in a suitable form.

The specific heat $c_p$ can also be written as a function of this index and the molecular weight of exhaust gases

$$c_p=\frac{\gamma}{\gamma-1}\frac{R}{M} \quad (4)$$

where $R$ is the universal gas constant and $M$ is the molecular weight of the exhaust gases. Knowing the exhaust velocity and the LOx-$LH_2$ mixture ratio, one can estimate the molecular weight and the temperature of the exhaust gases using the Figure 1.

Substituting for $T_e$ and $c_p$, the exhaust velocity can be expressed now as

$$u_e=\sqrt{2\frac{\gamma}{\gamma-1}\frac{RT_c}{M}\left[1-\left(\frac{p_a}{p_c}\right)^{\frac{\gamma-1}{\gamma}}\right]} \quad (5)$$

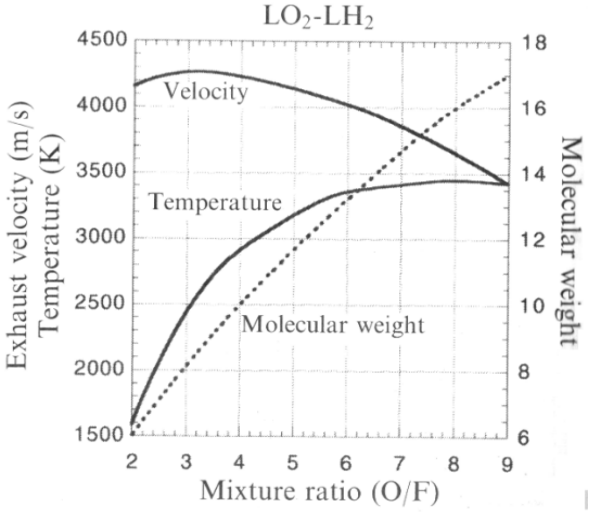


Figure 1. Variation of exhaust velocity, temperature and molecular weight for LOx-LH2 propellant

The mass flow rate $\dot{m}$ can be expressed as a function of the density, velocity and cross-sectional area at any particular point:

$$\dot{m}=\rho uA$$

Using the expression of the exhaust velocity to derive the velocity at any particular point, the mass flow rate can be written as

$$\dot{m}=pA\sqrt{2\frac{\gamma}{\gamma-1}\frac{RT_c}{M}\left[1-\left(\frac{p}{p_c}\right)^{\frac{\gamma-1}{\gamma}}\right]} \quad (6)$$

In the above relation the density $\rho$ is unknown and it needs to be expressed in terms of known parameters. Using the assumption of perfect gas and the isentropic expansion, the density at any particular point can be written as a function of combustion chamber parameters

$$\rho=\frac{p_c M}{RT_c}\left(\frac{p}{p_c}\right)^{\frac{1}{\gamma}} \quad (7)$$

Substituting in the mass flow rate equation, the following mass flow rate per unit cross-sectional area of the nozzle is obtained

$$\frac{\dot{m}}{A}=p_c\sqrt{2\frac{\gamma}{\gamma-1}\frac{M}{RT_c}\left(\frac{p}{p_c}\right)^{\frac{2}{\gamma}}\left[1-\left(\frac{p}{p_c}\right)^{\frac{\gamma-1}{\gamma}}\right]} \quad (8)$$

Differentiating the above relation, the peak value, which occurs at the throat of the nozzle, can be determined

$$\frac{\dot{m}}{A_t}=p_c\sqrt{\gamma\left(\frac{2}{\gamma+1}\right)^{\frac{\gamma+1}{\gamma-1}}\frac{M}{RT_c}} \quad (9)$$

Thus the mass flow rate can be determined mainly by the throat area $A_t$, the pressure and the temperature in the combustion chamber.

Substituting now the expressions for the exhaust velocity $u_e$ and the mass flow rate $\dot{m}$, the thrust equation can be written as

$$F=p_c A_t\sqrt{\frac{2\gamma^2}{\gamma-1}\left(\frac{2}{\gamma+1}\right)^{\frac{\gamma+1}{\gamma-1}}\left[1-\left(\frac{p_a}{p_c}\right)^{\frac{\gamma-1}{\gamma}}\right]}+ \quad (10)$$

$$+\left(p_e A_e-p_a A_e\right)$$

Using the relations presented above and the known data about the Vinci engine we have determined the density, the molecular weight $M$, the ratio of the specific heats $\gamma$, the throat cross-sectional area $A_t$ and the mass flow rate $\dot{m}$ of the exhaust gases which are needed to perform the numerical analysis of the exhaust gases [3].

## 3. NUMERICAL ANALYSIS OF EXHAUST GASES

The numerical model of the exhaust gas was computed using the CFD software ANSYS Fluent.

Using a structured multi-block strategy, the fluid domain has been meshed in the ICEMCFD meshing tool. The mesh was tuned with O-grid blocks close to the walls of the nozzle and the environment has been modeled as a cylinder. The final structured mesh had 2M hexahedral cells in 8 blocks.

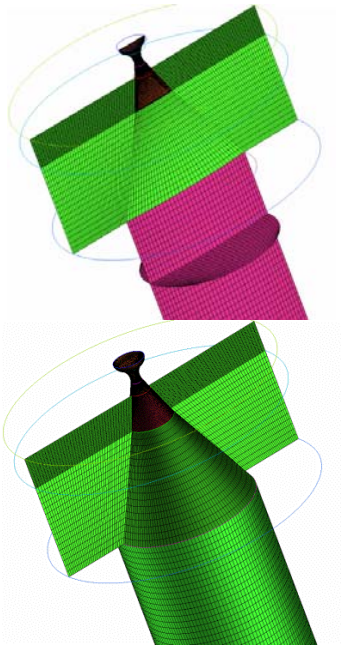

Figure 2. 3D multi-block structured mesh of the computational fluid domain

ANSYS Fluent has implemented two numerical methods for the computation of fluid flow solutions. One is a pressure-based solver and the other is a density-based solver. Both solvers can be used for a wide-ranging variety of flows but since the flow modeled here is a compressible and high speed flow, the chosen solver was density-based which solves the governing equations of continuity, momentum, energy and species transport simultaneously. Because the governing equations are non-linear (and coupled), several iterations of the solution loop must be performed before a converged solution is obtained. In each iteration the fluid properties are updated based on the current solution, the continuity, momentum, and (where appropriate) energy and species equations are solved simultaneously and the equations for turbulence are solved sequentially using the previously updated values of the other variables. The iterations continue until the convergence criteria are met.

The coupled governing equations were linearized implicitly with respect to all dependent variables in the set, specifically for a given variable, the unknown value in each cell is computed using a relation that includes both existing and unknown values from neighboring cells. This implicit formulation gives a system of linear equations for each cell in the domain.

The flow was modeled as viscous transport of species with the energy (heat transfer) equation enabled since the exhaust gases temperatures are essential to our simulation.

The effects of turbulent fluctuations of velocities and scalar quantities were modeled using the 2-equations k-eps "realizable" turbulence model which diverges from the standard k-eps model by certain mathematical constrains on the Reynolds stresses, consistent with the physics of turbulent flow. The near-wall modeling of the eps-equation uses the Enhanced Wall Treatment method which combines a two-layer model with enhanced wall functions. This choice of near-wall treatment reduces the computational time by allowing the use of coarse meshes with a $y^+$ greater than 1.

For the air/exhaust gases mixture transport simulation, a mixture of two non-reacting species was defined. The properties are defined in Table 1 where the exhaust gases properties (density, molecular weight and specific heat) were obtained from the analytical thermodynamics equations of the Vinci rocket engine described in the beginning of the text.

A pressure-inlet boundary condition was imposed at the combustion chamber/nozzle interface. The mixture has here a 1:0 ratio exhaust gases/air at a gauge total pressure of 60bar and 3500°K. The turbulence properties were imposed in terms of 1% turbulence intensity and 0.1 turbulent viscosity ratio. The same pressure-inlet boundary condition was imposed on the outer areas of the modeled environment. The mixture has here a 0:1 ratio of exhaust gases/air at a gauge pressure of 1atm and at a total temperature of 300°K. The turbulence properties were imposed in terms of turbulence intensity of 5% and turbulent viscosity ratio of 10. The outflow area was chosen far enough from the nozzle so that we could impose a pressure-outlet condition with standard atmosphere conditions at sea level (1atm and 288°K).

In order to accelerate the flow convergence, an initial "guess" solution was used at the start of the computations based on the Full Multigrid initialization.

During the solution process we monitored the convergence by plotting the residuals and the total mass imbalance between the inlet of the domain and the outflow.

Table 1 Air/Exhaust gases Mixture properties

| **Properties/Species** | **air** | **Exhaust gases** | **Mixture** |
|---|---|---|---|
| **Density (kg/m$^3$)** | ideal-gas | ideal-gas | ideal-gas |
| **Specific Heat (J/kg-K)** | 1006.43 | 4060 | mixing-law |
| **Thermal Conductivity (W/m-K)** | 0.0242 | 0.0261 | mass-weighted-mixing-law |
| **Viscosity (kg/m-s)** | 1.7894e-05 | 1.34e-05 | mass-weighted-mixing-law |
| **Molecular Weight (kg/kmol)** | 28.966 | 12.45 | mass-fractions |

| | | | |
|---|---|---|---|
| **Mass Diffusivity ($m^2/s$)** | - | - | kinetic-theory |
| **Thermal Diff. Coef. (kg/m-s)** | - | - | kinetic-theory |

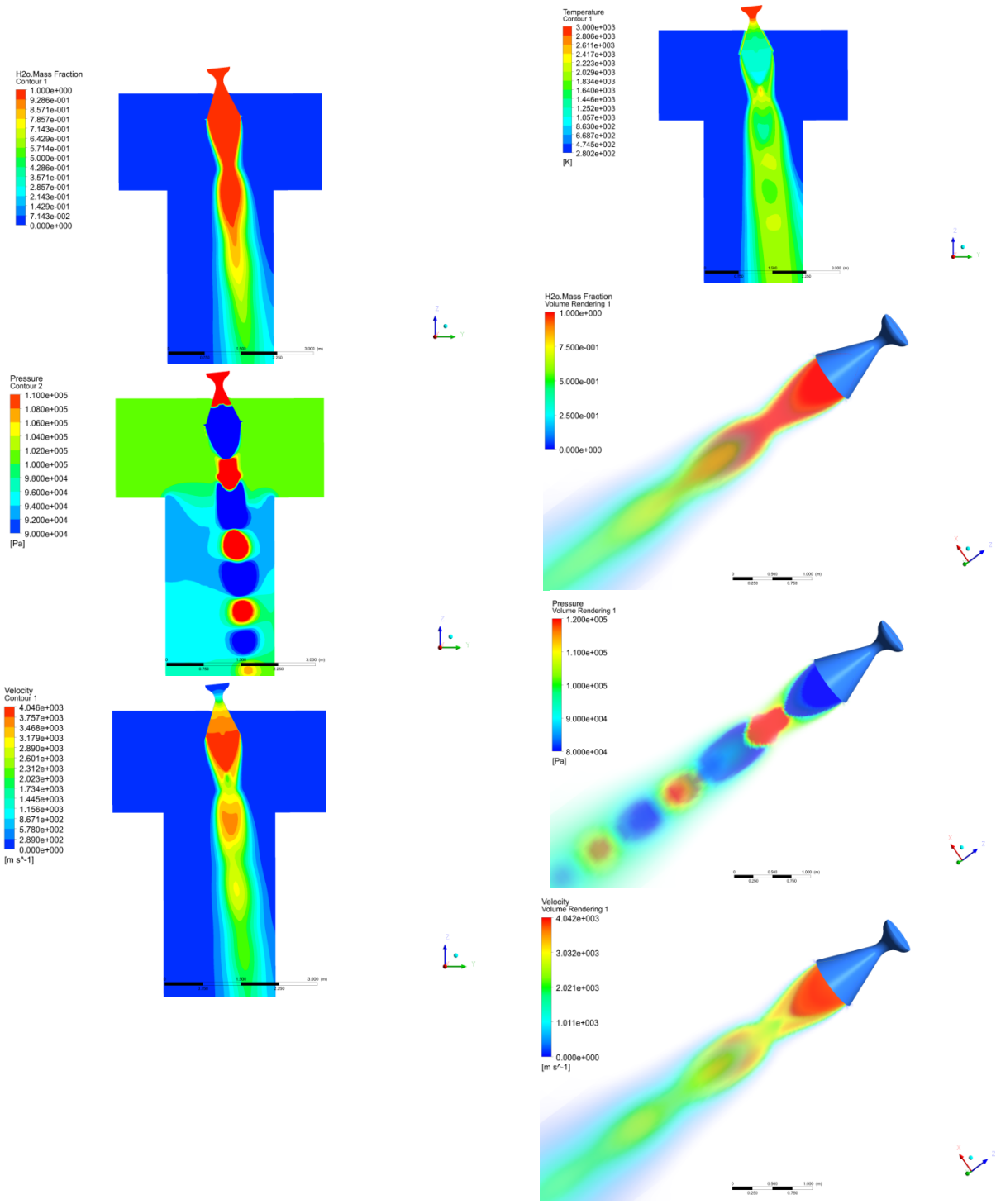

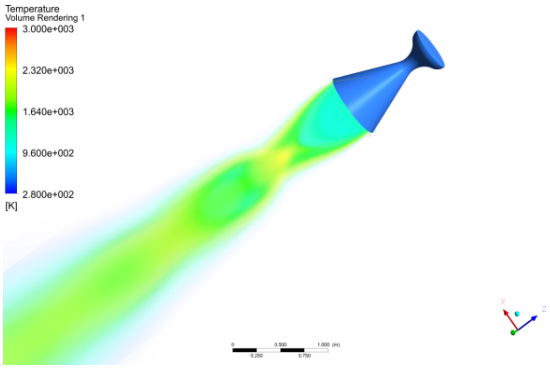


The converged solution is presented in the figures above where the rocket plume is very well defined. In the pressure distribution images one can notice the three shock diamonds that appear in the exhaust plume due to the slightly over-expanded supersonic flow at the nozzle exit [4]. The same behavior can be observed in the combustion chamber of a turbojet engine [5].

These are due to cyclic variations in the plume pressure relative to ambient creating shock waves that form the “Mach disks” [6,7]. At each shock diamond, the flow becomes compressed enough that it expands developing the expansion fan (which is a set of expansion waves). After the flow expands enough so that its pressure is again below ambient, the expansion fan reflects off the contact discontinuity creating the compression fan. The pattern of disks repeats itself three times before the turbulent shear at the contact discontinuity causes the wave pattern to dissipate. The corresponding increase and decrease in temperature can be observed in the contour plot of temperatures of the exhaust gas. In terms of exhaust gases velocity, the contour plot of velocities shows an exit velocity of gases at 4046m/s which has an error of 14% relative to the expected exit velocity of 4650m/s. The error can be attributed to a number of approximations we made in our numerical model (pseudo-transient analysis, estimated turbulence values, species transport, mesh quality, etc.).

## 4. CONCLUSIONS

In the present work the flow of exhaust gases from a liquid propellant rocket engine have been numerically modeled. In order to perform the appropriate simulations, the combustion chamber and the nozzle were the subject of an analytical study. Using known data about the Vinci cryogenic rocket engine we calculated the characteristics of the exhaust gases (molecular mass, specific heat and the mass flow rate) which were used to complete the boundary conditions for the numerical model. The solution for the simulation was calculated using the CFD software ANSYS where the flow was modeled as a pseudo-transient, turbulent, species transport, energy enabled flow. The results proved the feasibility of the complex model. Qualitatively we obtained the expected rocket plume and we were able to identify its characteristics. Quantitatively, the errors were acceptable for the degree of approximation introduced by the numerical model but opens new scopes for future studies. The mesh influence on precision, a better turbulence model and more accurate estimation of turbulence properties, a full transient analysis and a more complex multiphase model are all possible starting points for more accurate future simulations of rocket exhaust gases flow.

## REFERENCES

1. Mattingly J.D., Ohain H, *Elements of Propulsion: Gas Turbines and Rockets*, AIAA Education Series, Reston, Virginia (2006).

2. Sutton G.P., Biblarz O., *Rocket Propulsion Elements*, John Willey & Sons, Inc., New York (2001).

3. Hill, P., Peterson, C., *Mechanics and thermodynamics of propulsion*, Addison-Wesley Publishing Company, (2010).

4. Orlowska, M., Panas, A.J., Recko, K., Zyluk, A., *Numerical Modelling Of The Thermo-Mechanical Response Of A Rocket Motor To Exhaust Gases Load*, Journal Of Theoretical And Applied Mechanics, 52, 3, pp. 803-814, Warsaw (2014).

5. Rotaru C., Andres-Mihaila M., Matei P. G., *"An Extended Combustion Model for the Aircraft Turbojet Engine"*, International Journal of Turbo & Jet Engines, Volume 31, Issue 3, Pages 229-237 (2014).

6. Pandey, K. M. and Yadav, S. K., *CFD analysis of a rocket nozzle with two inlets at Mach 2.1*, Journal of Environmental Research and Development, Vol. 5 No. 2 (2010).

7. Georgiadis, N.J., Dalbello,T.W., Trefny, C.J. and Johns, A.L., *Aerodynamic Design and Analysis of High Performance Nozzle for Mach 4 Accelerator Vehicles*, 44th AIAA Aerospace Sciences Meeting & Exhibit, Reno, Nevada (2006).

# ENGINEERING SCIENCES

"HENRI COANDA"
AIR FORCE ACADEMY
ROMANIA

"GENERAL M.R. STEFANIK"
ARMED FORCES ACADEMY
SLOVAK REPUBLIC

INTERNATIONAL CONFERENCE of SCIENTIFIC PAPER
AFASES 2015
Brasov, 28-30 May 2015

# DESIGN OF A LSA AIRCRAFT USING ADVANCED SOFTWARE

**Angi Norbert*, Razvan Udroiu***

*Faculty of Technological Engineering and Industrial Management, Transilvania University of Brasov, Romania

***Abstract:*** *This paper is focused on the design of a light sport aircraft (LSA) in the university level. A market research and analysis study has been made and based on the General Aviation Manufacturers Association (GAMA) study, showing that 20-25% of light weight sport aircrafts are currently produced using reciprocating engines and within a few years this ratio could increase between 33% and 50%. A preliminary and conceptual design was done for a new lightweight, low-cost, low fuel consumption and long-range aircraft. The design process that covers by this paper is based on software tools like as Advanced Aircraft Analysis (AAA) and CATIA. Using the data from this paper, the design will follow a series of aerodynamic analysis in wind tunnel, and flight experiments to determine the real performance of the airplane.*

***Keywords:*** *preliminary and conceptual design, aircraft, lightweight structure, Computer Aided Design*

## 1. INTRODUCTION

The reason for choosing this theme was the result of an economic analysis of data from General Aviation Manufacturers Association (GAMA) [7] resulting that the global sales of various planes, best-selling aircraft are equipped with piston engine. "In 2013 the aircraft sold worldwide in 2256, 933 (41.4%)", which can be seen in fig. 1. At the same time range aircraft piston engine, the lightweight are in development, "the update of economic, figures seem to show that LSA is somewhere between 20% and 25% of sales piston GA and this share will increase with LSA becoming close to 33% to 50% of total sales piston engine airplanes" [7], fig. 2. "FAA issued a 20-year forecast for aviation in 2030, according to LSA aircraft sales will increase by 825 per year until 2013 and then increase to 335 per year" [7].

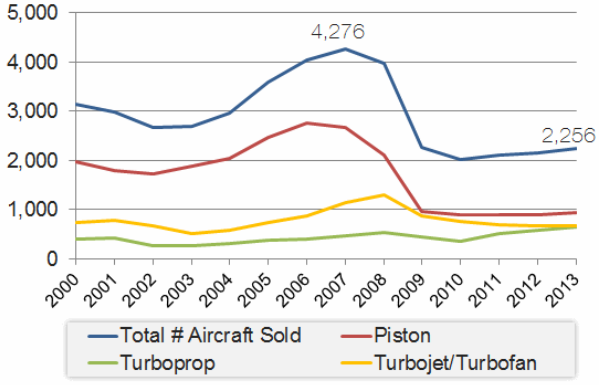


Fig,1. Aircrafts sold by category between 2000 -2013 [7]

According to the last year's market analysis, CS - LSA (Light Sport Aircraft) regulation allows an facile certification of

aircraft and the total investment for production is less compared to other category of airplanes. Because LSA aircrafts have a lower selling price than other aircrafts, 60.000$ – 190.000$ and lower fuel consumption, this type of airplanes becomes more and more attractive for people passionate about flight. Most modern airplanes from this category are capable for long flights, up to 1400 km without refueling. This type of airplanes are ideal for business and leisure flight, because their low fuel consumption, and the maintenance cost and taxes are lower than other categories of airplanes. According to the simplicity and flying cost of light sport aircrafts, it could be a market opportunity for Romania.

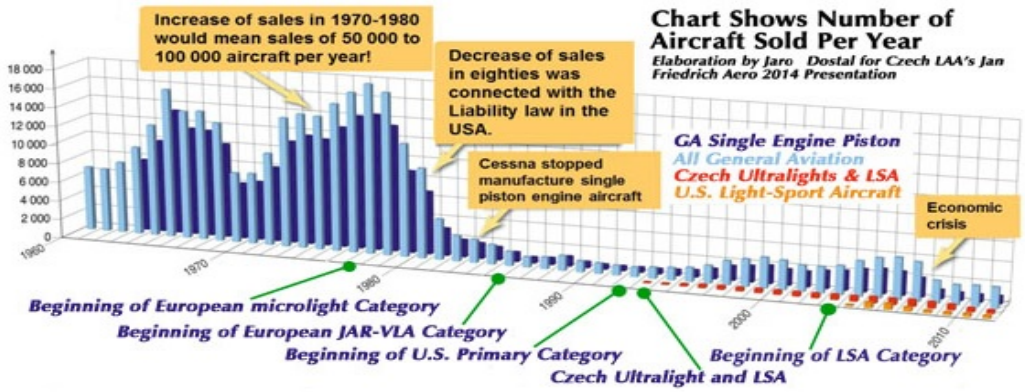


Fig. 2. Number of LSA sold per year, from 1960 to 2014 [1]

## 2. PRELIMINARY DESIGN OF THE AIRPLANE

Generally the aircraft development process consists in the following steps: market analysis and customer requirements, mission specifications, conceptual design, preliminary design, detailed design, prototype manufacturing, flight test, and finally the aircraft production.

In the conceptual design phase, the aircraft will be designed in concept without the precise calculations. The preliminary design phase tends to employ the outcomes of a calculation procedure. As the name implies, the parameters that are determined in the preliminary design phase, are not final and will be altered later. Also, in this phase, parameters are essential and will directly influence the detail design phase. One of the results of the preliminary design is used to define the geometry of the aircraft. These parameters will be used as input data to 3D modelling of the aircraft. In a modern design process, the 3D model of the aircraft plays a crucial role.

Designing an aircraft can be an overwhelming task for a new designer. The designer must strive for a better, lighter and optimal solution as the concept to be competitive with the best aircraft in the current market. An optimal design could mean lighter structure, lower fuel consumption or lower price.

The conceptual design of the aircraft was started by studying the current competitors in the same regulation class. After the studies between several possible configurations it was chosen the best configuration for the concept.

After collecting this data from other aircrafts, it starts the preliminary design of the airplane. The preliminary design of the aircraft was made by using a commercial aircraft design and analysis software, thus as Advanced Aircraft Analysis (AAA) from DAR corporation [6].

Table 1 General characteristics of the SkyDreamer airplane

| **Parameter** | **Value** |
|---|---|
| Crew | Two |
| Empty weight<br>Max. Takeoff weight | 315 kg<br>600 kg |
| Fuel capacity | 100 L |
| Powerplant | Rotax 912iS – 100 HP |
| Propelles | NEUFORM TXL3-65-47-101.6 |
| Maximum speed<br>Cruising speed | 290 km/h<br>205 km/h |
| Range | 1650 km |
| Service ceiling | 5500 m |

Generally, to design a new aircraft it is necessary a mission specification to be defined. Aircraft mission specifications come depending on the aircraft type and customer requirements [6].

The airplane presented in this paper is called SkyDreamer, having the general characteristics as shown in the table 1. The mission specification of the SkyDreamer aircraft consists in the following main segments: warm-up, taxi, take-off, climb, cruise, descend and land/taxi. The preliminary design of the aircraft was done using a design procedure, as seen from fig. 3.

The preliminary design phase is performed in the following steps, using AAA software:

- estimate aircraft maximum take-off weight,
- determine wing area and engine thrust (or power) simultaneously,
- aerodynamic consideration,
- estimation of the wing, flap, aileron, fuselage and tail dimensions,
- aircraft weight and balance and
- static stability.

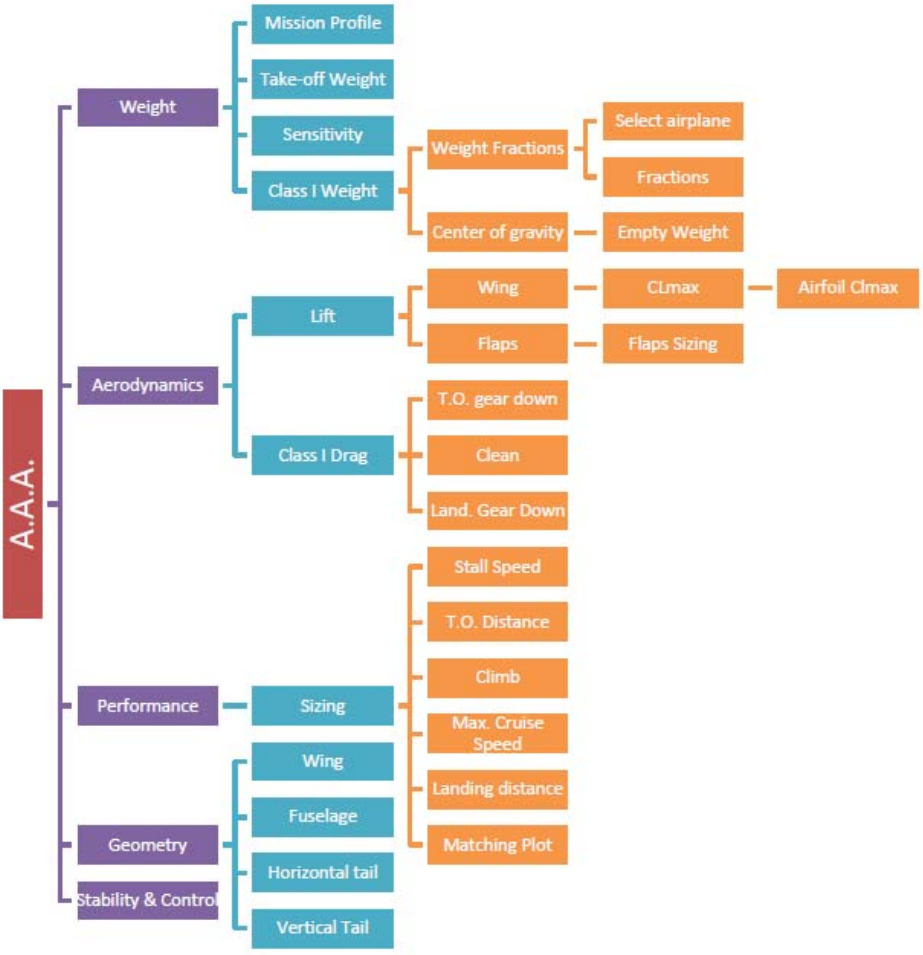


Fig. 3. The flowchart of preliminary design using AAA

According to achieve higher performance for the aircraft it was chosen a Rotax 912iS, 100 HP engine. Compared to other engines it has a lower fuel consumption, $CO_2$ emission and lower weight to horsepower ratio. For this type of engine it was choosen NEUFORM TXL3-65-47-101.6 proppeler having 1.65 m diameter.

The general technique to estimate the maximum take-off weight is as follows: the aircraft weight is broken into several parts. Some parts are determined based on statistics, but some are calculated from performance equations. Maximum take-off weight is broken into four elements: payload weight ($W_{PL}$), crew weight ($W_C$), fuel weight ($W_f$) and empty weight ($W_E$).

$$W_{TO} = \frac{W_{PL} + W_C}{1 - \left(\frac{W_f}{W_{TO}}\right) - \left(\frac{W_E}{W_{TO}}\right)} \quad (1)$$

In order to find $W_{TO}$, one needs to determine the three parameters (payload, crew, and fuel fraction) in a fairly accurately way, and the last parameter (i.e. empty weight fraction) from statistics.

The required amount of the total fuel weight necessary for a complete flight operation depends upon the mission to be followed, the aerodynamic characteristics of the aircraft, and the engine specific fuel consumption (table 2).

Table 2. Mission fuel weight calculation

| | Mission profile | $W_{begin}$ [N] | $\Delta W_{Fused}$ [N] | $W_{Fbegin}$ [N] |
|---|---|---|---|---|
| 1 | Warmup | 5967.3 | 29.8 | 720.6 |
| 2 | Taxi | 5937.4 | 17.8 | 690.8 |
| 3 | Take-off | 5919.6 | 11.8 | 672.9 |
| 4 | Climb | 5907.8 | 9.7 | 661.1 |
| 5 | Cruise | 5898.1 | 515.4 | 651.4 |
| 6 | Descent | 5382.6 | 37.7 | 136.0 |
| 7 | Land,Taxi | 5345.0 | 37.4 | 98.3 |

The general arrangement of the wing at the fuselage affects the parameters of the airplane. It was chosen a low wing configuration. The relative thickness of the wing is chosen according to a low cruise speed aircraft (V < 0.7 M), ε0=14-20% at the root chord of the wing and εe=7-9% at the tip chord of the wing.

The optimal value for the dihedral angle is between $\psi_v$=5-7° for a low wing configuration in order to obtain a good lateral stability for the airplane.

Some of the preliminary design results are presented below.

**a) The main configuration of the fuselage**

- The length of the fuselage, $L_f$ = 6.45m;
- Maximum height of the cabin, $h_{fmax}$ = 1.05 m;
- The maximum width of the fuselage, $l_f$ = 1.18 m.

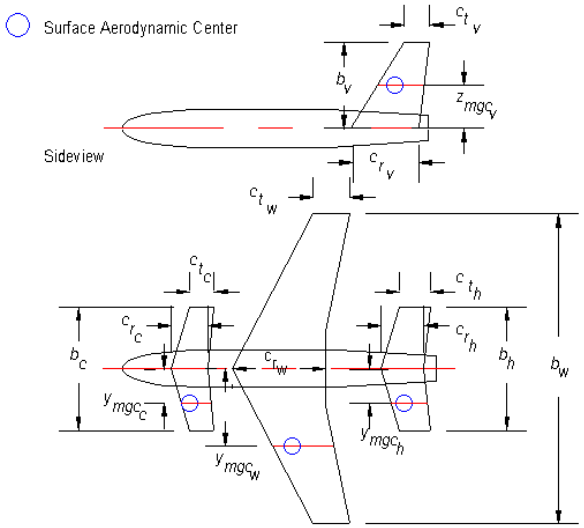


Fig. 4. Wing geometric parameters

**b) The main configuration of the wing.** The main parameters of the wing (fig. 4) are:

- airfoil type, Eppler 562 [2] having a relative thickness, (t/c)w =15% at 27.6% c;
- span, bw= 10.09 m;
- area, $S_w$=11.5m$^2$;
- aspect ratio, $AR_w$= 8.85;
- taper ratio, λ= 0.65;
- leading sweep angle, $\Lambda_{LE}$ = 3.86$^0$;
- trailing edge sweep angle, $\Lambda_{TE}$=-1.61$^0$;
- quarter chord sweep angle, $\Lambda_{c/4w}$ = 2.5$^0$;
- dihedral angle, ψ= 5$^0$;
- angle of attack, $i_W$= 1.5$^0$;
- root chord length, $c_{rw}$ =1.38 m;
- tip chord, $c_{tw}$= 0.9 m;
- mean geometric chord, $c_w$=1.16 m.

**c) The configuration of the tail.** The main parameters of the horizontal tail are:

- horizontal tail span, $b_h$= 2.79m;
- root chord, $c_{rh}$=0.92 m;
- tip chord, $c_{th}$=0.69 m;
- mean chord length, $c_h$=0.81 m

- sweept angle, $\Lambda = 2.5^0$;
- horizontal tail area, $S_h = 2.25\ m^2$;
- aspect ratio, $AR_h = 3.45$;
- taper ratio, $\lambda = 0.75$;

The main parameters of vertical tail are:

- tail span, $b_v = 1.22$ m;
- root chord, $c_{rv} = 1.29$m;
- tip chord, $c_{tv} = 0.84$ m;
- sweept angle, $\Lambda = 15^0$;
- vertical tail area, $S_v = 1.3 m^2$;
- aspect ratio, $A_{rv} = 1.15$;
- taper ratio, $\lambda = 0.65$;
- mean tail chord cv=1.08.

**d) Pre-dimensioning of the landing gear.** The main parameters of the landing gear (fig. 5) layout [3, 4, 6] are:

- X-coordinate of forward critical gear ground containing point, Xgear.for=0.745m;
- X-coordinate of after critical gear ground containing point, Xgear.aft =2.12m ;
- Y- coordinate of the after critical gear ground containing point, Ygear,aft=0.955m;
- lateral tip-over angle, $\psi = 44.220$.

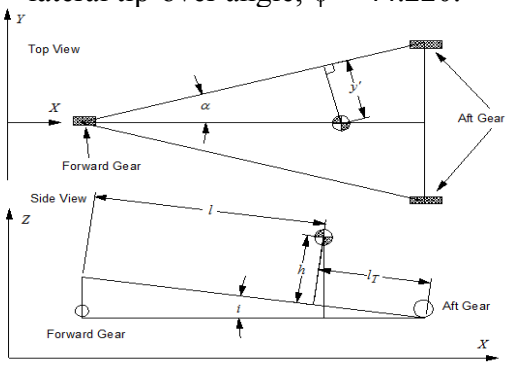


Fig. 5. Landing gear configuration

**e) Calculation of aerodynamic characteristics of the aircraft.** The aerodynamic characteristics for the airplane it was calculated for the following conditions: take off with gear down, climb with gear up, cruise, descent with gear up and landing with gear down. The drag polar plots are shown in the fig. 6.

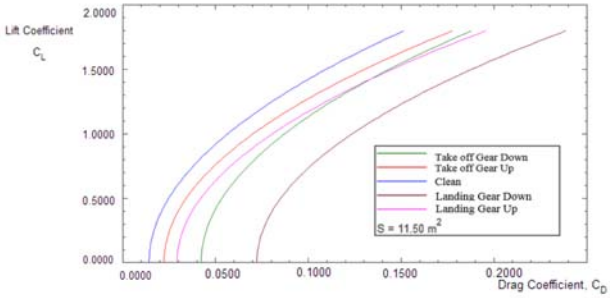


Fig. 6. Drag polar

## 3. DETAIL DESIGN OF THE AIRPLANE

Based on the dimensions obtained from AAA, the SkyDreamer aircraft was 3D designed using the advanced Computer Aided Design (CAD) software, CATIA [5]. The detail design of the airplane was started from the configuration of the cockpit. The layout of the cockpit is design to ensure maximum comfort for the pilot at long duration flight. The seats and the rudder pedals are adjustable to ensure access to the instrumental panel and flight commands, in function of the height of the pilots (1.63 m – 1.91m). The CAD models of the cockpit, fuselage, tail of the SkyDreamer aircraft are presented in the figures 7, 8, 9 and 10.

Fig.7 General layout of the cockpit

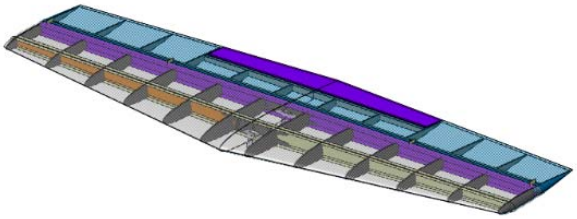

Fig.8. CAD model of horizontal tail

Fig. 9 CAD model of the fuselage

Fig. 10. Concept aircraft – SkyDreamer

## 4. CONCLUSIONS

This paper presents some steps of the SkyDreamer project. According to the estimated performance, the new concept could be competitive with the top sales light sport aircrafts in the current market. The estimated flight range of this new aircraft is 1650 km with 100 l fuel, which means 14.89 l/h fuel consumption, according to AAA results. Using advanced software tools (Advanced Aircraft Analysis, Catia), the design process of a new aircraft is made in a relative short time and it is simplified. The results of the present study reflect only the preliminary design of the airplane, which will be followed by further tests and design optimization, to obtain the final layout of the airplane. After wind tunnel analysis, flight tests and further optimizations, the aircraft could be passing towards to the production.

## REFERENCES

1. Dan Johnson Media Corp. 2013 Light-Sport Market Share Report & Analysis, (2014). Available: http://www.bydanjohnson.com/
2. Eppler, R. Airfoil Design and Data, (1990).
3. Curry, N. S. Aircraft Landing Gear Design Principles and Practices, American Institute of Aeronautics and Astronautics, (1984).
4. Roskam, J.,. Airplane Design, University of Kansas, (1985).
5. ***, User manual for Catia v5, Dassault Systemes (2012)
6.***, DARcorporation, http://www.darcorp.com/Software/AAA/ (2014).
7.***, General Aviation Manufacturers Association (GAMA), http://www.gama.aero/industry-documents-and-publications (2014).

"HENRI COANDA"
AIR FORCE ACADEMY
ROMANIA

"GENERAL M.R. STEFANIK"
ARMED FORCES ACADEMY
SLOVAK REPUBLIC

INTERNATIONAL CONFERENCE of SCIENTIFIC PAPER
AFASES 2015
Brasov, 28-30 May 2015

# THE BEHAVIOR OF AN $AL_2O_3$ COATING DEPOSITED BY PLASMA ELECTROLYTIC OXIDATION ON ALUMINUM ALLOYS AT HIGH TEMPERATURE REGIME

**Geanina Laura Pintilei*, Marioara Abrudeanu*, Corneliu Munteanu**, Ionuț Vasile Crîşmaru**, Mihaela Vladu* and Iustin Popa***

*Faculty of Mechanics and Technology, University of Pitesti, Romania, **Faculty of Mechanical Engineering "Gheorghe Asachi" Technical University, Iasi, Romania

***Abstract:*** *Aluminum alloy present numerous advantages like high specific strength and diversity which recommend them to a high number of applications from different fields. In extreme environments the protection of aluminum alloys is difficult and requires a high number of requirements like high temperature resistance, thermal fatigue resistance and corrosion fatigue resistance. To obtain these characteristics, coatings can be applied to the surfaces so they can enhance the mechanical and chemical properties of the parts. This paper analyses an $Al_2O_3$ coating deposited by plasma electrolytic oxidation on an AA2024 aluminum alloy. The sample was subjected to a temperature of 500 °C and after that slowly cooled to room temperature. The sample was analyzed by electron microscopy and X-ray diffraction to determine the morphological and phase changes that occurred during the temperature exposure. To determine the stress level in the parts due to thermal expansion a finite element analysis was performed in the same conditions as the tests.*

***Keywords:*** *$Al_2O_3$, PEO, AA2024*

## 1. INTRODUCTION

The purpose of this paper is to analyze the behavior of an AA2024 sample with an $Al_2O_3$ coating deposited by plasma electrolytic oxidation. The sample was subjected to high temperature. After the test the sample was analyzed by electron microscopy and X ray diffraction and also finite element analyses were done to determine the stress level that appears in the sample due to the different thermal expansion coefficients of the materials.

Yerokhin A. L. 1998, describes the fact that plasma electrolytic oxidation, also called micro arc oxidation represents a relatively new technique of surface modification which have a greater interest for achieving some ceramic oxide coating on Al, Ti and Mg alloys. [1-3]

The layer obtained by plasma electrolytic oxidation can enhance wear and corrosion properties as well as conferring other functional properties such as antifriction properties, thermal protection, optical and dielectric properties. Another used of plasma electrolytic oxidation is that of bond coating for other coating methods. [4]

Plasma electrolytic oxidation method is based on conventional anodic oxidation of metals with low density and their alloys in liquid electrolyte solution. This method works over voltage discharge which leads to micro

plasma discharge. Plasma electrolytic oxidation method allows the formation of oxides coatings made of substrate material as well as more complex oxides containing elements present in the electrolyte. [5]

## 2. MATERIALS, METHODS AND INSTRUMENTATION

The deposition of the coating was done by plasma electrolytic oxidation spraying. After deposition, the sample was subjected to a temperature of 500°C for a period of two hours. The sample was cooled slowly in atmospheric air at normal temperature.

Electron microscopy and X ray diffraction were used to analyze the effects of the high temperature exposure on the sample. Before the analyses, the sample was cut, polishes and cleaned in ultrasonic bath.

In table 1 the parameters used for the elecrtolitic plasma oxidation are presented. Electrolyte solution used in deposition composed of: sodium metasilicate ($Na_2SiO_3$), sodium hydroxide (NaOH) and distilled water.

*Table 1: Parameters of deposition*

| Technological parameters | $Al_2O_3$ |
|---|---|
| Time (min) | 2 |
| Tension (V) | 350 |
| Intensity (A) | 20 |

A finite element analysis was done to determine the mechanical stress that appears in the sample due to the thermal expansion of the materials. The mesh used in the finite element analyses is shouted in Fig 1. The mesh consisted of 50225 nodes and 25892 elements.

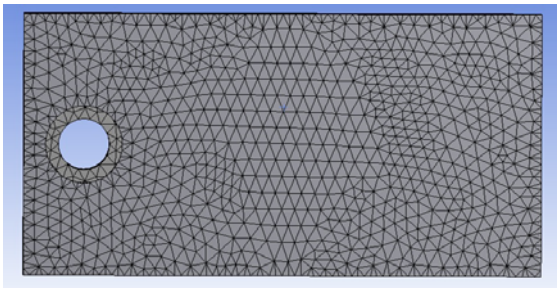

Fig. 1. The mesh used in the finite element analyses

## 3. RESULTS OF THE THERMAL EXPOSURE TESTS

In Fig. 2 a-b are presented images of the sample with an $Al_2O_3$ coating before and after the exposures to high temperature.

In Fig. 2 – a in cross section the microstructure of the layer obtained by plasma electrolytic oxidation after deposition can be observed. The layer obtained presents pores with different dimension and a very good compactness. Fig. 2 – b presents a SEM image in cross section of the layer obtained by plasma electrolytic oxidation after thermal exposure at 500ºC for two hours. In this case as well we can observe a compactness of the layer deposited. On the SEM image in cross section we can observe pores with different dimensions.

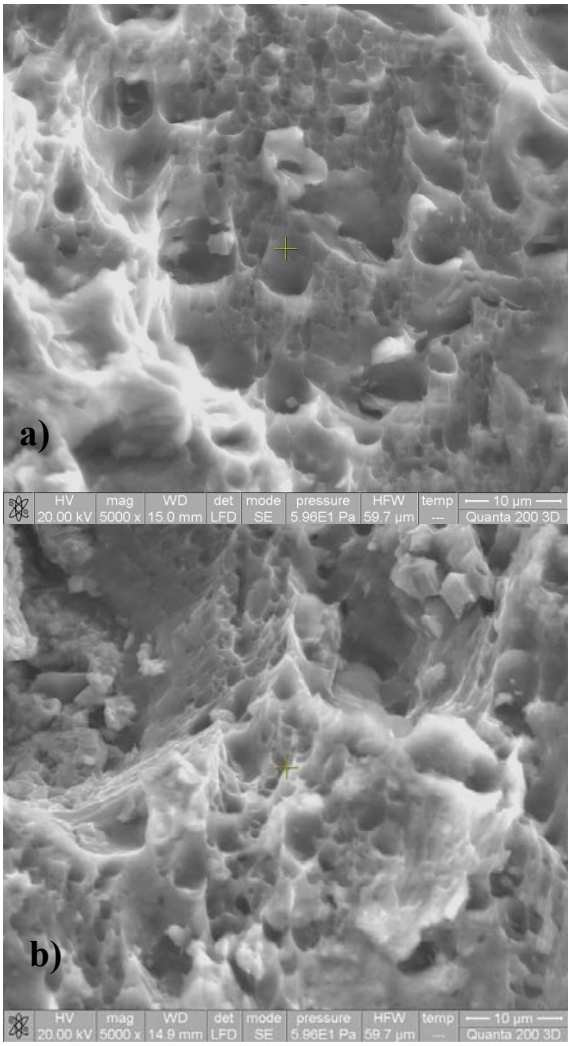


Fig. 2. SEM images at the magnification of 5000x of the $Al_2O_3$ coating: (a) before test, (b) after test

For the determination of the constituent phases of the layer obtained by plasma electrolytic oxidation we used X-ray diffraction method (Fig. 3.).

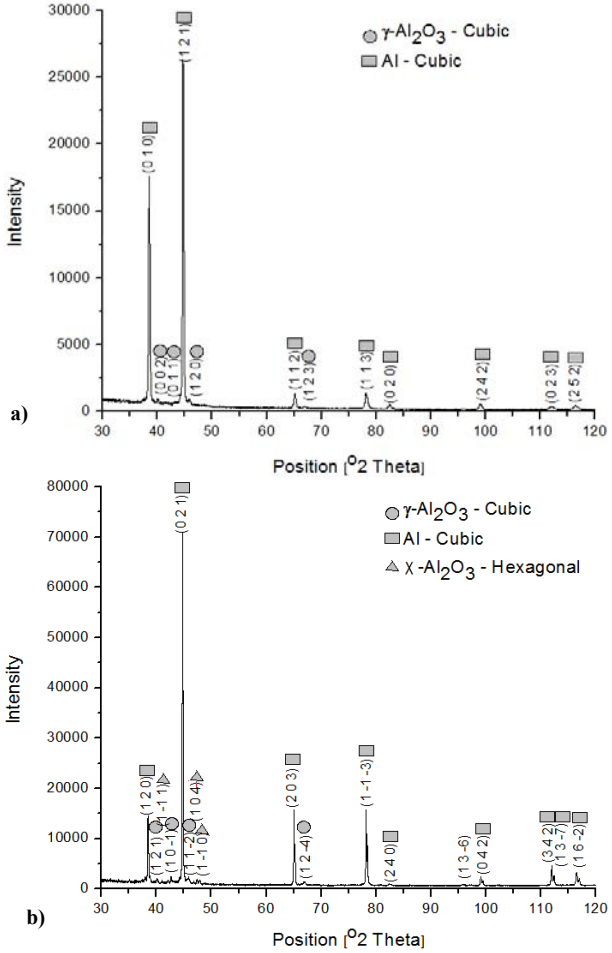


Fig. 3. XRD analyses of the $Al_2O_3$ coating: (a) after deposition, (b) after test

After plasma electrolytic oxidation deposition we can observe in the X-ray diffraction that the diffraction is made of one single phase namely is $\gamma$-$Al_2O_3$. The intensity peaks which determine Al phase on the surface is due to X-ray penetration through the coating, due to the pores obtained in coating after deposition. This Al phase is identified from the base material.

After thermal exposure at 500°C the Al phase which appears on the diffraction due to X - ray coating penetration remains unchanged, crystallizing in cubic system. In the case of the $\gamma$-$Al_2O_3$ phase, as well, in it unchanged the cubic system. Due to oxidation after thermal exposure appeared on the surface a new phase $\chi$-$Al_2O_3$ which crystallized in hexagonal system. The picks increased in intensity due to the coating being sintered.

Maximum equivalent stress appears on the clamping whole area. Its value is 252 MPa. On the surface of the sample the maximum equivalent stress is 200 MPa. In the cross section of the sample we can that the base material is less solicited mechanical, and the tension distribution on the surface is extended in all layer body (Fig. 4.).

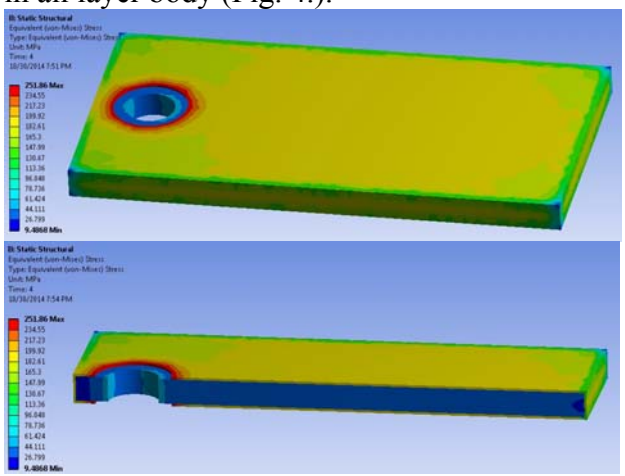

Fig. 4. Tensile stress distribution in the sample with an $Al_2O_3$ coating

The elastic strain distribution is presented in Fig. 5. The maximum value of the elastic strain on the clamping hole is 0.78%, and on the rest of the surface layer is 0.73%.

In Fig. 6 the plastic deformations of the sample is presented. The value of the plastic deformation is very small in the coating layer, except for clamping hole area where the value is 0,3%.

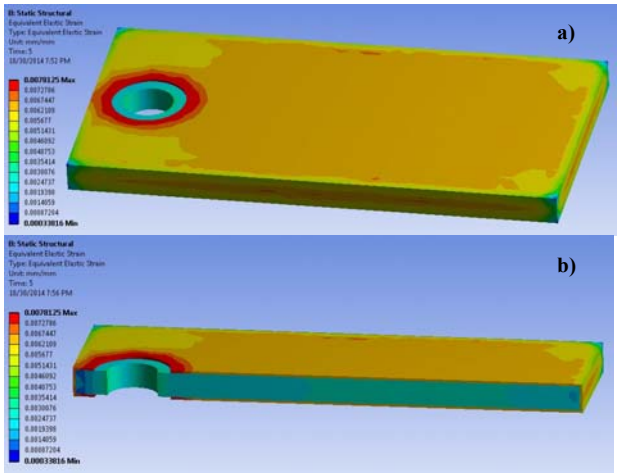


Fig. 5. Elastic strain distribution in the sample with an $Al_2O_3$ coating

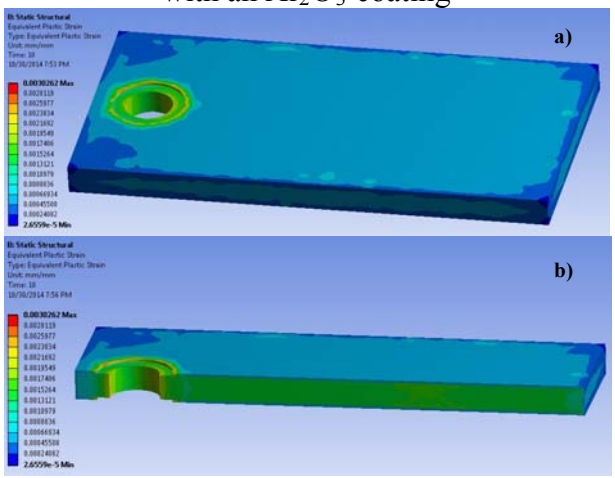


Fig. 6. Plastic deformations in the sample with an $Al_2O_3$ coating

Fig. 7 presents the total deformation which appears in the sample. The maximum value of the total deformation is 0.62 mm.

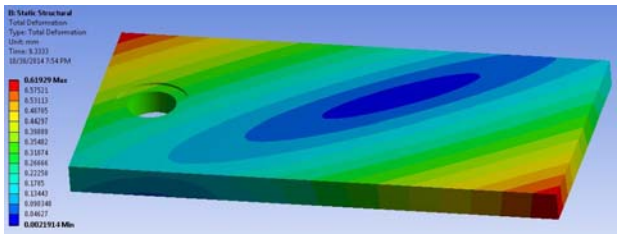

Fig. 7. Total deformation in the sample with an $Al_2O_3$ coating

## 5. CONCLUSIONS & ACKNOWLEDGMENT

The exposure of the sample with a coating of $Al_2O_3$ obtained by plasma electrolytic oxidation at a temperature of 500°C produced a higher level of compactness of the deposited coating. The volume of the pores and the thickness of the splats interfaces decreased.

This work of Pintilei Geanina Laura was supported by the strategic grant POSDRU/159/1.5/S/138963 - PERFORM, co-financed by the European Social Fund – Investing in People, within the Sectoral Operational Programme Human Resources Development 2007-2013.

## REFERENCES

1. Per-Lennart Larsson, On representative stress correlation of global scratch quantities at scratch testing of elastoplastic materials, Materials & Design, In Press, Accepted Manuscript, Available online 13 February 2013
2. Dipankar Ghosh, at. all, Scratch-induced microplasticity and microcracking in zirconium diboride–silicon carbide composite, Acta Materialia, Volume 56, Issue 13, August 2008, Pages 3011-3022
3. Aleksandar Vencl, at. all, Evaluation of adhesion/cohesion bond strength of the thick plasma spray coatings by scratch testing on coatings cross-sections, Tribology International, Volume 44, Issue 11, October 2011, Pages 1281-1288
4. Y Xie and H.M Hawthorne, On the possibility of evaluating the resistance of materials to wear by ploughing using a scratch method, Wear, Volume 240, Issues 1–2, May 2000, Pages 65-71
5. N. Schwarzer, Q.-H. Duong, at. all, Optimization of the Scratch Test for specific coating designs, Surface and Coatings Technology, Volume 206, Issue 6, 15 December 2011, Pages 1327-13354. Walter, N. Name of the fourth example paper. *Source.* [online]. Available: http://www.domain.extension (December, 2009).

"HENRI COANDA"
AIR FORCE ACADEMY
ROMANIA

"GENERAL M.R. STEFANIK"
ARMED FORCES ACADEMY
SLOVAK REPUBLIC

INTERNATIONAL CONFERENCE of SCIENTIFIC PAPER
AFASES 2015
Brasov, 28-30 May 2015

# THE INFLUENCE OF $AL_2O_3$ DEPOSITED COATING BY PLASMA ELECTROLYTIC OXIDATION TO THE BEHAVIOR OF AN ALUMINUM ALLOY SUBJECTED TO MECHANICAL SHOCK

**Geanina Laura Pintilei*, Marioara Abrudeanu*, Corneliu Munteanu**, Ionut Vasile Crismaru**, Iustin Popa*, Vladu Mihaela***

*Faculty of Mechanics and Technology, University of Pitesti, Romania, **Faculty of Mechanical Engineering, "Gheorghe Asachi" Technical University, Iasi, Romania

***Abstract:*** *This paper analysis the resilience of an Al-Cu-Mg aluminum alloy subjected to shock loads and the way how a coating can improve its behavior. For improving the behavior was used plasma electrolytic oxidation deposited of $Al_2O_3$ coatings. The samples without and with coating were subject to mechanical shock to determine the resilience of the materials. The cracks propagation was investigated using the QUANTA 200 3D DUAL BEAM electron microscope. To highlight the physical phenomenon that appears in the samples during the mechanical shock, explicit finite element analysis were done using Ansys 14.5 software.*

***Keywords:*** *Charpy test, $Al_2O_3$, AA2024*

## 1. INTRODUCTION

Electrolytic plasma oxidation, also called micro-arc oxidation, is a relatively new technique of surface modification. This method has a greater interest for achieving some ceramic coatings oxides on Al, Ti and Mg alloys. [1-5]

The layers obtained by micro arc oxidation can enhance wear resistance and corrosion properties as well as conferring other functional properties such as anti-friction, thermal protection, optical and dielectric properties. [6-8]

This research analyzes the influence of PEO coatings on aluminum alloys related to the energy needed to fracture the materials and also on the nature of the fracture. One type of coating was considered in this paper and a comparison was made relating to a sample without coating. To highlight the results, electron microscopy was used. This was achieved with the QUANTA 200 3D DUAL BEAM electron microscope.

## 2. MATERIALS AND METHODS

The impact test was done using the Charpy method on six samples, three samples with $Al_2O_3$ coating deposited by plasma electrolytic oxidation and three samples without coating.

After the tests, the samples were analyzed using the QUANTA 200 3D DUAL BEAM electron microscope to determine the fracture profile and the influence of the mechanical shock on the deposited coating.

A finite element analysis was done using the Explicit Dynamics module from Ansys 14.5 to determine the stress distribution inside the materials during the impact test. In Fig. 1

the meshes used for the finite element analysis are presented.

The mesh for the base material sample was composed of 2521 nodes and 3122 elements. The model with $Al_2O_3$ coating was composed of 6759 nodes and 7583 elements.

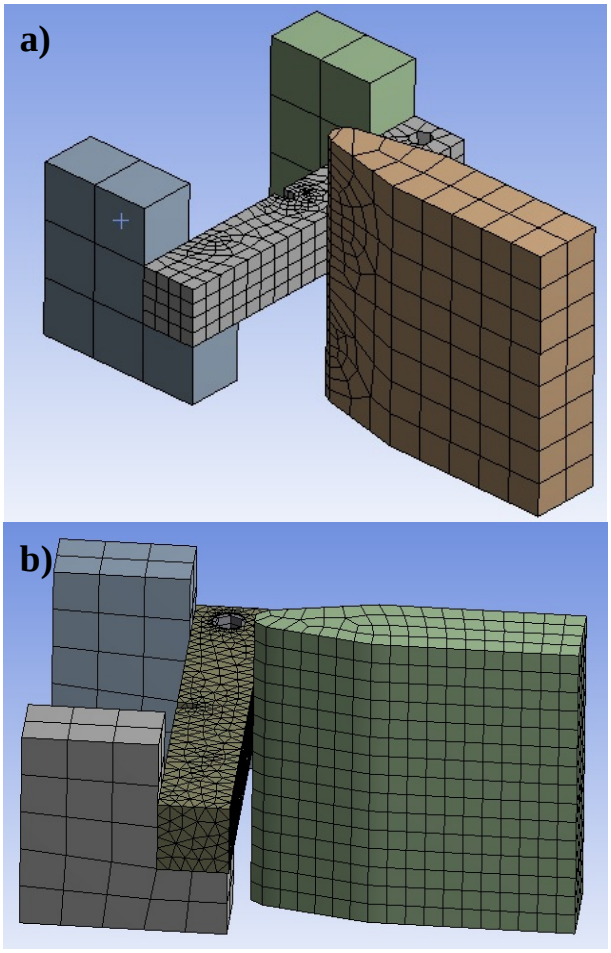


Fig. 1. The meshes used in the finite element analyzes: (a) sample without coating, (b) $Al_2O_3$ electrolytic plasma oxidation

Electrolyte solution used in deposition is composed of: sodium metasilicate ($Na_2SiO_3$), sodium hydroxide (NaOH) and distilled water.

## 3. RESULTS OF THE CHARPY IMPACT TESTS

**3.1. The results for the samples without coating.** In Fig. 2 SEM images of the sample without coating after the impact test can be observed. We can observe in SEM images that the fractures an irregular profile with large plastic deformation. This indicates that the sample suffered a ductile fracture due to mechanical shock. The energy needed for the fracture in impact test had the recorded values of: 188.7 J, 189.3 J and 189.23 J. It can be determined that the average plastic deformation energy for all three samples without coating is 289 J.

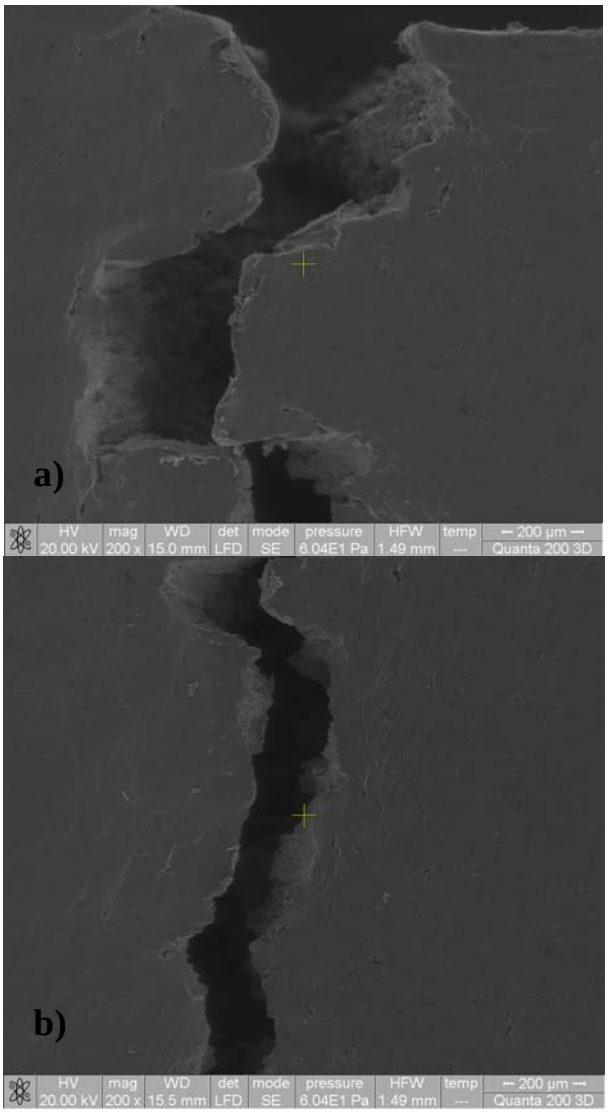


Fig. 2. SEM images for the 2024 sample: (a) the fracture propagation 200x, (b) cracks propagate in the material 200x

In Fig. 3a rezults after cracks propagation in samples are presented. The maximum stress which appears in the contact area with the supports is 303MPa. High value of stress is due to crushing of the material in that region. Maximum value of the stress which appear in contact area with pendulum is 281.4 MPa. We can observe that the crack is initiated in the U notch and its propagated to contact area with pendulum. Fig. 3b shows results at the end of the simulation and it can be observed that the sample was brocken. The profile of the

fracture in simulation is similar with the samples obtained experimentally.

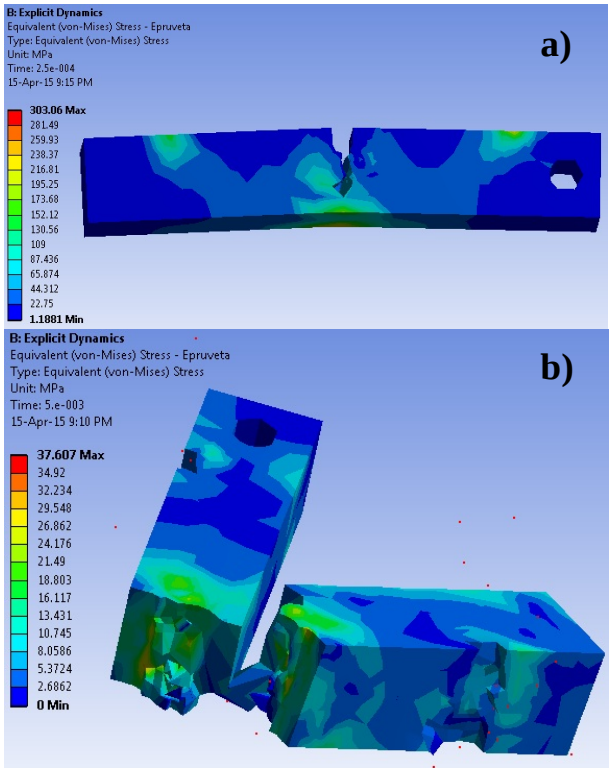


Fig. 3. The stress distribution in the impact test for the sample without coating: (a) the fractures initiation, (b) at the end of the simulation

**3.2. The results for the samples with $Al_2O_3$ coating obtained by electrolytic plasma oxidation.** In fig. 4 SEM images of the samples with $Al_2O_3$ coating after impact test are presented. The SEM analysis revealed that the sample fracture is similar with the samples without coating. The profile of the fractures is irregular and material base suffered big plastic deformation during the test. These results indicate that the samples suffered a ductile fracture. In the impact zone with the pendulum, in the area in contact with stands and in the area of U notch the coating exfoliated due to contact fatigue and intensive bending. The energy needed from the fracture of the samples had a value of 190.07 J, 191.37 J and 194.08 J. The average energy value for these samples is 192.08 J.

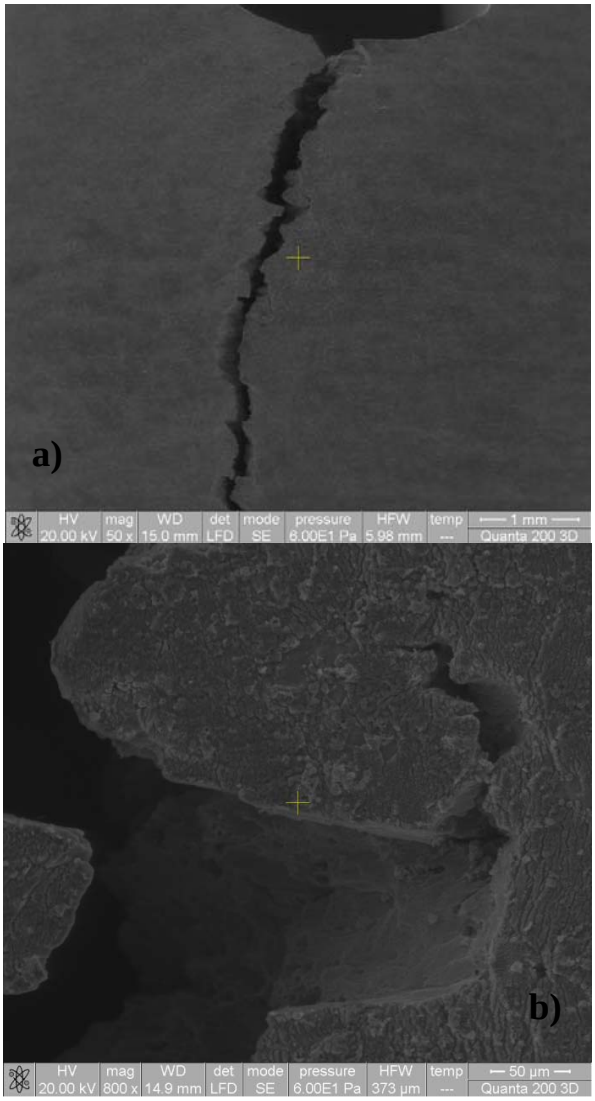


Fig.4. SEM images for the sample with $Al_2O_3$ coating: (a) the fracture propagation 50x, (b) cracks propagate in the material 800x

The EDAX analysis presented in fig. 5 showed a good adherence between $Al_2O_3$ coating and aluminum alloy material base. In

this analysis we can observe only chemical elements of the coating.

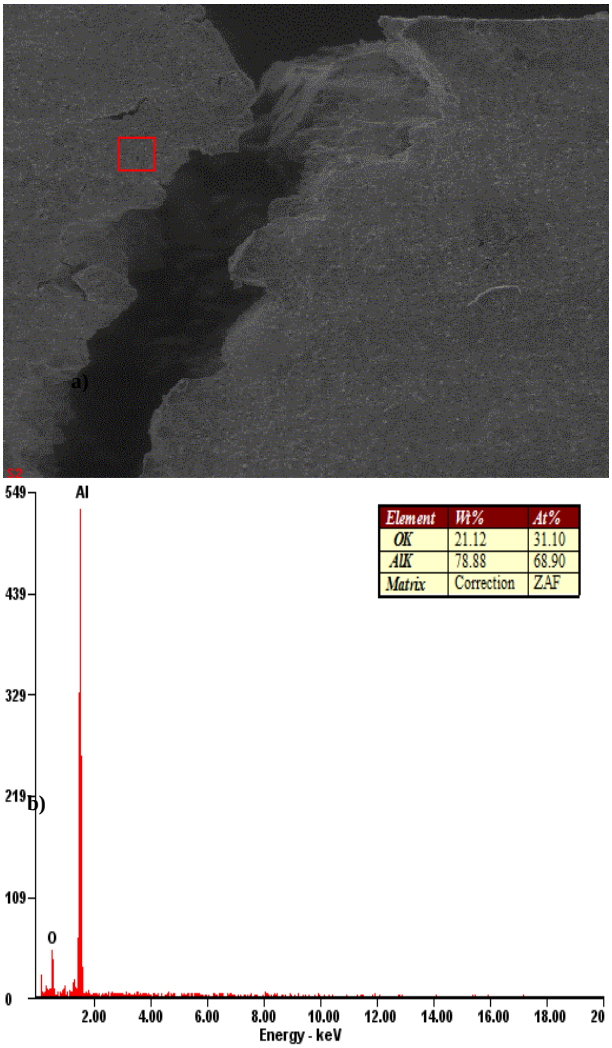


Fig. 5. The EDAX analyses for the sample with $Al_2O_3$ coating: (a) on the surface with the remained coating, (b) on the exfoliation surface

Maximum tensile stress achieved appears shortly before fracture initiation and has the value of 282 MPa (Fig. 6a). This value of the tensile occurs on the surface of the U notch. In the area of the notch with Charpy pendulum the coating exfoliated.

In Fig. 6b equivalent stress distribution to the end of the simulation is presented. The profile of the samples confirms the results obtained experimentally regarding its ductile fracture of it. On the samples we can observe area in which the layer presents coating exfoliation on the base material. But this exfoliation is not completed.

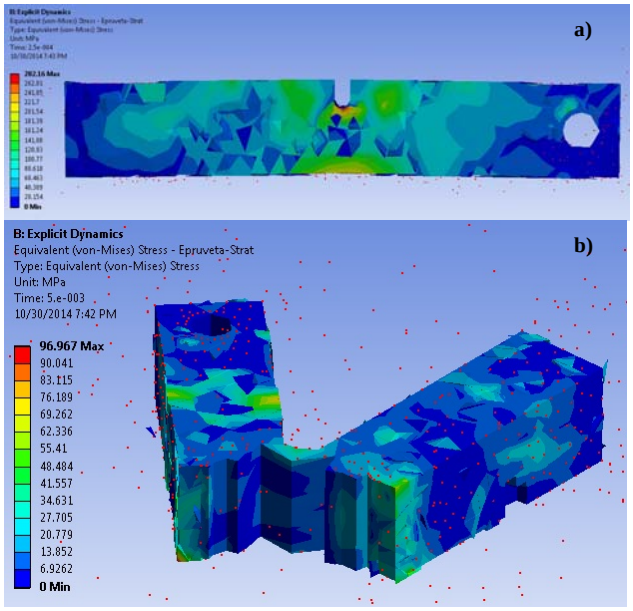


Fig. 6. The stress distribution in the impact test for the sample with $Al_2O_3$ coating: (a) the fractures initiation, (b) at the end of the simulation

## 4. CALCULATIONS OF THE KCU RESILIENCE

The results of the resilience test are defined by the ratio between the energy needed to fracture and the sectional area in the notch.

The average thickness of the $Al_2O_3$ coating is 173 µm. The measurement of the $Al_2O_3$ coating is presented in Fig. 7.

The sample with an $Al_2O_3$ coating has a resilience average value of 618.081 J/cm$^2$ and the sample without coating has a calculated average value of the KCU resilience of 630.233 J/cm$^2$.

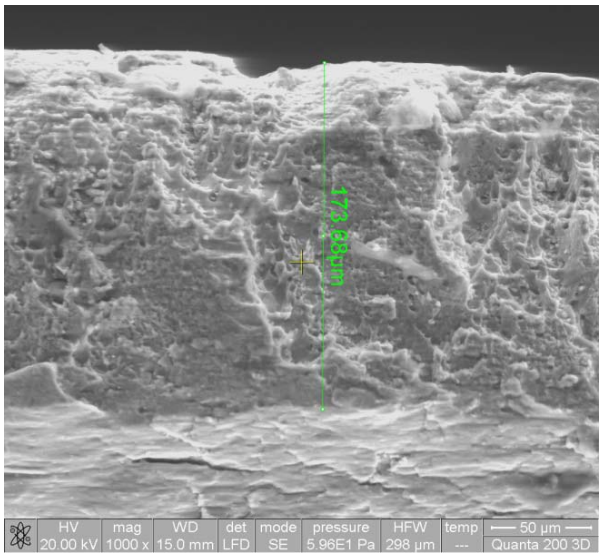

Fig. 7. Measurements of the coatings tightness $Al_2O_3$ PEO coating

## 5. CONCLUSIONS & ACKNOWLEDGMENT

Both results with finite element analysis and experimental tests confirm ductile fracture of the samples and a good adherence of $Al_2O_3$ coating layer with base material. Mechanical resistance required to break the sample was only 3.43% higher than the measured sample of AA2024.

Taking also in consideration the average of the coating tightness the variation of the KCU resilience is presented in Fig. 8.

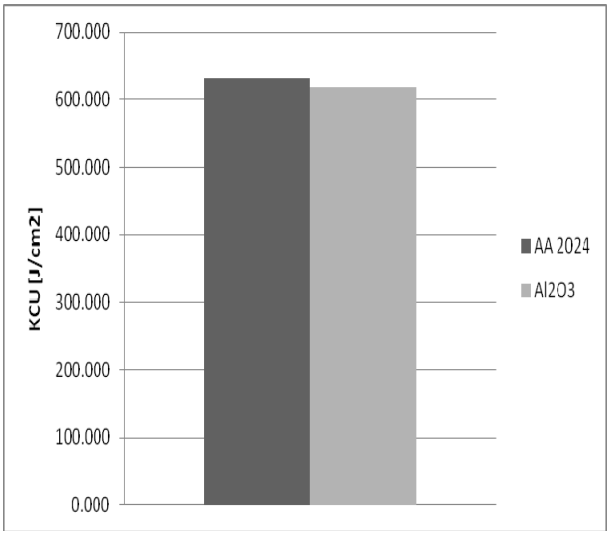


Fig. 8. The average KCU resilience values for the analyze samples

This work of Pintilei Geanina Laura was supported by the strategic grant POSDRU/159/1.5/S/138963 - PERFORM, co-financed by the European Social Fund – Investing in People, within the Sectorial Operational Programme Human Resources Development 2007-2013.

## REFERENCES

1. S.V. Gnedenkov, O.A. Khrisanfova, A.G. Zavidnaya, S.L. Sinebrukhov, P.S. Gordienko, S. Iwatsubo, A. Matsui, Surf. Coat. Technol. 145 (1–3) (2001) 146.

2. N. Godja, N. Kiss, C. Löcker, A. Schindel, A. Gavrilovic, J. Wosik, R. Mann, J.Wendrinsky, A. Merstallinger, G.E. Nauer, "Preparation and characterization ofspark-anodized Al-alloys: physical, chemical and tribological properties", Tribol.Int. 43 (2010) 1253–1261.

3. G. Sundararajan, L. Rama Krishna, "Mechanisms underlying the formation of thick alumina coatings through the MAO coating technology", Surf. Coat. Tech-nol. 167 (2003) 269–277.

4. Mehdi Javidi, Hossein Fadaee, "Plasma electrolytic oxidation of 2024-T3 aluminum alloy andinvestigation on microstructure and wear behavior" www.elsevier.com/locate/apsusc, Applied Surface Science 286 (2013) 212– 219.

5. Cui S H, Han J M, Du Y P and Li W J (2007), „Corrosion resistance and wear resistance of plasma electrolytic oxidation coatings on metal matrix composites", Surf Coat Technol, 201, 5306–5309.

6. Gerasimov M V, Nikolaev V A and Shcherbakov A N (1994), „Microplasma oxidation of metals and alloys", Metallurgist, 38(7–8), 179.

7. Guan Y J, Xia Y and Xu F T (2008a), „Interface fracture property of PEO ceramic coatings on aluminum alloy", Surf Coat Technol, 202, 4204–4209.

8. Jin F, Paul K C, Xu G D, Zhao J, Tang D L and Tong H H (2006), „Structure and mechanical properties of magnesium alloy treated by micro-arc discharge oxidation using direct current and high-frequency bipolar pulsing modes", Mat Sci Eng A, 435–436, 123–126.

"HENRI COANDA"
AIR FORCE ACADEMY
ROMANIA

"GENERAL M.R. STEFANIK"
ARMED FORCES ACADEMY
SLOVAK REPUBLIC

INTERNATIONAL CONFERENCE of SCIENTIFIC PAPER
AFASES 2015
Brasov, 28-30 May 2015

# ROBOTIC GRIPPERS FOR HANDLING BOOKS IN LIBRARIES

**Corina Monica Pop*, Gheorghe Leonte Mogan***

*Faculty of Mechanical Engineering, Transilvania University of Brasov, Romania

***Abstract:*** *Recent developments in robotics outside traditional industrial applications increasingly focus on robots operating in an unstructured environment and human vs. robot interactions. Among the most recent application fields for robots used in unstructured environments are personal and service robotics, space and underwater robotics, medical and rehabilitation robotics, construction robotics, agriculture robotics. However robots that are designed to perform specific library tasks are relatively rare. In this case a mobile robot arm is used to manipulate the books on a shelf. In this context, this paper describes the most relevant performances of prototypes designed for robotic manipulation of book material.*

***Keywords:*** *librarian robot, manipulation, service robots*

## 1. INTRODUCTION

Current trends in robotics research are focused especially on autonomous and semiautonomous robots. Some authors assign these robots to the class of service robots [1]. According to the International Federation of Robotics a service robot is designed for the well-being of humans and equipment, excluding manufacturing operations [2].

Service robots feature arm structures similar to industrial robots [3].

In terms of applications service robots are divided into professional service robots and personal service robots. In addition to service areas such as cleaning, surveillance, inspection and maintenance these robots are employed for hazardous, impossible or unacceptable manual tasks. Personal robots are service robots which include domestic robots that may perform daily chores, assistive robots for people with disabilities or elderly people, and robots used for entertainment [4].

Currently, very active researches are conducted in the field of service robots as results from the programmes of the most international conferences on Robotics (*International Conference on Robotics and Automation* – ICRA, *International Conference on Intelligent Robots and Systems* – IROS, etc.). However, robots that are designed to perform specific library tasks are relatively rare. In this case a robotic arm is used to manipulate books on a shelf [5].

## 2. BOOK MANIPULATION

The issue of object manipulation is solved by using standard, well-known geometries of articulated arms that can satisfy a wide area of conditions.

Considering the above, the problem of book manipulation can be approached like a standard manipulation problem.

The basic steps related to a complete automatic manipulation of a book can be described as follows:

- book identification (by title, author or subject) and automatic relation to its location;
- positioning of the manipulation system in front of the book to be picked up;
- pick-up from the shelf;
- motion towards a transfer unit (connection between the conservation area and the user area);
- release of the book and position reset.

The serviceable surface for pick-up is the back, considering also the adjacent books [6].

## 3. ROBOT-ENVIRONMENT INTERACTION

A robot can interact with the environment by ensuring adequate contact followed by the motion required by the task. Although robot manipulators have been successfully applied to various tasks, their versatility is limited. E.g. when a manipulator is assigned to pick up objects of different sizes and attributes, its end-effector needs to be adapted to the object's parameters.

## 4. GRIPPING OPERATION ANALYSIS

The design of a robot gripper is based on following parameters:

- maximum depth of the shelf;
- maximum book size;
- maximum book mass;
- minimum book thickness.

Book pick-up:

- the hand approaches the book, and one finger (often the forefinger) is used to tilt the book around its base;
- the other fingers grip the book;
- the book is drawn out.

Book repositioning:

- the gripped book approaches the shelf, in such a way the lower corner edges are the first to be positioned (between adjacent books);
- the book is pushed into the shelf;
- the body of the book is readjusted in vertical position.

The robotic unit is designed to simulate the human approach: when a book is correctly positioned into its shelf the only accessible surface is the back of the book. [6].

## 5. ROBOTIC GRIPPER FOR BOOK HANDLING IN LIBRARIES - STATE OF ART

With regard to robotic library systems, relevant research has been conducted. In this context, a remotely operated solution was presented by Tomizawa and coworkers [7], the University of Tsukuba, Japan. Their work was based on a robotics project from the Johns Hopkins University [8], ***C****omprehensive* ***A****ccess to* ***P****rint* ***M****aterial* (CAPM), who had built a robot limited to extract books from a shelf.

The robot uses a 7 DOF (***D****egrees* ***O****f* ***F****reedom*) manipulator of 1100 mm length in order to extract from and return books to a shelf [9]. The manipulator has a working range between 400 mm and 1100 mm above the floor (Fig. 1).

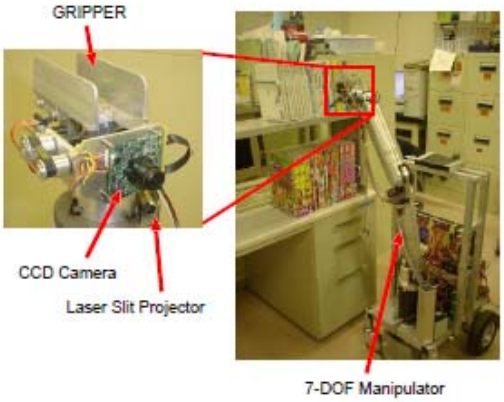


Fig. 1. 7 DOF manipulator and hand for book pick-up. (T. Tomizawa et al., 2003)

The hand consists of a gripper made of two flat fingers that can move right-and-left symmetrically; these fingers can hold books with a weight up to 400g, with a thickness under 50 mm [10].

UJI (i.e. the acronym of the ***U****niversity* ***J****aume-I,* ***C****astellón*, Spain,) Librarian Robot [11] is a service robot with a prototype mobile manipulator designed to assist in everyday tasks. The first application is its employment as an assistant in a public library to search

books in the bookshelves, pick them up and take them to specified locations [12, 13].

The experimental setup, presented in Fig. 2, requires a mobile platform (Nomadic), a robot arm (Mitsubishi PA-10, 7 DOF parallel-jaw gripper), and a camera in hand (MEGA-D Megapixel Digital Stereo Head) configuration. Moreover, a special design of the fingers in the parallel-jaw gripper was necessary.

The first tests with this system show good performance. For instance, the time necessary to localize a label from an initial image is always less than 1s. Moreover, the next image processing, including OCR (***O**ptical **C**haracter **R**ecognition*), to identify the label, is always within 5-10 s. A ratio of 5 s per each centimeter of book is needed before the book is grasped (e.g. a book of 4 cm thickness takes 20s). All tests have been conducted using a 266 MHz Pentium II Processor.

Recent experiments show that the system is robust enough to manipulate non-conventional books, as shown in Fig. 2 (right) [5].

Fig.2. The system in action.
(M. Prats et al., 2004)

The new experiments developed with this system, but with another mobile platform (ActivMedia PowerBot) show an important improvement [14] in terms of book locating, identifying and extracting. With regard to gripping, a ratio of 1.5 s per 1 cm of book will be needed (e.g. a book with a width of 4 cm requires 6 sec). All experiments used a 1.2 GHz Pentium IV Processor [15].

In another experiment a manipulator uses a three-fingered Barrett hand and a JR3 force/torque and acceleration sensor mounted at the wrist.

The researchers tested force/pressure control strategies in a real application: a robot that pulls out a book from a bookshelf.

By placing tactile sensors on the robot fingertips, the robot can estimate whether the initial contact is good. The current system is able to autonomously ensure a good initial contact on the top of the book even from a very rough initial estimation.

Fig. 3. The robot grasping the book.
Left: initial contact. Middle: Maximizing contact surface. Right: doing the task.
(A. Morales et al., 2007)

Three types of behaviors have been implemented as shown in Fig. 3. The first one controls the force that the manipulator applies on the book through the contact on the fingertip. The second one tries to maximize the contact area in order to assure that the reference force can be reached. Finally, the third behavior is to extract the book.

In the future new gripping actions will be implemented so that the UJI service robot would be able to handle objects of different shapes [17].

With ubiquitous robotics, distributed computing, and sensor networks evolving rapidly, robotics engineers are using the ambient intelligence concept as a basis for developing advanced robot technology. At the ***I**ntelligent **S**ystems **R**esearch **I**nstitute* (ISRI) of the Japan's National Institute of ***A**dvanced **I**ndustrial **S**cience and **T**echnology* (AIST), the researchers have been studying knowledge-sharing robot control associating

distributed objects in physical space with a knowledge database in virtual space using RFID tags as physical hyperlinks [18].

Fig. 4 The librarian robot system, the intelligent floor, and the intelligent bookshelf. (B. K. Kim et al., 2008)

The librarian robot consists of a manipulator which can recognize and manipulate books, and a mobile platform, which can localize and navigate itself using floor-embedded RFID tags [19].

The complete librarian robot system is shown in Fig.4. The intelligent floor for robot localization and the intelligent bookshelf for checking the book status are connected to a middleware-based network.

Fig. 5. Book handling. (B. K. Kim et al., 2008)

Fig. 5 shows the robot gripper handling a book. Here, the robot gripper developed in AIST was used, as shown in Fig.6. The robot system retrieves book parameters from the database using the attached RFID tag.

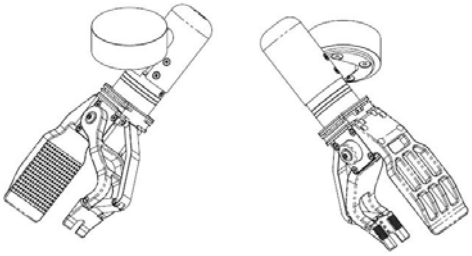

Fig. 6. Robotic hand designed to handle a book. (B. K. Kim et al., 2008)

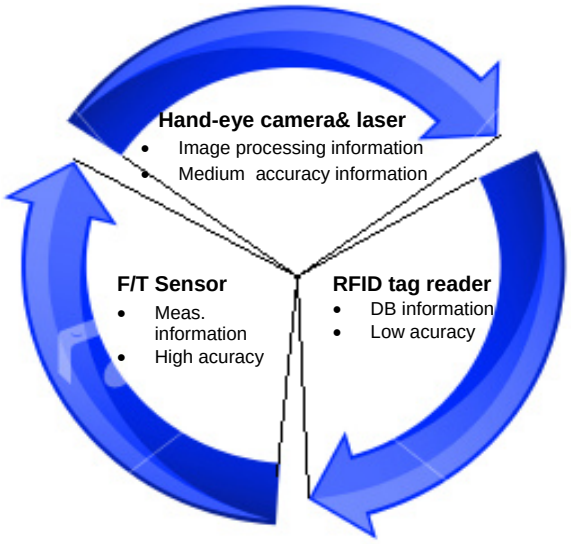


Fig. 7. The relationship among the sensors.

Hence, using the hand-eye vision and the laser installed on the gripper, the robot gets the image of the arranged books and then identifies the target book through image processing. Also, the robot detects the force variation signal from the gripper.

Fig. 7 shows the relationship between these sensors [20].

## 6. CONCLUSION

Developing a robot capable of handling all types of objects used in human living environment is extremely difficult.

This paper attempts a comparative analysis of two similar approaches and the solutions adopted regarding library robot systems designed to improve library user assistance.

With respect to this, AIST devised some methods, as part of environmental structuring for effective adaptation of robots to human living environment.

Here, following aspects should be emphasized:

- In both cases, the analyzed library robot systems were designed to perform similar book-handling tasks.
- Both robot systems were designed to include human-specific capabilities. However, the AIST-system is largely based on the wider concept of “intelligent ambient” whereas the UJI-system concentrates mainly on the combination of sensory/force aspects.

- The AIST-system can thus be viewed as part of a wider framework including advanced concepts such as ubiquitous robotics, distributed computing and sensor networks. This allows for increased robot versatility and adaptability to different library environments.
- The UJI-system focuses mainly on the robot's individual handling performance. It attempts to improve a number of specific tasks that relate to book handling capabilities through enhancing its force/vision coupling characteristics.

## REFERENCES

1. Bekey, G., Junku, Y.. The Status of Robotics. *IEEE Robotics & Automation Magazine.* Volume 15, Issue 1 (2008).
2. http://www.ifr.org
3. Chivarov, N., Shivarov N.. Mobile Robot for Inspection. *Robotics and Mechatronics,* Drjanovo, Bulgaria (2007).
4. Rybak, V.. Safety, Uncertainty, and Real-Time Problems in Developing Autonomous Robots. In *Proceedings of the 8th WSEAS International Conference on Signal Processing, Robotics And Automation* (2009).
5. Prats, M., Ramos-Garijo, R., Sanz, P.J., del Pobil, A.P.. Autonomous Localization and Extraction of Books in a Library. In: F. Groen et al. (Ed.), *Intelligent Autonomous Systems,* Amsterdam: IOS Press (2004).
6. Ravina, E.. A Pneumotronic Unit for Automatic Manipulation of Book Material. In *12th IFToMM World Congress,* Besançon, France, June 18-21 (2007).
7. Tomizawa, T., Ohya, A., Yuta, S.. Book Browsing System using an Autonomous Mobile Robot Teleoperated via the Internet. In *Proceedings of the IEEE International Conference on Intelligent Robots and Systems*, Lausanne (2002).
8. Suthakorn, J., Lee, S., Zhou, Y., Thomas, T., Choudhury, S., Chirikjian G.S.. A Robotic Libarary System for an Off-Site Shelving Facility. In *Proceedings of ICRA'01* (2001)
9. http://www.roboken.esys.tsukuba.ac.jp
10. Tomizawa, T., Ohya, AYuta, S.. Remote Book Browsing System using a Mobile Manipulator. In *Proceedings of the 2003 IEEE International Conference on Robotics and Automation* (2003).
11. del Pobil, A.P., Prats, M., Ramos-Garijo, R., Sanz P.J., Cervera E.. The UJI Librarian Robot: An Autonomous Service Application. In *Proceedings of the 2005 IEEE International Conference on Robotics and Automation* (2005)
12. Prats, M., Sanz, P.J., del Pobil, A.P.. *Model-based Tracking and Hybrid Force/Vision Control for the UJI Librarian Robot,* IEEE/RSJ International Conference on Intelligent Robots and Systems, Edmonton, Canada, Aug. (2005).
13. Prats, M., Sanz, P.J., del Pobil, A.P., Martinez, E., Marin, R.. Towards Multipurpose Autonomous Manipulation with the UJI Service Robot. *Robotica Journal*, Volume 25, Issue 2 (2007).
14. Ramos-Garijo, R., Prats, M., Sanz, P.J., del Pobil A.P.. An Autonomous Assistant Robot for Book Manipulation in a Library. In *Proceedings of IEEE International Conference on Systems, Man & Cybernetics*, Washington D.C., USA (2003).
15. Prats, M., Ramos-Garijo, R., Sanz, P.J., del Pobil A.P.. Recent Progress in the UJI Librarian Robot. In *Proceedings of IEEE*

*International Conference on Systems, Man & Cybernetics* (2004).

16. Prats, M., del Pobil, A.P., Sanz, P.J.. A Control Architecture for Compliant Execution of Manipulation Tasks. In *Proceedings of International Conference on Intelligent Robots and Systems*, Beijing, China, Oct. (2006).
17. Morales, A., Prats, M., Sanz, P., del Pobil A.P.. An Experiment in the Use of Manipulation Primitives and Tactile Perception for Reactive Grasping, in Robotics Science and Systems, Workshop on Robot Manipulation Sensing and Adapting to the Real World, Atlanta, USA (2007)
18. Miyazaki, M., Kim, B.K., Ohba, K., Chong, N.Y., Hirai, S., Mizukawa, M., Tanie, K.. Knowledge Distributed Robot System - Application of Multi-agent System. In *Proceedings of the 2004 SICE System Integration* (SI 2004) (2004).
19. Kim, B.K., Ohara, K., Kitagaki, K., Ohba K.. Design and Control of Librarian Robot System Based on Information Structured Environment. *Journal of Robotics and Mechatronics*. Volume. 21, Issue 4 (2009).
20. Kim, B.K., Ohara, K., Kitagaki, K., Ohba, K., Sugawara, T.. Design of Ubiquitous Space for the Robotic Library System and Its Application. In *Proceedings of the 17th IFAC World Congress* (IFAC 2008) Seoul, Korea (2008).

"HENRI COANDA"
AIR FORCE ACADEMY
ROMANIA

"GENERAL M.R. STEFANIK"
ARMED FORCES ACADEMY
SLOVAK REPUBLIC

INTERNATIONAL CONFERENCE of SCIENTIFIC PAPER
AFASES 2015
Brasov, 28-30 May 2015

# SPECIFIC TESTS FOR COMPOSITE STEERING COLUMNS

**Lucian Eugen Rad*, Thomas Heitz**, Anghel Chiru***

*Faculty of Mechanical Engineering, Transilvania University of Brasov, Romania, **Thyssenkrupp Presta, Eschen, Liechtenstein

***Abstract:*** *The work has a strong practical level, focusing on testing methods for composites based of carbon fiber and the results of tests for components of the steering column made by carbon fiber composites materials.*

***Keywords:*** *composite, test*

## 1. INTRODUCTION

As we known, in contrast to conventional materials, properties of the composites can be controlled to a high extent by the choice of components, the percentage of fiber, fiber orientation and geometry. One of the attributes of composites is that the design engineer can choose the material properties while the optimal shape of the product, arises.

The mechanical properties depend on several variables of the composite:

- properties of the fiber
- nature of the fiber surface
- the material properties of the matrix
- properties of any other phases
- volume fraction of the second phase (and any other phase)
- spatial distribution and alignment of the two phases (including fabric material)
- the nature of the interfaces.

Processing methods - in cycles of temperature, pressure, vacuum and other factors - provide a great variability in the properties of the final product.

Ability to create a composite in its final form is effective for production, but complicates the tests. Often there is no clear relationship between the properties of test samples (specimens) and properties of the final product. Therefore, attempts should be made at different stages of manufacture to measure the properties of both constituent materials and in the final component or structure.

## 2. SPECIFIC TESTS FOR STEERING COLUMN

**2.1 Test equipment.** Typically, each component of the steering column must fulfill several functions. These multi-axial requests can be determined only by testing entire system as a whole.

According to a defined plane, are made various test measurements, listed (Table 1), in order to determine the properties of the steering column. It is perform strength tests / life and / or safety testing of vehicle collisions or other tests. After the tests of resistance / life are always performed measurements of the

same kind as those before the test in order to ascertain any change in properties.

Table 1: Specific test for steering column

| **Preliminary measurements** | **Strength tests** | **Subsequent measurements for strength testing** |
|---|---|---|
| Weight | 2K Dynamic Test | Torque lock release lever |
| Force lock-release lever | Torsional wear test | Naturalfrequency horizontal and vertical |
| Natural frequency horizontal and vertical | Wear test of the locking mechanism | Stiffness horizontal and vertical |
| Stiffness horizontal and vertical | | Strenght adjustment in lenght and height |
| Strenght adjustment in lenght and height | | Maximum moment |
| Torsional stiffness | | Full rotation |
| Maximum moment | | Non-uniformity |
| Full rotation | | Mass flow |
| Non-uniformity | | |
| | | |
| **Vehicle collision tests** | **Testing for incorrect use** | **Other tests** |
| Maintenance force | Torque from incorrect use | Universal joints extraction force |
| Compression tests | Incorrect use of driver lever | Breakout force joints yoke |
| Freefall test | Limit checking end | Cardan bushings depressing force |
| Bodyblock | The effort required to operate the lever | Shaker Test |
| Dynamic limiters end test | | Climate testing |
| | | Saline mist test |

Test equipment and computer programs for data processing for testing, test conditions should enable vibration, oscillations, forces and maximum stresses, environmental, durability / reliability

The tests were made using following equipment:

- MTS Dual Rotary System (DRS)
    - Two torsional stations with single or dual rotary inputs

-160 Nm, 400º/sec capable rotary inputs

- MTS Rotary Vibration (RV)
    - 565 Nm ±45º, 50 Hz capable rotary input
    - 5 kN ±25 mm capable linear input
    - Combined linear and rotary inputs
- Tensile Machine MTS Insight 50
    - 50 kN capability
    - Column spacing of 405 mm
    - Vertical test space of 1,100 mm
- NVS (Noise,Vibration,Harshness) / BSR (Buzz,Squeak, Rattle) Testing
    - Electro-dynamic Shaker LDSv890
- Environmental Testing
    - Two environmental chambers with a soaking area of 1m x 0.9m x 0.9m
    - Soaking conditions ranging from -55º C to 155º C and 10% to 98% relative humidity
    - Soaking area can also include fixtures for testing purposes during the soak schedule – pneumatic controls available
- Instrumentation
    - Force and torque transducers
    - Digital and analog encoders
    - Pneumatic, hydraulic and electric actuators
- Data Acquisition and Data Analysis
    - MTS data acquisition system
    - Multiple computation models available to aid in system analysis

-Performance Curve Evaluation

-Torsional Rate, Lash, Stiffness and Damping

Structural Lash and Bearing Hysteresis

For mechanical tests, are required some force application devices with grips and other items to transfer load applied to the test specimen (Fig. 1). Specific standard tests of composite materials are: the tensile stresses (ISO 527, ISO 14129, ASTM 3039), compressive stresses (ISO 14126, ASTM 3410), shear stress (ISO14130, ASTM D

3846), bending stress (ISO 14125, ASTM D 4476), delamination.

Besides static mechanical tests, the operation and dynamic tests are made: impact test (ASTM D 7137) and fatigue test (ISO13003, ASTM D 3479).

The damages nondestructive inspection methods are microscopic, ultrasonic, radiography, thermography.


Fig. 1: Specific equipment static and dynamic mechanical testing and data acquisition software

Besides these standard tests, they can make a series of tests and experiments to explore the behavior of various composite materials and extreme environments. Test results should help the design engineer to correctly calculate different modules and resistant due to the high anisotropy of composite materials based on carbon fibers and to render a representation of the characteristics of composite materials tested.

To perform tests on specimens of composite materials were made plates 300x300mm from which specimens were cut according to the standards. To achieve the plates and specimens using RTM process, we used a standard resin produced by Hunstman standard epoxy resin XB3585 and XB3458 hardener and fiber Toray T700 and Tenax HTS40.

**2.2 Test results.** Reasons for traditional materials (steel), to achieve structural components of the steering column, are replaced with composite materials reinforced with carbon fiber, advantages of carbon fiber have:

-carbon fibers are very light, their density is $\rho \approx 1{,}8$ kg / dm³

-Stiffness and E modulus is high in fiber direction

-fatigue-stiffness to high dynamic loads

-acid-resistance and high biocompatibility

-stressed anisotropic behavior.

Composites steering column components must be lightweight, have a simple and cheap technology, to meet the requirements of the specifications and bring more innovation in vehicle technology.

The main requirements of the steering column extracted from the specification of the VW Golf 6 are presented below:

- Weight saving
- Natural frequency
  - Vertical > 50 Hz
  - Horizontal > 50 Hz
- Stiffness
  - Vertical ≤ 1.6 mm
  - Horizontal ≤ 1 mm
- Force control in climatic conditions of -30 to + 80 ° C
- Locking way and blocking force of action lever, including acoustic and a haptic behavior
- Maximum permissible torsional moment
- Torsional stiffness

According to DIN EN ISO 527-1 requires 5 or > 5 specimens and test results that the static tests are relevant.

In the following are shown force-displacement curves for the five specimens

tested and calculation parameters characterizing composite materials:

Tensile parallel on fiber EN ISO 527

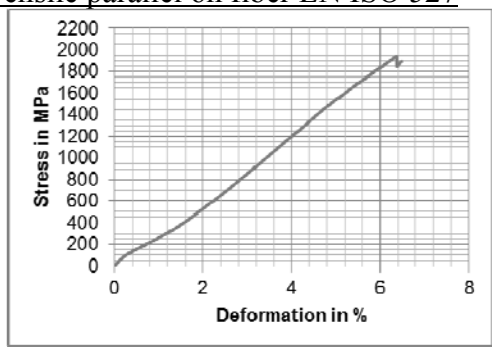


Fig. 2: Tensile stress-strain curve parallel to the fibers

Fig.3: Breaking standard specimen

After averaging measurements was made and the following parameters were calculated:

Table 2: Parameters calculated for fiber HTS40 and T700 for tensile parallel fiber

| HTS40 CFK | E modul [Mpa] | Break Strenght [Mpa] | Elongation Break [%] | Pois ratio |
|---|---|---|---|---|
| Average | 108.8 | 1.896 | 1,78 | 0,33 |
| Standard deviation | 7.390 | 54 | 0,11 | 0,05 |
| Coefficient variation | 6,8% | 2,8% | 6,4% | 14% |

| T 700 CFK | E-modulus [Mpa] | Breaking Strenght [Mpa] | Elongation Break [%] | Poiss ratio |
|---|---|---|---|---|
| Average | 98.879 | 1.782 | 1,75 | 0,28 |
| Standard deviation | 8.211 | 282 | 0,18 | 0,09 |
| Coefficient variation | 8,3% | 15,8% | 10,3% | 35% |

Composite materials are strong in axial tension, and tensile test specimen, must be gripped in some manner for testing. It is proper to calculate the minor Poisson ratio from the measured transverse modulus, the axial modulus and the major Poisson ratio.

Tensile perpendicular on fiber EN ISO 527

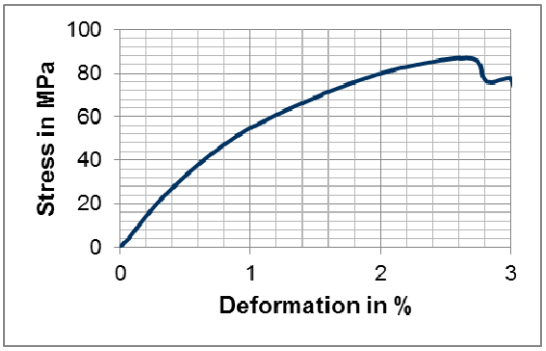


Fig.4: Tensile stress-strain curve ±45˚ fibers orientation

Fig. 5: The fracture pattern of the specimens

After averaging measurements was made and the following parameters were calculated:

Table 3: Parameters calculated for fiber TS40 and T700 for tensile perpendicular on fibers

| HTS40 CFK | E-modulus [Mpa] | Break Strenght [Mpa] | Elongation Break [%] |
|---|---|---|---|
| Average | 7.832 | 49 | 0,66 |
| Standard deviation | 1.017 | 2,3 | 0,05 |
| Coefficient variation | 13% | 4,7% | 7,6% |

| T700 CFK | E-modulus [Mpa] | Breaking Strenght [Mpa] | Elongation Break [%] |
|---|---|---|---|
| Average | 7.137 | 46 | 0,66 |
| Standard deviation | 716 | 4,9 | 0,06 |
| Coefficient variation | 10% | 10,7% | 9,2% |

For both carbon epoxy laminates, the axial compressive strength was nearly a constant value. The tests shows that, in case of both laminates, the values obtain are comparable and the different fiber nature, not interfere with the quality of the composite material.

Tensile tests (±45˚ fibers orientation) for determining shear characteristics DIN 65466

| HTS, CFK | Shear-modul [Mpa] | Shear Strenght [Mpa] | Shear Elongation at Break [%] |
|---|---|---|---|
| Average | 6 | 133 | 2,12 |
| Standard deviation | 678 | 2 | 0,39 |
| Coefficient variation | 10,9% | 1,5% | 18,4% |

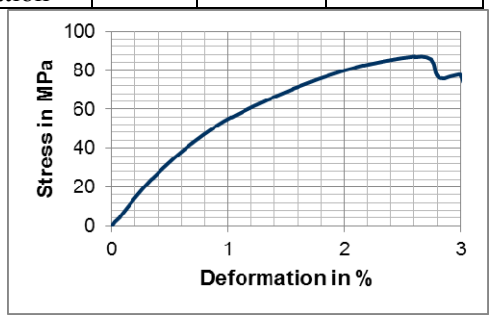


Fig.6: Tensile stress-strain curve ±45˚ fiber orientation

Compression perpendicular on fiber EN ISO 14126

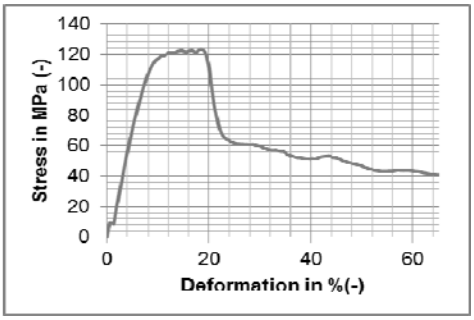


Fig.8: Stress-strain curve in compression perpendicular on fiber

Fig.7: The most common fracture pattern of specimens for ±45˚ fibers orientation

Table 4: Parameters calculated for fiber HTS40 and T700 for ±45˚ fibers orientation

| T700 CFK | Shear-modulus [Mpa] | Shear Strenght [Mpa] | Shear Elongation atBreak[% |
|---|---|---|---|
| Average | 5.619 | 121 | 2,15 |
| Standard deviation | 805 | 2,1 | 0,51 |
| Coefficient variation | 14,3% | 1,7% | 23,6% |

Fig.9: The most common fracture pattern of the specimens for compression perpendicular on fibers

Table 5: Parameters calculated for fiber T700

| HTS40 CFK | E-modul [Mpa] | Breaking Strenght [Mpa] | Elongation Break[%] |
|---|---|---|---|
| Average | 8.016 | 169 | 3,14% |
| Standard deviation | 901,4 | 4,1 | 0,40% |
| Coefficient variation | 11,2% | 2,4% | 12,8% |

and HTS40 for compression perpendicular on fibers

| T700 CFK | E-modulus [Mpa] | Breaking Strenght [Mpa] | Elongation Break [%] |
|---|---|---|---|
| Average | 8.265 | 185 | 3,61% |
| Standard deviation | 1.328,6 | 8,5% | 1,03% |
| Coefficient variation | 16,1% | 4,6% | 28,6% |

The existence of reliable material characteristics is an important basis for FEM calculations.

Having determined the characteristics of the material were made molds (Fig.10) to produce parts / specimens similar in structure with console steering column that we want to achieve.

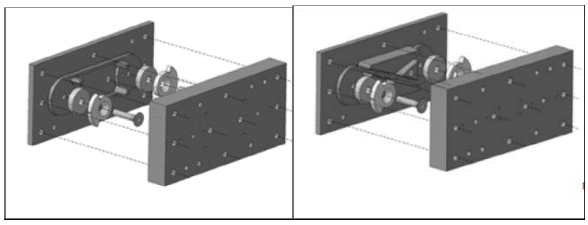

Fig.10: Right / cross molds for specimen

Specimens were made to highlight the behavior of composite materials based on carbon fiber for achieving steering column bracket.

The specimen is strained by means of a fork-like construction, which in turn is attached to the drive components of the machine. This mounting have to eliminate all movements of rotation and translation. The specimen shall apply only translation tensioning rails or to compare the effects of stress. In order to analyze as many cases of stresses and deformations, specimens required stress on three directions. Specimen mounted in the test machine, loaded after X direction, is shown in Figure 11. The image presents fork construction details.

The lengths x1 and x2 are defined analogously. The elongation of the sample results from the difference between the two lengths. This value is compared to the rate recorded for the test machine. After recording three measurements race-force it was measured for compare some of characteristic values among others for the spring constant, c. Each specimen was mounted in the test machine, tense and removed four times and subjected to five times to a task 7'000 N for right specimen and 6'000 N for cross specimen.

Table 6 shows that the reliability of the values measured by the test machine under 10% would be acceptable but the measured values of that machine test could not be confirmed by manual measurements.

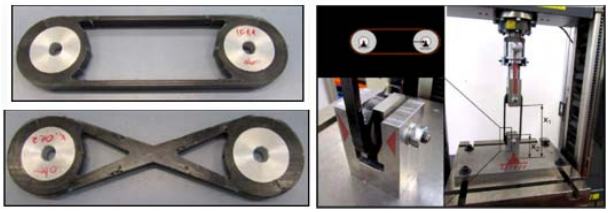

Fig. 11: Specimens for testing steering column and their test machine

In the specifications of the client is known the torque of the drive lever or driving force of drive lever.

The torque of the drive lever is made in dependence on the angle lever Force lock / unlock is determined by the length of the lever and the results recorded in a test report.

Tabel 6: Measured values

| | c [N/mm] by measuring on the test machine | | c [N/mm] by manual measuring | |
|---|---|---|---|---|
| Right specimen | 13.133 | ±848 | 25.586 | ±2387 |
| Cross specimen | 10.326 | ±984 | 15.054 | ±3413 |

Tests were performed using FEM to compare simulated results with real tests and measurements.

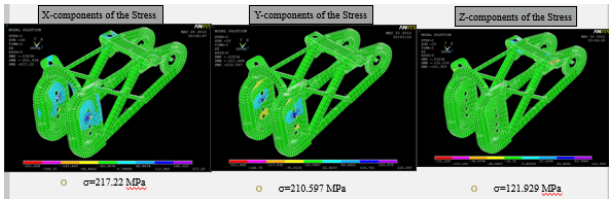


Fig.12: FEM simulation for console steering column

FEM simulation results for the steering column bracket and structural measurements and tests specimens were relatively similar.

Stiffness horizontal and vertical

A highly rigid steering column will have its own frequency higher than a less rigid column. As a measure of stiffness it is considered the ratio force / displacement [N/mm]. This report is the equivalent of elastic constant of the steering column. The value of the ratio is higher; we obtained the more rigid steering column. It is therefore desirable to achieve a high rigidity of the steering column. Radial stiffness measurement is made after the vertical and horizontal. Radial forces are applied to the end of the steering pipe. Here deflection is measured.

Table 7: Real measured values of stiffness and values of simulation results

| Stiffness[mm] | Real Test [mm] | FEM simulation [mm] |
|---|---|---|
| BS 1 Vertical (<1,6) | ±1,47 | ±0,96 |
| BS 1 Orizontal (<1,0) | ±0,71 | ±0,73 |
| BS 2 Vertical (<1,6) | ±1,45 | ±1,02 |
| BS 2 Orizontal (<1,0) | ±0,85 | ±0,75 |

For a defined radial force, resulting deflection should not exceed a certain limit (table 7). Tangent curve force/displacement is a measure of movements. The value of tangent at any point of the curve, there should be below a certain limit value (fig.13).

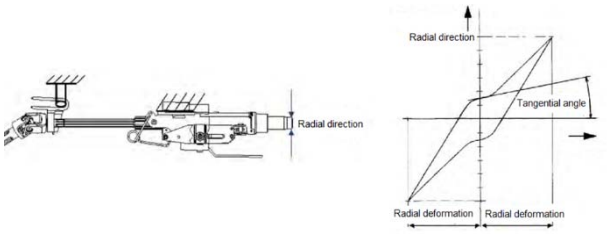


Fig. 13: Graphical representation of stiffness measurement and the resulting diagram

Natural frequency horizontal and vertical

The natural frequency of a complete steering column is measured on the vertical and horizontal. For this purpose the steering column is mounted on a rigid support. At the end piping steering column mounted a mass equivalent to multiple properties. Then, the steering column is brought into a specific position. On the board applies an acceleration transducer. The excitation frequency is effected by means of an impact hammer (Dirac pulse) in steering piping. If it is desired to measure the natural frequency in the vertical direction, the acceleration sensor is applied to the top or bottom surfaces of the equivalent mass, and the tubing is excited to vibration, to a mechanical impulse in the vertical direction. Measuring direction must correspond to the excitation.

Table 8: Frequency values and their real measured and values from the simulation results

| Natural frequency[>50Hz] | Real Test [Hz] | FEM simulation [Hz] |
|---|---|---|
| BS 1 Vertical | 47 | 45,6 |
| BS 1 Horizontal | 61,8 | 58,2 |
| BS 2 Vertical | 45,3 | 45,5 |
| BS 2 Horizontal | 59 | 57,9 |

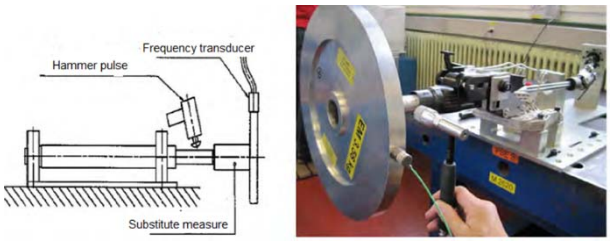

Fig. 14: Natural frequency measurement

## 3. CONCLUSIONS & ACKNOWLEDGEMENT

Mechanical tests are very important to describe the behavior of composite materials based on carbon fiber in various different applications and conditions.

Test results on specimens help choosing the correct material composition, mode of settlement of the fibers, their orientation, etc.

With the help of computer programs AlphaLam, LamiCens, LAP can calculate the dimensional characteristics of different stratifications. For CFK materials, transverse contraction coefficient becomes for certain angles, 0, an effect that can be exploited.

Both specimens and finished parts made of composite materials based on carbon fiber revealed that traditional materials can be successfully replaced by the new composite materials.

The quality of parts made of composite materials must be very good and constant in every section of the piece and manufacturing technology should allow the production of parts in high and very high series for automotive parts.

The next step is to optimize the production process to obtain high quality parts in a production time of less than 2 min / part for the high series production.

This work was partially supported by the strategic grant POSDRU/159/1.5/S/137070 (2014) of the Ministry of National Education, Romania, co-financed by the European Social Fund – Investing in People, within the Sectoral Operational Programme Human Resources Development 2007-2013.

## REFERENCES

1. T.Heitz-*Performantele fizico-mecanice ale pieselor din materiale compozite utilizate pentru coloana de direc□ie a autovehiculului*, Teză de doctorat, 2013, Brasov,România
2. C Soutis and N A Fleck, '*Static compression failure of carbon fibre T800/924C composite plate with a single hole*', Journal of Composite Materials, 1990 **24**(5) 536–58.
3. M B Gruber, J L Overbeeke and T W Chou,'A reusable sandwich beam concept for composite compression test', Journal of Composite Materials, 1982 **16**162–71.
4. N.Iosipescu, *Journal of materials*, 1967, 537-566
5. Heitz, T. und Chiru, A. *Analysis of using CFK material for steering columns components in passenger vehicles* - Part 2. Valancia : FISITA, 13th EAEC Automotive Congress, 2011. C54

"HENRI COANDA"
AIR FORCE ACADEMY
ROMANIA

"GENERAL M.R. STEFANIK"
ARMED FORCES ACADEMY
SLOVAK REPUBLIC

INTERNATIONAL CONFERENCE of SCIENTIFIC PAPER
AFASES 2015
Brasov, 28-30 May 2015

# NONLINEAR EFFECTS OF THE SIDEWASH GRADIENT ON AN AIRPLANE VERTICAL TAIL

**Constantin Rotaru*, Ionică Cîrciu*, Raluca Ioana Edu**, Oliver Ciuică*, Eduard Mihai***

*Faculty of Aeronautical Management, "Henri Coandă" Air Force Academy, Brasov, Romania,
**Faculty of Mechatronics and Integrated Armament Systems, Military Technical Academy, Bucharest, Romania

***Abstract:*** *This paper presents an analytical evaluation of the airplane yawing moment, based on the general theory of the aerodynamic design, with details leading first to the separate formulation of the Fourier coefficients in the series solution to the Prandtl's lifting-line theory, followed by the numerical calculation of the sidewash gradient of the vertical tail for a standard configuration of an airplane geometry. Several approaches of the vortex strength and vortex span factors were considered to choose the methodology that better predicts the airplane dynamic handling quality requirements.*

***Keywords:*** *aircraft stability, aerodynamics, Fourier transform*

## 1. INTRODUCTION

A rigid airplane in free flight has three translational and three rotational degrees of freedom. Small translational and rotational disturbances must all result in a return to the original equilibrium attitude. Any object moving through the air will experience drag that opposes the motion. If the angle of attack remains constant, this drag increases with increasing air velocity. The thrust developed by an aircraft engine is either constant with airspeed or decreases with increasing airspeed, so, when an airplane is in static equilibrium with regard to translation in the direction of motion, the forward component of thrust must balance the drag. Any disturbance in velocity in a direction normal to the equilibrium flight path will result in an aerodynamic force that opposes the disturbance. At some angles of attack beyond stall, the airplane must be unstable for disturbances in normal velocity. From an analytical point of view it is easier to design an unmanned aircraft with an autopilot than it is to design a good manned airplane [3].

Static stability in the rotational degrees of freedom is of primary importance for maintaining airplane trim. To be statically stable in rotation, any disturbance in roll, pitch or yaw must all result in the production of a restoring moment that will return the airplane to the original equilibrium attitude [1].

Longitudinal motion involves three degrees of freedom: axil translation, normal translation and rotation in pitch. The other three degrees of freedom, namely sideslip translation, rotation in roll and rotation in yaw are the lateral degrees of freedom which do not compose a planar motion and give the airplane a three dimensional movement. The airplane is defined to have a positive sideslip when the $y_b$ component of airplane velocity relative to

the surrounding air is positive. For equilibrium longitudinal motion, the net side force, rolling moment and yawing moment must all be zero. No airplane can be always perfectly symmetric. Asymmetric loading and thrust, propeller rotation or an asymmetric distribution of bugs on the wings can cause either aerodynamic or inertial asymmetry, thus, ever for level flight; some provision must be made for trimming the airplane in roll and yaw. For a standard configuration of airplane geometry, a yaw disturbance in a positive sideslip angle requires a positive yawing moment to restore the disturbance to zero, so, in mathematical terms, static stability in yaw requires that $C_{n,\beta} = \partial C_n / \partial \beta > 0$. Good handling qualities for a typical airplane configuration are normally found with $C_{n,\beta}$ in the range between 0.06 and 0.15 per radian. The size of the vertical tail is not usually fixed by consideration of static stability. When the vertical tail is sized based on control and dynamic handling quality requirements, sufficient static stability is normally provided.

## 2. LATERAL STATIC STABILITY

The yaw stability derivative is estimated by combining the contributions made by the various components of the airplane (fuselage, propeller and vertical tail). The contributions from the fuselage and propeller are typically destabilizing, but these are small and easily countered by the stabilizing effect of an aft vertical tail. The lift developed on the vertical tail as a result of a positive sideslip produces a side force from right to left (fig 1). Since the vertical tail is aft of the airplane center of gravity, this lift produces a positive yawing moment about center of gravity. This is a restoring moment, which tends to point the airplane into the relative wind and return the sideslip angle to zero [4].

If the vertical tail were isolated in a uniform flow field, the angle of attack for this lifting surface would be equivalent to the sideslip angle $\beta$. The magnitude of the airflow relative to the vertical tail can be decreased if the surface is in the wake of the wing or the fuselage.

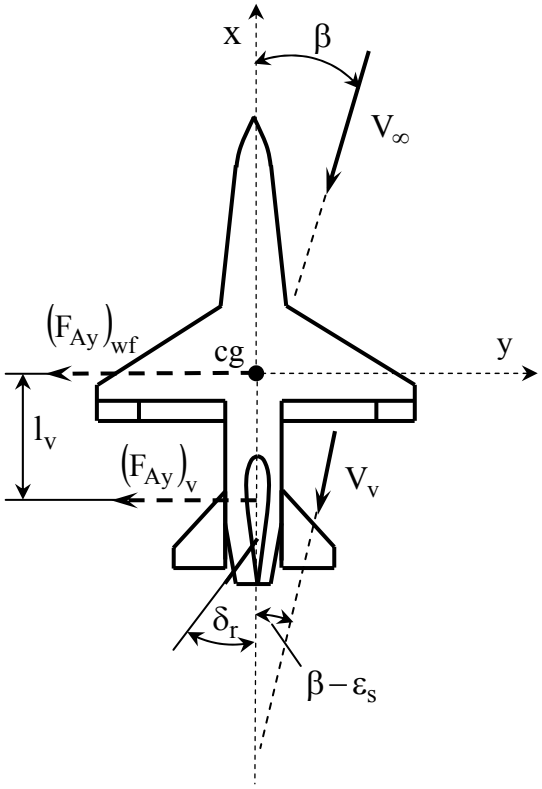


Fig. 1 Effect of sideslip on the aerodynamic yawing moment

This magnitude can be increased if the vertical tail is in the slipstream of a propeller or jet engine [5]. The angle of attack for the vertical tail can be modified by the slipstream of a propeller or by vorticity shed from the main wing. For small sideslip angle $\beta$, the sidewash on a vertical tail can be considered to be a linear function of $\beta$,

$$\varepsilon_s = \varepsilon_{s0} + \varepsilon_{s,\beta} \cdot \beta \qquad (1)$$

where $\varepsilon_{s0}$ is the sidewash angle at zero sideslip and $\varepsilon_{s,\beta}$ is the sidewash gradient,

$$\varepsilon_{s,\beta} = \partial \varepsilon_s / \partial \beta \qquad (2)$$

The lift developed on the vertical tail is linear for small angles of attack and rudder deflection. Positive deflection (leftward) of an aft rudder produces a rightward increment in the lift developed on the vertical tail and a negative increment in the aerodynamic yawing moment for the airplane [2]. Using standard sign convention, the contribution of the vertical tail to the yawing moment is

$$(\Delta n)_v = \frac{1}{2}\rho V_v^2 S_v \cdot \cdot \left[ l_v C_{Lv,\alpha} (\beta - \varepsilon_s - \varepsilon_r \delta_r) + \bar{c}_v C_{mv,\delta_r} \delta_r \right] \qquad (3)$$

where $V_v$ is the local magnitude of the relative airspeed at the position of vertical tail, $C_{Lv,\alpha}$ is the lift slope for the vertical tail, $\varepsilon_r$ is the rudder effectiveness, $\bar{c}_v$ is the mean chord length of the vertical tail and $C_{mv,\delta_r}$ is the change in the moment coefficient for the vertical tail with respect to rudder deflection.

The contribution of the vertical tail to the yawing moment coefficient is

$$(\Delta C_n)_v = \eta_v \frac{S_v l_v}{S_w b_w} C_{Lv,\alpha}\left[(1-\varepsilon_{s,\beta})\beta - C_{Lv,\alpha}\varepsilon_{s0}\right] - \quad (4)$$

$$-\eta_v \frac{S_v l_v}{S_w b_w} C_{Lv,\alpha}\left(\varepsilon_r C_{Lv,\alpha} - \frac{\bar{c}_v}{l_v} C_{m_v,\delta_r}\right)\delta_r$$

where $\eta_v$ is the dynamic pressure ratio for the vertical tail which is analogous to that for the horizontal tail. Equation (4) provides the contributions of the vertical tail and rudder to the yaw control derivative

$$(\Delta C_{n,\beta})_v = \eta_v \frac{S_v l_v}{S_w b_w} C_{Lv,\alpha}(1-\varepsilon_{s,\beta}) \quad (5)$$

$$C_{n,\delta_r} = -\eta_v \frac{S_v l_v}{S_w b_w} C_{Lv,\alpha}\left(\varepsilon_r C_{Lv,\alpha} - \frac{\bar{c}_v}{l_v} C_{m_v,\delta_r}\delta_r\right)$$

The aerodynamic derivative $C_{mv,\delta_r}$ is always negative, thus, the change in the airplane yawing moment coefficient with rudder deflection is always negative for an aft rudder, when leftward deflection of the rudder is considered to be positive [6]. The sidewash gradient, $\varepsilon_{s,\beta}$, is typically negative and thus it increases the stabilizing effect of the vertical tail. The lift slope for a vertical tail in combination with a horizontal tail can be estimated using the numerical lifting line method or from three dimensional panel code.

## 3. THE SIDEWASH GRADIENT ON VERTICAL TAIL

The sidewash induced on the vertical tail by the wingtip vortices has a significant effect on the static yaw stability of an airplane. For a vertical tail mounted above the wing, the sidewash gradient is negative and has a stabilizing effect on the airplane. The sidewash gradient produced by the wingtip vortices can be estimated using the vortex model (fig. 2)

According to Biot-Savart law, the y component of velocity induced by the pair of wingtip vortices at the arbitrary point in space $(x, y, z)$ can be written as

$$V_y = \frac{\Gamma_{wt}}{4\pi}\frac{z}{z^2+\left(y+\frac{1}{2}b'\right)^2}\left(1+\frac{x-\frac{1}{2}b'\tan\Lambda}{\sqrt{A}}\right) - \quad (6)$$

$$-\frac{\Gamma_{wt}}{4\pi}\frac{z}{z^2+\left(y-\frac{1}{2}b'\right)^2}\left(1+\frac{x-\frac{1}{2}b'\tan\Lambda}{\sqrt{B}}\right)$$

where

$$A = \left(x-\frac{1}{2}b'\tan\Lambda\right)^2 + z^2 + \left(y+\frac{1}{2}b'\right)^2$$

$$B = \left(x-\frac{1}{2}b'\tan\Lambda\right)^2 + z^2 + \left(y-\frac{1}{2}b'\right)^2 \quad (7)$$

The wingtip vortex strength is proportional to the product of the wing lift coefficient and airspeed. The vortex strength $\Gamma_{wt}$ and spacing $b'$ can be calculated from Prandtl's lifting line theory. Taking into account that the sidewash is positive from left to right (according to the sign convention) applying the small angle approximation, the sidewash angle can be written as

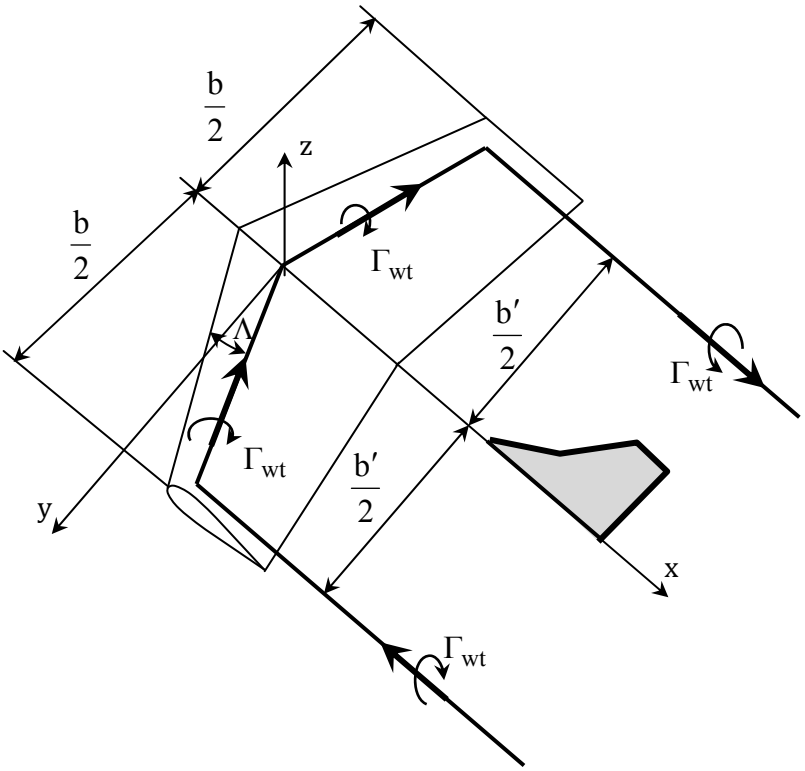


Fig. 2 Vortex model

$$\varepsilon_s = -\frac{V_y}{V_\infty} =$$
$$= \frac{C_{Lw} k_v}{\pi^2 \lambda_w} \frac{\bar{z}}{\bar{z}^2 + (\bar{y} - k_b)^2} \left(1 + \frac{\bar{x} - k_b \tan\Lambda}{\sqrt{\bar{A}}}\right) -$$
$$- \frac{C_{Lw} k_v}{\pi^2 \lambda_w} \frac{\bar{z}}{\bar{z}^2 + (y + k_b)^2} \left(1 + \frac{\bar{x} - k_b \tan\Lambda}{\sqrt{\bar{B}}}\right) \quad (8)$$

where $C_{Lw}$ and $\lambda_w$ are the lift coefficient and aspect ratio for the wing and

$$\bar{x} = \frac{x}{b_w/2},\ \bar{y} = \frac{y}{b_w/2},\ \bar{z} = \frac{z}{b_w/2}$$
$$\bar{A} = (\bar{x} - k_b \tan\Lambda)^2 + \bar{z}^2 + (\bar{y} - k_b)^2$$
$$\bar{B} = (\bar{x} - k_b \tan\Lambda)^2 + \bar{z}^2 + (\bar{y} + k_b)^2$$

The vortex strength factor $k_v$ is a ratio of the wingtip vortex strength to that generated by an elliptic wing having the same lift coefficient and aspect ratio. The vortex span factor $k_b$ is defined as the spacing between the wingtip vortices divided by the wingspan.

When the airplane has some component of sideslip, the wingtip vortices are displaced relative to the position of the vertical tail, as shown in fig. 3.

Using also the small angle approximation, the $y'$ coordinate is related to the y coordinate by the equation

$$\bar{y}'(\beta) = y\cos\beta - \left(x - \frac{1}{2} b' \tan\Lambda\right)\sin\beta \quad (9)$$

Within this small approximation, the sidewash gradient can be written as

$$\frac{\partial \varepsilon_s}{\partial \beta} = \frac{\partial \varepsilon_s}{\partial \bar{y}'} \cdot \frac{\partial \bar{y}'}{\partial \beta} \quad (10)$$

where

$$\frac{\partial \varepsilon_s}{\partial y'} =$$
$$- 2 \frac{C_{Lw} \cdot k_v}{\pi^2 \lambda_w} \frac{\bar{z}(\bar{y} - k_b)}{\bar{z}^2 + (\bar{y} - k_b)^2} \left(1 + \frac{\bar{x} - k_b \tan\Lambda}{\sqrt{\bar{A}}}\right) +$$
$$+ 2 \frac{C_{Lw} \cdot k_v}{\pi^2 \lambda_w} \frac{\bar{z}(\bar{y} + k_b)}{\bar{z}^2 + (\bar{y} + k_b)^2} \left(1 + \frac{\bar{x} - k_b \tan\Lambda}{\sqrt{\bar{B}}}\right) -$$
$$- \frac{C_{Lw} k_v \bar{z}}{\left[\bar{z}^2 + (\bar{y} - k_b)^2\right] \pi^2 \lambda_w} \frac{(\bar{x} - k_b \tan\Lambda)(\bar{y} - k_b)}{\bar{A}^{\frac{3}{2}}} +$$
$$+ \frac{C_{Lw} k_v \bar{z}}{\left[\bar{z}^2 + (\bar{y} + k_b)^2\right] \pi^2 \lambda_w} \frac{(\bar{x} - k_b \tan\Lambda)(\bar{y} + k_b)}{\bar{B}^{\frac{3}{2}}}$$

and

$$\frac{\partial \bar{y}'}{\partial \beta} = -(\bar{x} - k_b \tan\Lambda) \quad (11)$$

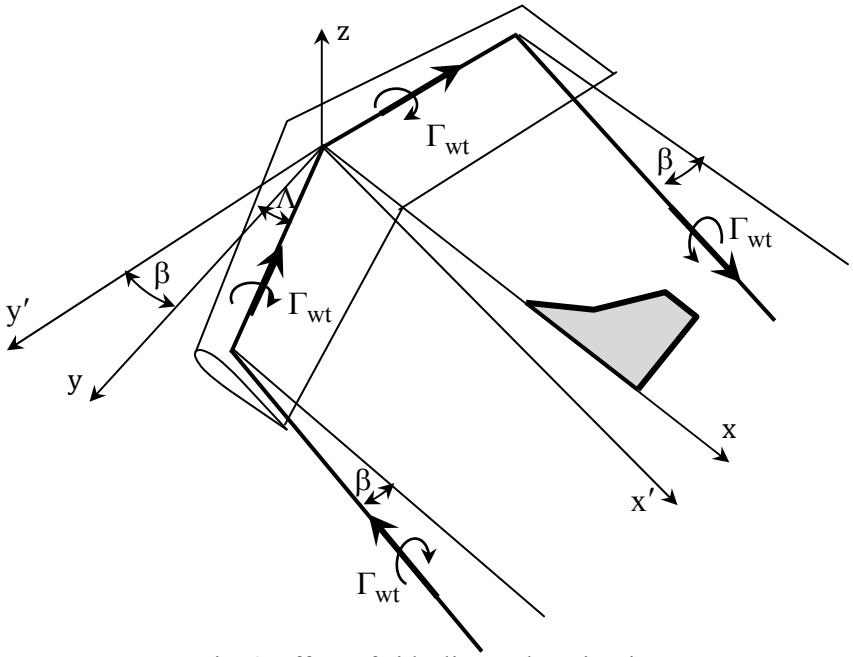


Fig. 3 Effect of sideslip on the wingtip

The sidewash gradient induced at an arbitrary point in space can be estimated by using the above equations. The tail sidewash factor $k_\beta$ depends on the platform shape of the wing and the position of the tail relative to the wing.

## 4. NUMERICAL RESULTS

The parameters $k_v$ and $k_b$ can be written in the form

$$k_v = 1 + \sum_{n=2}^{\infty} \frac{A_n}{A_1} \sin\left(n\frac{\pi}{2}\right)$$

$$k_b = \frac{\frac{\pi}{4} + \sum_{n=2}^{\infty} \frac{nA_n}{(n^2-1)A_1} \cos\left(n\frac{\pi}{2}\right)}{1 + \sum_{n=2}^{\infty} \frac{A_n}{A_1} \sin\left(n\frac{\pi}{2}\right)} \qquad (12)$$

where $A_1, A_2, \ldots A_n$ are the Fourier coefficients in the series solution to Prandtl's Lifting-line equation. The Fourier coefficients for a wing with geometric and aerodynamic twist are given by

$$A_n = a_n(\alpha - \alpha_{L0})_{root} - b_n\Omega \qquad (13)$$

where

$$\sum_{n=1}^{N} a_n \left[\frac{2\lambda(1+r)}{\tilde{C}_{L,\alpha}\left[1-(1-r)|\cos\theta|\right]} + \frac{n}{\sin\theta}\right]\sin(n\theta) = 1$$

$$\sum_{n=1}^{N} b_n \left[\frac{2\lambda(1+r)}{\tilde{C}_{L,\alpha}\left[1-(1-r)|\cos\theta|\right]} + \frac{n}{\sin\theta}\right]\sin(n\theta) = |\cos\theta|$$

$\lambda$ is the aspect ratio, r is the taper ratio, $\tilde{C}_{z,\alpha}$ is the section lift slope for the airfoil from which the wing was generated and $\theta = \cos^{-1}(2y/b)$.

In order to obtain N independent equations for the N unknown Fourier coefficients $a_n$ and $b_n$, the above equations can be written for each span-wise sections of the wing. With the first and last sections located at the wingtips and the intermediate sections spaced equally in $\theta$, this gives the system of equations

$$\begin{bmatrix} A_{11} & A_{12} & ... & A_{1N} \\ A_{21} & A_{22} & ... & A_{2N} \\ \vdots & \vdots & \vdots & \vdots \\ A_{N1} & A_{N2} & ... & A_{NN} \end{bmatrix} \cdot \begin{bmatrix} a_1 \\ a_2 \\ \vdots \\ a_N \end{bmatrix} = \begin{bmatrix} 1 \\ 1 \\ \vdots \\ 1 \end{bmatrix}$$

$$\begin{bmatrix} A_{11} & A_{12} & ... & A_{1N} \\ A_{21} & A_{22} & ... & A_{2N} \\ \vdots & \vdots & \vdots & \vdots \\ A_{N1} & A_{N2} & ... & A_{NN} \end{bmatrix} \cdot \begin{bmatrix} b_1 \\ b_2 \\ \vdots \\ b_N \end{bmatrix} = \begin{bmatrix} \cos(\theta_1) \\ \cos(\theta_2) \\ \vdots \\ \cos(\theta_N) \end{bmatrix}$$

where

$A_{1,j} = j^2,\ j = 1, N$

$A_{i,j} =$

$$\left[ \frac{2\lambda(1+r)}{\widetilde{C}_{L,\alpha}\left[1-(1-r)\left|\cos(\theta_i)\right|\right]} + \frac{j}{\sin(\theta_i)} \right] \sin(j\theta_i)$$

$\theta_i = \dfrac{(i-1)\pi}{N-1},\ i = 2, N;\ j = 1, N$

$A_{N,j} = (-1)^{j+1} j^2,\ j = 1, N$

For a wing platform with an aspect ratio of 8.8, a taper ratio of 0.5 and $S_w = 16\,m^2$, $b_w = 10\,m$, $\lambda = 6.25$, $\widetilde{C}_{Lw,\alpha} = 4.5$, $\Lambda = 10^\circ$ $l_v - l_w = 4\,m$, $\alpha = 5^\circ$, $\alpha_{L0} = -1.5^\circ$, $\bar{x} = 0.9$, and $\bar{z} = 1$, the Fourier coefficients are:

$$a = \begin{bmatrix} 0.198575 \\ 0 \\ 0.006929 \\ 0 \\ 0.009344 \\ 0 \\ 0.003888 \\ 0 \\ 0.003887 \end{bmatrix} \text{ and } b = \begin{bmatrix} -0.011237 \\ 0 \\ 0.008744 \\ 0 \\ 0.011790 \\ 0 \\ 0.004906 \\ 0 \\ 0.004905 \end{bmatrix}$$

The sidewash gradient is

$\varepsilon_{s,\beta} = -0.0043$ .

## 5. CONCLUSIONS

The numerical results show that the sidewash gradient on the vertical stabilizer increases rapidly with the distance aft of the wingtips. Also, there is an optimum in the trade-off between the area of the vertical stabilizer and its distance aft of the center of gravity. The numerical lifting line method gives very good results and can be used for accurately estimating the aerodynamic derivatives associated with tail configurations. The even Fourier coefficients in both $a_n$ and $b_n$ are identically zero for the plane tapered wing, so, the computation time can be reduced by forcing all even coefficients to be zero and solving the system of equations for the old coefficients using sections distributed over only one side of the wing.

## REFERENCES


1. Anderson, D. J., *Fundamentals of Aerodynamics,* McGraw-Hill Series in Aeronautical and Aerospace Engineering, New York (2007).
2. Katz, J., Plotkin, A., *Low Speed Aerodynamics,* Second Edition, Cambridge University Press, (2010).
3. Phillips, F. W., *Mechanics of Flight,* Jhon Wiley & Sons, Inc., New Jersey (2010).
4. Rotaru, C., Circiu, I., Boscoianu M. *Computational Methods for the Aerodynamic Design*, Review of the Air Force Academy, No 2(17), pp. 43-48 (2010).
5. Rotaru, C., Mihăilă M., Matei, P., Stefan, A., *Computing Nonlinear Characteristics of Helicopter Rotor Blades,* Review of the Air Force Academy, Vol. XI, No I(23), ISSN 2069-4733, pp.5-12 (2013).
6. Rotaru, C., Arghiropol A., *Maple soft solutions for nonlifting flows over arbitrary bodies,* Proceedings of the 3rd WSEAS international conference on FINITE DIFFERENCES - FINITE ELEMENTS - FINITE VOLUMES - BOUNDARY ELEMENTS, ISSN 1970-2769, pp. 270-274 (2010).

"HENRI COANDA"
AIR FORCE ACADEMY
ROMANIA

"GENERAL M.R. STEFANIK"
ARMED FORCES ACADEMY
SLOVAK REPUBLIC

INTERNATIONAL CONFERENCE of SCIENTIFIC PAPER
AFASES 2015
Brasov, 28-30 May 2015

# COUPLED TRANSIENT ANALYSIS OF A UAV COMPOSITE WING

**Amado Ştefan*, Ciprian Larco*, Radu-Călin Pahonie*, Ionuț Nicolaescu***

*Faculty of Mechatronics and Integrated Armament Systems, Military Technical Academy, Bucharest, Romania

***Abstract:*** *This article focuses on the flexibility influence over aerodynamic forces on a mini-airplane wing. For the flow around the flexible wing a transient structural analysis and a CFD analysis were coupled. The results were compared with the CFD analysis over a rigid wing structure.*

***Keywords:*** *coupled systems, FEM, aero-elasticity*

## 1. INTRODUCTION

Aero-elastic and loads considerations play a part across much of the design and development of an aircraft. The aero-elastic and loads behavior of the aircraft have an impact upon the concept and detailed structural design, aerodynamic characteristics, weight, jig shape, FCS design, handling qualities, control surface design, propulsion system, performance (effect of flight shape on drag), landing gear design, structural tests, etc.

A coupled system is one in which physically or computationally heterogeneous mechanical components interact dynamically.

The interaction is called one-way if there is not feedback between subsystems, as illustrated in Figure 1(a) for two subsystems identified as X and Y. The interaction is called two-way (or generally multiway) if there is feedback between subsystems, as illustrated in Figure 1(b). In this case, which will be the one of primary interest here, the response has to be obtained by solving simultaneously the coupled equations which model the system. "Heterogeneity" is used in the sense that component simulation benefits from custom treatment.

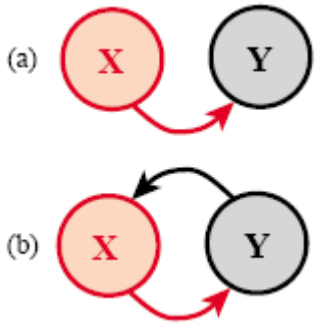


Fig. 1. Interaction between two subsystems X and Y: (a) one way, (b) two way.

As noted above the decomposition of a complex coupled system for simulation is hierarchical with two to four levels being common.

A coupled system is characterized as two-field, three-field, etc., according to the number of different fields that appear in the first-level decomposition.

For computational treatment of a dynamical coupled system, fields are discretized in space and time. A field partition is a field-by-field decomposition of the space

discretization. Asplitting is a decomposition of the time discretization of a field within its time step interval (Figure 2). In the case of static or quasi-static analysis, actual time is replaced by pseudo-time or some kind of control parameter.

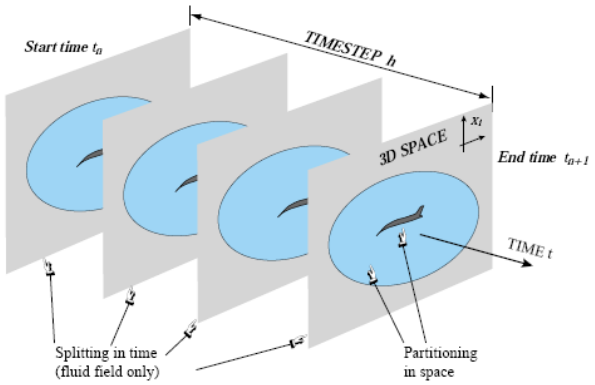


Figure 2. Decomposition of an aero-elastic FSI coupled system: partitioning in space and splitting in time. 3D space is shown as "flat" for visualization convenience.

Partitioning may be algebraic or differential. In algebraic partitioning the complete coupled system is spatially discretized first, and then decomposed. In differential partitioning the decomposition is done first and each field then discretized separately.

## 2. ANALYTICAL MODEL

One important interest in aircraft design is the aero-elastic deflections of the flexible wing, more specifically the aerodynamic influence on the effectiveness of the control surfaces in comparison to the rigid wing. It is known that as the speed increases the effectiveness reduces until at some critical speed – the reversal speed – there is no response to application of the control surface. At speeds greater than the reversal speed, the action of the controls reverses, a phenomenon known as control reversal. Although not necessarily disastrous, it is unacceptable that at speeds near to the reversal speed, the aircraft responds either very slowly or not at all to application of the controls, and that has the opposite response to that demanded occurred beyond the reversal speed.

Static aero-elasticity is the study of the deflection of flexible aircraft structures under aerodynamic loads, where the forces and motions are considered to be independent of time. Consider the aerodynamic lift and moment acting upon a wing to depend solely upon the incidence of each chord-wise strip. These loads cause the wing to bend and twist, so changing the incidence and consequently the aerodynamic flow, which in turn changes the loads acting on the wing and the deflections, and so on until an equilibrium condition is usually reached. The interaction between the wing structural deflections and the aerodynamic loads determines the wing bending and twist at each flight condition, and must be considered in order to model the static aero-elastic behavior. The static aero-elastic deformations are important as they govern the loads in the steady flight condition, the lift distribution, the drag forces, the effectiveness of the control surfaces; the aircraft trim behavior and also the static stability and control characteristics. The aero-elastic wing shape at the cruise condition is of particular importance as this has a crucial effect on the drag and therefore the range.

There are two critical static aero-elastic phenomena that can be encountered, namely divergence and control reversal. Divergence is the name given to the phenomenon that occurs when the moments due to aerodynamic forces overcome the restoring moments due to structural stiffness, so resulting in structural failure. The most common type is that of wing torsional divergence. In general, for aero-elastic considerations the stiffness is of much greater importance than the strength.

The static aero-elastic behavior is considered initially using an iterative approach and then a direct approach.

The rigid aero-foil section is symmetric (so has no inherent camber) and is attached to a torsional spring of stiffness $k_\theta$ at a distance $d$ aft of the aerodynamic center on the quarter chord. The lift-curve slope is $a_1$. The aero-foil has an initial incidence of $\theta_0$ and twists through angle $\theta$ due to the aerodynamic loading.

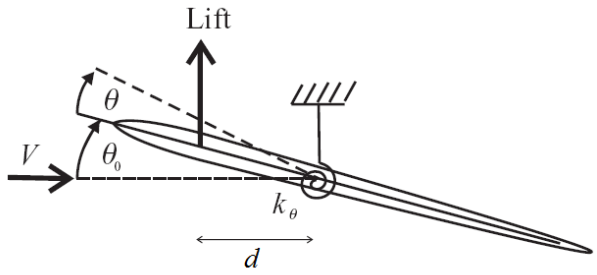


Figure 3. Two-dimensional aero-foil with a torsional spring

The lift acting on the aero-foil at air speed $V$ (true air speed, or TAS) and initial angle of incidence $\theta_0$ causes a pitching moment of

$$M = \left(\frac{1}{2}\rho V^2 c a_1 \theta_0\right)\cdot d = q d^2 a_1 \theta_0 \qquad (1)$$

to act about the flexural axis, where $q$ is the dynamic pressure and $\rho$ is the true air density. The equation for the aero-foil will be obtained using Lagrange's equations. Since only static aero-elastic effects are being considered, the kinetic energy term can be ignored. The potential (or strain) energy $U$ is found from the twist of the torsional spring, namely

$$U = \frac{1}{2}k_0\theta^2 \qquad (2)$$

The generalized moment may be obtained from the incrementalwork done by the pitching moment acting through the incremental angle $\delta\theta$ and is given by

$$Q_\theta = \frac{\partial(\delta W)}{\partial(\delta\theta)} = \frac{\partial\left(q d^2 a_1 \theta_0 \delta\theta\right)}{\partial(\delta\theta)} = q d^2 a_1 \qquad (3)$$

Then application of Lagrange's equations for coordinate $\theta$ gives

$$k_0\theta = q d^2 a_1 \theta_0 \qquad (4)$$

Consequently,

$$\theta = \frac{q d^2 a_1}{k_\theta}\theta_0 = qR\theta_0 \qquad (5)$$

where $R = d^2 a_1 / k_\theta$ .

Thus having applied the initial aerodynamic loading, the aero-foil has twisted by angle $\theta$, as determined in equation (5). In performing this calculation, it has been assumed that the pitching moment has not changed due to the twist. However, as a consequence of the twist, the aerodynamic moment now changes to allow for the new angle of incidence. This new loading, in turn, causes the aero-foil twist to change again, leading to a further modification in the aerodynamic loading, and so on.

The stepping between application of the aerodynamic load on the aero-foil, changing the aero-foil twist and then determining the new aerodynamic loading illustrates the fundamental interaction between a flexible structure and aerodynamic forces that gives rise to aero-elastic phenomena.

At first iteration, the incidence of the aero-foil includes the initial incidence and the estimate of twist, so the revised pitching moment becomes

$$M = q d^2 a_1\left(\theta_0 + qR\theta_0\right) \qquad (6)$$

and, since the potential/strain energy term remains the same as in equation (2), application of Lagrange's equations gives a revised elastic twist angle of

$$\theta = q d^2 a_1 \frac{1+qR}{k_\theta}\theta_0 = qR\left(1+qR\right)\theta_0 \qquad (7)$$

Repeating the above process continues by using the updated elastic twist value in the pitching moment and work expressions, leading to an infinite series expansion for the elastic twist in the form

$$\theta = qR\left[1 + qR + \left(qR\right)^2 + \left(qR\right)^3 + \cdots\right]\theta_0 \qquad (8)$$

Now, remembering that the binomial series is written as

$$(1-x)^{-1} = 1 + x + x^2 + x^3 + \cdots \quad (9)$$

in the limit, the aero-foil twist becomes

$$\theta = \frac{qR}{1-qR}\theta_0 \quad (10)$$

It should be noted, however, that the single step (strongly coupled) approach is only feasible if there is a direct mathematical relationship between the aerodynamic forces and the deflections. If advanced static aero-elastic calculations for an entire aircraft, involving the coupling of computational fluid dynamics (CFD) methods with finite element methods, are applied, then such an approach requires use of a loosely coupled approach somewhat similar to the iterative process shown above.

It should be remembered that there are a number of significant assumptions in the above analysis. Sweepback (or sweep-forward) will increase the aerodynamic interactions between different parts of the wing, which will make the strip theory aerodynamics more inaccurate. It has been assumed that the wing behaves as a beam-like structure, and consequently that the flexural axis remains parallel to the axis of sweep along the mid-chord line. In cases where the wing behaves more like a plate, such as for low aspect ratio tapered swept wings, the structural bending/torsion coupling effects for the swept wing must also be included.

## 3. NUMERICAL MODEL

The traditional approach to determining a mathematical model for aircraft with fairly slender high aspect ratio wings was to recognize that the structure is ‘beam-like’ and then to represent the major aircraft components (e.g. wing, front fuselage, rear fuselage, tail-plane, fin) by beams lying along reference axes positioned at, for example, the locus of shear centers (or flexural axis). The beams are capable of bending, shear, torsional and axial deformations. In such an approach, each beam is divided into several sections or elements. The combination of such ‘beams’ for all parts of the aircraft is called a ‘stick’ or ‘beam’ model.

The flexural rigidity *EI* and torsional rigidity *GJ* of the beam are traditionally estimated from the member section properties by classical structural analysis methods. The structural stiffness behavior of each element is represented by a stiffness matrix (effectively the finite element method employing beam elements).

The problem with employing beam elements directly for an aircraft structure is that for such a complex structure, the calculated stiffness distribution is rather inaccurate. It may be suitable for an aircraft in early design where the detailed structure has not yet been defined and where scaled stiffness and mass properties from previous aircraft might be employed, but not at the later stages of design and certification where structural detail is available and important.

It should be emphasized that the model employed for dynamics purposes may not be as detailed in structural representation as the model used for stress analysis. The dynamic idealization for an aircraft structure is relatively crude though the level of sophistication is continually growing.

When modelling a detailed component such as a machined bracket using ‘brick’ elements, say, the FE model will represent the load paths well and the stresses derived from the stiffness matrix and element deformations will be quite reliable. However, for a complex stiffened aircraft box structure, the level of detail that can be accurately modelled is limited and so the stress output can be rather unreliable. Therefore the FE method often tends to be used to determine load paths via nodal forces that can subsequently act as input loads to a more detailed FE model of a local structure or to a structural element where dedicated design formulae/programs are available.

The UAV wing is 100% composite materials, e-glass type woven fabric being used. These are plain weave balanced fabrics with 0/90 degrees fiber orientation. For the matrix material epoxy is used. The airfoil is E197, the wingspan is 1000 mm, root chord length has 150 mm, and the end chord is 80 mm (Figure 3). The wing has twenty ribs and two spars and two cylindrical reinforcement tubes.

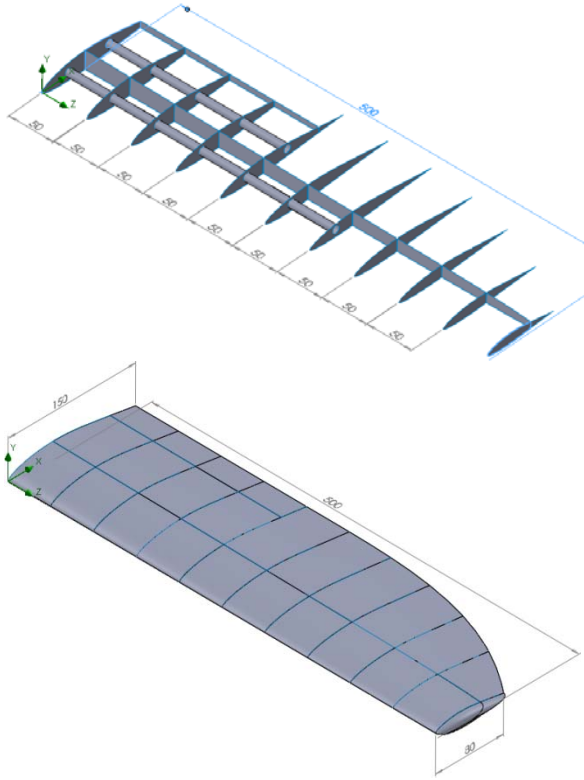

Figure 4. The wing structure – geometry model

To determine the loads, it is considered the air flow over the half of wing with the speed of 15 m/s, the airfoil attack angle at 5°. The solver calculate all the flow parameters, in figure 5 is presented the pressure field).

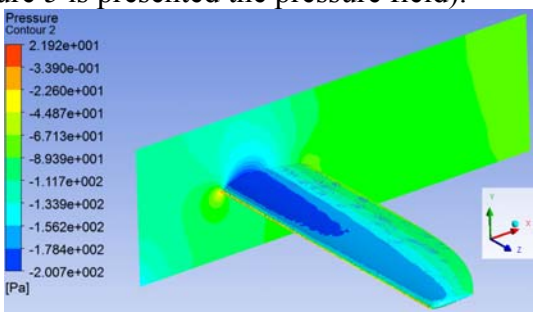


Figure 5. Flow analysis (pressures on the wing and in the symmetry plane)

The fibers used in the UAV are plain weave fabrics, which have a complicated structure and detailed meso scale models are required for the analysis. In this study, the method used for modeling the woven structure is to consider the woven lamina as a single equivalent layer by assuming $E_1 = E_2$. The numerical results from the structural analysis, at the last time step (2 sec), are presented below.

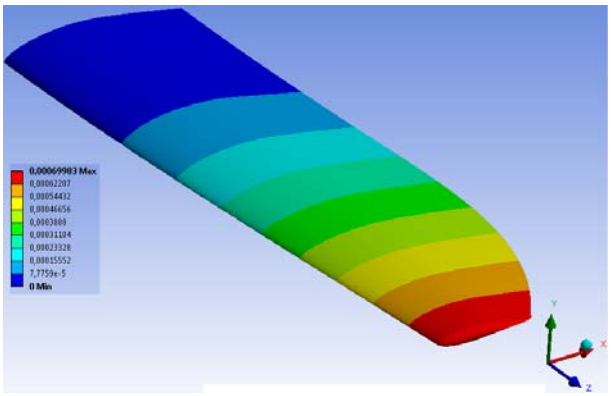

Figure 6. Total displacement field (mm)

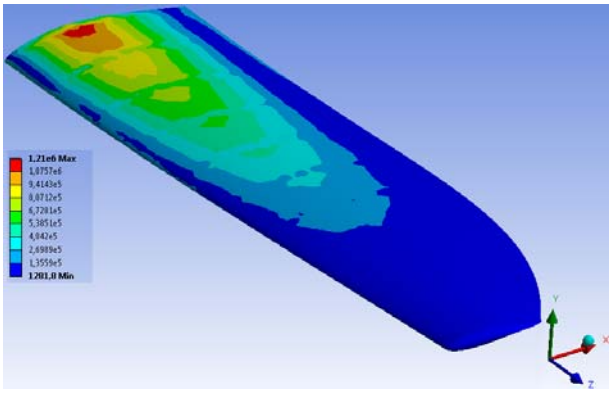

Figure 7. Equivalent Von Mises stress field (Pa)

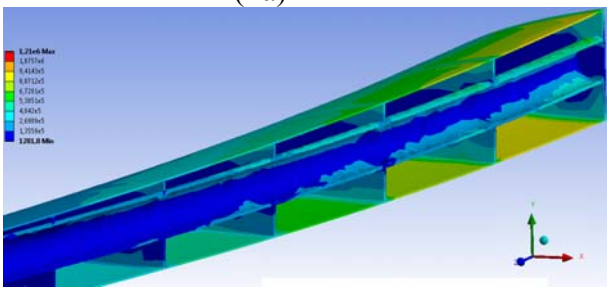

Figure 8. Equivalent Von Mises stress field (Pa) in section along the first spar

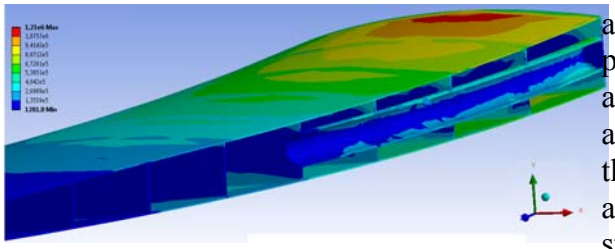

Figure 9. Equivalent Von Mises stress field (Pa) in section along the second spar

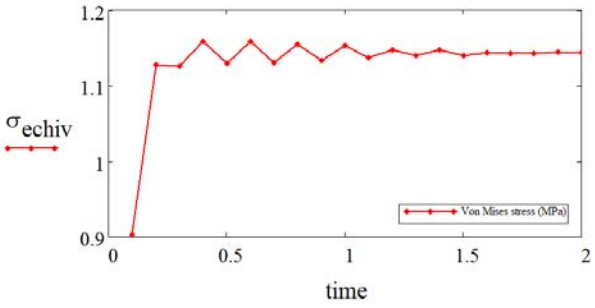


Figure 10. Time variation for maximum Von Mises stress (flexible wing)

Table 1: Aerodynamic forces on wing

| | Lift (N) | Drag (N) |
|---|---|---|
| Flexible wing | 6.456 | 0.708 |
| Rigid wing | 6.5 | 0.699 |

## 4. CONCLUSIONS & ACKNOWLEDGMENT

The results from the coupled transient structural analysis with flow analysis were compared this classic case of a flow over the rigid wing. The study was realized on a UAV composite wing with 1 m span.

By comparing the aerodynamics forces on the wing (table 1), it can be noticed that the wing deformation for the flexible wing case induces a very small decrease on lift (0.67%), and a slight increase of drag (1.25%). The differences are expected to be larger if the wing span increses.

The flight regime is stable (as can be seen in figure 10) because of wing stiffness.

This study involved a simplified composite airframe, considering equivalent material properties. However, for a complex stiffened aircraft structure, the level of detail that can be accurately modelled can be increased and so the stress output can be more realistic. This also implies using failures theories for structural analysis.

This paper has been financially supported within the project entitled "*Horizon 2020 - Doctoral and Postdoctoral Studies: Promoting the National Interest through Excellence, Competitiveness and Responsibility in the Field of Romanian Fundamental and Applied Scientific Research*", contract number POSDRU/159/1.5/S/140106. This project is co-financed by European Social Fund through Sectoral Operational Programme for Human Resources Development 2007-2013. Investing in people!

## REFERENCES

1. Megson, T.H.G., *Aircraft Structures for Engineering Students*, 5th ed, Elsevier (2012).
2. Park, K.C. Felippa, C.A., *Partitioned Analysis of Coupled Systems,* Chapter 3 in *Computational Methods for Transient Analysis*, Belytschko T. and Hughes T.J.R., eds., North-Holland, Amsterdam–New York (1983).
3. Hodges D.H., Chang, Pierce G.A., *Introduction to Structural Dynamics and Aeroelasticity, Second Edition*, Cambridge University Press, UK (2011).
4. NAFEMS, *A Finite Element Primer*, DTI, (1987)
5. Wright, J.R., Cooper, J.E., *Introduction to Aircraft Aeroelasticity and Loads*, John Wiley & Sons Ltd, West Sussex, UK, (2007)

.

"HENRI COANDA"
AIR FORCE ACADEMY
ROMANIA

"GENERAL M.R. STEFANIK"
ARMED FORCES ACADEMY
SLOVAK REPUBLIC

INTERNATIONAL CONFERENCE of SCIENTIFIC PAPER
AFASES 2015
Brasov, 28-30 May 2015

# CALCULATING TECHNICAL SCATTERING FULL ERROR FOR EXTERNAL SUSPENDED BOMBS AT FREE RELEASE

**Stoyko Stoykov*, Milen Atanasov****

*Institute for Research and Innovation, National Military University, Veliko Tarnovo, Bulgaria,
**Aviation Faculty, National Military University, Dolna Mitropolia, Bulgaria

***Abstract:*** *The error of aviation bombs mission use is sum of aiming error and technical scattering error. Technical scattering full error is sum of partial errors. Technical scattering full error of aviation bomb free release is determined.*

***Keywords:*** *technical scattering full error, bomb*

## 1. INTRODUCTION

The expression of the error of aviation bombs mission use $\xi$ can be written in the following way:

$$\xi = \xi_a + \xi_t, \qquad (1)$$

where $\xi_a$ is the error in solving the aiming problem;

- $\xi_t$ error caused by bombs technical scattering.

Diversions at the initial conditions of bombs movement are the main reason for technical scattering of the bomb explosion points [2, 3, 4]. Another important reason for technical scattering is diversion of ballistic bomb qualities from nominal ones [4].

Technical scattering caused by the setting is along the course of flight (in the longitudinal plane).

Technical scattering full error of the i bomb $\Delta\xi_t$ is presented as a sum of errors with partial reasons:

$$\Delta\xi_{ti} = \sum_{j=1}^{n} \Delta\xi_{tij}, \qquad (2)$$

where j is a symbol of partial reason;

n– the number of reasons.

Each partial error $\Delta\xi_{tij}$ is divided into a group error, equal for all bombs and expressed in shifting the whole bombs series and individual – displacing the length of the series and redistributing the bombs in the series.

Considerable partial errors are:

- $\Delta\xi_{tt}$, error of delay and "disorder" of the moment of dropping, caused by the errors of control system discharge and the errors in the time of moving at the initial section;

- $\Delta\xi_{t\theta}$, error of oscillation of bomb path, caused by diversion of bomb axis from the tangent in the process of discharge and causing angular velocity of the bomb;

- $\Delta\xi_{tн}$, error, caused by different levels between points of dropping and compartment (inner suspension);

- $\Delta\xi_{tv}$, error caused by the aircraft rate in value and direction in the process of successive bomb dropping and the change in bomb velocity at the initial part of moving.

The full technical scattering error caused by the discharge process is a sum of the partial errors.

$$\Delta\xi_{ti} = \sum_{j=1}^{n}\Delta\xi_{tij} = W_{\xi}\Delta t_i + \frac{\partial A}{\partial C_{x\delta}}\Delta C_{x\delta} + \frac{\partial A}{\partial V}\Delta V_i + \frac{\partial A}{\partial \lambda}\Delta\lambda_i, \quad (3)$$

where

$$\Delta V_i = \Delta V_i^{(1)} + \Delta V_i^{(2)}$$
$$\Delta\lambda_i = \Delta\lambda_i^{(1)} + \Delta\lambda_i^{(2)}.$$

## 2. MATHEMATICAL MODEL

The odd movement of each bomb at the initial part can be considered as a diversion of real values of initial parameters from predicted values.

Differences in corresponding values $x_b - x_b^r, y_b - y_b^r, \ldots\ldots$ and so on for the moment of time $t_d$ are diversion of real movement parameters from predicted at the surrounding aircraft area. They are caused by bomb disturbances. Outside disturbance zone and when there is a full bomb oscillation damping, real movement will be distinguished by predicted one only by difference in movement parameters at the surrounding aircraft area. That is why movement parameters at the surrounding aircraft area are considered as initial movement conditions.

Using the formula (3) we have technical scattering full error assessment for fighter bomber at horizontal flight with following data:

- airplane mass - m=15480 kg;
- airplane weight - G=mg=1.5186*$10^5$ N;
- wing area - S=34.5 $m^2$;
- airplane rate - V=250 m/s;
- flight altitude - H=1000 m.

The study is for practical aviation bomb P-50-75.

When there is bomb free release equations for mass center movement are [1]

$$\bar{x} = \left[\frac{1}{2}(n_{bx} - n_x)g\right]gt^2 + \frac{1}{3}\omega_z(n_{by} - n_y)gt^3;$$
$$\bar{y} = \frac{1}{2}(n_{by} - n_y)gt^2 - \frac{1}{3}[\omega_z(n_{bx} - n_x)]gt^3. \quad (4)$$

Having in mind that [1] $x_b=x_a+\bar{x}+x_0$, $y_b=y_a+\bar{y}+y_0$, where $x_0=y_0=0$, $x_a=Vt$, $y_a=0$ and using formula (4) we receive real parameters for bomb movement.

$$x_b = Vt - 4.57t^2 - 0.0007t^3;$$
$$y_b = 0.23t^2 - 0.014t^3;$$
$$\dot{x}_b = t - 9.14t - 0.0021t^2; \quad (5)$$
$$\dot{y}_b = 0.46t - 0.042t^2.$$

Bomb angle of pitch $\theta_b$ and angular velocity $\dot{\theta}_b$ are assessed by formulas [1]:

$$\theta_b = \omega_z t + Q\frac{t^2}{2};\ \dot{\theta}_b = \omega_z + Qt. \quad (6)$$

Bomb coordinates and their derivatives in the border of disturbance zone $t=t_d$ are:

- **real coordinates**

$$x_b = Vt_d - 4.57t_d^2 + 0.0111t_d^3;$$
$$y_b = -3.537t_d^2 - 0.0143t_d^3;$$
$$\dot{x}_b = V - 9.149t_d + 0.0332t_d^2;$$
$$\dot{y}_b = -7.074t_d - 0.043t_d^2;$$
$$\dot{\theta}_b = \omega_z + Qt_d;\ \theta_b = \omega_z t_d + Q\frac{t_d^2}{2},$$

- **predicted coordinates**

$$x_b^r = Vt_d;\ y_b^r = -4.905t_d^2;$$
$$\dot{x}_b^r = V;\ \dot{y}_b^r = -9.81t_d;$$
$$\theta_b^r = -0.0392t_d;$$
$$\dot{\theta}_b^r = -0.0392.$$

In the border of disturbance zone for coordinate $y= y_{bd}$ we define $t_d$:

- **real movement**

$$t_d = \sqrt{\frac{y_{bd}}{-3.537}},$$

- **predicted movement**

$$t_d^r = \sqrt{\frac{y_{bd}}{-4.905}}.$$

When $y_{bd}$= -1.5 m, V=250 m/s, $\omega_z$=-0.0047 $s^{-2}$, Q=0.16 [1] we have:

- **real movement**

$t_d$=0.7976;

$x_b = 196.49$ m;

$y_b = -2.25$ m;

$\dot{x}_b = 242.709$ m/s;

$\dot{y}_b = -5.669$ m/s;

$\theta_b = 0.0471$;

$\dot{\theta}_b = 0.123\ s^{-1}$.

- **predicted movement**

$t_d^r = 0.6773$;

$x_b^r = 169.321,\ y_b^r = -2.25$;

$\dot{x}_b^r = 250$ m/s, $\dot{y}_b^r = -6.644$ m/s;

$\theta_b^r = -0.0266$ ;

$\dot{\theta}_b^r = -0.0392\ s^{-1}$.

The difference between real and predicted bomb movement in the disturbance zone is assessed by formulas:

$$\Delta t_d = t_d - t_d^r;$$

$$\Delta x_b = x_b - x_b^r,\ \Delta y_b = y_b - y_b^r;$$

$$\Delta \dot{x}_b = \dot{x}_b - \dot{x}_b^r,\ \Delta \dot{y}_b = \dot{y}_b - \dot{y}_b^r;$$

$$\Delta \theta_b^r = \theta_b - \theta_b^r;$$

$$\Delta \dot{\theta}_b = \dot{\theta}_b - \dot{\theta}_b^r.$$

From where:

$\Delta t_d = 0.12$ s;

$\Delta x_b = 27.169$ m;

$\Delta \dot{x}_b = -7.29$ m/s;

$\Delta \dot{y}_b = 0.975$ m/s;

$\Delta \theta_b^r = 0.0737$;

$\Delta \dot{\theta}_b = 0.162\ s^{-1}$.

Technical scattering full error is assessed by formula (3) and airplane ground velocity $W_\xi$ is assessed by formula:

$$W_\xi = V + U, \quad (7)$$

where U is the wind velocity. We assume that U=10 m/s. Then airplane ground velocity is $W_\xi$=260 m/s.

Partial error $\Delta\xi_{tW}$:

$$\Delta\xi_{tW} = W_\xi \Delta t_d = 31.2 \text{ m}.$$

Resistance coefficient increasing $\Delta C_{xb}$ is received by formula:

$$\Delta C_{xb} = 3\% C_{xb} = 0.6146 * \frac{3}{100} = 0.0184.$$

After solving the ballistic problem we receive the partial error, caused by $\Delta C_{xb}$:

$$\Delta\xi_{tCxb} = \frac{\partial A}{\partial C_{xb}} \Delta C_{xb} =$$

$$= 813.587 * 0.0184 = 14.97 \text{ m}$$

When the flight is horizontal, errors $\Delta V^{(1)}=0$, $\Delta\lambda^{(1)}=0$, as aviation target system automatically reads the rate of flight , bomb weight is slightly less than airplane weight and the angle $\lambda$=0.

Errors $\Delta V^{(2)}$ and $\Delta\lambda^{(2)}$, caused by bomb movement in the disturbance zone are received by formulas:

$$\Delta V^{(2)} = \Delta \dot{x}_b = \quad (8)$$

$$= V_{bx}^r(t_d) - V_{bx}(t_d) = -7.29 \text{ m/s};$$

$$\Delta\lambda^{(2)} = \frac{\Delta \dot{y}_b - \Delta \dot{x}_b \operatorname{tg}\lambda}{\dot{x}_b} \cos^2\lambda = \quad (9)$$

$$= 0.22^0.$$

Partial error is calculated by formula (3):

$$\Delta\xi_{tv} = \frac{\partial A}{\partial V} \Delta V^{(2)} + \frac{\partial A}{\partial \lambda} \Delta\lambda^{(2)} = \quad (10)$$

$$= -19.9 - 14 = -33.9 \text{ m}.$$

Technical scattering full error is calculated by formula (3):

$$\Delta\xi_{tj} = \sum_{j=1}^{4}\Delta\xi_{tj} = W_{\xi}\Delta t_d + \frac{\partial A}{\partial C_{xb}}\Delta C_{xb} + \frac{\partial A}{\partial V}\Delta V^{(2)} + \frac{\partial A}{\partial \lambda}\Delta\lambda^{(2)} =$$
$$= 31.2 - 14.97 - 19.9 - 14 = -17.67\ \text{m}.$$

## 3. CONCLUSIONS

From so done calculations for partial errors for the used example with accepted conditions for bomb release we see that partial error $W_{\xi}\Delta t_d$ has positive sign. The others $\frac{\partial A}{\partial C_{xb}}\Delta C_{xb}$, $\frac{\partial A}{\partial V}\Delta V^{(2)}$, $\frac{\partial A}{\partial \lambda}\Delta\lambda^{(2)}$ have negative sign, i.e. there is compensation for partial errors and technical scattering full error is reduced.

## REFERENCES


1. А.В., Бухалев, Установки ракетного и бомбардировочного авиационного оружия част I, М, ВВИА (1966).
2. А. М., Краснов, Основы анаализа процесса прицеливания в авиационных системах управления вооружением, Электронный журнал „Труды МАИ“, Выпуск 61, (2012).
3. А.Г., Постников, В.С., Чуйко, Внешняя баллистика неуправляемых авиационных ракет и снарядов, Москва, Машиностроение, (1985).
4. M.N. Pravidlo, V.A. Nesterov, A.N. Belyaev, The Analisis of the Adaptive Closed-Loop Ejection System of Stores. Part 1, Мехатроника, автоматизация, управление, №2, (2014).

"HENRI COANDA"
AIR FORCE ACADEMY
ROMANIA

"GENERAL M.R. STEFANIK"
ARMED FORCES ACADEMY
SLOVAK REPUBLIC

INTERNATIONAL CONFERENCE of SCIENTIFIC PAPER
AFASES 2015
Brasov, 28-30 May 2015

# PROJECTILE'S DRAG COEFFICIENT EVALUATION FOR SMALL FINITE DIFFERENCES OF HIS GEOMETRICAL DIMENSIONS USING ANALYTICAL METHODS

**George Surdu***, **Ioan Vedinaş****, **Georgică Slămnoiu***, **Şomoiag Pamfil****

*Research Center for Navy, Constanta, Romania, **Military Technical Academy, Romania

***Abstract:*** *In this paper is described an algorithm for projectile's drag coefficient evaluation for small finite differences of projectile's geometrical dimensions. The algorithm is presented in projectile design bibliography as projectile's shape index evaluation using empirical relations. The study is useful for engineers who work in research and ammunition design when is necessary to evaluate the preliminary projectile shape index and his implication on trajectory. In the same time based on projectile's shape index the drag coefficient is calculated using the reference law's Siacci, 1943 and 1930. The paper offer an evaluation of projectile's drag coefficient/shape index in accordance with the small finite differences of projectile's geometrical dimensions of ogive and tronconical part. This study can be easily implemented in a standalone application as a module of projectile's drag coefficient evaluation.*

***Keywords:*** *drag coefficient, projectile's shape index, ammunition, aerodynamics, projectile, aerodynamic configuration, reference drag laws*

## 1. INTRODUCTION

Analytical methods are very useful for preliminary evaluation for aerodynamic parameters of projectiles and projectiles ballistic design. In this case is necessary a simple and expedite instrument to evaluate the influences for small differences of projectile's geometrical dimensions in drag coefficient evaluation or projectile's shape index. In addition, these small differences represent the accepted tolerance or accepted projectile's dimensions tolerances in ballistic design.

These types of studies offers to engineers or field test specialist of ammunitions an important standalone instrument which serves in: projectile geometrical modification evaluation, ballistic table evaluation, projectile's trajectory evaluation using drag coefficient modifications caused by small differences of projectile's dimensions.

This small differences/ tolerances of projectile's dimension are inherent and the only way is to accept them and evaluate the implication of them on projectile's aerodynamic coefficients, projectile's trajectory or projectile – target impact.

Some of these studies can represent a cheap and handy alternative for field-testing but cannot replace the experimental tests. Specialist for preliminary evaluation and implications can use these instruments.

This study presents projectile's shape index and drag coefficient evaluation using the method of the French researcher Hélie that has

established a relation for the shape index for projectile based on his ogive dimensions.

In addition, this relation is corrected using the projectile shape index correction made some relations obtained based in aerodynamic tunnel experiments made in U.S.A.

This study put together these relations for projectile's shape index and also evaluate projectile's drag coefficient in accordance with the standard drag law's Siacci, 1943 and 1930.

This study also contains and exemplification of how small differences in projectile's geometry can affect the value of projectile's shape or drag coefficient.

The study has two main objectives: projectile's shape index and drag coefficient evaluation using the proposed analytical algorithm and the influence of projectile's small geometrical tolerances on projectile's shape index.

The evaluated drag coefficient is for Mach values between 0.1 and 4.0.

The projectile aerodynamic configuration is similar to the 30 mm projectile presented in Fig.1.

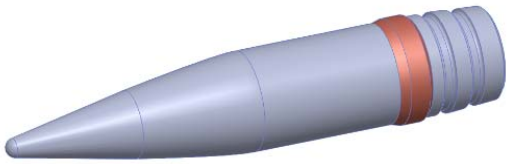

Fig. 1 Aerodynamic configuration of 30 mm caliber projectile used

The study uses some of the projectile's geometrical dimensions and his flight conditions.

## 2. MATHEMATICAL MODELS USED

The study has two main objectives as we mentioned before and for these objectives are reached by using simple empirical relations to evaluate the projectile's shape index and drag coefficient. In this case, the mathematical model for the analytical evaluation will be presented in the following.

The mathematical model [1, 2, 3] for drag coefficient estimation uses projectile's geometrical dimensions (Fig. 2).

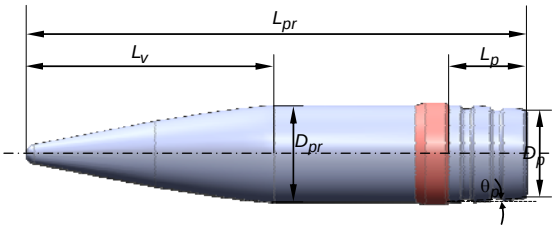


Fig. 2 Projectile's dimensions used

These dimensions are: $L_{pr}$ – projectile's total length, $L_v$ - ogive length, $L_p$ - tronconical length, $D_{pr}$ - transversal section diameter, $D_p$ projectile back – side diameter, $\theta_p$ – angle for projectile's tronconical part.

For the algorithm of shape index estimation, we use the following relations [2,3]:

$$\lambda_v = \frac{L_v}{D_{pr}} \tag{1}$$

$$\gamma_p = D_{pr} - 2 \cdot L_p \cdot tg(\theta_p) \tag{2}$$

$$\gamma_{pr} = 1 - \frac{\gamma_p^2}{D_{pr}^2} \tag{3}$$

Where $\lambda_v$ is ogive's relative length, $\gamma_p$ represents a geometrical coefficient for tronconical part, $\gamma_{pr}$ is a geometrical coefficient for projectile shape.

The preliminary projectile's shape index, taking into account the ogive's length, is estimated using relation [1]:

$$i_T = \frac{12 \cdot \lambda_v}{\sqrt{5} \cdot \left(4 \cdot \lambda_v^2 + 1\right)} \tag{4}$$

Using the above relation for projectile shape index evaluation we can obtain the final values for $i_{TC}$ [1]:

$$i_{TC} = i_T \cdot \left[1 - \left(0.6 + \frac{\lambda_v}{10}\right) \cdot \gamma_{pr}\right] \tag{5}$$

valid for projectile's velocities less than 250 m/s,

$$i_{TC} = i_T \cdot \left[1 - \eta_{pr} \cdot \gamma_{pr}\right] \tag{6}$$

valid for projectile's velocities greater than 205 m/s and less and equal with 400 m/s and

$$\eta_{pr} = 0.6 + 0.167 \cdot \lambda_v - 0.0027 \cdot \lambda_v \cdot V_0 \tag{7}$$

For projectile's velocities greater than 400 m/s we use for shape index evaluation following relation [1]:

$$i_{TC} = i_T \cdot \left[1 - 0.6 \cdot \left(1 + \frac{\lambda_v}{10}\right) \cdot \gamma_{pr}\right] \quad (8)$$

Once we evaluate the projectile index , $i_{TC}$, we calculate drag coefficient for projectile using the reference drag coefficient law's Siacci, 1930 or 1943 based on projectile relative length. The relation for projectile's drag coefficient is:

$$C_D = i_{TC} \cdot C_{Dref} \quad (9)$$

In which $C_D$ represents drag coefficient calculated and $C_{Dref}$ represents the value of drag coefficient used as reference.

Based on relations (5) to (8) we can evaluate the influence of projectile's small geometrical tolerances on projectile's shape index using the small differences hypothesis [3,4,5,6] or in mathematical terms, the shape index functions differentiation as follows:

$$\delta i_{TC} = \Delta\lambda_v + \Delta L_p + \Delta\theta_p \quad (10)$$

In which:

$$\Delta\lambda_v = \frac{\partial i_{TC}}{\partial\lambda_v} \cdot \delta\lambda_v \quad (11)$$

$$\Delta L_p = \frac{\partial i_{TC}}{\partial L_p} \cdot \delta L_p \quad (12)$$

$$\Delta\theta_p = \frac{\partial i_{TC}}{\partial\theta_p} \cdot \delta\theta_p \quad (13)$$

$$\delta\lambda_v = \frac{\partial\lambda_v}{\partial L_v} \cdot \delta L_v + \frac{\partial\lambda_v}{\partial D_{pr}} \cdot \delta D_{pr} \quad (14)$$

$$\frac{\partial\lambda_v}{\partial L_v} = \frac{1}{D_{pr}} \quad (15)$$

$$\frac{\partial\lambda_v}{\partial D_{pr}} = -\frac{L_{pr}}{D_{pr}^2} \quad (16)$$

In which $\frac{\partial i_{TC}}{\partial\lambda_v}$, $\frac{\partial i_{TC}}{\partial L_p}$, $\frac{\partial i_{TC}}{\partial\theta_p}$, $\frac{\partial\lambda_v}{\partial L_v}$, $\frac{\partial\lambda_v}{\partial D_{pr}}$ are partial derivatives.

As an example of projectile's shape index variation caused by $\lambda_v$ we have for index shape variation the following relations:

$$\delta i_{TC} = \frac{\partial i_{TC}}{\partial\lambda_v} \cdot \delta\lambda_v \quad (17)$$

where $\delta\lambda_v$ is from relation (14) and

$$\frac{\partial i_{TC}}{\partial\lambda_v} = \frac{i_{TC}}{\lambda_v \cdot \left(4 \cdot \lambda_v^2 + 1\right)} - \frac{6 \cdot i_{TC}}{100} \cdot \gamma_{pr} \quad (18)$$

Using relations (14), (17) and (18), we can evaluate the influence of projectile's ogive length on projectile's shape index and drag coefficient. In similar way can be evaluated, too, the influences on projectile shape index and drag coefficient caused by $\theta_p$ and $L_p$ variations.

## 3. NUMERICAL RESULTS

Initial data used to make the calculations for projectile shape index and drag coefficient are presented in Table 1.

Table 1. Initial data for calculation

| Parameter | Value |
|---|---|
| $D_{pr}$ [mm] | 30 |
| $L_{pr}$ [mm] | 150.75 |
| $L_v$ [mm] | 74.58 |
| $L_p$ [mm] | 5.2 |
| Mach number [-] | 0.1 to 4.0 |
| $\theta_p$ [deg] | 15 |

Drag coefficient values obtained for this initial data are exposed in Table 2. These drag coefficient values are calculated using the mathematical model presented in chapter 2.

Table 2. Numerical results for shape index and drag coefficient

| Mach number value | Shape index value | Drag coefficient after Siacci law | Drag coefficient after 1930 law |
|---|---|---|---|
| 0.1 | 0.4408 | 0.1124 | 0.0815 |
| 0.2 | 0.4408 | 0.1124 | 0.0815 |
| 0.3 | 0.4408 | 0.1128 | 0.0815 |
| 0.4 | 0.4408 | 0.1128 | 0.0815 |
| 0.5 | 0.4408 | 0.1133 | 0.0815 |
| 0.6 | 0.4408 | 0.1142 | 0.0815 |
| 0.7 | 0.4408 | 0.1172 | 0.0815 |
| 0.8 | 0.5936 | 0.1692 | 0.1098 |
| 0.9 | 0.6146 | 0.2489 | 0.1278 |
| 1.0 | 0.6356 | 0.3471 | 0.2276 |
| 1.1 | 0.6567 | 0.4196 | 0.2364 |
| 1.2 | 0.4499 | 0.3104 | 0.1602 |
| 1.3 | 0.4499 | 0.3230 | 0.1566 |
| 1.4 | 0.4499 | 0.3289 | 0.1525 |
| 1.5 | 0.4499 | 0.3302 | 0.1476 |
| 1.6 | 0.4499 | 0.3302 | 0.1417 |
| 1.7 | 0.4499 | 0.3275 | 0.1363 |
| 1.8 | 0.4499 | 0.3230 | 0.1318 |
| 1.9 | 0.4499 | 0.3181 | 0.1287 |
| 2.0 | 0.4499 | 0.3122 | 0.1260 |
| 2.1 | 0.4499 | 0.3064 | 0.1233 |
| 2.2 | 0.4499 | 0.3001 | 0.1201 |
| 2.3 | 0.4499 | 0.2938 | 0.1161 |
| 2.4 | 0.4499 | 0.2875 | 0.1125 |
| 2.5 | 0.4499 | 0.2812 | 0.1093 |
| 2.6 | 0.4499 | 0.2749 | 0.1062 |
| 2.7 | 0.4499 | 0.2686 | 0.1030 |
| 2.8 | 0.4499 | 0.2632 | 0.1003 |
| 2.9 | 0.4499 | 0.2573 | 0.0976 |
| 3.0 | 0.4499 | 0.2515 | 0.0949 |
| 3.1 | 0.4499 | 0.2456 | 0.0922 |
| 3.2 | 0.4499 | 0.2411 | 0.0904 |
| 3.3 | 0.4499 | 0.2357 | 0.0882 |
| 3.4 | 0.4499 | 0.2312 | 0.0859 |
| 3.5 | 0.4499 | 0.2263 | 0.0841 |
| 3.6 | 0.4499 | 0.2218 | 0.0819 |
| 3.7 | 0.4499 | 0.2173 | 0.0801 |
| 3.8 | 0.4499 | 0.2132 | 0.0783 |
| 3.9 | 0.4499 | 0.2088 | 0.0769 |
| 4.0 | 0.4499 | 0.2052 | 0.0751 |

Table 3. Numerical results for ogive relative length

| $\delta L_v$ | $\delta D_{pr}$ | $\lvert\delta\lambda_v\rvert$ | $\lvert\delta\lambda_v\rvert$ caused by $\delta L_v$ | $\lvert\delta\lambda_v\rvert$ caused by $\delta D_{pr}$ |
|---|---|---|---|---|
| 0.0007 | 0.0208 | 0.0017 | 0.0000 | 0.0017 |
| 0.0215 | 0.0341 | 0.0021 | 0.0007 | 0.0028 |
| 0.1078 | 0.0930 | 0.0041 | 0.0036 | 0.0077 |
| 0.1480 | 0.1136 | 0.0045 | 0.0049 | 0.0094 |
| 0.1638 | 0.1584 | 0.0077 | 0.0055 | 0.0131 |
| 0.2874 | 0.2683 | 0.0127 | 0.0096 | 0.0222 |
| 0.3080 | 0.3056 | 0.0151 | 0.0103 | 0.0253 |
| 0.3560 | 0.3483 | 0.0170 | 0.0119 | 0.0289 |
| 0.4140 | 0.3611 | 0.0161 | 0.0138 | 0.0299 |
| 0.4816 | 0.4127 | 0.0181 | 0.0161 | 0.0342 |
| 0.5528 | 0.4645 | 0.0201 | 0.0184 | 0.0385 |
| 0.6439 | 0.4765 | 0.0180 | 0.0215 | 0.0395 |
| 0.7238 | 0.4802 | 0.0157 | 0.0241 | 0.0398 |
| 0.7505 | 0.6683 | 0.0304 | 0.0250 | 0.0554 |
| 0.7759 | 0.7011 | 0.0322 | 0.0259 | 0.0581 |
| 0.8272 | 0.7212 | 0.0322 | 0.0276 | 0.0598 |
| 0.8538 | 0.7965 | 0.0375 | 0.0285 | 0.0660 |
| 0.9156 | 0.8968 | 0.0438 | 0.0305 | 0.0743 |
| 0.9628 | 0.9647 | 0.0478 | 0.0321 | 0.0799 |
| 0.9887 | 0.9705 | 0.0475 | 0.0330 | 0.0804 |

Calculated drag coefficient graph is presented in Figure 3. Results are obtained using the exposed analytical method.

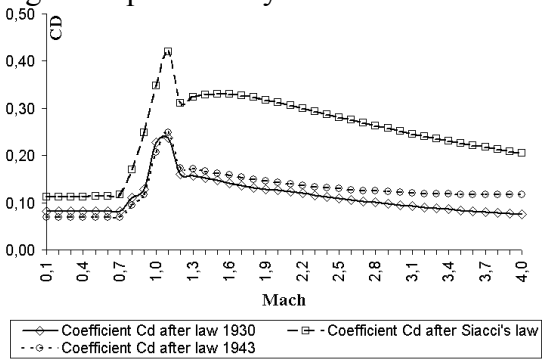


Fig. 3 Drag coefficient values vs. Mach using the algorithm presented

Results for projectile's ogive relative variation, $\delta\lambda_v$, caused by ogive length variation, $\delta L_v$, and projectile diameter variation, $\delta D_{pr}$, are presented in Table 3., Figure 4. to Figure 6.

Results for projectile's shape index variation with ogive length variations and ogive length and projectile's diameters variations are presented in Table 4., Figure 7. to Figure 9.

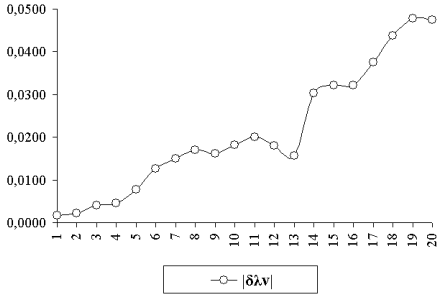


Fig. 4 $\lvert\delta\lambda_v\rvert$ for $\delta L_v$ and $\delta D_{pr}$ in the same time

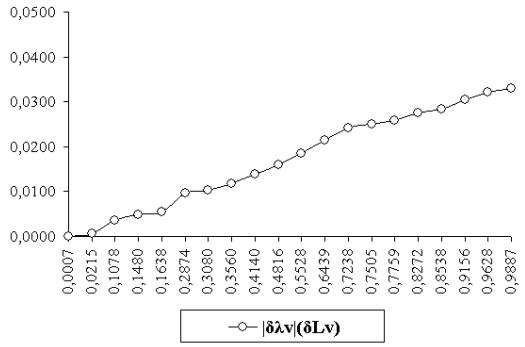


Fig. 5 $|\delta\lambda_v|$ only for $\delta L_v$

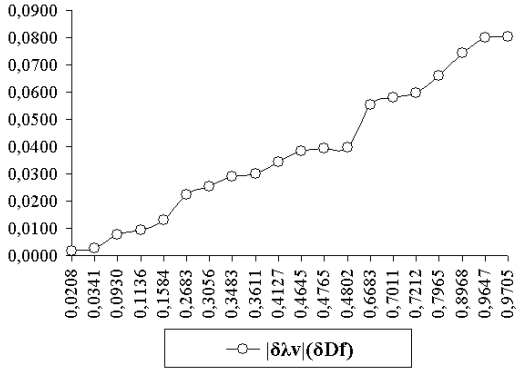


Fig. 6 $|\delta\lambda_v|$ only for $\delta D_{pr}$

Table 4. Numerical results for shape index

| $\delta i_{TC}(\delta\lambda_v)$ | $\lvert\delta i_{TC}\rvert(\delta L_v)$ | $\lvert\delta i_{TC}\rvert(\delta D_{pr})$ |
|---|---|---|
| 0.00030 | 0.000004 | 0.00030 |
| 0.00037 | 0.00013 | 0.00050 |
| 0.00072 | 0.00063 | 0.00135 |
| 0.00079 | 0.00087 | 0.00165 |
| 0.00135 | 0.00096 | 0.00230 |
| 0.00222 | 0.00168 | 0.00390 |
| 0.00264 | 0.00180 | 0.00444 |
| 0.00298 | 0.00208 | 0.00506 |
| 0.00283 | 0.00242 | 0.00525 |
| 0.00318 | 0.00282 | 0.00600 |
| 0.00352 | 0.00323 | 0.00675 |
| 0.00316 | 0.00377 | 0.00693 |
| 0.00275 | 0.00423 | 0.00698 |
| 0.00533 | 0.00439 | 0.00972 |
| 0.00566 | 0.00454 | 0.01019 |
| 0.00565 | 0.00484 | 0.01049 |
| 0.00659 | 0.00499 | 0.01158 |
| 0.00768 | 0.00536 | 0.01304 |
| 0.00840 | 0.00563 | 0.01403 |
| 0.00833 | 0.00578 | 0.01411 |

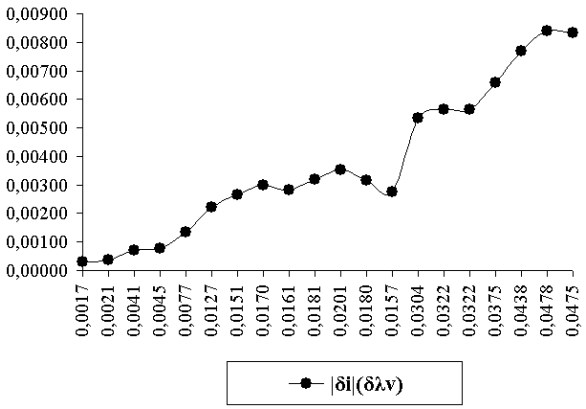


Fig. 7 $|\delta i_{TC}|$ only for $\delta\lambda_v$

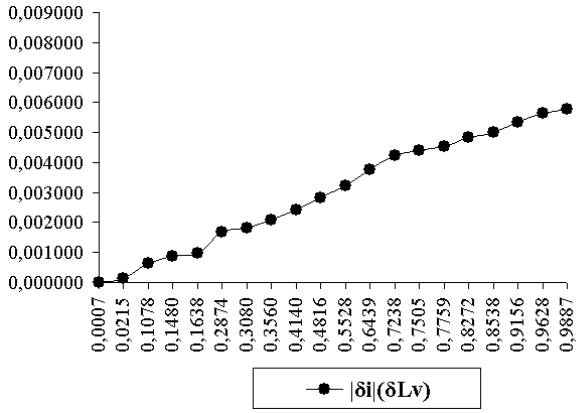


Fig. 8 $|\delta i_{TC}|$ only for $\delta L_v$

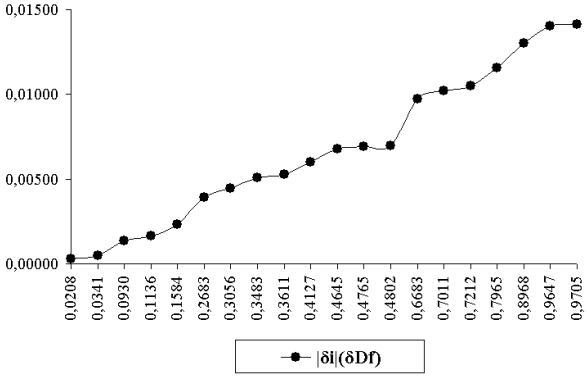


Fig. 9 $|\delta i_{TC}|$ only for $\delta D_{pr}$

As we can observe projectile's diameter variation introduce the highest variation of projectile's shape index.

We also can conclude that we can use for preliminary calculations this method to calculate the projectile's shape index and drag coefficient for aerodynamic configurations of projectiles. As a plus we can evaluate too drag coefficient variation caused by projectile's geometrical variations.

## 4. CONCLUSIONS & ACKNOWLEDGMENT

The drag coefficient was calculated, see Table 2 and Fig. 3 using the method presented in chapter 2.

On the other hand, the drag coefficient was calculated using the algorithm presented in chapter 2, and the results obtained for it were in accordance with preliminary design requirements.

In addition, reference [1] recommends this method to be used for preliminary projectiles design evaluations.

This kind of study can be used to implement the presented method as module for an exterior ballistic. The software module is a good ready-made instrument for evaluations instead of sheet preliminary calculations.

The usefulness of this type of study can be seen in teaching purposes, experimental testing and design of different type of products.

This paper has been financially supported within the project entitled "Horizon 2020 - Doctoral and Postdoctoral Studies: Promoting the National Interest through Excellence, Competitiveness and Responsibility in the Field of Romanian Fundamental and Applied Scientific Research", contract number POSDRU/159/1.5/S/140106. This project is co-financed by European Social Fund through Sectoral Operational Programme for Human Resources Development 2007-2013. Investing in people!

## REFERENCES

1. Antonescu, I. *Bazele proiectării proiectilelor*, Editura Academiei Militare, Bucure□ti (1977).
2. Niţă, M.M., Moraru, Fl., Patraulea, R., *Avioane şi rachete. Concepte de proiectare*, Editura Militară, Bucureşti (1985).
3. Moraru, Fl., *Elemente de teoria estimaţiei cu aplicaţii în balistică*. Editura Academiei Tehnice Militare, Bucureşti (1979).
4. Surdu. G., Slămnoiu. G., Moldoveanu C., Ciuculin. A., Şomoiag P., *Metode statistice şi instrumente software realizate in – house pentru aplicaţii în balistică cu scopul determinării valorii adevărate a parametrilor determinaţi experimental.* Sisteme energetice şi Balistice. Bucureşti (2013).
5. Şomoiag, C.E. Moldoveanu, *Numerical Research on the Stability of Launching Devices During Firing,* Defence Technology Elsevier Journal, Volum 9, Issue 4, decembrie 2013, pag. 242-248, ISSN 2214-9147.
6. C.E. Moldoveanu, A. Giovannini, H.C. Boisson, *Turbulence receptivity of longitudinal vortex-dominated flows*, Lecture Notes in Computational Science and Engineering, Vol. 69: BAIL 2008 - Boundary and Interior Layer Proceedings of the International Conference on Boundary and Interior Layers - Computational and Asymptotic Methods, Limerick, July 2008, Springer Verlag, Berlin, pag. 227 – 236, ISBN: 978-3-642-00604-3, 2009.

"HENRI COANDA"
AIR FORCE ACADEMY
ROMANIA

"GENERAL M.R. STEFANIK"
ARMED FORCES ACADEMY
SLOVAK REPUBLIC

INTERNATIONAL CONFERENCE of SCIENTIFIC PAPER
AFASES 2015
Brasov, 28-30 May 2015

# CONDUCTIVE THERMOPLASTIC POLYMER NANOCOMPOSITES WITH ULTRALOW PERCOLATION THRESHOLD

**Fulga Tanasa*, Madalina Zanoaga*, Yevgen Mamunya****

*"Petru Poni" Institute of Macromolecular Chemistry, Iasi, Romania, **Institute of Macromolecular Chemistry, Kiev, Ukraine

***Abstract:*** *The polymer composites with conductive properties are a subject of great interest due to their remarkable characteristics. Depending on their formulation, different morphologies can be achieved, yielding in composites with superior conductivity ranging from electrostatic dissipative to highly conductive. Conductive fillers able to give highly ordered distributions lead to composites with segregated morphology where the critical volume fraction of filler is ultralow, while the electrical resistivity reaches values of $10^{-4}$ Ω·cm. This articles aims to highlight a few advantages of segregated conductive composites versus random conductive composites, based on the value of their corresponding percolation threshold. Factors that can influence the critical volume fraction of filler and its distribution in the matrix, such as nature of filler and matrix, processing approach and specific parameters, etc., are also reviewed, as well as the range of applications.*

***Keywords:*** *segregated conductive polymer composites, ultralow percolation threshold, applications*

## 1. INTRODUCTION

Conductive polymer composites are a relatively new class of materials with highly interesting properties which recommend them for various applications. They have been the subject of both theoretical and experimental studies over the last decades due to their versatility, especially the possibility to tune some characteristics (electric conductivity) according to specific requirements by only adjusting the amount of the conductive filler and its distribution. Conductive carbon-based fillers (as carbon black, carbon nanotubes or nanowires, graphene, graphene oxide, etc.) are preferable because, unlike metal fillers, they do not get oxidized and subsequently covered with an insulating layer on the particles surface [1,2].

The major advantage of the conductive composites is that electrical properties are close to the fillers, while their mechanical characteristics and processing are typical for plastics. These composites have several other advantages over the conventional conductive materials, including processability, flexibility, light weight, ability to absorb mechanical shocks, low production costs. They can be used as antistatic materials and in applications such as switching devices, medical equipment, cables, transducers and gas sensors, as well as devices for electromagnetic radiation shielding and electrostatic discharge [1-7], as summarized in Fig. 1.

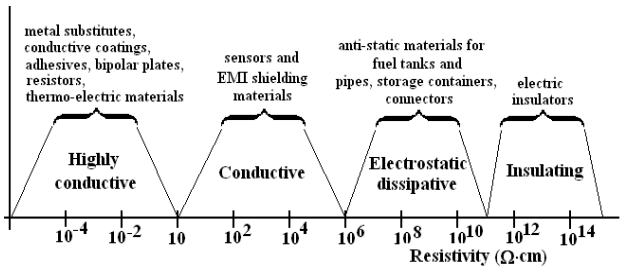


**Figure 1.** Classification and applications of conductive polymeric composites

As conductive composites can consist of randomly distributed conductive fillers (powders, nanoparticles, -wires, -sheets, -tubes, etc.) within the matrix, which can be a polymer or a polymer blend, either conductive or not, they hold a great deal of interest from a fundamental point of view when the filler content is ultralow and they can be considered as typical segregated systems. The specific thermal and electric properties are determined by the morphology and properties of the conductive phase and are the result of different factors acting synergistically during their processing. The influence of the matrix type and nature of filler on the electrical characteristics of the composite has been studied in many works [8-12].

The aim of this article is to highlight a few advantages of segregated conductive composites *versus* random conductive composites, based on the value of their corresponding percolation threshold. Factors that can influence the critical volume fraction of filler and its distribution in the matrix are also reviewed, as well as some applications.

## 2. NANOCOMPOSITES WITH ULTRALOW PERCOLATION THRESHOLD

**2.1 The percolation threshold and the critical volume fraction of the filler.** It is known that most of the common industrial polymers are basically insulating from electrical point of view. Therefore, they can be transformed into conductive media only by incorporating a conductive phase, conductive fillers, respectively. Basically, the electric conductivity of a segregated system can be empirically described using the equation 1,

$$\sigma = \sigma_0 (\varphi - \varphi_c)^t \quad (1)$$

where $\sigma$ *and* $\sigma_0$ are conductivity values, $\varphi$ and $\varphi_c$ are the filler volume fractions and $t$ is a critical exponent (for 2D networks, t=1.3; for 3D networks, t=2). When the volume filler fraction $\varphi$ reaches a critical value $\varphi_c$ (also called the percolation threshold), an infinite conductive cluster (IC) is formed and the composite becomes conductive [13]. In general, $\varphi_c$ depends on several factors, such as the shape of filler particles, the interaction between filler and host polymer and the spatial filler distribution. The more the shape of particles diverges from the spherical one; the lower is the percolation threshold. The interaction between the polymer matrix and filler influence on $\varphi_c$ through the capability of the polymer melt to wet the filler particles: the stronger this interaction, the better the wettability, the higher $\varphi_c$. As for the spatial distribution of the filler, it depends on the polymer-filler interaction, as well as on viscosity of polymer melt and the processing method: the polymer with the higher shear viscosity will generate the larger shear stress and enables a different particle size distribution [11].

A relationship between these factors was defined (equation 2),

$$\sigma = \sigma_c + (\sigma_m - \sigma_c)[(\varphi - \varphi_c)/(F - \varphi_c)]^t \quad (2)$$

where $F$ is the packing factor (a structural parameter that depends on the filler particles size and shape) and $\sigma_m$ is the maximum value of conductivity.

The conductive properties of composites thus obtained can be modulated by controlling the filler spatial distribution and, consequently, the percolation threshold which is a measure of the critical volume fraction of filler $\varphi_c$. At this specific point, a jump in conductivity can be recorded. Further addition of filler will yield in a gradually increase in conductivity, due to the formation of supplementary conductive pathways, up to a saturation that results in a plateau where the conductivity reaches the maximum value, $\sigma_m$.

The mechanism for the formation of a segregated conductive network relies on the capability of the polymeric matrix to provide exclusion micro-domains where the conductive filler particles are allowed a constrained volume, such as the interface

between immiscible polymers in a blend. This conditionality substantially increases the density of the ordered conductive pathways at ultralow filler volume fraction.

Conductive composites based on polymer blends bring out more interest because they combine the properties of all components. Thus, the co-continuous phase of polymer blends can simultaneously give the maximum contribution of the mechanical modulus of each component [14]. An illustrative example is the case of polyamide/polypropylene (PA/PP) blends successfully used as matrix for conductive composites due to the mechanical properties of PA and enhanced processability of PP. At the same time, heterogeneous polymeric systems made of immiscible components (such as PA/PP) have overall reduced mechanical characteristics due to their low adhesion at the interface. This is one fundamental factor which leads to segregated composites as the filler preferentially occupies certain areas, thus creating a highly ordered morphology with the minimum amount required. This phenomenon is driven by the following factors: thermodynamic (surface tensions between each polymer and filler, and between polymers), kinetic (the viscosity of the polymeric components at the processing temperature), processing (the method and parameters can influence on the thermodynamic and kinetic factors) and chemical (chemical interactions of the filler with one constituent of the blend) [15,16]. Studies performed on different polymeric blends (PP/PA, PP/PE, EVA/PE, HIPS/LLDPE, PET/PE, PE/POM) and fillers [17-27] revealed that the filler can be localized in one of the two polymer phases and/or at the interface bridging the phases, as schematically represented in Fig. 2.

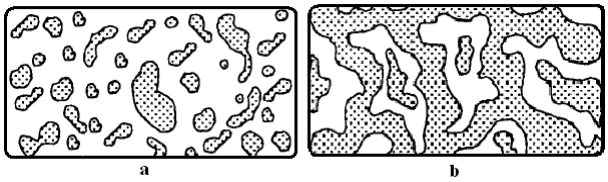


Figure 2. Spatial distribution of the filler in: a – random and b – segregated composites

This is an important issue in terms of load transfer through the matrix and it also yields in increased values for some specific properties, such as the complex viscosity, storage modulus and loss modulus of the blends.

**2.2 Processing strategies.** As for the processing, the conventional methods employed to obtain conductive composites are solution processing, melt mixing and *in situ* polymerization [28,29]. The melt mixing approaches (the twin-screw extrusion, internal mixing and injection molding) are the preferred ones since they are compatible with the industrial technologies for polymers and proved their effectiveness in terms of filler dispersion even considering the primary and secondary agglomeration of particles. Such composites generally have a percolation threshold close to the theoretic value calculated by the classical percolation theory [30,31]. Even nanometric fillers, such as carbon nanotubes or graphene nanosheets with high aspect ratio and able to favour highly ordered dispersions, can undergo abnormal aggregation (secondary agglomeration) that results in high value percolation thresholds (10–20 vol%). In the end, these conductive composites have some disadvantages, such as high melt viscosity, low economic affordability and poor mechanical properties (mainly ductility and toughness) [32,33].

Another approach to obtain segregated conductive composites with ultralow percolation threshold is based on compressing a mixture of polymer granules decorated with

conductive fillers via dry or solution mixing [34]. Despite its advantages (process simpleness, great variety of fillers, relatively good dispersion), only polymers with high melt viscosity can be used for this method in order to preserve the segregated morphology and the low critical volume fraction of the filler.

The latex technology can also be considered when such composites are envisaged [34]. It comprises a polymeric emulsion where the filler particles are allowed only in the constrained volume of the interstitial space surrounding the latex particles during the freeze-drying processing. The method provides a good dispersion of the filler, availability to almost any polymer–filler system, low production costs and an environmentally friendly processing when water is used as solvent. The main drawback of this approach is the complex manufacturing.

**2.3 Factors that influence the ultralow percolation behavior.** The challenges of tailoring the morphology of the segregated conductive composites resulted in specific methods to obtain ultralow critical volume fraction of the filler. The type and nature of the matrix, type and nature of filler, as well as processing method and parameters (kinetic and thermodynamic factors) can influence the percolation threshold.

**a. The polymer matrix.** The polymeric matrices influence the percolation behavior by the molecular weight and modulus. It was proven that polymers with high molecular weights and moduli better preserve the segregated morphology. When single polymers are employed, the preferred matrices are usually thermoplastic high melt viscosity polymers (such as UHMWPE [35-37], PS [38,39], natural rubber [40], PA66 [41], etc.), because they can keep the conductive pathways localized in the interfacial regions during processing. The high modulus polymers compel filler particles into the interstitial space, facilitating the segregated network; thus, using a copolymer based on methyl methacrylate (MMA), n-butyl acrylate (BA), methacrylic acid (MAA) and poly(vinyl alcohol) with a high modulus (~640 MPa), segregated conductive composites with ultralow percolation threshold (1.5 vol%) were obtained [42].

On the other hand, if the glass transition temperature ($T_g$) of the polymer matrix is lower than the processing temperature, the polymer modulus is too low and cannot promote the formation of the segregated conductive structure [43]. In such cases, the filler is easily mixed with the soft polymer particles, leading to a random conductive network. Therefore, polymers with high modulus and $T_g$ values are suitable matrices when emulsion methods are employed.

The polymer particle size also affects the segregated conductive composites formation by influencing the density of conductive pathways and the selective location of the conductive filler: the $\varphi_c$ value decreases along with the increasing particle size ratio polymer: filler [44].

The influence of the thermodynamic factor on the formation of segregated morphology is defined by the polymer surface tension. The high polymer surface tension leads to low polymer-filler interfacial tension and strong affinity between the conductive filler and matrix. Therefore, an insulating polymer layer can occur, that decreases the composite conductivity. For composites obtained by melt compounding, the high polymer-filler interfacial tension thermodynamically favors the aggregation of the conductive particles in the polymer melt, facilitating the formation of the segregated conductive structure [34]. Furthermore, a higher conductivity can be achieved using a semi-crystalline polymer matrix instead an amorphous one, because the conductive particles are expelled from the crystalline segments during crystallization; consequently, the amorphous phase accumulates most of the filler [45].

On the other hand, conductive composites with ultralow percolation threshold can be obtained using polymer blends as matrices. Thus, HIPS/UHMWPE [46], PC/ABS/ABS-*g*-MA [47], PE/PET [48], PE/PS [49],

PP/PS/ABS [50], UHMWPE/PMMA [51], PP/PA, PP/PE, EVA/PE, HIPS/LLDPE, PET/PE, PE/POM [17-27] are examples successfully illustrating the wide variety of available convenient combinations. A particular case deserves a special mention, namely the use of thermoplastic co-polyamides in the polymer blends used as matrix for conductive composites with ultralow percolation threshold. Studies [52-54] revealed the ternary co-polyamide coPA (PA6/PA66/ PA610) used in composite formulations with PP and CNTs, obtained by melt mixing, favored the formation of the segregated morphology in the corresponding conductive composites and enabled an ultralow percolation threshold (0.8-1.48 vol%) [52].

**b. Effect of the conductive fillers.** The nature of the conductive fillers has a decisive role in the electrical properties of conductive composites with ultralow percolation threshold. Considering a uniform dispersion of the conductive filler particles at the interface of the polymeric domains, the $\varphi_c$ values decrease along with the increasing aspect ratio of the filler, in concordance with the theory of the excluded volume [55]. On the other hand, it is known the high aspect ratio fillers have superior transport properties and effectiveness in forming segregated conductive morphologies. Thus, depending on the nature of the filler and the corresponding segregated morphology, different percolation thresholds can be reached for the same matrix: in the case of UHMWPE-based composites, it can vary from 0.003 vol% (graphene nanosheets as filler; method: solution mixing) to 0.5 vol% (fillers: carbon black and MWCNTs; method: dry mixing) [34].

Most of the conductive fillers are to be found at the interface of polymer domains, which requires a highly uniform dispersion, difficult to reach especially at relatively high loadings. This is a typical situation for MWNTs-based conductive composites, where secondary agglomeration is a common drawback [56,57]. Therefore, the high aspect ratio conductive nanofillers are not to be used for conductive composites with segregated structures without employing highly efficient dispersion methods.

Different segregated morphologies can be found in conductive composites due to disparities in the microstructure of the filler, be it nano-bundles, -sheets or -wires. Commonly, the nanosheets are frequently restacking forming a "plane-to-plane" conductive network which can be considered a 2D structure. Therefore, fillers like graphene nanosheets are less susceptible to generate highly branched networks as compared to CNTs [58], and the percolation threshold moves from ultralow to low values.

Besides the geometry, the chemistry of the conductive fillers surface also affects the properties of the segregated conductive composites through the corresponding changes in the inherent electrical conductivity [59].

**c. Processing method and parameters.** The processing approach and process parameters can dramatically influence the morphology of the segregated composites, with direct effect on their percolation behavior. The main approaches are already presented herein. While solution and dry mixing methods are costly and complex, and the results reported are sometimes arguable in terms of dispersion effectiveness and percolation threshold value, the melt mixing and latex approaches seem more appropriate, given that their characteristics favor the diffusive rearrangement of the conductive filler in the polymeric matrices (dynamic

percolation, formation of additional conductive channels and improving their electrical performance). The latex approach leads to composites with relatively high $\varphi_c$ (0.6 vol% [43,46], 0.9 vol% [41]) due to the difficulties to stabilize the filler particles in the constrained volume between matrix particles, as the molecular weight and modulus of the latex polymer is relatively low [60].

Considering the maximum conductivity $\sigma_m$ [S/cm] as analysis criterion, it can be noticed that its values depends on the same factors. Thus, the CNTs-containing composites showed higher conductivity than those containing graphene nanosheets due to the better transport properties of CNTs [38,40,60].

During latex processing in the presence of surfactants such as sodium-dodecyl sulfate (SDS), insulating gaps may occur inside the composite, creating high resistivity point along with segregated conductive channels [61]. When melt mixing is considered, the segregated morphology of the conductive filler prevents the diffusion of the macromolecular chains, obstructing the melting at high loadings [62]. Therefore, the filler amount cannot exceed 10% when these composites are prepared through dry compounding and melt blending, but can vary between 0 and 100 wt% if they are obtained by the latex technology, without any limitation due to the melt viscosity [34].

The high temperature processing lowers the melt viscosity of the host polymers yielding in significant mixing between the matrix and conductive filler, and thus prevents the formation of the segregated morphology.

The high pressure treatment can increase the packing factor *F*, up to a certain value, generating tightly packed networks [34]. Beyond this value, the network breaks into separate conductive segments.

The mechanical mixing is strongly related to the wettability of the filler particles by the polymer and this is affecting their coating and the composites percolation behavior, respectively. In addition, pre-mixing insulating polymers can generate static electricity that facilitates the absorption of the conductive fillers on the surfaces of the polymer granules [34]. Still, excessive mixing creates additional stress and reduces the conductive network, similar to high pressure. A critical mixing time must be established in order to optimize the processing/performance ratio.

The melt blending method is highly recommended when two incompatible polymers are used as matrix because segregated conductive structures with tuned properties are difficult to obtain by other approaches. There are two methods to obtain the segregated conductive composites by melt blending. One implies adjusting the thermodynamic parameter (interfacial tension) through the kinetics features (melt viscosity and compounding); thus, the conductive filler is initially dispersed into the polymer thermodynamically unfavorable (the polymer with the lower melt viscosity) and, subsequently, the master-batch is melt blended ("diluted") with the other polymer (the more favorable polymer having the higher melt viscosity). The thermodynamic driving forces favor the distribution of the conductive filler into the favorable polymer and at the interface [16,52]. The other method consists of the introduction of a third polymer with high affinity for the conductive filler, acting as compatibilizer for a selected pair of incompatible polymers. The percolated filler-compatibilizer phase will be selectively placed in the interfacial region of the polymer blend [34].

A successful example of optimization of all these factors acting synergistically is the system poly(3,4-ethylenedioxy-thiophene): poly(styrene-sulfonate)(PEDOT:PSS), used as the conducting surfactant for the dispersion of CNTs instead of the usual insulating stabilizers [34]; thus, $\sigma_m$ reached values comparable to pristine CNTs.

**2.4 Applications.** The electrical properties of the conductive composites with ultralow percolation threshold are directly connected with their sensing characteristics, given their capability to alter the conductive network under the action of some external stimuli, such as temperature, mechanical stress, and chemical environment. Therefore, these hi-tech materials are used for sensors and actuators, as well as in electronics as thermo-electric or EMI shielding materials.

The positive (PTC) and negative (NTC) temperature coefficients of these materials

depend on their resistivity around the melting point of the matrix polymer. Due to their strong interrelation, they are used for extremely high temperature protection devices, self-regulating heaters, micro-switch sensors, etc. [63,64].

The electrical response of the conductive composites toward mechanical stress (the piezo-resistive effect) occurs when the distance between the conductive particles changes to exceed the tunneling distance under the applied load [34]. Despite their interesting strain-resistivity behavior, the use of these bulky sensors is limited by necessity of reaching the high loadings of conductive filler in order to enable pathways for an effective charge transport [65].

The use of conductive polymer composites as materials for chemicals detection relies on their ability to swell when exposed to organic compounds, when vapors or liquids diffuse into the polymer matrix, yielding in increased distances between the conductive particles. This swelling process is often too slow causing a low response rate. Conductive composites with segregated morphologies are ideal for such applications because the conductive phase is located at the interfacial regions and allows the accelerate permeation of chemicals through the capillary effect [66,67].

The conductive polymer composites have been widely used for EMI shielding applications, but the high filler loadings required for adequate shielding properties (≥ 20 dB) negatively affect the production costs and mechanical characteristics due to their secondary aggregation [68,69].

## 3. CONCLUSIONS AND FUTURE DEVELOPMENT

The conductive thermoplastic polymer composites having segregated morphology have an efficient charge transport at very low content of filler, which entails unique advantages: the ultralow percolation threshold, high value maximum conductivity, sensing abilities, thermo-electric properties etc.

Comparing the percolation thresholds of conductive composites obtained by different methods, it can be concluded that segregated composites obtained by emulsion technique and melt blending have higher $\varphi_c$ values than those prepared *via* dry or solution mixing. The choice in terms of method and process parameters is made, ultimately, based on the nature and properties of the polymer or polymer blend and filler. Given that the lowest $\varphi_c$ (~0.0054 vol%) was obtained in a system made of CB/ABS after introducing large polymeric beads (~5 mm in diameter) as a scaffold for the segregated conductive morphology [34], one question remains: is low *versus* ultralow percolation threshold a competition toward segregated conductive composites with 0 vol% filler?

Significant efforts have been made in order to develop these materials for various applications. Yet, there are still certain challenges that must be addressed (wise selection of polymers for the mixed matrices, improved dispersion of the filler, avoid the formation of micro-voids, optimization of the processing parameters as a function of specific pairs matrix-filler, use of hybrid fillers instead of classic CNTs which are highly expensive

etc.) in order to make the transition from theory to application and enable the conductive thermoplastic polymer nanocomposites with ultralow percolation threshold multiple functionality.

## REFERENCES


1. 1. Zois, H., Apekis, L., Mamunya Y.P. Dielectric properties and morphology of polymer composites filled with dispersed iron. *Journal of Applied Polymer Science.* 88 (2003).
2. Huang, J.C. Carbon black filled conducting polymers and polymer blends. *Advances in Polymer Technology.* 21 (2002).
3. Gul, V.E. *Structure and Properties of Conducting Polymer Composites*. Utrecht: VSP (1996).
4. Ma, P.C., Siddiqui, N.A., Marom, G., Kim, J.K. Dispersion and functionalization of CNTs for polymer-based nanocomposites: a review. *Composites A*. 41 (2010).
5. Villmow, T., Pegel, S., John, A. Rentenberger, R., Pötschke, P. Liquid sensing: smart polymer/CNT composites. *Materials Today*. 14 (2011).
6. Antunes, R.A., Oliveira, M.C.L., Ett, C. Carbon materials in composite bipolar plates for polymer electrolyte membrane fuel cells: a review of the main challenges to improve electrical performance. *Journal of Power Sources*. 196 (2011).
7. Dang, Z.M., Yuan, J.K., Zha, J.W., Zhou, T., Li, S.T., Hu, G.H. Fundamentals, processes and applications of high-permittivity polymer–matrix composites. *Progress in Materials Science.* 57 (2012).
8. Lux, F. Models proposed to explain the electrical conductivity of mixtures made of conductive and insulating materials. *Journal of Materials Science.* 28 (1993).
9. Bridge, B., Folkes, M.J., Wood, B.R. Investigation into the DC conductivity of colloidally dispersed gold/polymer composites. *Journal of Physics D: Applied Physics*. 23 (1990).
10. Zhang, M.Q., Xu, J.R., Zeng, H.M., Huo, Q., Zhang, Z.Y., Yun, F.C., Friedrich, K. Fractal approach to the critical filler volume of an electrically conductive polymer composite. *Journal of Materials Science*. 30 (1995).
11. Mamunya, Y. Ch. 9: Carbon nanotubes as conductive filler in segregates polymer composites - electrical properties. in S. Yellampalli *Carbon Nanotubes – Polymer Nanocomposites*, Rijeka(Croatia): InTech (2011).
12. Carmona, F., Mouney, C. Temperature-dependent rezistivity and conduction mechanism in carbon particle-filled polymers. *Journal of Materials Science*. 27 (1992).
13. Stauffer, D. *Introduction to percolation theory.* London: Taylor and Francis (1985).
14. Potschke, P., Paul, D.R. Formation of co-continuous in melt mixed immiscible polymer blends. *Journal of Macromolecular Science, C: Polymer Reviews*. 43 (2003).
15. Fenouillot, F., Cassagnau, P., Majeste, J-C. Uneven distribution of nanoparticles in immiscible fluids: morphology development in polymer blends. *Polymer*. 50 (2009).
16. Mamunya, Ye., Levchenko, V., Boiteux, G., Seytre, G., Zanoaga, M., Tanasa F., Lebedev, E. Controlling morphology, electrical, and mechanical properties of polymer blends by heterogeneous distribution of carbon nanotubes. *Polymer Composites.* Article first published online: 21 mar 2015. DOI: 10.1002/pc.23434 (http://onlinelibrary.wiley.com/journal/10.1002/(ISSN)1548-0569/earlyview)
17. Zhang, L., Wan, C., Zhang, Y. Investigation on the MWCNTs reinforced PA 6/PP composites. *Polymer Engineering & Science*. 49 (2009).
18. Zhang, L., Wan, C., Zhang, Y. Morphology and electrical properties of PA 6/PP/MWCNTs composites. *Composites Science and Technology*. 69 **(**2009).
19. Potschke, P., Bhattacharyya, A.R., Janke, A. Morphology and electrical resistivity of melt mixed blends of polyethylene and carbon nanotubes filled polycarbonate. *Polymer*. 44 (2003).
20. Sun, X., Yu, Q., Shen, J., Gao, S., Li, J., Guo, S. *In situ* microfibrillar morphology and properties of PP/PA/CB

composites prepared through multistage stretching extrusion. *Journal of Materials Science*. 48 (2012).

21. Tchoudakov, R., Breuer, O., Narkis, M., Siegmann, A. Conductive polymer blends with low carbon black loading: PP/PA. *Polymer Engineering & Science*. 36 (1996).
22. Yui, H., Wu, G., Sano, H., Sumita, M., Kino, K. Morphology and electrical conductivity of injection-molded PP/CB composites with addition of high-density PE. *Polymer*. 47 (2006).
23. Foulger, S.H. Reduced percolation threshols of immiscible conductive blends. *Journal of Polymer Science Part B: Polymer Physics*. 37 (1999).
24. Breuer, O., Tchoudakov, R., Narkis, M., Siegmann, A. Segregated structures in CB-containing immiscible polymer blends: HIPS/LLDPE systems. *Journal of Applied Polymer Science*. 64 (1997).
25. Li, B., Xu, X.-B., Li, Z.-M., Song, Y.C. Manipulating the conductivity of CB-filled immiscible polymer composites by insulating nanoparticles. *Journal of Applied Polymer Science*. 110 (2008).
26. Mamunya, Y.P., Muzychenko, Y.V., Lebedev, E.V., Boiteux, G., Seytre, G., Boullanger, C., Pissis, P. PTC effect and structure of polymer composites based on PE/POM blend filled with dispersed iron. *Polymer Engineering and Science*. 47 (2007).
27. Gupta, S., Ou, R.Q., Gerhardt, R.A. Effect of the fabrication method on the electrical properties of poly(AN-*co*-butadiene-*co*-styrene)/CB composites. *Journal of Electronic Materials*. 35 (2006).
28. Wiley Encyclopedia of Composites, 1999-2014 by John Wiley and Sons, Inc. (Available at http://onlinelibrary.wiley.com/book/10.1002/ 9781118097298/homepage)
29. Bowen, D.H., Signorelli, R.A., De Luca, P.L., Williams, J.C., Kelly, A., Greer, A.L., Kelly, A. Manufacturing methods for composites: an overview. in A. Kelly, *Concise Encyclopedia of Composite Materials*, Oxford-New York-Tokio: Elsevier Ltd. (1994).
30. Scher, H., Zallen, R. Critical density in percolation processes. *Journal of Chemical Physics*. 53 (1970).
31. Tang, H., Chen, X.F., Luo, Y.X. Electrical and dynamic mechanical behavior of CB filled polymer composites. *European Polymer Journal*. 32 (1996).
32. Göldel, A., Kasaliwal, G., Pötschke, P. Selective localization and migration of MWCNTs in blends of PC and poly(styrene–acrylonitrile). *Macromolecular Rapid Communications*. 30 (2008).
33. Grady, B.P. Recent developments concerning the dispersion of carbon nanotubes in polymers. *Macromolecular Rapid Communications*. 31 (2010).
34. Pang, H., Xu, L., Yan D.X., Li, Z.M.. Conductive polymer composites with segregated structures. *Progress in Polymer Science*. 39 (2014).
35. Lisunova, M.O., Mamunya, Y.P., Lebovka, N.I., Melezhyk, A.V. Percolation behaviour of ultrahigh molecular weight PE/MWCNTs composites. *European Polymer Journal*. 43 (2007).
36. Pang, H., Chen, T., Zhang, G.M., Zeng, B.Q., Li Z.M. An electrically conducting polymer/graphene composite with a very low percolation threshold. *Materials Letters*. 64 (2010).
37. Ren, P.G., Di Y.Y., Zhang, Q., Li, L., Pang, H., Li, Z.M. Composites of ultrahigh-

molecular weight PE with graphene sheet sand/or MWCNTs with segregated network structure: preparation and properties. *Macromolecular Materials and Engineering.* 297 (2012).
38. Yu, J.R., Lu, K.B., Sourty, E., Grossiord, N., Koning, C.E., Loos, J. Characterization of conductive MWCNT/PS composites prepared by latex technology. *Carbon.* 45 (2007).
39. Long, G.C., Tang, C.Y., Wong, K.W., Man, C.Z., Fan, M.K., Lau, W.M., Lau, W.M., Xu, T., Wang, B. Resolving the dilemma of gaining conductivity but losing environmental friendliness in producing PS/graphene composite *via* optimizing the matrix-filler structure. *Green Chemistry*. 15 (2013).
40. Zhan, Y.H., Lavorgna, M., Buonocore, G., Xia, H.S. Enhancing electrical conductivity of rubber composites by constructing interconnected network of self-assembled graphene with latex mixing. *Journal of Materials Chemistry.* 22 (2012).
41. Linares, A., Canalda, J.C., Cagiao, M.E., Ezquerra, T.A. Conducting nanocomposites based on PA 6,6 and carbon nanofibers prepared by cryogenic grinding. *Composites Science and Technology.* 71 (2011).
42. Kim, Y.S., Wright, J.B., Grunlan, J.C. Influence of polymer modulus on the percolation threshold of latex-base composites. *Polymer*. 49 (2008).
43. Jurewicz, I., Worajittiphon, P., King, A.A., Sellin, P.J., Keddie, J.L., Dalton, A.B. Locking CNTs in confined lattice geometries – a route to low percolation in conducting composites. *Journal of Physical Chemistry B.* 115 (2011).
44. He, D., Ekere, N.N. Effect of particle size ratio on the conducting percolation threshold of granular conductive–insulating composites. *Journal of Physics D: Applied Physics.* 37 (2004).
45. Feng, J.Y., Chan, C.M. Double positive temperature coefficient effects of CB-filled polymer blends containing two semicrystalline polymers. *Polymer*. 41 (2000).
46. Breuer, O., Tchoudakov, R., Narkis, M. Electrical properties of structured HIPS/$\gamma$-irradiated UHMWPE/CB blends. *Polymer Engineering & Science*. 40 (2000).
47. Chen, J., Shi, Y.Y., Yang, J.H., Zhang, N., Huang, T., Chen, C., Wang, Y., Zhou, Z.W. A simple strategy to achieve very low percolation threshold via the selective distribution of CNTs at the interface of polymer blends. *Journal of Materials Chemistry.* 22 (2012).
48. Dai, K., Xu, X.B., Li, Z.M.. Electrically conductive CB filled in situ microfibrillar PET/PE composite with a selective CB distribution. *Polymer*. 48 (2007).
49. Gubbels, F., Jerome, R., Vanlathem, E., Deltour, R., Blacher, S., Brouers, F. Kinetic and thermodynamic control of the selective localization of CB at the interface of immiscible polymer blends. *Chemistry of Materials.* 10 (1998).
50. Al-Saleh, M.H., Sundararaj, U. An innovative method to reduce percolation threshold of CB filled immiscible polymer blends. *Composites, A.* 39 (2008).
51. Pang, H., Bao, Y., Xu, L., Yan, D.X., Zhang, W.Q., Wang, J.H., Li, Z.M. Double-segregated CNT-polymer conductive composites as candidates for liquid sensing materials. *Journal Materials Chemistry A.* 1 (2013).
52. Zanoaga, M., Mamunya, Ye., Tanasa, F. Conductive properties of some ternary thermoplastic nanocomposites filled with dispersed powders. A comparative study. *Revue Roumaine de Chimie*. 59 (2014).
53. Mamunya, Y., Levchenko, V., Boiteux, G., Lebedev, E., Zanoaga, M., Tanasa, F. Electrical and mechanical properties of novel nanocomposites based on copolyamide-polypropylene polymer blends containing carbon nanotubes. *Polymer Journal (Ukr.).* 32 (2010).
54. Boiteux, G., Mamunya, Y., Lebedev, E., Adamczewski, A., Boullanger, C., Cassagnau, P., Seytre, G. From conductive polymer composites with controlled morphology to smart materials. *Synthetic Metals*. 157 (2010).
55. Celzard, A., McRae, E., Deleuze, C., Dufort, M., Furdin, G., Marêché, J.F. Critical concentration in percolating systems containing a high-aspect-ratio

filler. *Physical Review. B, Condensed Matter.* 53 (1996).
56. Dorigato, A., Dzenis, Y., Pegoretti, A. Filler aggregation as a reinforcement mechanism in polymer nanocomposites. *Mechanics of Materials*. 61 (2013).
57. Lazzeri, A., Thio, Y.S., Cohen, R.E. Volume strain measurements on $CaCO_3$/PP particulate composites: the effect of particle size. *Journal of Applied Polymer Science*. 91 (2004).
58. Du, J.H., Zhao, L., Zeng, Y., Zhang, L.L., Li, F., Liu, P.F., Liu, P.F., Liu, C. Comparison of electrical properties between MWCNT and graphene nanosheet/HDPE composites with a segregated network structure. *Carbon.* 49 (2011).
59. Tan, Y.Q., Fang, L.J., Xiao, J.L., Song, Y.H., Zheng Q. Grafting of copolymers onto graphene by miniemulsion polymerization for conductive polymer composites: improved electrical conductivity and compatibility induced by interfacial distribution of graphene. *Polymer Chemistry*. 4 (2013).
60. Pham, V.H., Dang, T.T., Hur, S.H., Kin, E.J., Chung, J.S. Highly conductive PMMA-reduced graphene oxide composite prepared by self-assembly of PMMA latex and graphene oxide through electrostatic interaction. *ACS Applied Material Interfaces.* 4 (2012).
61. Tkalya, E.E., Ghislandi, M., With, G., Koning, C.E. The use of surfactants for dispersing CNTs and graphene to make conductive nanocomposites. *Current Opinions on Colloid Interface Science*. 17 (2012).
62. Pang, H., Yan, D.X., Bao, Y., Chen, J.B., Chen, C., Li, Z.M. Super-tough conducting CNT/UHMWPE composites with segregated and double-percolated structure. *Journal of Material Chemistry.* 22 (2012).
63. Zha, J.W., Li, W.K., Liao, R.J., Bai, J.B., Dang, Z.M. High performance hybrid carbon fillers/binary–polymer nanocomposites with remarkably enhanced PTC effect of resistance. *Journal of Material Chemistry A*. 1 (2013).
64. Xu, H.P., Dang, Z.M., Shi, D.H., Bai, J.B. Remarkable selective localization of modified nanoscale CB and PTC effect in binary–polymer matrix composites. *Journal of Material Chemistry.* 18 (2008).
65. Clark, A.C., Ho, S.P., LaBerge, M. Conductive composite of UHMWPE and CB as a dynamic contact analysis sensor. *Tribology International.* 39 (2006).
66. Pang, H., Piao, Y.Y., Ling, X., Bao, Y., Cui, C.H., Fu, Q., Li, Z.M. Tunable liquid sensing performance of conducting CNY–PE composites with a porous segregated structure. *RSC Advances.* 3 (2013).
67. Srivastava, S., Tchoudakov, R., Narkis, M. A preliminary investigation of conductive immiscible polymer blends as sensor materials. *Polymer Engineering & Science.* 40 (2000).
68. Al-Saleh, M.H., Sundararaj, U. EMI shielding mechanisms of CNT/polymer composites. *Carbon*. 47 (2009).
69. Yang, Y.L., Gupta, M.C., Dudley, K.L., Lawrence, R.W. Novel CNT–PS foam composites for EMI shielding. *NanoLetters*. 5 (2005).

# ENGINEERING SCIENCES

"HENRI COANDA"
AIR FORCE ACADEMY
ROMANIA

"GENERAL M.R. STEFANIK"
ARMED FORCES ACADEMY
SLOVAK REPUBLIC

INTERNATIONAL CONFERENCE of SCIENTIFIC PAPER
AFASES 2015
Brasov, 28-30 May 2015

# AERODYNAMIC CHARACTERISTICS OF AIRFOIL WITH SINGLE SLOTTED FLAP FOR LIGHT AIRPLANE WING

**Michael Damianov Todorov***

*Faculty of Transport, Technical University of Sofia, Bulgaria

***Abstract:*** *A numerical study was performed on a NACA 23012 airfoil with a single slotted flap to examine the aerodynamic coefficients at Reynolds number of $3\times10^6$, and for help to identifying the forces acting on a light airplane wing. Besides, in the paper the flow fields around the airfoil with single slotted flap were shown. All calculations were made using a CFD code Fluent. For a turbulent model the Spalart-Allmaras method was chosen. Conclusions were made about the aerodynamic efficiency of the proposed configuration wing-single slotted flap.*

***Keywords:*** *airplane wing, single slotted flap, aerodynamic characteristics, CFD, Fluent*

## 1. INTRODUCTION

Aircraft wing high-lift configuration design is an important and challenging part of the whole aircraft aerodynamic configuration design, even dealing with a 2-D high-lift configuration design task which is an essential step for the 3-D high-lift configuration design [10], [12], [13].

During the take-off and landing of an aircraft, the performance of high-lift devices has strong impact on the operating costs and environment around airports, such as improvements of payload, fuel consumption, and noise emission. Take-off and landing performance for very light airplanes are governed by the requirements as EASA CS-VLA [5]. The take-off and landing distances, and the important speeds as the stall speed with flaps retracted – $V_S$, the design maneuvering speed – $V_A$, the speed with flaps fully deflected – $V_F$, and the stall speed with flaps fully deflected – $V_{SF}$, depend on aerodynamic characteristics of the wing with a flaps deflected.

Nowadays, Computational Fluid Dynamics (CFD) is widely used for the prediction of the aerodynamic performance of the wing, at least in cruise flight. The computation of the flow over a multi-element wing in high-lift configuration remains however one of the most difficult problems encountered in CFD [3]. The computations normally include a comprehensive code, coupled to Euler or Navier-Stockes solvers. The examples for a successful application of CFD are the codes FLUENT, OVERFLOW of NASA, FLOWer and TAU of Deutshes Zentrum für Luft und Raumfahr [3], [12], elsA and WAVES of ONERA [6], CFD++ [15], Star-CCM+ [11], [8], TAS of Takoku University and UPACS of Japan Institute of Space Technology and Aeronautics [7, 8].

The high-lift configurations considerably complicate the flow physics by boundary layer transition, separations and reattachments.

Therefore it is very important to generate the appropriate mesh around it. The mesh can be structured, unstructured or hybrid. The structured mesh is identified by regular connectivity. The possible element choices are quadrilateral in 2D and hexahedral in 3D. This model is highly space efficient, i.e. since the neighborhood relationships are defined by storage arrangement. Some other advantages of structured mesh are better convergence and higher resolution. But obviously it cannot be used for very complicated geometry. The unstructured mesh is identified by irregular connectivity, [6], [9]. It cannot easily be expressed as a two-dimensional or three-dimensional array. This allows the usage of a solver for any possible element. Compared to structured meshes, this model can be highly space inefficient since it calls for explicit storage of neighborhood relationships. These grids typically employ triangles in 2D and tetrahedral in 3D. A hybrid mesh contains a mixture of structured portions and unstructured portions. It integrates the structured meshes and the unstructured meshes in an efficient manner, [12].

Another important step is the choice of a turbulent model. The turbulence is the most challenging area in fluid dynamics and the most limiting factor in accurate computer simulation of the flow. An overview of turbulence modeling is done in [2]. There are the following turbulent models, [16]:

- The *direct numerical simulation* (DNS) of Navier-Stockes equation can be applied only for very low Reynolds numbers and very simple and limited geometries, and practically no numerical solution for flows of interest to engineers can be obtained.
- *Large eddy simulation* (LES) solves the spatially averaged Navier-Stockes equations. Large eddies are directly resolved, but eddies smaller than the mesh are modeled. LES is less expensive than DNS, but the amount of computational resources and efforts are still too large for most practical applications.
- *Spalart-Allmaras* is a low-cost Reynolds-Averaged Navier-Stockes (RANS) model solving a transport equation for a modified eddy viscosity. It is designed specifically for aerospace applications involving wall-bounded flows. It embodies a relatively new class of one-equation models where it is not necessary to calculate a length scale related to the local shear layer thickness.
- The k-ε *turbulent models* are the most widely-used engineering turbulence model for industrial applications, which are a robust and a reasonably accurate. However they generally perform poorly for flows with strong separation, large streamline curvature, and large pressure gradient.
- The k–ω *turbulence models* have gained popularity mainly because the model equations do not contain terms which are undefined at the wall, i.e. they can be integrated to the wall without using wall functions, and they are accurate and robust for a wide range of boundary layer flows with pressure gradient. Reynolds stresses are solved directly using transport equations, avoiding isotropic viscosity assumption of other models. It is used for highly swirling flows. The quadratic pressure-strain option improves performance for many basic shear flows.

In [14], it was found the aerodynamic characteristics of an airfoil with single plain flap, as it is shown in Fig.1. For this purpose, first it was obtained numerical results for NACA 23012 airfoil which were compared with experimental wind tunnel data [1] to select density mesh and turbulent model. The aerodynamic characteristic were obtained by commercial CFD code FLUENT. It was generated structured mesh. The Spalart-Allmaras method gave closest results to the experimental data.

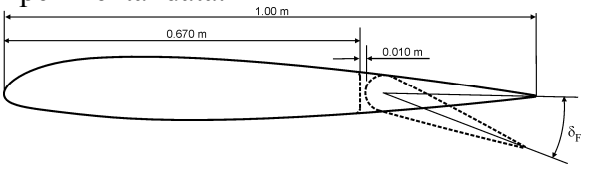


Figure 1. *NACA 23012 airfoil with single plain flap* [14]

Then the aerodynamic characteristics of NACA 23012 airfoil with single flap were calculated. It was generated multi-object hybrid mesh. The calculations were made for Reynolds number of $Re=3\times10^6$ (respectively $V$=43.81 m/s) at the sea level. The turbulent intensity and turbulent viscosity were 2.48% and 10 respectively. The flap deflection angle, $\delta_F$, was 20º.

The obtained results show that the chosen arrangement of wing-single plan flap is not sufficiently effective from an aerodynamic point of view, although it is attractive with the simple design.

Therefore, in the proposed paper another configuration will be studied: an airfoil with a single slotted flap, as it is outlined in Fig.2. A NACA 23012 airfoil with a 1.00 m chord has been used in all the CFD simulations. The single slotted flap with a 0.32 m chord, corresponding to 32% chord, has been constructed in such a way as to match the geometry of the baseline airfoil.

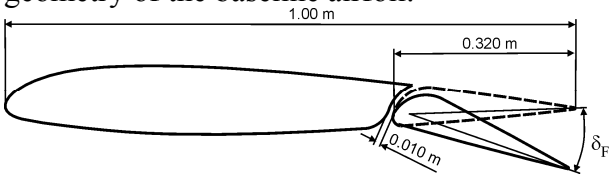


Figure 2. *NACA 23012 airfoil with single slotted flap*

## 2. AERODYNAMIC CHARACTERISTICS OF NACA 231012 AIRFOIL WITH A SINGLE SLOTTED FLAP

To calculate the aerodynamic characteristics of NACA 23012 airfoil with a single slotted flap, the multi-object hybrid O-mesh is generated. The circle has a 10*c* (*c*-airfoil chord) radius. Around the airfoil, the flap and downstream are provided with a high refinement, as it is shown in Fig.3. Thus the mesh has 711 754 nodes and 706 558 elements.

The calculations are made for Reynolds number of $Re=3\times10^6$ (respectively $V$=43.81 m/s) at the sea level. The turbulent intensity and turbulent viscosity are 2.48% and 10 respectively. The flap deflection angle, $\delta_F$, is 20º.

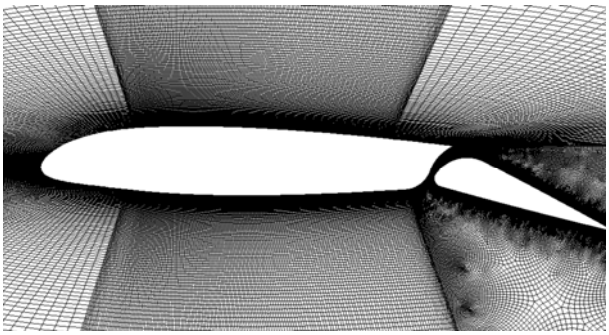

Figure 3. View of the mesh geometry of NACA 23012 airfoil with single slotted flap

Fig.4 and Fig.5 show $C_L$-α and $C_D$- α data of the numerical results for a NACA 23012 airfoil, NACA 23012 airfoil with a single plain flap, and NACA 23012 airfoil with a single slotted flap.

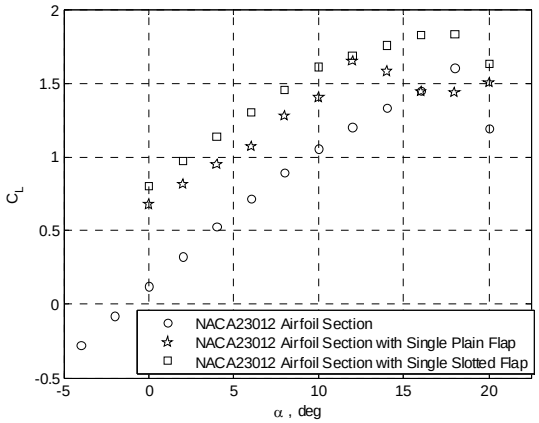


Figure 4. Lift coefficient $C_L$ plot over the range of angles of attack of the numerical results for a NACA 23012 airfoil, NACA 23012 airfoil with a single plain flap, and NACA 23012 airfoil with a single slotted flap

Figures 6, 7, and 8 show pressure coefficients, pressure, and velocity fields around NACA 23012 airfoil with a single slotted flap in the range from 0º to 20º angles of attack.

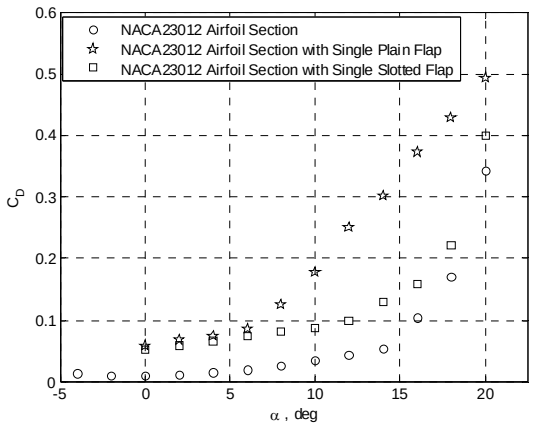


Figure 5. Drag coefficient $C_D$ plot over the range of angles of attack of the numerical results for a NACA 23012 airfoil, NACA 23012 airfoil with a single plain flap, and NACA 23012 airfoil with a single slotted flap

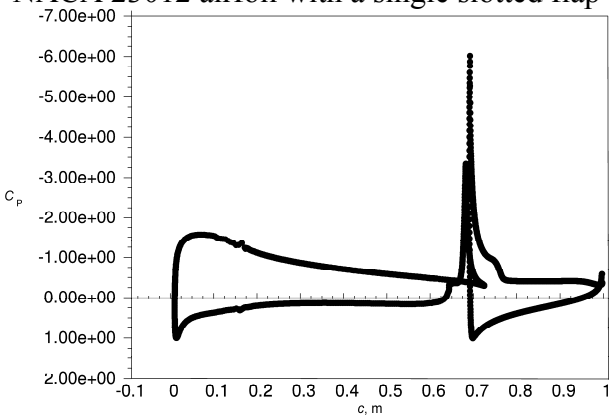


Figure 6a. Pressure coefficient of NACA 23012 airfoil with a single slotted flap at α=2º

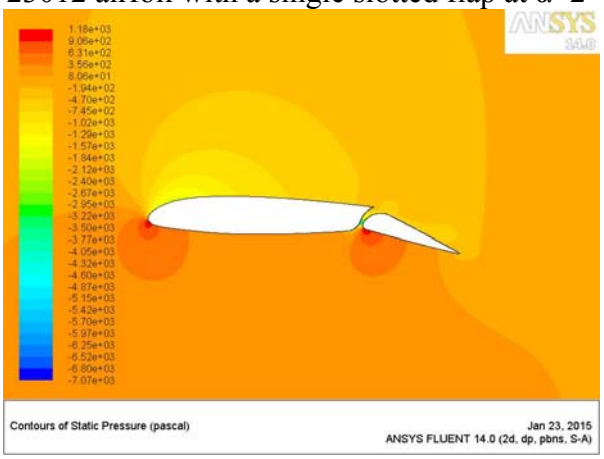


Figure 6b. Pressure around NACA 23012 airfoil with a single slotted flap at α=2º

## 3. DISCUSSION

The deflection of the single slotted flap results in an increase in the lift coefficient by about 38% compared to the baseline airfoil, in the range of angles of attacks from 0 to 10º (see Fig.4).

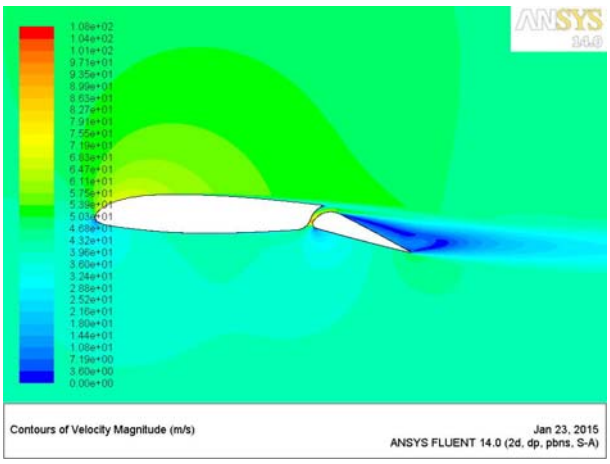


Figure 6c. Velocity fields around NACA 23012 airfoil with a single slotted flap at α=2º

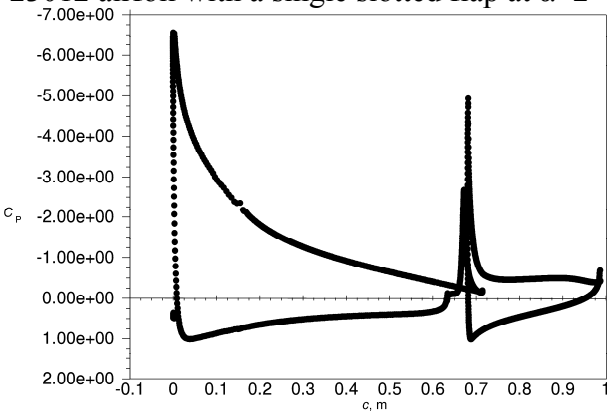


Figure 7a. Pressure coefficient of NACA 23012 airfoil with a single slotted flap at α=12º

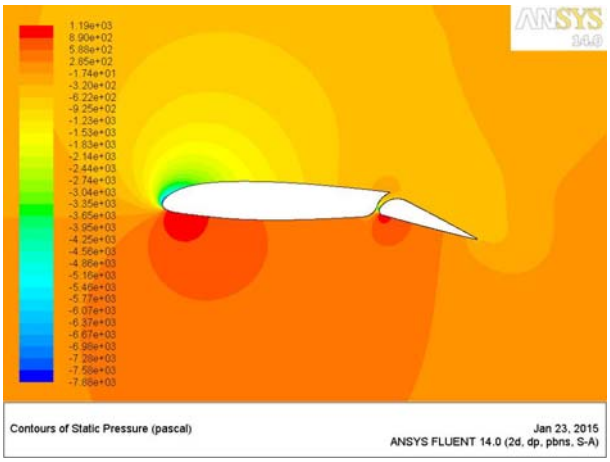


Figure 7b. Pressure around NACA 23012 airfoil with a single slotted flap at α=12º

This is about 8% higher lift coefficient than of the configuration with the single plain flap.

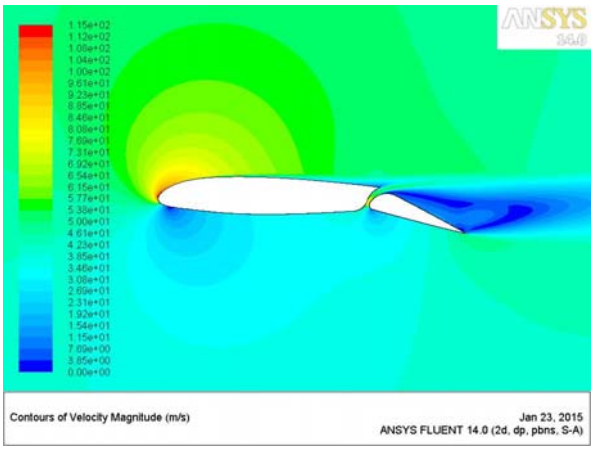


Figure 7c. Velocity fields around NACA 23012 airfoil with a single slotted flap at α=12º

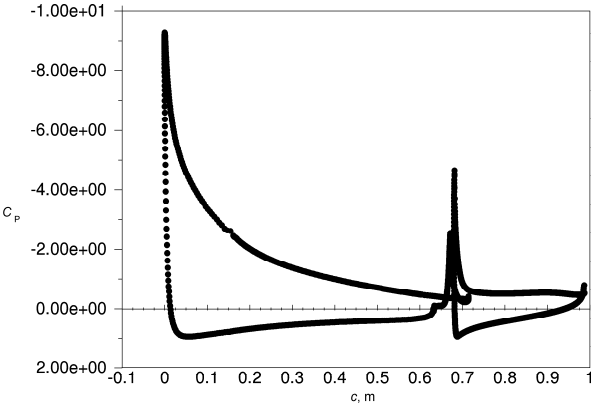


Figure 8a. Pressure coefficient of NACA 23012 airfoil with a single slotted flap at =18º

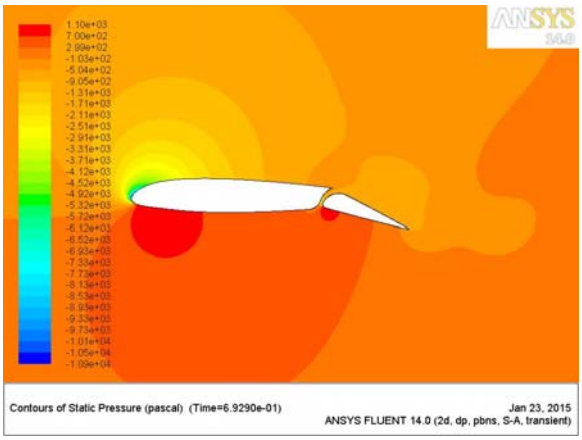


Figure 8b. Pressure around NACA 23012 airfoil with a single slotted flap at =18º

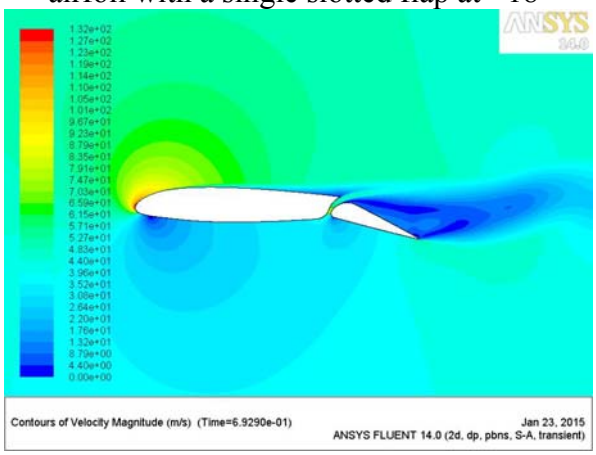


Figure 8c. Velocity fields around NACA 23012 airfoil with a single slotted flap at =18º

The maximum angle of attack in the case with a deflected single slotted flap is 18º. The maximum angle of attack of the baseline airfoil is the same, while in the case with the wing with a single plain flap it is 12º. This is because after α=12º the flow is fully detached to the upper surface, as it is shown in [14]. The bigger lift coefficient is due to the gap between the flap and the wing, and the selected geometry of the lower surface at the end of the wing airfoil.

They force high pressure air from below the wing over the flap helping the airflow to remain attached to the flap.

The deflection of the single slotted flap increases the drag coefficient at the high angles of attack less than the configuration with single plain flap. This is favorable since the flap is used in this configuration for take-off, i.e. at high angles of attack.

These results show that the chosen arrangement of a wing-single slotted flap is more effective than the configuration wing-single plain flap.

## 4. CONCLUSIONS

A numerical analysis was performed for a NACA 23012 airfoil with a single slotted flap. All calculations were performed with the Fluent code. It was used the Spalart-Allmaras turbulent method.

The analysis aimed to identify the aerodynamic forces acting on the proposed wing and flap at Reynolds number of $3\times10^6$.

The 2D CFD model was used to examine the major features around the proposed configuration wing-single slotted flap.

The obtained results were compared with those for the NACA 23012 baseline airfoil and configuration wing- single plain flap.

The CFD results for the proposed configuration wing-single slotted flap showed higher lift coefficient than the NACA 23012 baseline airfoil and configuration wing-single plain flap. The drag coefficient is less than that of the configuration wing-single plain flap. The obtained results are better from the aerodynamic point of view.

The further work is needed to investigate the influence of the gap and position of axis of rotation of the single slotted flap to improve of the aerodynamic characteristics of designed configuration airfoil-flap.

## REFERENCES


1. Abbott, I. H., von Doenhoff, A. E.. Summary of airfoil data, *NACA Report No. 824*, (1945).
2. Anderson, B., Anderson, R., Hakanson, L., Mortensen, L., Sudiyo, R., van Wachem, B.. Computation fluid dynamics for engineers, *Cambridge University Press*, (2012).
3. Brezillon, J., Dwight, R. P., Wild, J.. Numerical aerodynamic optimization of 3D high-lift configuration, *Proc. of 26th International Congress of The Aeronautical Sciences, ICAS* (2008).
4. van Dam, C.P.. The aerodynamic design of multi-element high-lift systems for transport airplanes, *Progress on Aerospace Sciences*, 38, 101-144, (2002).
5. EASA, Certification specifications for very light aeroplanes CS-VLA, Amendment 1, (March 2009).
6. Khare, A., Baig, R., Ranjan, R., Shah, S., Pavithran S., Moitra, A.. Computational simulation of flow over a high-lift trapezoidal wing, *Proc. of ICEAE* (2009).
7. Murayama, M., Yamamoto, K., Numerical simulation of high-lift configurations using unstructured mesh method, *Proc. Of 24th International Congress of The Aeronautical Sciences, ICAS* (2004).
8. Murayama, M., Yokokawa, Y., Yamamoto, K.. Validation study of CFD analysis for high-lift systems, *Proc. Of 25th International Congress of The Aeronautical Sciences*, *ICAS* (2006).
9. de Oliveira Neto, J. A., Cavali, D., Junior, C. B., Azavedo J.L.F., de Lima e Silva, A. L. F.. Computational simulations of high-lift configuration using unstructured grids, *Proceedings of the ENCIT 2006*, ABCM, Curitiba – PR, Brazil – Paper CIT06-0269 (2006).
10. Prabhar, A., Ohri, A.. CFD analysis on MAV NACA 2412 wing in high lift take-off configuration for enhanced lift generation, *J. Aeronautics & Aerospace Engineering*, volume 2, 1-8, issue 5, (2013).
11. Shankara, P., Snyder, D., Numerical simulation of high lift trap wing using STAR-CCM+, *AIAA 2012-2920*, (2012).
12. Schindler, K., Reckzech, D., Scholz, U., Aerodynamic design of high-lift devices for civil transport aircraft using RANS CFD, *AIAA 2010-4946*, (2010).
13. Steed, R. G. F.. High lift CFD simulation with an SST-based predictive laminar to turbulent transition model, *AIAA 2011-864*, (2011).
14. Todorov, M., Aerodynamic Characteristics of Airfoil with Single Plain Flap for Light Airplane Wing, *Proc. of ICMT*, (2015).
15. Vecchia, P. D., Ciliberty, D.. Numerical aerodynamic analysis on a trapezoidal wing with high lift devices: a comparison with experimental data, *XXII AIDAA Conference*, (2013).
16. www.fluentusers.com

"HENRI COANDA"
AIR FORCE ACADEMY
ROMANIA

"GENERAL M.R. STEFANIK"
ARMED FORCES ACADEMY
SLOVAK REPUBLIC

INTERNATIONAL CONFERENCE of SCIENTIFIC PAPER
AFASES 2015
Brasov, 28-30 May 2015

# MATHEMATICAL MODEL FOR A JET ENGINE WITH ANTI-STALL AUTOMATIC VALVE AIDED COMPRESSOR

**Alexandru-Nicolae Tudosie***

*Department of Electrical, Power Systems and Aerospace Engineering, Faculty of Electrical Engineering, University of Craiova, Romania

***Abstract:*** *The paper proposes a possible mathematical model for a jet engine, which operates together with its anti-stall valve system. The author has identified how the blow-off valve operating influences the engine's mathematical model. Furthermore, one has studied engine's behavior when its anti-stall valve is driven by a pneumatic automatic system and some simulations were also performed, concerning main engine's output parameter(s) time behavior. Results could be used for similar systems' studying, as well as for further studies of embedded engine control systems.*

***Keywords:*** *compressor, stall, BOV, control, command pressure, mathematical model, speed.*

## 1. INTRODUCTION

Jet engines for aircraft are built in a large range of performances and types (such as single- or double-spool, single jet or twin jets, with or without afterburning). For a high level thrust engine, there are necessary high compressors pressure ratios $\pi_c^*$, high combustor burned gas temperatures $T_3^*$, as well as alternative thrust augmentation methods (such as afterburning, compressor or combustor water injection).

The more important jet engine is and the bigger its compressor pressure ratio $\pi_c^*$ is, the more sensitive the compressor is, its sensitivity being represented by the possibility of stall.

Compressor's stall occurs when there is a disruption to the flow of air in the engine compressor, or when the pressure of air entering the engine drops below the pressure in the compressor or air within the compressor drops momentarily as a result of stalling air (disruption in air pressure). Consequently, the compressed air expands and travels quite fast toward the area of less pressure (toward the front and out the back) and it can be explosion-like.

An engine surge occurs when the compressor completely loses compression, phenomena which are more prominent in older jet engines.

Fortunately, nowadays compressor stalls or surges are extremely rare, but when present, they can cause harm to the engine or plane.

Compressor stall often will correct itself as soon as the flow of air in the engine is restored. Often times, the corrective action is given by the pilots by reducing engine power till the engine stabilizes.

Nowadays, following better compressor's gas-dynamic understanding ad with the use of

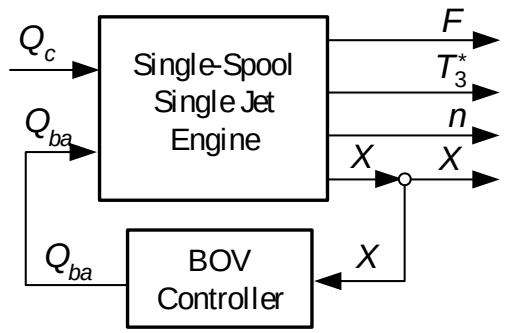


Fig. 1. Embedded system (engine + BOV diagram)

improved modern CAD design methods, this problem has virtually vanished.

One of the stall and surge prevention method for the high-pressure ratio compressors is the blow-off valve (BOV, also known as anti-stall valve) using. An automatic system for the BOV drive is presented in [15].

This paper aim is to introduce and study a possible mathematical model for a jet engine, which operates together with its BOV (as the block diagram in fig. 1 shows), when its working line intersects the surge line on the compressor's characteristic map.

## 2. SINGLE JET ENGINE MATHEMATICAL MODEL

**2.1. Jet engine as controlled object.** Aircraft jet engines as controlled objects are studied in [13] and [14], where the authors have identified, amongst a multitude of parameters, possible control parameters (inputs), controlled parameters (outputs), as well as theoretical command laws.

As input parameters, one has identified only three: a) the combustor fuel flow rate $Q_c$ (for all engine types); b) the exhaust nozzle's opening $A_5$ (only for engines with variable-area nozzles); c) the afterburner fuel flow rate $Q_p$ (only for the engines with afterburning). Other input parameters may be identified when the engine has new facilities/parts with special destination, which could introduce new control loops (see fig. 1), where the blew-off air mass flow $Q_{ba}$ is such an input. Meanwhile, BOV-controller uses as input another engine's output parameter (formally identified as $X$).

Single spool jet engine's most important outputs (controlled parameters) are: spool (shaft) speed (also called engine speed) $n$ and combustor hot gases temperature $T_3^*$. As inputs (control parameters), one may use the fuel flow rate $Q_c$ and, if the engine has a variable exhaust nozzle, its gases exhaust area $A_5$. Possible mixed control schemes, using the above-mentioned parameters, are presented in [12], [13] and [14].

Engine's model, as presented in [13] and [14] by a matrix description is

$$[A]\times(u)=(b), \tag{1}$$

where $[A]$ is engine matrix, $(u)-$output parameters vector and $(b)-$input parameters vector, as follows:

$$A=\begin{bmatrix} T_1 s+\rho_1 & -k_{1T3} & 0 & -k_{1p2} & k_{1p4} \\ k_{2n} & -k_{2T3} & 0 & k_{2p2} & 0 \\ 0 & -1 & 1 & -k_{3p2} & -k_{3p4} \\ 0 & k_{4T3} & k_{4T4} & k_{4p2} & k_{4p4} \\ k_{5n} & k_{5T3} & 0 & k_{5p2} & 0 \end{bmatrix} \tag{2}$$

$$u^T=\left(\bar{n} \quad \overline{T_3^*} \quad \overline{T_4^*} \quad \overline{p_2^*} \quad \overline{p_4^*}\right). \tag{3}$$

$$b^T=\left(0 \quad 0 \quad 0 \quad 0 \quad k_{5Qc}\overline{Q}_c\right). \tag{4}$$

The involved co-efficient are used with their expressions described in [13].

Engine's main output parameters are $\bar{n}$ and $\overline{T}_3^*$; their expressions should be issued by solving system (1) using the Cramer method:

$$X=\frac{det(A_X)}{det(A)}, \tag{5}$$

where $X$ is the generic annotation for each one of the output parameters vector's elements, $det(A)-$determinant of matrix $A$, $det(A_X)-$determinant of $A_X$-matrix, $A_X-$matrix corresponding to $X$-parameter, obtained by the appropriate replacing of its column with input $(b)$ column vector. The presence of a new loop, as in fig.1, modifies the model, by introducing a new input parameter, which is the evacuated air mass flow $Q_{ba}$.

**2.2. Updated model.** Because of the BOV operation, an air mass flow $Q_{ba}$ is evacuated from the compressor's air stream, which modifies engine's mass flow equation. So, the mass flow rate balance equation becomes

$$Q_a - Q_{ba} = Q_m, \tag{6}$$

where $Q_a$ is compressor mass air flow rate and $Q_m$ – combustor air flow rate (air involved in the fuel's combustion).

Consequently, one obtains $Q_{ba} = Q_a - Q_m$ which can be also written, using linear deviations, as

$$\Delta Q_{ba} = \Delta Q_a - \Delta Q_m, \tag{7}$$

or else

$$\Delta Q_{ba} = \left(\frac{\partial Q_a}{\partial p_2^*}\right)_0 \Delta p_2^* + \left(\frac{\partial Q_a}{\partial n}\right)_0 \Delta n - \\ - \left(\frac{\partial Q_m}{\partial p_3^*}\right)_0 \Delta p_3^* - \left(\frac{\partial Q_m}{\partial T_3^*}\right)_0 \Delta T_3^*. \tag{8}$$

Considering that, for a steady state regime, $p_3^* = \sigma_{cb}^* p_2^*$, where $\sigma_{cb}^*$ – combustor's pressure co-efficient, one obtains

$$\frac{Q_{ba0}}{Q_{a0}} \frac{\Delta Q_{ba}}{Q_{ba0}} = \left(\frac{p_{20}^*}{Q_{a0}}\right)\left(\frac{\partial Q_a}{\partial p_2^*}\right)_0 \frac{\Delta p_2^*}{p_{20}^*} + \left(\frac{n_0}{Q_{a0}}\right) \cdot \\ \cdot \left(\frac{\partial Q_a}{\partial n}\right)_0 \frac{\Delta n}{n_0} - \sigma_{cb}^* \left(\frac{p_{30}^*}{Q_{m0}}\right)\left(\frac{\partial Q_m}{\partial p_3^*}\right)_0 \frac{\Delta p_3^*}{p_{30}^*} - \\ - \left(\frac{T_{30}^*}{Q_{m0}}\right)\left(\frac{\partial Q_m}{\partial T_3^*}\right)_0 \frac{\Delta T_3^*}{T_{30}^*}, \tag{9}$$

which may be presented more simply as

$$k_{2ba}\overline{Q}_{ba} = \left(k_{2pc2} - \sigma_{cb}^* k_{2pt2}\right)\overline{p}_2^* + k_{2n}\overline{n} - \\ - k_{2T3}\overline{T}_3^*. \tag{10}$$

One can observe that the co-efficient $k_{2p2}$ in *A*-matrix in (2) should be replaced by the co-efficient $\left(k_{2pc2} - \sigma_{cb}^* k_{2pt2}\right)$, which can offer better information about BOV operating. Meanwhile, vector *b* should be adjusted, by adding the term $k_{2ba}\overline{Q}_{ba}$ as second element.

## 3. COMPRESSOR STALL

Technically speaking, stall occurs when the engine's working line intersects the surge line on the characteristic map, which means that gas stream through the combustor and/or the turbine is disrupted and the shallow border between surge line and working line is crossed, especially near the idle regime.

Fig. 2 shows a characteristic map of a compressor; formally, if stall occurs, one may consider that engine's working line become AS instead of AB. Point A, corresponding to idle regime, is located very close to the surge line, which makes the stall occurrence a high possibility.

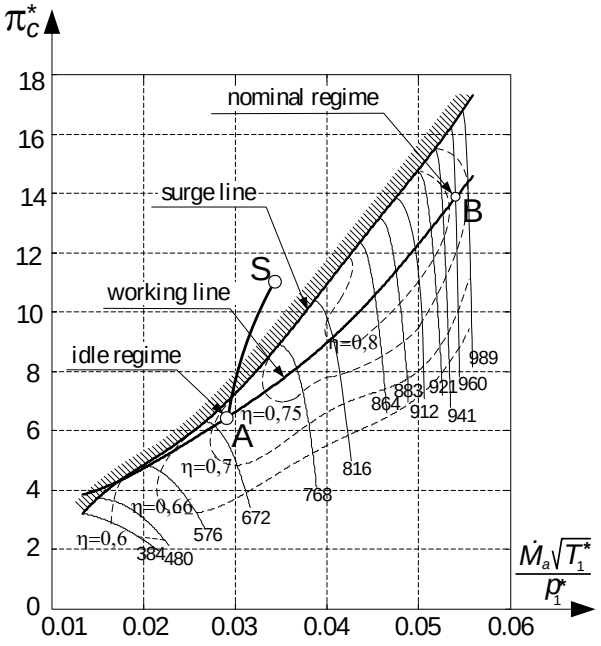


Fig. 2. Compressor characteristic map

In order to introduce the stall into the engine's model, one has to consider the new form of $k_{2p2}$, $k_{2p2}^{/} = k_{2pc2} - \sigma_{cb}^{*} k_{2pt2}$, where

$$k_{2pc2} = \left(\frac{p_{20}^{*}}{Q_{a0}}\right)\left(\frac{\partial Q_a}{\partial p_2^{*}}\right)_0, \quad (11)$$

$$k_{2pc2} = \left(\frac{p_{30}^{*}}{Q_{m0}}\right)\left(\frac{\partial Q_m}{\partial p_3^{*}}\right)_0. \quad (12)$$

First co-efficient should respect engine's normal operation, which means that the curve where the slope $\left(\frac{\partial Q_a}{\partial p_2^{*}}\right)_0$ is calculated will be the working line AB. Meanwhile, in order to simulate the flow disruption, one has to calculate the second co-efficient, in (12), using for the term $\left(\frac{\partial Q_m}{\partial p_3^{*}}\right)_0$ the AS-curve's slope value (crossing the surge line).

It leads to an important modifying of $k_{2p2}$ value and, together with the presence of $k_{2ba}\overline{Q}_{ba}$ between the elements of *b*-vector, to a new form of engine's mathematical model.

## 4. EMBEDDED SYSTEM'S MODEL

Jet engine operating with its BOV may be identified as controlled object by its new model, which consists of the updated jet engine model and the BOV model, as follows.

**4.1. Jet engine updated model.** It contains the new input $\overline{Q}_{ba}$, as well as the new form of the co-efficient $k_{2p2}$, so the fourth element in the second line in matrix *A* (formula (2) in section 2) becomes $k_{2p2}^{/}$ and the matrix becomes $A^{/}$; output vector remains the same, but the input vector $b^{T}$ becomes

$$b^{/T} = \left(0 \quad -k_{2ba}\overline{Q}_{ba} \quad 0 \quad 0 \quad k_{5Qc}\overline{Q}_c\right). \quad (13)$$

One can observe that air pressure behind the compressor $p_2^{*}$ is located amongst the engine secondary output parameters, so it becomes the inner feedback of the embedded system (see parameter *X* in fig. 1).

The new system

$$\left[A^{/}\right] \times (u) = \left(b^{/}\right) \quad (14)$$

shall be solved using Cramer-methods and one obtains for engine's speed parameter $\overline{n}$ and for the compressor's exhaust pressure $\overline{p}_2^{*}$ parameter new expressions

$$\overline{n} = \frac{k_{cc}\,\overline{Q}_c + k_{cb}\,\overline{Q}_{ba}}{\tau_m\, s + \rho_m}, \quad (15)$$

$$\overline{p}_2^{*} = \frac{\left(\tau_{cp}\, s + \rho_{cp}\right)\overline{Q}_c + \left(\tau_{pp}\, s + \rho_{pp}\right)\overline{Q}_{ba}}{\tau_m\, s + \rho_m}, \quad (16)$$

where co-efficient involved in eqs. (15) and (16) will be calculated using the new values for $k_{2p2}^{/}$ and $k_{2ba}$.

The parameters' expressions for temperature $T_3^{*}$ and thrust *F* have similar expressions (see [11], [13] and [14]) and may be calculated (and simulated) if necessary.

**4.2. BOV-model**. The anti-stall valve's model consists of the blew-off air mass flow equation, as well as of the BOV-controller equation, as follows:

a) $Q_{ba}$ mass flow equation

$$\overline{Q}_{ba} = k_{by}\,\overline{y} + k_{bp}\,\overline{p}_2^{*}, \quad (17)$$

where $k_{by} = \frac{\mu_b \sqrt{2}\pi d_b\, p_{20}^{*} y_0}{Q_{b0}\sqrt{\rho}}$ and

$$k_{bp} = \frac{\mu_b \pi d_b\, p_{20}^{*} y_0}{Q_{b0}\sqrt{2\rho\left(p_{20}^{*} - p_{H0}\right)}}; \quad (18)$$

b) BOV-controller equation, as determined in [15], with its annotations

$$\overline{y} = \frac{a}{b_2 s^2 + b_1 s + b_0}\,\overline{p}_2^{*}, \quad (19)$$

$$a = K_{yC}K_{p2}, b_2 = \tau_{CA}T_{\xi}, b_0 = \left(1 - K_D\right),$$

$$b_1 = \left(1 - K_D\right)T_{\xi} - K_{yC}\tau_{Cy} + \tau_{CA}. \quad (20)$$

Consequently, BOV mathematical model may be expressed as

$$\overline{Q}_{ba} = \left(\frac{k_{by}a}{b_2 s^2 + b_1 s + b_0} + k_{bp}\right)\overline{p}_2^{*}. \quad (21)$$

Embedded system operational block diagram is depicted in fig. 3, while system block diagram with transfer functions in fig. 4.

## 5. SYSTEM'S QUALITY

For a VK-1 type single-spool single-jet engine, *A*-matrix elements values are calculated in [11] and [13]. Based on these values, main parameter expression (engine's speed *n*) is

$$\bar{n} = \frac{1.352\,\bar{Q}_c - 0.269\,\bar{Q}_{ba}}{1.059\,s + 0.7102}, \qquad (22)$$

while secondary parameter $\bar{p}_2^*$ expression is

$$\bar{p}_2^* = \frac{(0.84\,s + 3.086)\,\bar{Q}_c - (0.975\,s + 7.13)\bar{Q}_{ba}}{1.059\,s + 0.7102} \qquad (23)$$

BOV controller equation, which co-efficient are calculated as presented in [15], has the form

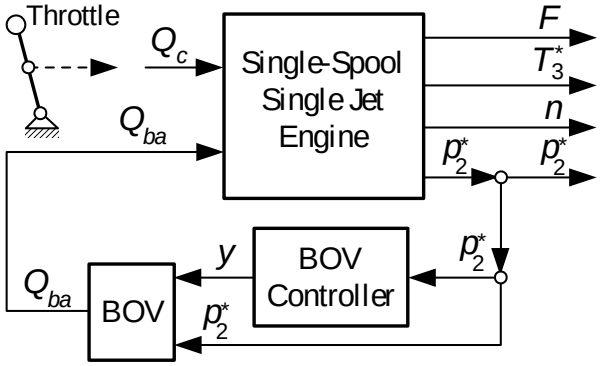


Fig. 3. Embedded system (engine+BOV) operational block diagram

$$\bar{y} = \frac{0.6237}{s^2 + 4.821s + 4.7823}\,\bar{p}_2^*. \qquad (24)$$

Based on the block-diagram with transfer functions in fig. 4 and on the above-determined forms for the system parameters, one has performed a simulation, considering as input parameter engine's fuel mass flow rate $\bar{Q}_c$ and as main output parameter engine's

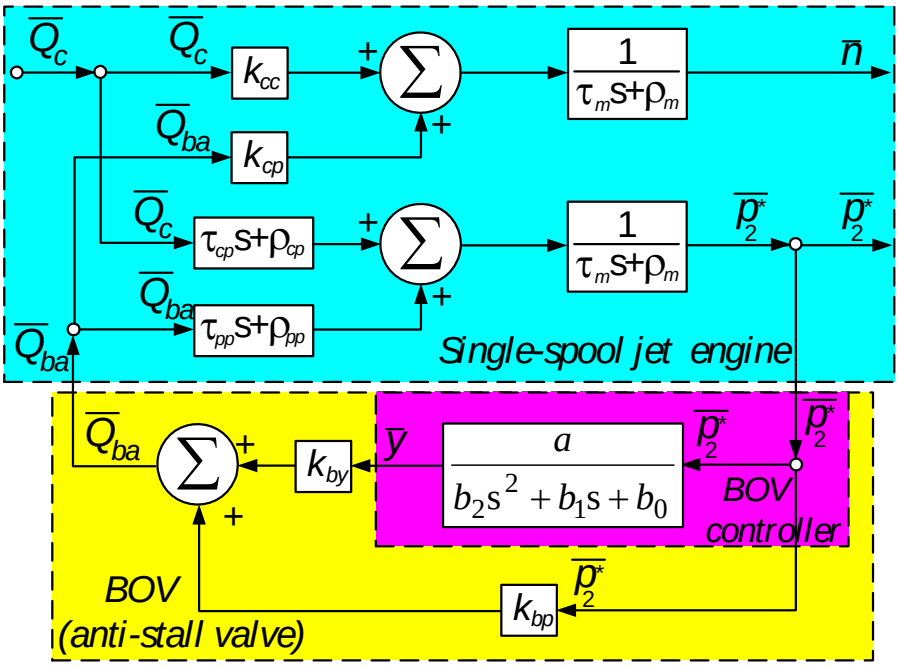


Fig. 4. Embedded system block diagram with transfer functions

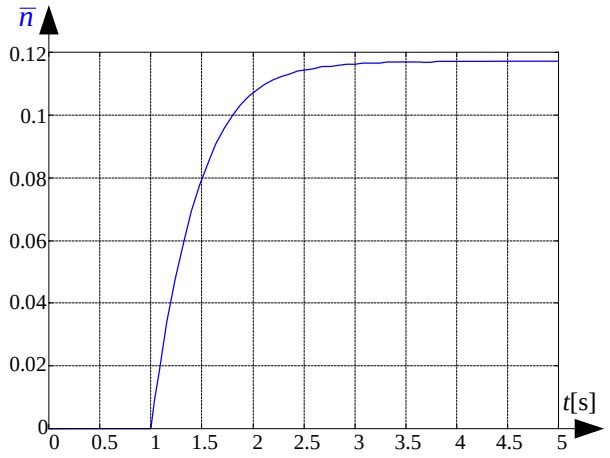


Fig. 5. Embedded system speed step response (fuel mass flow rate step input)

speed $\overline{n}$; meanwhile, one has studied both secondary output parameters (compressor pressure $\overline{p}_2^*$ and BOV opening $\overline{y}$) behavior.

One has considered a step input of the fuel mass flow rate parameter, so output parameters' behavior ($\overline{n}$, $\overline{p}_2^*$ and $\overline{y}$) is system's step response. System's time response (output parameters' values versus time) lays in figures 5, 6 and 7.

Fig. 5 presents main output parameter's (engine speed) behavior when the anti-stall system is active, while fig. 6 presents a comparison between the speed behavior in this situation (curve I) and the speed behavior when the engine is operating after the AS-working line in fig. 2 (curve II), so it become an unstable object. One can observe that BOV-operating makes the engine a stable object from the speed point of view, its stability being aperiodic.

Secondary parameters' ($\overline{p}_2^*$ and $\overline{y}$) time response is presented in fig. 7. One can observe that both output parameters are stable.

BOV opening parameter $\overline{y}$ is aperiodic, because of the chosen co-efficient of the (24) transfer function, in order to assure a smooth mass air flow evacuation; a periodic BOV opening isn't acceptable, being the reason of stall/surge engine behavior.

Air pressure $\overline{p}_2^*$ parameter's behavior is also stable, but one can observe a small initial override; is doesn't matter from the BOV opening point of view, which has an aperiodic behavior. However, if the override grows, or if the stability becomes periodic, it definitely may initiate compressor's stall-operating, because of the possibility of surge line crossing.

## CONCLUSIONS

In this paper one has proposed an approach of the unstable engine behavior, caused by the compressor's stall; meanwhile, one has introduced a possibility of correction, by using an anti-stall BOV for the compressor.

One has introduced a new single-spool single jet engine model, based on several existing mathematical models and on the author experience concerning co-efficient

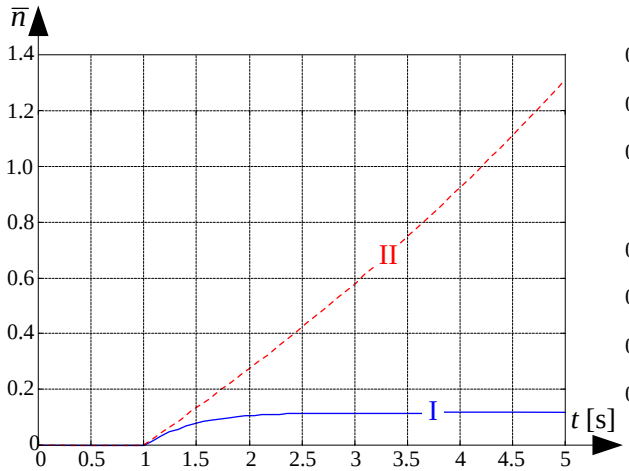


Fig. 6. System speed step response comparison (fuel mass flow rate step input)

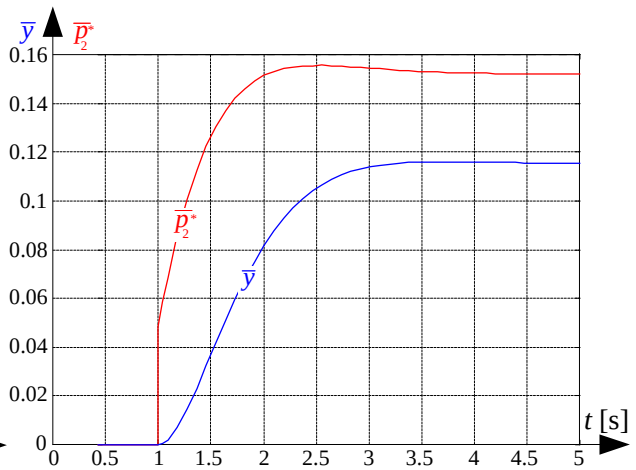


Fig. 7. System step response for secondary output parameters $\overline{p}_2^*$ and $\overline{y}$

calculation for various engine's regimes, different of the cruise regime, as is the idle regime.

BOV presence and operating means another compressor mass airflow balance, because of the evacuated (blew-off) air, which modifies the engine's working line, as well as mathematical model's co-efficient system. Meanwhile, it introduces another input parameter, $\overline{Q}_{ba}$, in addition to the already existing fuel mass flow rate $\overline{Q}_c$. In fact, the new input $\overline{Q}_{ba}$ is a parameter given by the BOV operating and it depends on $\overline{p}_2^*$, the air pressure parameter behind the compressor, which is a secondary engine output parameter; consequently, a new closed loop was added to the engine's model.

Based on another study, concerning a BOV-controller [15], one has built a control scheme for the embedded system (engine+ +BOV+controller), whose mathematical model was determined, as well as its block-diagram with transfer functions.

The above-mentioned elements were used during the simulations; one has considered a step input for the main input parameter $\overline{Q}_c$, while as output parameter one has considered engine's speed (which is the most illustrative parameter, being proportional to the engine thrust), as well as most important secondary output parameters: BOV opening $\bar{y}$ and compressor's pressure $\overline{p}_2^*$ (which is the cause of the studied phenomena and, in the same time, BOV-controller's input parameter).

As fig. 6 shows, when the stall/surge occurs, engine's speed becomes an unstable parameter (curve II). Applying the requested constructive measures (BOV installing) one obtains a stabilization of the engine, its speed parameter becoming aperiodic-stable (curve I), even if its secondary parameter $\overline{p}_2^*$ has a small override and seems to be periodic-stable (as fig. 7 shows). In spite of it, BOV-opening parameter $\bar{y}$ is aperiodic stable (fig. 7) and, consequently, a smooth air evacuation (blow-off) is assured.

Engine's speed parameter's behavior when the BOV-controller is active (fig. 5) shows an appropriate operating, an aperiodic stabilization and an acceptable response time (around 2.5 s), even if its static error is higher than usual (around 12%).

This paper is useful for aircraft engine and control specialists and students. Results could be used for similar systems' studying, as well as for further studies of embedded engine control systems.

## REFERENCES

1. Abraham, R. H. *Complex dynamical systems*, Aerial Press, Santa Cruz, California (1986).
2. Dinca, L. *On-board Hydro-pneumatic Equipment and Systems*, Universitaria Publisher, Craiova (2008).
3. Ispas, St., *Turbo-jet engine*. Tehnica Publisher, Bucuresti (1984).
4. Lungu, R., Tudosie, A., Dinca, L. *Fluid Mechanics and Technical Thermo-dynamics*. SITECH Publisher, Craiova (2004).
5. Lungu, R. *Flight Apparatus Automation*. "Universitaria" Publisher, Craiova (2000).
6. Mattingly, J. D. *Elements of Gas Turbine Propulsion*. McGraw-Hill, New York (1996).
7. Mattingly, J. D., Heiser, W. H., Pratt, D. T. *Aircraft Engine Design*. AIAA Education Series, Reston VA (2002).
8. Pimsner, V. *Thermical Plants with Blades*. Tehnica Publisher, Bucuresti (1988).

9. Stanciu, V., Boscoianu, M. *Kynetic compressor's stall*. MPM Edit Consult Publisher, Bucuresti (2002).
10. Stanciu, V., Crunteanu, D. *Subsonic Aerodinamic Compressor's Design*. Printech Publisher, Bucuresti (2009).
11. Stoenciu, D. *Aircraft Engines'Automation. Sigle Spool Single-jet Engine as Controlled Object.* Technical Military Academy Inprint, Bucuresti (1986).
12. Stoenciu, D. *Aircraft Engines'Automation. Automation Schemes Album.* Technical Military Academy Inprint, Bucuresti (1987).
13. Stoicescu, M., Rotaru, C. *Turbo-Jet Engines. Characteristics and Control Methods*. Military Technical Academy Publisher, Bucuresti (1999).
14. Tudosie, A. N. *Aerospace Propulsion Systems Automation*. University of Craiova Inprint, Craiova (2005).
15. Tudosie, A. N., Olteanu, M. C. *Pneumatic Anti-Stall Automatic System for a Jet Engine Compressor*. ( unpublished, 2015).
16. Vasiliu, N. et a. *Fluid Mechanics and Hydraulic Systems.* vol I and II, Tehnica Publisher, Bucuresti (1992).

"HENRI COANDA"
AIR FORCE ACADEMY
ROMANIA

"GENERAL M.R. STEFANIK"
ARMED FORCES ACADEMY
SLOVAK REPUBLIC

INTERNATIONAL CONFERENCE of SCIENTIFIC PAPER
AFASES 2015
Brasov, 28-30 May 2015

# PNEUMATIC ANTI-STALL AUTOMATIC SYSTEM FOR A JET ENGINE COMPRESSOR

**Alexandru-Nicolae Tudosie*, Mihai-Catalin Olteanu***

*Department of Electrical, Power Systems and Aerospace Engineering, Faculty of Electrical Engineering, University of Craiova, Romania

***Abstract:*** *The paper deals with a pneumatic system for the engine's compressor's anti-stall valve's automatic opening, in order to keep the compressor's operating enough far from the stall line. The authors have chosen an automatic opening system based on a pneumatic actuator and a pneumatic command system; starting from the non-linear motion equation, one has determined the linearized, adimensionalised mathematical model, as well as its simplified form. Based on it one has determined the block-diagram with transfer functions and one also has performed some studies concerning system's stability and quality. Results could be used for similar systems' studying, as well as for further studies of embedded engine control systems*

***Keywords:*** *compressor, stall, control, command pressure, air flow rate.*

## 1. INTRODUCTION

Jet engines for aircraft are built in a wide range of types, with respect to their thrust, constructive solutions and dimensions; no matter the solution were, they are equipped with compressors (centrifuge or axial).

The compressor is one of the most important engine's parts, which is responsible for the air pressure raise before the engine's combustor. Its pressure ratio, defined as $\pi_c^* = \frac{p_2^*}{p_1^*}$, depends on the total pressure values behind and before it, $p_2^*$ and $p_1^*$,.

However, the more important its task is and the bigger its pressure ratio is, the more sensitive the compressor is. Its sensitivity is represented by the possibility of stall operating, when the air flow rate through the compressor isn't co-related to the air necessities of the engine's combustor, especially during engine's transient (dynamical) operating regimes.

Obviously, in order to keep the compressor in the stable operational range, one has to assure the permanent correlation between the combustor's necessary air flow rate and the effective delivered compressor air flow rate, as well as the correlation with the injected fuel flow rate; that means that compressor's working line is enough far from the stall-line.

Stall is caused by the air flow stream's critical attack angle override, followed by stream's detachment and flow's spectrum alteration. In order to prevent it, an air valve is mounted on the compressor's crankcase, which role is to evacuate the excessive air, readjusting the air speed in the front of the compressor's blades.

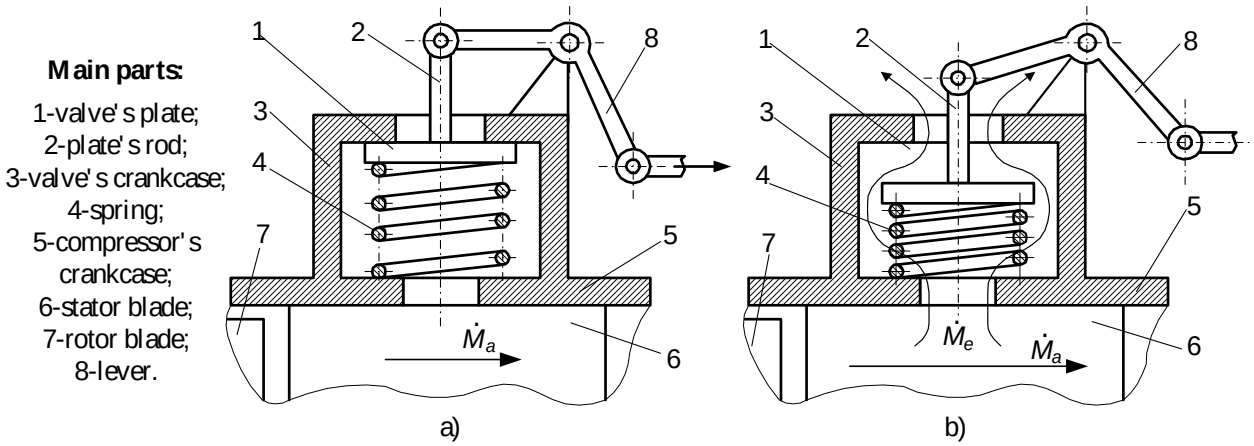


Fig. 1. Anti-stall valve

Compressor's stall is very difficult to be modeled, but some authors have explained it (see [10] and [11]) and have proposed some prevention methods, such as stator blades position adjustment and/or exhaust valves using. Blades position adjustment systems are described in [2], [13] and [14], while anti-stall valves using are described in [14] and [15].

In this paper the authors have studied an anti-stall valve's pneumatic command system.

## 2. COMMAND SYSTEM PRESENTATION

Anti-stall valve (see fig.1) operates by evacuating a small air mass flow (no more than 3 % of the total compressor's air mass flow $\dot{M}_a$) from jet engine's compressor towards the atmosphere, in order to avoid the stall. Valve's command systems are various, from the simplest version (consisting of a valve with spring) to the most complex, equipped by pneumatic, hydraulic, electric or combined actuators and sensors.

Figure 2 presents a pneumatic system consisting of a single active chamber actuator, a nozzle-flap distributor and a two sylphons pressure sensor.

Main input signal is the pressure captured from the last or from an intermediate "*k*" compressor stage ( $p_2^*$ or $p_k^*$); this pressure signal is converted into command pressure signal $p_C$, by using the nozzle-flap distributor, as well as the pressure sensor chambers A and B. The command pressure signal generates the actuator's rod displacement *y*, which is the output signal. The command system's rod (4) in fig. 2 should be connected properly to the lever (8) in fig. 1, in order to assure valve's opening when the input pressure $p_2^*$ reaches a certain value. The command pressure value would be presetted by the opening of the variable drossel (7).

One can observe that the command system's air supplying is realized by the controlled compressor and no other active fluid is involved.

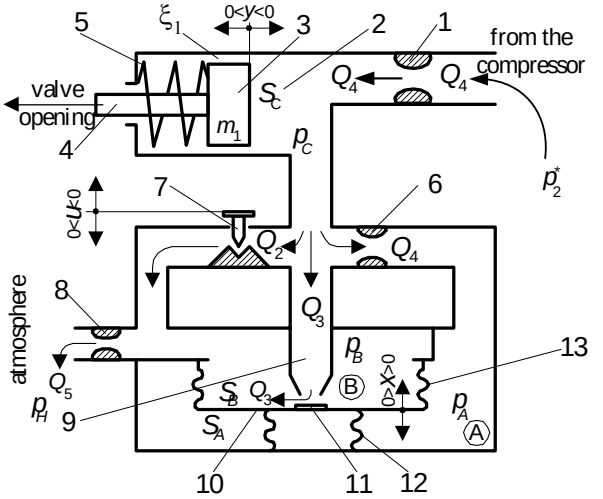


**System parts:** 1, 6, 8-drossels; 2-pneumatic actuator; 3-actuator's piston; 4-actuator's rod; 5-actuator's spring; 7-adjusting bolt; 9-nozzle; 10-plateau; 11-flap; 12, 13-silphon.

Fig. 2. Valve's opening command system

## 3. SYSTEM MATHEMATICAL MODEL

The studied system's mathematical model consists of the motion equation for each of its parts. The non-linear equation will be transformed, in order to bring them to an acceptable form for further studies, as well as for simulations.

### 3.1. Non-linear mathematical model.

System's non-linear motion equations are the following:

a) air mass flow equations:

$$Q_1 = \mu_{d1}\frac{\pi d_1^2}{4}\sqrt{\frac{2}{\rho}}\sqrt{p_2^* - p_C}\,, \tag{1}$$

$$Q_2 = \mu_7 b_7 (u_s - u)\sqrt{\frac{2}{\rho}}\sqrt{p_C - p_H}\,, \tag{2}$$

$$Q_3 = \mu_3 b_3 (x_s - x)\sqrt{\frac{2}{\rho}}\sqrt{p_C - p_B}\,, \tag{3}$$

$$Q_4 = \mu_{d6}\frac{\pi d_6^2}{4}\sqrt{\frac{2}{\rho}}\sqrt{p_C - p_A}\,, \tag{4}$$

$$Q_5 = \mu_{d8}\frac{\pi d_8^2}{4}\sqrt{\frac{2}{\rho}}\sqrt{p_B - p_H}\,, \tag{5}$$

b) nozzle-flap distributor equations:

$$V_A = V_{A0} + S_A x\,, \tag{6}$$

$$V_B = V_{B0} - S_B x\,, \tag{7}$$

$$Q_2 + Q_3 - Q_5 = \frac{\mathrm{d}V_B}{\mathrm{d}t} + \beta V_{B0}\frac{\mathrm{d}p_B}{\mathrm{d}t}\,, \tag{8}$$

$$S_B p_B - S_A p_A - (S_B - S_A)p_S = k_s x\,, \tag{9}$$

c) pneumatic actuator equations:

$$Q_1 - Q_2 - Q_3 - Q_4 = \frac{\mathrm{d}V_C}{\mathrm{d}t} + \beta V_{C0}\frac{\mathrm{d}p_C}{\mathrm{d}t}\,, \tag{10}$$

$$Q_4 = \frac{\mathrm{d}V_A}{\mathrm{d}t} + \beta V_{A0}\frac{\mathrm{d}p_A}{\mathrm{d}t}\,, \tag{11}$$

$$V_C = V_{C0} + S_C y\,, \tag{12}$$

$$m_1\frac{\mathrm{d}^2 y}{\mathrm{d}t^2} + \xi\frac{\mathrm{d}y}{\mathrm{d}t} + k_{el}y = S_C p_C\,, \tag{13}$$

where $d_1, d_3, d_6, d_8$ – drossels' diameters; $b_7$ – variable drossel (7) width; $\mu_{d1}, \mu_{d6}, \mu_{d3}, \mu_{d8}, \mu_7$ – mass flow co-efficient; $p_A$, $p_B$ – silphon chambers pressure; $V_C, V_A, V_B$ – chambers volumes; $m_1$ – piston and rod mass; $\xi$ – friction co-efficient; $k_{el}$ – spring (5) elastic constant; $k_s$ – silphons' elastic constant; $S_A, S_B$ – plateau (10) surfaces areas; $S_C$ – actuator's piston area.

The above determined non-linear equation system (equations (1) to (13)) is difficult to be used for further studies, so it can be brought to a linear form, using the small perturbation method, considering formally any variable or parameter $X$ as

$$X = X_0 + \Delta X\,, \tag{14}$$

where $X_0$ – steady state regime's value, $\Delta X$ – parameter's deviation and $\overline{X} = \frac{\Delta X}{X_0}$ the non-dimensional deviation.

### 3.2 Linearized mathematical model

In order to determine a linearized form for the above equation system, one has to identify the main parameters. The adjusting bolt displacement $u$ (performed during the ground testing period), has no relevance for the system dynamic behavior, so it should be excluded.

Expressing each one of the main parameters as in eq. (14) and introducing them into the equation system, after eliminating the terms containing the steady state regime, one obtains the system's linear form, as follows:

$$\Delta Q_1 = k_{1p2}\cdot\Delta p_2^* - k_{1C}\cdot\Delta p_C\,, \tag{15}$$

$$\Delta Q_2 = k_{2C}\Delta p_C - k_{2B}\Delta p_B - k_{2u}\Delta u\,, \tag{16}$$

$$\Delta Q_3 = k_{3C}\Delta p_C - k_{3B}\Delta p_B - k_{3x}\Delta x\,, \tag{17}$$

$$\Delta Q_4 = k_{4C}\cdot\Delta p_C - k_{4A}\cdot\Delta p_A\,, \tag{18}$$

$$\Delta Q_5 = k_{5B} \cdot \Delta p_B - k_{5H} \cdot \Delta p_H , \quad (19)$$

$$\Delta V_A = S_A \cdot \Delta x , \quad (20)$$

$$\Delta V_B = S_B \cdot \Delta x , \quad (21)$$

$$\Delta Q_2 + \Delta Q_3 - \Delta Q_5 = = \frac{\mathrm{d}}{\mathrm{d}t}\Delta V_B + \beta V_{B0}\frac{\mathrm{d}}{\mathrm{d}t}\Delta p_B , \quad (22)$$

$$S_B \cdot \Delta p_B - S_A \cdot \Delta p_A = k_s \cdot \Delta x , \quad (23)$$

$$\Delta Q_1 - \Delta Q_2 - \Delta Q_3 - \Delta Q_4 = = \frac{\mathrm{d}}{\mathrm{d}t}\Delta V_C + \beta V_{C0}\frac{\mathrm{d}}{\mathrm{d}t}\Delta p_C , \quad (24)$$

$$\Delta Q_4 = \frac{\mathrm{d}}{\mathrm{d}t}\Delta V_A + \beta V_{A0}\frac{\mathrm{d}}{\mathrm{d}t}\Delta p_A , \quad (25)$$

$$V_C = S_C \cdot \Delta y , \quad (26)$$

$$m_1 \frac{\mathrm{d}^2}{\mathrm{d}t^2}\Delta y + \xi \frac{\mathrm{d}}{\mathrm{d}t}\Delta y + k_{el}\Delta y = S_C \Delta p_C , \quad (27)$$

where the used annotations are:

$$k_{1p2} = \left(\frac{\partial Q_1}{\partial p_2^*}\right)_0 = \frac{\mu_{d1}\pi d_1^2\sqrt{2}}{8\sqrt{\rho\left(p_{2_0}^* - p_{C_0}\right)}} = \left(\frac{\partial Q_1}{\partial p_C}\right)_0 = k_{1C}$$

$$k_{2u} = \left(\frac{\partial Q_2}{\partial u}\right)_0 = \mu_7 b_7 \sqrt{\frac{2}{\rho}}\sqrt{\left(p_{C_0} - p_{B_0}\right)};$$

$$k_{3x} = \left(\frac{\partial Q_3}{\partial x}\right)_0 = \mu_3 \pi d_3 \sqrt{\frac{2}{\rho\left(p_{C_0} - p_{A_0}\right)}};$$

$$k_{2C} = \left(\frac{\partial Q_2}{\partial p_C}\right)_0 = \frac{\mu_7 b_7 \left(u_s - u_0\right)\sqrt{2}}{2\sqrt{\rho\left(p_{C_0} - p_{B_0}\right)}} = = \left(\frac{\partial Q_2}{\partial p_B}\right)_0 = k_{2B};\ k_{3C} = \left(\frac{\partial Q_3}{\partial p_C}\right)_0 = = \frac{\mu_3 \pi d_3 \left(x_s - x_0\right)\sqrt{2}}{2\sqrt{\rho\left(p_{C_0} - p_{B_0}\right)}} = \left(\frac{\partial Q_3}{\partial p_B}\right)_0 = k_{3B};$$

$$k_{4C} = \left(\frac{\partial Q_4}{\partial p_C}\right)_0 = \frac{\mu_{d6}\pi d_6^2\sqrt{2}}{8\sqrt{\rho\left(p_{C_0} - p_{A_0}\right)}} = = \left(\frac{\partial Q_4}{\partial p_A}\right)_0 = k_{4A};\ k_{5B} = \left(\frac{\partial Q_5}{\partial p_B}\right)_0 = = \frac{\mu_{d8}\pi d_8^2\sqrt{2}}{8\sqrt{\rho\left(p_{B_0} - p_{H_0}\right)}} = \left(\frac{\partial Q_5}{\partial p_H}\right)_0 = k_{5H} . \quad (28)$$

### 3.3 Non-dimensional linearized model

Using some appropriate chosen amplifying terms, the above-presented linearized mathematical model can be transformed in a non-dimensional one; after applying the Laplace transformation, one obtains the system's linear non-dimensional mathematical model, as follows:

$$K_{p2}\overline{p}_2^* + K_B\overline{p}_B + K_A\overline{p}_A + K_{uC}\overline{u} + + K_{xC}\overline{x} - \tau_C \mathrm{s}\overline{y} = \left(\tau_{yC}\mathrm{s}+1\right)\overline{y} , \quad (29)$$

$$K_{CB}\overline{p}_C + K_H\overline{p}_H - K_{uB}\overline{u} - - K_{xB}\left(\tau_x \mathrm{s}+1\right)\overline{x} = \left(\tau_B \mathrm{s}+1\right)\overline{p}_B , \quad (30)$$

$$K_{CA}\overline{p}_C - \tau_x \mathrm{s}\overline{x} = \left(\tau_A \mathrm{s}+1\right)\overline{p}_A , \quad (31)$$

$$\overline{x} = K_{Bx}\overline{p}_B - K_{Ax}\overline{p}_A , \quad (32)$$

$$\left(T_y^2 \mathrm{s}^2 + T_\xi \mathrm{s} + 1\right)\overline{y} = K_{yC}\overline{p}_C , \quad (33)$$

with the annotations

$$k_{AB} = k_{2B} + k_{3B};\ k_{BC} = k_{2C} + k_{3C};$$

$$k_{CA} = k_{1C} + k_{2C} + k_{3C} + k_{4C};$$

$$k_B = k_{5B} + k_{2B} + k_{3B};\ K_{p2} = \frac{k_{1p2}p_{20}^*}{k_{CA}p_{C0}};$$

$$K_B = \frac{k_{AB}p_{B0}}{k_{CA}p_{C0}};\ K_A = \frac{k_{4A}p_{A0}}{k_{CA}p_{C0}};$$

$$K_{uC} = \frac{k_{2u}u_0}{k_{CA}p_{C0}};\ K_{xC} = \frac{k_{3x}x_0}{k_{CA}p_{C0}};$$

$$\tau_{CA} = \frac{\beta V_{C0}}{k_{CA}};\ \tau_{yC} = \frac{S_C y_0}{k_{CA}p_{C0}};$$

$$\tau_B = \frac{\beta V_{B0}}{k_B};\quad \tau_x = \frac{S_B}{k_{3x}};\quad K_{xB} = \frac{k_{3x}x_0}{k_B p_{B0}};$$

$$K_H = \frac{k_{5H}p_{H0}}{k_B p_{B0}};\quad T_y^2 = \frac{m_1}{k_{el}};\quad T_\xi = \frac{\xi}{k_{el}};$$

$$K_{CB} = \frac{k_{BC}p_{C0}}{k_B p_{B0}};\ K_{Bx} = \frac{S_B p_{B0}}{k_s x_0};$$

$$K_{Ax} = \frac{S_A p_{A0}}{k_s x_0};\ K_{yC} = \frac{S_C p_{C0}}{k_{el} y_0} . \quad (34)$$

### 3.4. Simplified mathematical model

One can make some simplifications to the above-determined model, based on several experimental observations and determinations:

a) piston+rod mass is very small, so inertial effects could be neglected; consequently, the term $T_y^2 = \frac{m_1}{k_{el}}$ in equation (33) becomes null;

b) viscous friction is insignificant, so the friction co-efficient $\xi$ depends almost only on the mechanical friction;

c) if the $p_2^*$-pressure is enough high, the flow through the drossels (1), (6), (7) and (8) in fig.2 is critical, so pressures $p_A$ and $p_B$ become proportional to their supplying pressure, which is $p_C$. Consequently, the terms $\tau_A$ and $\tau_B$, depending on the compressibility co-efficient $\beta$ are becoming null;

d) for small values of (10)-plateau's areas and for small value of the (3)-drossel's diameter, the time constant $\tau_x = \frac{S_B}{k_{3x}} = \frac{\sqrt{2}S_B\mu_3\pi d_3}{\sqrt{\rho\left(p_{C_0} - p_{A_0}\right)}}$ can be considered as null;

e) if the flight regime (airspeed and altitude) remains the same, the pressure $p_H$ is constant, so $\bar{p}_H = 0$ and the terms containing it dissapears.

Consequently, the simplified mathematical model is

$$K_{p2}\bar{p}_2^* + K_B\bar{p}_B + K_A\bar{p}_A + K_{xC}\bar{x} - \\ -\tau_C s\bar{y} = \left(\tau_{yC}s+1\right)\bar{y}, \quad (35)$$

$$K_{CB}\bar{p}_C + K_H\bar{p}_H - K_{xB}\bar{x} = \bar{p}_B, \quad (36)$$

$$K_{CA}\bar{p}_C = \bar{p}_A, \quad (37)$$

$$\bar{x} = K_{Bx}\bar{p}_B - K_{Ax}\bar{p}_A, \quad (38)$$

$$\left(T_\xi s+1\right)\bar{y} = K_{yC}\bar{p}_C. \quad (39)$$

Based on it, one can build the system's block diagram with transfer functions, which lays in fig.3, as well as the system's transfer functions:

- with respect to the supply pressure

$$H_p(s) = \frac{\bar{y}(s)}{\bar{p}_2^*(s)} = \frac{K_{yC}K_{p2}}{\tau_{CA}T_\xi s^2 + \left[(1-K_D)T_\xi - K_{yC}\tau_{Cy} + \tau_{CA}\right]s + (1-K_D)}; \quad (40)$$

- with respect to the flight altitude

$$H_H(s) = \frac{\bar{y}(s)}{\bar{p}_H(s)} = \frac{K_{yC}K_H\left(K_B + \frac{K_{xC}}{1+K_{xB}}\right)\left(T_\xi s+1\right)}{\tau_{CA}T_\xi s^2 + \left[(1-K_D)T_\xi - K_{yC}\tau_{Cy} + \tau_{CA}\right]s + (1-K_D)}$$

where one has used the annotation

$$K_D = K_BK_{CB} + K_AK_{CA} - \\ - \frac{K_{CB} - K_{xA}\left(K_BK_{xB} - K_{xC}\right)}{1+K_{xB}}. \quad (42)$$

System's transfer functions, (40) and (41),

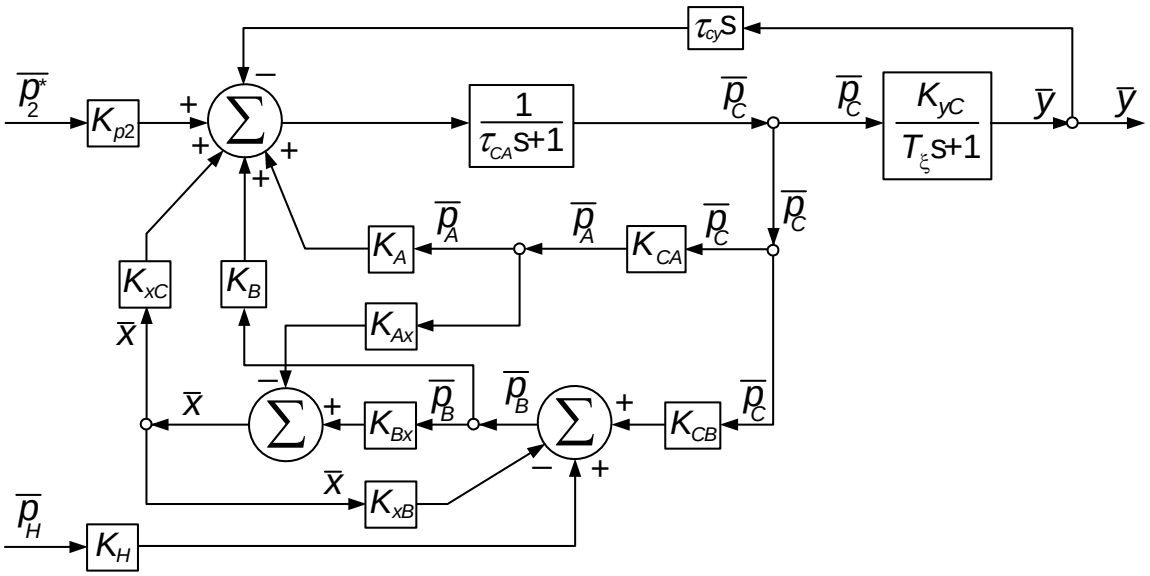


Fig. 3. Block diagram with transfer functions

have simplified forms; their characteristic polynomial is of second order.

## 4. SYSTEM'S STABILITY

According to algebraic Routh-Hurwitz criteria, system's stability is assured if the characteristic polynomial's co-efficient are strictly positive.

One can observe that, as long as $\tau_{CA}$ and $T_\xi$ are time constants and are strictly positives, the first polynomial co-efficient $\tau_{CA}T_\xi$ is always a positive one; although, the other co-efficient must be analyzed.

The third co-efficient, $1-K_D$, should also be a positive one. So,

$$1-K_BK_{CB}-K_AK_{CA}+ \\ +\frac{K_{CB}-K_{xA}\left(K_BK_{xB}-K_{xC}\right)}{1+K_{xB}}>0, \qquad (43)$$

which leads to

$$d_6^2 > a\times d_8^2 + b, \qquad (44)$$

where the used annotations are

$$a=\left[\mu_7 b_7 S_C\left(p_{C0}-p_{A0}\right)^2 y_0 Q_{10} - \right. \\ \left. -\mu_{d6}\pi S_A\left(p_{C0}-p_{B0}\right)^2 x_0 Q_{60}\right]: \\ : S_C{}^2 x_0\left(\mu_7 b_7 u_0-\frac{\pi}{4}\mu_{d1}d_1^2\sqrt{p_{H0}}\right)^2;$$

$$b=\frac{x_0 y_0\left(\mu_7 b_7 x_0-\frac{\pi}{4}\mu_{d6}S_A\sqrt{p_{H_0}}\right)}{\pi S_A\left(p_{C0}-p_{B0}\right)^2 x_0}\times \\ \times\left[k_{el}S_C-S_B{}^2 x_0\left(\mu_7 b_7 u_0-\frac{\pi}{4}\mu_{d1}d_1^2\sqrt{p_{H0}}\right)^2\right. \\ \left.+\left(p_{C0}-p_{A0}\right)^2\sqrt{\frac{2}{\rho}}y_0 Q_{10}\right]. \qquad (45)$$

The above-determined relation (44) may be graphically expressed as a domain of stability into a co-ordinates system $(d_6, d_8)$, as fig. 4.a shows. As far as these two drossel diameters are strictly positive, the diagram is relevant only in the positive side of its axis. It results a stability domain, as well as an instability domain on the diagram's surface. An observation may occur, concerning the (8)-drossel absence, when the drossel (8) should have a minimum value $(d_6)_{\min}$ in order to keep the system's stability.

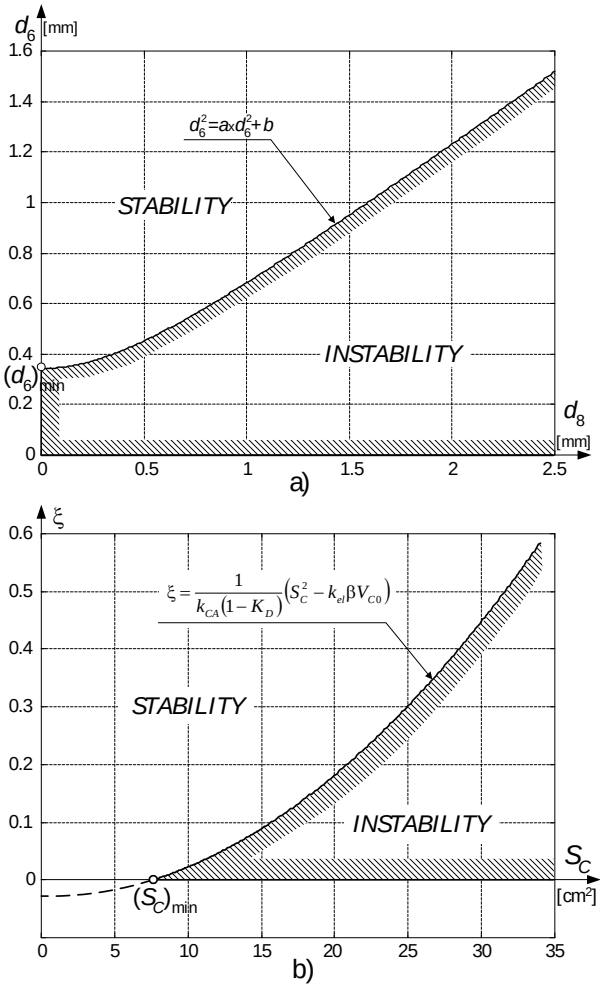


Fig. 4. System's stability conditions

The second characteristic polynomial's co-efficient must be also positive

$$\left(1-K_D\right)T_\xi - K_{yC}\tau_{Cy}+\tau_{CA}>0. \qquad (46)$$

Time constants $\tau_{CA}$ and $\tau_{Cy}$ are strictly positive, as well as the term $K_{yC}=\frac{S_C p_{C0}}{k_{el}y_0}$, determined by strictly positive factors. Moreover, one considers the first stability condition as fulfilled, meaning $1-K_D>0$, so condition (46) becomes $T_\xi > \frac{K_{yC}\tau_{Cy}-\tau_{CA}}{1-K_D}$.

Considering (28), (32) and (42) annotations one obtains for (46) the expression

$$\xi > \frac{1}{k_{CA}(1-K_D)}\left(S_C^2 - k_{el}\beta V_{C0}\right), \qquad (47)$$

which represents the second stability condition of the system; it could be graphically expressed as fig. 4.b) shows, which offers the possibility to choose the surface area of the actuator's piston $S_C$ with respect to the friction co-efficient $\xi$. The same diagram shows a minimum piston area $S_C$ – value, when piston motion would occur, hypothetically, frictionless.

For usual friction $\xi$ – values, actuator's piston area should be chosen in the range of $(30 \div 50)$ cm$^2$.

Stability studies may be extended, in order to determine the periodic/aperiodic stability domains; one has to verify the characteristic polynomial's discriminant sign as well as its roots locus.

## 5. SYSTEM'S QUALITY

Based on the block diagram in fig. 3, one has performed a simulation, concerning system's step response, for a constant flight regime. One has simulated a step input of $\bar{p}_2^*$, for two different situations, involving two $\xi$ – values and one has evaluate system's time response, depicted in fig. 5.

In both of the above-mentioned situations the system is a stable-one. When the friction co-efficient's value is small, system's stability is periodic-type, with an initial 10% override and a response time around 1.2 seconds, while when the friction grows, the stability becomes aperiodic and the response time increases too.

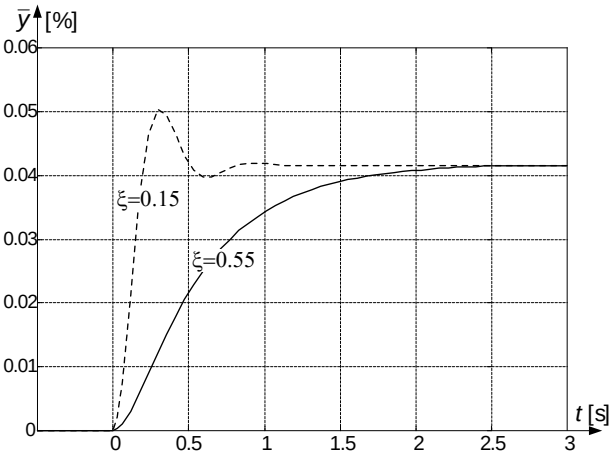


Fig. 5. System's quality

## 6. CONCLUSIONS

The studied pneumatic anti-stall valve's opening system is a second order control system, as its transfer function shows.

Because of its working fluid (air) compressibility, this kind of systems are less precisely, but very effective for a wide range of compressors. Compressibility factor β is found in many mathematical model co-efficient expressions (see (28)-expressions) and has an important influence above system's behavior.

Based on the simplified linearized mathematical model the authors have studied the stability of the system and, subsequently, have determined two graphic stability conditions, involving relations between constructive and functional parameters, which may be used by engine designers during the pre-design phases.

One has also performed a simulation, concerning system's quality, estimated through system's step response, for a step input of the main system parameter, $\bar{p}_2^*$. The conclusion is that system's behavior depends on the friction co-efficient values, which means that it depends on the materials

combination used for the actuator's manufacturing.

If the friction co-efficient is very low, even if the system is stable and its time response is small, its stability is periodically type, which is unacceptable from the compressor's operating point of view, because anti-stall valve's periodic opening induces itself an unstable flow through the compressor, acting contrary to its main objective.

If the friction co-efficient is enough high, system's stability becomes aperiodic, which is acceptable, even if the stabilization time increases (from 1.2 seconds to 2.5 seconds), which means that the system becomes slower. Consequently, a very important aspect of the system design is the choice of manufacturing materials, especially concerning the friction co-efficient between actuator's piston and cylinder materials.

The study is useful for aerospace students, engineers and professionals and may be extended for similar systems' analysis, as well as for further studies concerning axial compressors control systems, or embedded jet engine control systems.

## REFERENCES


1. Abraham, R. H. *Complex dynamical systems*, Aerial Press, Santa Cruz, California (1986).
2. Aron, I., Tudosie, A. Automatic system for the control of the axial compressor's blades with respect to the engine's throttle's position. *XVI-th Teaching Staff Scientific Contribution Session*, "Mircea cel Batran" Naval Academy, Constanta, 3-5 June 1999, vol. III, pp.177-184.
3. Dinca, L. *On-board Hydro-pneumatic Equipment and Systems*, Universitaria Publisher, Craiova (2008).
4. Ispas, St., *Turbo-jet engine*. Tehnica Publisher, Bucuresti (1984).
5. Lungu, R., Tudosie, A., Dinca, L. *Fluid Mechanics and Technical Thermo-dynamics*. SITECH Publisher, Craiova (2004).
6. Lungu, R. *Flight Apparatus Automation*. "Universitaria" Publisher, Craiova (2000).
7. Mattingly, J. D. *Elements of Gas Turbine Propulsion*. McGraw-Hill, New York (1996).
8. Mattingly, J. D., Heiser, W. H., Pratt, D. T. *Aircraft Engine Design*. AIAA Education Series, Reston VA (2002).
9. Pimsner, V., Berbente, C., Stanciu, V. s. a. *Blades Thermical Plants Processus*. Tehnica Publisher, Bucuresti (1986).
10. Pimsner, V. *Thermical Plants with Blades*. Tehnica Publisher, Bucuresti (1988).
11. Stanciu, V., Boscoianu, M. *Kynetic compressor's stall*. MPM Edit Consult Publisher, Bucuresti (2002).
12. Stanciu, V., Crunteanu, D. *Subsonic Aerodinamic Compressor's Design*. Printech Publisher, Bucuresti (2009).
13. Stoenciu, D. *Aircraft Engines'Automation. Automation Schemes Album.* Military Academy Inprint, Bucuresti (1977).
14. Stoicescu, M., Rotaru, C. *Turbo-Jet Engines. Characteristics and Control Methods*. Military Technical Academy Publisher, Bucuresti (1999).
15. Tudosie, A. N. *Aerospace Propulsion Systems Automation*. University of Craiova Inprint, Craiova (2005).
16. Vasiliu, N. et a. *Fluid Mechanics and Hydraulic Systems.* vol I and II, Tehnica Publisher, Bucuresti (1992).

"HENRI COANDA"
AIR FORCE ACADEMY
ROMANIA

"GENERAL M.R. STEFANIK"
ARMED FORCES ACADEMY
SLOVAK REPUBLIC

INTERNATIONAL CONFERENCE of SCIENTIFIC PAPER
AFASES 2015
Brasov, 28-30 May 2015

# FATIGUE LIFE SIMULATION OF THE SPECIMENS MADE OF MECHANICAL COMPONENT

**Sebastian Marian Zaharia***

*Faculty of Technological Engineering and Industrial Management, Transilvania University of Brasov, Romania

***Abstract:*** *This paper describes the validation of a Monte-Carlo simulation and finite element analysis of a practical application (mechanical component) using the fatigue testing techniques. Fatigue testing techniques investigate how the component structure reacts to stress over a long period of time and during different levels of its operations. The importance of implementing the Monte Carlo techniques in fatigue life analysis is motivated by the growing evolution of statistical methods for defining fracture and fatigue of mechanical components. The practical application was simulated with a Monte Carlo method and the statistical analysis was realized using the Weibull 9 software. Fatigue life prediction was simulated using finite element analysis with Ansys 15 software.*

***Keywords:*** *mechanical component, fatigue testing, simulation, Monte Carlo method, FEA*

## 1. INTRODUCTION

Fatigue failure is defined as the progressive degradation of the strength of a material or structural component during use such that failure can occur at much lower stress levels than the ultimate stress level. Fatigue is a dynamic aspect which initiates small (micro) cracks in the material or component and causes them to grow into large (macro) cracks; these, if not detected, can result in catastrophic failure. Fatigue damage can be produced in a variety of ways. Cyclic fatigue is caused by repeated fluctuating loads [4].

Fatigue design life implies the average life to be expected under average aerospace apparatus utilization and loads environment. To this design life, application of a fatigue life scatter factor accounts for the typical variations from the average utilization, loading environments, and basic fatigue strength allowable. This leads to a safe-life period during which the probability of a structural crack occurring is very low. With fail-safe, inspectable design, the actual structural life is much greater. The overall fatigue life of the aerospace apparatus is the time at which the repair of the structure is no longer economically feasible [3].

As a means of transportation, the helicopter has witnessed a significant progress in the past 10 years. We must take into account that by its construction alone, the helicopter is subjected continuously to periodical loads; therefore it must withstand a considerable high number of fatigue cycles. The most susceptible elements at these stresses during the construction of the helicopter are the main and the tail or anti-torque rotor assembly, in which the blades and

their mechanical fastening elements play a key role.

The blades and the rotor's component elements, but also the supple platinum, enter in the category of the vital parts of the helicopter, parts that by their failure or their loss, cause inevitably the destruction of the entire flying apparatus. A vital part is a piece that fulfils the following 3 conditions:

- Is a part that can't be doubled and whose breaking entails or could entail a serious accident;
- From the standpoint of exploitation (as part of the helicopter), the piece is subjected to significant alternate stresses (fatigue stress);
- The current technique of designing helicopters can't ensure very significant security coefficients.

## 2. EXPERIMENTAL STUDY

**2.1 Description of material specimens.** The French helicopter constructors introduced the system for reducing the vibrations like supple platinum. Supple platinum (Fig. 1) is made of a titanium alloy and is placed between the inferior part of the main transmission box and the mechanical board at the helicopter. Supple platinum is a vital part and has the role to reduce the vertical vibrations produced by the main rotor's blade.

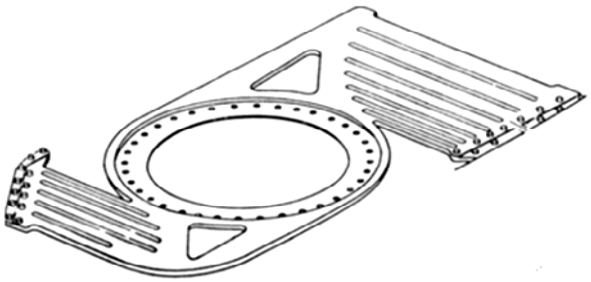

Figure 1. Mechanical component - supple platinum

Due to its configuration, mechanical component (supple platinum) cannot be subjected to stress tests. That's why the tests are being made on specimens, with standardized dimensions, made of the same material as supple platinum (a titanium alloy known in the aviation as TA 10).

**2.2 Testing specimen.** The tests of the specimens made of supple platinum consist of the repeated stress using a bending force, on a test bench that includes a fixation device for the specimen; the device for the tensioning of the specimen; the energy installation; the command installation; the electronic installation.

The experimental research has been performed on specimens made out of supple platinum, specifically from removed portions that result from the technological processing. Figure 2 shows the constructive model of the specimen used in fatigue tests and, also, the placement of strain gages [5].

Figure 2. Specimen for fatigue life testing

## 3. SIMULATION FATIGUE TESTS

**3.1 Fatigue life predictions using finite element analysis.** The finite element analysis is a numerical method for solving problems of engineering and mathematical physics and it is useful for problems with complicated geometries, loadings, and material properties where analytical solutions cannot be obtained [2].

Engineers design today's mechanical components using structural mechanics solutions that compute the response to applied forces and displacements. Fatigue simulation expands on structural analysis to account for extended real-life loadings. Fatigue life simulation is based on a single static structural FEA result and an expected loading history while the part is in use. Engineers have used the ANSYS Fatigue module for simple geometries and loadings for many years. For the majority of realistic geometries and real-life loading, ANSYS nCode DesignLife is the ideal choice. Images show static structural results (above) and fatigue life results (right) [1].

Figure 3 shows the constructive model of the specimen used in fatigue life tests, design in SolidWorks 2014 software.

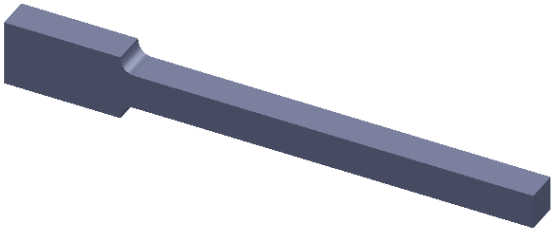

Figure 3. Specimen for fatigue life testing

The model with finite elements was realized in the Ansys 15 software. Approximately 771 hexahedron elements and 1488 nodes have been used for mesh discretization the specimen. The load was simulated by applying on the free end of a force of 500 N. In figure 4 is described Total Deformation of specimens and in figure 5 is presented Equivalent Elastic Strain.

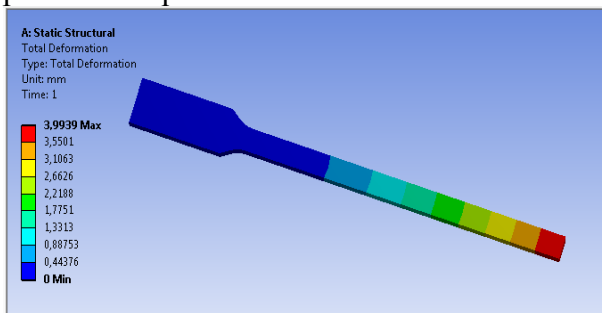


Figure 4. Total deformation

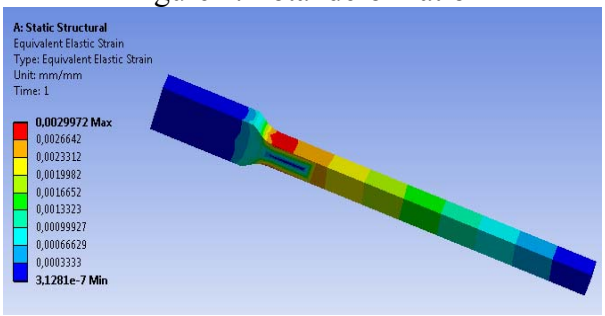


Figure 5. Equivalent Elastic Strain

Figure 6 illustrated the distributions of Equivalent (Von Mises) Stress.

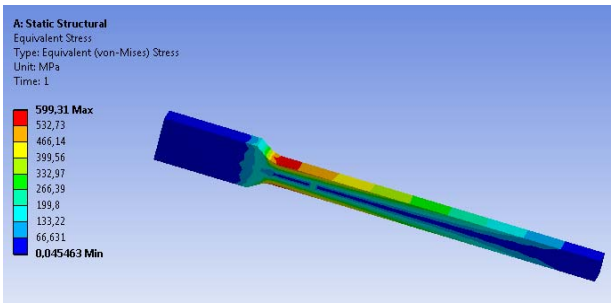


Figure 6. Distributions of Equivalent Stress

The main purpose of the analysis with finite elements of the specimens is to validate the fatigue life (figure 7) that occurs in normal testing on specimen.

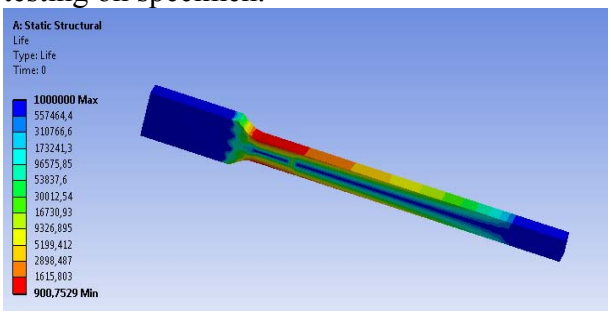


Figure 7. Fatigue life estimation

The distributions of Fatigue Damage is a contour plot of the fatigue damage at a given design life. Fatigue damage is defined as the design life divided by the available life (figure 8).

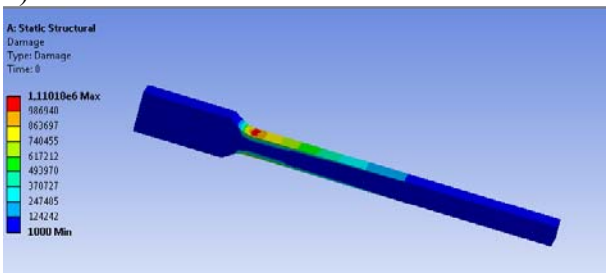


Figure 8. The distributions of Fatigue Damage

**3.2 Fatigue life predictions using Monte Carlo method.** Using the Monte Carlo method, we simulated N stages of a mechanical component with the help of a

statistical distribution (Weibull) which are suited to the analyzed case study (figure 9).

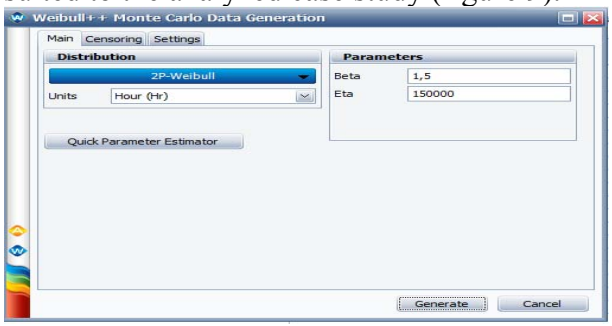


Figure 9. Monte Carlo simulation

Using the previously determined parameters (β=1,5; η=150000) we simulated with the help of Weibull 9 software the values for the number of cycles to failure in fatigue testing condition (figure 10).

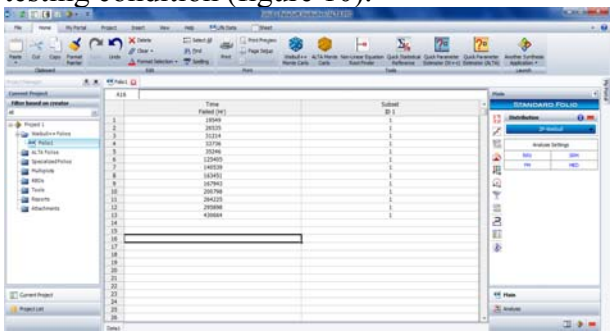

Figure 10. Data using the Monte Carlo method

Mean time to failure describes the expected time to failure for a mechanical component. The Mean Life (MTTF) can be calculated in the Quick Calculation Pad (figure 11).

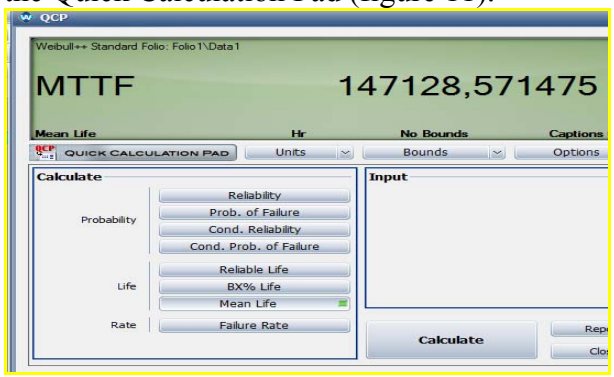


Figure 11. The distributions of Fatigue Damage

## 4. CONCLUSIONS & ACKNOWLEDGMENT

For the case study under analysis, figure 12 shows the number of cycles to failure from finite elements analysis, the simulation with the Monte Carlo method and the data from the fatigue testing. We can observe that, by using the simulation methods (FEA and Monte Carlo) of fatigue life, can be obtain a good results even in early stage Product Design and Development.

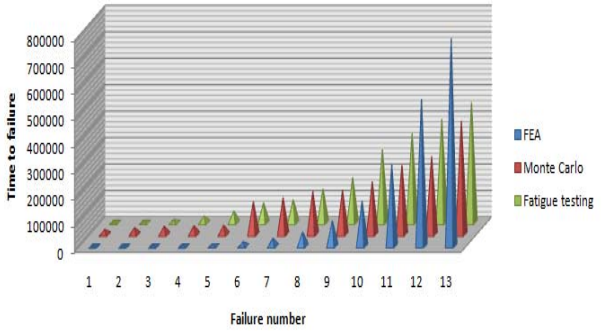


Figure 12. Comparative study of simulation methods

We hereby aknowledge the structural founds project PRO-DD (POS-CCE, O.2.2.1., ID 123, SMIS 2637, ctr. No 11/2009) for providing the infrastructure used in this work.

## REFERENCES

1. Lee, H-H., *Finite Element Simulations with ANSYS Workbench 14,* SDC Publications (2012).
2. Logan, D., *A First Course in the Finite Element Method (5th Edition)*, Cengage Learning (2011).
3. Kroo, I., *Aircraft Design: Synthesis and Analysis,* Desktop Aeronautics Inc (2001).
4. Megson, T.H.G., *Aircraft Structures for Engineering Students.* Elsevier Aerospace Engineering (2012).
5. Zaharia, S.M., Martinescu, I., Morariu, C.O., Life time prediction using accelerated test data of the specimens from mechanical element, *Eksploatacja i Niezawodnosc – Maintenance and Reliability*, 14 (2012) 99-106.

"HENRI COANDA"
AIR FORCE ACADEMY
ROMANIA

"GENERAL M.R. STEFANIK"
ARMED FORCES ACADEMY
SLOVAK REPUBLIC

INTERNATIONAL CONFERENCE of SCIENTIFIC PAPER
AFASES 2015
Brasov, 28-30 May 2015

# RELIABILITY AND STATISTICAL ANALYSIS OF THE FATIGUE LIFE OF THE TAPERED ROLLER BEARINGS

**Sebastian Marian Zaharia***

*Faculty of Technological Engineering and Industrial Management, Transilvania University of Brasov, Romania

***Abstract:*** *This paper presents the results of the reliability analysis and fatigue life on tapered roller bearings. Consider the aspects regarding the statistical analyzing of data we determined the main reliability indicators, which in turn determine the main characteristics regarding the performance and the warranty period of the tapered roller bearing. The obtaining information regarding the reliability of tapered roller bearings is usually done either by following the behavior of the products during operation or during the reliability tests.*

***Keywords:*** *tapered roller bearing, reliability, fatigue life, reliability indicators*

## 1. INTRODUCTION

The selection of the proper bearings for all mechanical systems is essential to the functional and commercial success of that system. The bearings must not only be of the right type, but also the correct size to assure reliability and cost effectiveness. The bearings must be installed properly, supplied with the correct lubricant, and provided with a compatible environment for the system to be successful. The number of revolutions under load determines the fatigue life of a rolling bearing that bearing experiences prior to the initiation of rolling contact fatigue. Because of the natural scatter of lives in a group of bearings operating under identical conditions, the life of the group is specified at some reliability level, usually 90% [1].

The obtaining information regarding the reliability of industrial products is usually done either by following the behavior of the products during operation or during the reliability tests. A reliability test is represented by an experiment performed to determine the parameters of reliability for a well-defined product. The main reliability parameters during reliability tests is mean time to failure (MTTF), knowing that, based on the existing relations between reliability parameters, they can be easily deduced from one in other [2].

The most used reliability tests are the following [3]:

• Complete tests (type n out of n) - in these tests n products of the same kind, the experiment being considered finished when all of the n products have failed. This kind of tests can't be applied in all the situations, because in the case of expensive products is uneconomical, and in the case of products that have a relatively long life time by nature, the experiment will take too long.

• Censored tests (type r out of n) - are commonly used and they consist of subjection

to testing of n products of the same type, the experiment being considered finished after the failure of r<n tested products; obviously, the r number is previously determined, usually by technical, economical and statistical considerations. At this type of experiments, the testing duration is random, because it's unknown when the r-th product will fail; the information here is incomplete, because in the end we will have only r, instead of n experimental data

• Truncated tests (with a fixed testing time) - a n number of products are subjected to testing, but the experiment doesn't stop according to the number of failed elements, but according to a tr time, previously set, a period during which the testing takes place. After this testing time (previously set) has passed, the experiment is considered finished.

The reliability of bearings depends on [4]:

- The design, which can be elementary, for normal requirements of reliability, and optimized, for certain operating conditions;
- The materials being used, this can present changes of the chemical structure, of the micro or macrostructure, in relation to the recommended specifications, with consequences on the product;
- The technology of execution, which, despite all the details and recommendations associated with the modern technologies for ball bearings, the complexity of the systems, machines, devices, tools and testers, because of the difficulties of continuous qualification of the personnel, still leaves room for errors, out of which the majority are eliminated through automatic control, the forced regime of adjustment leading to the reduction of the capacity of resistance at contact fatigue;
- The montage, which often weighs in with multiple factors of disturbance of the reliability;
- The operation conditions (the variations in load, the number of revolutions, the temperature, the contamination or aging of the lubricant, the humidity conditions), which manifest their influence in extremely complex ways.

## 2. EXPERIMENTAL SETUP

The reliability tests realized on bearings offer a multitude of data concerning the reliability and quality of essential and auxiliary materials, the technological and constructive design, the methods of processing being used, the accuracy of execution and, of course, their durability. Therefore, the methodology of accelerated testing of the ball bearings represents a complex process, which takes place in several stages (figure 1) [6].

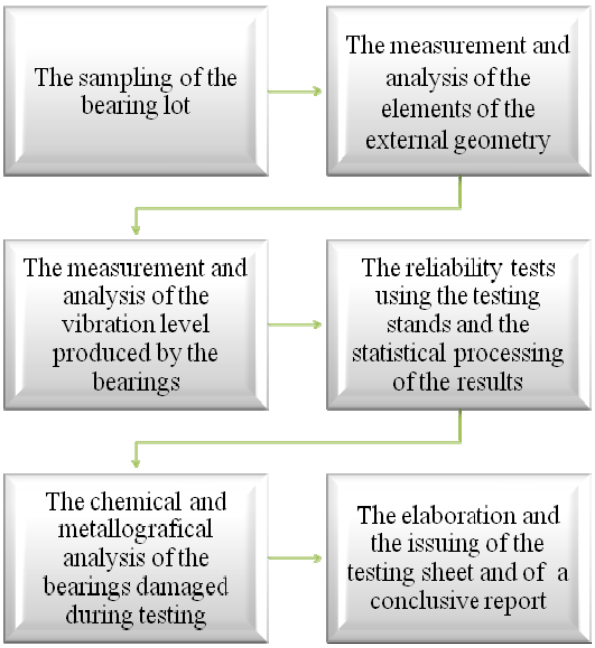


Figure 1. The testing methodology of the bearings

Table 1 describes the geometric and constructive aspects of the tapered roller bearings type, used for the reliability testing [5].

Table 1. The characteristics of the tapered roller bearings type 30205

| | |
|---|---|
| Type | Tapered |
| Cage Material | Steel |
| Dynamic Load Rating | 33.5kN |
| End Type | Open |
| Fatigue Limit Load | 3.45kN |
| Inside Diameter | 25mm |
| Limiting Speed | 13000rpm |
| Material | Metal |
| Number of Rows | 1 |
| Outside Diameter | 52mm |
| Race Width | 16.25mm |
| Reference Speed | 11000rpm |
| Roller Bearing Type | Taper |
| Static Load Rating | 33.5kN |

The tapered roller bearings type 6205 2RS are described in figure 2.

Figure 2. Tapered roller bearings type 30205

## 3. RELIABILITY AND STATISTICAL ANALYSIS

For the results obtained from the reliability testing of the tapered roller bearings for the use level stress (30 bars) we verified the hypothesis that the distribution law of the hours is Weibull (the Kolmogorov - Smirnov test was used). For this verification, we measured the spacing between empirical distribution function of the sample and the cumulative distribution function of the reference distribution. We compared these results with a level of confidence of the Kolmogorov – Smirnov test. Following the statistical processing of the experimental data for levels of stress the Weibull distribution was accepted (figure 3).

**Goodness of Fit - Details** [hide]

**Weibull** [#59]

Kolmogorov-Smirnov

| | | | | | |
|---|---|---|---|---|---|
| Sample Size | 15 | | | | |
| Statistic | 0.12328 | | | | |
| P-Value | 0.95523 | | | | |
| Rank | 27 | | | | |
| α | 0.2 | 0.1 | 0.05 | 0.02 | 0.01 |
| Critical Value | 0.26588 | 0.30397 | 0.3376 | 0.37713 | 0.4042 |
| Reject? | No | No | No | No | No |

Figure 3. Kolmogorov-Smirnov Goodness-of-Fit Test

After the introduction of data into the Weibull 9 software program (figure 4), we calculated the parameters corresponding to the Weibull distribution by using the maximum likelihood estimation method. For the data resulted from the reliability testing of the tapered roller bearings, the two determined parameters have the following values: shape parameter β=2,679; scale parameter or characteristic life η= 1569.

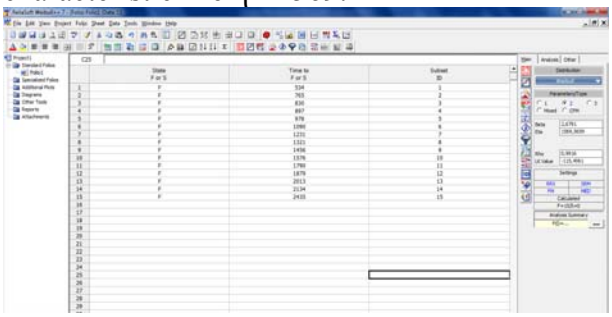

Figure 4. Introduction dates in Weibull 9 software

The basic reliability indicators followed during the reliability tests of the ball bearings are: B10 line, the mean operating time, the reliability function, the unreliability function, the failure rate, the probability density function [6]. Reliability/unreliability function is described in figure 5 and figure 6.

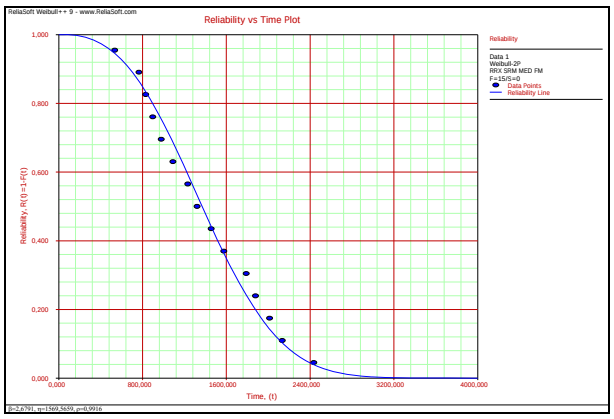


Figure 5. Reliability function

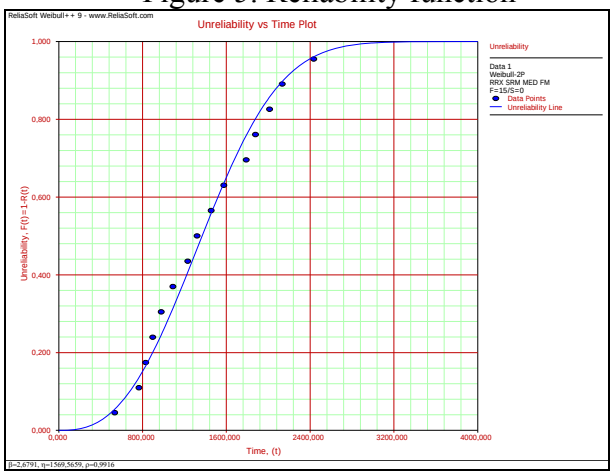


Figure 6. Unreliability function

Following is a plot of the probability density function - pdf 2D (figure 7) and 3D (figure 8) for our data, using the Weibull distribution.

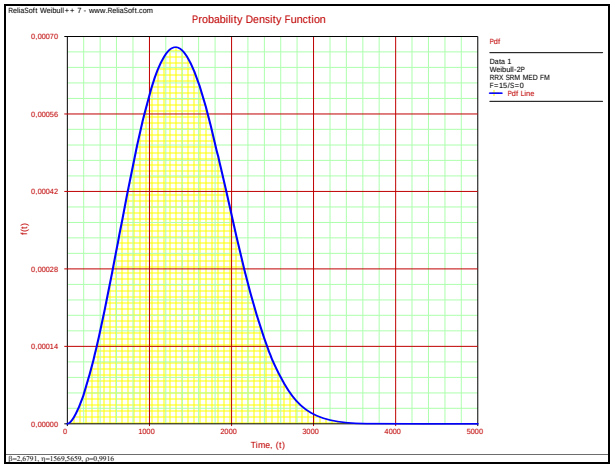


Figure 7. Probability density function

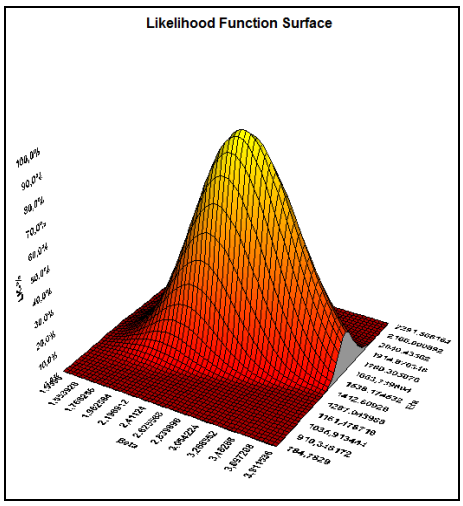


Figure 8. Probability density function – 3D

The number of failures per unit time that can be expected to occur for the tapered roller bearings is failure rate (figure 9).

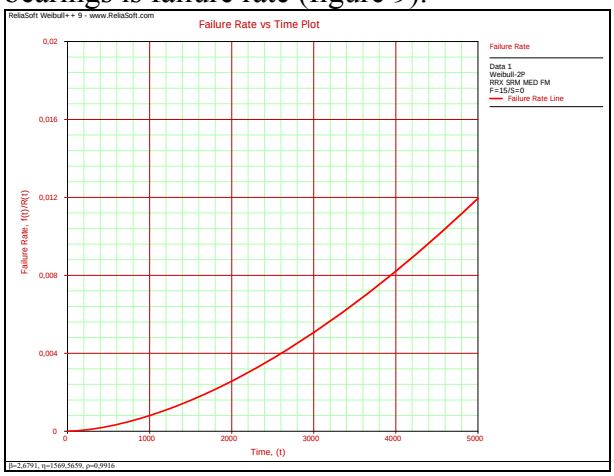


Figure 9. Failure rate plot

MeanLife (figure 10) is the average time that the tapered roller bearings in the data are expected to operate before failure.

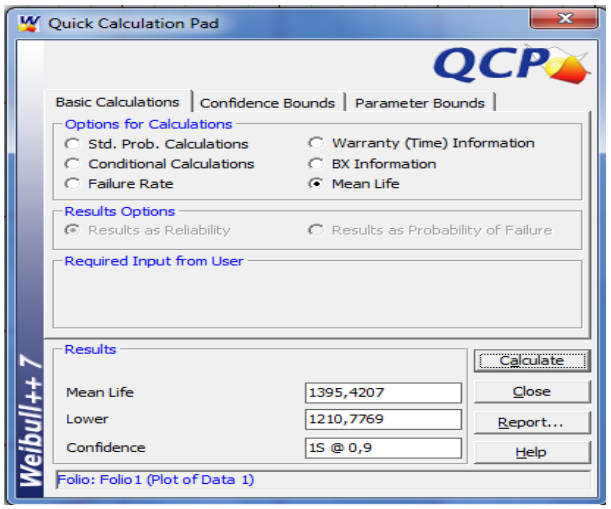


Figure 10. Fatigue life of tapered roller bearings

The BX (figure 11) is derived from the terminology used by bearing manufacturers, specifically the B10 life. B10 life refers to the time by which 10% of the bearings would fail.

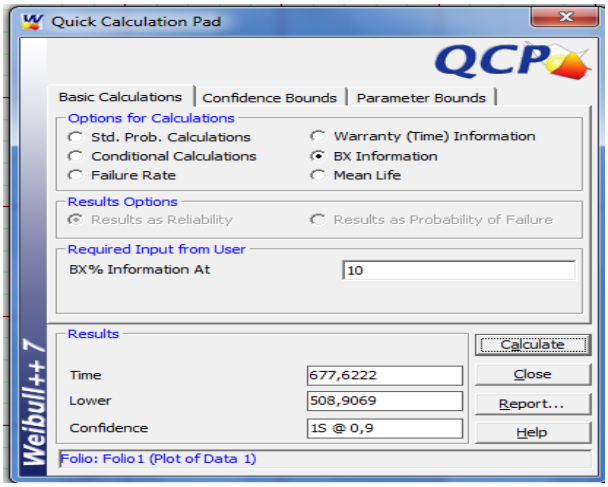


Figure 11. B10 life of tapered roller bearings

F/S Timeline plot (figure 12) displays the values for each failure and suspension of tapered roller bearings.

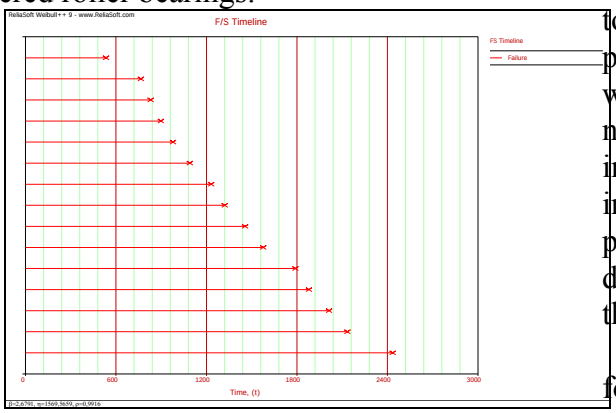


Figure 12. B10 life of tapered roller bearings

Histogram plot (figure 13) shows the number of failures/suspensions at a given time interval. Users can set the time interval at the control panel.

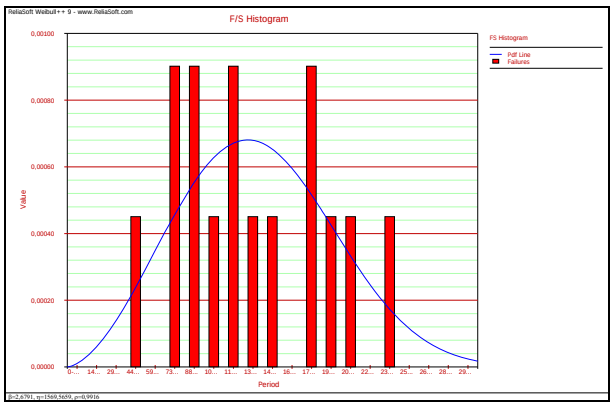


Figure 13. B10 life of tapered roller bearings

## 4. CONCLUSIONS & ACKNOWLEDGMENT

Many of the industrial products produced today for complex technical systems have very high reliability under normal use conditions. The main purpose of the reliability tests is to determine the reliability indicators for use level. The reliability tests have a great importance, aiming either to determine, either to check the reliability characteristic of a product, if this is established in a predictive way. The reliability tests are extremely necessary and they have a decisive role in improving the technical solutions and in increasing the performances. The essential problem of reliability tests is the testing duration, which is generally comparable with the product's useful lifetime.

We hereby aknowledge the structural founds project PRO-DD (POS-CCE, O.2.2.1., ID 123, SMIS 2637, ctr. No 11/2009) for providing the infrastructure used in this work.

## REFERENCES

1. http://www.ntnamericas.com/en/.
2. Zaharia, S.M., Martinescu, I., *Încercări de fiabilitate*, Editura Universită□ii Transilvania Bra□ov (2012).

3. Morariu, C.O., Zaharia, S.M. A New Method for Determining the Reliability Testing Period Using Weibull Distribution, Life time prediction using accelerated test data of the specimens from mechanical element, *Acta Polytechnica Hungarica,* 10 (7), 171-186.
4. Gafi□anu, M., *Rulmenti – Proiectare □i tehnologie*, Volumul 1, Editura Tehnică, Bucuresti (1985).
5 Changsen, W., *Analysis of Rolling Element Bearings*, Wiley (2005).
6. http://www.reliasoft.com/Weibull/index.htm

"HENRI COANDA"
AIR FORCE ACADEMY
ROMANIA

"GENERAL M.R. STEFANIK"
ARMED FORCES ACADEMY
SLOVAK REPUBLIC

INTERNATIONAL CONFERENCE of SCIENTIFIC PAPER
AFASES 2015
Brasov, 28-30 May 2015

# NOVEL POLYPROPYLENE-CLAY HYBRID MATERIALS FOR AUTOMOTIVE INDUSTRY. EFFECT OF THE COMPATIBILIZING AGENT

**Madalina Zanoaga*, Fulga Tanasa*, Raluca Darie***

*"Petru Poni" Institute of Macromolecular Chemistry, Iasi, Romania

***Abstract:*** *Novel polypropylene-clay (PP-clay) hybrid materials were prepared in preset ratios using an organically modified layered silicate, namely Cloisite® 20A, and maleic anhydride-grafted polypropylene (MA-g-PP) as compatibilizing agent. The compatibilizer was employed in order to obtain a better dispersion of the clay into the PP matrix, which was evidenced by the means of X-ray diffraction spectrometry (XRDS). The thermal stability of these new materials was assessed by thermal gravimetric analysis (TGA) and their rheological behavior was also investigated.*

***Keywords:*** *PP-clay nanocomposites, compatibilizer, characterization*

## 1. INTRODUCTION

Polymer nanocomposites, as hi-tech engineering materials, have attracted great attention due to their superior properties higher than those of conventional composites and comparable with those of metals. The effect of nanofillers on the polymer properties is different from what was predicted by classic thermodynamically studies for the reduced particle size fillers [1] and only using continuum mechanics it was possible to reveal that the properties of polymer nanocomposites are strongly dependent on the particular features of nanofiller (content, aspect ratio etc.) [2]. The automotive industry benefited of these advances (Fig. 1) since it used polymer nanocomposites to enhance the level of performance of their products (mechanical, thermal, electrical and chemical properties of various components) [3].

Polymer-clay nanocomposites are a special type of hybrid materials due to the fact that initially the filler is of micrometer dimensions, but allows nanocomposites with highly dispersed nanometric particles due to the strong interactions between the matrix and clay that occur during processing.

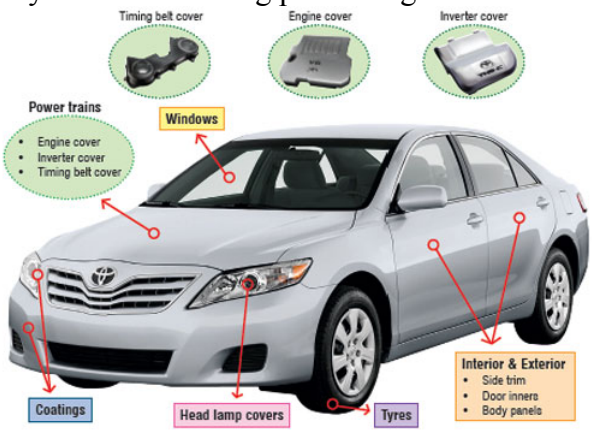


Fig. 1. Polymer nanocomposites in the automotive industry

This renders new materials improved properties as compared to initial polymers. As result of the good dispersion of the clay tactoids into the polymer matrix and the exfoliation of platelets, these new materials become lighter, have increased mechanical strength and scratching resistance, display flame retardancy properties, can be easily painted, and, in some cases, they can be recycled [4].

But for polymers with low polarity, such as polyolefin, the improvements are not always significant due to the very low compatibility between clays and polyolefin. Given the immiscible character of clays in relation to polyolefin, in general, and their particular layered structure, several approaches are to be considered in order to enhance the interfacial interactions between these components: (1) the use of organically modified clays to favor clays penetration among macromolecular chains [5,6]; (2) compatibilizing agents (functionalized oligomers) are employed due to their ability to form hydrogen bridges between the polymer matrix and the =O, -OH and/or -COOH groups of the silicate [6,7]; (3) appropriate processing – melt mixing was proven to be the most effective method in terms of thermoplastics; (4) combined approaches [8]. In common practice it is impossible to reach a wholly exfoliated morphology, due to various factors (*e. g.*, the secondary agglomeration of platelets as result of the electrostatic charges that can appear during processing), therefore, most of the nanocomposites have a mixed morphology where the exfoliation is preponderant as against intercalation.

Polypropylene (PP) is widely used for many applications due to its low cost, low density, high thermal stability and resistance to corrosion, and processability. The polypropylene-clays nanocomposites dis-played improved mechanical and barrier properties, flame retardant characteristics [9-11] as compared to raw PP.

This study focuses on novel PP-clay nanocomposites obtained by melt compounding and using MA-g-PP as compatibilizer in order to assess its effect on some properties of these new materials.

## 2. EXPERIMENTAL

**2.1 Materials.** The polypropylene used in experiments was an isotactic polypropylene (Malen-PF 401), a product supplied by Petrochemia Plock S.A. Poland. Polymer has a melt temperature of 170°C; decomposition temperature range 250–430°C, Vicat softening point 148°C; melt flow index (2.16 kg/230°C) 2.4–3.2 g/10min; volatile matter 0.3%wt.; isotactic index 95%.

Three different types of PP-g-MA (Crompton Corporation, USA) compatibilizers having different amounts of MA in their formulation were used, as follows: Polybond 3002 (0.2wt% MA) – C1, Polybond 3150 (0.5wt% MA) – C2, and Polybond 3200 (1.0wt% MA) – C3.

The organophilically modified clay Cloisite® 20A (Southern Clay, USA), assigned in this paper as C20A, was used as received. It was modified with a dimethyl dehydrogenated tallow quaternary ammonium salt where the anion was chloride ($Cl^-$). Particles size: 13μm (>90%); cationic exchange capacity: 95 meq/100 g clay; density: 1.77 g/cm$^3$; interlayer distance 2.10 nm.

The PP-clay nanocomposites were prepared by a two-step process. First, the compatibilizer was melt mixed with clay in a twin-screw extruder (HAAKE RHEOCORD 9000 mixer, $\Phi$=19 mm, L/$\Phi$=40, 200°C), in a preset ratio (90:10 wt%). The masterbatch samples were assigned as C1-C20A, C2-C20A and C3-C20A, respectively. In the second stage, the master-batch was melt mixed with neat PP (20:80 wt%) at 200°C. Thus, nanocomposites of PP/PP-*g*-MA/clay (2wt% clay) were obtained and the corresponding samples were assigned as PP-C1-C20A, PP-C2-C20A and PP-C3-C20A, respectively.

**2.2 Characterization.** The X-ray diffraction (XRD) measurements were run on a Bruker AD8 Advance X-ray diffractometer with Cu K$\alpha_1$ radiation, with a wavelength of 1.54 Å, operated at 40 mA and 40 kV. The XRD patterns were recorded in the range 2°-40° (2θ), at a scanning rate of 1°/min and the step interval was 0.02°. The interlayer spacing of the sample was derived from the peak position ($d_{001}$-reflection) in the XRD

diffractograms according to the Bragg equation ($\lambda = 2d\sin\theta$).

The thermal gravimetric (TG) analysis was performed on a Mettler Toledo TGA-SDTA 851 device, in air stream, with a heating speed of 10K/min, in the temperature range of 25-700°C, using samples of 4-6 mg.

The rheology study was performed on an Anton Paar rheometer equipped with CTD450, in plate-plate geometry, oscillatory mode, at a testing temperature of 200°C.

## 3. RESULTS AND DISCUSSION

**3.1 Morphology.** The changes of the interlayer distance in different polymer-clay hybrid materials can be estimated from XRD data by monitoring the position, shape and intensity of the basal reflections corresponding to the silicate layers. The intercalated morphologies are evidenced when the diffraction peak is shifted toward small angles, but the wholly exfoliated structures are confirmed when the XRD diffractograms no longer contain any diffraction peak of the clay.

In Fig. 2 are presented the XRD patterns of the master-batch samples C1,C2,C3-C20A (a) and the PP-clay nanocomposites (b), respectively.

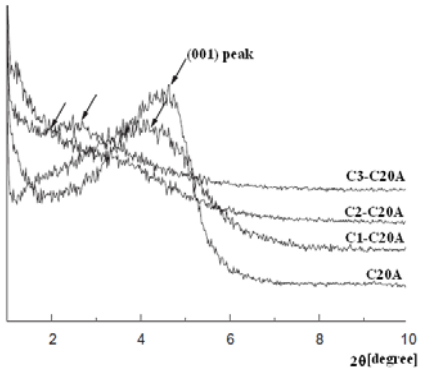


**a**

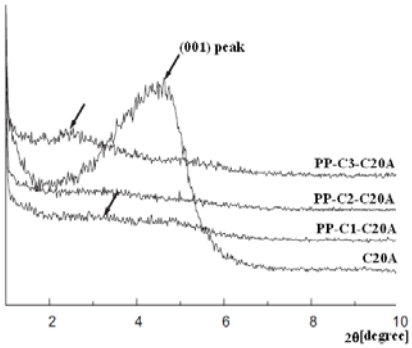


**b**

Fig. 2. XRD diffractograms of the master-batch (a) and nanocomposites (b) samples

The organically modified clay showed a distinct peak at 4.741, indicated in both images, but for the master-batch samples (Fig. 2a) the peaks position and intensity differ. The angle lowest value was obtained for the sample that contains 0.5wt% MA (C2-C20A, 1.95), which is an indication of an highly intercalated/exfoliated morphology. But the intensity of this peak is low compared to the one corresponding to the sample C1-C20A (4.160), which contains the lowest amount of MA (0.2wt%), this peak intensity being close to the pristine clay. As for the C3-C20A sample (1.0wt% MA), the peak position is intermediary (2.50), but the intensity is close to C2-C20A. This can be explained taking into consideration the various content of MA in the structure of the compatibilizing agent: the higher the amount of MA, the higher the degree of ramification of the polymer, the better dispersion of clay tactoids and polymer-clay intercalation/exfoliation.

All nanocomposite samples (Fig. 2b) showed peaks at lower values and of very low intensity, except for the sample PP-C2-C20A where no peak appeared. This clearly indicates that the clay tactoids and platelets are better dispersed, but when C2 (0.5wt% MA) was employed in the formulation; a complete

exfoliation seemed to occur. A higher content of MA (C3, 1.0wt%) favored a secondary aggregation of clay particles, since the sample displayed a rather significant peak, although the basal distance is still greater in comparison with the neat C20A.

**3.2 Thermal stability.** The thermal stability of hybrid materials is a key element in their processing, as well as applications. Therefore, it is necessary to study the thermal behavior and degradation mechanisms of polymer-clay nanocomposites, given the specific influence of the clay which acts as a thermal insulator: it reduces the diffusion of volatiles out of the matrix and renders the corresponding hybrids thermal and mass barrier properties [9].

In Fig. 3 are represented the curves corresponding to the pure PP and nanocomposites samples as obtained from the thermal gravimetric analysis (TGA).

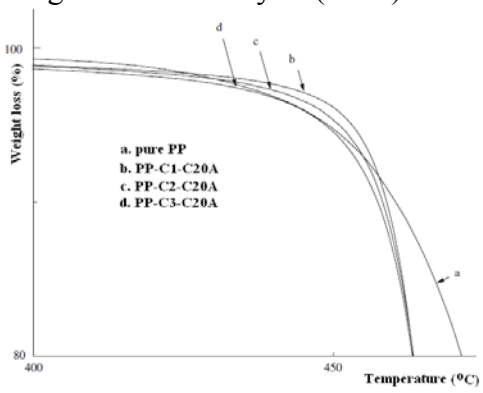


Fig. 3. TGA curves of nanocomposites samples as compared to neat PP

The first observation was the increase of the onset of degradation for all nanocomposites as compared to neat PP, which confirms the role of clay as thermal insulator and is consistent with literature data previously reported [6,13]. The weight losses of PP and its nanocomposites measured up to 250°C were found to be very small and correspond to the loss of water and some volatiles.

Assessing the influence of the compatibilizer on the thermal stability of hybrids, it is noticeable that the higher amount of MA has a negative effect on the samples thermal stability. The branching, that occurs subsequently to grafting, contributes to the clay dispersion, but, at the same time, it favors the thermal degradation of small chains and promotes the decomposition. Moreover, the thermal degradation of the organic modifier from the structure of the compatibilizers can be added to this phenomenon.

**3.3 Rheology.** The rheological properties of polymer-clay nanocomposites are related to their distortion or deformation. The rheological properties can be an indication of melt-processing behavior in certain procedures (*e. g.*, injection molding). Since the rheological characteristics of particulate suspensions are sensitive to the structure, particle size, shape, and surface features of the dispersed phase, the rheology studies potentially offer the means to assess the dispersion of nanocomposites in the molten state [14].

The shear viscosity of the considered nanocomposites samples as a function of the shear rate, at 200°C, as shown in Fig. 4.

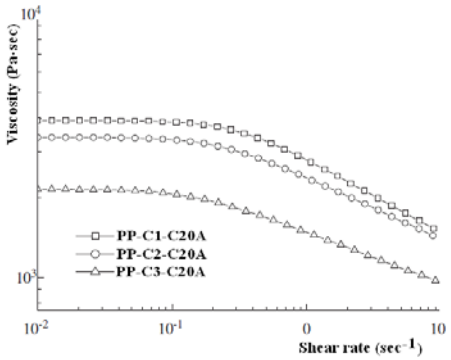


Fig. 4. The rheology data for the nanocomposites samples

It is noteworthy the significant decrease in shear viscosity, as a general trend for all studied nanocomposites. Considering the content of MA in compatibilizers as a criterion, it was concluded that a higher amount of MA entails a pronounced decrease in shear viscosity, as illustrated for sample PP-C3-C20A. Given the lower molecular weight of PP-*g*-MA compared to the neat PP, its shear viscosity is correspondingly lower. Thus, it enhances the general effect by adding a supplementary shear-thinning behavior [6]. Furthermore, some thermal and oxidative degradation secondary reactions may occur during melt processing which are also contributing to the overall effect.

Still, this specific behavior is a result of the preferential orientation of the clay tactoids and

platelets as well, effect enhanced by the presence of the compatibilizing agents.

## 4. CONCLUSIONS

Novel (PP-clay) hybrid materials were prepared using an organically modified layered silicate, namely Cloisite® 20A, and various compatibilizers (MA-*g*-PP with different content of MA) in order to investigate the effect of compatibilization on some properties of the nanocomposites.

The morphology study confirmed the improved dispersion of the clay into the PP matrix and the exfoliation of the clay platelets in the case of PP-C2-C20A (0.5 wt% MA). The higher amount of MA was proven to have negative effect on the thermal stability of the nanocomposites due to certain degradation processes, such as thermal and oxidative reactions, or secondary aggregation of the clay platelets. Nevertheless, the rheology study evidenced that PP-clay nanocomposites are allowed to simultaneously achieve higher moduli and improved processability if their formulation includes compatibilizing agents. Further investigation will aim to optimize the PP: compatibilizer: clay ratio, in relation to processing parameters.

## REFERENCES

1. Gacitua, W.E., Ballerini, A.A., Zhang, J. Polymer nanocomposites: synthetic and natural fillers, A review. *Ciencia technologia*. 7 (2005).
2. Sheng, N., Boyce, M.C., Parks, D.M., Rutledge, G.C., Abes, J.I., Cohen, R.E. Multiscale micromechanical modeling of polymer/clay nanocomposites and the effective clay particle. *Polymer*. 45 (2004).
3. http://nanowerk.com/spotlight/spotid=23934.php
4. Leaversuch, R. Nanocomposites Broaden Roles in Automotive, Barrier Packaging. *Plastics Technology Online*. Available at http://www.ptonline.com/articles/nanocomposites-broaden-roles-in-automotive-barrier-packaging (April 2014).
5. Lee, J.-H., Jung, D., Hong, C.-E., Rhee, K.Y., Advani, S.G. Properties of polyethylene-layered silicate nanocomposites prepared by melt intercalation with a PP-g-MA compatibilizer. *Composites Science and Technology*. 65 (2005).
6. Park, J.H., Lee, H.M., Chin, I.-J., Choi, H.J., Kim, H.K., Kang, W.G. Intercalated polypropylene/clay nanocomposite and its physical characteristics. *Journal of Physics and Chemistry of Solids.* 69 (2008).
7. Sanporean (Potârniche), C.G., Donescu, D., Vuluga, Z., Christiansen, J. D., Jensen, E. A., Paven, H. Compatibilizing agents influence on mechanical properties of PP/clay nanocomposites. *U.P.B. Sci. Bull., Series B*. 75 (2013).
8. Hwang, T.Y., Lee, S.M., Ahn, Y., Lee, J.W. Development of polypropylene-clay nanocomposite with supercritical $CO_2$ assisted twin screw extrusion. *Korea-Australia Rheology Journal*. 20 (2008).
9. Hasegawa, N., Kawasumi, M., Kato, M., Usuki, A. and Okada, A.. Preparation and Mechanical Properties of Polypropylene-Clay Hybrids using a Maleic Anhydride-Modified Polypropylene Oligomer, *Journal of Applied Polymer Science.* 67(1998).
10. Azza M. Mazrouaa. Polypropylene Nanocomposites, in Polypropylene, Fatih Dogan (Ed.), ISBN: 978-953-51-0636-4, InTech (2012). Available at:

http://www.intechopen.com/books/polypropylene/polypropylenenanocomposites (April 2015)
11. Gilman, J.W., Jackson, C.L., Morgan, A.B., Harris, R., Manias, E., Giannelis, E.P., Wuthenow, M., Hilton, D., Phillips, S.H. Flammability properties of polymer–layered silicate nanocomposites. Polypropylene and polystyrene nanocomposites. *Chemical Materials.* 12 (2000).
12. Gilman, J.W. Flammability and thermal stability studies of polymer layered-silicate (clay) nanocomposites. *Applied Clay Science.* 15 (1999).
13. Alexandre, M., Dubois, P. Polymer-layered silicate nanocomposites: preparation, properties and uses of a new class of materials. *Materials Science and Engineering: R: Reports*. 28 (2000).
14. Gu, S.-Y., Ren, J., Wang, Q.-F. Rheology of Poly(Propylene)/Clay Nanocomposites. *Journal of Applied Polymer ScienceI*. 91 (2004).

"HENRI COANDA"
AIR FORCE ACADEMY
ROMANIA

"GENERAL M.R. STEFANIK"
ARMED FORCES ACADEMY
SLOVAK REPUBLIC

INTERNATIONAL CONFERENCE of SCIENTIFIC PAPER
AFASES 2015
Brasov, 28-30 May 2015

# THE LIFE CYCLE AS AN OFFSHORE PIPELINE

**Timur Chis***

*Faculty of Applied Science and Engineering, Ovidius University, Constanta, Romania

***Abstract:*** *The life of offshore oil and gas pipeline, included different phases like: predesign (prefeasibility study), design, construction, commissioning, operation, maintenance, decommissioning and disposal (or abandonment). Each one of these actions may originate project and or specific activity. The jobs of offshore oil and gas pipeline is to transport oil, gas, water and biphasic products, for offshore oil fields to refinery and products exploitation, located to shore. This paper, provide information by the life and operation of offshore oil and gas pipeline, based to the optimization of engineering and economic activity.*

***Keywords:*** *offshore oil and gas pipelines, life cycle, environmental protection*

## 1. INTRODUCTION

In the feasibility studies of oil and gas pipelines, transport offshore products to shore industry is a very important activity of the offshore industry. Because the oil and gas price are variable depending of the market manufacturers want minimal investment in the offshore equipment. This tendency is justified by the reduction of time life of constructions as well as the reduction of the equivalent maximum investments period of production. In the period corresponding to the first phases (engineering, construction and start-up of transport in first years of oil and gas exploration) the total value of capital investments is higher the total income. The analysis assumes different perspectives in the mind term but specialty in the long term, when the control of the operating, production and maintenance costs of the plants is of fundamental importance to increase income and profit of offshore oil and gas pipelines. During the activity of oil and gas pipelines life the profitability of pipelines is function by the technical solutions during the engineering and purchasing stage. The selection of a better equipment and solution result a small investment in first stage but is necessary to investment in maintenance activity of platform. It's very important in this first stage to investment in environmental and security of oil and gas pipelines because every accident in environmental area is necessary to investment in activity of company (see to Oil platform accident in Houston, 2010 and Exxon Valdez accident) [1].

The Life Cost of oil and gas pipelines is a total sum of all cost sustained for the equipment beginning with purchase, throughout their life operation and up until the end of their service life. The problems in the defined life cost is to defined whit is time to operation the oil and gas pipelines for the structure of oil and gas exploration and production (the life of oil and gas pipelines is function by the oil and gas quantities, price of the oil and gas, the government legislation and

the price of maintenance). The choice of one or the other is a very significant impact of economic investments as it makes the determination of the operating costs difficult. In this paper is presenting the minimum investment policy of the life of oil and gas pipelines.

## 2. OIL AND GAS PIPELINES

The physical life of offshore oil and gas pipelines is averaging 20 to 40 years. The cost of offshore oil and gas pipelines is function by complexity (diameter, type of products transport, length, and type of the pipelines). The cost depends by the environment in which it operates the complexity of seabed or structures by oil and gas, the market condition and/or specific requirements of operator [2].

The environmental condition is:

- The seabed depth,
- The latter's lithological condition,
- The seismic characteristic of area,
- The marine meteorological condition.

The oil and gas exploitation condition conditioned the pipelines by the following elements:

- The life of oil and gas exploitations,
- The type of hydrocarbons (oil or gas or rich gas) and their composition (to possibility to transport in biphasic conditions),
- The weight and complexity of the topsides for processing oil and gas reserves,
- The need to continuously controlling oil and gas pipelines,
- The performances of oil and gas pipelines equipment's and corrosion preventions.

The market conditions and the specific inputs of the operating company is:

- Daily rate oil and gas transportation,
- The need to maintain a constant work load for national industries,
- A system to export production (eventually requirement for integrated storage),
- A price of oil and gas,
- Priority on time and cost of getting production started,
- A tendency by the companies to repeat and extrapolate known structural schemes and to use standard conditions.

Oil and gas offshore pipelines are used for:

-transport products from Jackets to Central Platform,

- transport water from Central Platform to fields for injection,

-transport biphasic products to shore facilities,

-transport oil and gas from platforms to shore facilities,

-transport oil from platforms to vessel from transportation and storage,

## 3. THE LIFE CYCLE OF OFFSHORE STRUCTURES

The life cycle of oil and gas pipelines can be broken down into following six main phases:

- Conceptual design,
- Outline design and feed,
- Detailed design,
- Construction, Installation and Commissioning,
- Operation, Production and Maintenance,
- Decommissioning and Disposal.

The Conceptual design (Feasibility Study), includes:

- Comparison of the major techniques of offshore oil and gas activity,
- Processing, delivery procurement, operation and support options,
- Cost benefits analysis for the conceptual design and alternative/optional,
- Safety and environmental activity and impact,
- Legal frameworks (International, Regional and Local Rules).

The Outline design and feet is function by Requirements Analysis, based to identification and examination of the technical solution and option for the facilities, processes and delivery to the preferred technical solution.

In the stage, detailed design is presented specifications for the equipment, process control and optimization of the offshore structures.

The Construction, Installation and Commissioning phase concerns the carrying out of the project's plan in order to perform the construction task, to install the plant and to build the operating structure to run.

The Operation, Production and Maintenance phase is the most extensive the life cycle.

The Decommissioning and Disposal phase in the last few years assumed an ever increasing importance. The OSPAR CONVENTION (Oslo-Paris, 1992) defined guidelines for the execution of all activities in this stage.

## 4. THE CONCEPT OF LIFE CYCLE COSTING

Evaluating the cost over the lifetime of an asset will provide the opportunities of improving the decision to performing the investments to create value. This is a very important to decide the investment function by price to the oil barrel.

Because the oil barrel price decreased since the last few year, and environmental and law is creasing the barrier to the major risk of oil and gas exploration, the maximum revenues to the investments is very difficult to defined and obtain.

In this case of improving the Concept of life costing, the companies are required to understand:

- The type of oil and gas pipelines that best suits for the exploitation of oil and gas field,
- The type equipment configuration of the terms related to Life Cycle Costs.

In the ISO/TC 67/WG 9 LIFE CYCLE COSTING, the differences between Life Cycle Cost and Life Cycle Costing:

- The Life Cycle Costing means a systematic analytic process where different alternatives are evaluated with the goal to find the best way to use scarce resources,
- The Life Cycle Cost means the consideration of all cost that are connected to procurement and ownership of a product over a defined period of the products lifetime.

The ISO Standard defined the Life Cycle Costing: "systematic consideration of all relevant cost and revenues associates with the acquisition and ownership of alternative options required to full an asset need. It is a iterative process of estimating, planning and monitoring cost and revenues differences throughout an asset's life. It is used to support the decision making process by evaluating alternative options and performing trade off studies. While the largest benefits can be achieved in the early project stages evaluating major configuration options, it is equally applicable to all stage of the life cycle and many levels of details".

Based to the ISO standards has been planned into the parts [1,2]:

- Methodology,
- Calculation methods,
- Project Implementation Guidelines.

In Part 1 of the Life Cycle Coasting process are this steeps [3]:

- Diagnostics and scoping,
- Data collection and structured breakdown of costs,
- Analysis and modeling,
- Reporting and decision.

## 5. THE CONCEPT OF LIFE CYCLE COSTING

The continuous decrease of oil price new technology and financial crises have forced the

Oil and Gas Industry to review the financial investments procedure, the production policies and the operations. The need for maximizing revenues across the asset's Life Cycle has shown that it is no longer possible to pursue the optimization of each phase of a life cycle.

## 6. CONCLUSIONS & ACKNOWLEDGMENT

The oil and gas offshore pipelines are the parts of investments to transport energy products from offshore fields to shore facilities. Because the oil price decreases in this moment, new investments are difficulty to implement.

In this case many company decided to modify the existent pipelines to new products.

## REFERENCES

1. ISO/TC 67/WG 9 LIFE CYCLE COSTING-ISO ASSOCIATION, (2007).
2. The Convention for the Protection of the marine Environment of the North-East Atlantic (1992).
3. T. Chis-Life cycle of Offshore System, SGEM, 2011,

"HENRI COANDA"
AIR FORCE ACADEMY
ROMANIA

"GENERAL M.R. STEFANIK"
ARMED FORCES ACADEMY
SLOVAK REPUBLIC

INTERNATIONAL CONFERENCE of SCIENTIFIC PAPER
AFASES 2015
Brasov, 28-30 May 2015

# INNOVATIVE POSSIBILITIES TO REPRESENT THE BAIA MARE URBAN SYSTEM SOILS POLLUTION WITH HEAVY METALS USING G.S. SURFER

**Bogdan Cioruța*, Mirela Coman****

*Faculty of Science, Technical University of Cluj-Napoca, Baia Mare, Romania, **Faculty of Engineering, Technical University of Cluj-Napoca, Baia Mare, Romania

***Abstract:*** *The mining activity, practices in Baia Mare has led to pollution and economic sealing of large areas of land; it has adversely affected the environment and now poses a significant risk to human health. The mining activities left over wide areas ponds, mine waste dumps and the undergroundwaters that come across the existing mine galleries springout contaminated and sometimes in an uncontrolled manner. Heavy metals are present in the environmental factors from this area and significantly affect local ecosystems and human health. This paper proposes to use the G.S. Surfer software in analyzing the concentration variations of the heavy metals recorded in Baia Mare urban system soils in order to present the real situation of the mining activity and the degree of historical pollution of the studied area. There are presented the preliminary results obtained from investigation of the pollution degree made by heavy metals such as arsenic, copper, iron, lead and zinc in the area with a long metallurgical activity; the analysis performed established that the soil of the studied area is worst polluted with concentrations that are higher than the normal values admitted by the Romanian laws. Also from the 2D and 3D pollution graphics is reflected an accumulation of heavy metals in soils especially during the last 30-50 years correlated with depth. So the G.S. Surfer pollution models have a special ecological and technical implication, ensuring the knowledge of the pollutants behavior in soil.*

***Keywords:*** *mining activities, heavy metals, historical polluted soils, G.S. Surfer*

## 1. INTRODUCTION

Baia Mare urban system is an area of contact between the Someş Platform and The Eastern Carpathians, on the southern side of the eruptive Neocene Gutâi and □ibleş. These massive mountains of volcanic rocks are made up of goldsilver ores and nonferrous metals such as lead, zinc, copper etc [1].

The mining activity, practices in Baia Mare, for over 150 years as the main activity over the centuries, has led to pollution and economic sealing of large areas of land - most mining perimeters today being in storage; it has adversely affected the environment and now poses a significant risk to human health.

The mining activities left over wide areas ponds, mine waste dumps and the undergroundwaters that come across the existing mine galleries springout contaminated and sometimes in an uncontrolled manner [1].

The Industrial and mining activities have been recognized as the major sources of soil heavy metal contamination [6].

Heavy metals are present in the environmental factors from this area and significantly affect local ecosystems and human health [2].

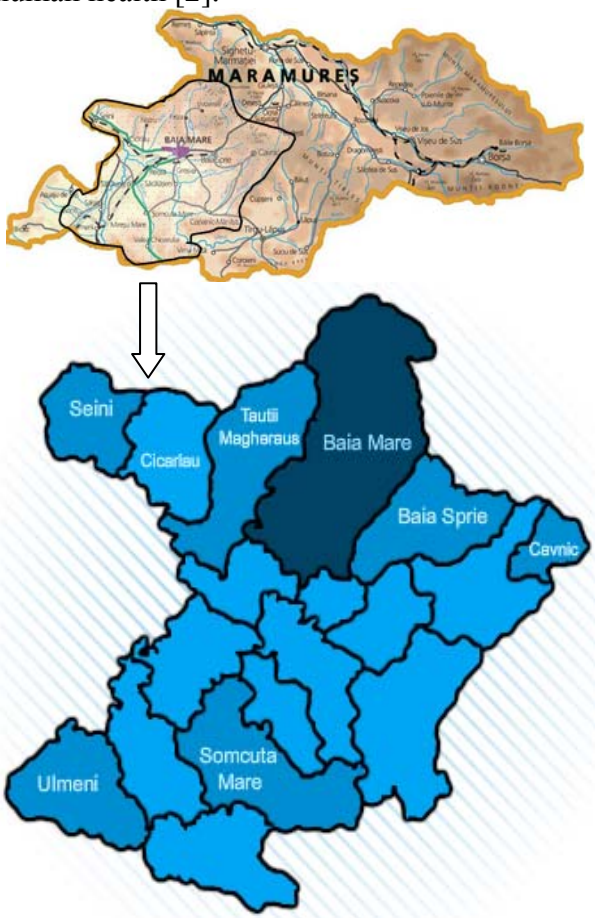


Fig. 1. The position of Baia Mare urban system in Maramure□ County [8]

The paper presents details on soil pollution with heavy metals, problem that has gradually found a solution in the environmental rehabilitation projects, activities that requiring investment of time and specialists in this field.

This paper proposes to use the G.S. Surfer 9.0 software [3] in analyzing the concentration variations of heavy metals recorded in Baia Mare's urban system soils, the spatial distribution of the contamination level and ecological risk, in order to present the real situation of the mining activity and the degree of historical pollution in the studied area [2].

There are presented preliminary results (Fig. 9-12), in form of 2D and 3D representations, obtained from investigation of the pollution degree made by heavy metals ions especially in the area with a long metallurgical activity.

The analyses performed established that the soil of the studied area is worst polluted with As, Co, Cu, Ni, Pb, Zn and many others, with concentrations that are higher than the normal values admitted by the Romanian law in the 0-20 and 20-40 cm depth interval [4]. Also is reflected an accumulation of heavy metals in soils, especially during the last 30 years, correlated with depth.

## 2. BAIA MARE DEPRESION - CURRENT STATUS OF POLLUTION ACTIVITIES

In Baia Mare Depression were identified 7 classes of soils and 13 soil types [6], with different weights depending on the type of use (table 1). The quality of soil has been affected over time primarily through mining activities, ore preparation and nonferrous iron metallurgy. The mining activities have generated large areas ponds and mine waste dumps and as a consequence, when the underground waters cross the existing mine galleries spring up contaminated and often in an uncontrolled manner. These facts led to the estimation that an area of approx. 25 000 ha is polluted with heavy metals (lead, copper, zinc, cadmium, nickel, cobalt, manganese, chromium) [1].

Table 1. Classes and soil types in Baia Mare Depression [1]

| Soil use type | Class and soil type | Area (Ha) |
|---|---|---|
| Forest soil | Cambisoils (eutricambisol, districambisol) | 25220.3 |
| | Luvisoils (preluvosol, luvosol, luvosol Albic) | 13519 |
| | Spodisoils (prepodsoluri) | 631.9 |
| | Cernisoils (rendzinic) | 383.2 |
| | Protisoils (litosol, aluviosol) | 64.1 |
| | Pelisoils (pelosol) | 9.3 |
| | **Total forest land** | **39827.8** |
| Agricultural soil | Hidrisoils (gley, stagnosol) | 15728 |
| | Luvisoils (luvosol, preluvosol) | 14175 |
| | Protisoils (aluviosol, regosol) | 13283 |
| | Cambisoils (eutricambisol) | 1054 |
| | **Total agricultural land** | **44240** |

The degree of intensity of heavy metal pollution of this area is shown in table 2. On territory of Baia Mare Depress ion have been built 6 tailing ponds and 55 waste dumps [5]. In terms of perimeter distribution of the metal extraction and processing of Baia Mare Depression, the areas where these dumps have formed are considered "hot spots", spots that exist even in the Baia Mare city.

Table 2. Fields polluted with heavy metals (Source:Report 2012, EPA Maramureş)

| Total | Areas affected by pollution with heavy metals | From which | | | |
|---|---|---|---|---|---|
| | | weak | moderately | strong | excessive |
| Ha | 25 140 | 15310 | 4910 | 2500 | 2420 |
| % | 100 | 61.00 | 19.50 | 9.90 | 9.60 |

Among the physical characteristics of soils from sites studied for the present project were pursued: soil texture in the upper horizon, degree of compaction (DC, % v/v), hydraulic conductivity (HC, mm/h), resistance to penetration (RP, kgf/cm$^2$) for several layers: 0-25 cm, 25-35 cm and 35-50 cm.

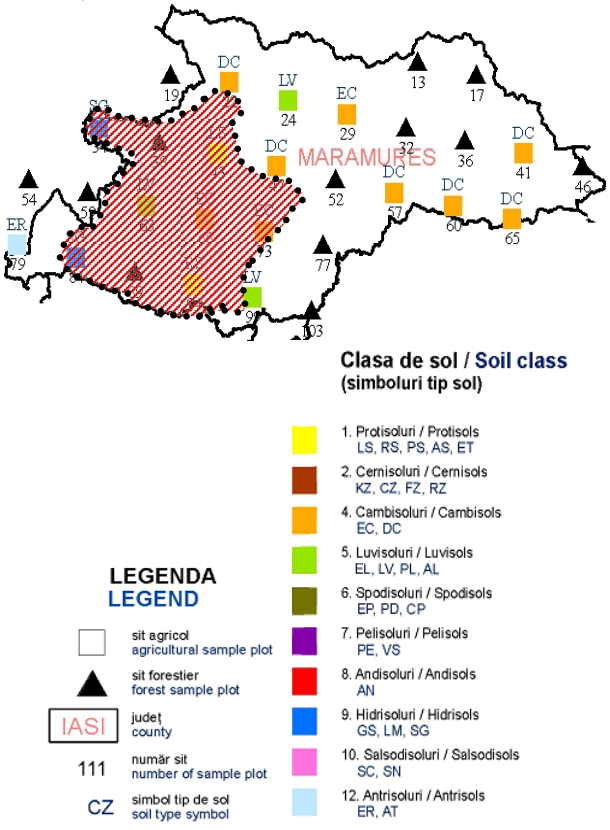


Fig. 2. Maramure county soil classes [9]

Texture or composition of the mineral part of the soil particle size is defined by the percentage of various fine mineral fractions, mainly sand, dust, clay, size and specific properties.

Depending on the dominance of a component are set textural classes and subclasses. In practice, currently, soils are grouped into five major classes.

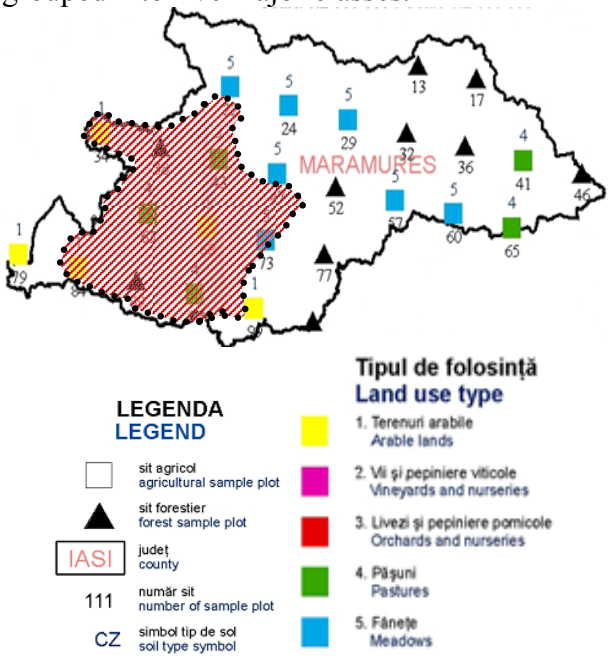


Fig. 3. Maramure county land use types [9]

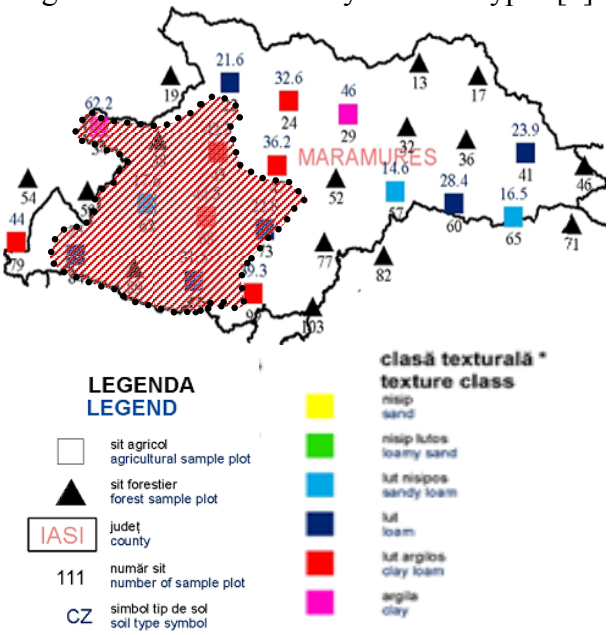


Fig. 4. The texture in the upper horizon for Maramures county soils [9]

The degree of compaction, hydraulic conductivity and resistance to penetration is determined in layers 0-25 cm, 25-35 cm 35-50 cm and shown in the following.

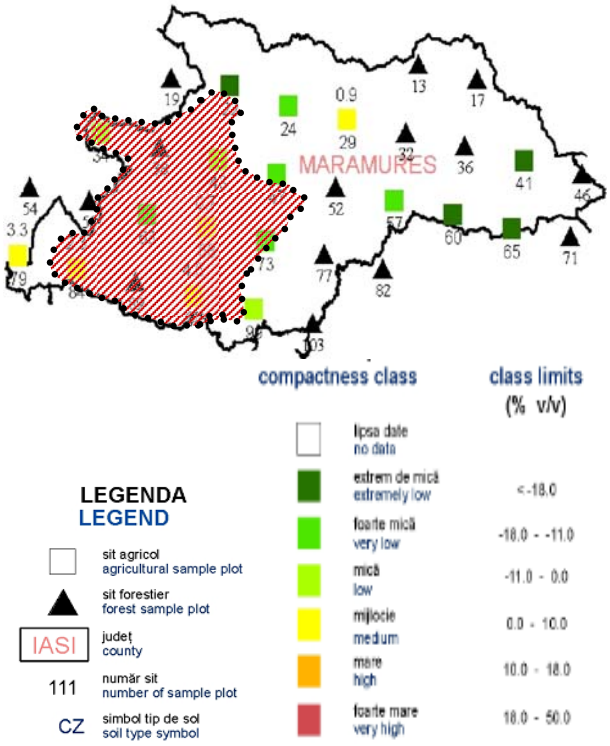


Fig. 5. The degree of compaction for Maramures county soils (0-25 cm) [9]

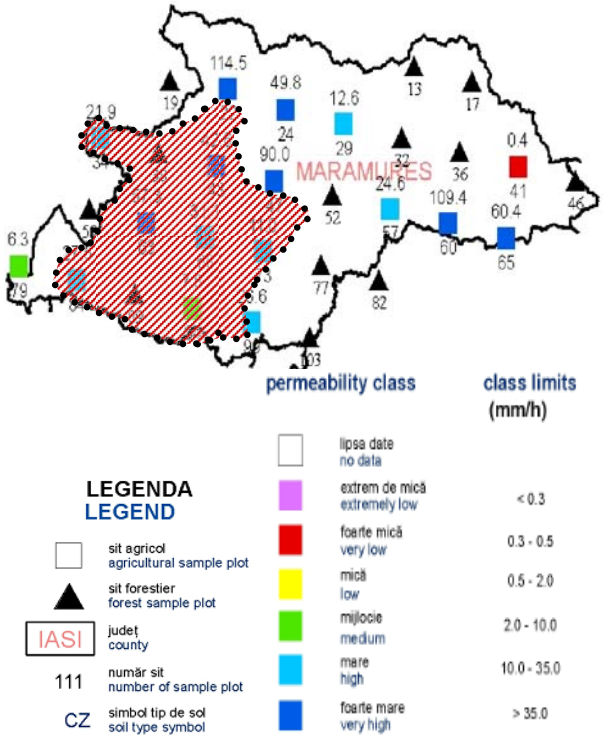


Fig. 6. The hydraulic conductivity for Maramures county soils (0-25 cm) [9]

## 3. MATERIAL AND METHODS

The soil is a dynamic system where short-term fluctuations occur, such as variations in humidity and pH levels, in redox conditions; it is also the place where the organic matter gradually decomposes as a consequence of changes in nature [5].

Through field and laboratory tests, soils can be characterized from a physical, chemical and biological perspective.

The total metal content of soils is the result of varied metal input – parental material, atmospheric deposits, chemical fertilizers and improvements, organic fertilizers and other organic and inorganic polluting substances – minus metal output resulted from cropping or from leaching and volatilisation [6].

Problems generated by soil contaminations with different pollutant substances have recently interested more and more researchers worldwide. Nowadays, one of the major problems of environment in industry is the historical pollution. It has dramatically consequences on the environment, especially on the ecosystems and regarding life quality and health of the peoples living in or near the affected areas [5].

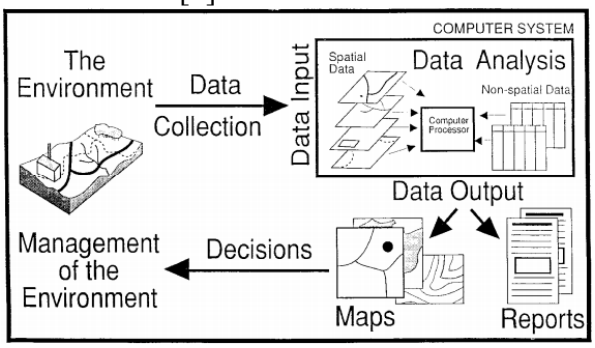


Fig. 7. The methodology for studying the heavy metals concentration in soils [5]

At the onset and maintenance of pollution effects due to industrial emissions, a special role has the combinations of heavy metals with soil strata. In this area, the processing activities of metal concentrates carried over the last years led to pollution of great-seed surfaces of terrain and adversely affected the environment and the quality of life [6].

The accumulation of heavy metals (Zn, Pb, Cr, Mn, Fe, Cu, Cd, As) in soils has a special ecological implication because of their toxicity and their compounds, but also because of the

form of the chemical bindings which affect the soil reaction. Ensuring the protection of soil quality, as a mean to enhance soil resources and the environmental protection, foresees, among other things the use of remediation methods and the technologies designed to neutralize or block the flow of pollutants required to ensure the desired efficiency and enforcement of laws regarding soil quality protection.

Soil sampling procedures from the research area were conducted according to Order 184/1997 [7]. The soil samples were gathered from different depths depending on the vegetation of the respective soil: 0-20 cm for arable land and grass, 20-40 cm for orchards and vineyards. For each material studied, we used the specific methods mentioned in our literature and complied with the experimental parameters and requirements of our study procedures.

The analytical data referring to the content of heavy metals in the studied soil revealed a wide variation of heavy metals contents. The concentration of heavy metals determined at the assays from Baia Mare area were compared with the average value of the normal contents with the maximum allowable values and with the values of the warning threshold and intervention one, for soil less sensible according to Order 756/1997 [4] law regarding soil quality protection and volatilisation.

Surfer software, registered as a trademark of Golden Software Inc., is a powerful contouring, gridding and surface mapping program for scientists, hydrologists, engineers, geologists, archeologists, oceanographers, biologists, foresters, geophysicists, medical researchers, climatologists, educators, students or anyone who needs to generate maps quickly and easily [3].

## 4. RESULTS AND DISCUSSIONS

Expansion of cultivated areas, intensification of agricultural production, irrational exploitation of forests, industrialization, urbanization etc are all causes of soil no longer be able to fulfill, in part or in full, its basic functions.

Currently soil is subjected to a wide range of impacts increasingly becoming more intense, causing or intensifying its quality harmful phenomena and processes, including erosion, salinisation, acidification and alkalinization or nutritional disequilibrium. All these phenomena constitutes land degradation meaning the whole range of harmful soil processes and phenomena, if we refer to the introduction in the soil or land of substances or energy characteristics that can cause changes in its physical, chemical or biological, affecting current or future use of it.

Although the soil pollution is an old phenomenon, closely linked to many human activities conducted throughout the different stages of the development of civilization, because of the problems involved at present it require special attention and management.

The indicators, that were considered, were determined in accordance with the analysis standards in force, and the obtained values have been reported to the values from Order no. 756/1997 - Annex no.1, for soils use.

In terms of legislation in force concerning the methods for determining the specific toxic pollutants from soil, the metals are determined by atomic absorption spectrophotometry, in accordance with the standard analysis ISO 11047-1999 - the total form and the values were reported at the values specified in the Order no. 756/1997 [4]. For the present paper we consider the case of the soil pollution with Cu, Pb, Zn, Mn.

In soils, the natural copper content may be 20 mg/kg of dry matter; for the Baia Mare depresion case were established about 4500 ha of land with higher copper content of 300 mg/kg and 15500 ha with a content between 100 - 300 mg/kg.

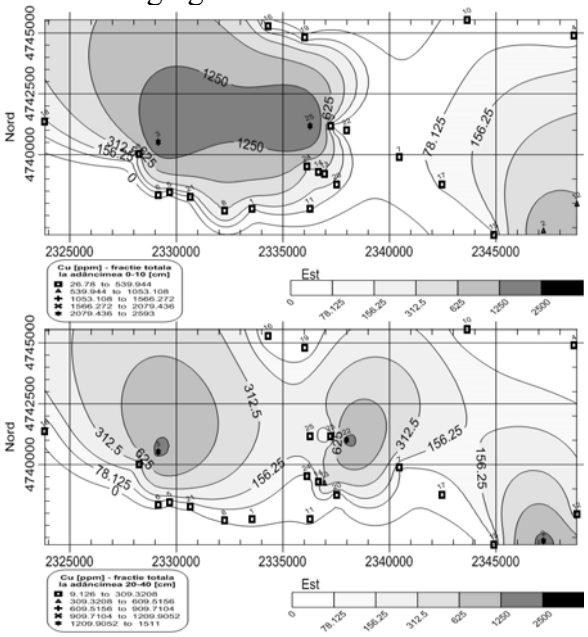


Fig. 8. The soils pollution with copper (Cu) in Baia Mare urban system

In soils lead falls can be reached by air or contaminated landfill (waste mining, metallurgy) being circulated by air or by water runoff from rainfall.

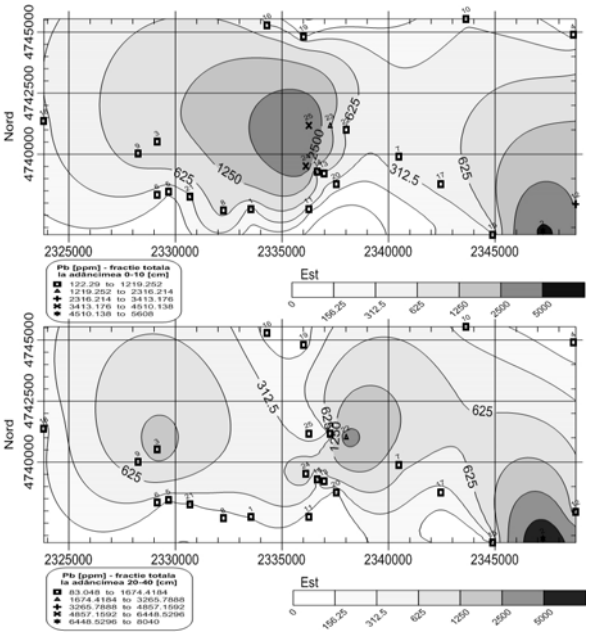


Fig. 9. The soils pollution with lead (Pb) in Baia Mare urban system

## 5. CONCLUSIONS

Current state of soil pollution inside Baia Mare area - is the result of 150 years of processing different heavy metals concentrates especially lead and zinc. The used technologies have excessively polluted the environment and affected the human health.

The concentration levels with heavy metals in uncontaminated dry soil mentioned in literature are: chrome 50 mg/kg, copper 12 mg/kg, lead 526 mg/kg, magnesium 450 mg/kg, cadmium 0,4 mg/kg, zinc 40 mg/kg.

As a result, environmental agencies are placed in charge in remediating, monitoring and mitigating the soil contamination sites. According to actual trend, Surfer software is used to monitoring the metal contaminants in the soil horizons, so the G.S. Surfer pollution models have a special ecological and technical implication.

## REFERENCES

[1]. Coman M., Oros V., Fălău B., Pop R., (2010) *Soil Pollution with Heavy Metals - Specific Issues for Baia Mare Area*, ProEnvironment 3, 29-32

[2]. Yang G., Chaofeng S., Meiting J., (2014) *Heavy Metal Contamination Assessment and Partition for Industrial and Mining Gathering Areas*, IJERPH, 11, 7286–7303

[3]. ***,www.goldensoftware.com

[4]. Order 756/1997 - approve the regulation of environmental pollution assessment

[5]. Coman M. (2006) *Depresiunea Baia Mare – Protecția mediului din perspectiva dezvoltării durabile*, Ed. Risoprint, Cluj-Napoca

[6]. Fodor D. (2001) *Impactul industriei miniere asupra mediului*, Ed. Infomin, Deva

[7]. Order 184/1997 - soil sampling procedures

[8]. www.subm.ro/SUBM.html

[9]. www.unibuc.ro/Monitoring_sol_2011.pdf

"HENRI COANDA"
AIR FORCE ACADEMY
ROMANIA

"GENERAL M.R. STEFANIK"
ARMED FORCES ACADEMY
SLOVAK REPUBLIC

INTERNATIONAL CONFERENCE of SCIENTIFIC PAPER
AFASES 2015
Brasov, 28-30 May 2015

# CONSIDERATIONS REGARDING THE SOIL POLLUTION WITH OIL PRODUCTS IN SĂCEL - MARAMUREŞ

**Marcela Hreniuc*, Mirela Coman*, Bogdan Cioruța****

*Faculty of Engineering, Technical University of Cluj-Napoca, Baia Mare, Romania, **Faculty of Science, Technical University of Cluj-Napoca, Baia Mare, Romania

***Abstract:*** *Extraction and transport of crude oil by developing environmentally friendly processes both themselves and by some unwanted accidents, such as discharges from tanks, underground or above ground pipe breakages, etc. The phenomenon of environmental pollution produced fluids from wells (oil, gas, condensate, salt water, sludge, sand) occurred with the start of oil exploitation and use as an energy source. Problems of environmental pollution by hydrocarbons has recently become more and more relevant. Each year brings us the increasing number of hydrocarbons' sources in the environment as well as innovative solutions to this problems. For the present paper the results of the given studies, established in database, come to bring to the attention of the interested public a clear image of the actual situation of the state of soil contamination with petroleum products.*

***Keywords:*** *cross-border project, oil products, contaminated sites, pollution management*

## 1. INTRODUCTION

Problems of environmental pollution by hydrocarbons has recently become more and more relevant, due to the high cost of work during the use of mechanical, physical, chemical and thermal methods of cleaning, as well as their limited capabilities. In addition, each year brings us the increasing number of hydrocarbons' sources in the environment [2].

Their list includes almost all automobile enterprises, pipelines, petrochemical and oil and gas company industry. Accidents associated with the release of hydrocarbons occur as a result of equipment failure (usually electrochemical corrosion and biological) and unauthorized entry into pipelines [3].

During the construction of the wells potential pollutants include: oil-well drilling fluids and solutions; drilling waste water and drill cuttings; reservoir fluids; fuel and lubricants and other waste building wells.

These effects are seen various components of the environment, including species, formation water, groundwater, soil and surface water.

Consequently, there is a gradual filtering pollution component of the environment.

The sources of soil's contamination within Maramure region are:

- oil and gas production refineries or facilities and different objects of oil and gas production;
- compressor stations;
- gas distribution stations and points;
- automobile company;
- gas and oil stations;
- aviation company, rail and enterprise.

The results of the given studies established in database [1,3], showing the pollution of soils by oil products in Maramure region and conducted peer review of possible levels of soil contamination due to the sources with oil activity [4].

The greatest likelihood of soil's contamination with oil products within the given area are: refineries, pipelines and pumping stations [3].

In areas along the oil fields and pipelines, ground and surface waters are being contaminated by oil products and related toxic substances that bring soil to environmentally critical ecosystems.

The oil and oil products along with pesticides internationally recognized priority pollutants. Their negative effect on soil and vegetation, air, surface and ground water, ecological systems and human health observed at all stages of the industrial use of these products from refining, storage, transportation and elimination of equipment [3].

## 2. THE ACTUAL STATE OF SOILS IN MARAMURE COUNTY

One of the recipients of oil pollution is soil. The contamination of soil is closely associated with increased negative impact of pollutants on vegetation and fauna. The oil and gas pollution is caused the powerful negative impact from various chemicals and highly wastewater.

The main reason for the ecological situation's aggravation in the areas of enterprise production and refining of oil spills are a result of the technical facilities and equipment wear and tear as a result of emergencies, and the soil quality in the respectively region.

Thus, reduction of anthropogenic impact on the environment is achieved by a complex – as prevention measures emergency situations and the modern methods of response, which firstly differ under the soil classes and land use type, and secondly after the following atributes:

- average annual temperature and rainfall - indirect factor;
- gleyzation and pseudo-gleyzation;
- salinization / alkalinization;
- texture, slope and landslides;
- total porosity compaction or restrictive horizon;
- humus reserve;
- $CaCO_3$ content;
- the reaction (pH), debazification;
- excess moisture from the surface.

Regarding Maramures county, but especially the Săcel, below shows some of the most important characteristics of soils that determine one way or the other emphasizing pollution or printing a key environmental behavior change.

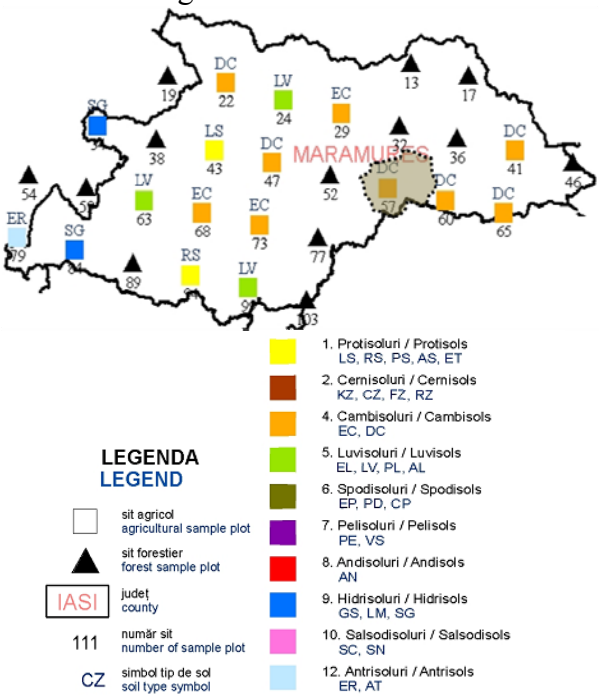


Fig. 1. The representation of the Maramures soil classes [7]

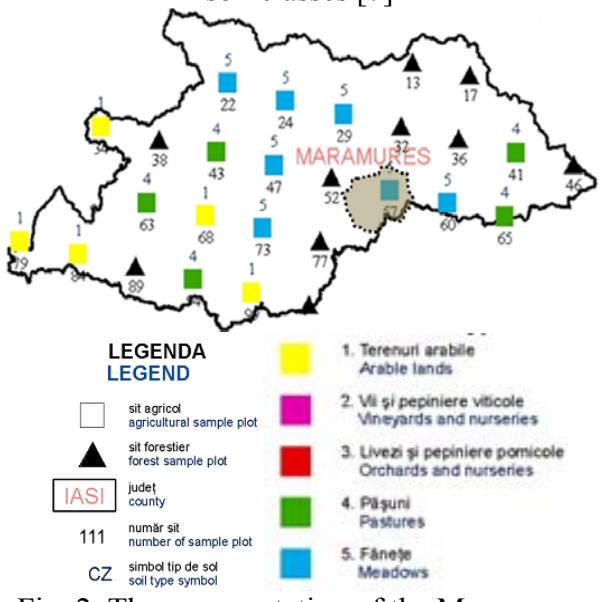


Fig. 2. The representation of the Maramures land use type [7]

## 3. MIGRATION AND BEHAVIOUR OF OIL PRODUCTS POLLUTANTS IN SOILS FROM SĂCEL - MARAMURE□

**3.1. General aspects of migration and behavior of oil pollutants in soil.** Following the physical configuration of the underground is found that the surface soil pollution produced in one area generates system-wide risks. Thus, if an area contaminated by the discharge of a pollutant oil, more or less viscous, the migration of pollutants from surface to depth is likely to be affected aquifer, and vice versa.

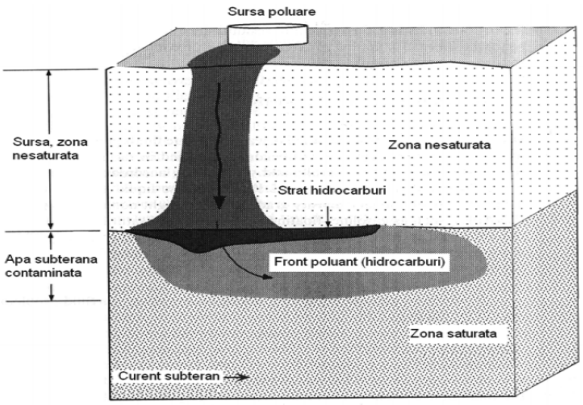


Fig. 3 Scheme of oil pollutants migration

If a contaminated aquifer through a borehole depth, for example, as by vaporization and the capillary rise of water contaminated is likely to be contaminated ground. This type of connection is evident in any other environment components, but each medium presents peculiarities of diagnosis, monitoring and treatment.

**3.2. Aspects of migration and behavior of oil pollutants in Săcel area soils.** Regarding the migration of pollutants in the underground's correspondence stands visible from one activity to another, so that even if oil exploration activity pollutant behavior remains the same.

In the county of Maramures presented below are images where possible migration of pollutants from the unsaturated zone to the saturated zone.

Fig. 4 Physical migration forms of oil products pollutants in Săcel soils

The discharge of a pollutant oil in a field immediately lead to the formation of unsaturated soil zone of a body soak. Its shape and penetration depth will be controlled by convection phenomena and specific pollutant dispersion and adsorption capacity and soil biological activity.

The direction and speed of the pollutant will mainly depend on its viscosity, the morphology of the land and soil permeability and aquifer rocks roof.

Fig.5 Soil profile from Săcel area

The main force acting on the pollutant in this area is gravity. Therefore, if the soil is slightly permeable soil pollutant infiltrate predominantly by a vertical component. Also, there will be a side impregnation of the pollutant more or less obvious due to its dispersion. Advancing to the aquifer, soil horizons pollutant meets physicochemical and biological properties different, so the different possibilities of absorption and biodegradation. As a result, the pollutant will be partially filtered by soil particles, partly absorbed volatilized and biodegraded in a greater or lesser extent.

The presence of impermeable barriers in the unsaturated zone can divert or halt the migration of pollutants to the saturated zone.

A not insignificant aspect is that the storm water pollutants can detach retaining matrix involving them into shallow groundwater. Because of this mathematical modeling of pollutants in soil full migration is difficult and requires remediation practice, together with mathematical models of dispersion and empirical methods to estimate the following parameters:

- impregnation body shape pollutants;
- the maximum depth of penetration of pollutants;
- the volume of pollutants retained in the unsaturated zone;
- the time required to reach the aquifer pollution.

Laboratory research conducted to estimate the behavior of pollutants in soil in the unsaturated zone, reduce the number of variables in the field.

The research conducted by EPA Baia Mare [5] analyzed the percentage by volume of hydrocarbons retained sand, depending on the mean diameter and size distribution thereof.

For other textural fractions (clay, loam) modest results are expressed:

- research conducted for evidence of oil pollutants ability to be retained in the soil make available a series of coefficients valid only in dry soils;

Fig.6 Laboratory investigations on polluted soils from Săcel area

- concret situations of land or soils with varying degrees of moisture and land use are proposed reduction percentages depending on the physical and geographical concrete and vegetation;
- research conducted to estimate the time of transfer of oil pollutants in the unsaturated zone to the saturated zone established as a standard water permeability of the soil type for which the experimenter; a series of spreads come closer then proposed model so diverse situations on the ground.

## 4. CONCLUSIONS

Based on data obtained from both the light field measurements and observations made and through other reliable sources of information (EPA Maramures [5], OSPA Maramures [6], Maramures County Council) we noticed that the quality status of soil resources from the County Maramures is a little known and publicized, at least in the eyes inventory and mapping of sites potentially contaminated with petroleum products.

Among the physical characteristics of soils from sites studied for the present project were pursued: soil texture in the upper horizon and the horizon intermediate structural instability index, the degree of compaction, saturated hydraulic conductivity, penetration resistance and edaphic volume.

These elements were helpful in discerning the extent to which soil is polluted or not /

contaminated with hazardous substances or wastes which can to a disease that is subject to the population or the occurrence of undesirable effects in the environmental factors.

Aware of the fact that the extraction and transport of crude oil - research objective pursued during the project - both by developing environmentally friendly processes themselves, and by some unwanted accidents, such as discharges from tanks, underground or aboveground piping burglary etc, I tried to perceive the phenomenon of environmental pollution produced fluids from wells (oil, gas, condensate, brine, sludge, sand) in a completely different way.

Therefore extrapolation to research in other fields we used the specific applications of new information and communication technologies, including mobile technology in data acquisition and field observations.

## REFERENCES

1. Cioru□a B., (2014) *Cercetări aplicative în domeniul Informaticii Mediului. Proiectul RoUaSoil*, (lucrare de diserta□ie), CUN Baia Mare
2. Coman M., Dăscălescu A., Cioru□a B., (2014) *Buletin informativ privind starea de calitate a solurilor din jude□ul Maramure□*, proiectul RoUaSoil, CUN Baia Mare
3. Coman M., Cioru□a B., Dăscălescu A., (2014) *Manual privind depoluarea □i fertilizarea solurilor poluate cu produse petroliere*, proiectul RoUaSoil, Baia Mare
4. Coman M., Dăscălescu A., (2013) *Regarding Romania-Ukraine cross-border management of contaminated sites with oil products*, Scienrific Papers series E - Land Reclamation, Earth Oservation & Surveying, Environmental Engineering, vol. II, pg. 123-126, ISSN 2285-6064
5. ***Agenția pentru Protecția Mediului Maramureş - http://apmmm.anpm.ro
6. ***Colec□ia de Studii ICPA, Oficiul de Studii Pedologice □i Agrochimice, 2013 - Maramure□
7. www.unibuc.ro/Monitoring_sol.pdf

# ENGINEERING SCIENCES

"HENRI COANDA"
AIR FORCE ACADEMY
ROMANIA

"GENERAL M.R. STEFANIK"
ARMED FORCES ACADEMY
SLOVAK REPUBLIC

INTERNATIONAL CONFERENCE of SCIENTIFIC PAPER
AFASES 2015
Brasov, 28-30 May 2015

# SOME PATTERNS OF APPLICATION OF FMEA METHOD FOR STUDYING THE QUALITY OF A PRODUCT

**Raluca Nicolae (Mănescu)*, Anişor Nedelcu***

*Manufacturing Engineering Department, Transilvania University of Brasov, Romania

***Abstract:*** *In the front is intended as FMEA method to ensure a process for ensuring quality in industrial projects, which may apply to products and manufacturing process, through recognition of failure, issues/their effects, as well as the likelihood of their occurrence in order to reduce the substantial failure as well as the consequences thereof. The article will look like the following: to establish the potential of failure of the products or components of products and not only; determination of potential effects of different modes of failure; application analysis of failure modes, effects and failure criticity. You can apply for a product FMEA method and not only. All these actions will lead to warning of potential product-related problems since the beginning. Warning actions can turn into animation techniques of group work and creativity.*

***Keywords:*** *Method FMEA, minimize risk, preventive actions, potential defects*

## 1. INTRODUCTION

FMEA method is a procedure in the product development and operations management of analysis of potential failure modes within a system of classification and probability of failure. Originated from English Failure Mode and Effects Analysis, means Analysis of the Failure mode and effects (AMDE) [1]. Product quality and reliability are of critical importance in all existing systems. Such as the reliability and quality of a product is to be built since the early stages of product design. FMEA method is desired to begin the first stages of conceptual design and continues throughout the life span of the product. Designers and technologies will start to think about the quality and reliability of the product, because no product even last generation no matter how optimized is not likely to result in a better product than the designed [1]. The main idea which does this method is that the flaws that does not produce nor are removed. The concept is not a new one. By developing the method, FMEA is carried out as a tool of systematic analysis of quality and quality of planning which can be easily understood and applied by anyone. Used correctly the FMEA enables the discovery of problems with quality and avoiding their occurrence through appropriate measures [2].

The control of the traditional inspection after the process of the production must be preceded by systems that have planned the quality from the very beginning and be followed by continuous improvement of the product [3].

A corresponding activity type FMEA reliability team to help identify potential failure modes based on previous experience in

developing similar products. In this way all failures can be removed from the system with the minimum possible effort and resources [4].

## 2. ANALYSES

At the stage of manufacture of the product, information on the process, or the means of production are particularly important and come in more efficient application of FMEA method already achieved, which may also evolve.

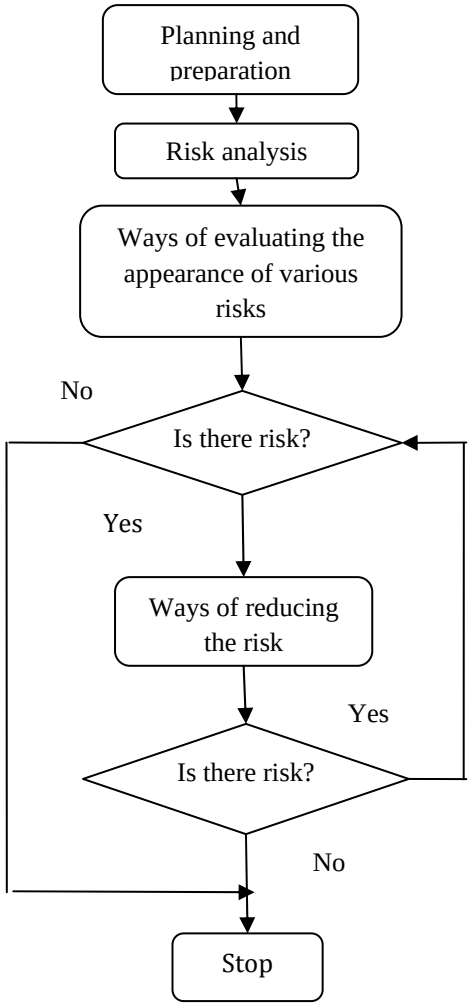


Figure 1: The logic of the FMEA analysis for a product.

Even in the use phase of products, information products and processes come in addition to the already completed FMEA however leading to minimize risks, figure 1. In figure 1, by applying FMEA method will minimize the potential risks and analysis. It will be carefully scrutinizing all kinds of defects and risks of potential as well as their causes and effects.

FMEA method must be used before the completion of the product. If the customer subsequently requests such a method are useless effects being null and void. This shows that it is necessary for this method to be within the organization.

The product is systematically broken down through a "top-down" in components or functions, and subsequently studied with respect to construction requirements, and keep these requirements in the course of production. Systematic analysis procedure is supported through the use of a corresponding form. In figure 2 you see that all the departments involved in delivering products bring their experience in analyzing and FMEA success.

At the same time the success of FMEA depends largely on the creative team. The FMEA analysis necessary for the nomination of a coordinator who guided a team of basic: product designer, technologist, personnel from quality assurance, auditor and team of experts made up of: master programmer, worker, N.C., vendor and customer. This team of experts helps the team to deepen analysis FMEA.

During this phase, the guidelines have been established that will be subject to analysis of FMEA in the light of the criteria for use [2]. This team of experts helps the team to deepen analysis FMEA.

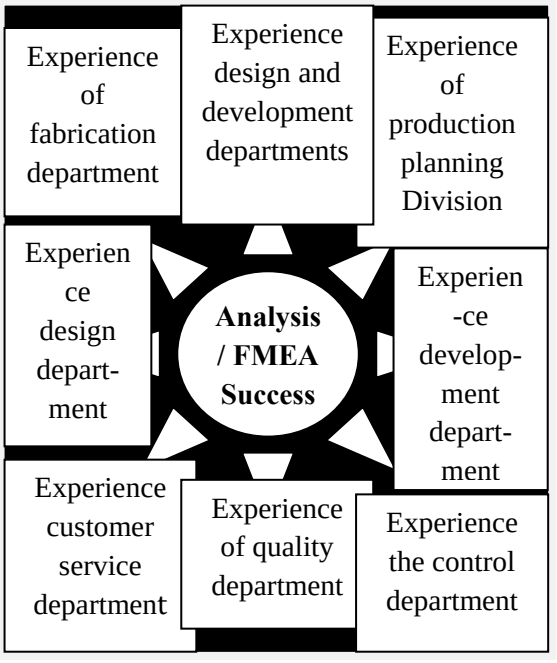


Figure 2: Analysis/ Fmea's success in order to ensure the quality of a product.

After establishing the functions and potential defects, the next step of the analysis is to identify the potential aftermath of FMEA defects. This requires a review of the team. Identification of the need to start with potential defects has the most serious track potential.

According to [4], the use of FMEA method has some advantages and disadvantages presented in table 1.

Table 1: Advantages and disadvantages of FMEA

| ADVANTAGES | DISADVANTAGES |
|---|---|
| -Early identification of potential failures;<br>-Improve the quality, reliability and safety of products/processes;<br>-Improving manufacturing company;<br>-Increasing customer satisfaction;<br>-Reducing the time and resources involved in product development;<br>-The development of appropriate data bases in the prevention of future disks;<br>-Reduction of expenditure in respect of the warranty of the product;<br>-Increasing the efficiency of production;<br>-Reducing electrical on the turnover. | -Is limited by the experience analysis team members;<br>-Can only identify major failure of a system;<br>-Cannot find the failures of a complex system or subsystem;<br>-By taking the product of the three indices of risk, a failure with an index of greater severity can obtain a lower risk than another failure. |

The final step of risk analysis is done the list of measures to prevent and/or the discovery of the defect or fault of the case and/or in order to limit the effects of its prosecution.

Within it all the defects, potential consequences of potential flaws and potential causes of defects shall be assessed with reference to the importance of monitoring of potential customer, the probability of the probability of discovery of potential defects. An FMEA analysis must change with technological process and to adapt to any problem that arises. FMEA analysis is done and to verify the problem is taken into account in the analysis and what solutions or actions are expected to apply. So will watch if the actions envisaged by the FMEA were well implemented, figure 2.

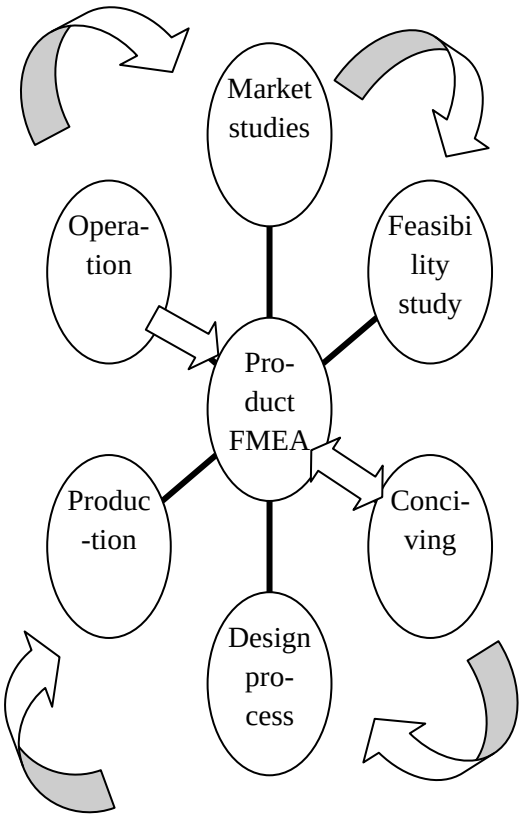


Figure 2: The application of FMEA process stages in the life cycle of the product

FMEA analysis target of a product is to determine potential or existing failures and classification according to risk levels, outcome

analysis consisting of triggering corrective or preventive actions to minimize the risk of each level failures.

## 3. CONCLUSIONS & ACKNOWLEDGMENT

In this article, FMEA method is an effective tool to quantify the risks, so that they can be analyzed, prioritized, mitigated or eliminated. FMEA can be applied both for study quality of a product as well as in all types of organizations, including manufacturing and services.

The method applied, may lead to lower production costs and improve products. Process FMEA provides an alternative approach to performing a Failure Mode and Effect Analysis. Occurrence, severity and detection rankings replace apportionments and failure rates. According to Crosby, while raising the quality of registers and a reduction of costs and as a result, not the quality, but the cost of non-quality. This idea led him to affirm: Crosby's "quality does not cost, but it is not a gift" [5]. FMEA method is created by specialists and applies to using specialized software. FMEA method determines and ensures efficient quality management and technological progress and economic.

This paper is supported by the Sectoral Operational Programme Human Resources Development (SOP HRD), ID134378 financed from the European Social Fund and by the Romanian Government.

## REFERENCES

1. Dumitrascu, A-E., Ciobanu, V., Borz, S-A., *Ingineria şi managementul riscurilor*, Editura Lux Libris, ISBN 978-973-131-247-7, Brasov, Romania, (2013).

2. Fulea, G-L., Borzan, M., Bulgaru, M., Herciu, D., Onetiu, G., *Aplicarea metodei FMEA pentru studiul calitatii pieselor injectate*, A XII-a Conferinta Nationala Multidisciplinara- cu participare internationala ”Profesor Dorin Pavel- fondatorul hidroenergeticii romanesti”, Sebes, Romania, pp. 283 -284, (2012).

3. Juran, J-M., *Planificarea calitatii*, Editura Teora, Bucuresti, Romania, (2000).

4. Ivana, B., Teza de doctorat, *Contributii la implementarea managementului fiabilitatii si mentenabilitatii in proiectarea instalatiilor,* Bucuresti, Romania, (2014).

5. Crosby, P-B., *Quality is Free- The Art of Making Quality Certain,* McGraw Hill, (New York, 1979).

"HENRI COANDA"
AIR FORCE ACADEMY
ROMANIA

"GENERAL M.R. STEFANIK"
ARMED FORCES ACADEMY
SLOVAK REPUBLIC

INTERNATIONAL CONFERENCE of SCIENTIFIC PAPER
AFASES 2015
Brasov, 28-30 May 2015

# NEED TO IMPLEMENT A HIGHLY-PERFORMING INTELLECTUAL-PROPERTY MANAGEMENT IN THE TECHNICAL-ENGINEERING FIELD

**Ramona Pakocs*, Nouraş Barbu Lupulescu***

*Department of Manufacturing Engineering, Transylvania University of Brasov, Romania

***Abstract:*** *In the last 20 years, many industrial companies, both at a national, and at an international level, have been confronted to a serious problem, namely: fight against unfair competition. In this article, we will elucidate which are the most threatening activities in counterfeiting, piracy, fake etc.; and, at the same time, we will explain why the implementation of a new type of management is needed, within the industrial enterprises, to wit: intellectual-property management. We will explain what supposes the training of a highly-performing intellectual-property management. Likewise, we will propose a few useful tools of highly-performing intellectual-property management, applicable within the industrial companies, which will find their solution, after a brainstorming session, organized with experts and with experienced academic teaching staff. Then, all solutions presented within the brainstorming session will undergo a multi-criteria analysis; and, in the end, the solution with the highest score will be chosen.*

***Keywords:*** *counterfeiting, piracy, fake, protection, brainstorming, multi-criteria analysis, solutions*

## 1. INTRODUCTION

The management is the art and science to make the others act so that an organization's objectives should be attained; it is the process whereby the goals are determined and fulfilled, through the achievement of basic, specific, functions, in guiding and enhancing the human resources. [5]

Making decisions is a critical part of all managerial activities [5]; the decisions as regards the protection measures against intellectual-property rights should be part of a modern and absolutely necessary management modern, called: intellectual-property management.

The managers' incorrect and unconscious decisions, with respect to the protection measures against unfair-competition activities may cause great losses, inclusively the bankruptcy of the industrial companies; and not only.

In the following, we will explain which are the unfair-competition facts, as well as what supposes combating them, with a view to protecting the industrial companies against counterfeiting, piracy, fakes etc.

## 2. FIGHT AGAINST UNFAIR COMPETITION

In the recent years, the definition of the *counterfeit* concept has been modified several times. Even in the best-known specialized dictionaries, this notion is explained in relatively vague terms. No distinction appears

anywhere, between the notions of piracy, counterfeit and fake. In most specialized dictionaries, all three notions are linked to the intangible "brand". This fact limits the detection of this crime. [4]

As previously explained, the definitions afferent to the notion of *counterfeit* are numerous; therefore, we have chosen a few sources, such as dictionaries and special industrial-property laws [3]

In this way:

**A. In the Explanatory Dictionary of Business Terms** [6], "**Counterfeit** is [only] the unauthorized representation of a trademark, which occurs in the case of identical or similar goods, as the goods for which the trademark is registered, with a view to deluding the consumer that (s)he purchases original merchandise."

**B. According to DEX `98** [2], "**to counterfeit** means to reproduce an original document, an object, preparation, with fraudulent purposes, presenting it as authentic; to falsify."

**C. According to the "Dictionary of Synonyms** "**to counterfeit** means to falsify, to distort, to simulate."

**D. According to WEBDEX** [7], "**to counterfeit** means to purposefully distort, presenting as authentic; to falsify."

Although the specialized dictionaries only managed to define briefly the concept of *counterfeit*, we will show that nor do the special laws manage to define the notion, clearly and completely.

As a result of the analysis on the **Law no. 66/2010**, one can see that the Art. 83 specifies three sorts of crime (counterfeiting; unlawfully putting into circulation a product with either an identical or a similar mark to a trademark; and putting into circulation products with geographic indications), yet, in the art. 35, par. 2, the definition of the action of *counterfeit* includes not only putting into circulation, but also other activities. [4]

Only the Law no. 296 from June 28$^{th}$, 2004, as regards the Code of Consumption, greatly amends the presentation of these notions. The art. 9 stipulates: [4] "There are forbidden the importation, manufacture, distribution, as well as the commercialization of the products - which are falsified or counterfeited, which are dangerous, whose security parameters are noncompliant; possibly affecting therefore the consumers' life, health or security".

Nevertheless, in DEFINITIONS, the same gap appears: both the counterfeited product and the falsified product only refer to the brand: [4] "In the sense of the legislation as regards consumer protection, the terms and expressions below are defined in this way:

...*32.* COUNTERFEIT PRODUCT – "any good, including its package, in whose case, an identical mark to a trademark is used without authority; or the product that cannot be differentiated, in its essential aspects, from a branded product, whereby the lawful rights incumbent on the legal holder of the respective mark are infringed".

*33.* FALSIFIED PRODUCT – "product in whose case the brand identification elements – name, logo or industrial design – lawfully registered, were altered, with a view to deceiving upon its origin, from products that were not manufactured by the legal holder of the brand or a duly authorized agent; or, on whose case, the trademark was used without the owner's assent;..." Obviously, from these definitions, no difference results between COUNTERFEIT and FAKE. [4]

Nor does the law no. 344 from 29/11/2005 as regards some measures meant to ensure the observance of the intellectual-property rights, in the case of the customs-clearance operations bring the desired amendment: Art. 3. - (1) In the sense of this law, the terms and expressions below have the following meaning:

...11. COUNTERFEIT GOODS:

a) "any commodity, including its package, which bears an identical mark or an undistinguishable mark, in its essential aspects, from a trademark for a product or a service, legally registered for the same type of goods; infringing, therefore, the rights incumbent on the legal holder of the respective mark."

b) "any symbol of a trademark, for a product or a service (including logo, label, self-adhesive, brochure, instructions for use or guarantee document, which bear such a symbol) even if it is presented separately and

which is in the same situation with the goods mention at letter a);"

c) "any package that bears brands of counterfeited products, presented separately, under the same conditions as the goods defined at letter a)."

12. PIRATED GOODS:

"All copies manufactured without the consent given by the right holder or by the duly authorized agent, in the manufacturing country – which are manufactured, directly or indirectly, after a product bearing the copyright or related rights; or of a right on the industrial designs and models; if making such copies constituted an infringement of the respective intellectual-property right;"

13.GOODS INFRINGING AN INTELLECTUAL-PROPERTY RIGHT

a) counterfeit goods;

b) pirated goods;

c) "goods infringing the rights upon a patent or an additional protection certificate or a geographical indication or a variety patent."

(2) "To the goods mentioned at paragraph (1) point 13, where applicable, any mold or die shall be assimilated, destined or adapted to manufacturing such goods, that infringe an intellectual-property right, provided that the use of such molds or dies should infringe the right holder."

The complete and comprehensive definition as regards combating unfair competition (counterfeit, piracy, fake), based on the references made by the Law no. 298/2001, is: "manufacturing, offering for sale, sale, importation, in general commercial exploitation, storage, use or putting into circulation, reproduction, with a view to manufacturing products with an identical aspect – unlawfully, to wit without the assent given by the holder of the industrial property right, during its validity and after its having been rendered public." [4]

This definition can be schematically shown, as follows, in figure 1: [4]

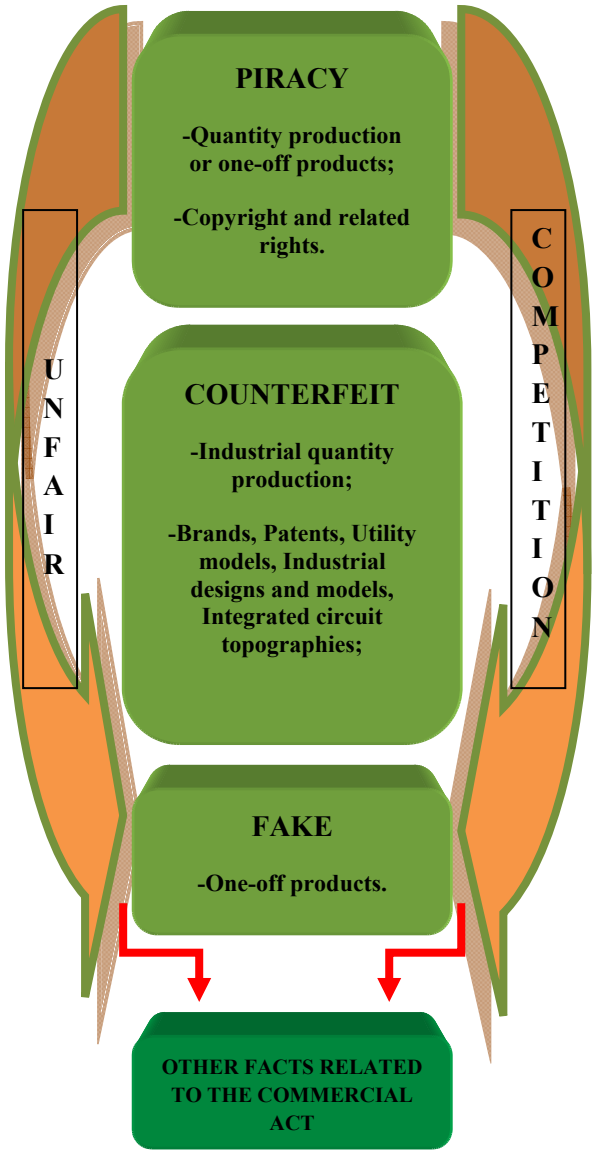


Figure 1. Correct understanding of the notions of counterfeit / piracy / fake, in integrated form.

## 3. NEED TO TRAIN A HIGHLY-PERFORMING INTELLECTUAL-PROPERTY MANAGEMENT

In order to define the intellectual-property management, we propose the following definition:

**Intellectual - Property Management** represents the sum of the knowledge referring to the legislation afferent to the protection of the intellectual property, the awareness of the preventive active forms, as well as the awareness of the legislation afferent to the action taken against the activities of unfair competition, counterfeit, piracy etc. as well as their application, with a view to diminishing the risks specific to intellectual property.

The actions of: intellectual theft, unfair competition, counterfeit, unauthorized use, plagiarism, bankruptcy, economic espionage, piracy, fake etc., "threaten" the product to be launched on the market. After the launch of the product on the market, it runs the risk of suffering from all these actions. In order to prevent the risks specific to intellectual property, a new type of modern management, to wit **intellectual-property management** is needed**.**

Forming a highly-performing intellectual property management supposes the following steps: [4]

1. Knowledge of the protection legislation;
2. Knowledge of the preventive active forms;
3. Knowledge of the legislation afferent to the action taken against unfair competition, counterfeit, piracy, fake etc.

In terms of the legislation afferent to the protection of intellectual property, we will mention the most important laws, namely:

- Law no. 64/1991 as regards the patents;
- Law no. 11/1991 as regards combating unfair competition;
- Law no. 129/1992 as regards the protection of industrial models and designs;
- Law no. 8/1996 as regards the copyright and related rights;
- Law no. 84/1998 as regards the trademarks and geographic indications;
- Law no. 350/2007 as regards the utility models;
- Law no. 337/2005 for amending and supplementing the Law. 16/1995 as regards the protection of the integrated-circuit topography.

## 4. STUDY ON THE IMPLEMENTATION OF THE INTELLECTUAL-PROPERTY MANAGEMENT

In previous works [4], five main categories of risks specific to intellectual property were identified, to wit:

1. Risks of conception/creation;
2. Risks of specific production P.I.;
3. Risks of marketing;
4. Risks of administration;
5. Social risks.

With a view to implementing a highly-performing intellectual-property management, within each organization, an analysis of the intellectual-property risks, as well as the application of some useful intellectual-property management tools are needed. Hence, the risks will be diminished

Therefore, in order to analyze the risks specific to intellectual property, we propose the achievement of a SWOT analysis, which might be adapted and used, as useful tool, within the industrial companies.

In order to apply the **SWOT analysis, specific to the intellectual-property risks,** within industrial enterprises, a **Brainstorming session** was organized**,** where the following solutions were proposed:

- **Elaboration of a working panel** of the probable intellectual-property risks, meant to help managers identify these risks, in time.
- **Achievement of a general scheme afferent to the SWOT analysis** on the risks specific to intellectual-property, which might be adapted to needs of all industrial companies.
- **Elaboration of a working scheme** with technical and economic solutions of intellectual-property protection, applicable within the industrial companies.
- **Organization of periodical meetings** with a view to analyzing and assessing the intellectual-property risks, in time.

- **Implementation of a managerial strategy** afferent to intellectual property, with a view to protecting the intellectual capital, within the industrial companies.
- **Clinching collaboration contracts** with the intellectual-property experts.

Table 1. Determination of the weight of each criterion.

| | PIDA | PCMF/P/S | PCDI | PCIB | s/S EAI | PPACN | Points | Level | Y1 |
|---|---|---|---|---|---|---|---|---|---|
| **PIDA** | 1/2 | 1 | 0 | 0 | 0 | 1 | 2.5 | 4 | 3.33 |
| **PCMF/P/S** | 0 | 1/2 | 1 | 1/2 | 1 | 1 | 4 | 1 | 3.66 |
| **PCDI** | 1 | 0 | 1/2 | 1/2 | 1 | 0 | 3 | 3 | 3.5 |
| **PCIB** | 1 | 1/2 | 1/2 | 1/2 | 1 | 0 | 3.5 | 2 | 3.6 |
| **s/S EAI** | 1 | 0 | 0 | 0 | 1/2 | 0 | 1.5 | 5 | 4 |
| **PPACN** | 0 | 0 | 1 | 1 | 1 | 1/2 | 3.5 | 2 | 3.6 |

In order to carry out a comparative evaluation of all these solutions found within the Brainstorming session, **a multi-criteria analysis** was proposed**.**

This **multi-criteria analysis** can be achieved in **five stages**, which are not necessarily successive.

**Stage 1: Criteria determination:**

A "criterion" is the expert's clear and well defined viewpoint, whereby (s)he defines, individuates and defines certain characteristics or properties imposed on the object of analysis: [1]

With reference to our study, the following **criteria to characterize risk, in intellectual property,** were identified**:**

1.Probability to infringe the copyrights **(PIDA);**

2.Probability to counterfeit the trademarks of company or of products/services **(PCMF/P/S);**

3.Probability to counterfeit the industrial design **(PCDI);**

4.Probability to counterfeit the patented inventions **(PCIB);**

5.Under/overestimations of the intangible assets **(s/S EAI);**

6.Probability to produce the unfair-competition acts **(PPACN).**

After the identification of the risk-characterization criteria, in intellectual-property, the weight coefficients for each criterion will be calculated, as shown in table 1.

According to our study, several variants were chosen to reduce specific risks of intellectual property. The grade will be granted to each variant, according to each criterion. One variant will be analyzed, in turn, in the light of each criterion, until all variants are treated. This calculation shall be done in a table, called matrix of consequences.

Identification of variants to reduce the risks specific to intellectual property:

**Variant 1. Elaboration of a working panel** of the probable intellectual-property risks, meant to help managers identify these risks, in time.

**Variant 2. Achievement of a general scheme afferent to the SWOT analysis** on the risks specific to intellectual-property, which might be adapted to needs of all industrial companies.

**Variant 3. Elaboration of a working scheme** with technical and economic solutions of intellectual-property protection, applicable within the industrial companies.

**Variant 4. Organisation of** periodical **meetings** with a view to analyzing and assessing the intellectual-property risks, in time.

**Variant 5. Implementation of a managerial strategy** afferent to intellectual property, with a view to protecting the intellectual capital, within the industrial companies.

**Variant 6. Clinching collaboration contracts** with the intellectual-property experts.

In the following, a grade will be given to each variant, in the light of each criterion.

Then, the consequence of the different weight, afferent to each criterion, will be considered; the table 2, then the table 3 will be filled in: the grades will be magnified (by lines) with the importance coefficient.

| | PIDA | PCMF/P/S | PCDI | PCIB | s/S EAI | PPACN |
|---|---|---|---|---|---|---|
| Variant 1 | 8 | 8 | 9 | 8 | 8 | 9 |
| Variant 2 | 10 | 10 | 10 | 10 | 10 | 10 |
| Variant 3 | 8 | 10 | 8 | 8 | 8 | 8 |
| Variant 4 | 8 | 8 | 8 | 9 | 9 | 9 |
| Variant 5 | 9 | 10 | 10 | 10 | 10 | 10 |
| Variant 6 | 8 | 8 | 10 | 9 | 9 | 10 |

Table 2. Giving a grade to each variant.

In table 3, we made the following notations: **C-** criterion; **V-** variant; **Y1-** weight coefficent.

According to table 3, we multiplied the grades for each variant in table 2, by the weight coefficient obtained in **table 1.**

**RESULT INTERPRETATION:**

As a result of the calculation effectuated in table 3, we noticed that the greatest sum (216.9) ranks variant 2 first, followed by variants 5 with a score of 213.57, variant 6 ranks third with a score of 195.32, variant 4 ranks fourt, with a score of 184.72, variant 3 ranks fifth, with a score of 180.84 and variant 1 ranks sixth with a score of 180.62.

In line with the result interpretation, the variant with the highest score was chosen, to wit variant 2, which referred to the **Achievement of a general scheme afferent to the SWOT analysis** on the risks specific to intellectual-property, which might be adapted to the needs of industrial companies, which is meant to help managers identify these risks in time, with a view to implementing a managerial strategy specific to intellectual property.

| | C 1 | C1 x Y1 | C 2 | C2 x Y1 | C 3 | C3 x Y1 | C 4 | C4 x Y1 | C5 | C5 x Y1 | C6 | C6 x Y1 | TOTAL |
|---|---|---|---|---|---|---|---|---|---|---|---|---|---|
| V. 1 | 8 | 26.64 | 8 | 29.28 | 9 | 31.5 | 8 | 28.8 | 8 | 32 | 9 | 32.4 | 180.62 |
| V. 2 | 10 | 33.3 | 10 | 36.6 | 10 | 35 | 10 | 36 | 10 | 40 | 10 | 36 | 216.9 |
| V. 3 | 8 | 26.64 | 10 | 36.6 | 8 | 28 | 8 | 28.8 | 8 | 32 | 8 | 28.8 | 180.84 |
| V. 4 | 8 | 26.64 | 8 | 29.28 | 8 | 28 | 9 | 32.4 | 9 | 36 | 9 | 32.4 | 184.72 |
| V. 5 | 9 | 29.97 | 10 | 36.6 | 10 | 35 | 10 | 36 | 10 | 40 | 10 | 36 | 213.57 |
| V. 6 | 8 | 26.64 | 8 | 29.28 | 10 | 35 | 9 | 32.4 | 9 | 36 | 10 | 36 | 195.32 |

Table 3. Raising grades with importance coefficient.

| SWOT ANALYSIS OF THE RISKS SPECIFIC TO INTELLECTUAL-PROPERTY | | | |
|---|---|---|---|
| **Internal factors of P.I. risks:** | | | |
| **STRENGTHS:**<br><br>Efficient management of a modern enterprise;<br>Right to produce/ commercialize;<br>Quality/ assortment of manufactured goods;<br>Protection of I.P. rights; | **Exploitation modalities:**<br>Highly-performing management of I.P.;<br>Protection measures specific to I.P.; | **WEAKNESSES:**<br>Inexistence of highly-performing management of I.P.;<br>Lack of protection measures specific to I.P.;<br>Managers' lack of awareness on the possible I.P. risks. | **Reduction modalities:**<br>Managerial strategies of protection against unfair-competition acts, piracy, fake, intellectual theft etc. |
| **External factors of P.I. risks:** | | | |
| **OPPORTUNITIES:**<br><br>Rise in intangible assets, by the enhancement of patents, utility models, integrated-circuit topography models etc.<br>Assignment contracts. | **Exploitation modalities:**<br>Long-term profits, as well as stability of the enterprise and employees.<br>Investment in the company's intellectual property. | **THREATS:**<br><br>Abusive protection (confusion +association) of an industrial design / model vs. trademark;<br>Piracy in design /cct ;<br>Counterfeit in design /cct<br>Intellectual fraud in design / cct;<br>Abusive protection of a trademark vs. business name;<br>Abusive protection (confusion +association) of a field vs business name;<br>Abusive protection of a business name vs. trademark;<br>Plagiarism in design /cct;<br>Production of goods infringing DPI;<br>Unfair competition in production;<br>Unfair competition in trade;<br>Commercialisation of goods infringing DPI. | **Reduction modalities:**<br>patent;<br>utility model certificate;<br>industrial design-model certificate;<br>integrated-circuit topography circuit;<br>specific provisions in the legislation against unfair competition;<br>business name;<br>trademark certificate;<br>specific provisions in the legislation against unfair competition ;<br>competition law, normative acts referring to consumer protection etc. |

Table 4. SWOT analysis of the risks specific to I.P.

## 5. CONCLUSIONS & ACKNOWLEDGMENT

The general scheme of the SWOT analysis on the risks specific to intellectual property, which may be adapted to the needs of highly-performing management, namely: Intellectual-Property Management, is a useful tool, meant to help managers identify the intellectual-property risks in time, and to implement one or

several strategies, with a view to combating them, likewise resorting to the risk-reduction modalities (according to the scheme), by patent, by utility model certificate, by industrial design-model certificate, by integrated-circuit topography certificate, by business name, by trademark certificate, by specific provisions in the legislation afferent to unfair competition etc.

„This work was partially supported by the strategic grant POSDRU/159/1.5/S/137070 (2014) of the Ministry of National Education, Romania, co-financed by the European Social Fund – Investing in People, within the Sectoral Operational Programme Human Resources Development 2007-2013".

## REFERENCES

1. Bobancu, S., *Creativity and Invention. Course Notes,* electronic publication (2012).
2. Explanatory dictionary of the Romanian language (1998).
3. Fantana, R. S., *A chrestomathy the notion of infringement in Romanian legislation. Consequences*. Scientific Session of the National Chamber of Industrial Property Attorneys in Romania , 3rd Edition , Bucharest (2007 ).
4.Fantana, R. S., *Research on integrated management of intellectual property risk technical and economic*, Thesis, Brasov, (2008).
5. Ursachi I., *Management,* ASE, Bucharest (2001).
6. Walter G., *Explanatory Dictionary of Terms of Business,* World Trade Organization , IRECSON Publishing Institute, (2006).
7.www.webdex.ro/online/noul_dictionar_explicativ_al_limbii_romane.

"HENRI COANDA"
AIR FORCE ACADEMY
ROMANIA

"GENERAL M.R. STEFANIK"
ARMED FORCES ACADEMY
SLOVAK REPUBLIC

INTERNATIONAL CONFERENCE of SCIENTIFIC PAPER
AFASES 2015
Brasov, 28-30 May 2015

# RISK MANAGEMENT AND ASSESSMENT OF THE MANUFACTURING AND MARKETING RISK-FACTORS WITHIN INDUSTRIAL COMPANIES

**Ramona Pakocs*, Nouraş Barbu Lupulescu***

*Department of Manufacturing Engineering Transylvania University of Brasov, Romania

***Abstract:*** *This paper is consecrated to a study referring to the manufacturing and marketing risk factors, specific to intellectual property; an analysis has been conducted upon case studies, within some companies manufacturing spare parts for cars, tractors, trucks etc., in Romania. By means of this paper, an alarm signal is given, referring to the counterfeit or "industrial piracy" actions, as well as to their consequences, when the counterfeit amplifies and extends masswide. As a result of the study conducted upon the "recovery of the intellectual-property rights, upon the spare parts, at a national level"[5,8], the losses of the damaged companies become obvious, in terms of economic efficiency; just as the stipulations the law become relevant, in the case of the situations under analysis, within companies manufacturing spare parts for cars, tractors, trucks etc.*

***Keywords:*** *intangible, assessment, mark, risk, counterfeit/fake, crime.*

## 1. INTRODUCTION

The economic efficiency of any industrial company may be diminished by whatsoever counterfeit or "piracy" action.

The industrial companies make great efforts, in order to reduce the counterfeiting of their products.

Hence the final cost of the product manufactured by the owner of rights is higher than the cost of a licensed product.

The licensee does not include, among others, the market tracking costs [5,8].

By this article, we intend to clarify the following aspects:

- how the counterfeit influences the economic efficiency of the industrial company;
- what says the law, in the case the counterfeit is masswide; and the one who should deal with the protection is negligent;
- which is the social impact, as a result of this counterfeit. [5]

## 2. ANALYSIS OF THE RISK FACTORS WITHIN A COMPANY

**2.1. Risk Management.** Risk management is the main component of any company's strategic management, ensuring an efficient administration of the possibilities and of the adverse effects generated by the various types of risks [5,8].

A highly performing risk-management supposes comprehending the factors that may

affect the smooth functioning of the organization [5,8].

The organizations have adapted a formal risk-management process, for each type of risk, under different circumstances [1,2,4,6].

**2.2. Study of the risk factors within a company.** We introduced the risks specific to intellectual property in a scheme (shown in table 1) wherein we systematized the general risks that may be run by an organization, as well as the main internal and external factors that determine them.

Table 1. Internal and external risk factors.

| FACTORS | INTERNAL | EXTERNAL |
|---|---|---|
| **INTELLECTUAL PROPERTY RISKS** | -failure to supervise the market;<br>- contracts;<br>-unfair competition;<br>- underestimation / overestimation;<br>- copyright;<br>-brand;<br>- patents;<br>- industrial design etc. | - failure to supervise the market ;<br>- contracts;<br>- unfair competition;<br>- underestimation / overestimation ;<br>- copyright;<br>- brand;<br>- patents;<br>- industrial design etc. |
| **FINANCIAL RISKS** | - liquidities;<br>- cash-flow. | - interest rates;<br>- exchange rates;<br>- credits. |
| **STRATEGIC RISKS** | -research-development; | - competition;<br>- market;<br>- demand. |
| **OPERATIONAL RISKS** | - financial control;<br>- IT system;<br>- recruitment;<br>- logistics. | - regulations;<br>- culture;<br>- management. |
| **HAZARD RISKS** | - wage-earners;<br>- properties;<br>- products;<br>- services. | - contracts;<br>- suppliers;<br>- environment. |

There is a multitude of events, which may negatively influence the activity of an enterprise/organization, and which can be split into two categories, namely: [5,8]

**1. External factors with negative influence:**

**a. Economic factors:**

-competition;

-market;

-macroeconomic/ microeconomic conditions.

**b. Natural factors:**

-earthquakes, draught, natural disasters etc.;

**c. Political factors:**

-change of government, after the elections;

-implementation of new legislative regulations.

**d. Social factors:**

-increase/decrease in the living standard;

-demographic changes.

**e. Technological factors:**

-access to information;

-reduction of the infrastructure costs;

-evolution of technology.

**2. Internal factors with negative influence:**

**a. Infrastructure:**

-equipment noncompliant with the production demands;

-incurred repair costs, which have not been taken into account.

**b. Staff:**

-ever more frequent labour accidents;

-human errors;

-fraudulent behaviour.

**c. Processes:**

-qualitative errors;

-non-compliance with the deadlines afferent to the manufacture of the products;

-delays in service.

**d. Technology:**

-problems with the data integrity;

-update of the working technologies etc.

I showed these internal and external factors with negative influence in figure 1, as follows:

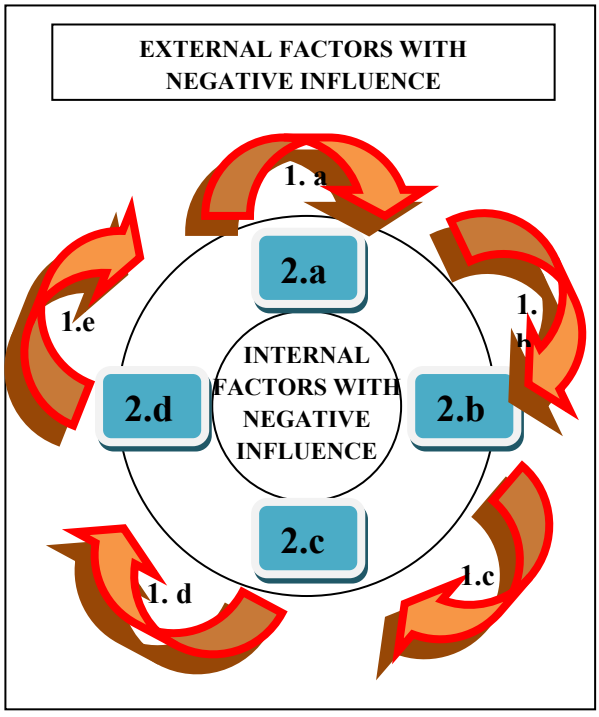


Figure 1. Internal / External factors with negative influence.

**2.3. Analysis of the manufacturing and marketing risks, specific to intellectual property.** As a result of an analysis conducted within an industrial company, a series of production risks and marketing risks, specific to intellectual property resulted, such as:

**A. Manufacturing risks specific to intellectual property: [5,8]**

-Risk related to the inexistence of a highly-performing quality management;

-Risk related to the management's unresponsiveness towards the infringement of P.I. rights, for one's own products;

-Risk of inefficient promotion on the market of the P.I. (brand) for new products;

-Risk of unjustified expenditure on the promotion of old, outdated products;

-Risk of trademark production infringing the P.I. rights ;

-Risk of unfair competition in production;

-Risk related to the disclosure of know-how, production information, manufacturing secrets;

-Risk related to failure to promote the managerial skills;

-Risk related to failure to promote the employees' skills;

-Technological risk related to the lack of protection for inventions/patents;

-Technological risk related to the lack of protection for utility models;

-Technological risk related to the lack of protection for industrial drawings – models;

-Technological risk related to the lack of protection for integrated circuit topographies;

-Risk of product non-standardization etc.

**B. Marketing risks specific to intellectual property: [5,8]**

-Risk related to the unfair protection of the business name;

-Risk related to the abusive protection of a product by patent;

-Risk related to the abusive protection of a trademark vs. business name;

-Risk related to the abusive protection of a business name vs. trademark;

-Risk related to the abusive protection (confusion + association) of an industrial design/ model vs. trademark;

-Risk related to the abusive protection (confusion + association) of a trademark vs. industrial design/model;

-Risk related to the abusive protection of a utility model;

-Risk related to the abusive protection of an integrated-circuit topography;

-Risk related to the abusive protection (confusion + association) of a field vs. business name;

- Risk related to the abusive protection (confusion + association) of a field vs. trademark;

-Risk related to the lack of protection of the client list and information;

-Risk related to the absence of market information;

-Risk related to the absence of marketing strategies;

-Risk related to the lack of protection for the distribution network;

-Risk related to the lack of protection for contracts;

-Risk of clinching non-protective contracts in PI;

-Risk related to the loss of reputation and credibility;

-Risk related to the lack of advertising / promotion;

-Risk related to the lack of protection for the database;

-Risk to commercialize goods infringing PI rights – [11] and others;

-Risk of unfair competition in trade – crime [14];

-Risk related to the lack of protection for the trademark of factory, commerce and services;

-Risk related to the lack of protection for the origin indications;

-Risk related to the lack of protection for the plant and animal species etc.

Regardless of the types of risks, the treatment thereof with negligence, by the organization's management, may lead to enormous losses, even bankruptcy.

In the following, we will analyze a case study referring to the "recovery of the intellectual-property rights upon the spare parts, at a national level", in the case of two companies, manufacturing spare parts for cars, tractors, trucks etc., in Romania.

In order to keep the data confidentiality, we named the former company" SIGMA" and the latter, "OMEGA".

## 3. ANALYSIS OF THE CASE STUDY UPON THE MANUFACTURING AND MARKETING RISK FACTORS, WITHIN THE INDUSTRIAL COMPANIES „S.C. SIGMA S.A." AND „S.C. OMEGA S.A."

At a national level, starting with the `90-ies, based on H.G. 1213 din 20.11.1990, the industrial plants were abolished; ad many joint stock companies were established, in order to "take over" their assets and liabilities. [5,8]

The "satellite" enterprises, set up in the '70-ies, with a view to producing spare parts for the internal market – as a result of the suffocation of the enterprises, to cover the external market – changed overnight into joint stock companies, detaching themselves from the parent undertaking. [5,8]

Besides, many influential people set up companies, which turned subsequently into basic pillars of the industry manufacturing spare parts for cars, tractors, trucks etc.

Currently, in our country, there are approximately 100 units manufacturing spare parts for cars, tractors, trucks etc.

In line with the imposed international legislation, referring to environment and quality, the Romanian Auto Registrar (RAR), homologated and certified all manufacturers of spare parts, throughout our counter, according to the legislation in force. [8,10,12,13].

After an analysis on the case study referring to the patrimonial evaluation of the first company manufacturing spare parts for cars, tractors and trucks, called S.C. SIGMA S.A., a drop in the value of the company and product brands was noticed, which could not be calculated, as this assessment of the trademarks, within the evaluation of the intangible assets, would not have been profitable, in economic terms.

The explanation would be the low volume of the sales and the economic inefficiency.

In this case, the tangible patrimonial assets were evaluated, with some connections to the intangible assets, by calculating the good-will.

In figure 2, we will present the graph of the total sales for the company S.C. SIGMA S.A. in the period 1990-2000, and in figure 3, the graph afferent to the evolution of the total spare-part sale, for the same company:

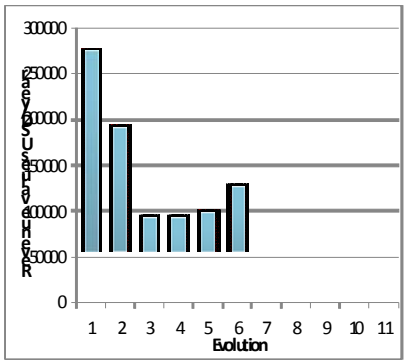


Figure 2. Graph of the sales evolution at S.C. SIGMA S.A.[5]

The analysis of the graph afferent to the evolution of the total sales at S.C. SIGMA S.A., shows a light drop in sales, during the years 3, 4; then an increase, in the years 5,6,7; afterwards a dramatic drop, in the years 8,9,10 which affected the entire company – consequences suffered after the penetration on the market, of the industrial "counterfeit", or "piracy" phenomenon.

According to [3], "there is counterfeit, if an element of the original work has been reproduced, even if there is no risk of confusion. The essential criterion of the counterfeit resides in the exemption from

personal creative effort, represented by the loan."

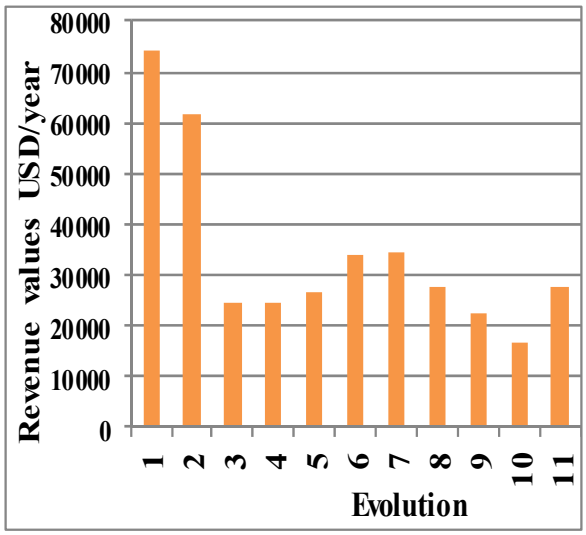


Figure 3. Graph afferent to the evolution of the total spare-part sale for S.C. SIGMA S.A.[5]

According to [7], "By reproduction, there is understood, a perpetration whereby the author… conveys or imitates something". The socially dangerous consequence of this crime is a concrete result, namely counterfeit products..."

Art.13/Law no. 8-96 stipulates: [9] "the use or the exploitation of a work engenders the author's distinct and exclusive rights to authorize:

a) the reproduction, either integral or partial, of the work; … Art. 14. - (1) By reproduction, in the sense of this law, there is understood the achievement of one or several copies of the work, in any material form …"

At the end of 1990, the latter company manufacturing spare parts for cars, trucks and tractors, called S.C. OMEGA S.A., requests a study referring to the "recovery of the intellectual-property right upon the spare parts, at a national level" [5,8], which study was subsequently demanded also by S.C. SIGMA S.A. [5,8]

As a result of the two studies conducted at S.C. SIGMA S.A and S.C. OMEGA S.A., the following resulted:

- as a consequence of the great demand of spare parts, at a national level, 12 enterprises manufacturing spare-parts for trucks, cars and tractors were established, the design for the pieces being transmitted; yet no document of non-exclusive license assignment was ever signed. The manufacture was achieved at the level of the plant, after clear orders, according to the criterion part/ no. items;
- since the abolishment of the plant, so far, these companies have clinched no contract of non-exclusive cession;
- all production of spare parts for cars, tractors and trucks, at a national level, was counterfeited, excepting the pieces manufactured and sold by the right holders S.C. SGMA S.A. and S.C. OMEGA S.A. [5,8]
- a few companies in the country were interested to become legal;
- a non-exclusive cession contract was negotiated, by law nr. 8/1996 as regards the copyright and related rights, which stands for the first contract clinched by the right owners S.C. SIGMA S.A. and S.C. OMEGA. S.A. It was concluded and signed by the future beneficiary, the company S.C. X S.A. (called according to the confidentiality procedure); this contract being stopped by AGA.
- no knowledge exists of some summons to court for the recovery of the rights, as the expertise was not continued.

## 4. CONCLUSIONS & ACKNOWLEDGMENT

1. Unless the “pirate” companies existed, with a high production level, both S.C. SIGMA S.R.L. and S.C. OMEGA S.R.L. would have been the first companies manufacturing spare parts, at a national level.
2. If S.C. SIGMA S.R.L. and S.C. OMEGA S.R.L. recovered their copyright, the great value of their trademarks would be proven.
3. Laws were issued (Law no. 202/2000 as regards the intellectual-property in customs) which disadvantages the right holder (owner).
4.The efficiency of these enterprises enormously dropped; the marker losing by intellectual theft; the right holder having not sued against the counterfeit.

„This work was partially supported by the strategic grant POSDRU/159/1.5/S/137070 (2014) of the Ministry of National Education, Romania, co-financed by the European Social Fund – Investing in People, within the Sectoral Operational Programme Human Resources Development 2007-2013”.

## REFERENCES

1. Băbuț, G., Moraru, R., *Environmental risk characterisation principles*, Proceedings of the 6th Conference on Environment and Mineral Processing, part. I, pag. 17-21, VŠB-TU Ostrava, Czech Republic, (2002).
2. Beer, T., Ziolkowski, F., *Environmental risk assessment: An Australian perspective*, Supervising Scientific Report 102, Australia, (1995).
3. Eminescu, I., *Unfair competition.Roman Law and compared.,* Publisher " LUMINA LEX" , Bucharest (1993 ).
4. Ene, C.N., *Comparisons on international approaches to risk management.,* Economia Journal, Management series , (year VIII , no. 2/2005 , pp. 77-88).
5. Fântână, R.S., *Research on integrated quality-risk management of technical-economic intellectual property*, PhD Thesis, "Transilvania" University. Brasov Faculty of Technological Engineering (2008).
6. Hillson, D., *Project Risk Management: Future Developments,* (2004). Available: (www.risk-doctor.com/pdf-files/fut0798.pdf).
7. Lazăr V., Offences against intellectual property rights, Publisher „ALL BECK”, LEGAL, Collection " LEGAL STUDIES ", Bucharest (1999 ) .
8. Secara G., Fântână R. S., *General Management*, Publisher Pro Universiataria, Bucharest (2010).
8. Resolution no . 394 of 8 June 1995 on the obligations of economic agents - individuals or legal – the marketing of durable consumer (Official Gazette no. 122 of 19 June 1995).
9. Law no. 8 of 14 March 1996 on Copyright and Related Rights ( Official Gazette No. 60 of 26 March 1996).
10. Decision no. 786 of 10 September 1996 amending and supplementing Government Decision no . 394/1995 concerning the obligations payable by companies-natural or legal persons, in the marketing of products from consumer use of long (d. OF No 222 of 17 September 1996).
11. Law no. 84 of 15 April 1998 on trademarks and geographical indications (Official Gazette no. 161 of 23 April 1998).
12. Order No.. 170 of 25 March 1999 for completing the regulations on the certification and/or approval of equipment, spare parts and materials used in road vehicles and allow economic agents which provides services repairs or carries reconstruction of road vehicles approved by order of the Minister of transport no. 536/1997, (m. OF. No. 224 of 20 May 1999).
13. Ordinance no. 82 of 24 August 2000 concerning the authorization of economic agents that provide repair services , regulation and / or carries on reconstruction of vehicles (Of. No. 413 of 30 August 2000).
14. Law no. 298 of 7 June 2001 amending the Law no. 11/1991 on Unfair Competition ( Official Gazette . Part I no. 313 of 12 June 2001).

"HENRI COANDA"
AIR FORCE ACADEMY
ROMANIA

"GENERAL M.R. STEFANIK"
ARMED FORCES ACADEMY
SLOVAK REPUBLIC

INTERNATIONAL CONFERENCE of SCIENTIFIC PAPER
AFASES 2015
Brasov, 28-30 May 2015

# EFFECTS OF THE LASER POWER ON WOOD COLOURATION

**Adrian Petru*, Aurel Lunguleasa****

*Faculty of Wood Engineering, Transilvania University of Brasov, Romania

***Abstract:*** *This paper present a study about influence of the laser power on wood colour change. An application of this study is artistic wood burning. The tests were made on beech wood. The results show that the laser power influence on wood is not linear. It found four variations areas defining this influence. It observed differences in colour uniformity between low and high laser power, also. In that way was defined the interval value limits in area in which the colour variation is large and uniformity is better.*

***Keywords:*** *pyrography, wood burning, laser technology, beech*

## 1. INTRODUCTION

Laser radiation processing is gaining more and more followers because of the advantages which it has this technology. One of this is easy availability of equipment. One of the laser processing applications is the wood pyrography. Laser technology is well suited for high-volume automated manufacturing owing to the high processing speed, low waste, precision of operation, and high quality of engraved products [7].

Operational laser parameters that affect wood colour are: laser output power, feed speed, and scan gap. It keeps constant feed speed and scan gap for this study.

Dumitras proposed for permanent materials engraving the power of the $CO_2$ lasers less than 15 W [2]. These values depend on the other work parameters (especially speed), and on the material. The material to be processed is the most important influence factor.

Research on Moso bamboo wood showed that engraved surface darkens more and more with increasing laser power [7]. There have been other studies regarding the influence of laser power on wood colour, comparing several woody species [10].

## 2. OBJECTIVE

The aim of this study is to define the laser power variation range used for wood engraving. The study proposes itself to obtain more colour nuances between natural colour of the wood and black without pronounced degradation of the wood.

## 3. MATERIAL, METHOD, AND EQUIPMENT

The methodology consists in more tests about using more power values, and keep the others work parameters at the same values. For this study, it was used beech wood (*Fagus Sylvatica* L.) veneer. This wood is one of the most used species, recommended as support for pyrography by others authors [3,4,5,6,8,10]. Beech is a specie with light natural colour and an uniform structure. The

"HENRI COANDA"
AIR FORCE ACADEMY
ROMANIA

"GENERAL M.R. STEFANIK"
ARMED FORCES ACADEMY
SLOVAK REPUBLIC

INTERNATIONAL CONFERENCE of SCIENTIFIC PAPER
AFASES 2015
Brasov, 28-30 May 2015

pale colour provides the possibility to obtain a large colour gradient by burning. The experiments were made on rectangular specimens with 105 mm wide and 225 mm depth (Fig. 1).

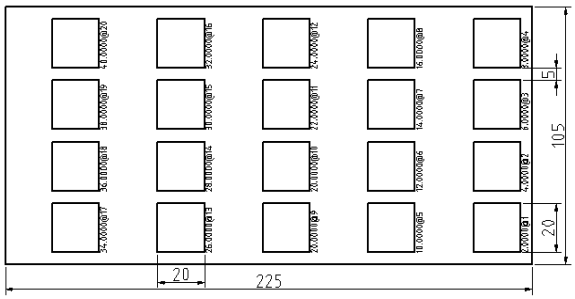


Fig. 1. Sample shape and size.

In order to analyse the wood colour, the radially section of samples were used. This section allowed the study of colour difference between early wood and late wood. These two areas of wood growth are distinguished by hardness.

The specimens was dried at 12% moisture content and conditioned at 20ºC temperature and 65% relative humidity [1]. Prior to manufacture, the wood specimens was sanded mechanical with 80 grained sand paper and then it sanded with 120 grained sand paper. The used equipment contains: Laser Engraving Machine 4030lsct equipment for laser processing, HP LaserJet 3055 all-in-one for image scanning, and PC for image processing and colour measurement. The specimens were burned by laser.

Original image is a linear draw processed by computer. This draw contains 20 squares. Each square was rasterised with different power value. The power values were chosen starting from minimum value of the engraving machine (2 W). Each square was burned at a range of powers from 2 to 40 W with incremental changes of 2 W (Fig. 1). A software application was developed for ease of data entry. This application helps to setting the process parameters.

The work parameters are:

- Focused distance: 73 mm;
- Scansion speed: 400 mm/s;
- Spot Size at working distance: 0.0254 mm;
- Laser Wavelength: 10.6 µm.

Engraved surface was scanned with HP LaserJet 3055 all-in-one printer, fax, copier, and scanner. The used parameters for this study are:

- Colour mode;
- Resolution 600 dpi;
- Bitmap image format;
- Scan scale 1:1.

The file with scanned image was transferred to a computer in order to analyse the image. Pyrographed image was converted to large-scale nuances in order to correlate the colour measured values.

The colour was measured using the digital colour analysis method [9]. The measured values were converted in to CIEL*a*b* system [11].

Each filled square was measured with a 100 pixels circular surface diameter. It resulted 7957 pixels for each square and 159140 measured pixels for each image using this parameter. It was calculated the average value for each measured round surface.

## 4. RESULTS AND DISCUSSION

In Fig. 2 are shown experimental research results. It observes that L* parameter is the most influenced by burning. A* and b* parameters define especially the natural colour of the wood. This is the reason why the values of these parameters have initial an upward trend, while L* decreases. This study analyses

L* parameter only. It observes several areas of change on its variation:

- Up to 4 W is the range in which the wood is not affected by laser radiation. It seems that under this power, the laser does not have energy to bring the temperature which burning the wood.
- Area between 4 and 10 W is the range in which we see great colour changes (darkening) of the surface. It seems that this is the recommended range for pyrography.
- Area between 10 and 24 W is the range in which the resulting colour variation is small, although the power increases mostly. This interval is not economical because it requires high energy consumption with a little colour effect.
- Area over 24 W is the range in which the brightness decreases significantly again. The wood is degrading strongly at these working parameters. It is not recommend to use these values for pyrography because burning wood is deep and it loses its mechanical properties. The colour varies randomly because the material becomes unstable and burned parts are removed from the surface by the cooling system.

Point where the trichromatic components meet is characteristic for grey colour. The black colour is represented in trichromatic components by 0 value for all components.

Another important aspect is related to how to the wood is coloured. At low power staining, the colour is uniform, with no major differences between early and late wood. With increasing laser output power, there appear differences between early and late wood. Late wood is denser and darker than early wood. Due to higher density, the late wood burns slower than early wood. Therefore, with the increasing laser output power, the burning

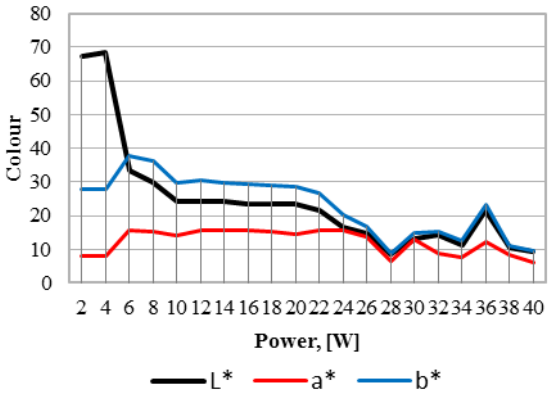


Fig. 2. Colour variation depending on laser power.

wood turns into a negative image of a natural design.

The laser power influences the wood temperature, because a higher power has a greater impact on processed wood. This impact is translating into higher impact forces which cause increasing processing temperature.

## 5. CONCLUSIONS & ACKNOWLEDGMENT

Because the pyrography represents a wood reaction under temperature influence, the work piece is very important for colour obtaining. It cannot obtain the black colour into strongly degrades wood phase by laser power variation only. This colour is important because it defines the number of nuances which it can be made by pyrography. The black is the limit of this interval.

It was defined the laser output power variation interval for pyrography. This is between 4 and 10 W. It was visually studied the surfaces aspect. The coloration is uniform in the mentioned range above.

The results can be used for mathematical modelling of the studied phenomenon. This

"HENRI COANDA"
AIR FORCE ACADEMY
ROMANIA

"GENERAL M.R. STEFANIK"
ARMED FORCES ACADEMY
SLOVAK REPUBLIC

INTERNATIONAL CONFERENCE of SCIENTIFIC PAPER
AFASES 2015
Brasov, 28-30 May 2015

model will be used for work process optimising.

The colour modifications it obtains by varying the others working parameters (scan gap, feed speed), also.

This paper is supported by the Sectoral Operational Programme Human Resources Development (SOP HRD), ID134378 financed from the European Social Fund and by the Romanian Government.

## REFERENCES

1. Cismaru M.,. *The phisics of wood and other wooden materials (in Romanian)*. Brasov: Transilvania Publishing House (2003).

2. Dumitra□, C. Dan,. *The laser beam engineering*. Bucure□ti: Editura BIC ALL (2004).

3. Easton, S.,. *Wood burning with style*. East Petersburg, PA: Fox Chapel Publishing Company, Inc. (2010).

4. Haller P., Beyer E., Wiedemann G., Panzner M., Wust H.,. Experimental study of the effect of a laser beam on the morphology of wood surfaces. *First International Conference of the European Society for Wood Mechanics*. Lausanne, Switzerland. (2001)

5. Hinescu A.,. *The book of universal carpenter (in Romanian)*. Bucharest: Technical Publishing House (1989).

6. Kacík F., Kubovsky I.,. Chemical changes of beech wood due to CO2 laser irradiation. *Journal of Photochemistry and Photobiology A: Chemistry*. 222 (2011).

7. Lin, C.J., Wang, Y.C., Lin, L.D., Chiou, C.R., Wang, Y.N. and Tsai, M.J.,. Effects of feed speed ratio and laser power on engraved depth and color difference of Moso bamboo lamina. *Journal Of Materials Processing Technology*. 198 (2008).

8. Năstase V.,. *Equipment and technology for furniture and other wooden products manufacturing*. Bucharest: Didactic and Pedagogical Publishing House (1991).

9. Petru, A., Lunguleasa, A.,. Colour measurement using digital image analysis. *International Conference of Scientific Paper AFASES*. Bra□ov (2014)

10. Petutschnigg A., Stöckler M., Steinwendner F., Schnepps J., Gütler H., Blinzer J., Holzer H., Schnabel T.,. Laser Treatment of Wood Surfaces for Ski Cores: An Experimental Parameter Study. *Advances in Materials Science and Engineering*. 2013 (2013).

11. Popa, E., Popa, V.,. *Alder, Poplar, Robinia Wood. Properties, Coloration*. Bra□ov: Transilvania University Publishing House (2004).

"HENRI COANDA"
AIR FORCE ACADEMY
ROMANIA

"GENERAL M.R. STEFANIK"
ARMED FORCES ACADEMY
SLOVAK REPUBLIC

INTERNATIONAL CONFERENCE of SCIENTIFIC PAPER
AFASES 2015
Brasov, 28-30 May 2015

# MATHEMATICAL MODEL FOR PORK BONELESS NECK TENDERIZING TO PRODUCE ROMANIAN TRADITIONAL PRODUCT "*CEAFĂ PERPELITĂ*"

**Adrian Roşca*, Petre Cîrdei****

*Faculty of Agriculture and Horticulture, University of Craiova, Romania, **National Institute of Research - Development for Machines and Installations Designed to Agriculture and Food Industry (INMA), Bucharest, Romania

***Abstract:*** *The paper presents a mathematical model to produce Romanian traditional cured-cooked-smoked pork boneless neck product "Ceafă Perpelită" type made after raw meat's mechanical tenderizing. The tenderizing process performed to decrease the duration of cured marinating period consists in passing several times the raw boneless neck among rollers with cutting prongs, and cyclic impulsive pressing of the meat, respectively. The mathematical model is based on force - extension diagrams obtained by using Werner - Bratzler testing method both for raw boneless neck and cured-cooked-smoked final product, too, for no tenderized raw boneless neck and after raw boneless neck mechanical tenderizing. The mathematical model consists in the geometric linear transforming of the characteristic diagrams obtained by using Werner-Bratzler method for the tenderized meat in comparison with the initial no tenderized meat. The model can be used to predict the mechanical characteristics of "Ceafă Perpelită", after boneless neck mechanical tenderizing.*

***Keywords:*** *mathematical model, meat tenderizing, Ceafă Perpelită, Warner-Bratzler testing method*

## 1. INTRODUCTION

To estimate tenderizing machine's and process' performances, is necessary to determine tenderized meat's mechanical characteristics, which could describe the meat qualitative transformations [12,13]. In principle, meat's tenderization represents the resultant of dynamic interdisciplinary processes consisting in chemical, biochemical and mechanical phenomena [8]. Thus, a mathematical model, represented by a complex system of variables and relationships, could be recommended to analyze meat's mechanical tenderizing [1,11].

In previous paper, Graiver proposed a mathematical model for the absorption of curing salts in pork's meat [2].

According previous research papers, the variables parameters of the mathematical model have to be based on experimental research data of meat diagrams determined by using Warner-Bratzler test method [6,7-9, 12,15].

Taking into account only the mechanical phenomena, a dynamic system involves different transformations of its internal parts under the action of given external forces. The mathematical models of the meat tenderizing process could be studied in further theoretical researches by applying automatic systems theory [3].

According to international and Romanian legislation, sodium nitrite, sodium or potassium nitrate ($NaNO_2$); $NaNO_3$/ $KNO_3$), are not permitted in traditional cured-smoked-

cooked products usual processing, and no brine injection is allowed [4,10]. In principle, the processing technology of these traditional cured-smoked-cooked product in small enterprises consists in: wet curing phase of entire pieces of muscle meat in 15% curing salt concentration, during 2-3 weeks; drying / ripening phase in cold air ventilation for 6-8 hours; cold smoke phase (20°C) for 2-3 days, followed by a short sequence of hot smoke phase (80°C), for 4-6 hours [10]. In order to reduce the wet curing phase, two types of tenderizing machines were used: *four roller tenderizer machine*, and *cyclic impulsive pressing machine* [9,10].

## 2. MATERIALS AND METHOD

**2.1. Experimental method and equipment.** In order to determine the influence of mechanical tenderizing method on raw pork bone-less neck tenderness, two different methods / machines were used: *four roller tenderizer machine*, and *cyclic impulsive pressing machine.*

*Four roller tenderizer machine* (FRT) is designed to increase the effective surface area for the extraction of meat proteins during subsequent compression and stretching processes. In its operation, the machine performs superficial or deep cuts in the piece of meat that passes through two pairs of tenderizer roller. In principle, the machine consists of two pairs of parallel tenderizing rollers (provided with a number of cutting prongs), located at a certain distance, that are rotated in opposite directions by an electromechanical transmission [9,10].

*Cyclic impulsive pressing machine* (CIP) is a semi-continuous meat press machine for meat's pressing before marinating [10]. If meat pieces are pressed with a significant amount of force applied more or less evenly throughout the piece of meat, it will tenderize the meat piece and condition the meat fibers so that marinade will be absorbed into the meat fibers (with no vacuum or pressure influence).

CIP consists in mechanical-pneumatically equipment, and a programmable automat. In principle, this mechanical-pneumatically equipment consists in an electro-pneumatically system (air compressor, solenoid valve), and two pressing plates (a fixed lower plate, and mobile upper plate). To improve the tenderizing process, each of the two plates (covered with food grade Teflon pad) has pyramidal prongs (6 · 6 · 6 mm) [9,10].

In order to determine the tenderizing process influence on pork boneless neck used to produce traditional cured – smoked - cooked product *"Ceafă Perpelită"*, 6 samples (raw pork boneless neck, and *"Ceafă Perpelită"* final product) were processed according four methods:

- no tenderized pork boneless neck (NO TEND);
- pork boneless neck tenderized by ten times successive passing amongst the cutting prongs of the FRT (FRT 10x);
- pork boneless loin tenderized by CIP in 30 pressing cycles, each consisting in 0,5s pressing periods, and 0,5s pauses periods (CIP 30-0,5 -0,5);
- pork boneless neck tenderized by CIP in 30 pressing cycles, each consisting in 10s pressing periods, and 0,5s pauses periods (CIP 30-10-0,5).

To produce *"Ceafă Perpelită"* by using no-tenderized pork boneless neck, the following traditional phases were used: wet curing phase of entire pieces of muscle meat (12% curing salt concentration), during 2 weeks; drying / ripening phase in cold air ventilation 6 hours; cold smoke (approx. 20°C) 10 hours, followed by 4 hours hot smoke (approx. 80°C).

To produce *"Ceafă Perpelită"* by using tenderized pork boneless neck, the tenderized pork boneless neck was processed in the following phases: wet curing (12% curing salt concentration), during *4 days*; drying / ripening phase in cold air ventilation for 6 hours; cold smoke (approx. 20°C) for 10 hours, followed by 4 hours hot smoke (approx. 80°C).

**2.2. Tenderness evaluation by using Warner-Bratzler method.** One of the most relevant and utilized methods to estimate meat's tenderness is Warner - Bratzler (W-B) shear test method. During W-B test the shear blade acts simultaneously compression and slicing/ shearing of the product [4, 7,8,11-15]. To perform experimentally researches concerning general texture and tenderness analysis, universal testing machine *Lloyd Instruments*

*LRXPlus 5* (Unconventional Technologies and Equipment for Agro-Food Industry Lab. - UTEFIL, within Faculty of Agriculture and Horticulture in Craiova) was used. Due to collaboration between UTEFIL and Environmental Eng. Lab. within Faculty of Electrical Engineering, a *Warner - Bratzler experimental equipment* was made: special rigid frame (food- grade Teflon) that permits fast fitting of interchangeable W-B shear blades (W1.4571) [7,8].

During these experiments, 100mm/min cutting speed was used.

Representative W-B test diagrams for pork boneless neck tenderized by using FRT 10 x methods, and for *"Ceafă Perpelită"* obtained by using this tenderized pork boneless, are presented in Figure 1 and Figure 2, respectively.

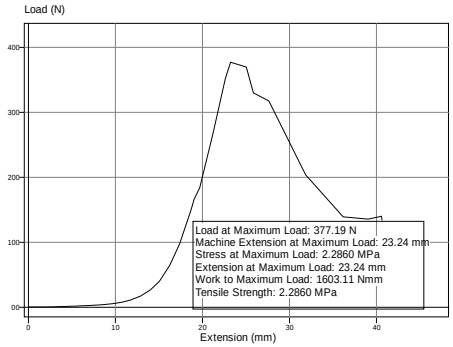


Figure 1. W - B test diagram for tenderized pork boneless neck by using FRT 10x

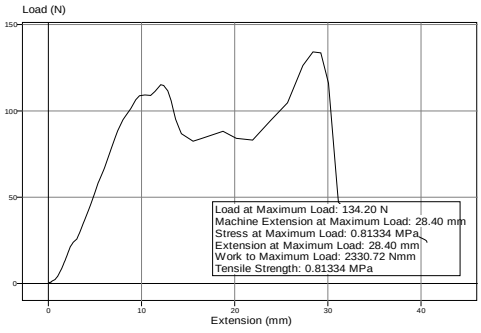


Figure 2. W - B test diagram for "*Ceafă Perpelită*" tenderized by using FRT 10x

## 3. RESULTS

**3.1. Mathematical model for meat tenderizing.** The mathematical model to study the influence of tenderizing method on meat tenderness is based on the hypothesis that any meat's final product material can be characterized by numerical curves obtained by mechanical characteristics experimentally determined for each tenderizing method. Resulting numerical curves could differ more or less from those of no tenderized meat samples.

In Figure 1 and Figure 2 is observed the maximum shear force that characterizes each type of pork boneless neck, and *"Ceafă Perpelită"* tenderness'.

Due to the inhomogeneous character of the meat's tissues, the maximum shear force cannot describe all the cutting / shearing process.

Therefore for each untenderized and tenderized pork boneless neck sample, and for each *"Ceafă Perpelită"* obtained by using these meat pieces, too, average curves that describe all evolution of the shearing diagrams obtained by using W - B method were numerical determined (in Figure 3 and Figure 4, for FRT 10x).

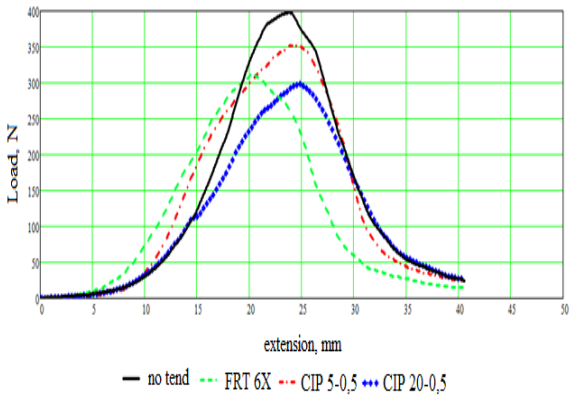


Figure 3. Numerical determined average curves of the four types of pork boneless neck samples NO TEND; CIP 30-0,5-0,5; CIP 30-10-0,5; FRT 10x

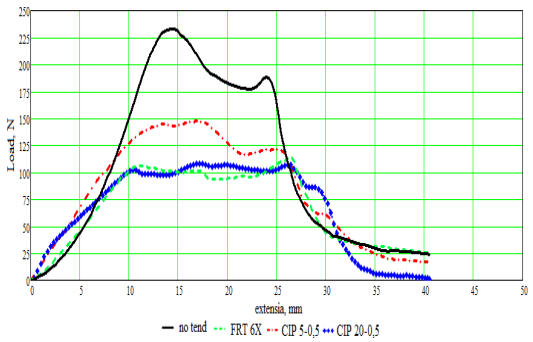


Figure 4. Numerical determined average curves of the four samples "*Ceafă Perpelită*" CEP-NO TEND; CEP-CIP 30-0,5-0,5; CEP-CIP 30-10-0,5; CEP-FRT 10x

The proposed mathematical model is based on the hypothesis that the characteristic curve of the sample (no tenderized, or tenderized by using mechanical methods), is obtained as a linear transformation that can be described by the vectorial equation [10]:

$$\begin{pmatrix} x' \\ F' \end{pmatrix} = T \begin{pmatrix} x \\ F \end{pmatrix} \quad (1)$$

where: $F$ is the shear force in N, $x$ is the cutting length / extension in mm, before tenderizing (characteristic curve coordinates of the meat sample, before tenderizing); $F'$ and $x'$ represent the shear force and the cutting length/ extension of the same meat sample type (characteristic curve coordinates, after tenderizing).

$T$ is the linear transformation given by the matrix [10]:

$$T = \begin{pmatrix} t_{1,1} & t_{1,2} \\ t_{2,1} & t_{2,2} \end{pmatrix} \quad (2)$$

where $t_{ij}$, $i$ =1,2; $j$ =1, 2 are real numbers.

It must be noticed that each force $F$ is represented by a pair of coordinates ($x_i$, $F_i$), $I$ = 1, $N$, and each force $F'$ is represented by a pair of coordinates ($x'_I$, $F'_i$), $i$ = 1, $N$. The matrix elements $T$ are calculated with relation [10]

$$\Im(t_{1,1}, t_{1,2}, t_{2,1}, t_{2,2}) = \sum_{i=1}^{N} [(t_{1,1}x_i + t_{1,2}F_i - x_i')^2 + (t_{2,1}x_i + t_{2,2}F_i - F_i')^2] \quad (3)$$

The solutions of relation (3) are determined by canceling the partial derivate in rapport with matrix coefficients' witch defines the linear transformation [10]

$$t_{1,1} = \frac{\left(\sum_{i=1}^{n} x_i^{(0)} x_i^{(1)}\right)\left(\sum_{i=1}^{n} F_i^{(0)2}\right) - \left(\sum_{i=1}^{n} x_i^{(1)} F_i^{(0)}\right)\left(\sum_{i=1}^{n} x_i^{(0)} F_i^{(0)}\right)}{\left(\sum_{i=1}^{n} x_i^{(0)2}\right)\left(\sum_{i=1}^{n} F_i^{(0)2}\right) - \left(\sum_{i=1}^{n} x_i^{(0)} F_i^{(0)}\right)^2} \quad (4.1)$$

$$t_{1,2} = \frac{\left(\sum_{i=1}^{n} x_i^{(1)} F_i^{(0)}\right)\left(\sum_{i=1}^{n} x_i^{(0)2}\right) - \left(\sum_{i=1}^{n} x_i^{(1)} x_i^{(0)}\right)\left(\sum_{i=1}^{n} x_i^{(0)} F_i^{(0)}\right)}{\left(\sum_{i=1}^{n} x_i^{(0)2}\right)\left(\sum_{i=1}^{n} F_i^{(0)2}\right) - \left(\sum_{i=1}^{n} x_i^{(0)} F_i^{(0)}\right)^2} \quad (4.2)$$

$$t_{2,1} = \frac{\left(\sum_{i=1}^{n} x_i^{(0)} F_i^{1}\right)\left(\sum_{i=1}^{n} F_i^{(0)2}\right) - \left(\sum_{i=1}^{n} F_i^{(1)} F_i^{(0)}\right)\left(\sum_{i=1}^{n} x_i^{(0)} F_i^{(0)}\right)}{\left(\sum_{i=1}^{n} x_i^{(0)2}\right)\left(\sum_{i=1}^{n} F_i^{(0)2}\right) - \left(\sum_{i=1}^{n} x_i^{(0)} F_i^{(0)}\right)^2} \quad (4.3)$$

$$t_{2,2} = \frac{\left(\sum_{i=1}^{n} F_i^{(0)} F_i^{(1)}\right)\left(\sum_{i=1}^{n} x_i^{(0)2}\right) - \left(\sum_{i=1}^{n} x_i^{(0)} F_i^{(1)}\right)\left(\sum_{i=1}^{n} x_i^{(0)} F_i^{(0)}\right)}{\left(\sum_{i=1}^{n} x_i^{(0)2}\right)\left(\sum_{i=1}^{n} F_i^{(0)2}\right) - \left(\sum_{i=1}^{n} x_i^{(0)} F_i^{(0)}\right)^2} \quad (4.4)$$

Based on described linear transformation, for pork boneless neck tenderized by using each method, the matrix $T$ elements are:

- pork boneless neck tenderized by CIP 30-0,5-0,5

$$T = \begin{pmatrix} 0.993 & -0.0002658 \\ -0.816 & 0.846 \end{pmatrix}$$

- pork boneless neck tenderized by CIP 30-10-0,5

$$T = \begin{pmatrix} 1.005 & -0.00005879 \\ 0.165 & 0.816 \end{pmatrix}$$

- pork boneless neck tenderized by FRT 10x

$$T = \begin{pmatrix} 0.999 & 0.0000962 \\ -0.449 & 0.723 \end{pmatrix}$$

The numerical tenderizing curves for pork boneless neck obtained by using the mathematical model are presented in Figure 5, Figure 6 and Figure 7, respectively.

In these three figures it can be observed that the configurations and the maximum amounts of the numerical tenderizing curves are similar with the average curves experimentally determined (Figure 3).

All these similarities validate the mathematical model based on proposed linear transformation.

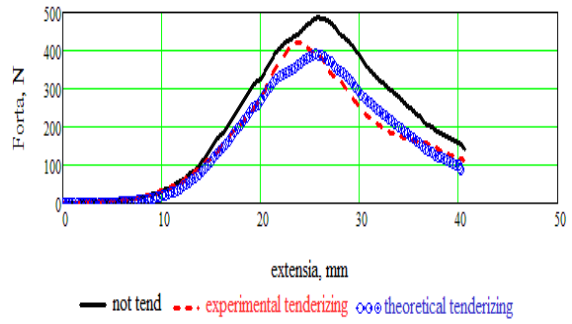


Figure 5. Numerical curves obtained by using the mathematical model for CIP 30-0,5-0,5 tenderizing

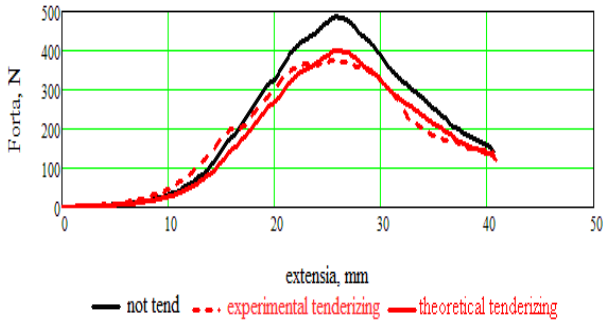


Figure 6. Numerical curves obtained by using the mathematical model for CIP 30-10-0,5 tenderizing

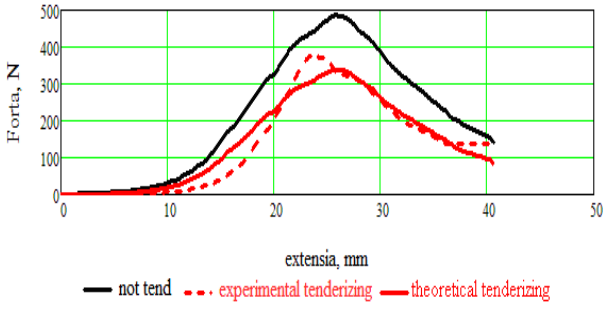


Figure 7. Numerical curves obtained by using the mathematical model for FRT 10x tenderizing

Based on described linear transformation, for *"Ceafă Perpelită"* tenderized by using each method, the matrix $T$ elements are:

- *"Ceafă Perpelită"* tenderized by CIP 30-0,5-0,5

$$T = \begin{pmatrix} 0.999 & 0.0004562 \\ 1.446 & 0.529 \end{pmatrix}$$

- *"Ceafă Perpelită"* tenderized by CIP 30-10-0,5

$$T = \begin{pmatrix} 1.001 & -0.0008085 \\ 1.446 & 0.529 \end{pmatrix}$$

- *"Ceafă Perpelită"* tenderized by FRT 10x

$$T = \begin{pmatrix} 0.992 & -0.000661 \\ 1.096 & 0.451 \end{pmatrix}$$

The numerical tenderizing curves for *"Ceafă Perpelită"* obtained by using the mathematical model are presented in Figure 8, Figure 9 and Figure 10, respectively.

In these three figures, it is observed that the maximum amounts and configurations of the numerical tenderizing curves are similar with the average curves experimentally determined (Figure 4). All these similarities validate the correctness of mathematical model based on proposed linear transformation.

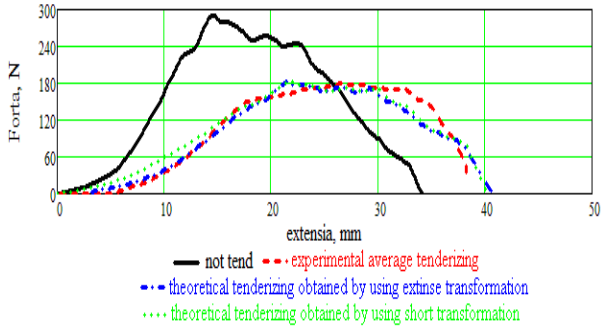


Figure 8. Numerical curves obtained by using the mathematical model for "*Ceafă Perpelită*" CIP 30-0,5-0,5 tenderizing

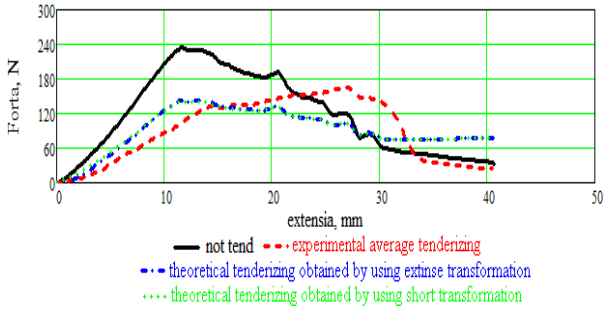


Figure 9. Numerical curves obtained by using the mathematical model for "*Ceafă Perpelită*" CIP 30-10-0,5 tenderizing

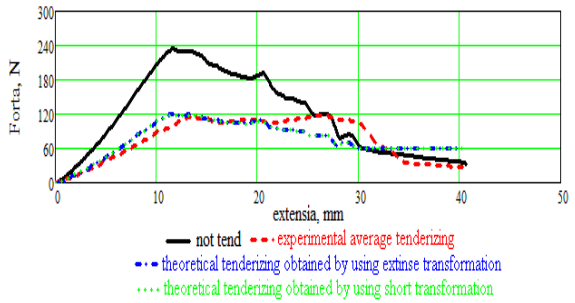


Figure 10. Numerical curves obtained by using the mathematical model for "*Ceafă Perpelită"* FRT 10x tenderizing

## 4. CONCLUSIONS

Mechanical tenderizing is a process that has to reduce the meat's mechanical characteristics amounts of the final product.

Each tenderizing method determines significant changes of specific strain within the meat's tissues, which determines the "*Ceafă Perpelită"* tenderness' improvement.

The main conclusion drawn in this paper refers the correctness of the mathematical model based on proposed linear trans-formation, proved both by the curves' configurations and the maximum amounts similarities' between the numerical tenderizing curves, too, and the average curves experimentally determined, respectively.

Further general and specific conclusions could be draw after this mathematical model will be applied for other types of meat, before and after the same or other mechanical tenderizing methods.

The data presented in this paper can be important for all the specialists interested in decreasing the wet curing period of the traditional meat products.

## REFERENCES

1. Bobancu, V., Mihaileanu, N., Gheorghita, S., Brezuleanu, A., Stefanescu, A., Balanescu, T., *Dictionary of general mathematics*. Bucharest: Romanian Enciclopedic Publishing (2007).
2. Graiver, N., Pinotti, A., Clifano, A., Zaritzky, N., Mathematical modeling of the uptake of curing salts in pork meat, *Journal Food Engineering*, Vol. 95/4 (2009).
3. Ionescu, V., Varga, A., *Systems Theory*. Bucharest: ALL Publising House (2009).
4. Institute of Food Technologists, Sensory evaluation guide for testing food and beverage products. *Food Technology*, 35/11(1981).
5. McGee, H., *On food and cooking: the science and lore of the kitchen.*Scribner (2004).
6. Roffel, B., Betlem, B., *Process Dynamics and Control, Modelling for Control and Prediction.* John Wiley & Sons Ltd. Pubsh. House (2006).
7. Roşca, A., Roşca, D., Instrumental texture evaluation - An objective measuring method for quality assurance in food industry. *Annals of the University of Craiova, Biology, Horticulture, Food produce processing technology, Environmental engineering Series*, vol. XLI (LII) (2011), Universitaria Pubsh. House Craiova. Available: http://cis01.central.ucv.ro/analele_universitatii
8. Roşca, A., Roşca, D., Instrumental texture evaluation - An objective method to evaluate fresh vegetables quality. *Journal Progress of Cryogenics and Isotopes Separation*, ICSI-ICIT Rm. Valcea, Vol. 16 (1) (2013).
9. Roşca, A., Roşca, D., Simion, A. D., Tenderizing machines for traditional meat products processing. *Journal Progress of Cryogenics and Isotopes Separation*, ICSI-ICIT Rm.Valcea, Vol. 18 (1) (2014).
10. Simion, A. D., Cârdei, R. P., Roşca, A., Bădescu, M., Roşca, D., Mathematical model based on Warner - Bratzler analyze method concerning tenderized pork boneless loin in order to produce Romanian traditional product "Cotlet Perpelit" type. *International Symposium ISB-INMA-TEH Bucharest* (2014).
11. Shewfelt, R. L., Consumer friendly specifications to meet the demands of a global market, *Food Australia*, vol. 52(2000).
12. Tyszkiewicz, I., Klossowska, B.M. Mechanical Tenderization of Pork Meat: Protein and Water Release due to Tissue Damage. *Journal of the Science of Food and Agriculture*, Vol. 73(2) (1996).
13. Xargayó, M., Lagares, J., Fernández, E., Borrell, D., Sanz, D., The impact of tenderization on increased slicing yield. Available: http://en.metalquimia.com/upload/document
14. Xianzhong, X., Shaofang, Y., An examination of the force generated from incisor penetration into foods with different textural properties. Part I: Experimental observation, *Journal of Texture Studies*, Special Issue, Vol. 42 (3)(2011).
15. www.lloyd-instruments.co.uk (2013).

"HENRI COANDA"
AIR FORCE ACADEMY
ROMANIA

"GENERAL M.R. STEFANIK"
ARMED FORCES ACADEMY
SLOVAK REPUBLIC

INTERNATIONAL CONFERENCE of SCIENTIFIC PAPER
AFASES 2015
Brasov, 28-30 May 2015

# THE INFLUENCE OF CYCLIC VACUUMING AND PRESSURING PROCESS ON TENDERIZING *SHEEP PASTRAMI*

**Daniela Roşca*, Adrian Roşca****

*Faculty of Electrical Engineering, University of Craiova, Romania, **Faculty of Agriculture and Horticulture, University of Craiova, Romania

***Abstract:*** *The paper presents the mechanical characteristics of Romanian traditional cured-smoked product "Sheep Pastrami", made by using sheep raw meat tenderized after successive cyclic vacuuming and pressuring process. These characteristics are based on the shear force diagrams obtained by using Werner - Bratzler testing method of the final product, before and after tenderizing process by using cyclic vacuuming and pressuring process. To decrease the duration of curing / marinating period, the performed tenderizing process is represented in 24 min pressuring and vacuuming cyclic processes consisting in successive pressuring and de - pressuring cyclic processing (0…10 bar), followed by vacuuming and de - vacuuming cyclic processing (0…-0,85 bar). The paper presents characteristic shear force amount obtained by using Werner - Bratzler testing method for the tenderized and cured-smoked final product, in comparison with pastrami made with no tenderized sheep raw meat sample.*

***Keywords:*** *cyclic vacuuming and pressuring process, sheep meat tenderizing, Warner-Bratzler test method*

## 1. INTRODUCTION

*Pastrami* (Turkish: *pastırma*, Romanian: *pastramă*, Yiddish: *pastróme*) is a popular delicatessen meat usually made from beef, and sometimes from pork, sheep, mutton or turkey.

The raw meat is brined, partially dried, seasoned with various herbs and spices, then smoked and/or steamed. The method for making *pastrami* was originally used to preserve beef from spoiling in a time before modern refrigeration. The word *pastramă* is etymologically rooted in the Romanian *a păstra* which means "to keep" or "to preserve". But the word is maybe more ancient and come from the Latin *pastor* who means *shepherd*; so *Pastramă* is *shepherd's meat* of lamb or mutton. The first versions of this preparation date back to the Ottoman Empire, where Turkish people salted and dried beef and sheep. Beef and sheep plates are the traditional primal cut for making *pastrami*, but these days it is more common to see made from beef's and sheep's brisket and breast [7-9].

The Romanian specialty was first introduced to the United States in a wave of Romanian Jewish immigration from Bessarabia and Romania in the second half of the 19th century, via the Yiddish (pronounced *pastróme*). Early references in English used the spelling "*pastrama*", closer to the Romanian original. Among Jewish Romanians, goose breasts were commonly made into *pastrami* because they were inexpensive.

Beef navels and briskets, and sheep brisket and breast were cheaper than goose meat in America, so the Romanian Jews in America adapted their recipe and began to make the cheaper beef and sheep *pastrami*, as they usually done in Romania [7-9].

Traditional *Pastrami* is a cured meat, that it has been quickly injected with brine usually containing preservation additives (in industrial process) or otherwise infused for long time with brine (in homemade or small enterprise process). Both sheep brisket and sheep breast are tenderless parts of the animal's carcass. Therefore in the industrial process the meat is tenderized 4-6 hours in massaging intermittent vacuum equipment (maximum relative vacuum -0,65 bar) [1]. American and West - European meat tenderizing recent research papers recommend increasing the vacuum level up to -0,95 bar, or high pressure process up to 5000 bar [5].

For the same reason, in homemade or small enterprise process, the meat is tenderized for 1-2 weeks in high concentration brine containing additional flavors added (marinated).

Mechanical tenderization action produces complex modifications of the meat tissues in order to increase the surface area and thereby facilitate extraction and solubilization during the massaging phase. Softening of the muscle is also obtained, making the meat more adaptable for cooking process.

Tenderization, pre-massage and massage are closely interrelated, and not all products require the same mechanical action. Thus the mechanical action must be intensified and adapted in order to compensate for some of the negative consequences that may result in the product's quality. This will depend on the rest of the process and, above all, on the presentation and final quality of the product itself [2,4].

In low-injection products where meat content represents more than 80% of the final composition, meat quality is a determining factor in mastication, while in more highly injected products, this is not as important as the process and technology used [13].

Then, traditional *pastrami* is cold smoked, and finally dried in ventilated cold air [7].

In order to reduce the duration of the wet - curing step as much is possible, and even to eliminate it, in some recent papers are presented considerations concerning the influence of pressuring cyclic process, and vacuuming cyclic process on cured-smoked final product tenderness [7-9].

This paper presents a new tenderizing method based on both pressuring and vacuuming cyclic process.

## 2. MATERIAL AND METHOD

In order to produce *Sheep Pastrami*, 10 pieces of sheep brisket and breast were used (Animal Slaughter Certificate: 2 sheep, 16 - 18 months, 26 -27 kg in carcass, individual small farm). Two of these pieces were used to produce *Sheep Pastrami* respecting traditional homemade or small enterprise process: the meat was pierced for 4 times (Figure 2), then infused for 5 days in 12% concentration brine, then cold smoked in several steps during 1 day, and finally, dried 24 hours in free ventilated cold air.

The piercing step was realized by using the *Multi-needle piercing device*, that in principle consists in 120 needles (ø5; edge $20^0$ conical sharp) disposed in the same shape and reciprocity distance as into the industrial brine injection equipment (Figure 1) [7-9].

The novel tenderizing method proposed in this paper consists in several cyclic pressuring and de - pressuring step, followed by cyclic vacuuming and de - vacuuming step of the raw meat and brining, too, into a vessel.

Figure 1. Sheep brisket manually pierced

During the pressuring process, the pressure level is 3-4 times higher than during brine injection in industrial equipment, and 2-3 times than the dynamic pressing during the massaging industrial process.

In order to put in evidence the influence of pressuring cyclic and vacuuming cyclic process

(PV-CP) on meat tenderization, *Experimental Equipment* (EE- PV-CP) was used.

*Experimental Equipment for PV-CP* and *Multi-needle piercing device* were designed and made by Environmental Protection in Industry Laboratory (EPIL) within Faculty of Electrical Engineering, in collaboration with Unconventional Technologies and Equipment for Agro-Food Industry Laboratory (UTEFIL) within Faculty of Agriculture and Horticulture, within the University of Craiova.

In principle, EE-PV-CP is composed in a pressuring and vacuuming process hydraulic cylinder (PV-HC) consisting in a cylindrical vessel (inner ø 80; length 180 mm) made in W1.4571 and a food grade Teflon made piston (Figure 2). PV-HC is provided with a manometer gauge (0…12 bar) for pressuring process monitoring, and a mano-vacuumeter gauge (-1… 1,5 bar) when vacuuming process is actuated. In order to evacuate the liquid / gas excess before and after PV-CP, the piston is provided with G1/4" tap connected to ø8 Rilsan tube [7-9].

In order to actuate the pressuring and vacuuming process into EE-PV-CP, universal testing machine *LBG 10* (within EPIL), was used.

Pressuring and vacuuming cyclic method consists in the following processing steps:

- The sheep brisket manually pierced (4 times, as was presented above) is introduced into the PV-HC of the EE-PV-CP that contains 12% concentration brine (proportion 1:1 for sheep brisket, and salt brine, respectively).

- Each pressuring and vacuuming cycle lasts 24 min consists in 4 successive steps, each lasting 6 min (Figure 3):

- pressuring cycle (3 minutes): slow pressuring (during 1 min) up to 10 bar; maintaining for 1 min at 10 bar, followed by fast depressuring up to the ambient atmosphere; maintaining for 1 min at the ambient atmosphere pressure;

- vacuuming cycle (3 minutes): slow vacuuming (during 1 min) up to -0,85 bar; maintaining for 1 min at -0,85 bar, followed by fast de-vacuuming up to the ambient atmosphere; maintaining for 1 min at the ambient atmosphere pressure.

For this paper were used 2, 3, 4 and 5, respectively, pressuring and vacuuming cycles that last 48 min (PV-CP 48), 72 min (PV-CP 72), 96 min (PV-CP 96), and 120 min (PV-CP 120), respectively. For each pressuring and vacuuming cycle process lasting 48 min, 72 min, 96 min and 120 min, respectively, two pieces of sheep brisket were used.

All the eight sheep brisket tenderized by using pressuring and vacuuming cyclic process were smoked and dried in the same time (and technological conditions) with the pieces used to obtain *Sheep Pastrami* by using traditional method.

The most relevant and utilized texture and tenderness tests is Warner - Bratzler shear test. The shear force behavior gives information about tenderness, as well as the bite characteristic products. The shear blade realizes compression for slicing / shearing tests on products [3,6,10-13].

Figure 2. Experimental Equipment for PV-CP

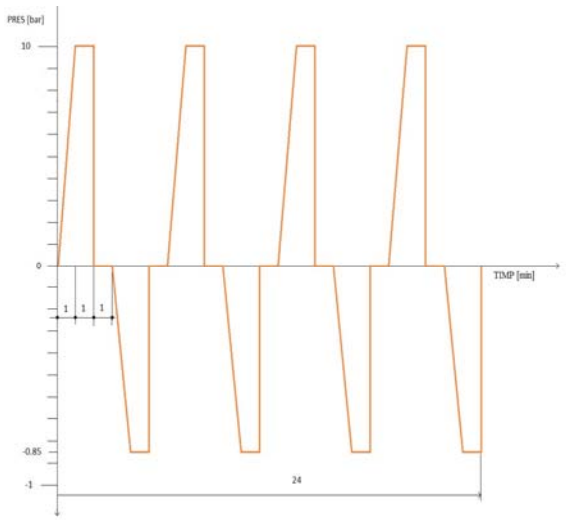


Figure 3. Pressuring and vacuuming cyclic process diagram

To perform interdisciplinary researches concerning general texture and tenderness analysis, universal testing machines *Lloyd Instruments LRXPlus 5* (within UTEFIL), was used since several years ago to perform comparative texture tests [6-9].

Due to collaboration between UTEFIL and EPIL, *experimental Warner - Bratzler equipment* was made: special rigid frame (made in food-grade Teflon) supporting a shear bar that permits interchangeable Warner - Bratzler shear blades sliding (square plate cut blade made in DIN W1.4571) into the frame [6-9].

During the experiment presented in this paper, 100mm/min cutting speed was used.

Warner - Bratzler testing sheer force of *Sheep Pastrami* obtained by using beef brisket tenderized by using PV-CP 96, is presented in Figure 4.


Figure 4. *Sheep Pastrami* obtained by using PV-CP 96, during Warner - Bratzler testing shear force

## 3. RESULTS AND DISCUSSIONS

In order to determine the influence of tenderizing process on the final product tenderness', *Sheep Pastrami* pieces made by using traditional homemade method, and tenderized pieces by using PV-CP, respectively, were tested by using Warner - Bratzler shear force method. During the Warner - Bratzler shear force tests, each of all 10 pieces of *Sheep Pastrami* were sliced in 6 parts. Warner - Bratzler shear force diagrams are presented in Figure 6 and Figure 7.

In Table 1 are presented: the maximum shear force amount and the shear force average for each of the five of *Sheep Pastrami* types; the de-crease of percentage average shear force (in comparison with traditional homemade *Sheep Pastrami*'s tenderness) by using each process method, that demonstrate the tenderness' increase of the final product, that was tenderized by using pressuring and vacuuming cyclic process.

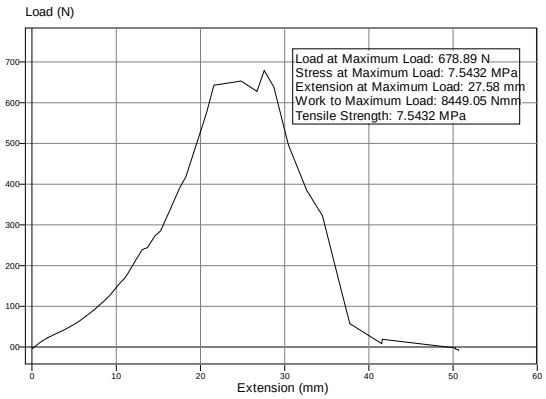


Figure 5. Warner - Bratzler shear force test diagram for *Sheep Pastrami* made by using traditional method

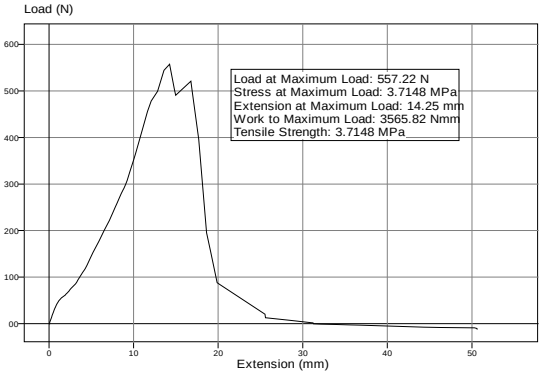


Figure 6. Warner - Bratzler shear force test diagram for *Sheep Pastrami* made by using PV-CP 72 method

Table 1 presents a synthesis of the influence of pressuring and vacuuming cyclic process on *Sheep Pastrami* final tenderness':

- in comparison with traditional homemade *Sheep Pastrami*'s tenderness, PV-CP 48 method determines a small tenderness' increasing of the final product (7,65%);
- in comparison with traditional homemade *Sheep Pastrami*, an important fast increasing (from 18,97% to 30,98%) of the final product tenderness' is observed when PV-CP 72 and PV-CP 96 were used;
- instead, very large increase (from 30,98% to 36,57%) of the final product *Sheep Pastrami* tenderness' is observed when PV-CP 96 and PV-CP 120, in comparison with traditional home-made *Sheep Pastrami*'s tenderness.

The influence of pressuring and vacuuming cyclic process on raw meat to obtain *Sheep Pastrami* determines 3-7% smaller amounts of the shear force than when pressuring cyclic process is used for tenderizing *Sheep Pastrami* [7].

Warner - Bratzler shear force for Sheep *Pastrami*

Table 1

| Sample code | Maximum shear force min…max amount, N | Shear force average, N | Decrease of shear force average, % |
|---|---|---|---|
| TRAD | 634,56...718,31 | 673,34 | - |
| PV-CP 48 | 587,23...642,78 | 621,85 | 7,65 |
| PV-CP 72 | 502,45...593,56 | 545,57 | 18,97 |
| PV-CP 96 | 447,67...509,11 | 464,73 | 30,98 |
| PV-CP 120 | 385,17...449,82 | 427,12 | 36,57 |

## 4. CONCLUSIONS

Cyclic pressuring and vacuuming process represents a novel method to obtain increasing of *Sheep Pastrami* tenderness'. Due to pressure and vacuuming amount levels, and fast pressuring and de - pressuring steps, and vacuuming and de-vacuuming, too, cyclic pressuring and vacuuming process effect's determines much faster osmosis phenomena that realizes the brine infusion into the meat' tissues, and *no other wet salting / brining is necessary*.

The method presented in this paper is better in efficiency term than pressuring cyclic processing and represents a much more intensively tenderizing method than massaging vacuum equipment in industrial processing [7].

As one of the most recommended analyze method, the Warner - Bratzler shear force test offered objective results concerning the influence of cyclic pressuring and vacuuming process on meat final products tenderness'.

The method and the results presented in this paper opens further experimental researches concerning the influence of similar cyclic pressuring and vacuuming process (higher pressure level, shorter or longer pressuring and de-pressuring, vacuuming and de-vacuuming, too) to produce *Sheep Pastrami*, by using other much more tenderless parts of animal's carcass.

## REFERENCES

1. Institute of Food Technologists, Sensory evaluation guide for testing food and beverage products. *Food Technology*, 35/11(1981).
2. McGee, H., *On food and cooking, the science and lore of the kitchen*. Scribner (2004).
3. Huidobro, R. de F., Miguel, E., Blazquez, B., Onega, E., A comparison between two methods (Werner-Bratzler and texture profile analysis) for testing either raw meat or cooked meat, *Meat Science*, Vol. 69, Issue 3 (2005).
4. Maddock, R., *Mechanical Tenderization of Beef*, Research RKM & Knowledge Management (2008).
5. *Larousse Gastronomique*, Hamlyn Publishing House, (2000)
6. Roşca, A., Roşca, D., Instrumental texture evaluation - An objective measuring method

for quality assurance in food industry. *Annals of the University of Craiova, Biology, Horticulture, Food produce processing technology, Environmental engineering Series*, vol. XLI (LII) (2011), Universitaria Pubsh. House Craiova. Available: http://cis01.central.ucv.ro/analele_universitatii/

7. Roşca, A., Roşca, D., The influence of pressuring cyclic process on tenderizing Sheep Pastrami, *Annals of the University of Craiova, Biology, Horticulture, Food produce processing technology, Environmental engineering Series*, Vol. XIX (LV) (2014), Available: http://cis01.central.ucv.ro/analele_universitatii/

8. Roşca, A., Roşca, D., The influence of pressuring cyclic process on tenderizing Beef Pastrami, *Annals of University of Craiova, Biology, Horticulture, Food produce processing technology, Environmental engineering Series*, Vol. XIX (LV) (2014), Universitaria Pubsh. House Craiova. Available: http://cis01.central.ucv.ro/analele_universitatii/

9. Roşca, D., Roşca, A., The influence of pressuring and vacuuming cyclic process on tenderizing Beef Pastrami, *Annals of the University of Craiova - Agriculture, Montanology, Cadastre Series*, Vol. XLIV/1 (2014), Universitaria Pubsh. House Craiova. Available: http://cis01.central.ucv.ro/analele_universitatii/

10. Rui, M. S. Cruz, Khmelinskii, I., Vieira, M., *Methods in Food Analysis*, CRC Press, Taylor and Francis Group, LCC (2010).

11. Shackelford, S. D., Morgan, J. B., Cross, H. R., Savell, J. W., Identification of threshold levels for Werner - Bratzler Shear force in beef top loin steaks, *Journal of Muscle Foods*, Vol. 2, issue 4 (1991).

12. Wheeler, T. L., Shackelford, S. D., Koohmaraie, M., Warner-Bratzler Shear Force Protocol, *USDA-ARS U.S. Meat Animal Research Center* (1995). Available: http://www.ars.usda.gov/SP2UserFiles/Place/54380530/protocols/Warner-BratzlerShearForceProtocol.pdf

13. Wheeler, T. L., Shackelford, S. D., Miller, M.F., Johnson, L.P., Miller, R.K., Koohmarie, M., Standardizing collection and interpretation of Warner-Bratzler shear force and sensory tenderness data, *Journal of Animal Science*, Vol. 75, no. 9 (1997).

"HENRI COANDA"
AIR FORCE ACADEMY
ROMANIA

"GENERAL M.R. STEFANIK"
ARMED FORCES ACADEMY
SLOVAK REPUBLIC

INTERNATIONAL CONFERENCE of SCIENTIFIC PAPER
AFASES 2015
Brasov, 28-30 May 2015

# THE INFLUENCE HEAT TRANSFER COEFFICIENT ON WOOD CONSTRUCTION

**Cosmin Spîrchez*, Aurel Lunguleasa***

*Faculty of Wood Engineering, Transilvania University of Brasov, Romania

***Abstract:*** *The paper presents types of insulation materials and their importance on wooden construction. Using computer software allowed the determination of heat transfer coefficient. The heat transfer coefficient has great importance for wood construction.*

***Keywords:*** *insulation material, wood, heat transfer coefficient*

## 1. INTRODUCTION

Green buildings are considered to be those that simultaneously meet the following conditions [1]:

- Have a constructive and functional structure and a process for achieving that don't contribute to environmental degradation (built and natural) and environmental factors.
- Allows efficient use of resources (water, energy) throughout the entire lifecycle.
- Meeting the technical requirements of the design and use, as well as the strength and stability, fire protection, health protection.
- Can carry and use with costs borne by investors.
- Meet the needs or expectations of the user from the sustainability, efficiency, comfort, and aesthetics.

Natural constructions are a similar concept in practice applied mainly small-scale and are characterized by:

- The use of natural buildings materials.
- Using materials and methods, manufacturing techniques near the place of their establishment and functioning.

Natural building concept corresponds to practice organic architecture and green architecture [1].

## 2. INSULATION MATERIALS USED TO WOOD CONSTRUCTION

**Natural fiber insulation**:

- sheep wool insulation;
- hemp fiber insulation;
- wood fiber insulation.

**Sheep wool insulation** is manufactured from natural wool fibers, washed and treated. These wool fibers are held either mechanically or using a maximum of 12% polystyrene fibers to form sheets or rolls.

Wool insulation is used as heat and sound insulation. Wool is a hygroscopic material which means that it is designed to absorb up to 30-40% of its own weight in moisture content. Thermal conductivity is between 0.0356

W/mK-0,040 W/mK. Sheep wool insulation is fire resistant[1].

**Hemp fiber insulation.** Insulation is manufactured from hemp fiber plus 10-12% Biko fibers for excellent dimensional stability.

Recently appeared insulation that is 100% natural hemp fibers Biko optional when natural fibers are replaced with corn[1].

Hemp is capable of absorbing up to 20% of its weight in moisture content. Hemp fiber insulation has low conductivity of 0.040 W/mK.

**Wood fiber insulation.** Raw materials for manufacture of insulated panels are wood fiber waste from wood chips.

Wood fibers obtained from wood chips can be treated by up to 2% paraffin.

Roofs are building elements serving the protection at the top of the building against climate action.

To perform this operation, the roof must ensure the collection and removal of meteoritic water, in order to prevent damages that may occur in their penetration into the building.

Roofs are divided into 2 groups: framing roofs, terrace roofs [2].

Roof framing type includes the following elements are: roof covering, elements accessories.

In fig.1 presents longitudinal framing walls for 11.00 m < L < 13.00 m.

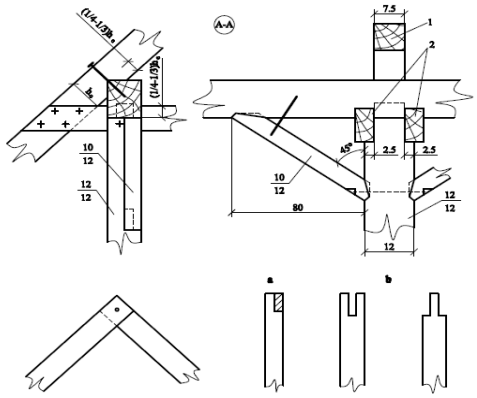

Fig. 1 Longitudinal framing walls for 11.00 m < L <13.00 m

1- rafter;
2- plier (7.5 * 15);

In fig.2 presents longitudinal framing walls for 11,00 m < L < 13,00 m.

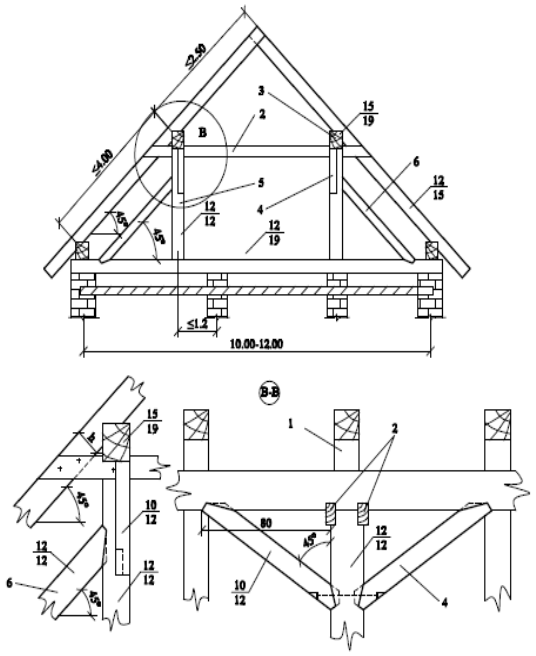

Fig.2 Longitudinal framing walls for 11.00 m < L <13.00 m

1- rafter;
2- plier (7.5 * 7.5);
3- base;
4- truss;
5- post.

In fig. 3 presents median longitudinal framing walls.

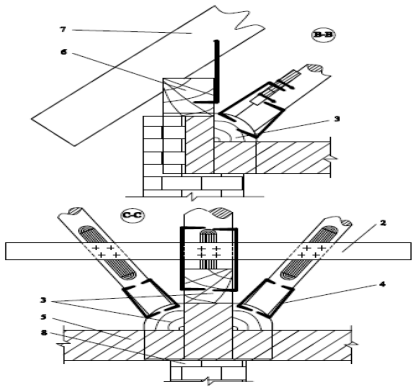

Fig.3 Longitudinal framing walls for 9.00 m < 11.00 m

In fig. 4 presents median longitudinal framing walls.

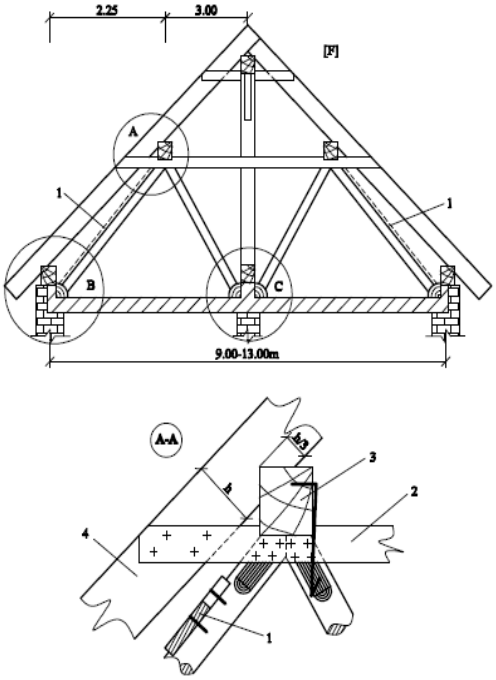


Fig. 4 Longitudinal framing walls for 9.00 m < L < 13.00 m

## 3. OPTIMIZATION STRUCTURE FOR PASSIVE ENERGY HOUSE

The paper has been taken to study three structures of insulation for passive energy house.

With software from German company (www.u-wert.net) were mapped graphics on temperature variation profiles coefficients from moisture and heat [3].

The structure of 1 taken for analysis is made of MDF (thickness 16 mm, coefficient of thermal conductivity of 0.13 W / mK), hamp (thickness 100 mm, coefficient of thermal conductivity of 0.04 W / mK), OSB (thickness 12 mm, coefficient of thermal conductivity of 0.11 W / mK), climacell (thickness 200 mm, coefficient of thermal conductivity of 0.04 W / mK).

Figure 5 shows the temperature variation of structure 1.

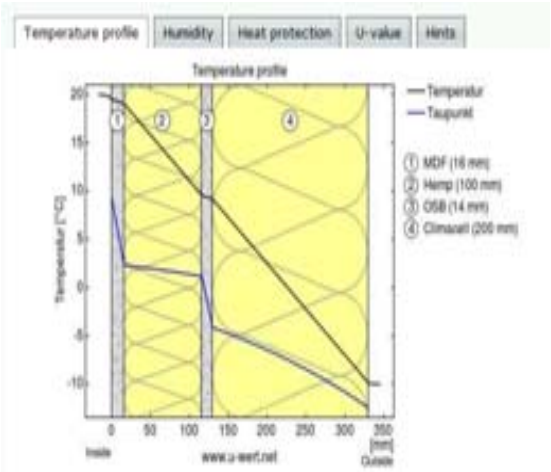


Fig. 5 Temperature variation for structure 1

In fig. 6 shows the variation thermic protection coefficients for structure 1.

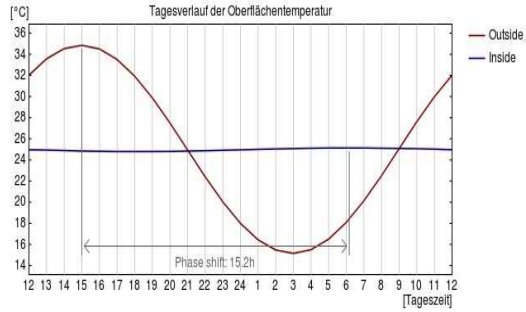


Fig. 6 Variation thermic protection coefficients for structure 1

The structure of 2 taken for analysis is made of gypsum fiberboard (thickness 16 mm, coefficient of thermal conductivity of 0.32 W/mK), KnaufTecTem (thickness 100 mm, coefficient of thermal conductivity of 0.045 W/mK), Gutex Multhiterm (thickness 14 mm, coefficient of thermal conductivity of 0.042 W / mK), Isocell (thickness 200 mm, coefficient of thermal conductivity of 0.04 W / mK).

Figure 7 shows the temperature variation of structure 2.

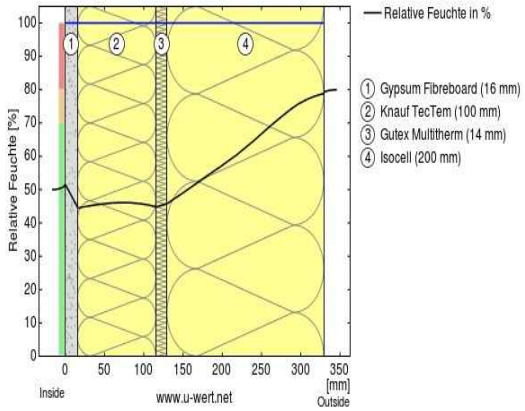


Fig.7 Temperature variation for structure 2

In fig.8 shows the variation thermic protection coefficients for structure 2.

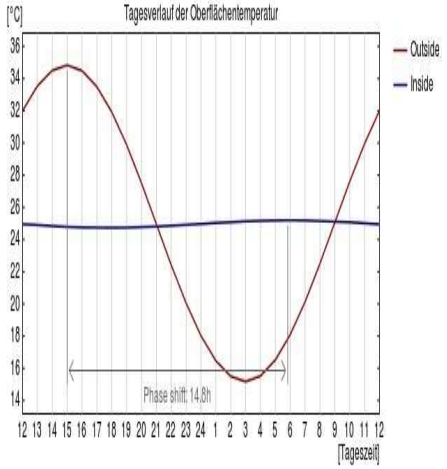


Fig.8 Variation thermic protection coefficients for structure 2

The structure of 3 taken for analysis is made of wool (thickness 16 mm, coefficient of thermal conductivity of 0.04W/mK), mineral (thickness 100 mm, coefficient of thermal conductivity of 0.045W/mK), cellulose (thickness 14 mm, coefficient of thermal conductivity of 0.04 W/mK), folio (thickness 200 mm, coefficient of thermal conductivity of 0.22 W / mK).

Figure 9 shows the temperature variation of structure 3.

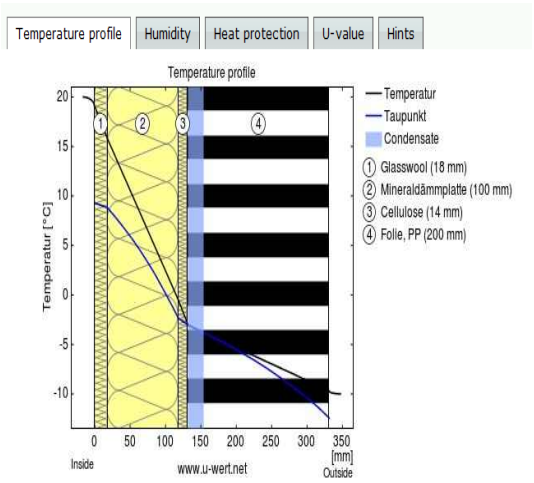


Fig.9 Temperature variation for structure 3

In fig.10 shows the variation thermic protection coefficients for structure 3.

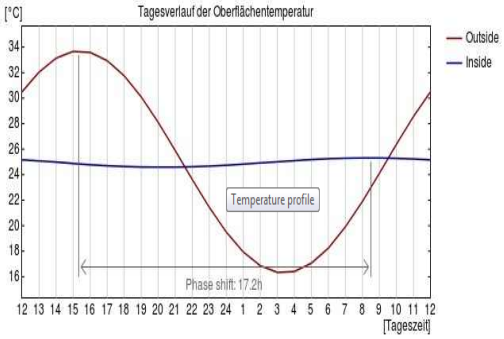


Fig. 10 Variation thermic protection coefficients for structure 3

## 4. CONCLUSIONS

Given that structure 1 heat transfer coefficient U = 0.127 W/m$^2$K, structure 2 is the heat transfer coefficient U = 0.128 W/m$^2$K, structure 3 is the heat transfer coefficient U = 0.244 W/m$^2$K. The optimum structure is 1.

A low U-value indicates a high level of insulation.

## REFERENCES

1. Bucur, I., *Eco managementul cladirilor*. City Constanta: Publishing House (2002).
2. Lazarescu C-tin., *Constructii din lemn*, Brasov, Transilvania University of Brasov, Publishing House (2008).
3. Tutorial Program *www.u-wert.net*

"HENRI COANDA"
AIR FORCE ACADEMY
ROMANIA

"GENERAL M.R. STEFANIK"
ARMED FORCES ACADEMY
SLOVAK REPUBLIC

INTERNATIONAL CONFERENCE of SCIENTIFIC PAPER
AFASES 2015
Brasov, 28-30 May 2015

# TRANSMISSION CODING SYSTEM USING HAMMING ENCODING FHSS

**Gabriel ANASTASIU*, Elena ANASTASIU****

*Faculty of Electrical Engineering and Computer Science, University of Suceava, Romania,
**"Alexandru cel Bun" College, Gura Humorului, Romania

***Abstract:*** *Current issues facing many communication systems, especially the unauthorized interception requires solving by various methods against jamming type. These methods range from sub-level coding and coding to mixed. In this article I present a mixed method that can be used in various transmission systems.*

***Keywords:*** *jamming, hamming, coding level.*

## 1. INTRODUCTION

In current systems need the possibility of transmission observed "hide" or encoding information using different coding elements.

This signal encoding is required when sending confidential data or maximum security, such as a military system.

In this article I will try to present their own contribution and that makes a double coding of data, which provides a good security system to intercept and a small cost. The system presented below is an experiment conducted on a small scale but can be extended to other professional type systems using other modules such as performing Intel Intel Edisson or Galileo.

## 2. SYSTEM DESCRIPTION

The system is based on two elements modular development board Arduino Leonardo [6] and Pololu Wixel radio [7].

Leonardo Arduino development board is made by people from Arduino and is a board based on ATMEGA32U4. It has 20 pin digital input / output (of which 7 can be used as PWM outputs and 12 analog inputs and a micro USB connection. It also has 6 analog inputs / outputs that can connect different sensors, figure 1:


Figure 1. Arduino Leonardo parts.

Pololu Wixel transceiver type plate, Figure 2 [6] is a development board radio operating at 2.4 GHz frequency and allows multiple applications among which one you will use this material, i.e. FHSS (Frequency Hopping Spread Spectrum). Implementation plate modulation is done by programming the micro

USB port and then the communication between Arduino board and Wixel.

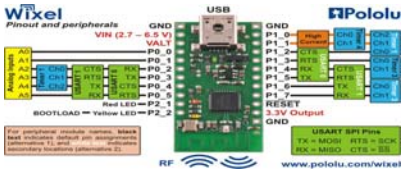


Figure 2. Pololu Wixel Board.

Block diagram of the proposed system is given in Figure 3:

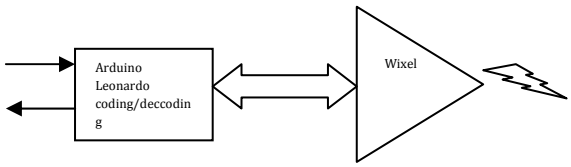


Figure 3. Block diagram.

## 3. CODING SYSTEM IMPLEMENTATION DECODE Hamming FHSS

From the block diagram it can be seen that the application source coding system is the module Arduino Leonardo. Following tests using NRZ coding or Hamming [1] revealed that only encoding that provides secure is indeed a model Hamming coding.

Hamming encoding is defined in the literature as correcting code and error detector and two errors.

The code contains four data bits d1, d2, d3, d4 and 3 parity bits p1, p2, p3. Parity bits are calculated as follows:

p1 sums d1, d2, d4
p2 sums d1, d3, d4
p3 sums d2, d3, d4

Organize bits in the code-word is:

p1 p2 d1 p3 d2 d3 d4

The encoding: code-word is determined by calculating the corresponding parity using both look how odd parity and parity.

The decoding: Calculated parity check with the appropriate and correct actually sums and correct parity and check showing 0.

An example of Hamming coding based on which system you implement an algorithm for Arduino Leonardo is:

The encoding enters the code-word 1001. We calculate:

p1 = 1+0+1 = 0
p2 = 1+0+1 = 0
p3 = 0+0+1 = 1

resulting Hamming code 0 0 1 1 0 0 1 s are represented by the underlined parity bits.

The decoding: 0011001. We assume that you received without errors. We will reconstruct the data bits: 1 0 0 1

Parity should be checked:

p1 + d1 + d2 + d4 = 0 + 1 + 0 + 1 = 0
p2 + d1 + d3 + d4 = 0 + 1 + 0 + 1 = 0
p3 + d2 + d3 + d4 = 1 + 0 + 0 + 1 = 0

How these values are 0 results that there was error. We implemented an application that supplied after running the Arduino environment Arduino Sketch_apr17a [2], the example shown above, the result provided below:

***this works for message of 4bits in size***
***enter message bit one by one: 1 2 3 4***
***the encoded bits are given below:***
***1 2 3 0 4199040 7 6 4201166 4***

Code will be forwarded obtained board transceiver type Pololu Wixel is scheduled to work FHSS mode. Spread Spectrum modulation techniques such techniques are defined as the bandwidth of the transmitted signal is much larger than the bandwidth of the original message, and the bandwidth of the transmitted signal is determined by the message to be transmitted and an additional signal known as the spreading code. Spectrum technology was first used during World War II by the army, which has experienced extended spectrum, low interference because it offered much-needed security. Are two ways to achieve spread: frequency hopping and direct sequencing? Frequency hopping is one of the variants of spread spectrum techniques that allow the coexistence of multiple networks (or other devices) in the same area. Frequency hopping is resistant to attempts to decode multiple frequencies by multiplying mechanism. Frequency hopping radio transmission is a technique where the signal is divided into several parts and then transmitted through the ether using a random pattern of jumping or "jump" frequencies. The frequency hopping may be several times a second to a few thousand times per second. Frequency

hopping is the most easy to use spread spectrum modulation model. Any radio with digital control type frequency synthesizer can theoretically be used in a radio system with frequency hopping. This conversion requires the addition of a generator pseudo noise (PN) code to select frequencies for transmission or reception. The best type FHSS systems using a uniform frequency hopping band. FSS subsystem produces an effect of spreading pseudo random jump RF carrier frequency over disponibile. The RF frequencies are denoted f1 ... FN where N may represent several radio harmonics made or more. An illustration of a FHSS system type is given in Figure 5:

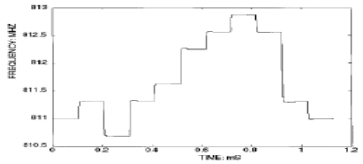

## 4. EXPERIMENTAL RESULTS

To achieve a real implementation of a software module to perform a FHSS Pololu Wixel [7] we started from a dedicated algorithm which comply with the elements of Figure 5, Figure 6:

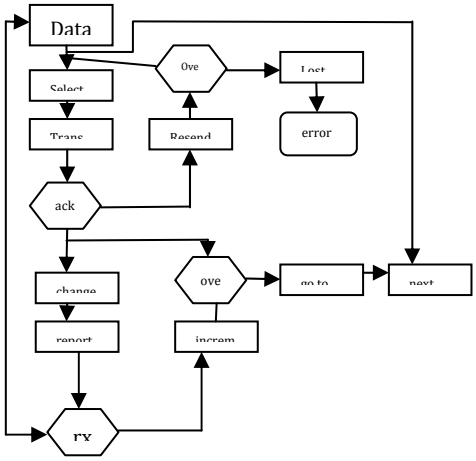


Figure 6. Algorithm model FHSS WIXEL.

The implementation of this algorithm translates as the workings of the FHSS Wixel plate. So the result is a signal output which theoretically cannot be decoded unless known mathematical models applied, where it can be seen mixing Hamming coded signal over-bearing.

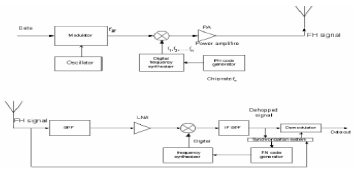

Figure 7. Wixel signal output.

If assume 1-bit error:

1. If 1 check bit bad:
   Data is good, check bit itself got corrupted.
   Ignore check bits. Data is good.
2. If more than 1 check bit bad:
   Data in error (single-bit error in data). *Which* check bits are bad shows you exactly where the data error was. They point to a *unique* bit which is the bit in error. In figure 9 is the FHSS over Hamming function of time.

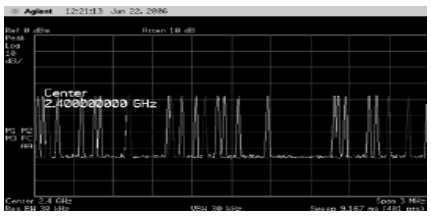


Figure 9. Wixel output signal.

Implementation scheme is illustrated in Figure 10 and can see two basic components development board Arduino Leonardo Pololu Wixel.

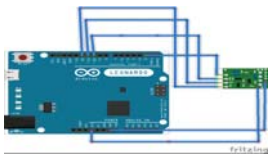

Figure 10. Schematics implementation.

Software implementation results in part described in chapter three of this article are measurable and can be highlighted and achieve primary receiving system that logically plays decoder. To achieve a simulation of the transmission system described in the article we used a number of lines of code containing information that a wanted transmitted. View information from the system I viewed it on the Arduino Leonardo serial interface, results are outlined in chapter 3, figure 11:

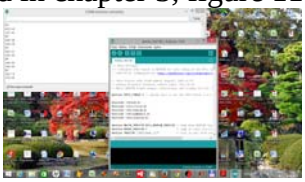

Figure 11. Data representation Serial Terminal.

The implementation of this algorithm and combining with FHSS modulation coding type Hamming we got a system that is difficult to decode, at least theoretically but can be studied and implemented other more advanced systems such as Intel development board Galileo or Intel Edison. Such a system can provide a coding system to satisfy the requirements of civil and military.

## 5. CONCLUSIONS & ACKNOWLEDGEMENT

Applying this dual coding system can be very useful because FHSS is highly resistant to both the jamming systems, simply because the algorithm to achieve the “frequency hopping” allows "insurance" in front of potential intruders but also because of coding Hamming type that allows error correction.

This paper was supported by the project "Sustainable performance in doctoral and post-doctoral research PERFORM - Contract no. POSDRU/159/1.5/S/138963", project co-funded from European Social Fund through Sectorial Operational Program Human Resources 2007-2013.

## REFERENCES

1. Micolau, J., Juvilla, O., "Hamming Block Codes”, Raymond Hills, January (2000).
2. R.Petraru, and A.Velicu, “Basic practical elements in the deployment of embedded microprocessors using Arduino,” Ed.Techno Media Sibiu, 2014 (*references*)
3. Robofun, Arduino for beginers
4. R.Santos, “Random Nerd Tutorials”
5. www.robofun.ro .
6. http://www.pololu.com .
7. http://www.arduino.cc .
8. http://www.ee.unb.ca/tervo/ee4253/Hamming.htm.

"HENRI COANDA"
AIR FORCE ACADEMY
ROMANIA

"GENERAL M.R. STEFANIK"
ARMED FORCES ACADEMY
SLOVAK REPUBLIC

INTERNATIONAL CONFERENCE of SCIENTIFIC PAPER
AFASES 2015
Brasov, 28-30 May 2015

# USING BIG DATA FOR INTELLIGENT BUSINESSES

**Cristian Bucur***

*University of Economic Studies, Bucharest & Petroleum and Gas University, Ploiesti, Romania

***Abstract:*** *Big data changes the way organizations use their data infrastructure and data analytics software platforms. This article presents an overview of the current technologies involved and is presented the use cases of big data systems. Also is presented a general architecture and how data analytics system evolved from traditional data warehouses. Are discussed the main challenges a company is faced when implementing a big data system and how the new technology is perceived by organizations.*

***Keywords:*** *big data, business intelligence, data warehouse, nosql.*
***MSC2010*:** *97P30, 97R10, 97R50.*

## 1. INTRODUCTION

We face today an extraordinary revolution of communications, which lead to a staggering quantity of data available. Apart from technical evolution that made possible to store and compute these data, an important role is played by improved statistical and computational methods that made possible to analyze and discover knowledge.

Big data is the term used to describe this massive volume of structured or unstructured data collected that is too large to be processed with traditional methods.

According to Gartner (http://www.gartner.com /doc/code/235055 ?ref=ddisp) the definition of big data is: a high volume, velocity and variety of information assets that necessitates innovative forms of processing in order to enhance process optimization or business insights and decision making. To the "three Vs" definition of analyst Doug Laney from Gartner, SAS added two more dimensions: variability and complexity [18]. Data flows can be inconsistent and vary in time, so it can be complicated to deal with peaks and also data has multiple sources, so necessitates be matching and transforming to acquire correlations.

## 2. USE CASES

A big data system is capable to generate complex processes and deeper business insights than existing data warehouse and business intelligence systems. These systems are not limited to providing support for decision making, could be also used for:

- Marketing and sales growth - One use is developing a recommendation engine for making purchasing suggestions to customers based on their interests compared with comportment of millions of other customers. Another is to optimize sale conversion process by tracking the actions of customer and getting insights on how can be improved. Also big data could help obtain customer segmentation for companies, helping them to make personalized offers and targeted campaigns.
- Risk and compliance management - insurance or credit companies could use a big data system to detect specific associations or

comportments associated with lower risks of default.

- Behavioral analytics - in sociology the scientists can learn about specific people habits and customs.
- Allocation of resources - in public services determining the efficient allocation of people by predicting where is most likely to need them, reduction of costs or optimizing the consumption of resources in a city by monitoring data received from sensors.
- Improvement of performance in operational department - by analyzing companies entire data you can detect the non-functional areas.
- Improving financial performance of enterprise - one example would be the reduction of maintenance costs by determining exactly which equipment is likely to fail.
- Monetization of data - studies made on a specific domain market and customers could be sold to other players in the same domain.
- Fraud detection - in case of financial firms' big data could be used to detect fraud schemes and anomalies in operations by analyzing multiple sources of data in real time.
- Innovation of new services or products - by analyzing the sentiment and expectation of customers regarding companies or competition products.

## 3. ARCHITECTURE OVERVIEW

Big data analytics systems apply analytic capabilities to large and varied datasets. Such new systems combined to traditional data warehouses or online analytical processing OLAP, enlarged the domain of application for decision support systems. Studies show that big data implementations would not replace data warehouses but due to new specifications in terms of volume, speed and variety of data, the traditional model would be modified to logical data warehouses LDW, which integrates multiple structures and types of data sources interconnected [6].

A typical enterprise data warehouse architecture [11] showed in the figure below is made of several sources of data that provides information for a staging area from where data is transformed and stored in EDW. The presented architecture assumes that data marts are part of EDW and the application know which database to query for data. Is also introduced a sandbox optional area for storing uncertified data.

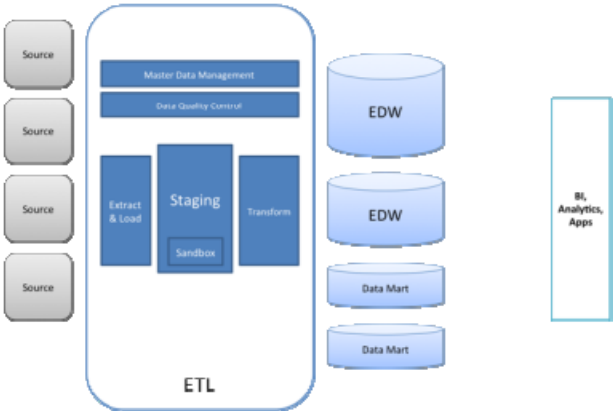


Fig. 1 Typical Enterprise Data Warehouse (EDW) architecture (source: http://cognilytics.com/blog1-php/)

A modern EDW architecture would necessitate replacing of staging area with a data lake based on Hadoop. A data lake (http://en.wiktionary.org/wiki/data_lake) is a term which defines a massive repository for storing big data. Unlike data marts designed to perform analysis and storing only some attributes of data, a data lake is designed to keep all the data attributes. It is designed to be easy accessible and made from relatively cheap hardware for storing massive data.

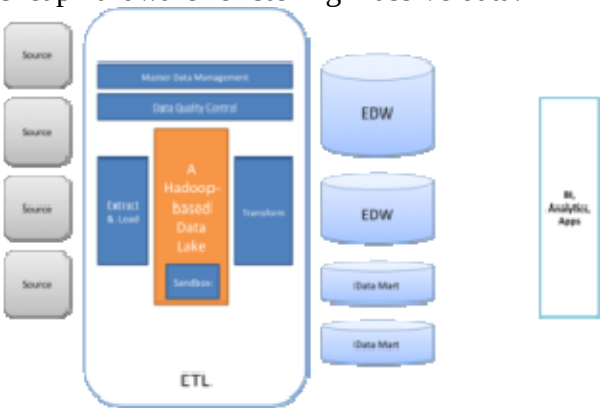


Fig. 2 Changes in EDW architecture caused by big data (source: http://cognilytics.com/blog1-php/)

Hadoop (https://hadoop.apache.org/) is an open source software developed by Apache for distributed computing. It is a framework that manages processing large volume of data in clusters of computers utilizing simple programming models, designed to scale to multiple servers and detect and handle failures

at application layer to deliver high-availability. It is written in Java and was developed after Google's MapReduce and Google File System (GFS)[1].

According to [11] some characteristics of a data lake are:

- Raw data can be stored permanently not just temporary
- It include tools used to make analysis on raw data
- Can store semi structured or unstructured data
- Provides effective and extensible platform for sandboxes
- Reduces costs of storage and processing

Apart from above advantages, Hadoop used in a data lake could solve one important problem of traditional architectures, the lack of agility.

In the figure below we present a general infrastructure for Big Data [14]. It includes layers for data management usually solved by cloud and analytics, requiring computing clusters.

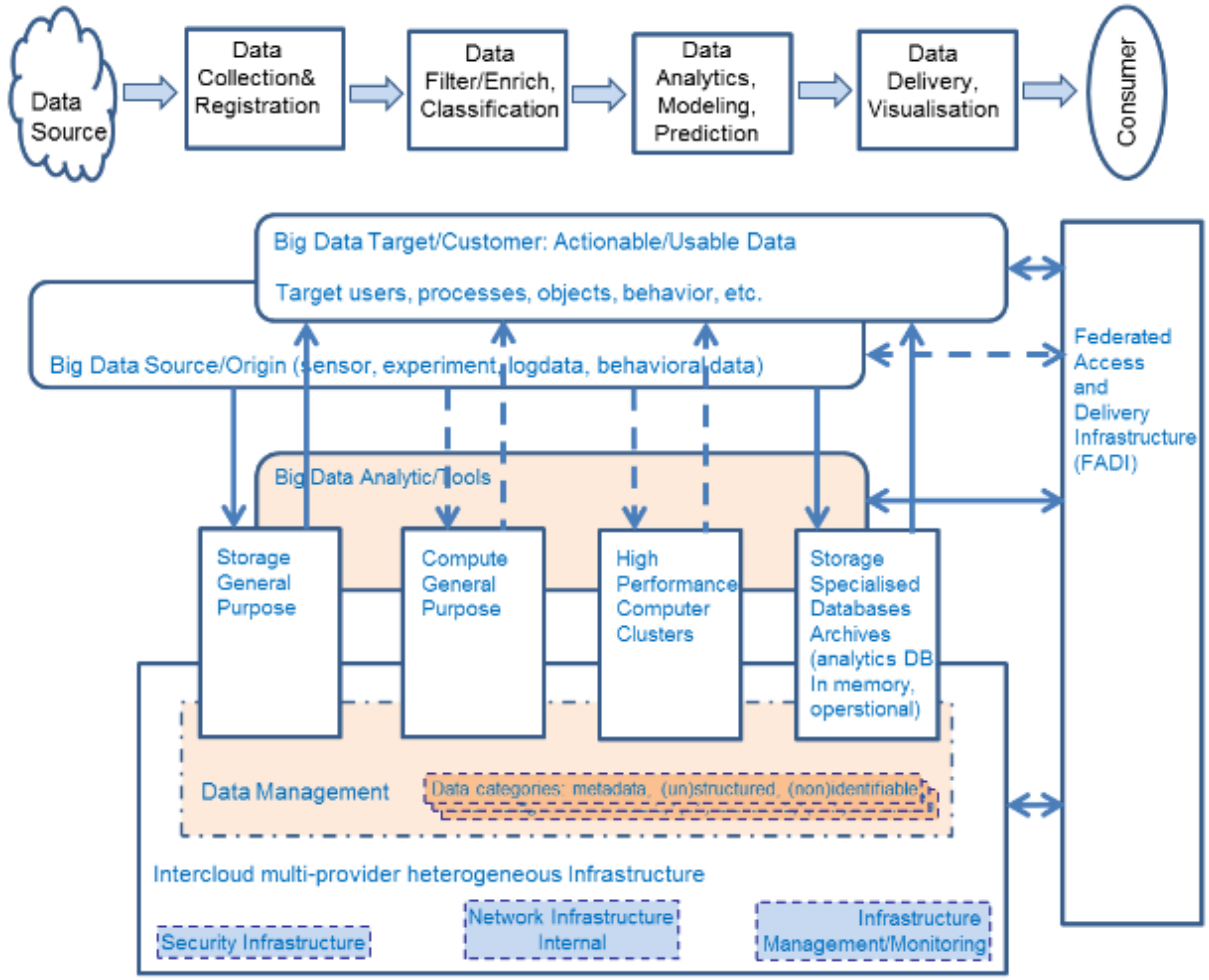


Fig. 3 Big Data infrastructure functional components (source: http://www.uazone.org/demch/worksinprogress/sne-2013-02-techreport-bdaf-draft02.pdf )

The infrastructure include: big data management tools, registries, indexing, semantics, namespaces, security infrastructure, collaborative environment, cluster services, Hadoop framework, Data analytics tools, Sql and nosql databases, Parallel processing databases.

A study [12] about Big Data architectures outline that all include the following areas:

- Big data analytics
  - Descriptive, Predictive and Spatial, Real-time, Interactive, Batch Analytics, Reporting, Dashboard
- Big Data Management/Data Store
  - Structured, semi-structured and unstructured data, Velocity, Variety and Volume, SQL and noSQL, Distributed File System
- Big Data Infrastructure
  - In Memory Data Grids, Operational Database, Analytic Database, Relational Database, Flat files, Content Management System, Horizontal scalable architecture

## 4. DATA SOURCES

The range of data used in big data projects varies from internal companies' operational data extended with sensors and instruments data, to external data from syndicated data providers and public data. An important source of data is social media from which could be extracted the sentiment regarding products or services, consumers perception about using their products or competition ones.

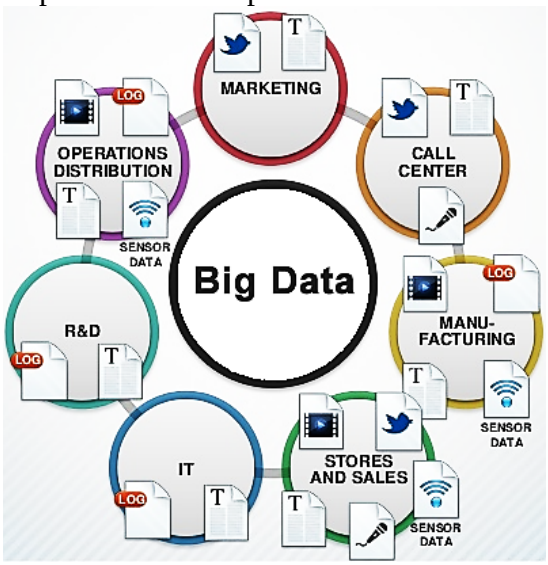


Fig. 4 Big Data sources

(source: adapted from http://www.hds.com/solutions/big-data/?WT.ac=us_mg_sol_bigdat)

There is also a less used source of data that now become a subset of big data - the dark data. Dark data is usually human generated enterprise data, produced by employees such as emails, internal reports, contracts and other document in readable format that has been archived. This data could be analyzed for patterns and correlations.

In a survey conducted by IDG [16] in the first trimester of 2015 is revealed which are the most common sources of data used in big data systems. The percent shows the proportion of systems that use the resource:

- customer databases - 63%
- emails - 61%
- transactional data - 53%
- worksheets - 51%
- word document - 48%

The survey notices that from last year, the percent of systems that use customer databases increased from 49% to 63% and a more notable increase is in case of transactional data, from 33% to 53%.

## 5. CHALLENGES

The main challenges companies have to manage in dealing with Big Data are [17]:

- Having a strategy to discover valuable information in multiple sources and being capable of collecting data. The companies must be ready to adapt to business transformations imposed by information trend. Information will improve the decision making process and help determine the investment with bigger profit. Gartner predicts that in 2015 will be around 4.4 millions of jobs in domains related to big data.
- Extract knowledge from data - finding new ways to analyze the collected data for predicting trends and outcomes. Business intelligence software platforms perform now predictive and real time analysis in multiple business domains, and should be capable to use all kind of unstructured information, and also new typed of data like clickstream, video, images, sentiment data. It is important to know

how to use all data to gain more competitiveness.

- Enterprise information management - the information volume is constantly growing and companies need to adapt to new requirements for storing and processing it. Also companies must manage the need to extend the access of employees to big data software platforms and this must be made fast and cost effective. This has great impact on companies' data centers.

Due to these challenges not all the companies will be able to benefit from the advantages of big data solutions. A Gartner study shows that through 2015, only 15% percent of Fortune 500 companies will be able to benefit, the other 85% percent would not be capable to gain competitive advantage from exploiting such technologies.

But despite this situation the companies are interested in investing in big data systems. According to IDG survey [16], 27% of respondents already implemented a big data solution and 14% are in the process of implementing/testing the solution. Also 12% have plans to implement in the next 12 month, 8% in the next 13-24 month and 8% are likely to implement a solution in future, but with no specific timeframe. Only 30% of respondents said they have no plans in implementing a big data solution.

The growing trend is also revealed in 2015 Big Data study made in [15], which states that in the last year the number of companies that adapted data analytics solutions increased by 125%. The study was made on 1139 respondents and was conducted online on IDG Enterprise websites.

The majorities of companies expects to gain business values from these solutions and are investing in them. Yet, more importance is accorded to structured data as 32% percent of subjects do not intend to use unstructured data in their solutions in near future. Also large companies invest over ten times more than SMBs in data solutions ($13.8 million compared to $1.6 million). In the picture below are presented the most important criteria, according to customers, in evaluating an offering from a data and analytics vendor:

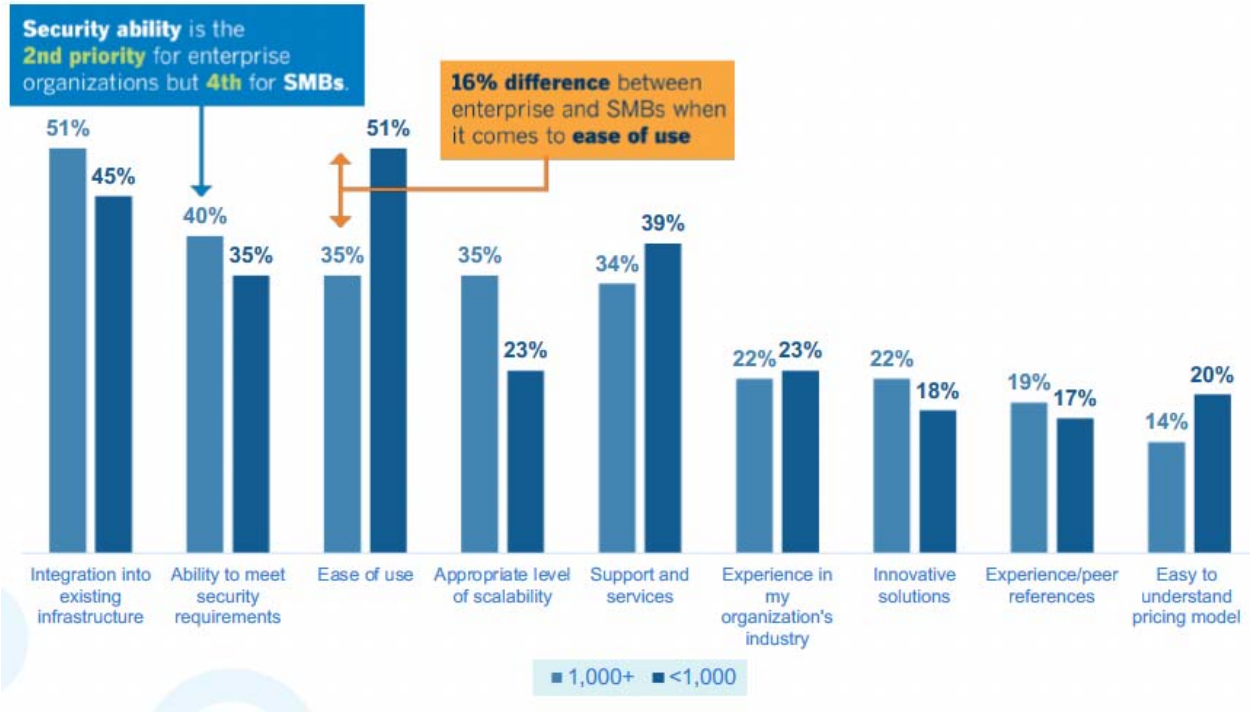


Fig. 5 Top criteria for acquiring a big data solution in case of enterprises and SMBs (source: http://www.idgenterprise.com/report/2015-big-data-and-analytics-survey)

We can see that the most important criteria in acquiring a data and analytics solution are integration into existing infrastructure, ability to meet security requirements, the ease of use, scalability and support and services. There are significant differences in importance of these criteria between large enterprises and small companies. The ease of use is one of the top criteria for small companies but only third for enterprises (16% difference), also there is an important difference in scalability which is not as important for SMBs as for large companies. Support and service is more important for SMBs even than security, being the 3rd priority and 4th security while in case of large companies security is 2nd priority. Moreover the study shows that the confidence in security solutions for company data increased from 49% to 66% in the last year.

## 6. CONCLUSION & ACKNOWLEDGEMENT

Big data refers to the technology an organization may require to deal with large amount of data and storage facilities. The first that had to deal with such problems were the web search companies that had to process very big volumes of distributed loosely structured data. Dealing with such datasets impose difficulties in manipulating and managing the big data. In current paper we presented an overview of the technologies involved and the use cases of big data systems. Also is presented a general architecture and how data analytics system evolved from traditional data warehouses. The main challenges a company is faced when implementing a big data system are presented and how the new technology is perceived by organizations. We concluded that the main factors involved in acquiring a data analytics solution in an organization are integration into existing infrastructure, ability to meet security requirements, the ease of use, scalability and support and services

This work was co-financed from the European Social Fund through Sectorial Operational Programme Human Resources Development 2007-2013, project number POSDRU/159/1.5/S/134197 „Performance and excellence in doctoral and postdoctoral research in Romanian economics science domain”.

## REFERENCES

1. Art Lindsey, *The Origins of Hadoop*, [online], (March, 2015), http://siliconangle.com/ blog/2010/10/14/the-origins-of-hadoop/

2. Bucur Cristian (2014a), "*Aspects regarding detection of sentiment in web content*", International Journal of Sustainable Economies Management (IJSEM), Volume 3: 4 Issues (2014), p.24-32, ISSN: 2160-9659

3. Bucur Cristian (2014b), „*Opinion mining platform for intelligence in business*", Economic Insights – Trends and Challenges, Vol. III LXVI, No. 3/2014, ISSN 2284-8576

4. Cristian BUCUR, „*Implications and Directions of Development of Web Business Intelligence Systems for Business Community*", Economic Insights – Trends and Challenges, Vol. LXIV, No. 2/2012 p. 96 – 108, ISSN 2284-8576

5. David Floyer, *Enterprise Big-data*, [online], (March, 2015), http://wikibon.org/wiki/v/Enterprise_Big-data

6. Douglas Laney, Alexander Linden, Frank Buytendijk et all, *Answering Big Data's 10 Biggest Vision and Strategy Questions*, [online] 12 August 2014, http://www.gartner.com/doc/2822220

7. Krish Krishnan, *Data Warehousing in the Age of Big Data*, Morgan Kaufmann, 2013, ISBN: 0124058914
8. Matt Turk, *A chart of the big data ecosystem, take 2*, [online], accessed march 2015, http://mattturck.com/2012/10/15/a-chart-of-the-big-data-ecosystem-take-2/

9. Nik Bessis, Ciprian Dobre, *Big Data and Internet of Things: A Roadmap for Smart Environments*, Springer, 2014, ISBN: 3319050281

10. Rajendra Akerkar, "*Big Data Computing*", CRC Press, 2014, ISBN-10: 1466578378

11. Rob Klopp, *A Modern Data Warehouse Architecture Part 1 – Add a Data Lake*, [online], (March, 2015), http://cognilytics.com/blog1-php/

12. Sanjay Mishra, *Survey of Big Data Architecture and Framework from the Industry*, NIST Big Data Public Working Group, 2014

13. Vangie Beal, *Big data*, [online], (March, 2015), http://www.webopedia.com/TERM/B/big_data.html

14. Yuri Demchenko, Canh Ngo, Peter Membrey, *Architecture Framework and Components for the Big Data Ecosystem*, System and Network Engineering Group, UvA, 2013

15. ***, *2015 Big Data and Analytics Survey*, [online], (March, 2015), http://www.idgenterprise.com /report/ 2015-big-data-and-analytics-survey

16. ***, *Big Data and Analytics: The Big Picture*, [online], (March, 2015), http:// www.idgenterprise.com/report/big-data-and-analytics-the-big-picture

17. ***, *Big Data Management & Analytics*, [online], (March, 2015), http://www.gartner.com/technology/topics/big-data.jsp

18. ***. *Big data*, [online], accessed March 2015, http://www.sas.com/en_be/insights/big-data/what-is-big-data.html

19. ***, *Ten Practical Big Data Benefits*, [online], http://datascienceseries.com/stories/ten-practical-big-data-benefits

"HENRI COANDA"
AIR FORCE ACADEMY
ROMANIA

"GENERAL M.R. STEFANIK"
ARMED FORCES ACADEMY
SLOVAK REPUBLIC

INTERNATIONAL CONFERENCE of SCIENTIFIC PAPER
AFASES 2015
Brasov, 28-30 May 2015

# THE EQUATION OF DISPERSION AND THE DISPLACEMENT VECTOR IN THE ANTISYMMETRIC CASE

**Mihaela Dumitrache*, Camelia Gheldiu***

*Faculty of Mathematics and Computer Science, University of Pitesti, Romania

***Abstract:*** *In this paper we study the propagation of the Lamb waves and we find the equation of dispersion and the equations of the displacement vector in the antisymmetric case.*

***Keywords:*** *nonlinear eigenvalue problems, second order hyperbolic equation, wave equation.*
***MSC2010:*** *35P30, 35L10, 35L05.*

## 1. INTRODUCTION

We are under the same conditions of the article [1], so we consider an elastic, isotropic, continuous and homogeneous medium and we study the propagation of the antisymmetric Lamb waves through it.

Using the results from [1], [2] and [3], we obtain the equation of dispersion and the equations of the displacement vector in the symmetric case.

## 2. PROBLEM FORMULATION

We consider the normal guided Lamb waves that appear in a plate of thickness $2h$ comparable with the wavelength, due to coupling between the components longitudinal $L$ and the transverse components of the wave $TV$. Thus, two types of wave Lamb can be produced, but, in this paper, we study the antisymmetric waves which are depicted in Figure 1, where for each side of the middle of the plate, the transverse components are equal and the longitudinal components are opposite.

Just like in the article [4], we assume homogeneous and isotropic elastic plate bounded by two parallel planes located at a short distance $2h$, and we find the equation of dispersion and the equations of the displacement vector, but in the antisymmetric case.

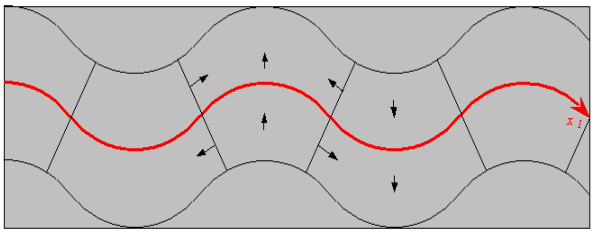


Figure 1: The antisymmetric Lamb waves

## 3. PROBLEM SOLUTION

In the article [1] we started from the equation of the displacement vector $\boldsymbol{u}$ for a material point

$$\mathbf{u} = \nabla\varphi + \nabla\times\psi \qquad (1)$$

where $\varphi$ is a scalar potential and $\psi$ is a vectorial potential. In expression (1) the two potentials should verify the following two equations of wave

$$\nabla^2\varphi - \frac{1}{v_L^2}\frac{\partial^2\varphi}{\partial t^2} = 0, \tag{2}$$

where

$$v_L = \left(\frac{c_{11}}{\rho}\right)^{\frac{1}{2}} = \left(\frac{\lambda + 2\mu}{\rho}\right)^{\frac{1}{2}}$$

is the phase velocity of the longitudinal waves and

$$\nabla^2\psi - \frac{1}{v_T^2}\frac{\partial^2\psi}{\partial t^2} = 0, \tag{3}$$

where

$$v_T = \left(\frac{c_{44}}{\rho}\right)^{\frac{1}{2}} = \left(\frac{\lambda}{\rho}\right)^{\frac{1}{2}}$$

is the phase velocity of the transversal waves.

The scalar and the vectorial potentials are trigonometric functions of time *t*, with the same frequency $\omega$. However, they can be expressed as follows, with the wave number *k*:

$$\begin{aligned} &\phi = \phi_0\left(x_2\right)e^{i(\omega t - kx_1)}, \\ &\psi = \psi_{0j}\left(x_2\right)e^{i(\omega t - kx_1)}, \quad j = 1,2,3. \end{aligned} \tag{4}$$

The equation of dispersion has the following relation [1]:

$$\frac{\tan\left(qh + \alpha\right)}{\tan\left(ph + \alpha\right)} = -\frac{4k^2pq}{\left(q^2 - k^2\right)^2} \tag{5}$$

where the constants $p$ and $q$ are defined as follows:

$$p^2 = \frac{\omega^2}{v_L^2} - k^2, \tag{6}$$

$$q^2 = \frac{\omega^2}{v_T^2} - k^2,$$

and the constant angle $\alpha = 0$ (the symmetric case studied in [4]) and $\alpha = \frac{\pi}{2}$, this is the case that we study in this paper, the antisymmetric case.

Further, using the results from [3], we know that we have three regions with respect to the phase velocity. So, we write the equation of dispersion (5) and the equations of the displacement vector for each subdomain of wave number *k* taking into account the type of values that can be taken the constants *p* and *q*, for the case $\alpha = \frac{\pi}{2}$ ( the antisymmetric case) .

The first case is obtained for $k < \frac{\omega}{v_L} < \frac{\omega}{v_T}$ $\Leftrightarrow V > v_L > v_T$, and we have $p$ and $q$ real numbers, so the dispersion equation is

$$\frac{\tan\left(qh + \frac{\pi}{2}\right)}{\tan\left(ph + \frac{\pi}{2}\right)} = \frac{\tan\left(ph\right)}{\tan\left(qh\right)} = -\frac{4k^2pq}{\left(q^2 - k^2\right)^2}, \tag{7}$$

and the equations of the displacement vector are:

$$\begin{aligned} u_1 &= qA\left[-\sin\left(qx_2\right) + \frac{2k^2}{k^2 - q^2}\cdot\frac{\sin\left(qh\right)}{\sin\left(ph\right)}\cdot\sin\left(px_2\right)\right] \\ &\quad\cdot\cos\left(\omega t - kx_1\right), \\ u_2 &= -kA\left[\cos\left(qx_2\right) + \frac{2pq}{k^2 - q^2}\frac{\sin\left(qh\right)}{\sin\left(ph\right)}\cdot\cos\left(px_2\right)\right] \\ &\quad\cdot\sin\left(\omega t - kx_1\right). \end{aligned} \tag{8}$$

The second case is obtained for $\frac{\omega}{v_L} < k < \frac{\omega}{v_T}$ $\Leftrightarrow v_L > V > v_T$ and we have $p$ an imaginary number, i.e. $p = ip$ and $q$ a real

number, so the dispersion equation has the form:

$$\frac{\tan\left(qh+\frac{\pi}{2}\right)}{\tan\left(ph+\frac{\pi}{2}\right)}=\frac{\tan(ph)}{\tan(qh)}=\frac{4k^2pq}{\left(q^2-k^2\right)^2}, \qquad (9)$$

and the equations of the displacement vector are:

$$u_1 = qA\left[-\sin(qx_2)+\frac{2k^2}{k^2-q^2}\frac{\sin(qh)}{\sinh(ph)}\sinh(px_2)\right]\cdot\cos(\omega t-kx_1),$$

$$u_2 = -kA\left[\cos(qx_2)+\frac{2pq}{k^2-q^2}\frac{\sin(qh)}{\sinh(ph)}\cosh(px_2)\right]\cdot\sin(\omega t-kx_1). \qquad (10)$$

The third case is obtained for $\frac{\omega}{v_L}<\frac{\omega}{v_T}<k \Leftrightarrow v_L>v_T>V$, and we have $p$ and $q$ imaginary numbers, i.e. $p=ip$ and $q=iq$, so the dispersion equation is

$$\frac{\tan\left(qh+\frac{\pi}{2}\right)}{\tan\left(ph+\frac{\pi}{2}\right)}=\frac{\tan(ph)}{\tan(qh)}=\frac{4k^2pq}{\left(q^2+k^2\right)^2} \qquad (11)$$

and the equations of the displacement vector are the following form:

$$u_1 = qA\left[\sinh(qx_2)-\frac{2k^2}{k^2+q^2}\frac{\sinh(qh)}{\sinh(ph)}\cdot\sinh(px_2)\right]\sin(\omega t-kx_1),$$

$$u_2 = -kA\left[\cosh(qx_2)-\frac{2pq}{k^2+q^2}\frac{\sinh(qh)}{\sinh(ph)}\cdot\cosh(px_2)\right]\sin(\omega t-kx_1), \qquad (12)$$

where $A$ is a constant factor.

## 3. CONCLUSIONS

In this paper we use the antisymmetric Lamb waves in an elastic, isotropic, continuous and homogeneous medium and we find the equation of dispersion and the equations of the displacement vector for every subdomain of the wave number $k$ in the antisymmetric case.

## REFERENCES

1. Dumitrache, M., Gheldiu C, *High-frequency waves. The equation of the displacement vector*. The Proceedings of the International Session of 15-th Scientific Papers "Scientific Research and Education in the Air Force", AFASES 2013, 23-25 mai Braşov, ISSN, ISSN-L 2247- 3173, pg. 329-332.
2. Dumitrache, M., Gheldiu C, *High frequency waves and the equation of dispersion.* International Scientific Conference "Mathematics & IT: Research and Education (MITRE-2013)" Chisinau, August 18-22, 2013, at the Moldova State

University (MSU), Faculty of Mathematics and Computer Science.
3. Dumitrache, M., Gheldiu C, *The curve of dispersion in the plane* $(\omega, \not{k})$, Buletin Ştiinţific-Universitatea din Piteşti, Seria Matematică şi Informatică, Nr. 19 (2013).
4. Dumitrache, M., Gheldiu C, *The equation of dispersion and the displacement vector in the symmetric case*. The Proceedings of the International Session of 16-th Scientific Papers "Scientific Research and Education in the Air Force", AFASES 2014, 22-24 mai Braşov, ISSN, ISSN-L 2247-3173,pg.345-347.

"HENRI COANDA"
AIR FORCE ACADEMY
ROMANIA

"GENERAL M.R. STEFANIK"
ARMED FORCES ACADEMY
SLOVAK REPUBLIC

INTERNATIONAL CONFERENCE of SCIENTIFIC PAPER
AFASES 2015
Brasov, 28-30 May 2015

# SUBJECT INFORMATION TECHNOLOGY IN MILITARY EDUCATION

**Miroslav Hrubý***

*Faculty of Military Technology, University of Defence, Brno, Czech Republic

***Abstract:*** *The paper deals with the first experience in realization of a new Master's degree program at the Faculty of Military Technology, University of Defense, Brno, Czech Republic. This Master's degree program named Military Technology was prepared according to the new requirements of the Czech Ministry of Defense. The author's attention is focused on the subject "Information Technology" (IT) which plays an important role not only from the Department of Communication and Information Systems point of view. The subject IT was for the first time realized at the Faculty of Military Technology in the winter semester of the academic year 2014/2015. The content, teaching methods and assessment of the subject IT are described. Finally a few important points for the future of the subject IT are formulated.*

***Keywords:*** *algorithms, computer networks, engineering education, programming.*
***MSC2010*****:** 68W01,68N15, 68P05, 97Q60.

## 1. INTRODUCTION

In the last years the Faculty of Military Technology, University of Defense, Brno, Czech Republic offered to its military students Bachelor's degree programs and follow-up Master's degree programs. Since 2013, the Faculty of Military Technology has been preparing, according to the new requirements of the Czech Ministry of Defense, its new five-year Master's degree program named Military Technology.

This new Master's degree program has only one field of study. This field of study is also named Military Technology. Subjects and study duties in the first 5 semesters are the same for all military students but from the 6th semester this study field is internally divided into 15 modules that correspond to the names of the required military specialties. These are: as follows:

- Automated Command and Control Systems;
- Combat and Special Vehicles;
- Communications and Information Systems – Information Technology (IT);
- Communication and Information Systems – Communication Technology (CT);
- Aircraft – Avionics and Armament;
- Aircraft – Airframes and Engines;
- Air Radio Navigation systems;
- Air Staff Officer;
- Airbase Engineering Support;
- Radar Technology and Electronic Warfare;
- Air Traffic Control;
- Military Geography and Meteorology;
- Military Pilot;

- Weapons and Ammunition;
- Military Engineering.

In the winter semester of the first year of studies the subject IT is included. The current specification of this subject is derived from [2] and [3] in the first part of its content.

The goal of the article is to introduce a study plan of the subject IT, its teaching methods and rules for granting the credit. The findings from the first semester of the subject teaching are included.

## 2. SUBJECT "INFORMATION TECHNOLOGY"

**2.1 Goals of the subject.** First of all it is necessary to keep in mind that new military university students are coming from various types of secondary schools. Their IT knowledge and digital competences can radically differ. The course especially builds on secondary school knowledge of mathematics and physics, improves skills for PC usage and forms algorithmic thinking necessary for technically educated military professionals. Gained knowledge is useful for next subjects being studied in curriculum.

Due to the obvious characteristics of new students the goals of the subject were specified in two main aims:

- Algorithms and programming (32 teaching hours);
- Computer networks (16 teaching hours).

Students should gain knowledge of problem analysis ways, basics of programming techniques, principles and practical usage of the event programming, the meaning of IT technical terms and principles of operation of various types of computer networks. They should be able to divide the problem into sub-processes, to create applications in particular development environment, to solve simple applications as a support for engineering activities, to assess the basic network components configuration for workstations, to design simple local computer network, to design methods of obtaining the status of network components in workstations. Students should be acquainted with the basics of analytical and programming work on a local computer and within a computer network. It was planned that laboratory topics from programming should be implemented using selected higher programming language (Python, Java Script, C# or Visual Basic).

Finally, JavaScript programming language was selected as the most suitable tool for the practicing of programming skills. This programming language was evaluated at the department level as a modern and popular tool which is available free of charge as a component of contemporary web browsers. Teachers and students can access many good information sources at the Internet [1,4,5].

**2.2 Content of the subject.** The first part of the subject is focused on algorithms and programming. Firstly, three lectures (3 x 2 teaching hours) are provided:

- Introduction into algorithms;
- Data types and data structures;
- Statements of a high level programming language, structure of a program.

Secondly, 26 teaching hours are given in the form of laboratory practicing of the topics such as:

- User interface of the program (application);
- Programming of the input and output;
- Usage of an array;
- String processing;
- Subroutines and user defined functions.

Thirdly, the second part of the subject focused on computer networks is started by three lectures (2 + 4 + 2 teaching hours):

- Introduction to computer networks, network architecture reference model ISO/OSI, model TCP/IP;
- Ethernet, fundamental suite of TCP/IP protocols;
- Planning the address space, CIDR, VLSM, routing.

Fourthly, 8 teaching hours in laboratory are focused on:

- Addressing in a simple network, (configuring user devices and basic network devices);
- Realization of simple network and their diagnostics (configuration of simple networks in practice, their diagnostics and troubleshooting).

**2.3 Teaching methods.** Lectures are provided in a high capacity lecture hall for all

students at the same time. Lectures focused on algorithms and programming and lectures focused on computer networks are realized by two vocational specialist. Laboratory exercises are provided for the groups of 25 students. In the academic year 2014-2015 five members of CIS Department academic staff took part in laboratory exercises. The teaching process was coordinated by the guarantor of the subject.

For clarification, the three examples of tasks from programming are as follows:

- One-dimensional array (vector) named Charles has 13 elements. Give each element random whole number from the interval <10; 99>. Find out how many numbers which are stored in the array Charles meet the interval which limits are set by the user. Display all used data in the form which you find as the most suitable.
- Two-dimensional array (matrix) contains the results of written work from the subject Math. The work was done by a group of 24 students. According to the position of a teacher's desk and each student's place in the classroom, the results of students are characterized as:
  Teacher
  1 2 2 3 3 1
  1 3 2 1 2 2
  3 4 2 2 4 1
  2 3 2 3 1 4
  Find occurrence of each classification levels. Display all used data in the form which you find as the most suitable.
- Declare and check a user defined function which has to make a calculation of the monthly cost of water for swimming pool cuboids with dimensions l (length) / w (width) / d (depth), which will be filled to p %. The pool water is completely changed n-times per month. The price of water is x CZK per $m^3$. Realize displaying the pool parameters and calculated costs on a web page. Suggest this listing in the form which you find as the most suitable.

From the three examples above it is evident that programming tasks are especially focused on the array data structure and statements of branching, switch and cycles.

The students should be familiarized with three basic control structures (sequence, branching and cycle) and their use in writing algorithms by a high level programming language (in its integrated development environment).

**2.4 Subject assessment.** The students' knowledge and skills assessment is realized independently in two phases. Firstly, in the first part of the subject the students have to accomplish the tasks from algorithms and programming. Secondly, later in the second part of the subject they have to accomplish the tasks from computer networks. The tasks are set by the teaching academic staff and each group of students has to fulfil the goals during their laboratory exercises.

Finally, the students, who fulfil the stated goals in both two parts of the subject, receive the course credit.

## 3. CONCLUSIONS & ACKNOWLEDGMENT

The subject "Information Technology" is a mandatory subject for all military students at the Faculty of Military Technology, University of Defense, Brno Czech Republic in the first semester of their Master's degree program since 2014. It is a subject of so-called core knowledge. In previous study programs realized at the Faculty of Military Technology was no subject of such content which was mandatory for all students.

The students are warned that it requires significantly different demands due to the previous knowledge and skills of students in the ICT field, especially focused on algorithms and programming. Both students and teachers have to keep in mind this fact.

The first experience from the teaching process is the follows:

- Inclusion of the subject "Information Technology" in the education of all Faculty of Military Technology students is very important for their future studies.
- Teaching of the subject in the 1st semester of military students' studies is the optimal time.
- The content of the subject, focused on algorithms and programming and computer networks, seems to be well done but it will be suitable to be prepared to slightly modify the subject content appropriate to the experience gained.
- The current number of 25 students in the laboratory exercises would be reduced to the number of 10 to 15 students in the interest of better communication and individual approach which is sometimes needed.
- If possible, it is necessary to encourage students to use their own notebooks because of these students can make better progress thanks to the usage of devices they are familiarized with.
- It is suitable to install and use the same web browser by all students. It makes better conditions for discussions among students and their teacher about various solutions of programming tasks.
- The topics of programming tasks should be selected carefully according to the contemporary knowledge of students in the laboratory groups and their interests.
- The teachers should creatively use connections to the problem areas of other subjects, e.g. work with vectors and matrices in mathematics.
- The author assumes that evaluation of different high level programming languages usage according to the teachers' offer and students' selection could bring interesting results for the subject guarantor.

Acquiring of the algorithmic thinking skill is sometimes a long distance run but this type of thinking is a necessary prerequisite for successful studies at the military technical faculty and the important element of a contemporary military professional profile.

The author assumes that students' assessment should always consist of a written part and a practical part of assessment. From the algorithms and programming point of view the written part should be focused on understanding of key concepts and connections among key terms used in this vocational field, including understanding of simple parts of the code. On the other hand, in practical part of assessment the students should demonstrate their current programming skill. They should be capable to create required code and explain their thinking process which led to this code.

## REFERENCES

1. Haverbeke, M.. Eloquent JavaScript: A Modern Introduction to Programming. [online]. Available: http://eloquentjavascript.net/ (2015).
2. Hrubý, M.. Počítačová podpora práce s daty. In *XXX International Colloquium on the Management of Educational Process. Proceedings, Science.* Brno: University of Defence (2012).
3. Hrubý, M.. Předmět „Informační technologie" při přípravě „Akreditace 2014". In *XXXI International Colloquium on the Management of Educational Process.* Brno: University of Defence (2013).
4. JavaScript Tutorial. *W3Schools Home.* [online]. Available: http://www.w3schools.com/js/default.asp (2015).
5. Moncur, M.. Sams Teach Yourself JavaScript in 24 Hours. *Pearson Education, Informit.* [online]. Available: http://www.informit.com/library/library.aspx?b=STY_JavaScript_24_hours (2015).

"HENRI COANDA"
AIR FORCE ACADEMY
ROMANIA

"GENERAL M.R. STEFANIK"
ARMED FORCES ACADEMY
SLOVAK REPUBLIC

INTERNATIONAL CONFERENCE of SCIENTIFIC PAPER
AFASES 2015
Brasov, 28-30 May 2015

# SIMPLE SOFTWARE FOR EDUCATION

**Hošek Jaromír*, Alexandr Štefek***

*Faculty of Military Technology, University of Defense, Brno, Czech Republic

***Abstract:*** *The paper deal with education of the students of technical branches. The one of the basic subjects for most technical branches in technical colleges is subject Automatic control. The teaching is focused on theory of automatic control and next revision theoretical knowledge in practical laboratory exercises. It is very suitable to make another experiment or "playing" with basic elements of automatic control for better understanding automatic control lectures. The aim of this paper is to show possibilities of the experimenting and better understanding of the theoretical and practical lessons for every student without using very expensive software.*

***Keywords:*** *automatic control, practical experiences, simulating program.*

## 1. INTRODUCTION

The University of Defense prepare students to three main branches: commanders for fighting units of Czech Army, technical experts for the Czech Army and the last branch prepare general practitioners for health service of Czech Army. The technical branches like construction and maintenance of aircraft, pilots, construction and maintenance of control systems of the rocket, radar engineering and antiaircraft systems have the Automatic Control subject like one of the basic subject. The aim of the lectures in that subject is to grasp a core of control systems and understand relation in control techniques by the students. There is presumption that these future professionals which will operate with military equipment can use capabilities of that equipment at maximum level.

Another benefit is the noticeable amount of these technical specialists leave army after fulfilment their contract. These technicians have good reputation in civilian factories and they are good valued. These professionals have big experiences with management team in extreme conditions and knowledge and skills from control engineering.

## 2. THE SIMPLE SOFTWARE FOR EDUCATION

**2.1 The basic idea for design the software.** The knowledge gained from lectures and exercises must be verifies using practical lectures – laboratory exercises. Laboratory is equipped with devices from company Feedback. The Feedback is verified kit used at many schools, colleges and universities. The electro kit and pneumatic kit is mainly used. Nowadays a low-cost LEGO Mindstorm NXT system is used for teaching modern control theories. Theoretically counted examples are verified on those kits. Students must set calculated parameters and they watch changes in behavior of the kit immediately. The higher

level of laboratory exercise then combines calculations and settings a combination of more parameters of the regulated circuit. Laboratory equipment is expensive and setting of kits parameters is limited. The most of those kits operate with excellent but expensive software, for example MATLAB software. In this case students have not expensive kits or software, but they can verify their knowledge at laboratory even during breaks between lectures.

The frequent teaching in laboratory, mean less time for students experiments. This leads to decision to design simple single-purpose tools which enables exploration and testing automatic control principles for students. Described tool allows simulate simple system with P control and change parameter of regulated system. The students are not limited neither to classrooms nor expensive licensed software. Developed software can be used on widely available computers like home computers are. The software allows not only set P parameter but also partially change structure of the regulated system.

This single-purpose program has simple and intuitive operation. The students can concentrate on study and experimenting and they do not waste time by another problems like study manuals. This program can students use on their private computer without any license and it do not require any special software.

**2.2 Software and its ability.** The software is based on freely available language C# (CSharp). This language use object-oriented design patterns (OOP language). Basic version of developer environment can use everybody, but it is limited to nonprofit applications. Programs created with these language runs safety with common computers e.g. home computers.

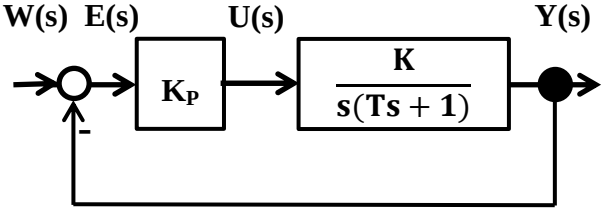


Fig.1 Scheme of the simple system

Example of possible simulated system structure is on Fig.1.

This is a negative feedback circuit with proportional element that is commonly used.

As shown in Fig.1 (compare with Fig. 2), students can set gain of a proportional element $K_P$ from 0 to 50, they can set gain K of a regulated element, order of astatic and time constant T. The element $K_P$ can be set by mouse, click to circle and move by pointer or after click to circle can set by keyboard and key + or -. To set other simulation parameters constant user must click to chart and rewrite numbers, Fig2.


Fig.2 Setting gains and constants

On the bottom of the screen Fig.3, are the classic controls of the program stop, play, fast move and back to start. The data of the measuring exercise we can save in Microsoft Excel ®, associated icon is in the right of controls.

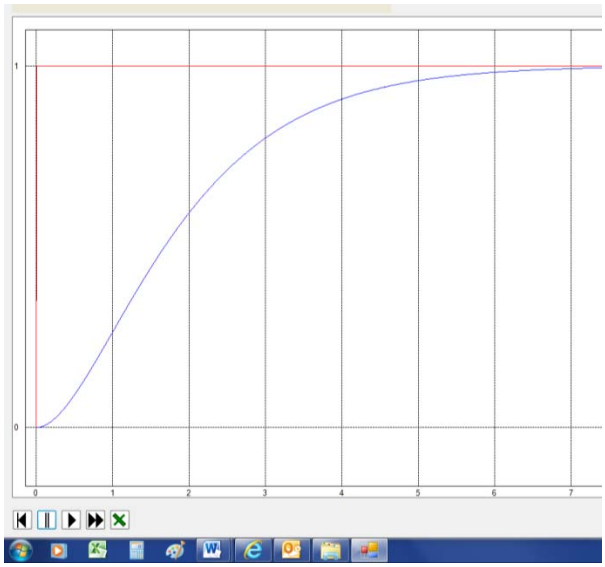

Fig.3 Print screen of the characteristic $K_P$=10, K=0.5, T=0.05

The interface allows change gain (P control parameter) during the simulation. This functionality offers to users some kind of

interactivity and observation of system behavior.

**2.3 Calculation of the shown example.** The calculation of the shown figure3 is very easy, but in comparison to available laboratory kit the proposed solution (software) an user can set system parameters and see resolution immediately.

Parameters are:

$$\mathbf{K_P} = 10; \mathbf{K} = 0.05; \mathbf{T} = 0.5$$

Now students have to calculate Transfer function of open and closed circuit:

$$\mathbf{G_O(s)} = \frac{0.05\mathbf{K_P}}{\mathbf{s}(0{,}5\mathbf{s}+1)}; \mathbf{G(s)} = \frac{1}{\mathbf{s}^2 + 2\mathbf{s} + 1}$$

The step response function is:

$$\mathbf{H(s)} = \frac{1}{\mathbf{s}} - \frac{1}{(\mathbf{s}+1)^2} - \frac{1}{\mathbf{s}+1}$$

Now application of inverse Laplace transformation to step response function give function in time domain.

$$\mathbf{h(t)} = 1 - \mathbf{te}^{-\mathbf{t}} - \mathbf{e}^{-\mathbf{t}}$$

We can see that transition process is aperiodical.

The program enables to insert steps in any time arbitrarily by clicking on icon step in the input of the chart. The new steps are red lines. The new characteristic is funny, fig4.

The students must calculate one example according to instructions to know what parameters set at first and then can make experiments and change all changeable parameters and explore substance of regulated systems.

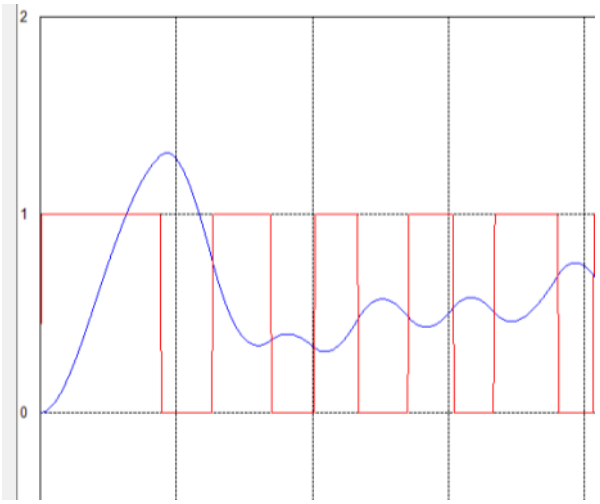


Fig.4 Print screen of the funny characteristic $K_P$=10, K=0.5, T=0.5

**2.4 Practical experiences** Practical part of a teaching, laboratory exercises is focused to use Feedback kit. The students are divided to group and every of that must evaluate own task. Practice shows that some students "fear" our laboratory kit and because of that they don´t understand some parts of that subject so good. The students can use special computer classrooms where they can train automatic control problems in common simulators (like MATLAB software is). The laboratory and computer classrooms are accessible only in breaks and afternoon. Laboratory availability creates space for this special software. The hesitant students obtain simple program and can explore secrets of automatic control. They can play with program in the comfort of their home and are not fixing on schools laboratory or classrooms. The additional homework for students is to identify unknown system according to the characteristic.

During checking tests students have deeper knowledge about automatic control problems. They are not afraid to discuss about that problems and they have bigger certainty in

their answers. The final examines are evaluated better and students are less feared.

The students start aware importance of differential equations and role of the coefficients. We can say that it is comeback to stage where they studied mathematic (nearly a year back). Here we apply the motto "the school of the game" but at a higher level than in elementary school.

The aim was not to design some new software (what is time-consuming) but to design very simple application with ability to run anywhere. The user has not worry about setting incorrect values to damage laboratory tool. As usually, during playing with that program students meet some problems or something interesting behavior, for example unusual characteristic. During solving this problem they understand setting values and connections in regulated system much more than during reading or counting of the examples.

After passing laboratory lesson of that subject students can depend on their skill and knowledge.

**2.4 Extended use.** The software is provided with source code. As it does not use any special external libraries students are encouraged to try understand simulation problems deeply. Nearly same approach can be used in control system software on embedded microcontrollers.

## 3. CONCLUSIONS & STUDENTS KNOWLEDGE

It was very pleasing and interesting after ending this subject when answer on question what was the subject give you the answer was: "I finally understood importance of the differential equations, their creating on base of the physical principles. I know how coefficients of linear differential equations are created and their influence on behavior of the regulated systems." and others. The students changed their sight on mathematics and physics. Those lessons are not boring counting loads of examples but they gain ability to interpret (explain) meaning of a calculated results.

At the end we can say that except deeper understanding automatic control problems, setting parameters of a regulated systems and their behavior, the students change opinion on other previous subjects like mathematics, physics and others and understand their place in technics.

## REFERENCES

1. Alkin, O.,. Teaching System Simulation Using Student –Expandable Software, In *Frontier In Education Confewrence – Global Engineering: Knowledge Without Borders, Opportunities Without Passports*, IEEE 2007.
2. Bonert, R.,. Interactive Simulation of Dynamic Systems on a Personal Computer to Support Teaching, Power Systems, *IEEE Transactions on* (Volume:4, Issue:1, 2002).
3. Zhang, Y., Wang, Z., Liu, X., Chen, L.,. C4ISR Capability Analysis Based on Service-Oriented Architecture, *Service Oriented System Engineering (SOSE),* IEEE 2010.
4. Tutorialspoint, available: http://www.tutorialspoint.com/csharp/

.

"HENRI COANDA"
AIR FORCE ACADEMY
ROMANIA

"GENERAL M.R. STEFANIK"
ARMED FORCES ACADEMY
SLOVAK REPUBLIC

INTERNATIONAL CONFERENCE of SCIENTIFIC PAPER
AFASES 2015
Brasov, 28-30 May 2015

# AIRPLANES OR RACKETS FLIGHT STABILIZATION OPTIMAL CONTROL IN CASE OF PITCH PERTURBATIONS

**Mircea Lupu*, Cristian-George Constantinescu**, Gheorghe Radu****

*Corresponding member of Romanian Scientists Academy, Faculty of Mathematics and Computer Science, Transilvania University of Brasov, Romsnia, **Faculty of Aeronautical Management, "Henri Coandă" Air Force Academy, Brasov, Romania

***Abstract:*** *In this paper the study of horizontal flight stabilization by using an automate system to control the pitch perturbations will be approached. This optimal control method is based on the extreme principle of Pontreaghin, finding the control function via the minimum transfer time from the initial (disrupted) position in the final position (target). The optimal control $U^*$ is determined, as well as the optimal trajectories which solve the optimal control problem (O.C.P.), by using a relay-type regulator with rapid action to stabilize this controllable system, suitable for aircrafts of rockets equipped with autopilot.*

***Keywords:*** *optimal control, control function, minimum transfer time.*
***MSC2010*:** 76B07, 49Q10, 35J25, 35F15, 45E05.

## 1. INTRODUCTION

In case of horizontal flight, pitch (longitudinal) perturbation may occur, pitch angle $\psi$ varying in this way. Considering an axis system Oxyz, the origin O being the CoG (mass center) of the aircraft, with Ox the horizontal flight axis, Oz as vertical axis and Oy as lateral axis, the pitch perturbation are characterized by the pitch angle $\psi$, (the rotation angle around Oy), lateral perturbations characterized by the rolling angle $\theta$ (the rotation angle around Ox) and yaw angle $\varphi$ (the rotation angle around Oz). These angles, together with their corresponding moments, are shown in figure 1.

In previous studies, [1], [2] it was presented the automate control and absolute stabilization for a linearised dynamic system by using two (equivalent) methods:

- the Lurie method, finding the Liapunov function [4-6, 9];
- the frequencial method V. M. Popov, using the transfer function, [8].

In this paper the study of horizontal flight stabilization by using an automate system to control the pitch perturbations will be approached. This optimal control method is based on the extreme principle of Pontreaguine, [7], finding the control function via the minimum transfer time: $\min(t_1 - t_0) = t^*$, from the initial (disrupted) position: $P_0\left(X^0; t_0\right)$ in the final position (target): $O\left(X^1; t_1\right)$.

So, the optimal control $U^*$ is determined, as well as the optimal trajectories $X\left(X^0; X^1; t_0; t_1; t\right)$ which solve the optimal control problem (O.C.P.), by using a relay-

type (on-off) regulator with rapid action to stabilize this controllable system, suitable for aircrafts of rockets equipped with autopilot.

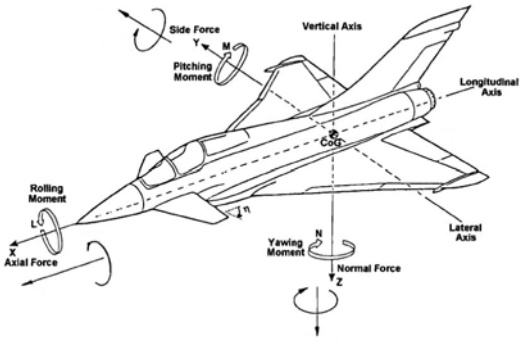


Fig. 1: The axial moments and angles of an airplane

In the previous study it was determined the Liapunov function $V \geq 0$, with $\dot{V} \leq 0$, ensuring the absolute global stabilization towards the point O in the phase space $(x_1; x_2; x_3) \leftrightarrow (z_1; z_2; z_3)$ and finding the parameters r, $C_1$, $C_2$ and the control function $\sigma = C^{'} z - r\varphi$:

$$V = -\frac{z_1^2}{2r_1} - \frac{z_2^2}{2r_2} + \frac{a}{2} z_3^2 + \int_0^{\sigma} f(\sigma) d\sigma$$

where $a = \frac{C_1}{b_3 \lambda_1 \lambda_2} > 0$, and $\varphi$ is an arbitrary non-linear control function; $\varphi(\sigma)$ respects the sector conditions. The system is fully controllable because the rank $R = (b; Ab; A^2 b) = 3$

## 2. MATHEMATICAL DETERMINATION

In the following section of the paper it will be presented the optimal control in the space $Oz_1z_2z_3$ for the diagonal system (see [3]), as: $\dot{z} = rz + bu \qquad \varphi = u$, detailed in the form:

$$\begin{cases} \dot{z}_1 = r_1 z_1 + bu \\ \dot{z}_2 = r_2 z_2 + bu \\ \dot{z}_3 = bu \end{cases} \tag{1}$$

where:

$$b = \begin{pmatrix} b_1 \\ b_2 \\ b_3 \end{pmatrix}; u = \begin{pmatrix} u_1 \\ u_2 \\ u_3 \end{pmatrix}; u_1 = u_2 = u_3 := u;$$

$$r_2 < r_1 < 0; r_3 = 0; b > 0$$

$$\left\{ \dot{z} = \frac{\partial H}{\partial \lambda}; \dot{\lambda} = -\frac{\partial H}{\partial z} \right\} \tag{2}$$

$$H = 1 + \lambda_1 \dot{z}_1 + \lambda_2 \dot{z}_2 + \lambda_3 \dot{z}_3 \tag{3}$$

$$H = \begin{Bmatrix} 1 + \{\lambda_1 r_1 z_1 + \lambda_2 r_2 z_2 + \lambda_3 r_3 z_3\} + \\ + bu\{\lambda_1 + \lambda_2 + \lambda_3\} \end{Bmatrix} \tag{4}$$

$$H \geq 0 \Rightarrow H_{min} = H(t^*, u^*, z^*, \lambda^*) = 0$$

$$|u| \leq 1 \Rightarrow u^* = \pm 1$$

As a function of u, the Hamiltonian H is a linear dependence:

$$H = H(u) = Bu + C$$

$$|u| \leq 1 \Rightarrow H_{min} = H(u^*) = 0$$

If $u = u^* = -1$, it results that H is an increasing function, and if $u = u^* = 1$, it results that H is a decreasing function, as shown in figure 2.

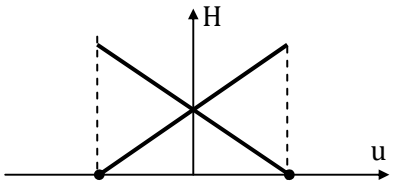


Fig. 2: The dependence H = H(u)

$$u^* = -\text{sign}(\lambda_1 + \lambda_2 + \lambda_3); b > 0$$

$$F = \lambda_1 + \lambda_2 + \lambda_3$$

$$\dot{\lambda} = -\frac{\partial H}{\partial z} \Rightarrow \begin{cases} \dot{\lambda}_1 = -\lambda_1 r_1 \\ \dot{\lambda}_2 = -\lambda_2 r_2 \\ \dot{\lambda}_3 = 0 \end{cases}; \frac{d\lambda}{\lambda} = -r \tag{5}$$

$$\begin{cases} \lambda_1 = C_1 e^{-r_1 t} \\ \lambda_2 = C_2 e^{-r_2 t} \\ \lambda_3 = C_3 \end{cases}; \lambda_i|_{t=0} = C_i \tag{5'}$$

$$F = F(t) = C_1 e^{-r_1 t} + C_2 e^{-r_2 t} + C_3$$

$$C_{1,2,3} \in R, C_1 C_2 C_3 \neq 0$$

$$u^* = -\text{sign}(F(t))$$

Remark:

The regulator is a relay-type one, so $u^* = \pm 1$. For $t \in [0; t^*]$ the sign of F may be constant, so $u^*$ keeps its value $(\pm 1)$ along the whole above mentioned time interval. It means that in this case no relay commutation will occur. This situation is possible if $C_1$, $C_2$ and

$C_3$ are simultaneously either positive or negative.

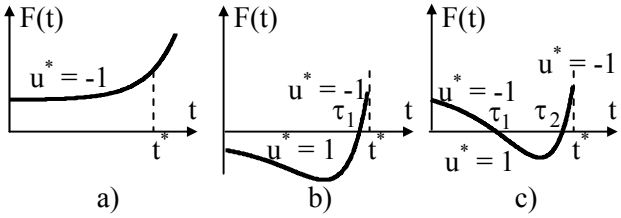


Fig. 3: Relay commutation
a) no commutation;
b) one commutation;
c) two commutations.

By varying the signs of $C_1$, $C_2$ and $C_3$, the function F(t) may have one or maximum two sign changes for $t \in [0; t^*]$, so $u^*$ will change its value too, accordingly to these. So one or maximum two relay commutations may occur in the time interval.

In figure 3 are presented 3 examples of the commutation function F(t).

In this case the Hamiltonian $H(t, u^*, z, \lambda)$ is computed by splitting the time interval:

- $t \in [0;\tau_1] \cup [\tau_1; t^*]$ if F(t) has a single sign change (in the moment $t = \tau_1$), as shown in figure 3b;
- $t \in [0;\tau_1] \cup [\tau_1;\tau_2] \cup [\tau_2; t^*]$ if F(t) has a double sign change (in the moments $t = \tau_1$ and $t = \tau_2$), as shown in figure 3c.

Trajectories $z_i = z_i(t, u^*)$ must be computed in accordance to the above mentioned.

In conclusion, the control possibilities depend on analysis of relay commutation, computing procedures for F(t) being necessary. As shown in figure 3, a such procedure must be able to solve the equation $F(t) = 0$, and to assign the correct values to the commutation variable: $u^* = -\text{sign}(F(t))$.

The compatibility of choosing $C_1$, $C_2$, $C_3$ and initial conditions (the starting position of the flying object) with the trajectory equations will be conditioned by positive values of time $(t \geq 0)$ and $H(t^*, u^*, z^*, \lambda^*) = 0$.

**2.1. Un-commutated Trajectory**. It results from (1) the trajectory equations:

$$\begin{cases} z_1 = \dfrac{1}{r_1}\left[(\alpha_1 r_1 + bu^*)e^{r_1 t} - bu^*\right] \\ z_2 = \dfrac{1}{r_2}\left[(\alpha_2 r_2 + bu^*)e^{r_2 t} - bu^*\right] \\ z_3 = bu^* t + \alpha_3 \end{cases} \quad (7)$$

where $A_0(\alpha_1, \alpha_2; \alpha_3)$ is the initial position.

By eliminating the time between the 3 above equations: $t = \dfrac{z_3 - \alpha_3}{bu^*}$, the trajectory results as the intersection of two surfaces, starting in the moment $t = 0$ from $A_0$:

$$\begin{cases} z_1 = \dfrac{1}{r_1}\left[(\alpha_1 r_1 + bu^*)e^{r_1 \frac{z_3 - \alpha_3}{bu^*}} - bu^*\right] \\ z_2 = \dfrac{1}{r_2}\left[(\alpha_2 r_2 + bu^*)e^{r_2 \frac{z_3 - \alpha_3}{bu^*}} - bu^*\right] \end{cases} \quad (8)$$

It may be noticed that the surfaces $z_1 = z_1(z_3)$ and $z_2 = z_2(z_3)$ are crossing the planes $(z_1Oz_3)$ and $(z_2Oz_3)$ respectively.

The goal for this trajectory $(z = z(t;\alpha))$ is to reach the target in origin: $z_i(t^*) = 0, i = \overline{1,3}$.

From $z_3(t^*) = 0$ it results:

$$t^* = -\frac{\alpha_3}{bu^*} \quad (9)$$

As time must be positive, the following restriction is obvious:

$$\frac{\alpha_3}{bu^*}<0 \xrightarrow[b>0]{} \begin{cases} \alpha_3>0; u^*=-1 \\ \text{or} \\ \alpha_3<0; u^*=1 \end{cases}$$

Similar, $z_1$ and $z_2$ from (8) must be null in the same time with $z_3$.

$$\begin{cases} z_1\big|_{z_3=0} \Rightarrow \alpha_1=\dfrac{bu^*}{r_1}\left(1-e^{-\frac{r_1\alpha_3}{bu^*}}\right) \\ z_2\big|_{z_3=0} \Rightarrow \alpha_2=\dfrac{bu^*}{r_2}\left(1-e^{-\frac{r_2\alpha_3}{bu^*}}\right) \end{cases} \quad (10)$$

In conclusion, if the initial coordinates $\alpha_1$ and $\alpha_2$ respect the constraints (10), and with an arbitrary value of $\alpha_3$, the ending point of the trajectory will be the origin O(0; 0; 0).

The trajectory may be plotted, either by using its parametric equations (7) or as intersection of two surfaces (8).

The mathematical determination of the parametric link between $C_1$, $C_2$, $C_3$ having the same sign (in the non-commutated case) is worked out by recalling the condition:

$$H\left(t^*,u^*,z^*,\lambda^*\right):=H_{min}=0$$

The optimal trajectories $A_0O$ are $\Gamma=\{\Gamma^+\}\cup\{\Gamma^-\}$, corresponding to the values $u=1$ and $u=-1$, respectively.

Two possible trajectories are shown in figure 4.

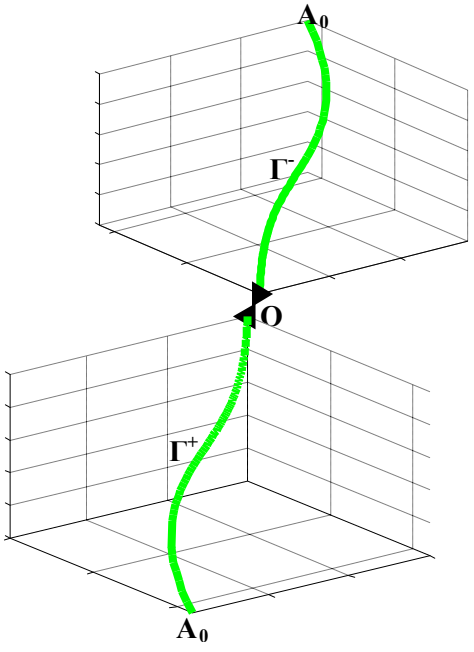


Fig. 4: Un-commutated trajectories

Finally, it comes out that:

$$H\left(u^*=\pm1\right)=0\Leftrightarrow$$
$$\Leftrightarrow 1\mp b\left(C_1e^{-r_1t^*}+C_2e^{-r_2t^*}+C_3\right)=0 \quad (11)$$

where $\mp$ must be the opposite sign of sign(F), defined in (5). So, it results a relationship involving $C_1$, $C_2$, $C_3$, that has to be respected. The conclusion is that only two of these three constants are arbitrary.

A non-commutated case that may be effectively approached is $C_3=0$, $C_1, C_2>0$, and linked by (11).

**2.2. One-commutation trajectory**.

In this case the relay switches at a moment $\tau^*<t^*$. The case $C_3=0, C_1<0$, $C_2>0$ is studied further.

Considering $r_2<r_1<0$, and denoting $r_2=-n$, $r_1=-m$, with $0<m<n$, F becomes:

$$F=C_1e^{mt}+C_2e^{nt}=0 \text{ for } 0<\tau^*<t^*,$$

where $\tau^*$ is the switching moment, and it may be computed as it follows:

$$t^*=\frac{1}{m-n}\ln\left(-\frac{C_2}{C_1}\right)=\frac{1}{r_2-r_1}\ln\left(-\frac{C_2}{C_1}\right)$$

It's obvious that $t^*>0\Leftrightarrow\left|\dfrac{C_2}{C_1}\right|<1$.

In this case, the starting point is $B(\beta_1;\beta_2;\beta_3)$, at the moment $t=0$, with the command $u^*=-\text{sign}(C_1+C_2)\underset{|C_1|>|C_2|}{\overset{C_1<0;C_2>0}{=}}1$.

This trajectory - $\Gamma^+$ - will commutate $\left(u^*=-1\right)$ at the moment $t=t^*$, in the point $Q(\gamma_1;\gamma_2;\gamma_3)$. From this moment on, the trajectory will go on with the curve $\Gamma^-$, till the target $O(0;0;0)$. The point $Q\left(\gamma;\tau^*\right)$ is similar to $A_0$, the starting point in the previous (un-commutated) case, but with the initial moment $t_0$ changed from $t_0=0$ to $t_0=\tau^*$ and with recalculated the final time, $t^*$.

So, the minimal final time will be $t^*=t_1^*+\tau^*$, for the trajectory described above: $\Gamma=\{\Gamma^+\}\cup\{\Gamma^-\}=[BQ]\cup[QO]$.

The phenomena are the same if $C_3 = 0, C_1 > 0,\ C_2 < 0$, when in the initial moment $t_0 = 0$ the command becomes $u^* = -1$. The trajectory starts from a point B', switches to $u^* = 1$ in the $t = \tau^*$ moment and will continue till the final point, O: $\Gamma = \{\Gamma^-\} \cup \{\Gamma^+\} = [B'Q'] \cup [Q'O]$.

The trajectory $\Gamma$ must end in O (a fix point) respecting the compatibility conditions. In the following lines, the appropriate mathematical approach will be described.

The solutions for the first curve, BQ, with $t_0 = 0$, are of type (7):

$$\begin{cases} z_i = \dfrac{1}{r_i}\left[\left(\beta_i r_i + bu^*\right)e^{r_i t} - bu^*\right], i = 1;2 \\ z_3 = bu^* t + \beta_3 \end{cases} \quad (7')$$

or of type (8):

$$\begin{cases} z_i = \dfrac{1}{r_i}\left[\left(\beta_i r_i + bu^*\right)e^{r_i \frac{z_3 - \beta_3}{bu^*}} - bu^*\right] \\ i = 1;2 \end{cases} \quad (8')$$

The coordinates of the point Q are obtained from (7'), at the moment $t = \tau^*$:

$$\begin{cases} \gamma_i = \dfrac{1}{r_i}\left[\left(\beta_i r_i + bu^*\right)e^{r_i \tau^*} - bu^*\right] \\ \gamma_3 = bu^* \tau^* + \beta_3 \end{cases} \quad (7'')$$

The solutions for the second curve, QO, with $t_0 = \tau^*$ and $u^* \to -u^*$ corresponding to the first curve, BQ, are of type (7) too:

$$\begin{cases} z_i = \dfrac{1}{r_i}\left[\left(\gamma_i r_i - bu^*\right)e^{r_i\left(t - \tau^*\right)} + bu^*\right] \\ z_3 = -bu^*\left(t - \tau^*\right) + \gamma_3 ; t \ge \tau^* > 0 \end{cases}$$

When the trajectory reaches the origin, its parametric equations must nullify:

$$z_i\left(t^*\right) = 0, i = \overline{1;3}$$

$$z_3\left(t^*\right) = 0 \Rightarrow t^* = \tau^* + \frac{\gamma_3}{bu^*}$$

The coordinates $\gamma_i$ must respect the compatibility constraints:

$$z_i\left(t_f\right) = 0, i = 1;2 \Rightarrow$$

$$\Rightarrow \left(\gamma_i r_i - bu^*\right)e^{r_i\left(t_f - \tau^*\right)} + bu^* = 0$$

It results:

$$\gamma_i = \frac{bu^*\left(e^{r_i\left(t_f - \tau^*\right)} - 1\right)}{r_i e^{r_i\left(t_f - \tau^*\right)}} \quad (12)$$

Similar compatibility constraints must be respected by the coordinates $\beta$, which has to be computed from (7"), replacing $\gamma_i$ with the one computed with (12).

## 3. CONCLUSIONS

The authors consider that their contribution is important because:

1. It synthesizes the a.r.a.s. method and system optimal control;
2. The approached application belongs to hydro aerodynamics (ballistics) as a critical case, one (characteristic) root being null $(r_3 = 0)$;
3. This dynamic system was optimal controlled, the optimizing parameter being the minimum stabilization time, and using a relay-type (on-off) regulator.

## REFERENCES

1. Lupu, M., Florea, Ol., Criteria and applications regarding the absolute stability for the ships autopilot route adjustment, *Proceedings of the 13th International Conference "AFASES-Scientific Research and Education in the Air Force", Braşov, May 26-28, 2011, pp.*

*pp.546-556, (ISSN, ISSN-L: 2247-3173), (2011).*

2. Lupu, M., Florea, Ol., Lupu, C., Studies and Applications of Absolute Stability of the Nonlinear Dynamical Systems. *Annals of the Academy of Romanian Scientists*, Serie Science and Technology, vol. 2, 2(2013), pp. 183-205.
3. Lupu, M., Radu, Gh., Constantinescu, C.G., Airplanes or Rackets Flight Stabilization Optimal Control in Case of Rolling Perturbation, *Review of the Air Force Academy, The Scientific Informative Review, Vol. XIII, No. 2(29)/2015* (to be appear).
4. Lurie, A.Y., *Nonlinear problems from the automatic control.* Moskow: Ed. Gostehizdat, in Russian, (1951).
5. Merkin, D.R., *Introduction in the movement stability theory.* Moskow: Ed. Nauka, in Russian, (1987).
6. Nalepin, R.A. & Co., *Exact methods in the nonlinear system control in case of automatic regulation.* Moskow: Ed. M.S. (2004).
7. Pontreaguine, L. & Co., *Theorie mathematique des processus optimeaux.* Moscou: Editions Mir (1974).
8. Popov, V.M., *The hyperstability of automatic systems.* Bucharest: Ed. Academiei Romane (1966). Moskow: Ed. Nauka (1970). Berlin: Springer Verlag (1973).
9. Rouche, N., Habets, P., Leloy, M., *Stability theory by Liapunov's direct Method.* Springer Verlag (1977

"HENRI COANDA"
AIR FORCE ACADEMY
ROMANIA

"GENERAL M.R. STEFANIK"
ARMED FORCES ACADEMY
SLOVAK REPUBLIC

INTERNATIONAL CONFERENCE of SCIENTIFIC PAPER
AFASES 2015
Brasov, 28-30 May 2015

# MATHEMATICAL MODELING BY USING A C++ SOFTWARE

**Ioan Milosan***

*Faculty of Materials Science and Engineering, Transilvania University of Brasov, Romania

***Abstract:*** *The aim of the study is to achieve a easy calculation of the linear regression (mathematical modeling) using of a C++ software. This application focused on the fitting and checking of linear regression models, using small and large data sets, with computers. Were constructed logical steps of the procedure and software based on their achievements C++ was made. The performance of regression analysis methods in practice depends on the form of the data generating process, and how it relates to the regression approach being used. It was used some statistical criteria as: Cochran, Student and Fischer criteria. After solving statistical analysis of the linear regression models, in the end there was obtained an applied statistical analysis of the linear regression model through the use of C++ software.*

***Keywords:*** *analytical models; computer aided software engineering, heat treatment, input variables, mechanical properties.*
***MSC2010:*** *15A06, 49K05, 68N17, 97P30, 97Q60, 97R30.*

## 1. INTRODUCTION

Mathematical modeling aims to de- scribe the different aspects of the real world, their interaction, and their dynamics through mathematics [1].

Today, mathematical modeling has an important key role in industrial fields and especially in complex metallurgical processes.

Linear regression is a statistical technique that is used to learn more about the relationship between a dependent variable and one or more independent variables [2, 3].

Linear regression equations with one or more variables were obtained under the assumption that the formula $\tilde{Y} = f(X_1, X_2 \ldots X_n)$ was known in relationships physical analysis of the problem. There are many situations in industrial processes in which this assumption not confirmed; therefore equations obtained by regression analysis are subject to a statistical analysis of the regression equation to determine whether or not consistent with experimental data [4, 5, 6, 7].

The aim of the study is to achieve a easy calculation of the linear regression (mathematical modeling) using of a C++ software for all industrial processes and in particularly for the statistical analysis of the regression equation applied to the mechanical results of a special S.G. cast iron.

## 2. METHOD OF CALCULATING

Solving statistical analysis of the linear regression models is done in the following steps:

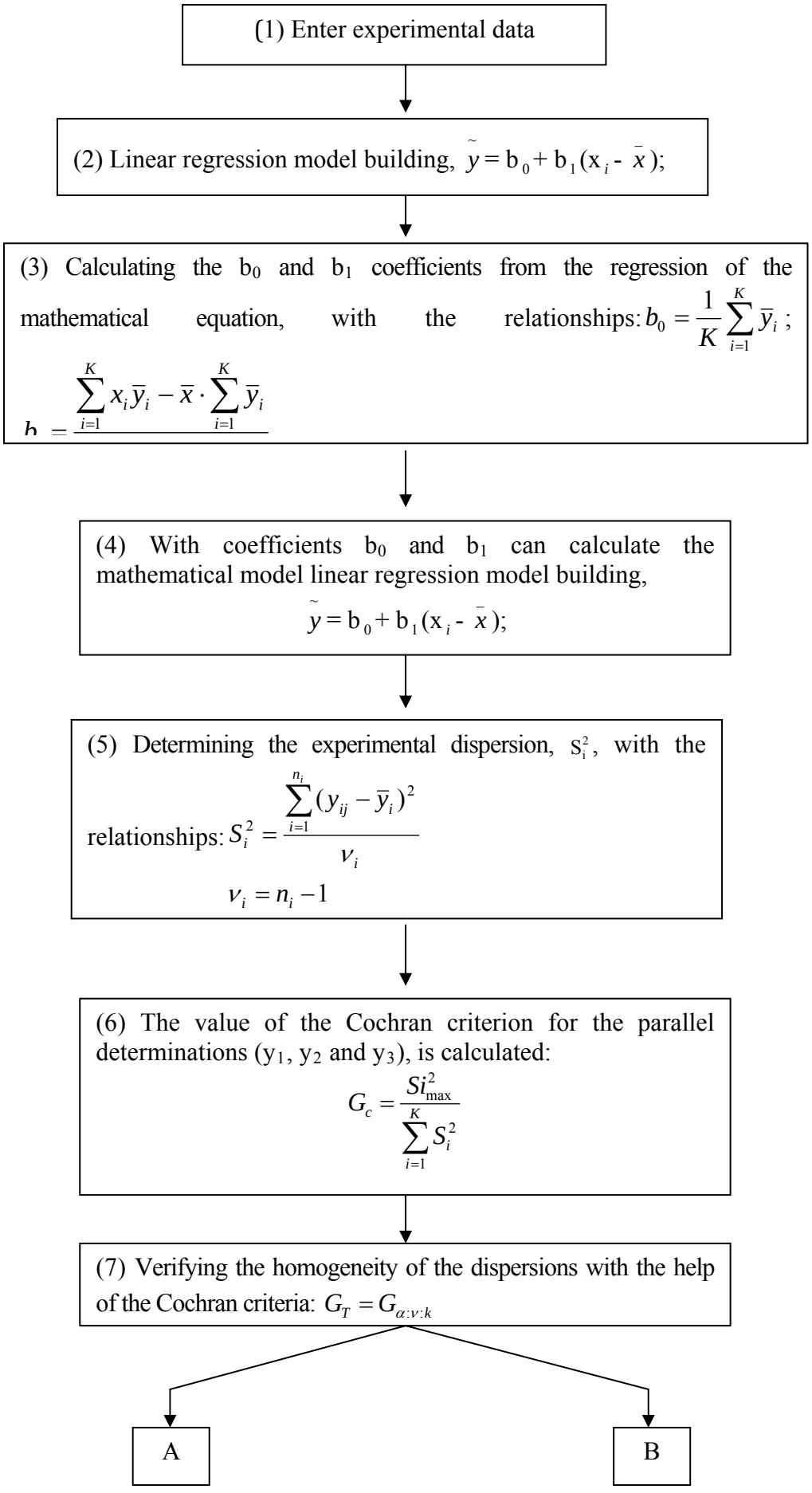
(1) Enter experimental data
(2) Linear regression model building, $\tilde{y} = b_0 + b_1(x_i - \bar{x})$;
(3) Calculating the $b_0$ and $b_1$ coefficients from the regression of the mathematical equation, with the relationships: $b_0 = \frac{1}{K}\sum_{i=1}^{K}\bar{y}_i$;
$b_1 = \frac{\sum_{i=1}^{K} x_i\bar{y}_i - \bar{x}\cdot\sum_{i=1}^{K}\bar{y}_i}{}$
(4) With coefficients $b_0$ and $b_1$ can calculate the mathematical model linear regression model building,
$\tilde{y} = b_0 + b_1(x_i - \bar{x})$;
(5) Determining the experimental dispersion, $S_i^2$, with the relationships: $S_i^2 = \frac{\sum_{i=1}^{n_i}(y_{ij} - \bar{y}_i)^2}{\nu_i}$
$\nu_i = n_i - 1$
(6) The value of the Cochran criterion for the parallel determinations ($y_1$, $y_2$ and $y_3$), is calculated:
$G_c = \frac{Si^2_{\max}}{\sum_{i=1}^{K} S_i^2}$
(7) Verifying the homogeneity of the dispersions with the help of the Cochran criteria: $G_T = G_{\alpha:\nu:k}$
A
B

A

B

(8.a) If $G_C < G_T$, the dispersions are homogeneous

(8.b) If $G_C > G_T$, the dispersions are not homogeneous, *calculation stops*

(9) Will determine the reproducibility dispersion $S_0^2$, with the relationship:

$$S_0^2 = \frac{1}{k} \cdot \sum_{i=1}^{K} S_i^2$$

(10) The value of the Student criteria is calculated:

$$t_{b0} = \frac{|b_0|}{Sb_0};\ t_{b1} = \frac{|b_1|}{Sb_1};\ Sb_0 = \sqrt{Sb_0^2};\ Sb_1 = \sqrt{Sb_1^2};\ Sb_0^2 = \frac{S^2}{N};$$

$$S^2 = \frac{1}{N-l} \cdot \sum_{i=1}^{K} \sum_{j=1}^{n_i} \left(y_{ij} - \tilde{y}_i\right)^2;\ N = k \cdot n_i;\ Sb_1^2 = \frac{S^2}{\sum_{i=1}^{k} n_i (x_i - \bar{x})^2}$$

(11) Verifying the coefficient signification $b_o$ and $b_1$ with the help of the critical value of the Student criteria, $t_T$ :

$$t_T = t_{\alpha,\nu}$$

C

D

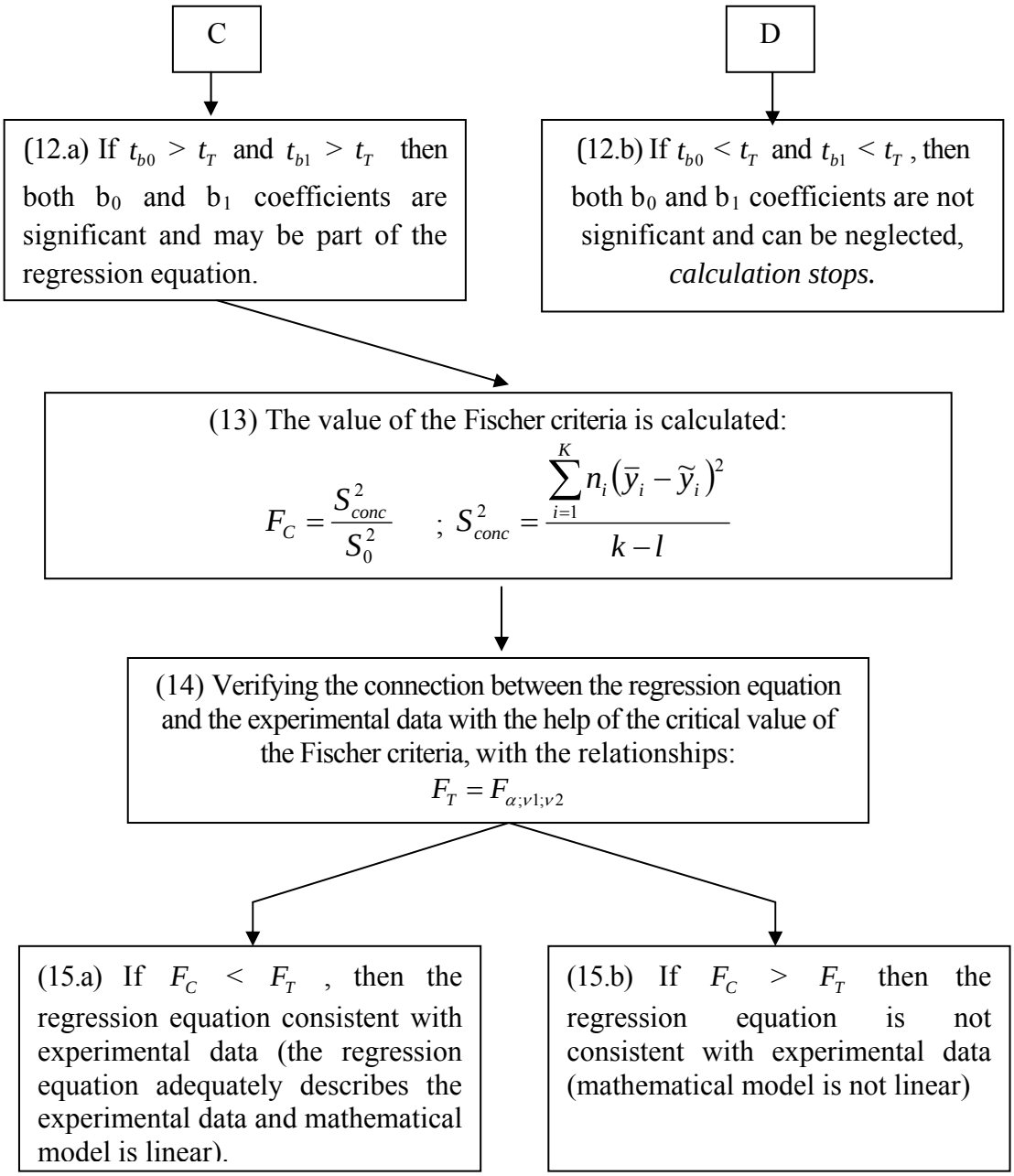


Fig. 1. Steps for calculating the statistical analysis of the linear regression models.

where:

- $\tilde{y}$ is the mathematical model;
- $x_i$ is the process variable;
- $\bar{x}$ is the average of process variables;
- $b_0$ is the slope coefficient from the regression of the mathematical equation, indicating the magnitude and direction of that relation;
- $b_1$ is the intercept coefficient from the regression of the mathematical equation, indicating the status of the dependent variable when the independent variable is absent.
- $b_0$ is the slope coefficient from the regression of the mathematical equation, indicating the magnitude and direction of that relation;
- $b_1$ is the intercept coefficient from the regression of the mathematical equation, indicating the status of the dependent variable when the independent variable is absent;
- K is the number of experimental points;
- $\bar{y}_i$ is the average of process performances;
- $S_i^2$ is the experimental dispersion;

- $Y_{ij}$ is the process performances;
- $\bar{y}_i$ is the average of process performances;
- $\nu$ is the number of degrees of freedom;
- $n_i$ is the number of parallel determinations performed each experimental points k.
- $G_c$ is the calculated value of the Cochran criteria;
- $G_T$ is the critical value of the Cochran criteria;
- $S^2_{i\,max}$ is the maximal experimental dispersion from the K number of experimental points;
- $S_i^2$ is the experimental dispersion;
- $\alpha = 0{,}05$ is the coefficient of statistical significance level;
- $\nu$ is the number of degrees of freedom, $\nu = n_i - 1$;
- $n_i$ is the number of parallel determinations performed each experimental points k.
- $Sb_0^2$ is the dispersion of $b_0$ coefficient;
- $Sb_1^2$ is the dispersion of $b_1$ coefficient;
- $S^2$ is the theoretical dispersion;
- $N$ is the total number of determinations;
- $l$ is the number of coefficients of the regression equation (l = 2)□
- $\tilde{y}_i$ is the mathematical model for each "i" point;
- $Y_{ij}$ is the process performances;
- $t_T$ is the critical value of the Student criteria;
- $\alpha = 0{,}05$ is the coefficient of statistical significance level;
- $\nu$ is the number of degrees of freedom, $\nu = N-2$;
- $S^2_{conc}$ is the dispersion according;
- $n_i$ is the number of parallel determinations performed each experimental points k.
- $\bar{y}_i$ is the average of process performances;
- $\tilde{y}_i$ is the mathematical model for each "i" point;
- $F_T$ is the critical value of the Fischer criteria;
- $\alpha = 0{,}05$ is the coefficient of statistical significance level;
- $\nu_1$ is the number of degrees of freedom, $\nu_1 = k-l$;
- $\nu_2$ is the number of degrees of freedom, $\nu_2 = k$;

## 3. EXPERIMENTAL RESEARCHES

The results were obtained after performing some KCU properties tests on samples pieces in the case of an austempered ductile iron. The studied cast iron has the following chemical composition (% in weight): 3.75% C; 2.14% Si; 0.4 % Mn; 0.012%P; 0.003%S; 0.05%Mg; 0.40% Ni, 0.42%Cu. This cast iron was made in an induction furnace.

The parameters of the heat treatment done were the following: the austenizing temperature, $t_A$ = 900[°C], the maintained time at austenizing temperature was, $\tau_A$ = 30 [min]; the temperature at isothermal level, $t_{iz}$ = 300[°C]; the maintained time at the isothermal level, $\tau_{iz}$ = 10, 20, 30, 40, 50 and 60 [min]. The experimental samples were performed at isothermal maintenance in salt-bath, being the cooling after the isothermal maintenance was done in air.

After the heat treating there were used 18 samples for each determining the impact strength (KCU).

The values of experimental points, the process variable, the average of process variable and the process performances (the values of impact strength, KCU) are presented in table 1. The process variable (xi) was the maintaining time at isothermal heat treatment and for each six samples it was made three parallel determinations ($y_1$, $y_2$ and $y_3$).

Table 1. The values of experimental points, the process variable, the average of process variable and the process performances (the values of impact strength)

| Experimental points | Process variable | Average of process variables | Process performances, KCU [ J / cm$^2$] | | |
|---|---|---|---|---|---|
| k | $x_i$ | $\bar{x}_i$ | $y_1$ | $y_2$ | $y_3$ |
| 1 | 10 | | 22 | 24 | 23 |
| 2 | 20 | | 28 | 26 | 27 |
| 3 | 30 | | 32 | 30 | 31 |
| 4 | 40 | 35 | 35 | 36 | 35 |
| 5 | 50 | | 38 | 39 | 39 |
| 6 | 60 | | 41 | 43 | 43 |

For easy calculation of the statistical analysis regression equation will work spreadsheet, considering the above six steps work, which is presented in table 2.

Table 2. Tabular presentation of data taken into account

| k | $\bar{y}_i$ | $x_i\bar{y}_i$ | $(x_i-\bar{x}_i)^2$ | $(y_{ij}-\bar{y}_i)^2$ | $S_i^2$ | $\hat{y}_i$ | $(y_{ij}-\hat{y}_i)^2$ | $(\bar{y}_i-\hat{y}_i)^2$ |
|---|---|---|---|---|---|---|---|---|
| 1 | 23 | 230 | 625 | 2.0000 | 1.0000 | 3.699 | 23.1746 | 0.0305 |
| 2 | 27 | 540 | 225 | 2.0000 | 1.0000 | 4.375 | 27.0603 | 0.0036 |
| 3 | 31 | 930 | 25 | 2.0000 | 1.0000 | 5.051 | 30.9460 | 0.0029 |
| 4 | 35.3333 | 1413.3333 | 25 | 0.6667 | 0.3333 | 5.727 | 34.8317 | 0.2516 |
| 5 | 38.6667 | 1933.3333 | 225 | 0.6667 | 0.3333 | 6.403 | 38.7175 | 0.0026 |
| 6 | 42.3333 | 2540 | 625 | 2.6667 | 1.3333 | 7.079 | 42.6032 | 0.0728 |
| Σ | 197.333 | 7586.6666 | 1750 | 9.3334 | 4.6666 | 32.334 | 197.3333 | 0.3640 |

Solving statistical analysis of the linear regression models in this case is done using the 15 steps above.

## 4. CALCULATING THE STATISTICAL ANALYSIS OF THE REGRESSION EQUATION WITH C++ SOFTWARE

Solving statistical analysis of the linear regression models with C++ software is done in the following steps:

(1) Input data into the program, actually presented in figure 2.

(2) Output data into the program, actually presented in figure 3.

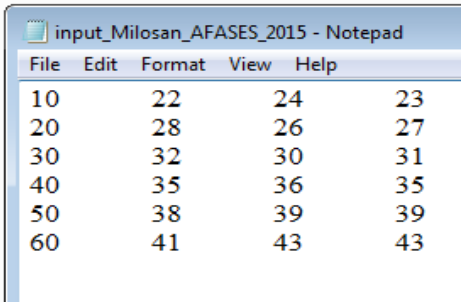


Fig. 2. Input data into the program

(3) Running Windows Commander data to determine all values in accordance with the working steps of the method, presented in figure 4.

output_Milosan_AFASES_2015 - Notepad

File Edit Format View Help

Linear regression with an independent variable

==========

1. The regression equation (mathematical model): y = b0 + b1 * (x - x_average)

2. Calculation b0 and b1 coefficients.

==========

| | | | | | | | | | | | | |
|---|---|---|---|---|---|---|---|---|---|---|---|---|
| 1 | 10.0000 | 35.0000 | 22.0000 | 24.0000 | 23.0000 | 23.0000 | 230.0000 | 625.0000 | 2.0000 | 1.0000 | 23.1746 | 2.0915 | 0.0305 |
| 2 | 20.0000 | 35.0000 | 28.0000 | 26.0000 | 27.0000 | 27.0000 | 540.0000 | 225.0000 | 2.0000 | 1.0000 | 27.0603 | 2.0109 | 0.0036 |
| 3 | 30.0000 | 35.0000 | 32.0000 | 30.0000 | 31.0000 | 31.0000 | 930.0000 | 25.0000 | 2.0000 | 1.0000 | 30.9460 | 2.0087 | 0.0029 |
| 4 | 40.0000 | 35.0000 | 35.0000 | 36.0000 | 35.0000 | 35.3333 | 1413.3333 | 25.0000 | 0.6667 | 0.3333 | 34.8317 | 1.4214 | 0.2516 |
| 5 | 50.0000 | 35.0000 | 38.0000 | 39.0000 | 39.0000 | 38.6667 | 1933.3333 | 225.0000 | 0.6667 | 0.3333 | 38.7175 | 0.6744 | 0.0026 |
| 6 | 60.0000 | 35.0000 | 41.0000 | 43.0000 | 43.0000 | 42.3333 | 2540.0000 | 625.0000 | 2.6667 | 1.3333 | 42.6032 | 2.8851 | 0.0728 |

b0 = 32.8889

b1 = 0.3886

Ymodel = 32.888889 + 0.388571 * (x - 35.000000)

Fig.3. Output data into the program.

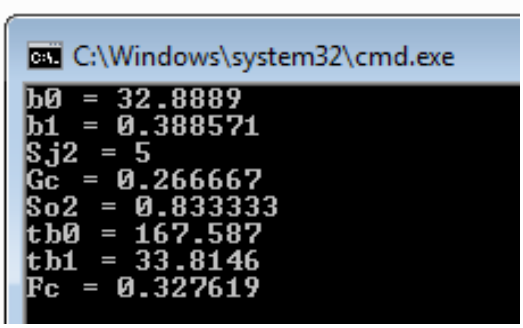


Fig. 4. Running Windows Commander data.

Solving statistical analysis of the linear regression models in this case is done in the following six steps, considering the data presented in figure 2 and calculated with the C++ software:

(1) Linear regression model building,

$$\tilde{y} = b_0 + b_1(x_i - \bar{x});$$

(2) After calculating the $b_0$ and $b_1$ coefficients from the regression of the mathematical equation, there has been obtained the following results: $b_0 = 32.8889$; $b_1 = 0.388571$, and the mathematical model is: $\tilde{y} = 19.288904 - 0{,}388571 \cdot x_i$

(3) After calculating the experimental dispersion, $S_i^2$ there has been obtained the following results: $S_i^2 = 5$;

(4) After calculating the homogeneity of the dispersions with the help of the Cochran criteria, there has been obtained the following results: $G_c = 0.266667$ and $G_c < G_T$ respectively $0.4266667 < 0.6161$. Because $G_C < G_T$ the dispersions are homogeneous and the dispersion value was determined: $S_0^2 = 0.833333$.

(5) After verifying the coefficient signification $b_o$ and $b_1$ with the help of the Student criteria, there has been obtained the following results: $t_{b0} > t_T$ result $167.587 > 2.12$ and $t_{b1} > t_T$, result $33.8146 > 2.12$, and then both $b_0$ and $b_1$ coefficients are significant and may be part of the regression equation.

(6) After verifying the connection between the regression equation and the experimental data with the help of the Fischer criteria, there has been obtained the following results: $F_C < F_T$ result $0.327619 < 4.53$, therefore the regression equation consistent with experimental data (the regression equation adequately describes the experimental data and mathematical model is linear).

## 5. CONCLUSIONS

(a) The regression analysis is one of the most widely used statistical tools to understand which among the independent variables are related to the dependent variable, and to explore the forms of these relationships.

(b) The performance of regression analysis methods in practice depends on the form of the data generating process, and how it relates to the regression approach being used.

(c) After verifying the connection between the regression equation and the experimental data with the help of the Fischer criteria, it is noted that the regression equation consistent with experimental data (the regression equation adequately describes the experimental data and mathematical model is linear).

(d) By using C++ software we obtained more accurate results and the application time was reduced by several hours (for the classical calculation) to 2-3 minutes.

## REFERENCES


1. Quarteroni, A., Mathematical Models in Science and Engineering, *American Mathematical Society*, 56, 1, 10-19 (2009).
2. Evans, J.R., Olson, D.L. *Statistics, Data Analysis and Decision Mo*deling, 2nd edition, Prentice Hall, New Jersey, USA (2003).
3. Akaike, H., A New Look at Statistical Modek Identification, *IEEE Trans. Auto Control*, 19, 716-723 (1974).
4. Lind, D.A., Marchal, W.G., Mason, R.D., *Statistical Techniques in Busines & Economics,* 11th edition, Mc Graw Inc., New York, USA (2005).
5. Kenkel, J.L., *Introductory Statistics for Management and Economics*. 4th edition. Duxbury Press, Wadsworth Publishing Company, New York, USA (1996).
6. Taloi, D., *Metallurgical Process Optimization- Applications in metallurgy*, E.D.P. Publishing Company, Bucharest, Romania (1984).
7. Crossman, A., Linear Regression Analysis. Linear Regression and Multiple Linear Regression, *Source* [online]. Available from: http://sociology.about.com/od/Statistics/a/Linear-Regression-Analysis.htmm (March, 2015).
8. Eijndhoven, S. Mathematical models in industrial context, Design of mathematical models, *Source* [online]. Available: https://static.tue.nl/uploads/media/2.1_Mathematical_models_in_industrial_context.pdf , (March, 2015).

"HENRI COANDA"
AIR FORCE ACADEMY
ROMANIA

"GENERAL M.R. STEFANIK"
ARMED FORCES ACADEMY
SLOVAK REPUBLIC

INTERNATIONAL CONFERENCE of SCIENTIFIC PAPER
AFASES 2015
Brasov, 28-30 May 2015

# OPTIMIZATION OF INDUSTRIAL PROCESSES USING A SPECIAL SOFTWARE

**Ioan Milosan***

*Faculty of Materials Science and Engineering, Transilvania University of Brasov, Romania

***Abstract:*** *The aim of the study is finding the best solution from all the industrial solution and this is a problem that can be solved with the help of the optimization calculation. The paper presents an experimental study regarding the utilization of a special Digital Sky Simplex Software for solving the production optimization of a hypothetical industrial process, using the Phases I problem of the Simplex algorithm. The number of unknowns components of calculation using the classical method is large, difficult, requiring a large volume of work and are insufficiently precise, all work was done whit the optimization by the linear programming, using a personal Digital Sky Simplex Software.*

***Keywords:*** *canonical forms, heat treatment, input variables, integer linear programming, optimization.*
***MSC2010:*** *15A06, 15A21, 15A39, 49J21, 49J30, 49K10, 68N17, 97P30, 97Q60, 97R30.*

## 1. INTRODUCTION

In optimization problems, we have to find solutions which are optimal or near-optimal with respect to some goals. Usually, we are not able to solve problems in one step, but we follow some process which guides us through problem solving. Often, the solution process is separated into different steps which are executed one after the other. Commonly used steps are recognizing and defining problems, constructing and solving models, and evaluating and implementing solutions [1].

In Optimization of Industrial Unit Processes, the term "optimization" means the maximizing of productivity and safety while minimizing operating costs. In a fully optimized plant, efficiency and productivity are continuously maximized while levels, temperatures, pressures, or flows float within their allowable limits [2].

The main optimization criteria are economic, technical and economic nature.

Planning processes to solve planning or optimization problems have been of major interest in operations research [3, 4].

Planning is viewed as a systematic, rational and theory-guided process to analyze and solve planning and optimization problems. The planning process consists of several steps:

1. Recognizing the problem,
2. Defining the problem,
3. Constructing a model for the problem,
4. Solving the model,
5. Validating the obtained solutions, and
6. Implementing one solution.

## 2. STEPS FOR OPTIMIZATION BY USING A LINEAR PROGRAMMING

A first stage of optimization is to determine the mathematical model and the second step is finding the optimum coordinates in the multifactorial space.

This means determining the extreme values (maximum or minimum) optimized parameters and factors, which receives the optimized parameter values, this step is even calling optimization.

Optimizing a process in terms of technological restriction require the use of a mathematical model which contains the optimized and restrictions of type equality and inequality [5].

If the optimized function and the restrictions are linear, then linear programming is used and when the optimized function and constraints are used nonlinear programming [6, 7].

The most used method to optimize the restriction is the Simplex algorithm method. The method described is a simple total solving linear program and is used frequently when the number of equations (m) and number of variables (n) is small.

Simplex algorithm applies when the number of equations (m) and number of variables (n) is large and full description of the method is cumbersome.

Steps for optimization by using a linear programming are:

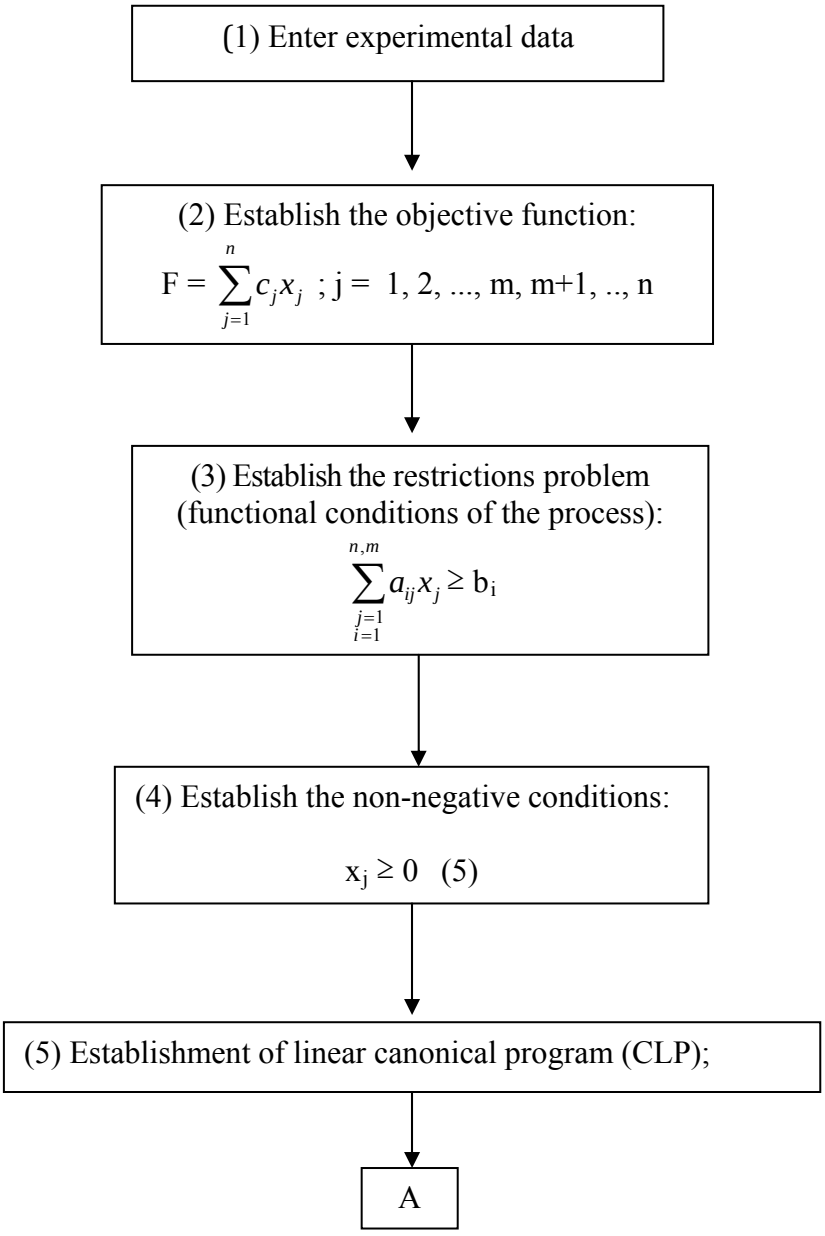

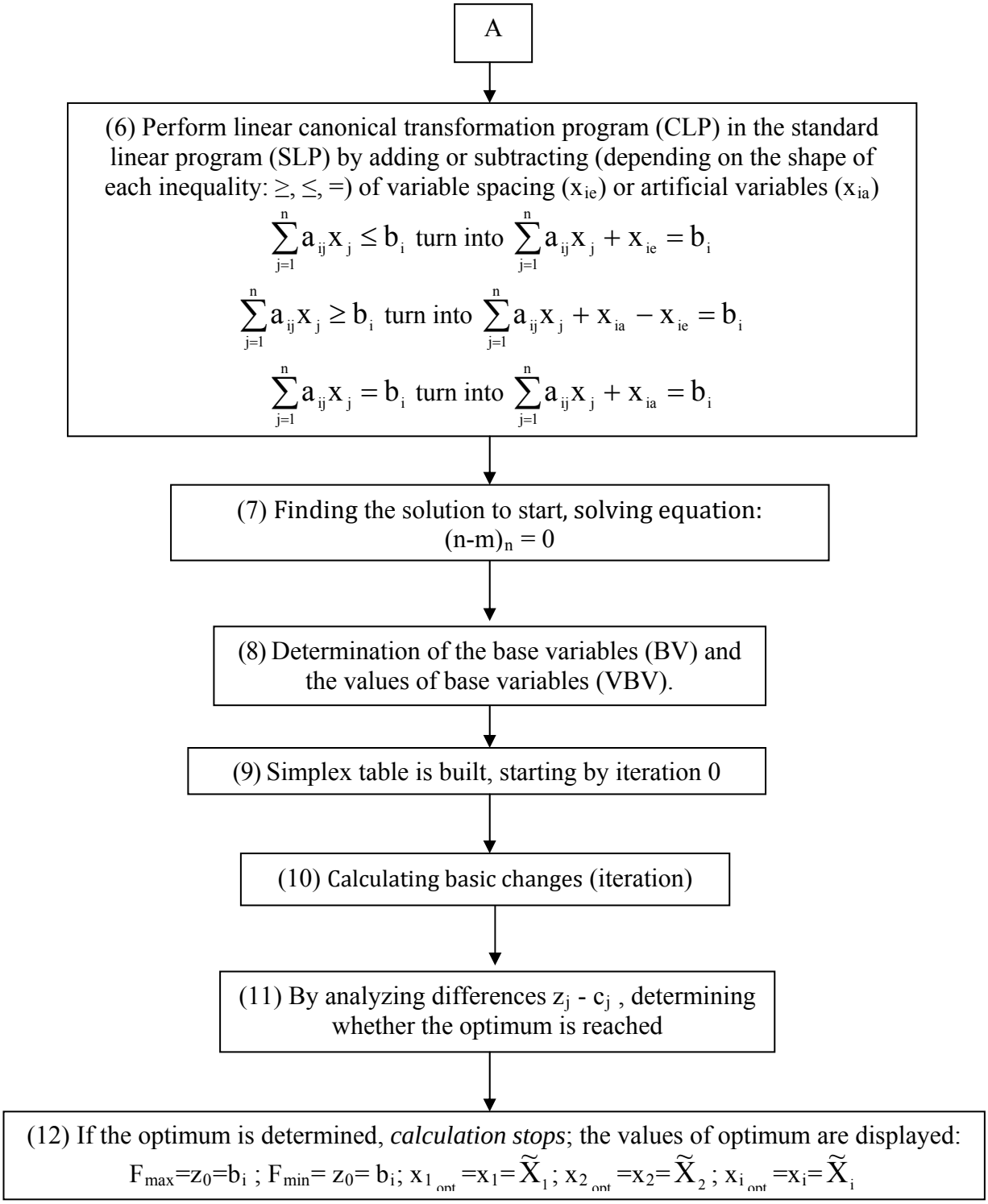


Fig. 1. Steps for optimization by using a linear programming.

where:

$x_j$ ($x_1$ , $x_2$ ,.....$x_n$ ) = system variables-process's parameters;

$c_j$ - connection coefficients;

j = n; i = m. (m < n)

$a_{ij}$ are called coefficients technology and can be each positive, negative or null.

$b_i$ = calculated coefficients;

$x_{ie}$ = variable spacing;

$x_{ia}$ = artificial variables;

n = number of the unknown of the problem

m = number of the equations

BV = the base variables;

VBV = the values of base variables;

$z_0$ = objective function;

$F_{max}$ = the maximum value of the objective function, F;

$F_{min}$ = the minimum value of the objective function, F;

## 3. EXPERIMENTAL RESEARCHES

In this experiment it was intended to study the heat treatment of C45 steel grade component parts treated in two heat treatment furnaces [5].

For this process it was calculate the optimization of the specific hourly productivity and the cost of each line in hand, aiming to achieve maximum benefit, using the Simplex algorithm - the One Phases' Method [7].

The optimization of this heat treatment production processes is made in relation to an economic criterion, so the function is an objective indicator of economic efficiency of the process analyzed [4]. The two heat treatment furnaces (F1, F2) for the two specific automotive component ($AC_1$, $AC_2$) made by C45 steel grade, are presented in Table 1.

Table 1. The optimized data for the heat treatment of the two specific automotive component ($AC_1$, $AC_2$) made by C45 steel grade.

| Heat treatment furnaces | Specific hourly productivity for automotive component parts (kg/h) | | Maximum production furnace / month, [t] |
|---|---|---|---|
| | $AC_1$ ($x_1$) | $AC_2$ ($x_2$) | |
| F 1 | 2 | - | 4 |
| F 2 | - | 1 | 1 |
| Benefit (million RON) | 3 | 1 | - |

### 3.1. Classical calculation steps for optimization by using a linear programming

The steps of the classical calculation are:

1) Establishment of linear canonical program (CLP)

a) The objective function (function to be optimized is the Benefit):

$$F= 3x_1 + x_2 = max \quad (1)$$

b) The restrictions problem are:

$$2 x_1 \leq 4 \quad (2)$$

$$X_2 \leq 1 \quad (3)$$

c) Non negativity conditions:

$$x_1 \geq 0 ; x_2 \geq 0 \quad (4)$$

2) Perform linear canonical transformation program (CLP) in the standard linear program (SLP) by adding or subtracting (depending on the shape of each inequality: ≥, ≤, =) of variable spacing ($x_{ie}$) variables are added in this care in order to easily get value system (for finding the solution to start).

$$F= 3x_1 + x_2 = max$$

$$2 x_1 + x_{1e} = 4 \quad (5)$$

$$x_2 + x_{2e} = 1 \quad (6)$$

$$x_1 \geq 0; x_2 \geq 0; x_{1e} \geq 0 ; x_{2e} \geq 0; \quad (7)$$

3) From the relation presented, it was determine the base variables (BV) and the

values of base variables (VBV), presented in Table 2.

Table 2. Base variables (BV) and values of base variables (VBV).

| BV | VBV |
|---|---|
| $x_{1e}$ | 4 |
| $x_{2e}$ | 1 |

The values from VBV are considered to be an admissible basic solution [8];

4) Simplex table is built, starting by iteration 0 (iteration= changing of base), presented in table 3.

Table 3. Simplex Table, Phase I, iteration 0.

| $c_J$ / $c_i$ | BV | VBV | 0 | 0 | 3 | 1 |
|---|---|---|---|---|---|---|
| | | | $x_{1e}$ | $x_{2e}$ | $x_1$ | $x_2$ |
| 0 | $x_{1e}$ | 4 | 1 | 0 | **2** | 0 |
| 0 | $x_{2e}$ | 1 | 0 | 1 | 0 | 1 |
| | $z_j$ | 0 | 0 | 0 | 0 | 0 |
| | $z_j - c_j$ | | 0 | 0 | - 3 | - 1 |

Because is an maximum program optimization, it was analyzed all differents $z_j - c_j$

- establish a procedure that allows moving from one base to another;
- basic changes are made by decreasing values (problem solved is maximum) optimization function;
- stops the iteration process (moving from one base to another), when it is not possible to increase the value of optimization function, results presented in Table 4.

Table 4. Simplex table, iteration 1.

| $c_J$ / $c_i$ | BV | VBV | 0 | 0 | 3 | 1 |
|---|---|---|---|---|---|---|
| | | | $x_{1e}$ | $x_{2e}$ | $x_1$ | $x_2$ |
| 3 | $X_1$ | 2 | - | 0 | 1 | 0 |
| 0 | $x_{2e}$ | 1 | - | 1 | 0 | **1** |
| | $z_j$ | 6 | - | 0 | 3 | 0 |
| | $z_j - c_j$ | | - | 0 | 0 | - 1 |

Stops the iteration process (moving from one base to another) when it is not possible to decrease the value of optimization function, so to reach the optimal solution, F=max, with solution $x_{i\ optimum}$ and all differents $z_j - c_j \geq 0$, so it reached the optimal solution, results presented in Table 5.

Table 5. Simplex table, iteration 2.

| $c_J$ / $c_i$ | BV | VBV | 0 | 0 | 10 | 20 |
|---|---|---|---|---|---|---|
| | | | $x_{1e}$ | $x_{2e}$ | $x_1$ | $x_2$ |
| 3 | $x_1$ | 2 | - | - | 1 | 0 |
| 1 | $x_2$ | 1 | - | - | 0 | 1 |
| | $z_j$ | 7 | - | - | 3 | 1 |
| | $z_j - c_j$ | | - | - | 0 | 0 |

Because all differents $z_j - c_j \geq 0$, so it reached the optimal (maximum) solution

The mathematical results of the optimal solutions are: $z_0 = F_{max} = 7$, with solutions:

$x_{1\ optimum} = 2; x_{2\ optimum} = 1;$

### 3.2. Calculation with Digital Sky Simplex Software.

Enter experimental data (figure 2).

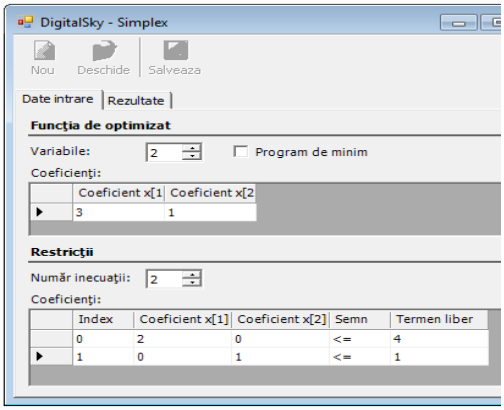


Fig. 2. Enter experimental data.

The values of Simplex Table, Phase I, Iteration 0 and Iteration 1 are presented in figure 3.

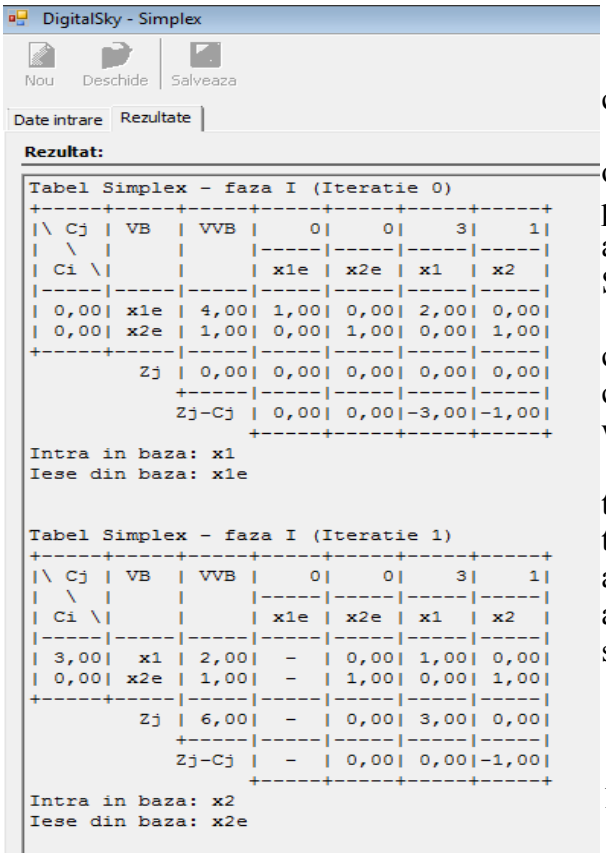


Fig. 3. The values of Simplex Table, Phase I, Iteration 0 and 1.

The values of Simplex Table, Phase I, Iteration 2, optimal (maximum) solution are presented in figure 4.

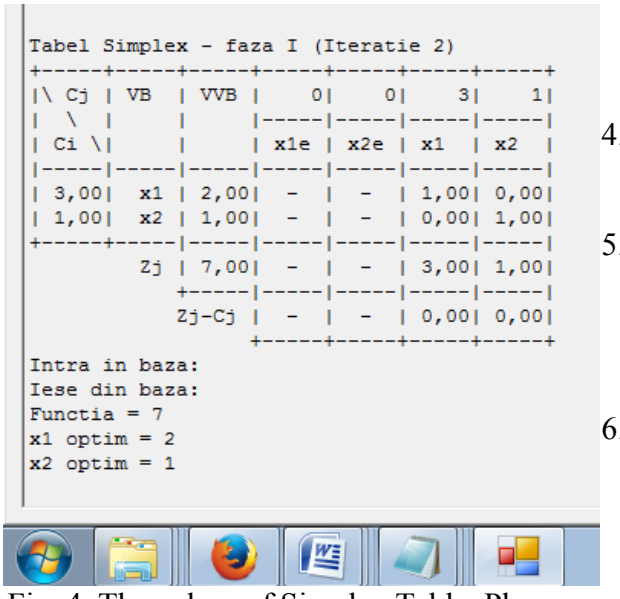


Fig. 4. The values of Simplex Table, Phase I, Iteration 2, optimal (maximum) solution.

## 3. CONCLUSIONS

Analyzing all data taken into account, there can say the following:

- For this process it was calculate the optimization of the specific hourly productivity and the cost of each line in hand, aiming to achieve maximum benefit, using the Simplex algorithm the One Phases' Method.

- In this case, because the number of components is large, the above methods are cumbersome, requiring a large volume of work, using the classical calculation.

- By using this software in place, reduce the computing time to several hours using traditional method to 2-3 minutes, getting an accurate result, respecting both the economic and technical component, without affecting the smooth running of the metallurgical process.

## REFERENCES

1. Anderson, C., G., *Applied metallurgical process testing and plant optimization with design of experimentation software,* Minerals, Metals & Materials Society, part I, 1-26, (2006).
2. Liptak, B., G., *Optimization of Industrial Unit Processes-Second Edition,* CRC Press, Boca Raton, (1998).
3. Babu, B., V., Angira, R., *Optimization of Industrial Proceses Using Improved and Modified Differential Evolution,* Springer-Verlag, Berlin, (2008).
4. Deb, K., *Multi-objective optimization using evolutionary algorithms*, John Wiley & Sons, Chichester, (2001).
5. Hartescu, F., Danilov, C., Process optimization system used in metallurgical plants. *1998 IEEE International Conference on Systems, Man, and Cybernetics,* vol. 4, 3989 – 3992, (1998).
6. Klemes, J., Friedler, F., Bulatov, I., Varbanov, P. *Sustainability in the Process Industry: Integration and Optimization*, Green Manufacturing & Sistem Engineering, Manchester, (2011).
7. Taloi, D. *Optimization of metallurgical processes. Application in metalurgy,* E.D.P. Bucharest, (1987)

"HENRI COANDA"
AIR FORCE ACADEMY
ROMANIA

"GENERAL M.R. STEFANIK"
ARMED FORCES ACADEMY
SLOVAK REPUBLIC

INTERNATIONAL CONFERENCE of SCIENTIFIC PAPER
AFASES 2015
Brasov, 28-30 May 2015

# COMPARATIVE ANALYSIS OF QUANTUM KEY DISTRIBUTION PROTOCOLS WITH TWO, THREE AND FOUR-STATE SYSTEMS

**Gabriela Mogos***

* Facultad de Informatica y Electronica, Escuela Superior Politecnica de Chimborazo, Riobamba, Ecuador

***Abstract:*** *Cryptographic protocols can be classified by the type of security against eavesdropping which they provide. There exist mathematically secure schemes whose security relies on mathematical proofs or conjectures about the complexity of deciphering the message without possessing the correct key. The majority of current secure public Internet connections rely on such schemes. Alternatively, a cryptographic setup may provide a physically secure method for communicating. In these setups the security is provided by the physical laws governing the communication protocol.This paper presents a comparative study of three quantum key distribution protocols with two, three and four-state systems, respectively. Starting with the same dimension of input data, the percentage of errors is analyzed by comparison with the dimensions of the cryptographic keys obtained in the case of each protocol.*

***Keywords:*** *security, qubits, qutrits, ququarts, quantum cryptography.*
***MSC2010*****:** 81P45, 94A15.

## 1. INTRODUCTION

Quantum information theory describes the communication and processing of information with symbols encoded in quantum mechanical systems, that is, as quantum signs, which by their nature are subject to physical constraints differing from those on classical signs. The development of quantum information theory has involved the replacement or generalization of traditional information-theoretic concepts so as to describe situations involving such signs, something that is necessary because quantum mechanical systems are described by non-standard probability distributions.

A central theme of such a study is the ways in which quantum mechanics opens up possibilities that go beyond what can be achieved classically.

This paper presents a comparative study of three quantum key distribution protocols: Bennett-Brassard; Bechmann-Pasquinucci, and Peres and Chen, Yan-Song, Deng, and Long, concerning the percentage of errors from the key compared with the dimensions of cryptographic keys obtained, and initial data.

It is important to mention that the protocols studied use for encoding the information of two, three, and four-state quantum systems.

For the performance of this study we developed software applications simulating each protocol, and we used the same dimension of input data at the measurement of the errors.

The applications simulating the protocols were realized in C++ language. The equipment used in the simulation process consists of two computers connected by a switch.

The modules of the application will run on each of the two computers: *the Sender* and *the Receiver*. In the research, we did not take into consideration the errors appeared due to the equipment and the presence of an eavesdropper.

## 2. THE QUANTUM KEY DISTRIBUTION PROTOCOLS

**2.1 The Quantum Key Distribution protocol with Two-State Systems.** In 1984 by Bennett-Brassard [8], using quantum bi-dimensional systems (*qubits*) realized the first quantum distribution key protocol.

The quantum bi-dimensional systems are represented by states of photon polarization, forming two orthonormal bases: linear and diagonal.

$$L = \{|0^0\rangle, |90^0\rangle\} \quad \text{- linear}$$
$$D = \{|45^0\rangle, |135^0\rangle\} \quad \text{- diagonal} \qquad (1)$$

**2.2 The Quantum Key Distribution protocol with Three-State Systems.** In 2000, Helle Bechmann-Pasquinucci and Asher Peres [9] (BPP) extended the quantum key distribution protocol for the three-state systems, the so-called *qutrits*. For qutrits, bases called Mutually Unbiased Bases (MUB) are used, obtained by the application of transformed Fourier discrete. For the protocol BPP, four measurement bases are used, each having three individual vectors.

$$\begin{aligned} A &= \{|\alpha\rangle, |\beta\rangle, |\gamma\rangle\} \\ B &= \{|\alpha'\rangle, |\beta'\rangle, |\gamma'\rangle\} \\ C &= \{|\alpha''\rangle, |\beta''\rangle, |\gamma''\rangle\} \\ D &= \{|\alpha'''\rangle, |\beta'''\rangle, |\gamma'''\rangle\} \end{aligned} \qquad (2)$$

**2.3 The Quantum Key Distribution protocol with Four-State Systems.** In 2006, a research team from China [7] proposed a key distribution scheme using quantum systems with four-dimensions (*ququarts*).

The Quantum Key Distribution protocol with Four-State Systems [7] uses twelve orthogonal states in a four-state quantum system. Hilbert space associated to these systems has four-dimensions, and the three mutually unbiased bases (MUB), each with four eigenvectors, are defined as follows:

$$Z - MUB = \begin{cases} |Z\rangle_0 = |0\rangle \\ |Z\rangle_1 = |1\rangle \\ |Z\rangle_2 = |2\rangle \\ |Z\rangle_3 = |3\rangle \end{cases}$$

$$X - MUB = \begin{cases} |X\rangle_0 = \frac{1}{\sqrt{4}}(|0\rangle + |1\rangle + |2\rangle + |3\rangle) \\ |X\rangle_1 = \frac{1}{\sqrt{4}}(|0\rangle + e^{2\pi i/4}|1\rangle + e^{4\pi i/4}|2\rangle + e^{6\pi i/4}|3\rangle) \\ |X\rangle_2 = \frac{1}{\sqrt{4}}(|0\rangle + e^{4\pi i/4}|1\rangle + e^{8\pi i/4}|2\rangle + e^{12\pi i/4}|3\rangle) \\ |X\rangle_3 = \frac{1}{\sqrt{4}}(|0\rangle + e^{6\pi i/4}|1\rangle + e^{12\pi i/4}|2\rangle + e^{18\pi i/4}|3\rangle) \end{cases} \qquad (3)$$

$$Y - MUB = \begin{cases} |Y\rangle_0 = \frac{1}{\sqrt{4}}(e^{-\pi i}|0\rangle + |1\rangle + |2\rangle + |3\rangle) \\ |Y\rangle_1 = \frac{1}{\sqrt{4}}(e^{-\pi i}|0\rangle + e^{2\pi i/4}|1\rangle + e^{4\pi i/4}|2\rangle + e^{6\pi i/4}|3\rangle) \\ |Y\rangle_2 = \frac{1}{\sqrt{4}}(e^{-\pi i}|0\rangle + e^{4\pi i/4}|1\rangle + e^{8\pi i/4}|2\rangle + e^{12\pi i/4}|3\rangle) \\ |Y\rangle_3 = \frac{1}{\sqrt{4}}(e^{-\pi i}|0\rangle + e^{6\pi i/4}|1\rangle + e^{12\pi i/4}|2\rangle + e^{18\pi i/4}|3\rangle) \end{cases}$$

## 3. COMPARATIVE ANALYSIS

Quantum Bit (Trit) Error Rate consists in the calculation of the percentage of errors from the key, obtained at the end of the quantum transmission, after the step of communication of the measurement bases from the public channel. Quantum Bit (Trit) Error Rate method may be applied to most of the key distribution systems, for detection of the enemy. Each system has its own accepted error rate, and exceeding it means the intervention of an enemy.

By quantum key distribution [1,2], two entities, *the Sender and the Receiver*, establish together a unique and secure key, which may be used with a secure encryption algorithm, like *one-time pad* [3,4].

A classical scheme of quantum key distribution uses two communication channels, a classical one, and a quantum one, and it has the following main steps:

1. *The Sender and the Receiver* generate random and independent sequences of bits/trits;

2. *The Sender and the Receiver* use a quantum key distribution protocol to compare the sequences of bits/trits, and to establish together a unique and secret key;
3. *The Sender and the Receiver* perform a procedure of error correction.
4. *The Sender and the Receiver* appreciate (according to the error rate) if the transmission was intercepted by *the enemy;*
5. *The Sender and the Receiver* communicate through a public channel and perform a procedure called *privacy amplification* [5,6];
6. *The final secret unique and secure key* is obtained.

We tested the applications on a variable number of input data (quantum systems), and studied how the quantum errors varied.

The first important step of the protocol is when *the Receiver* measures the quantum systems received from *the Sender*. Taking into account that the Receiver chooses the measurement bases randomly, we may speak of the appearance of significant errors in the protocol.

After running 10 times each application, we obtained the results shown in fig.1., fig.2. and fig.3., for an initial key with dimensions ranging from 160 to 2560 quantum systems.

| Nr crt | Initial qubits = 160 | | Initial qubits = 320 | | Initial qubits = 640 | | Initial qubits = 1280 | | Initial qubits = 2560 | |
|---|---|---|---|---|---|---|---|---|---|---|
| | Final bits | QBER (%) | Final bits | QBER (%) | Final bits | QBER (%) | Final bits | QBER (%) | Final bits | QBER (%) |
| 1 | 81 | 50 | 166 | 49 | 298 | 54 | 669 | 48 | 1312 | 49 |
| 2 | 86 | 47 | 160 | 50 | 327 | 49 | 664 | 49 | 1338 | 48 |
| 3 | 91 | 44 | 157 | 51 | 319 | 51 | 617 | 52 | 1267 | 51 |
| 4 | 70 | 57 | 181 | 44 | 309 | 52 | 652 | 50 | 1331 | 49 |
| 5 | 78 | 52 | 169 | 48 | 317 | 51 | 640 | 50 | 1344 | 48 |
| 6 | 75 | 54 | 149 | 54 | 314 | 51 | 645 | 50 | 1234 | 52 |
| 7 | 82 | 49 | 158 | 51 | 316 | 51 | 644 | 50 | 1300 | 50 |
| 8 | 84 | 48 | 176 | 45 | 329 | 49 | 626 | 52 | 1254 | 52 |
| 9 | 91 | 44 | 159 | 51 | 317 | 51 | 633 | 51 | 1288 | 50 |
| 10 | 81 | 50 | 162 | 50 | 313 | 52 | 641 | 50 | 1337 | 48 |
| | 81.41 | 49.20 | 163.21 | 49.13 | 315.68 | 51.00 | 642.75 | 50.17 | 1299.44 | 49.66 |

Fig. 1. Quantum Key Distribution protocol with Two-State Systems.

In the case of Quantum Key Distribution protocol with Two-State Systems - Bennett-Brassard – the Receiver needs to choose between the two measuring bases (linear and diagonal), therefore the probability to choose correctly is 1/2. After running the software application, we obtained an average error of 49.83%.

| No. crt | Initial qutrits = 160 | | Initial qutrits = 320 | | Initial qutrits = 640 | | Initial qutrits = 1280 | | Initial qutrits = 2560 | |
|---|---|---|---|---|---|---|---|---|---|---|
| | No. final trits | QTER (%) | No. final trits | QTER (%) | No. final trits | QTER (%) | No. final trits | QTER (%) | No. final trits | QTER (%) |
| 1 | 40 | 75 | 84 | 74 | 162 | 75 | 338 | 74 | 639 | 76 |
| 2 | 39 | 76 | 77 | 76 | 170 | 74 | 353 | 73 | 641 | 75 |
| 3 | 38 | 77 | 75 | 77 | 170 | 74 | 353 | 73 | 661 | 75 |
| 4 | 41 | 74 | 77 | 76 | 161 | 75 | 335 | 74 | 648 | 75 |
| 5 | 40 | 75 | 79 | 76 | 154 | 76 | 332 | 75 | 683 | 74 |
| 6 | 38 | 77 | 91 | 72 | 171 | 74 | 341 | 74 | 681 | 74 |
| 7 | 40 | 75 | 85 | 74 | 156 | 76 | 330 | 75 | 667 | 74 |
| 8 | 39 | 76 | 91 | 72 | 154 | 76 | 332 | 75 | 659 | 75 |
| 9 | 41 | 74 | 85 | 74 | 158 | 76 | 356 | 73 | 668 | 74 |
| 10 | 42 | 73 | 81 | 75 | 149 | 77 | 358 | 73 | 636 | 76 |
| | 39.76 | 75.18 | 82.15 | 74.56 | 160.17 | 75.29 | 342.28 | 73.89 | 657.91 | 74.79 |

Fig.2. Quantum Key Distribution protocol with Three-State Systems.

In the case of Quantum Key Distribution protocol with Three-State Systems - Bechmann-Pasquinucci and Peres – the Receiver needs to choose among the 4 measuring bases (A, B, C, D), the probability of choosing correctly is 1/4.

After running the software application, the error rate in the case of this protocol is of approximately 74.73%.

| No. crt | Initial ququarts = 160 | | Initial ququarts = 320 | | Initial ququarts = 640 | | Initial ququarts = 1280 | | Initial ququarts = 2560 | |
|---|---|---|---|---|---|---|---|---|---|---|
| | No. final bits | QQqER (%) | No. final bits | QQqER (%) | No. final bits | QQqER (%) | No. final bits | QQqER (%) | No. final bits | QQqER (%) |
| 1 | 92 | 72 | 240 | 63 | 384 | 70 | 840 | 68 | 1692 | 67 |
| 2 | 96 | 70 | 216 | 67 | 400 | 69 | 816 | 69 | 1696 | 67 |
| 3 | 88 | 74 | 232 | 65 | 408 | 69 | 816 | 69 | 1692 | 67 |
| 4 | 100 | 70 | 212 | 68 | 404 | 69 | 860 | 67 | 1648 | 68 |
| 5 | 104 | 68 | 200 | 69 | 412 | 68 | 864 | 67 | 1676 | 68 |
| 6 | 84 | 75 | 188 | 71 | 428 | 67 | 876 | 66 | 1702 | 67 |
| 7 | 104 | 69 | 208 | 68 | 412 | 68 | 816 | 69 | 1652 | 68 |
| 8 | 108 | 67 | 224 | 66 | 444 | 66 | 872 | 66 | 1640 | 68 |
| 9 | 92 | 72 | 188 | 71 | 404 | 69 | 844 | 68 | 1656 | 68 |
| 10 | 100 | 70 | 200 | 69 | 396 | 69 | 852 | 67 | 1660 | 68 |
| | 96.23 | 70.62 | 209.49 | 67.61 | 408.60 | 68.38 | 845.02 | 67.58 | 1671.12 | 67.60 |

Fig.3. Quantum Key Distribution protocol with Four-State Systems.

In the case of Quantum Key Distribution protocol with Four-State Systems, the Receiver needs to choose among the 3 measuring bases, therefore the probability of choosing correctly is of 1/3. The average error obtained after running the application is of 68.35%.

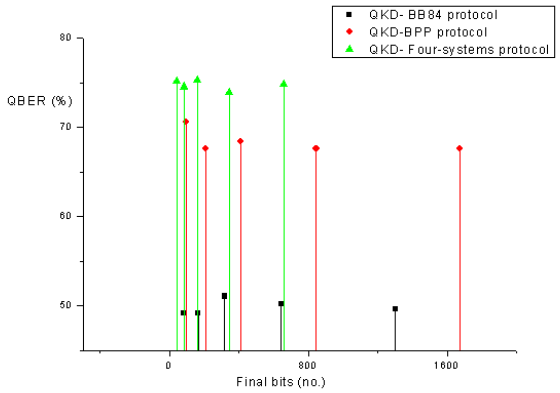


Fig.4. Variation of the error according to the dimension of the input data for all protocols.

We can see that the biggest errors are obtained in the case of Quantum Key Distribution protocol with Three-State Systems, when the Receiver needs to choose among several measuring bases than in the case of the other two protocols.

Quantum Key Distribution protocol with Four-State Systems is the most efficient of the three presented previously, because a quantum system with four-states transports two classical bits.

Consequently, even if the error rate registered by Quantum Key Distribution protocol with Four-State Systems is higher than for Quantum Key Distribution protocol with Two-State Systems, the dimension of the cryptographic key is bigger in the case of the protocol with four-state systems (average value of 257.8 bits) than in the case of two-state systems (average value of 209.17 bits).

## 4. CONCLUSIONS & ACKNOWLEDGMENT

Quantum Key Distribution (QKD) was demonstrated only for mathematical models of quantum key distribution systems. In practice, this unconditional security cannot be reached, due to technical imperfections of the devices used for polarization, and reading of photon polarization, respectively, involved in quantum key exchange.

The results obtained highlighted first the agreement between the theoretical model and the practical one in what concerns the average error of each protocol, and secondly, the dimension of the cryptographic key obtained in ideal working conditions.

This work was financed by the Prometeo Project of the Ministry of Higher Education, Science, Technology and Innovation of the Republic of Ecuador.

## REFERENCES

1. Bouwmeester D., Ekert A. & Zeilinger A., The Physics of Quantum Information. Quantum Cryptography, Quantum Teleportation, Quantum Computation, *Springer*, p. 314, (2000).
2. Bruss D., Optimal Eavesdropping in Quantum Cryptography with Six-States, *Physical Review Letters*, vol. 81, nr. 14, pp. 3018-3021, (1998).
3. Vernam G., Secret signaling system, *U.S. patent No. 1310719*, (1919).
4. Vernam G., Cipher printing telegraph system for secret wire and radio telegraphic communications, *Journal of IEEE*, vol. 55, pp. 109-115, (1926).
5. Bennett C.H., Brassards G. & Jean-Marc R., Privacy amplification by public discussions, *Siam Journal on Computing*, vol. 17, no. 2, pp. 210-229, (1988).
6. Bennett C.H., Bessette F., Brassard G., Salvail L., & Smolin J., Experimental quantum cryptography, *Journal of Cryptology*, vol. 5, no. 1, pp. 3-28, (1992).
7. Chen Pan, LI Yan-Song, Deng Fu-Guo, and Long Gui-Lu, Measuring-Basis Encrypted Quantum Key Distribution with Four-State Systems, *Commun. Theor. Phys.* (Beijing, China) 47, pp. 49–52, (2007).
8. Bennett C.H. and Brassard G., Proceedings IEEE Int. Conference on Computers, *Systems and Signal Processing, IEEE*, New York, (1984).
9. Bechmann-Pasquinucci H. and Peres A., Quantum Cryptography with 3-state systems, *Physical Review Letters 85*, 3313, (2000).

"HENRI COANDA"
AIR FORCE ACADEMY
ROMANIA

"GENERAL M.R. STEFANIK"
ARMED FORCES ACADEMY
SLOVAK REPUBLIC

INTERNATIONAL CONFERENCE of SCIENTIFIC PAPER
AFASES 2015
Brasov, 28-30 May 2015

# SOME FEATURES ABOUT STATIONARY DISTRIBUTION OF PROBABILITIES AND APPLICATIONS

**Ana-Maria Rîtea*, Sorina-Mihaela Stoian***

* Faculty of Mathematics and Computer Science, Transylvania University, Braşov, Romania

***Abstract:*** *An important aspect of the distribution is that of the stationary. Please note that here we consider only a special class of Markov chains, and indeed, the term Markov chain should always be described by adding the clause of the constant probabilities of transition. We present an application as a result of the study about the Markov chains and the stationary distribution of the probabilities.*

***Keywords:*** *probability distribution, recursive estimation, state estimation, stationary distribution.*
***MSC2010:*** *60A10, 03B48, 28D99, 30D35, 60E05, 62E10, 11K99, 97K50, 60J10, 60J20.*

## 1. INTRODUCTION

The natural significance of stationary of a probability distribution becomes apparent if we imagine a large number of processes that occur simultaneously. Let it be, for example, $N$ particles that are running independently the same type of random motion. At time $n$ the medium number of particles in the state $E_k$ is $Na_k^{(n)}$. With a stationary distribution these mean values remain constant and let observe (if $N$ is large enough for applying the law of large numbers) a macroscopic equilibrium state maintained by a large number of passes in opposite directions. In physics, many statistical equilibriums are of this kind, ie they are the exclusively simultaneous result observing of many independent particles. It is a typical case of a symmetric random motion (or diffusion); if more particles are observed then, after a sufficiently long time, about half of them will be to the right of the origin, and the rest to the left of them. However, it is known (citing law sinus) that most individual particles do not behave such that, spending a greater part of the time on the same side of the origin.

## 2. SOME FEATURES ABOUT STATES OF A MARKOV CHAIN

**Definition 1.** [1], [4] *The state $E_i$ leads to state $E_j$ and we note $E_i \to E_j$ if there exist a number $n > 0$ such that $p_{ij}^{(n)} > 0$. We say that the state $E_i$ communicate with the state $E_j$ and we note that with $E_i \leftrightarrow E_j$ if $E_i \to E_j$ and $E_j \to E_i$ .*

**Definition 2.** [1], [2], [5]. *A set of states C is closed if no state outside of C can not be touched by any $E_j$ of the states of C. The smallest closed set that contains the C is called the **closure** of C.*

**Definition 3.** [1], [2], [5] *A state* $E_k$ *which forms a single closed set is called* ***absorbing state***.

A Markov chain is called ***irreducible*** if there is no other closer set than the set of all states.

Obviously, $C$ is closed if and only if $p_{jk} = 0$ whenever $j$ is on $C$ and $k$ is outside of $C$, in this case, from Chapman-Kolmogorov equations we can see that $p_{jk}^{(n)} = 0$ for each $n$. So, it follows:

**Theorem 1.** [3], [7], [9] *If in* $P^n$ *matrix we cut all the lines and columns that correspond to the outside states of the set C, we will obtain stochastic matrix which continues to maintain the fundamental relations of Chapman-Kolmogorov.*

That means that we can define on C a Markov chain and this subchain can be studied independently of all other states.

**Remark 1.** The state $E_k$ is absorbing if and only if $p_{kk} = 1$; in this case the matrix of the last theorem is reduced to only one element.

The closure of a state $E_j$ is the set of all states that can be reached from it (inclusive $E_j$). This remark can be reformulated as follows:

**Definition 4.** [8] *A Markov chain is* ***irreducible*** *if and only if each state can be reached from every other state.*

**Application 1.** [8] In order to determine all closed sets is sufficient to know which $p_{jk}$ tend to zero and which are positive. Therefore, we use an asterisk to indicate the positive elements and we will consider the matrix

$$P = \begin{pmatrix} 0 & 0 & 0 & * & 0 & 0 & 0 & 0 & * \\ 0 & * & * & 0 & * & 0 & 0 & 0 & * \\ 0 & 0 & 0 & 0 & 0 & 0 & 0 & * & 0 \\ * & 0 & 0 & 0 & 0 & 0 & 0 & 0 & 0 \\ 0 & 0 & 0 & 0 & * & 0 & 0 & 0 & 0 \\ 0 & * & 0 & 0 & 0 & 0 & 0 & 0 & 0 \\ 0 & * & 0 & 0 & 0 & * & * & 0 & 0 \\ 0 & 0 & * & 0 & 0 & 0 & 0 & 0 & 0 \\ 0 & 0 & 0 & * & 0 & 0 & 0 & 0 & * \end{pmatrix}$$

Bet on the fifth line an asterisk appears in fifth place and, so $p_{55} = 1$; the state $E_j$ is absorbant. The third and the eighth lines contain only a positive element each, and it is obvious that $E_3$ and $E_8$ form a closed set. The crossings from $E_1$ are possible in $E_4$ and $E_9$, and from there only in $E_1$ , $E_4$ , $E_9$ . Consequently, the three states $E_1$ , $E_4$ , $E_9$ form another closed set.

We order now the states as follows:

$E_1' = E_5, E_2' = E_3, E_3' = E_8, E_4' = E_1, E_5' = E_9,$

$E_6' = E_4, E_7' = E_2, E_8' = E_7, E_9' = E_6$.

Elements of the matrix P are arranged in this way and, then, P takes the form

$$P' = \begin{pmatrix} * & 0 & 0 & 0 & 0 & 0 & 0 & 0 & 0 \\ 0 & 0 & * & 0 & 0 & 0 & 0 & 0 & 0 \\ 0 & * & 0 & 0 & 0 & 0 & 0 & 0 & 0 \\ 0 & 0 & 0 & 0 & * & * & 0 & 0 & 0 \\ 0 & 0 & 0 & 0 & * & * & 0 & 0 & 0 \\ 0 & 0 & 0 & * & 0 & 0 & 0 & 0 & 0 \\ * & * & 0 & 0 & * & * & * & 0 & 0 \\ 0 & 0 & 0 & 0 & 0 & 0 & * & * & * \\ 0 & 0 & 0 & 0 & 0 & 0 & * & 0 & 0 \end{pmatrix}$$

In this form the closed sets $(E_1')$, $(E_2', E_3')$ and $(E_4', E_5', E_6')$ appear clearly. From $E_7'$ it is possible a pass in each of the three closed sets and, therefore, the closure of $E_7'$ is the set of states $E_1'$, $E_2'$, $E_3'$, $E_4'$, $E_5'$, $E_6'$, $E_7'$. From $E_8'$ it is possibile a pass in $E_7'$ and in $E_9'$ and, so, in every closed set. The closures of $E_8'$ and of $E_9'$ consist of all nine states.

Suppressing all the lines and all the columns from the outside of a closed set we get three stochastic matrices

$$(*), \begin{pmatrix} 0 & * \\ * & 0 \end{pmatrix}, \begin{pmatrix} 0 & * & * \\ 0 & * & * \\ * & 0 & 0 \end{pmatrix}$$

and $P'$ does not contain any other stochastic submatrix.

We consider a fixed state $E_j$ and we suppose that, initially, the system is in state $E_j$. Whenever the system passes through the state $E_j$ the process is repeated from the beginning as it has been the first time. It is clear,

therefore, that a return to $E_j$ is a recurring event. If the system starts from a different state $E_i$ then, passing through $E_j$ becomes a *recurring event* delayed. Therefore, Markov chains appear as a special case of recurrent events simultaneously.

Each state $E_j$ is characterized by its *recursive time distribution* $\{f_j^{(n)}\}$. Here $f_j^{(n)}$ is the probability that the first return to $E_j$ occur at time *n*. From $p_{jj}^{(n)}$, we can calculate the probability $f_j^{(n)}$ using obvious recurrent relations

$$f_j^{(1)} = p_{jj},\ f_j^{(2)} = p_{jj}^{(2)} - f_j^{(1)} p_{jj},\ \dots,$$
$$f_j^{(n)} = p_{jj}^{(n)} - f_j^{(1)} p_{jj}^{(n-1)} - f_j^{(2)} p_{jj}^{(n-2)} - \dots - f_j^{(n-1)} p_{jj} \quad (1)$$

Relationships (1) express the fact that the probability of a *first* return to the state $E_j$, at the moment *n*, is equal with the probability of a return at the time *n*, minus the probability that the first return to take place at a time *v = 1,2, ..., n - 1*, and is followed by a repeated returning at time *n*.

The sum

$$f_j = \sum_{n=1}^{\infty} f_j^{(n)} \quad (2)$$

is the probability that, starting from the state $E_j$, the system to get back to the state $E_j$.

**Theorem 3.** [6] *In an irreducible Markov chain, all of the states belong to the same class: they are all transitory, all zero-persistent states, or all non-zero persistent states. In each case they have the same period. In addition, each state may be achieved from any other state.*

**Corollary 1.** [6] *In a finite Markov chain there is no zero state and it is impossible that all of the states to be transient.*

## 3. ERGODIC PROPERTIES OF THE IRREDUCIBLE CHAINS

**Definition 5.** [8] *A probability distribution* $\{v_k\}$ *is called stationary if*

$$v_j = \sum_i v_i p_{jj} \quad (3)$$

If the initial distribution $a_k$ is going to be stationary, then the absolute probabilities $\{a_k^{(n)}\}$ are independent of the time *n*, ie $a_k^{(n)} = a_k$.

The following theorem is often described as *a tendency towards equilibrium*.

**Theorem 4.** [7] *An irreducible periodically Markov chain belongs to one of the two classes:*

*i) All states are either transient or are all null state; in this case* $p_{jk}^{(n)} \to 0$ *when* $n \to \infty$ *for each pair j, k and there is no stationary distribution.*

*ii) All the states are ergodic, ie*

$$\lim_{n\to\infty} p_{jk}^{(n)} = u_k > 0 \quad (4)$$

*Where* $u_k$ *corresponds to the medium recursive time of* $E_k$. *In this case* $\{u_k\}$ *is a stationary distribution.*

A weaker formulation can highlight the implications of this theorem. Thus, if (4) takes place, then for an arbitrary initial distribution $a_k$

$$a_k^{(n)} = \sum_j a_j p_{jk}^{(n)} \to u_k \quad (5)$$

Therefore, if there is a stationary distribution it is necessarily unique and the distribution at the time *n* tends to her independently from the initial distribution. The only alternative to this situation is that $p_{jk}^{(n)} \to 0$.

*Demonstration*

By the theorem 3, the relation (4) is keeping any time as long as its states are ergodic. For proofing the affirmation (ii), the above, we point out, first of all, that

$$\sum u_k \le 1 \qquad (6)$$

This follows directly from the fact that, for fixed $j$ and $n$, the quantities $p_{jk}^{(n)}(k = 1,2,3,...)$ have the sum equal with unity, such that $u_1 + u_2 + ... + u_N \le 1$ for each $N$. For $n = 1$ and $m \to \infty$ we have the left side tending to $u_k$, and the general term from the right side of the sum tending to $u_v p_{vk}$. Adding an arbitrary number, but finite of terms we observe that

$$u_k \ge \sum_v u_v p_{vk} \qquad (7)$$

Summing these inequalities for all $k$ we obtain, in each part the finite quantity, $\sum u_k$

This shows that in (7) the inequality is not possible and, therefore,

$$u_k = \sum u_j p_{jk} \qquad (8)$$

If we put $v_k = u_k \left(\sum u_j\right)^{-1}$ we find that $v_k$ is a stationary distribution, such that there exist at least one distribution like that.

Let $\{v_k\}$ a certain distribution satisfying equality (3). Multiplying (3) by $p_{jk}^{(n)}$, and summing after $j$, we deduce, by induction, that

$$v_r = \sum_v v_k p_{vr}^{(n)} \qquad (9)$$

If $n \to \infty$, we obtain

$$v_r = (v_1 + v_2 + ...)u_r = u_r \qquad (10)$$

which completes the proof of point (*ii*). If states are transient or zero state and $\{v_k\}$ is a stationary distribution then equations (9) remain valid and $p_{vr}^{(n)} \to 0$ which is obviously impossible.

As a consequence, a stationary distribution may exist only in the ergodic case and the theorem is proved.

## 4. APPLICATION

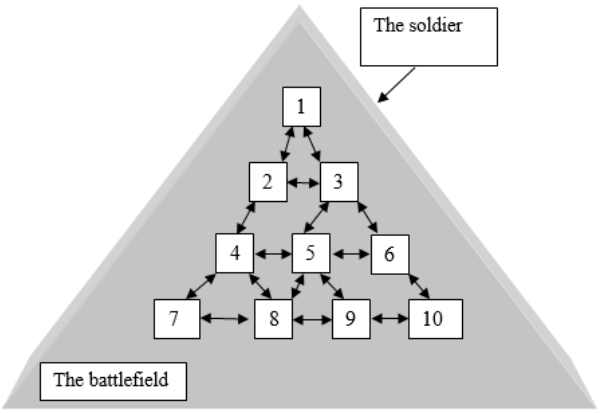


Fig. (1)

A soldier enters on the battlefield which contains 10 charging points of weapons. From each power point he can move to another point neighbor. He chooses with equal probabilities either supply points which are available. For example, from the no.1 building he moves with the same probability $\frac{1}{2}$, in the no. 2 and no. 3 buildings. From no.2 buildings he moves with the probability $\frac{1}{4}$ in buildings no.1, no.3, no.4 and no.5 etc.

We will determine the stationary distribution of probabilities (the limit probability) with each soldier is arming in every collecting point.

We note with $E_n$ the collecting point in which one the soldier will arm at the time $n$. The chain $\{E_n\}$ is Markov, with the set of states 1, 2, … 10 and transition probabilities

$$\begin{pmatrix}
0 & \frac{1}{2} & \frac{1}{2} & 0 & 0 & 0 & 0 & 0 & 0 & 0 \\
\frac{1}{4} & 0 & \frac{1}{4} & \frac{1}{4} & \frac{1}{4} & 0 & 0 & 0 & 0 & 0 \\
\frac{1}{4} & \frac{1}{4} & 0 & 0 & \frac{1}{4} & \frac{1}{4} & 0 & 0 & 0 & 0 \\
0 & \frac{1}{4} & 0 & 0 & \frac{1}{4} & 0 & \frac{1}{4} & \frac{1}{4} & 0 & 0 \\
0 & \frac{1}{6} & \frac{1}{6} & \frac{1}{6} & 0 & \frac{1}{6} & 0 & \frac{1}{6} & \frac{1}{6} & 0 \\
0 & 0 & \frac{1}{4} & 0 & \frac{1}{4} & 0 & 0 & 0 & \frac{1}{4} & \frac{1}{4} \\
0 & 0 & 0 & \frac{1}{2} & 0 & 0 & 0 & \frac{1}{2} & 0 & 0 \\
0 & 0 & 0 & \frac{1}{4} & \frac{1}{4} & 0 & \frac{1}{4} & 0 & \frac{1}{4} & 0 \\
0 & 0 & 0 & 0 & \frac{1}{4} & \frac{1}{4} & 0 & \frac{1}{4} & 0 & \frac{1}{4} \\
0 & 0 & 0 & 0 & 0 & \frac{1}{2} & 0 & 0 & \frac{1}{2} & 0
\end{pmatrix}$$

All the states communicate with each other such that they form a single class (obviously positive). We have $p_i = y_i$; $y_i$ obtained from the solving the system (8) with the conditions (10):

$$\begin{cases}
y_1 + y_2 + y_3 + ... + y_{10} = 1 \\
y_1 = \frac{1}{4}y_2 + \frac{1}{4}y_3 \\
y_2 = \frac{1}{2}y_1 + \frac{1}{4}y_3 + \frac{1}{4}y_4 + \frac{1}{6}y_5 \\
y_3 = \frac{1}{2}y_1 + \frac{1}{4}y_2 + \frac{1}{6}y_5 + \frac{1}{4}y_6 \\
y_4 = \frac{1}{4}y_2 + \frac{1}{6}y_5 + \frac{1}{2}y_7 + \frac{1}{4}y_8 \\
y_5 = \frac{1}{4}y_2 + \frac{1}{4}y_3 + \frac{1}{4}y_4 + \frac{1}{4}y_6 + \frac{1}{4}y_8 + \frac{1}{4}y_9 \\
y_6 = \frac{1}{4}y_3 + \frac{1}{6}y_5 + \frac{1}{4}y_9 + \frac{1}{2}y_{10} \\
y_7 = \frac{1}{4}y_4 + \frac{1}{4}y_8 \\
y_8 = \frac{1}{4}y_4 + \frac{1}{6}y_5 + \frac{1}{2}y_7 + \frac{1}{4}y_9 \\
y_9 = \frac{1}{6}y_5 + \frac{1}{4}y_6 + \frac{1}{4}y_8 + \frac{1}{2}y_{10} \\
y_{10} = \frac{1}{4}y_6 + \frac{1}{4}y_9
\end{cases}$$

$$\Leftrightarrow \begin{cases}
y_1 = y_7 = y_{10} = \frac{1}{18} \\
y_2 = y_3 = y_4 = y_6 = y_8 = y_9 = \frac{1}{9} \\
y_5 = \frac{1}{6}
\end{cases}$$

## 5. CONCLUSIONS

So if the soldier is in the initial point *i* with probability $p_i = y_i, 1 \le i \le 10$, then in every minute there exist the same probability $y_i \left( p_i^{(n)} = p_i = y_i \right)$ that the soldier to be in *i* point. On the other hand, even if the initial probabilities $p_i$ are different of $y_i$ the ergodic

character of the chain assures us that after many moments, probability that the soldier to be the point *j* will be close to the limit probability, $y_j$. He will be found most frequently in the no.5 weapons collection point where he returns on average every 6 considered moments.

In conclusion we can say that it is usually easy in terms of comparison, to decide whether there is a stationary distribution and therefore if a given irreducible chain is ergodic.

## REFERENCES


1. Capinski, M, Kopp, E., *Measure, Integral and Probability*, Berlin: Springer – Verlag (2003).
2. Cenuşa, Gh., Burlacu, V., Sacuiu, I., *Teoria probabilităţilor şi statistică matematică*, Bucureşti: Editura ASE (1999).
3. Feller, W., *An introduction to probability theory and its applications*, Third Edition, Vol. I, New York: John Wiley & Sons (1968).
4. Geiss, Ch., Geiss, St., *An Introduction to probability theory*, Jyväskylän: Department of Mathematics and Statistics University of Jyväskylän (2004)
5. Iosifescu, M., *Lanţuri Markov finite şi aplicaţii*, Bucureşti: Editura Tehnică (1977).
6. Klebaner, F. C., *Introduction to Stochastic Calculus with Applications*, London: Imperial College Press (2004)
7. Orman, G.V., *Capitole de matematici applicate*, Cluj-Napoca: Editura Albastră (1999).
8. Orman, G.V., *Handbook of limit theorems and stochastic approximation*, Braşov: Transilvania University Press (2003).
9. Pletea, A., Popa, L., *Teoria probabilităţilor*, Iaşi: Editura Universităţii Tehnice Gh. Asachi (1999).

"HENRI COANDA"
AIR FORCE ACADEMY
ROMANIA

"GENERAL M.R. STEFANIK"
ARMED FORCES ACADEMY
SLOVAK REPUBLIC

INTERNATIONAL CONFERENCE of SCIENTIFIC PAPER
AFASES 2015
Brasov, 28-30 May 2015

# PERFORMANCE ANALYSIS OF PARALLEL SVM TRAINING ON CLUSTER HAVING SIMILAR IBM ROADRUNNER ARCHITECTURE

**Ştefania-Iuliana Şoiman*, Gheorghe Radu**, Ştefan-Gheorghe Pentiuc*, Ionuț Balan*****

*Faculty of Electrical Engineering and Computer Science, "Stefan cel Mare" University, Suceava, Romania, ** Faculty of Aeronautical Management, "Henri Coandă" Air Force Academy, Brasov, Romania, ***Faculty of Economics and Public Administration, "Stefan cel Mare" University, Suceava, Romania

***Abstract:*** *The paper presents an analysis of the efficiency of parallelization of the SVM training algorithms. The researches were focused on computing time reduction in the training stage, and on good accuracy of the resulted classifier. Firstly it was described the algorithm Parallel Cutting Plane Support Vector Machines (PCPSVM) that ensures the parallelism of both data and calculations. Another approach for training SVM was based on the evolutionary algorithms (EASVM). These algorithms are very suitable for parallelization at data level. The experiments were conducted on a supercomputer having a similar architecture to the IBM Roadrunner supercomputer from DOE of USA, the first supercomputer that surpassed 1 petaflops barrier. The experimental results validated the fact that the parallelization of the two different training algorithms of SVM led to very good time performances and a very good accuracy of the solutions.*

***Keywords:*** *Parallel algorithms, Parallel computation, Classification and discrimination; cluster analysis, IBM Roadrunner cluster, Support Vector Machines training.*
***MSC2010*:** *68W10, 65Y05, 62H30, 68M99.*

## 1. INTRODUCTION

Support Vector Machine (SVM) is a successfully method applied in pattern recognition supervised learning on large data sets with a great number of patterns to be classified and/or having a large number of features thereof. SVM classification method was derived from statistical learning theory by Vapnik et al. in 1992 [1]. Initially used for handwriting character recognition, it is increasingly used so that in the last decade emerged many new and diverse applications using SVM.

The method involves a quadratic problem (QP) solving and generally produces a binary classifier usually for linear separable classes, but may be applicable for multi-class classification or for nonlinear separable classes. SVM is trained to find the optimal separation hyper-plane in the pattern space that ensures an area as large as possible for classes' separation. One of the disadvantages of SVM training algorithm is the large amount of memory required for classification of huge data sets.

Undertaken researches are focused on improving the classification accuracy and

reducing the computation time during the training stage.

An efficient algorithm for training the SVM is presented in the paper of Dai and Fletcher [2], about Quadratic Programs subject to Lower and Upper Bounds which demonstrated the usefulness on the medium and large training sets. Another interesting approach may be found in [3] that uses the solution of the problem division into several smaller quadratic sub problems in SVM training.

The Evolutionary Optimization technique enables the adaptation of the decision hyper-plane to the available training patterns, directly solving the optimization of the primary problem. It is considered the basic idea of SVM, geometric concept of training [4], but the proposed approach deviates from the standard mathematical treatment. In addition, this technique open the way of evolutionary generalizations involving non-standard, nonlinear decision surfaces. It proposes a new approach: the training follows the standard SVM, while the optimal hyper-plane coefficients (*w* and *b*) are determined directly by an evolutionary algorithm with a balance between classification accuracy and generalization ability [5, 6].

## 2. PARALLEL ALGORITHM FOR TRAINING SVM

**2.1. The Parallel Cutting Plane Support Vector Machines algorithm.** The PCPSVM algorithm was proposed in [7], and represents a parallel implementation of the training algorithm of SVM [8].

*Problem Formulation*

Given the training set $(x_i,y_i)$ with $i=1,n$ where $x_i=(x_{i1},x_{i2},..,x_{ip})$ is an input pattern vector from a real space $X \subseteq \mathcal{R}^m$, and $y_i \in \{-1,1\}$ is the output, representing the class label, SVM will find the separation hyper-plane (between the two classes) $f_{(x)} = w^T\phi(x_i) + b$ by solving the optimization problem:

$$min_{w,b,\xi}\ (\frac{1}{2}w^Tw + C\sum_{i=1}^{n}\xi_i) \quad (1)$$

with the conditions:

$$y_i(w^T\phi(x_i)+b) \geq 1-\xi_i i = 1..n, \xi_i \geq 0 \quad (2)$$

The discriminant function may have the form of

$$f_{w(x,y)}=w^T\Psi(x,y) \quad (3)$$

where the parameter $w \in \mathcal{R}^m$ is the weight vector, and $\Psi(x,y)$ is the feature vector of the input pattern $x$ and the output $y$ as in [8]. The flexible definition of $\Psi$ allows to the SVM to create models for various problems: natural language analysis, bioinformatics (Sequence alignment of proteins), feature selection, image segmentation.

The dual problem may be formulated as follows:

$$max_\alpha W_{(\alpha)} = \sum_{i=1}^{n}\alpha_i - \frac{1}{2}\sum_{i,j=1}^{n}y_iy_j\alpha_i\alpha_jk(x_i,x_j)$$

with the conditions $0 \leq \alpha_i \leq C$, $i=1,n$

$\sum_{i=1}^{n}\alpha_i y_i = 0$.

The Cutting-Plane algorithms as presented by Joachims et al. in [7] starts from an empty set of constraints W=0. At the first iteration w and ξ are set to zero (5). The algorithm iteratively builds the working set $W = W_1 \cup ... \cup W_n$, within the constraints imposed by (2) and (4), reformulating the optimization problem as follows:

$$min_{w,\xi>0}\ \frac{1}{2}w^Tw + C\xi,\ \xi = \frac{1}{n}\sum_{i=1}^{n}\xi_i \quad (5)$$

with the conditions:

$$\frac{1}{n}w^T\sum_{i=1}^{n}[\Psi(x_i,y_i) - \Psi(x_i,\overline{y_i})] \geq \frac{1}{n}\sum_{i=1}^{n}\Delta(y_i,\overline{y_i}) - \xi, \forall(\overline{y_1}..\overline{y_n}) \in W \quad (6)$$

where $W = \{-1,1\}^n$.

The solution found by the algorithm is the couple (w, ξ) in the condition of a classification error ε.

The algorithm needs a number of iterations (C / ε), until reaching the optimum solution, which means that the working set W is independently of the size of the pattern training set.

Parallel Cutting Plane Support Vector Machines algorithm (PCPSVM) divides the input set of available processors ensuring so the parallelism of both data and calculations. PCPSVM algorithm was tested on the cluster RedPower from the Laboratory of High Performance Computing USV Suceava.

2.2. **Evolutive Algorithm for Training SVM**. The general problem of finding the separation hyper-plane between 2 classes is solved using systematically an evolutionary algorithm. The main elements of this evolutionary approach are as follows.

*Representation*: hyper-plane coefficients, $w$ and $b$ are coded in a chromosome structure: $c = (w_1 \ldots, w_n, b)$. Initially, the chromosomes are generated randomly, so $w_i \in [-1,1]$ for i=1,..,n and $b \in [-1,1]$.

*Assignment of fitness function*. The fitness function derives from the objective function and is subject to restrictions of the optimization problem. Departing, however, from standard SVM, for the fitness function is derived a different nonlinear formulation. The parameter is mapped from $\Phi$ in $H$. It follows, then, that the quadratic norm involved in the generalization condition becomes $\|\Phi(w)\|^2$, and the equation of the separation hyper-plane is

$$\langle \Phi(w), \Phi(x_i) \rangle - b = 0 \qquad (7)$$

It is used the notation $\langle u, w \rangle = u^T w$ and the nucleus is used to turn the rule into a scalar product. The formulation of the fitness condition (function) to be minimized incorporates the objective function. The restrictions are formulated by penalizing chromosomes that are incorrectly classified by a *t()*function that returns the value of the argument if it is negative, and 0 otherwise. For classification, the expression of the fitness function is

$$f(w,b) = \frac{1}{2} K(w,w) + C \sum_{i=1}^{m} \xi_i + \sum_{i=1}^{m} [t(y_i (K(w,x_i) - b) - 1 + \xi_i)]^2 \qquad (8)$$

The *selection* and *variation operators*: are applied the most commonly used coding scheme: the tournament selection, intermediated crossing and mutation by disruption of normal distribution.

*Stop condition*: the algorithm stops after a predefined number of generations.

Once the closest values to the optimal values of hyper-plane coefficients are found, a new pattern can be classified directly, using the equation:

$$class(x_i) = \text{sgn}(K(w, x_i) - b) \qquad (9)$$

*Classification accuracy* is defined as the ratio of the number of cases / patterns correctly labeled and total test examples.

The optimization problem solving requires the treatment of errors indicators that were included in the representation in the initial version of evolutionary algorithm. The proposed algorithm (EASVM) provides interactively the hyper-plane coefficients at any time, so it is possible to calculate the errors on each iteration. In this way the error indicators may be removed from the representation of the evolutionary algorithm.

As a consequence, the representation of an individual (hyper-plane) contains only $w$ and $b$. In addition, all indicators will be calculated in reference to their fitness function. Regarding the classification, the current individual (separating hyper-plane) is taken and the support hyper-planes are determined by the proposed mechanism of Bosch and Smith, as in the paper [9].

By using evolutionary algorithms to solve such a problem, the results are obtained in a fairly large time, with a significant consumption of resources. Due to the fact that this type of algorithms can be easily parallelized, we resorted to this embodiment, firstly in order to achieve better results in a shorter training time.

The parallelization of the algorithm for SVM training in the evolutionary approach is presented in the paper [10]. The parallelization

was performed upon the general stages of an evolutionary algorithm: generation of the initial population, selection, crossover, mutation being executed in individual loops on each node. The parallelization is mainly achieved at data level: the population being equally divided between MPI processes running on each node of the cluster.

## 3. EXPERIMENTAL RESULTS

The experiments were conducted on a supercomputer from the High Performance Computing Laboratory in the „Stefan cel Mare" University of Suceava. This supercomputer has a very similar architecture as the supercomputer IBM Roadrunner installed at Los Alamos National Labs, New Mexico, USA, the first supercomputer in the world that surpassed 1 petaflops [11].

The endowment of the University "Stefan cel Mare" Suceava, is a computer cluster consisting of 48 blade servers QS22 (nodes) with 96 PowerXCell 8i processors at 3.2 GHz and 8 server blades (LS22) with AMD Opteron. The storage capacity is 10 TB cluster, and the theoretical processing power is 9.98 TFlops and was able to sustain a rate of 6.53 TFlops for LINPACK operations). Each PowerXCell 8i processor consists of 8 units of account SPE (Synergistic Processor Element) and a computing unit PPE (PowerPC Processor Element). The PPE processor contains a PowerPC core 64-bit. On this core can run operating systems and 32 and 64 bits applications? SPE processor is optimized for applications requiring intensive calculations, like SIMD (Single Instruction Multiple Data). These cores are not created for the implementation of operating systems. SPEs are independent processing elements, each running threads or individual applications. SPEs depend on the PPE sites in that the latter run the operating system and some applications are controlled, while the PPE utilize SPEs to achieve higher speeds in data processing.

*Experiments with PCVSM*

The results validate the fact that the parallelization of the algorithm reduces the complexity of $O(n)$ to $O(n/p)$, for $p$ processors and $n$ the size of the training set. The training of the SVM classifiers was implemented by using the MPICH platform. The PCPSVM algorithm was parallelized on one level (without using the SPE processors).

The speed-up factor was calculated by reference to the PCPSVM algorithm running time on a single PowerXCell 8i processor, using a single thread.

**Table 1**

| Training set | Number of Patterns | Number of Features |
|---|---|---|
| covtype | 581012 | 54 |
| ijcnn1 | 49990 | 22 |
| realsim | 72309 | 20958 |
| web-a | 49479 | 300 |

It was selected 4 sets of binary data (Table 1) to evaluate the proposed parallel algorithm for training SVM: *covtype* (areas covered by forests), *real-sim* (articles discussion groups on real vs simulated) [12], *ijcnn1* - IJCNN 2001 (International Joint Conference on Neural Networks)] *web-a* (the web page classification) [13,14].

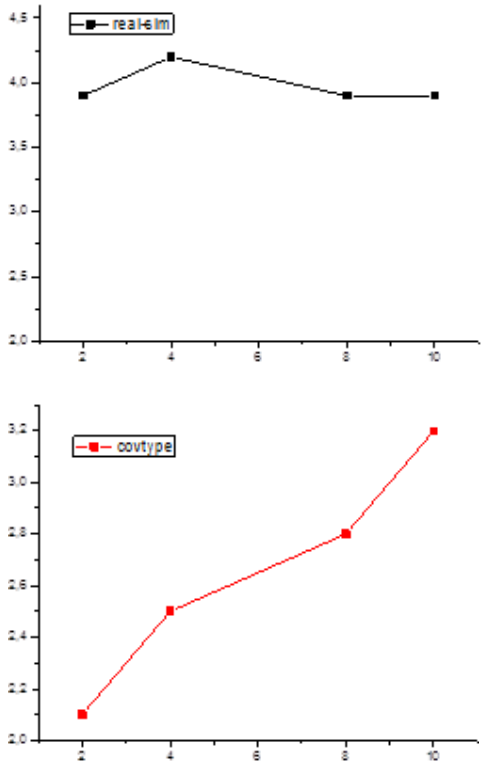


Figure 1. The speed-up obtained by PCPSVM algorithm for *covtype* and *real-sim* databases.

Tests show an increase execution speed of the parallel algorithm in relation to the number of processors involved in training the classifier

on the MPI platform. The results in Figure 1 show a linear growth of the acceleration factor obtained after the parallel execution of the program at the training with *covtype* database.

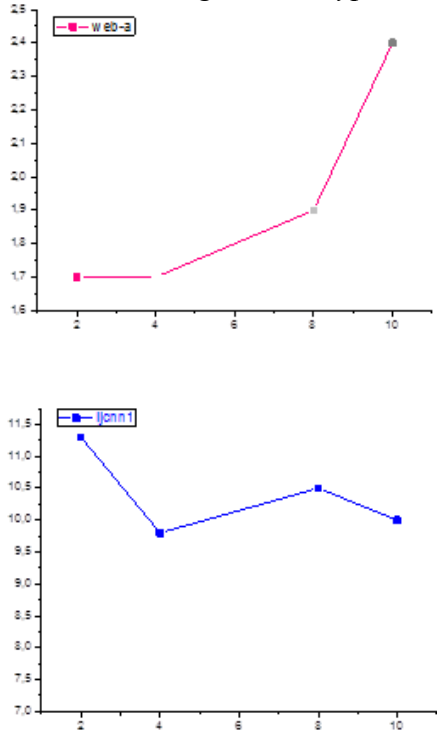


Figure 2. The speed-up for *web* and *ijcnn1* database.

The results in Figure 2 show an acceleration factor of 11 obtained by the program execution PCPSVM on 2 PPE processors using the training data set *ijcnn1* containing 50,000 patterns with 22 features. Lowest acceleration factor, 2.5, is obtained from the classification of web pages; an average acceleration factor of 4, is obtained by the PCPSVM algorithm during the tests with *real-sim* database containing 72,309 patterns.

*Experiments with EAVSM*

For the experiments were chosen four test problems from UCI Repository of Machine Learning Databases [15], their characteristics are shown in Table 2. In each case of these 4 databases many runs were made, taking into account the average values of the results.

**Table 2.**

| **Database** | **Kernel** | **Size of training set** | **Size of test set** |
|---|---|---|---|
| Pima | polynomial | 576 | 192 |
| Iris | radial | 105 | 45 |
| Spambase | polinomyal | 3451 | 1150 |
| Soybean | polinomyal | 30 | 17 |

The population size in each case was 200 individuals; the number of generations evolves these populations being 250, while the probability of recombination and the mutation is 0.4.

The average accuracy obtained in each case is shown in the following table.

**Table 3**.

| Nodes | Iris (%) | Spam (%) | Pima (%) | Soybean (%) |
|---|---|---|---|---|
| 1 | 95,11 | 76,08 | 71,09 | 91,76 |
| 2 | 96,88 | 78,23 | 76,82 | 94,11 |
| 4 | 98,66 | 78,32 | 79,43 | 98,82 |
| 8 | 98,22 | 79,00 | 79,68 | **100** |
| 20 | **100** | 80,48 | 80,21 | **100** |

It may be observed that on the studied datasets, the parallelization of the evolutionary algorithm led to improved results in most considered cases.

## 3. CONCLUSIONS

The parallelization of the training algorithms of SVM proves to be an extremely promising approach, both in terms of computing time performance shown in solving the very large problems, and in terms of solution accuracy.

Tests aimed at training SVM classifier recorded the execution times when used only the PPE processors of PowerXCell 8i processors. Better results for the speed-up of

SVM algorithm may be obtained by activating accelerators SPE of the PowerXCell 8i processors.

The evolutionary solution of the optimization problem provides on every execution step the function coefficients. The EASVM algorithm performance is comparable to that of SVM canonical one, and in some cases offers better results, being widely applicable [~~14,~~15,16].The evolutionary approach to SVM training proves to be a promising method leading to good performance in solving large problems with very good solution accuracy.

## REFERENCES


1. Boser, B.E., Guyon, I., Vapnik, V.N. (1992). A training algorithm for optimal margin classifiers. In Proceedings of the *Fifth Annual Workshop of Computational Learning Theory*, 5, 144-152, Pittsburgh, ACM.
2. ai, Y.-H. & Fletcher, R., New algorithms for singly linearly constrained quadratic programs subject to lower and upper bounds. *Math. Program.,* 106**,** 403-421 (2006).
3. Zanghirati, G. & Zanni, L. A parallel solver for large quadratic programs in training support vector machines. *Parallel Comput.*, 29, 535-551 (2003).
4. Gheorghe Radu, Ştefan-Gheorghe Pentiuc, Ionuţ Balan – Paralelizarea algoritmilor evolutivi pentru instruirea maşinilor cu vector suport, *Sisteme distribuite, Suceava, 2011*, ISSN 1842-6808, p. 24-26 (2011).
5. R. Stoean, M. Preuss, C. Stoean, D. Dumitrescu, Evolutionary Support Vector Machines and their Application for Classification, *Technical Report Nr. CI-212/06,* Collaborative Research *Center on Computational Intelligence, University of Dortmund* (June, 2006).
6. S.H. Jun, K.W. Oh, An evolutionary statistical learning theory, in *Comput. Intell*, 3(3): 249-256 (2006)
7. Yuan, G., PCPSVM: A parallel cutting plane algorithm for training SVMs. *Computer Engineering and Technology (ICCET), 2010 2nd International Conference on (Volume:4 )*, pp. V4-655 to V4-659 (2010).
8. oachims, T., Finley, T. & Yu, C.-N. J. 2009. Cutting-plane training of structural SVMs. *Mach. Learn.,* 77,27-59 (2009).
9. R.A. Bosch, J.A. Smith, Separating Hyper-planes and the Authorship of the Disputed Federalist Papers, *American Mathematical Monthly*, Volume 105, Number 7, pp. 601-608, (1998).
10. Gheorghe Radu, Ionuţ Balan, Ştefan-Gheorghe Pentiuc – Learning Support Vector Machine Using Parallelized Evolutionary Algorithms*, Acta Universitas Apulensis, Mathematics-Informatics*, Nr. Special, ISSN 1582-5329, p. 331-240 (2011).
11. arker, K. J., Davis, K., Hoisie, A., Kerbyson, D. K., Lang, M., Pakin, S. & Sancho, J. C. Year. Entering the petaflop era: The architecture and performance of Roadrunner. In: *High Performance Computing, Networking, Storage and Analysis*, 2008. SC 2008. International Conference for, 15-21 Nov. 2008 2008. 1-11 (2008).
12. McCallum, A. K., Data for binary classification separating real from simulated, and auto from aviation. *http://people.cs.umass.edu/~mccallum/data.html* .
13. Prokhorov D., IJCNN 2001 neural network competition. Ford Research Laboratory, *http://www.geocities.com/ijcnn/nnc_ijcnn01.pdf,* (2001).
14. Platt, J. C. (1998). Fast training of support vector machines using sequential minimal optimization. MIT Press**:** 185-208.
15. A. Frank, A. Asuncion, UCI Machine Learning Repository, University of California, Irvine, School of Inform. and Comp. Sc., *http://archive.ics.uci.edu/ml/* .
16. Schipor, O.A., Pentiuc, S.G., Schipor, M.D., Improving Computer Based Speech Therapy Using a Fuzzy Expert System, *Computing and Informatics* Volume: 29 Issue: 2 Pages: 303-318 (2010)